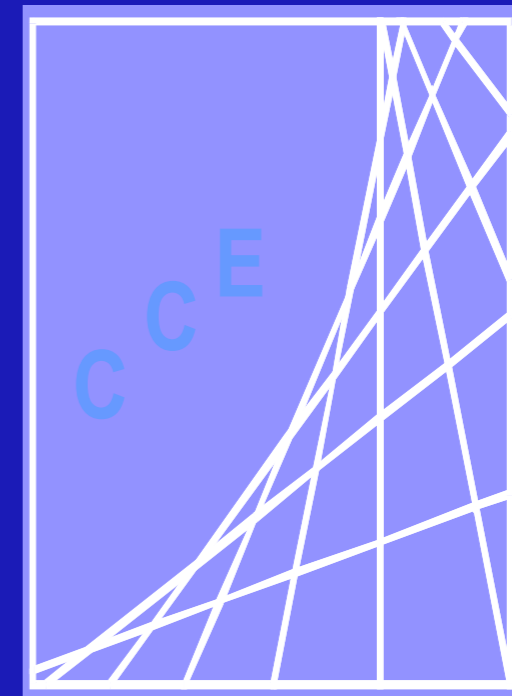


CCE 2012

Computational Civil Engineering International Symposium Iasi, Romania - May 25th, 2012

CCE 2012 International Symposium Iasi, Romania - May 25th, 2012



COMPUTATIONAL CIVIL ENGINEERING

2012



Editura Societatii Academice "MATEI - TEIU BOTEZ"

All rights reserved, © Societatea Academica "Matei - Teiu Botez", Iasi, România, 2012

Proceedings of the 10th International Symposium
"Computational Civil Engineering"
Iasi, Romania - May 25th, 2012

Scientific publication
ISSN 2285-2735, ISSN-L 2285-2735
Director, prof.dr.ing. Constantin Ionescu
Editor in Chief, dr. Rodian Scînteie

Table of Contents

1. Rodian Scinteie, Mihai Budescu, Andrei-Ionut Stefancu Evolution, Refinements, and New Concepts in Computational Civil Engineering	1-8
2. Hamed Amouzegar, Hossein Tajmir Riahi, Maryam Daei Application of Endurance Time Method in Structural Optimization of the Dampers for Seismic Design of Concrete Structures	9-24
3. Sergiu Andrei Baetu, Ioan Petru Ciongradi Cyclic nonlinear analysis of reinforced concrete slit walls with shear connections	25-42
4. Alex H. Barbat, Yeudy F. Vargas, Lluís G. Pujades, Jorge E. Hurtado Probabilistic assessment of the seismic damage in reinforced concrete buildings	43-61
5. Renáta Bašková Modelling of the line construction of building by the method network analysis	62-71
6. Gheorghita Boaca, Cristian-Claudiu Comisu Composite materials in bridge consolidation	72-79
7. Mihai Budescu, Silviu Cristian Melenciuc, Andrei-Ionut Stefancu Experimental study regarding the induced ductility at the steel column base by the baseplate’s flexibility	80-90
8. Omar D. Cardona, Mabel C. Marulanda, Martha L. Carreño, and Alex H. Barbat Probabilistic Seismic Risk Assessment of Barcelona, Spain	91-108
9. Cristina Cosma Integration of web-enhanced teaching tools in undergraduate construction and civil engineering higher education	109-122
10. Ciprian Cozmanciuc, Ruxandra Oltean Analytical method for axial– flexural interaction diagram in case of reinforced concrete columns confined with fibre reinforced polymers	123-133

11. Ciprian Cozmanciuc, Ruxandra Oltean Finite element analysis of square reinforced concrete columns confined with composite membranes subjected to eccentric compression	134-142
12. Gabriela Dascalu Nonlinear analysis in finite element program Abaqus	143-149
13. Laura Dumitrescu, Dan Preda Stefanescu Computer based assessment of building energy performance	150-160
14. Augustin-Ionut Gavrilă, Neculai Scîntei Improvement proposal for URGENT1 - Software for planning and simulation of emergency evacuation using auto transport	161-166
15. Adrian Haiducu, Elena Poida The effects of the seismic actions on bridge structures and structure control system	167-177
16. Vasile Iacob Aspects on building demolition waste and their impact on the environment	178-183
17. Vasile Iacob Improving mechanical and durability performances of air-placed concrete. Laboratory and situ researches.	184-189
18. Dorina Isopescu, Andrei-Ionut Stefanescu, Silviu-Cristian Melenciuc Nonlinear finite element analysis of masonry infill walls	199-202
19. Ludovic Gheorghe Kopenetz, Dragos Florin Lisman Monitoring Steel Bearing Cables Using a Sound Scanning Technique	203-211
20. Marek Krajnák Possibilities of using the genetic algorithms to solve optimization tasks in construction projects	212-219
21. Daniel Lepadatu, Adrian Iacob, Adrian-Alexandru Ciobanu Design of Experiment Application in Thermal Bridges Assessment	220-234
22. Dragos Florin Lisman, Ludovic Gheorghe Kopenetz Intelligent Sensor Networks Used for the Assessment of Structural Health	235-251
23. Ana Nicuta, Razvan Mircea Chirila, Daniela Grigore Principles for design of wind turbine foundations. Case Study	252-261
24. Cerasela-Panseluta Olariu Dynamic response of a wind turbine considering soil - structure interaction	262-272
25. Ruxandra Oltean Finite element analysis of bonding between carbon fibers reinforced polymeric composites (CFRP) and concrete	273-279

26. Ruxandra Oltean, Ciprian Cozmanciuc
Bond behavior between fibers reinforced polymeric (FRP) strips and concrete – An analytical and numerical investigation 280-290
27. Ioana Olteanu, Alexandru Stanila
Computer aided optimization of a mixed structure 291-300
28. Radu-Aurel Pescaru, Georgeta Vasies, Hasan Ali Ahmad Akileh, Adrian Radu
Numerical simulation approach to estimate the ground level wind action near a prismatic building 301-309
29. Elena Poida, Adrian Haiducu
Seismic hazard of Romania: overview for the probabilistic approach 310-318
30. Irina Radinschi, Bogdan Aignatoiaei
Maple 12 a Reliable Tool for Physics Learning 319-325
31. Victoria-Elena Rosca, Elena Axinte, Elena-Carmen Teleman
Optimization methods for steel girders using EUROCODE 3 326-339
32. Octavian Victor Rosca
Some Considerations Regarding the Complex Eigenvalues in Structural Analysis 340-347
33. Neculai Scîntei, Augustin-Ionut Gavrilă
URGENT1 - Software for planning and simulation of emergency evacuation using auto transport 348-354
34. Ana-Luciana Tofan, Vasile Musat
Implementation of a Geotechnical GIS Database for 3D Modeling of the Layer Limit Surfaces 355-367
35. Ana-Maria Toma, Gabriela Maria Atanasiu, Ionut-Ovidiu Toma
Numerical Evaluation of the Seismic Behavior of a Load-Bearing Masonry Condominium Structure Specific for Romanian Urban Areas 368-377
36. Georgeta Vasies, Elena Axinte, Claudiu Romila, Adrian Radu
Numerical simulation of wind action on solar panels inclined with 30° and different wind directions 378-392
37. Georgeta Vasies, Elena Axinte, Elena Carmen Teleman
Wind action on solar panels placed on flat roofs with parapets 393-401
38. Vasile-Mircea Venghiac
Multidirectional energy dissipative columns 402-409

**THE 10th INTERNATIONAL SYMPOSIUM
"COMPUTATIONAL CIVIL ENGINEERING 2012"**

ORGANIZERS

**Faculty of Civil Engineering and Installations
Academic Society "Matei - Teiu Botez"
Spanish Association of Seismic Engineering**

Co-ordination committee

Prof. Eng. Mihai Budescu
Prof. Eng. Alex. Horia Barbat
Prof. Eng. Constantin Ionescu

Scientific commission

Prof. Eng. Doina Stefan
Prof. Eng. Elena Axinte
Dr. Eng. Rodian Scînteie
Dr. Eng. Gabriela Covatariu
Dr. Eng. Mihai Petru

Organizing commission

Eng. Nicoleta Pasehonov

Evolution, Refinements, and New Concepts in Computational Civil Engineering

Rodian Scinteie, Mihai Budescu, and Andrei-Ionut Stefancu
Department of Structural Mechanics, Gheorghe Asachi” Technical University of Iasi
Faculty of Civil Engineering and Building Services, Iasi, 700050, Romania

1. INTRODUCTION

Held each year in Iasi at the Faculty of Construction and Building Services from the Technical University “Gheorghe Asachi” the Symposium became a tradition. 80 authors are participating from universities from Columbia, Slovakia, Iran, Spain, SUA and of course Romania. This edition the scientific committee selected 37 articles grouped in four themes:

- Computer aided design and engineering;
- Computer based education;
- Computational methods in civil engineering;
- Computer aided management in civil engineering.

2. COMPUTER AIDED DESIGN AND ENGINEERING

Ten articles are part of this section.

Mircea Venghiac discusses in the article titled “Multidirectional energy dissipative columns”, the opportunity of using the Slimdek composite flooring system in conjunction with multidirectional dissipative columns as a method to absorb seismic energy.

By means of Computational Fluid Dynamics (CFD) Georgeta Vasies et al. examines the wind effect on the design of support systems for solar panels. In the study, the wind pressure on 12 solar panels in an arrayed configuration, mounted on ground level, with an angle of 30° and seven wind directions (0°, 30°, 45°, 60°, 90°, 135°, 180°) have been analyzed using ANSYS 12 CFX computer code.

The problem of wind action on solar panels placed on flat roofs with parapets is tackled by Georgeta Vasies, Elena Axinte, and Elena Carmen Teleman. The aim of the article is to highlight the shielding effect produced by the building, respectively by building and parapet on the pressure distribution on the solar panels surface. Numerical simulations are performed using ANSYS 12 CFX, for an incidence wind angle of 135°.

Due to the fact that Romania is located in a seismic area, when evaluating the response of a wind turbine to seismic action soil - structure interaction should be considered. In her paper Cerasela-Panseluta Olariu presents a dynamic analysis of a 70 meters tall wind turbine considering 4 different types of soils and using the finite element method.

Budescu, Melenciuc and Stefancu present the results of an experimental study regarding the induced ductility at the steel column base by the baseplate's flexibility. The overall structural behavior is described and the parameters involved in the connection design of two exposed rigid baseplates are evaluated. The connections have been analyzed by means of full-scale tests that lead to failure modes validated by finite element models.

Energy regeneration is a special problem both for Europe and the entire world. Designing the foundations for the wind turbines – that generate eco-friendly energy – is a challenging task. Nicuta, Chirila and Grigore present issues related to the design of foundations for wind turbines located in two different areas of Romania, with different geotechnical characteristics.

Problems in Civil Engineering are more complex and challenges are raised whenever optimization of solutions is required. Wide spread of computer use and development of algorithms provide proper conditions for introduction of the Artificial Intelligence within construction projects. An interesting approach of the subject is made by Marek Krajnák from the Institute of Civil Engineering Technology and Management at the Faculty of Civil Engineering, Technical University of Kosice, Slovakia in his paper "Possibilities of using the genetic algorithms to solve optimization tasks in construction projects". The article presents the state of the art in the area, detailing on evolutionary algorithms, use, advantages, and disadvantages of genetic algorithms.

The optimization problems that may be solved using GA as found into literature are:

- resource optimization,
- process optimization,
- optimization of construction products, and
- optimization of customer service.

A review of software tools available for convenient use within construction projects is also performed. Although the GAs are resource consuming tools, the development of the information technology allows this approach and the future increase makes this inconvenient even less significant. Their versatility and simplicity produce a large potential for full exploit in the area. In addition, GAs do not impose great demands on the user.

Modern architecture tends to propose structures with challenging shapes for the structural designers. In their paper Ioana Olteanu and Alexandru Stanila study the structural configuration of an innovative flexible 5-storey building. The analyses were performed using SAP2000 computer program and lead to the most suitable configuration that satisfied strength, serviceability and stability requirements

Amouzegar et al. evaluate the concrete moment-resisting frames strengthened using dampers by Incremental Dynamic Analysis (IDA) and Endurance Time (ET) analysis. A special attention is given to the results' accuracy assessment and application of ET analysis in estimating structural optimization by using damper. Optimization results of dampers characteristics and their positions in the structures obtained by ET analysis are the same as the results of IDA in most cases.

Standard optimal design formulation of steel plate girder respecting Class restriction is discussed by Rosca, Axinte and Telesman. Efficient procedures for minimum weight design of unstiffened steel plate girders using analytical and numerical approach are presented. The nonlinear optimization problem is formulated also on the basis of the current Eurocode 3 specification. Results of numerical calculations for optimal shapes of three steel-grades and various beam length are presented

3. COMPUTER BASED EDUCATION –

This section includes 2 articles.

Throughout time, there has always been a constant need to improve students' learning process. To meet this goal Radinschi and Aignatoiaei suggest the use of Maple 12 as a mean to assist first year students in the learning physics. Examples of 2d and 3d plotting of physical quantities from Classic Mechanics are presented in their article. The plots use important physical quantities like the mechanical work, force, momentum, wave vector, period and pulsation.

Cristina Cosma describes and analyzes in her paper the three steps used in implementing webenhanced teaching in one of the Wentworth Institute of Technology' courses (CCEV 206 - Heavy Construction). The advantages and

disadvantages of using such novel instructional methods are assessed based on students' evaluations and comments and also on student performance. The paper particularly outlines the challenges encountered in building the on-line course content, class assignments and student learning assessment tools.

4. COMPUTATIONAL METHODS IN CIVIL ENGINEERING

This section has 16 articles.

The effects of the seismic actions on bridge structures and structure control system is assessed by Haiducu and Poida. Advantages and disadvantages of different types of isolators applied to bridge structures are highlighted and a numerical example is presented.

Radu-Aurel Pescaru in paper titled "Numerical simulation approach to estimate the ground level wind action near a prismatic building" presents some numerical results, regarding the pedestrian level wind environmental conditions around single rectangular shape buildings. The research was carried on at the Building Aerodynamics Laboratory of the Faculty of Civil Engineering and Building Services from Iasi.

Strengthening of reinforced concrete elements (RC) and structures with externally bonded fiber reinforced polymers (FRP) is becoming an increasingly popular technique in civil engineering community. In respect to this trend, Cozmanciuc and Oltean evaluate the behavior of RC elements wrapped with carbon fiber polymeric (CFRP) sheets by means of a finite element analysis using Ansys package software. Their paper presents the results of the analysis for a RC column before and after confining it with one layer of CFRP

Ruxandra Oltean presents in her paper the experimental program that has been carried out at the Technical University of Iasi, Romania and studied the interfacial behavior between carbon fibre reinforced polymer (CFRP) composite sheets and concrete. Furthermore finite element analysis that supported the experimental results was performed

Reinforced concrete (RC) structures, due to a wide range of reasons often need to be strengthened. Fiber reinforced polymer (FRP) composites in the form of bonded strips applied to the external surface can be a convenient strengthening solution. One major drawback of such a strengthening technique is the unpredictability of the bonding between FRP and concrete. Oltean and Cozmanciuc's article provide a full review of existing bond strength and bond – slip models and conducts a

research aimed at simulating the bond behavior of external FRP reinforcement and concrete substrate

Ciprian Cozmanciuc and Ruxandra Oltean present, in their article, a procedure that allows the development of a simplified axial– flexural interaction diagram for FRP-confined RC columns. In the proposed method, the analysis of FRP-wrapped columns is carried out based on principles of equilibrium and strain compatibility equivalent to that of unconfined RC columns.

Masonry or masonry infill walls have been widely used in the past and are still a common design solution for low rise building nowadays. Isopescu, Stefancu and Melenciuc analyze, using the finite element method, the influence of the design solutions and the infill materials on the overall behavior of a reinforced concrete frame.

Laura Dumitrescu and Dan Preda Stefanescu briefly present a detailed comparative study of a thermal bridge calculation using two programs for thermal field simulation. A simplified method to include the thermal bridge effect into the assessment of the building energy performance is also proposed.

A new approach to an economical design of buildings based on performance criteria is addressed by Sergiu Andrei Baetu and Ioan Petru Ciongradi. The solution is to create an improved structure for tall multi-storey buildings that has a rigid behavior at low seismic action and turns into a ductile one in the case of a high intensity earthquake

Numerical evaluation of the seismic behavior of a load-bearing masonry condominium structure is performed by Toma et al. The analysis is performed by means of SAP2000 computer software, the numerical model closely follows the geometry and loading conditions of a real structure. The results show that there are minor degradations in the structure and, therefore, the safety of the occupants is not jeopardized.

A nonlinear finite element analysis using the Abaqus program is performed by Gabriela Dascalu. The author seeks to enhance the way that the elastic-plastic response of structural assemblies is addressed

Seismic risk and seismic effects are important concerns in civil engineering. The subjects are largely studied all over the world in order to reduce potential damages. Several articles presented to the symposium are the expression of this present involvement.

In the article “Probabilistic Seismic Risk Assessment of Barcelona, Spain” the authors Omar D. Cardona, Mabel C. Marulanda, Martha L. Carreño and Alex H. Barbat present the assessment of seismic risk for the city of Barcelona using CAPRA (Comprehensive Approach for Probabilistic Risk Assessment) which

involves the evaluation of probabilistic losses of the exposed elements using probabilistic metrics.

The paper performs a seismic risk assessment of the city of Barcelona, Spain using CAPRA, which is considered to be the most robust for this type of modeling and identifies the most important aspects of catastrophe risk from the financial protection perspective according to the fiscal responsibility of the states. The probabilistic earthquake risk model is built on the following modules:

- Hazard module,
- Exposure module, and
- Vulnerability module.

The outputs of these three modules are further process by Risk module to produce data for end users or applications. All the modules have probabilistic formulation to cover the uncertainty of all events. Using the model the paper develops maps to clear specify the loss in case of catastrophic events. The risk is of maximum importance not only for insurance industry which may impose different premiums but also for the government whom, as last resort, is the risk taker for the uninsured or uninsurable risk. Also, maps may help for decision makers to save not only money but also lives. These measures are of particular importance for the future design of risk retention (financing) or risk transfer instruments, and therefore they will be a particularly valuable contribution to further studies to define a strategy for financial protection to cover the fiscal liability of the state.

In the same direction, the article “Seismic hazard of Romania: overview for the probabilistic approach” of Elena Poida and Adrian Haiducu from Department of Structural Mechanics at Technical University of Civil Engineering, Bucharest – Romania, is dealing with the analysis of probabilistic seismic hazard analysis (PSHA). The application is developed for territory of Romania using CRISIS2007 v7.2 computer software. A description of the software and data used for model is made in the article. The analysis is made for the main seismic source in Romania: Vrancea Region. The seismicity of the source was selected as Poisson process.

As Romania is one of the world countries exposed to a persistent, periodical and severe seismic regime produced by various tectonic type sources use of powerful analysis tools is a must. The results obtain with Crisis were validated through the preview hazard analysis studies and proved to be an interesting tool in performing a probabilistic hazard analysis.

A probabilistic assessment of the seismic damage in reinforced concrete buildings by using Monte Carlo simulation is described by Barbat et al.

Some considerations regarding the complex eigenvalues in structural analysis are drawn by Rosca. Numerical problem of the complex eigenvalues are dealt with. A structural case study of a 3 storey frame tested on the master shaking table of the

Laboratory of Earthquake Engineering from the Structural Mechanics Department of the Faculty of Civil Engineering and Building Services from Iasi is presented. The analysis lead to the complex eigenvalues and modal shapes of vibration.

In their work, Composite materials in bridge consolidation, Gheorghita Boaca and Cristian-Claudiu Comisu present the technical solution for the rehabilitation of an arches bridge on a national road in Romania. The consolidation solution of bridge for taking current and future loads were made with composite materials based on carbon fibers arranged to take over sectional efforts. In order to determine the amount of material, static calculation was made for the entire bridge structure. The values for sectional efforts determined the carbon fiber amount necessary.

5. COMPUTER AIDED MANAGEMENT IN CIVIL ENGINEERING

Nine articles were selected for this section.

Using heuristics for a better time schedule of evacuation and with a final purpose of mineralizing risk taking Gavrila and Scînteii improve the previously developed software URGENT1. The program is used for planning and simulation of emergency evacuation using auto transport

Using URGENT1 program Scînteii and Gavrila performed a case study that simulated and planned decisions regarding population evacuation in case of an emergency. It resolved issues related to: transportation plan, convoys' assembly, displacement itineraries, population evaluation and other.

“Implementation of a Geotechnical GIS Database for 3D Modeling of the Layer Limit Surfaces” is the title of the article submitted by Ana-Luciana Tofan, Vasile Musat. The paper present a method for integration of geotechnical data in a Geographical Information System and it also highlights the changes in 3D surface models of stratification limits.

Dragos Florin Lisman and Ludovic Gheorghe Kopenetz present a solution for complex monitoring systems. The system uses complex sensors capable of detecting cracks, crack propagation, linear displacements and image capturing sensors and is designed to continuously assess the structural health of different categories of bearing structures

Vasile Iacob summarizes in his paper the Romanian and European concerns on the recovery of demolition waste.

The same author presents a modern and efficient method for air-placing low W/C ratio concrete. A modified traditional Romanian installation for dry mix air-placing

is proposed. The changes improve its reliability and increase its quality and performances thus leading to significant costs and material savings.

In the context of Energy Performance of Buildings Directive (EPBD) implementation in national regulations, Lepadatu et al. present a statistical study emphasizing on the significance of different factors involved in the effect of thermal bridges. The study uses a nonlinear regression model.

Ludovic Kopenetz and Dragos Lisman propose a sound scanning technique to detect the initial rupture in steel bearing cables. The entire system depends on a set of accurate sound acquisition devices. The authors try to prove by several tests that this is a feasible and cost-competitive method for cable structure monitoring.

The mathematic apparatus of various methods of network analysis and its conformity with the requirements for planning, debugging, tracking and automatic update of the scheduling line construction are dealt by Bašková.

Application of Endurance Time Method in Structural Optimization of the Dampers for Seismic Design of Concrete Structures

Hamed Amouzegar, Hossein Tajmir Riahi and Maryam Daei

Department of Civil Engineering, University of Isfahan, Isfahan, Iran

Summary

Optimization techniques play an important role in structural design. These methods help a designer to find the best solutions in order to maximize benefits derivation from the available resources. Additionally, to mitigate damage resulting from seismic hazard, an alternative design approach is to introduce seismic isolation systems or supplemental energy dissipation which can distribute energy dissipation within a structure when subjected to seismic ground motions. The optimization design of structure by using damper, including the optimization of damper characteristics and its position in structure, is an accurate function since mentioned parameters have fundamental effect on the structural energy absorption. The main goal of this paper is the evaluation of concrete moment-resisting frames strengthened using dampers by Incremental Dynamic Analysis (IDA) and Endurance Time (ET) analysis. ET analysis is a new dynamic pushover procedure in which structures are subjected to gradually intensifying acceleration functions and their performances are assessed based on their responses. This has been performed using OpenSees software. In order to model deteriorating connections, frames are modeled using concentrated plastic hinges. Therefore the material model with stiffness degradation and strength deterioration characteristic is considered in this study. To perform incremental dynamic analysis a set of ground motion accelerograms is selected from the database of the records used in FEMA 695. In this paper special attention is given to the results accuracy assessment and application of ET analysis in estimating structural optimization by using damper. It is clearly observed that structural responses resulted from endurance time analysis are compatible with those obtained from Incremental Dynamic analysis (IDA). Optimization results of dampers characteristics and their positions in the structures obtained by ET analysis are the same as the results of IDA in most cases. Also it is shown that ET analysis can clearly identify the structure with a better performance even in the case study of structures with a relatively complicated nonlinear behavior.

KEYWORDS: Damper Devices, Structural Optimization, Endurance Time Method, Incremental Dynamic Analysis, Concrete Structures.

1. INTRODUCTION

Analytical and experimental studies show that by using dampers in structures the structural damping is increased notably and damages to the structures due to strong earthquakes can be reduced significantly. Optimum design of structures with damper, including optimization of dampers' parameters and optimization of dampers' location in the structure, is a major task, because rational parameters and proper location of dampers will lead to most effective energy dissipation [1].

Endurance time method is basically a dynamic pushover method that tries to predict seismic response of structures by analyzing their performance when subjected to predesigned intensifying acceleration functions [2]. If ET acceleration functions can assemble the major characteristics of real ground motions with different intensities, they can provide a good estimate of the real response of the structures to be used in performance based engineering [1]. Therefore this method can be used to check the performance of different systems and find the one with the best performance. In this research, half of provisions of ASCE/SEI 41-06 [3] have been considered for setting design objectives and acceptance criteria, the Basic safety earthquake 1 (BSE-1) and Basic safety earthquake 2 (BSE-2).

On earthquake intensities, BSE-2 hazard level represents the most intensive probable earthquake having the probability of exceedance of 2% in 50 years or return period of 2475 years and BSE-1 hazard level has the probability of exceedance of 10% in 50 years or return period of 474 years. These hazard levels are defined as acceleration response spectra or acceleration time-histories which are scaled according to corresponding 5% damped design spectrum ASCE-07 [4]. In this paper it is tried to find the optimum arrangement of viscous dampers in Reinforced Concrete (RC) Special Moment Frame (SMF) to reach the expected performance by using ET method as the analysis tool along with the genetic algorithm as the optimization tool.

The frames with nonlinear behavior and controlled design drift in initial design are modeled using OPENSEES [5]. Using genetic algorithm, the arrangement of dampers along the altitude of structure is assigned such that the structure satisfies the half of two allowable code performances in the two levels of BSE-1 and BSE-2 at the least sum of required damping coefficients. In this paper the acceleration functions using in ET method have a matched response spectrum with the 5% damped design spectrum ASCE-07. For evaluating ET method the results are compared with the results of incremental dynamic analysis [6] with spectrum matched records.

2. ET ACCELERATION FUNCTIONS AND SPECTRUM MATCHED RECORDS

A major factor in the success of the endurance time method is in the availability of suitable intensifying excitation functions. Previous studies show that usable intensifying excitations (i.e. acceleration functions in this study) can actually be designed [7]. Acceleration functions are designed in such a way that each window from zero to time t produces a response spectrum that is proportional to the template spectrum with proportionality factor that is linearly increasing with time and equal to unity at particular time called t_{Target} . To achieve this goal, the target acceleration response of ET acceleration function can be defined as in Eq (1):

$$S_{aT}(T, t) = \frac{t}{t_{\text{Target}}} S_{aC}(T) \quad (1)$$

Where $S_{aT}(T, t)$ is the target acceleration response spectrum at time t and period of vibration T . $S_{aC}(T)$ is the template acceleration response spectrum. Acceleration functions used in this study (ETA40g or series g) have been optimized in such a way that, the response spectrum of SDOF system with 5% damping for the window from zero to 10 (t_{Target}) seconds of ETA40g is fit to design spectral acceleration ASCE-07 (2005) code for soil type C with $S_s=1.5$, $S_1=0.6$, $F_a=1.0$, $F_v=1.3$ and $TL=8$. The response of SDOF system to the acceleration function series ETA40g with a window from zero to any other time have a linear relation with ASCE-07 spectrum. For example for time 5 sec or 15 sec the spectrum will be equal to 0.5 or 1.5 times to ASCE-07 spectrum.

Optimization of these acceleration functions is for 200 periods in 0 to 5 seconds plus 20 points from period = 6 to period = 50 seconds. The whole time of these acceleration functions is 40.96 seconds. Figure 1 shows one of these acceleration functions.

Seven near fault ground motions (series OGM) were selected from the series of fourteen near-field pulse records subset listed in FEMA P695 [8]. The specifications of the ground motions of this set are shown in Table 1. The records have been spectrum matched to the same design earthquake spectrum ASEC-07 that acceleration functions ETA40g are optimized to fit. The spectrum matching procedure is applied in time domain using wavelet method. The wavelet used in this study is reverse impulse presented by Abrahamson (1992).

After using impulse reverse wavelet for prevention of non-zero displacement and velocity at the end of the time series a linearly base line correction has been applied to the spectrum matched results. This procedure has the advantage that the shape and frequency content of time series after spectrum matching are almost the same before [9].

Figure. 2. shows the arias intensity, fourier amplitude and acceleration time history of record DZC before and after of spectrum matching. Figure. 3. shows the mean

response acceleration of acceleration functions ETA40g at $t = 10$ and 15 seconds, OGM set with scale factor 1 and 1.5 and spectrum matched set (GM) with scale factor 1 and 1.5. The obtained coefficients for GM set and ET acceleration functions proportionate with the performance levels are shown in Table 2 .

Table 1. Description of the GM set of ground motions used in this study.

Date	Name	Magnitude (Ms)	Station Name	PGA (g)	Component (degree)	Epical (km)	Abbreviation
1999	Duzce, Turkey	7.1	Duzce	0.52	270	1.6	DZC
1992	Erzican, Turkey	6.7	Erzincan	0.49	N-S	9	ERZ
1979	Imperial Valley-06	6.5	El Centro Array #6	0.44	230	27.5	H-E
1999	Kocaeli, Turkey	7.5	Izmit	0.22	90	5.3	IZT
1992	Landers	7.3	Lucerne	0.79	0	44	LCN
1992	Cape Mendocino	7	Petrolia	0.63	90	4.5	PET
1994	Northridge-01	6.7	Rinaldi Receiving Sta	0.87	228	10.9	RRS

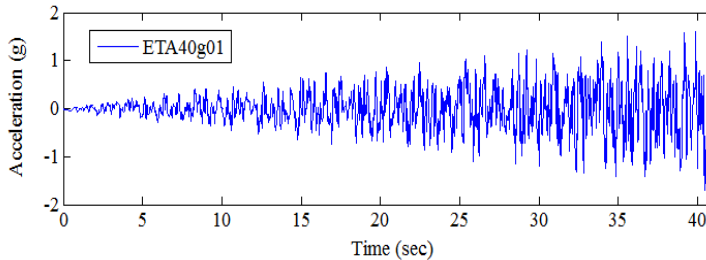


Figure 1. Acceleration Function ETA40g01

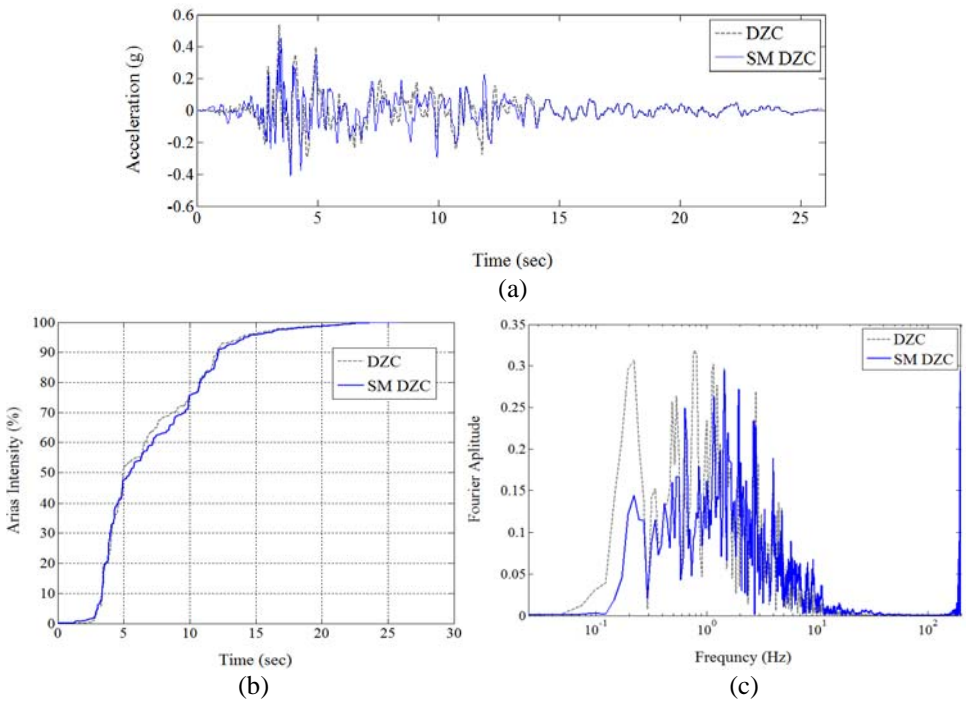
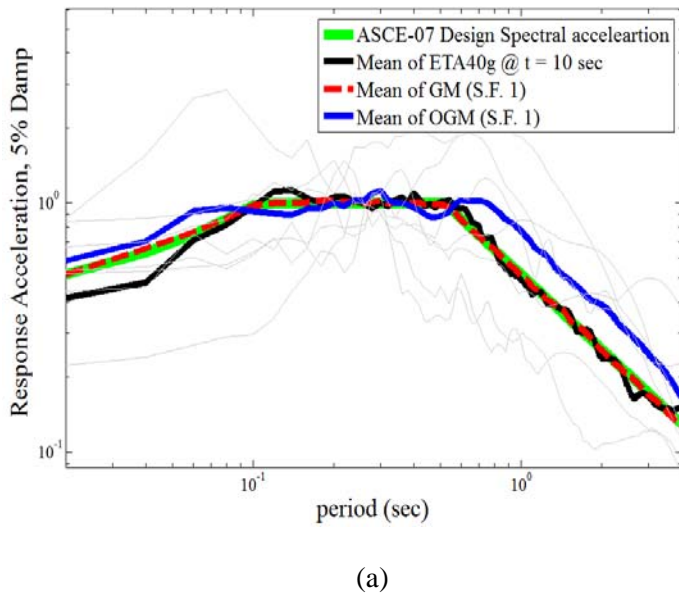
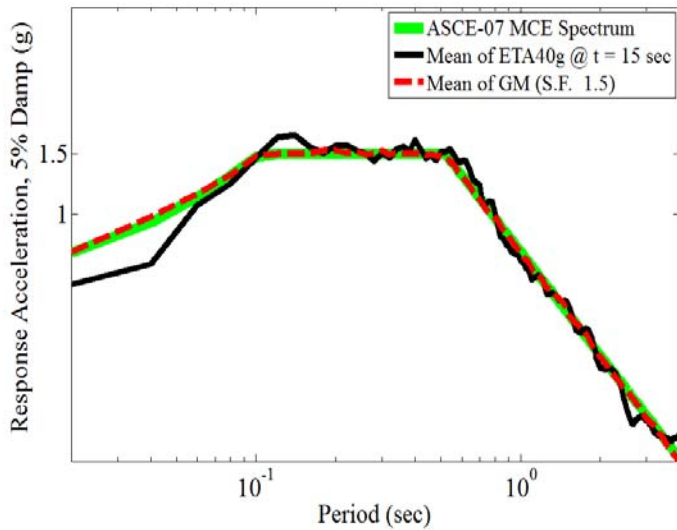


Figure 2. a) apparent shape, b) Arias intensity and c) Fourier amplitude of record DZC before and after spectrum matching.



(a)



(b)

Figure 3. Response spectrum acceleration a) of ETA40g at time 10 sec, GM and OGM sets with scale factor 1 b) of ETA40g at time 15 sec, GM set with scale factor 1.5.

Table 2. Scale factors for GM1 and ET time in 3 hazard levels.

Performance levels	Scale factor	ET time (sec)	Maximum interstory drift ratio (MIDR)
BSE-1 (Basic safety earthquake 1) ASCE-07 design earthquake (L.S.)	1.00	10	1.25 % (1/2 * 2.5 %)
BSE-2 (Basic safety earthquake 2) ASCE-07 maximum considered earthquake (C.P.)	1.50	15	2.5 % (1/2 * 5 %)

3. STRUCTURAL MODELS AND VISCOUS DAMPERS

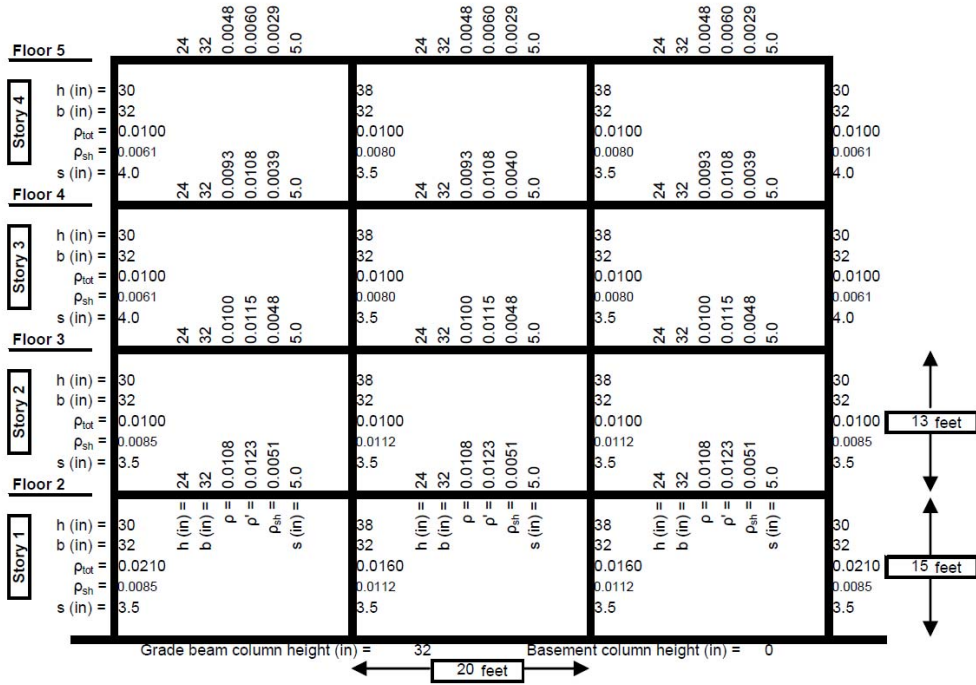
In this study three Reinforced Concrete Special Moment Frame (RC-SMF) with two, four and eight story and three bays are considered. The generic frames are adopted from the models developed by Haselton (2011) [10]. These frames are designed according to ASCE7-02 and ACI318-02. The geometry and specifications of four story model is depicted in Figure 4 and The specifications of frames are shown in Table 3. Height of story one in all frames is 15 feet and the height of the all other stories is 13 feet. Length of each bay is 20 feet. For the two story, Column size concrete strength are designed to satisfy joint shear requirements, specifically the column widths were increased to increase column area. Beams strength were

controlled by force demand, but four beams had additional reinforcement added to keep the same rho ratio between the floors. Column strengths are controlled by strong-column weak-beam (SCWB) except two exterior lower columns that were controlled by flexural demands and two upper story exterior columns controlled by minimum the reinforcement requirement. Beam stirrups were controlled by the minimum requirement. The column stirrups were controlled by confinement requirement. For the four and eight story, Initial member sizes (beam depths, column dimensions) were determined mostly by joint shear and minimum size requirements, in addition to column-beam compatibility considerations. The depth of the grade beams was increased to help alleviate joint shear concerns. Beam strengths were controlled by force demands, particularly lateral forces. Fourth floor beam strength was increased slightly to help reduce SCWB ratio at affected joints. Column strengths were determined by strong-column weak-beam (SCWB) ratios except in the first story, where flexural demands controlled. Concrete strength was increased to 7.0 ksi for four story and was stepped up to 6.0 ksi for eight story in the lower columns to help meet joint shear requirements. Beam stirrups were controlled by shear capacity design. The column stirrups were controlled by both the shear capacity design and the confinement requirements. The frames are modeled in OPENSEES (2011). A primary frame and Grade Beam at the basement has been considered in all frames. The joints were defined as joint shear panel zones. Modeling Flexural Behavior of Reinforced Concrete Beam-Column Elements is shown in figure 5.

Viscous dampers are widely used in mechanical systems. The force induced in viscous damper depends on velocity; therefore, the maximum damper force in an earthquake is always $\pi/2$ out of phase with respect to displacement, and the maximum speed occurs at the time that the displacement is zero. This is an advantage for these kinds of dampers because when the structure endures great internal forces due to displacements created by earthquakes, they induce least extra forces on the structure. To model viscous dampers as bracing, viscous material available in OPENSEES is used. The induced stress in this material is acquired from this equation:

$$\sigma = C_0 |\dot{\epsilon}|^\alpha \text{sign}(\dot{\epsilon}) \quad (2)$$

Where σ represents the induced stress in the material, $\dot{\epsilon}$ strain rate, C_0 damping ratio and α damping exponent.



Design base shear = 0.092g, 386 k **f_c** beams = 5ksi **f_c** cols, upper = 5ksi
f_c cols, lower = 7ksi, **f_y** rebar, nom = 60ksi

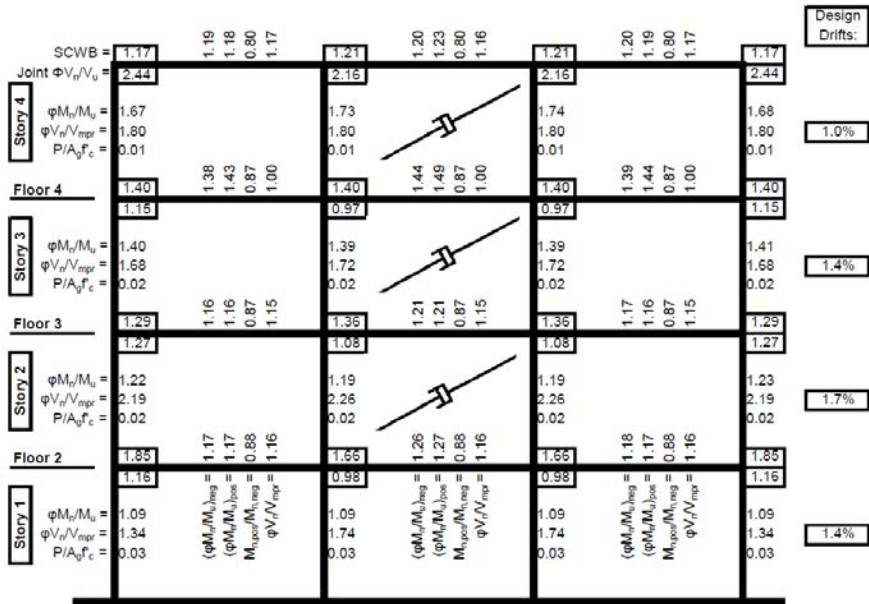


Figure 4. Schematics of four story frame under investigation.

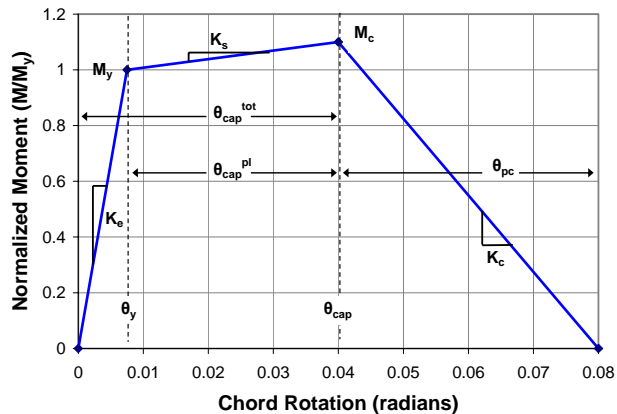


Figure 5. Modeling Flexural Behavior of Reinforced Concrete Beam-Column Elements

Table 3. Specification of the frames.

ID Number	No. of stories	Fundamental Period (sec)	Strength/Stiffness Distribution Over height	Foundation Fixity Assumed in Design
2064	2	0.66	A*	GB**
1003	4	1.12	A	GB
1011	8	1.71	A	GB

* Expected practitioner design; strength and stiffness stepped over height as would be done in common design practice.

** "Grade Beam" - this considers the rotational stiffness of the grade beam and any basement columns.

4. ANALYSIS AND OPTIMIZATION PROCEDURE

The problem is going to find optimized damper coefficients in each story so that the MIDR of the frame in two level of ASCE-07 satisfy the limit levels of half of ASCE41-06 (MIDR = 1.25 % for design earthquake and MIDR = 2.5 % for maximum considered earthquake (MCE)). At first step some value should be assigned to the dampers and in the next step OPENSEES is running and then it's got to be check that MIDR has satisfied the limit levels or not. So this problem needs an optimization procedure. It seems that the genetic algorithm is a good optimization procedure for this problem. In genetic algorithm a primary population is randomly generated then after generation the fitness function will be check. The good population will be remain with a cross over rate and remain are killed. After that a new population will be generated from the good ones. For prevention of stick answer in a local space, the algorithm is doing a mutation. In this specific problem the fitness function is defined sum of damping coefficients in all stories. Before checking fitness function the constraint (MIDR should have an acceptable difference with the Limits) should be controlled. If primary population satisfy the

constraint the algorithm can go on, if not the population should change. Because of negligible changes in MIDR under primary population, the algorithm may never converge, so the first population should be potential for the solution. The convergences criteria may be defined algorithm halts after a specified number of iteration or converge in damping coefficient. After generation organisms (coefficient), the structure is analyzed under ETA40g. Then ET curve corresponding to MIDR is drawn. MIDR correspond to time 10 sec is equivalent to MIDR for design earthquake (Life Safety (LS)), and at time 15 sec is equivalent to MCE (Collapse Prevention (CP)). After checking both MIDR of LS and CP levels with limit levels, if feasible solution is obtained then genetic algorithm tries to find optimal solution. Else new population of organisms should be reproduced.

5. ANALYSIS AND OPTIMIZATION RESULTS

5.1. ET acceleration functions and ground motions

The response spectrum of seven records and ETA40g are exactly match to the ASCE-07 spectrum (target spectrum). So any scale factor multiplied by the records produce a spectrum that is scale factor times to target spectrum. The performance criterion for BSE-1 level is considered to be LS (1.25% MIDR) and for BSE-2 level is considered to be CP. So for controlling MIDR at BSE-1 level, the scale factor is 1 and for controlling BSE-2 (2.5% MIDR) level the scale factor is 1.5 respectively. In the endurance time method particularly for ETA40g the dynamic analysis is going to the last time of the acceleration function that is here 40.96. Then the ET curve is drawn correspond to MIDR. MIDR at time 10 sec should be compared with BSE-1 level and at time 15 sec should be compared with BSE-2 level.

5.2. ET analysis and optimization

In this research, according to the code, the design objectives 'p' and 'k' are assigned as the rehabilitation objectives. Therefore, the structure should satisfy the CP performance level in BSE-2 hazard level and LS level in BSE-1 hazard level. This would be the basic safety objective or BSO. According to ASCE41-06, the allowable transient interstory drift ratio is 5 % for the CP level or 2.5 % for those structures that without damper satisfy the limits levels and 2.5 % for the LS level. In this paper because the frames satisfied the limits so they are considered relatively 1.25 % and 2.5 % for BSE-1 and BSE-2. By drawing the performance curve similar to the curve in Figure. 6 and comparing with the allowable limits of the code, the vulnerability of each structure can be distinguished [11]. In this stage using the genetic algorithm with the purpose of reaching the acceptable

performance stated in the code, which is equivalent to make the performance curve (ET curve) below the allowable limit of the code presented in Figure. 8 to Figure. 10, the required damping for each structure is evaluated (Figure. 7). For example, for the eight frame, the required damping in the first and sixth stories is more than the other stories and the second and fifth stories have least influence on controlling MIDR rather than other stories.

The performance curves of the structures before and after the rehabilitation are compared in Figure. 8 to Figure. 10. As shown, the performance curve of the structure after rehabilitation (damper installation) is quite close to allowable limit of the code and the smoothed curve has contacted it at a point, this indicates the optimal use of structure capacity.

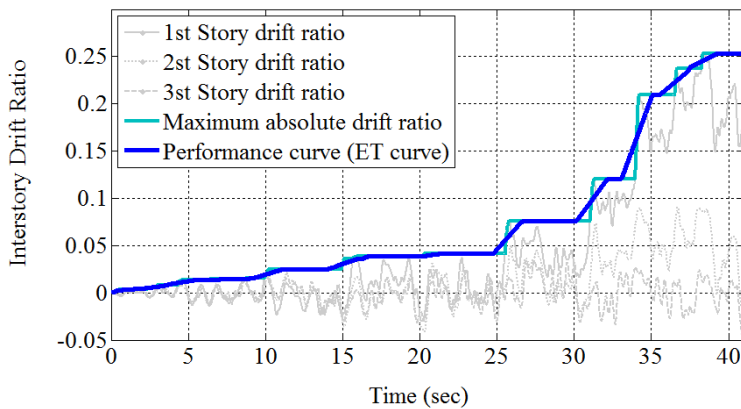


Figure 6. Generating performance curve (ET curve) for FM03B1RGW based on interstory drift ratio.

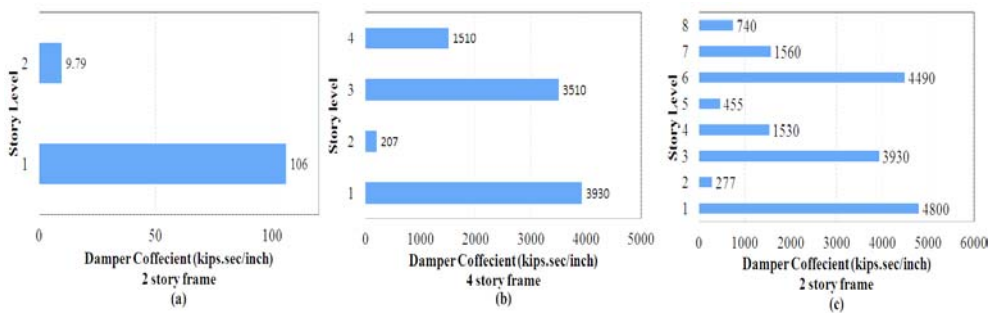


Figure 7. Optimum damper distribution for (a) 2 story frame (b) 4 story frame (c) 8 story frame.

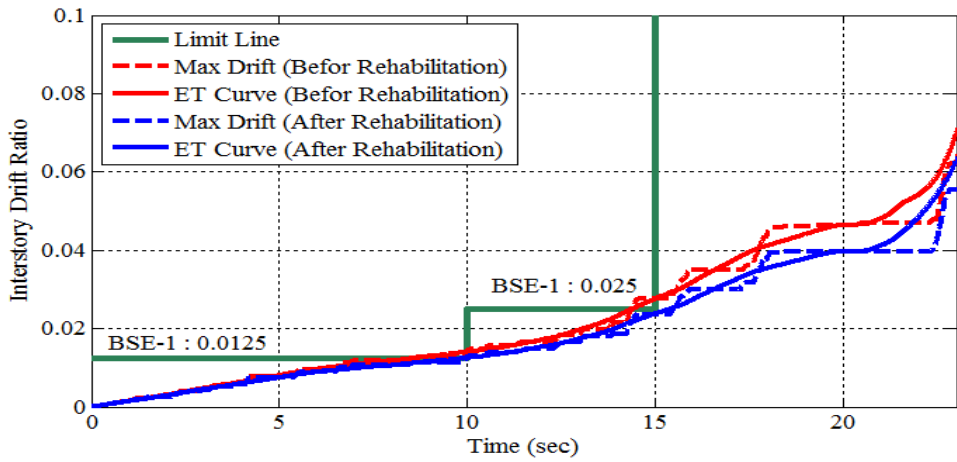


Figure 8. Performance curve (ET curve) for 2 story frame before and after rehabilitation.

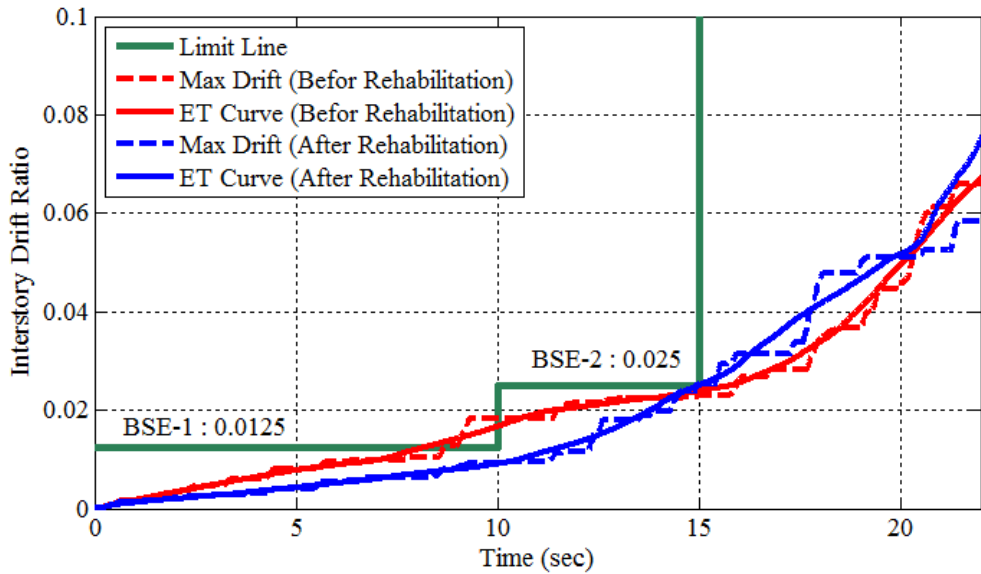


Figure 9. Performance curve (ET curve) for 4 story frame before and after rehabilitation.

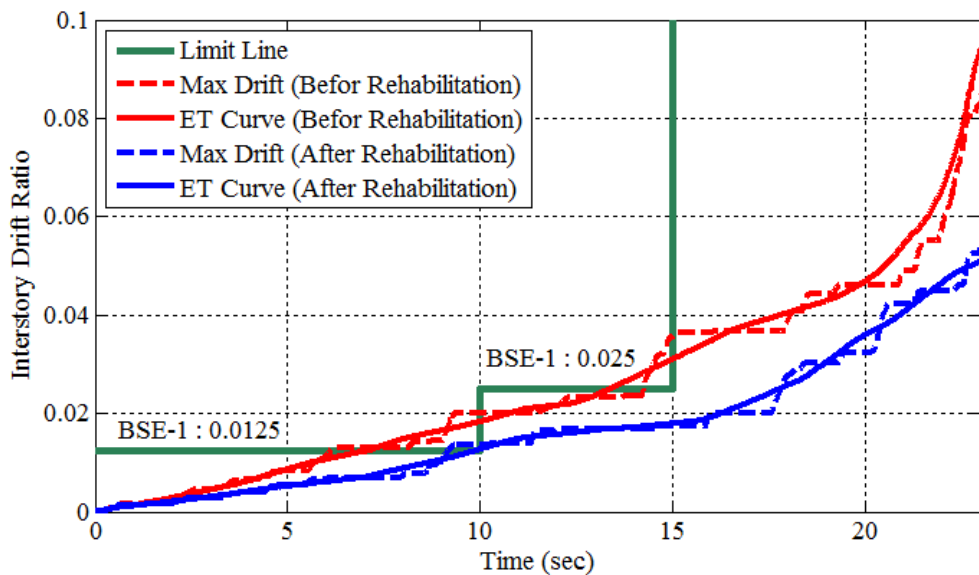


Figure 10. Prformance curve (ET curve) for 8 story frame before and after rehabilitation.

5.3. Verification and comparative study

In order to investigate the structure behavior under earthquake records and to compare them with the ET method estimation, the average response of the structure to seven earthquake records and also the response of the structure to the ET acceleration function before and after the rehabilitation in the frames are compared in Figure. 11 to Figure. 13.

As figures show there is a good compatibility between the results of two method, especially in 4 and 8 story frames. In 4 and 8 story frames, It can be seen that ET analyses properly estimate the response of the structure under GM set of ground motions in both hazard levels. The structure’s behavior after rehabilitation is also acceptable according to time-history analyses of the considered limits. In two story frames, although the interstory drift ratio line is over the limit line but almost it’s difference between ET result and limit line is negligible. In four story frame, at the BSE-1 hazard level MIDR (the second story) considerably reduced in two method and after rehabilitation it has a acceptance amount whereas there is no difference between MIDR (second story) before and after rehabilitation the BSE-2 hazard level.

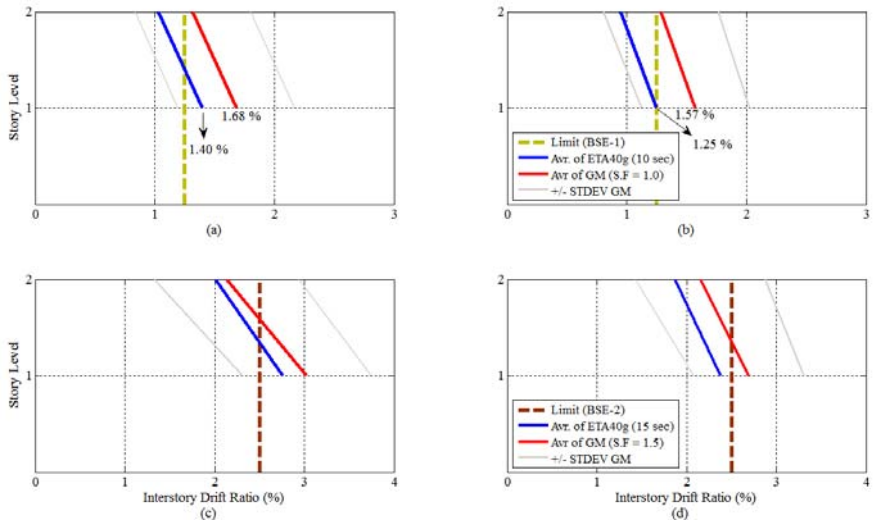


Figure 11. Average interstory drift ratios of 2 story frame under GM set of ground motions and ET estimation a) before rehabilitation in BSE-1 b) after rehabilitation in BSE-1 c) before rehabilitation in BSE-2 d) after rehabilitation in BSE-2

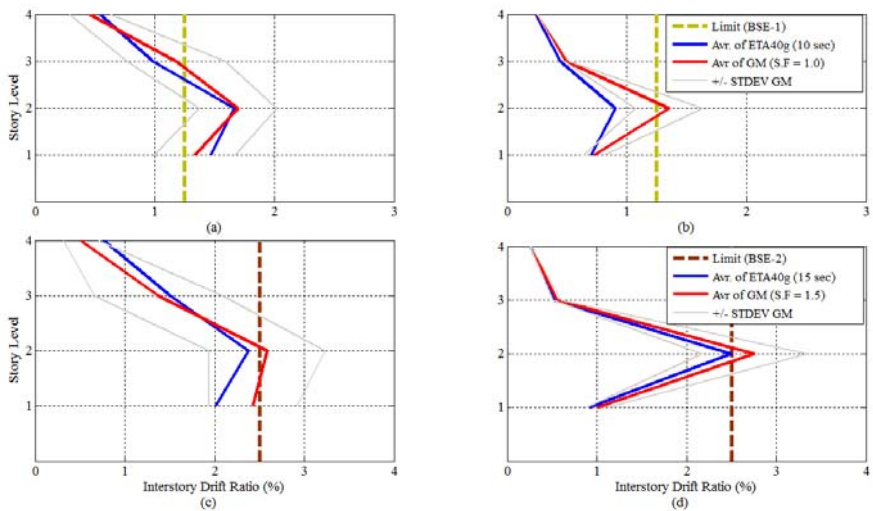


Figure 12. Average interstory drift ratios of 4 story frame under GM set of ground motions and ET estimation a) before rehabilitation in BSE-1 b) after rehabilitation in BSE-1 c) before rehabilitation in BSE-2 d) after rehabilitation in BSE-2

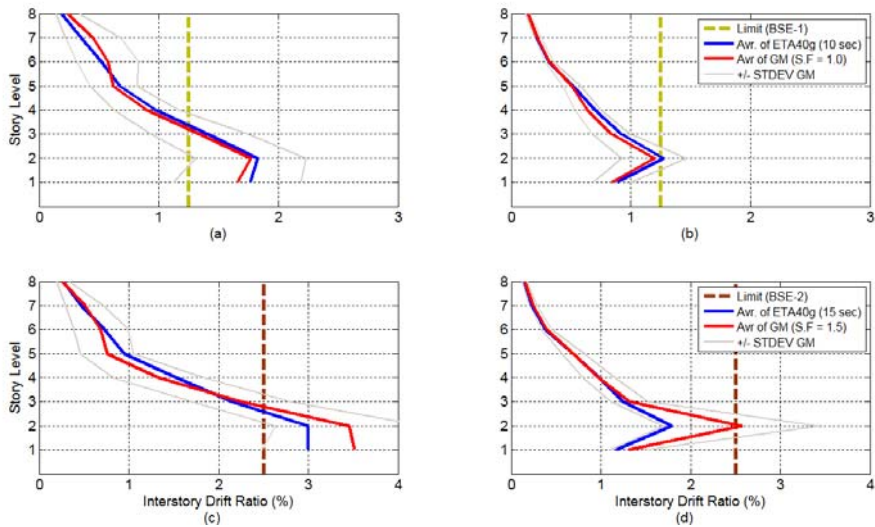


Figure 13. Average interstory drift ratios of 8 story frame under GM set of ground motions and ET estimation a) before rehabilitation in BSE-1 b) after rehabilitation in BSE-1 c) before rehabilitation in BSE-2 d) after rehabilitation in BSE-2

6. CONCLUSIONS

ET method can be considered an effective procedure in performance based optimum design of structures hugely reducing the required computational effort. This reduction of the number of required time-history analyses is accompanied by some loss of accuracy, suggesting classical procedures to be used for final verification of the design. Thus, the ET method can play a role in making the response-history analysis performance based seismic optimization a practical design alternative. Results show that ET analysis with acceleration functions series g has a good compatibility with IDA analysis with spectrum matched records on Reinforced Concrete (RC) Special Moment Frame (SMF) with and without dampers. By waiving the negligible difference between the results of two method it is be reasonable to use acceleration functions and ET method in optimization instead of IDA with with more much time for analyzing. Although yet this is not clear that which records and how many should be used for in IDA analyzing.

Acknowledgements

The authors would like to thank University of Isfahan for their support on this research.

References

1. Estekanchi, H. E., Riahi, H. T. and Vafai, A., Application of Endurance Time Method in Seismic Assessment of Steel Frames, *Engineering Structures*, 33:9, 2535-2546, 2011.
2. Riahi, H. T. and Estekanchi, H., E.Seismic Assessment of Steel Frames with Endurance Time Method, *Journal of Constructional Steel Research*, 66:6, 780-792, 2010.
3. ASCE/SEI 41-06, ASCE standard, Seismic rehabilitation of existing buildings, American Society of Civil Engineers, New York, 2007.
4. ASCE/SEI -07, ASCE standard, Minimum Design Loads for buildings and other Structures, American Society of Civil Engineers, New York, 2005.
5. OpenSees (2011), Open system for earthquake engineering simulation. Pacific Earthquake Engineering Research Center, <http://peer.berkeley.edu/>
6. Vamvatsikos D., Cornell C.A., Incremental dynamic analysis, *Earthquake Engineering and Structural Dynamics*, 31:3. 491–514, 2002.
7. Estekanchi, H. E. and Basim, M. Ch., Optimal damper placement in steel frames by the Endurance Time method, *The Structural Design of Tall and Special Buildings*, 20:5, 612-630, 2011.
8. FEMA P695, Quantification of Building Seismic Performance Factors, Federal Emergency Management Agency. Washington DC, 2009.
9. Hancock J, Watson-Lamprey J, Abrahamson NA, Bommer JJ, Markatis A, McCoy E, Mendis R., An improved method of matching response spectra of recorded earthquake ground motion using wavelets, *Journal of Earthquake Engineering*; 10, 67–89, 2006.
10. <http://myweb.csuchico.edu/>
11. Riahi, H. T. and Estekanchi, H. E., Seismic Assessment of Steel Frames with Endurance Time Method, *Journal of Constructional Steel Research*, 66:6, 780-792, 2010.

Cyclic nonlinear analysis of reinforced concrete slit walls with shear connections

Sergiu Andrei Baetu¹, Ioan Petru Ciongradi¹

¹Department of structural mechanics, "Gheorghe Asachi" Technical University, Jassy, Romania

Summary

An economical design of buildings based on performance criteria takes into account the dissipation of the seismic energy accumulated in the structure. In a tall structural wall, plastic hinges appear only at the base of the wall and the rest of the wall has not ductility resources and remains undamaged. A solution to increase the seismic performance of a reinforced concrete structural wall is to create a slit zone with short connections. Yielding of this shear connections increases the energy dissipation. The objective of these solutions is to create an improved structure for tall multi-storey buildings that has a rigid behavior at low seismic action and turns into a ductile one in the case of a high intensity earthquake. In this article, a comparative nonlinear cyclic analysis between slit walls and a solid wall is performed in the finite element software ANSYS and our main objective is to evaluate the nonlinear behaviour of the proposed walls.

KEYWORDS: reinforced concrete slit walls, short connections, cyclic nonlinear analysis, ductile behavior, energy dissipation capacity.

1. INTRODUCTION

Reinforced concrete walls are structural elements used in multi-story buildings in earthquake prone countries like Romania, Turkey, Chile, Mexico, China, Japan, USA, Peru etc., because they have a high capacity of resisting lateral loads. Nevertheless, such walls also require sufficient ductility to avoid brittle failure under the action of strong seismic loads. When a structure is subjected to strong earthquakes, it is necessary to assure, for economical design reasons, inelastic deformations without the failure of the building; this is because the design of buildings based on performance criteria takes into account the dissipation of seismic energy accumulated in the structure. The fact is that, in a tall structural wall, plastic hinges appear only at the base of the wall and the rest of the wall remains undamaged. There is an alternative solution which overcomes this

drawback, consisting of creating a slit zone with short connections introduced into the wall structure. The solution proposed in this paper –structural reinforced concrete slit walls– changes the behavior of a the solid wall and provides to the structure more ductility, energy dissipation and adequate crack patterns (Figure 1).

The first precast slit panel was patented by Professor K. Muto, in Japan, in 1973 (Figure 1a) [1]. This is the first energy dissipation system used in Japan. This solution consisted of precast RC vertical strips introduced in the steel frames. Other solutions of slit walls have been proposed by Chinese, Korean, Iranian and Russian researchers. The Korean researchers proposed a slit panel used for reinforced concrete framed buildings in which strips are anchored into the beams (Figure 1b) [2]; in China was proposed a cast-in situ structural slit wall with a slit zone with short connections or inserted rubber belts (figures 1d and 1e) [3 – 5]; in Iran was proposed a cast-in situ reinforced concrete slit walls with a variable number of slits on the height (Figure 1f) [6, 7]; and in Russia it has been patented a precast panel with concrete strips assembled by post-stressing (Figure 1c) [8]. These solutions have been used to construct high-rises buildings up to 38 floors in Japan [9] and China [5], buildings that behaved very well during recent seismic events. The slab in these types of buildings can be cast-in situ or precast, and the structural walls are positioned at the border of the building or into the core, in order to reduce the influence of the slab stiffness.

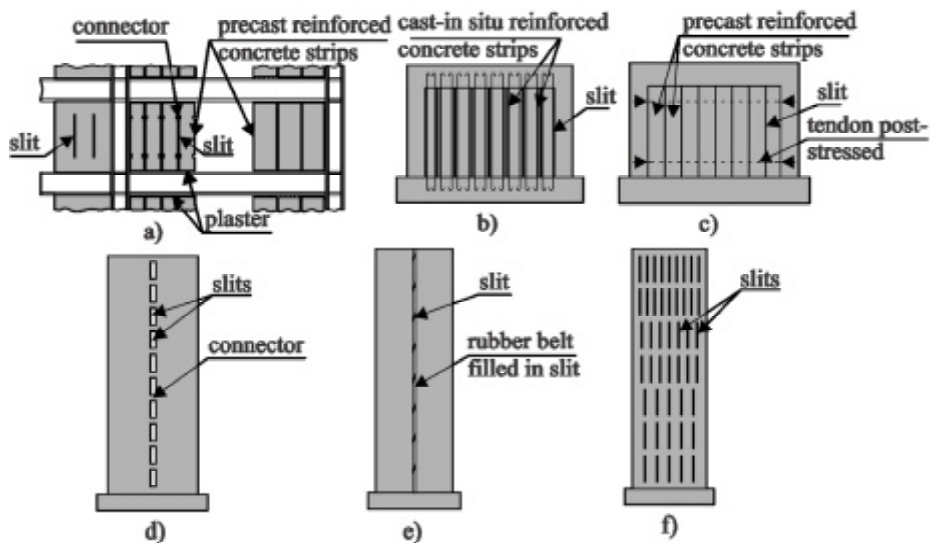


Figure 1. Slit panels and walls: a) precast slit panel with strips introduced in steel frames [1], b) slit panel with strips anchored in beams [2], c) precast panel with strips assembled by post-stressing [8], d) cast-in situ slit wall with a slit zone with short connections [3], e) cast-in situ slit wall with rubber belts inserted in slit zone [4] and f) cast-in situ reinforced concrete slit walls with a variable number of slits on height [6]

The reasons for introducing these solutions are related to the effects of soft soil – stiff structure interaction and the reduction of seismic design forces. In the case of a soft soil and a stiff building, the soil will absorb the seismic energy through deformations that can cause the overturning of the building [10]. By reducing the lateral stiffness, the fundamental natural period of vibrations is increased and resonance can be avoided. With this solution, the seismic demands can be significantly reduced and an economical design can be reached.

A case study corresponding to a 20 levels building designed for a seismic area with a dual reinforcement is analysed and discussed. A structural wall is extracted from this building and its detailed nonlinear structural analysis is performed. The same wall is then modified into a slit wall with short connections, in order to study the improvement if its behaviour when compared with that of the original wall. We performed the cyclic nonlinear analyses of RC structural walls studied in this article by using the finite element software ANSYS 12. This software allows calculating the behaviour of short connections with a realistic finite element model able to handle complex geometries and to describe precisely the complex stress state and the cracking pattern.

2. STRUCTURE DESCRIPTION

The case study considers a multi-storey building in a seismic area from which a reinforced concrete structural wall is isolated. The building is located in the city of Iasi, Romania, which has the following site characteristics: design ground acceleration $a_g = 0.2g$, control period $T_c = 0.7s$, ductility class H, importance factor $\gamma_I = 1$ [11]. The building has dual reinforced concrete structure and regular form in plan and elevation. The seismic lateral loads applied upon the building are absorbed by the concrete core and, in the short direction, by the border walls. It has 20 levels with a height of 3m each. In plan, the building has 31 m in length and 21 m in width (Figure 2). The concrete used in the analysis is C32/40. The fundamental period of the structure is $T_1 = 1.077s$. The study is focused on a lateral wall with a length of 10m (Figure 3). The design analysis was performed with the computer program SAP2000 with which a thickness of the wall of 40 cm was obtained; the wall is reinforced with vertical bars $\phi 14/15$ and horizontal bars $\phi 10/15$ and, at the boundary it has $8\phi 28$ bars [12, 13]. The number of short connections is varied along the wall height. The height of each connection is 0.40m and the thickness of the slit is 5cm. Comparative analyses were conducted on the slit walls and on a solid wall.

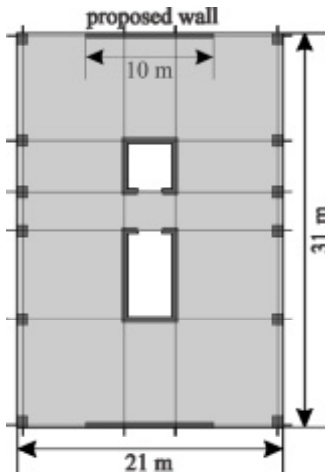


Figure 2. Dimensions of the studied building

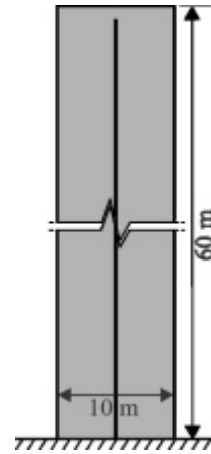


Figure 3. Dimensions of the studied slit wall

3. FINITE ELEMENT ANALYSIS BY ANSYS 12 SOFTWARE

The concrete used in the analysis is C32/40. In the analysis of the short connection performed with the ANSYS 12 computer program, the finite element used for concrete is Solid 65 with cubic shape and the dimension of 50 mm (Figure 4a). Solid 65 elements are capable of plastic deformation, cracking in three orthogonal directions, and crushing. The loading is applied in the y direction through a steel plate in order to prevent stress concentrations. The steel plate is meshed with finite element Solid 45 (Figure 4b) with the same dimensions as concrete. The rebars were modeled by using the smeared model (Figure 4a) [14 – 20].

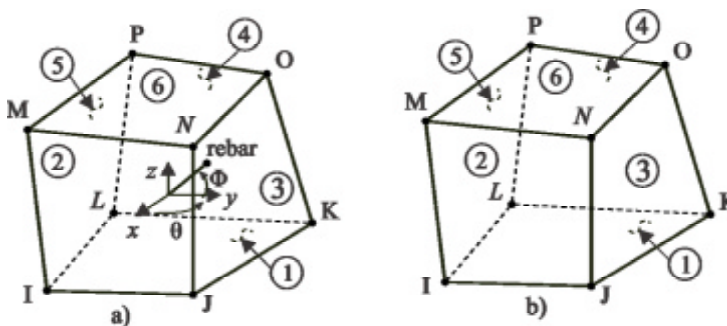


Figure 4. Finite elements used in analysis: a) Solid 65 for concrete and c) Solid 45 for steel plate [18]

The multilinear isotropic material uses von Mises failure criterion along with the Willam and Warnke (1974) model to define the failure of the concrete. For the boundary elements a confined concrete was set. The compressive uniaxial stress-strain curve for the unconfined and confined concrete is shown in the Figure 5 [15, 16, 18]. The multilinear isotropic stress-strain curve for unconfined concrete is computed with equations proposed by Desayi and Krishnan in 1964 [21], and for confined concrete can be used the curve used for unconfined concrete with increased strength and deformations according to SR EN 1992-1-1:2004 [22].

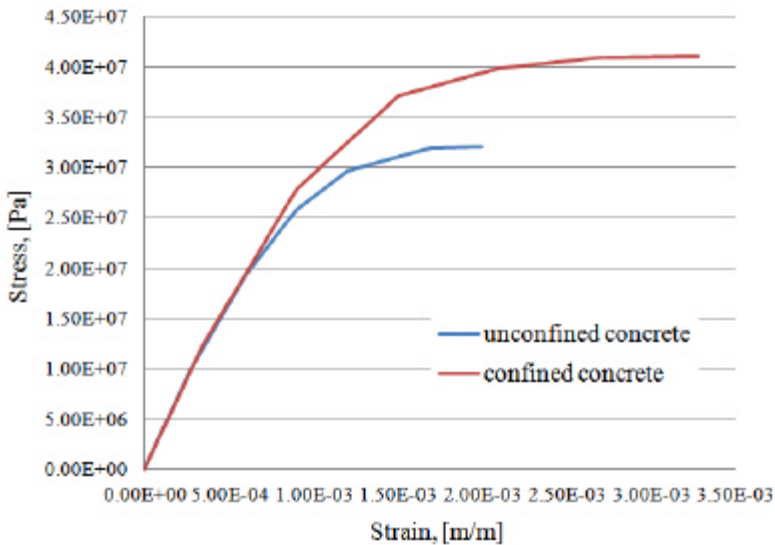


Figure 5. Uniaxial stress-strain curve for the unconfined and confined concrete

Implementation of the Willam and Warnke material model in ANSYS requires different constants be defined (Table 1) [17].

Table 1. Concrete Properties

1	Shear transfer coefficients for an open crack (b_t)	0.4
2	Shear transfer coefficients for an closed crack (b_c)	0.8
3	Uniaxial tensile cracking stress (f_r)	2.2E+006 Pa
4	Uniaxial crushing stress (f_c)	unconfined concrete
		confined concrete

For the reinforcement definition, parameters to be considered are material number, volume ratio and orientation angle (θ and F) in X and Y directions respectively (Table 2). Volume ratio refers to the ratio of steel to concrete in element.

Table 2. Real constants for concrete

Particulars	Constants		
	Real constant for rebar 1 (vertical rebar)	Real constant for rebar 2 (horizontal rebar)	Real constant for rebar 3 (vertical rebar-boundary element)
Material number	2	2	2
Volume ratio	0.00513	0.00377	0.0308
Orientation angle θ	90	0	90
Orientation angle F	0	90	0

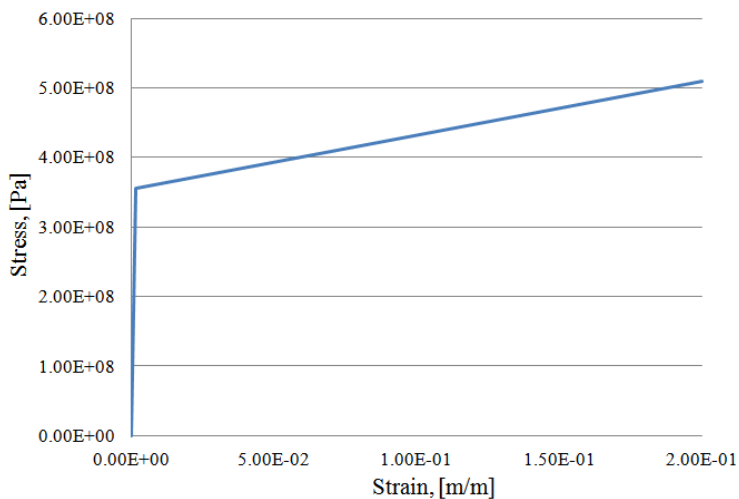


Figure 6. Stress-strain curve for reinforcement

In Figure 6 is shown the stress-strain curve of reinforcement used in this study. The bilinear kinematic hardening model (BKIN) was used [18, 21]. The bilinear model requires the yield stress ($f_y = 3.55E+008$ Pa) and the hardening modulus of the steel ($E'_s = 2.1E+009$ Pa).

4. CYCLIC ANALYSIS

4.1 Loading and boundary conditions

The structural wall is fully restrained at the base (Figure 8). Cyclic analysis is done with forces that are disposed uniform along the height of wall. In Figure 7 are presented the load patterns for each studied wall.

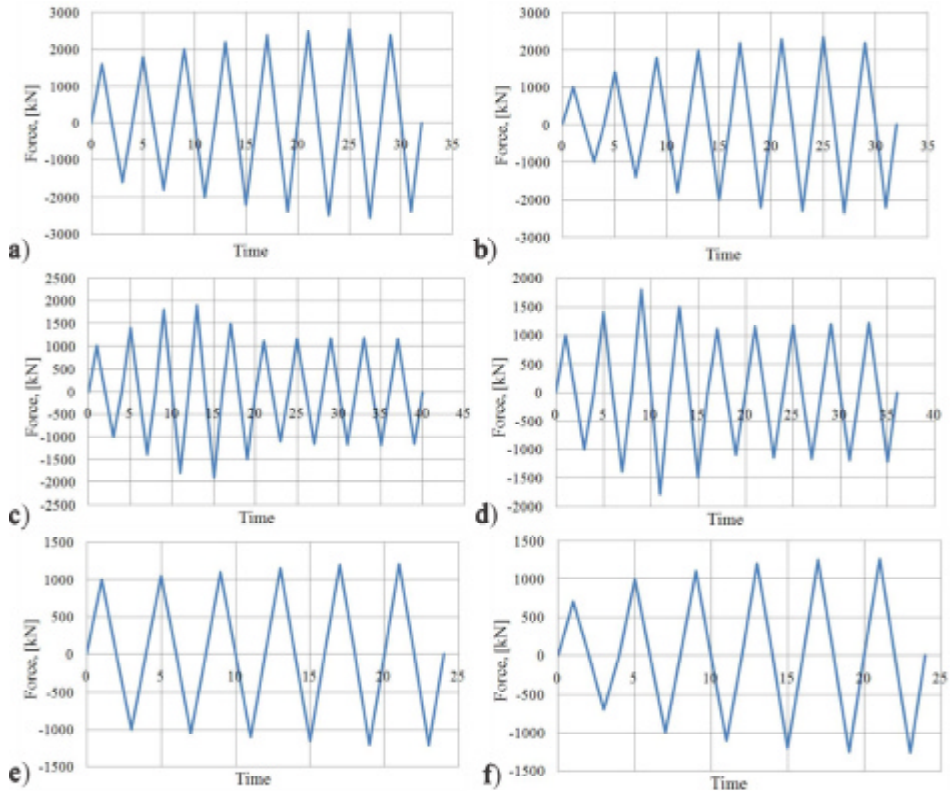


Figure 7. Load pattern for the studied walls: a) solid wall and slit wall with 20 connections, b) slit wall with 10 connections, c) slit wall with 5 connections, d) slit wall with 4 connections, e) slit wall with 3 connections and f) slit wall with 2 connections

Concentrated forces are applied at each level through steel plates to avoid the stress concentrations. The gravity loads include structural wall weight which is taken by the program and loads from floor connected to the wall 47.3 kN divided on each node of the slab zone.

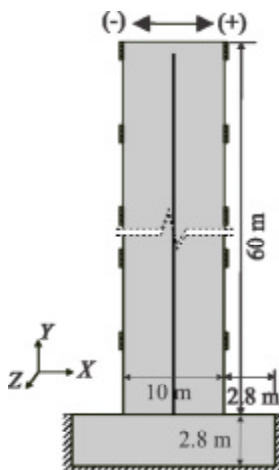
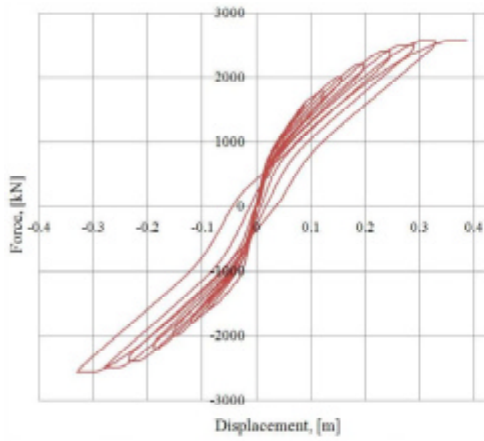


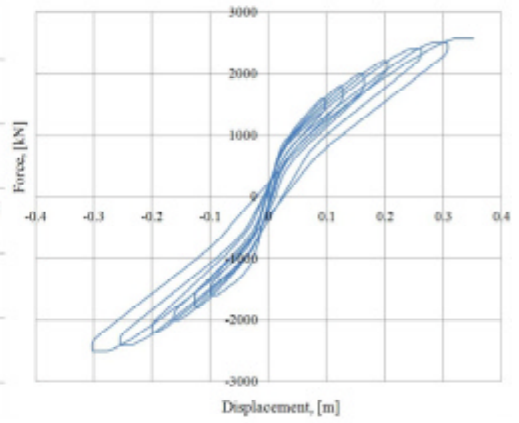
Figure 8. Boundary conditions

4.2 Comparative analysis of the slit and solid walls

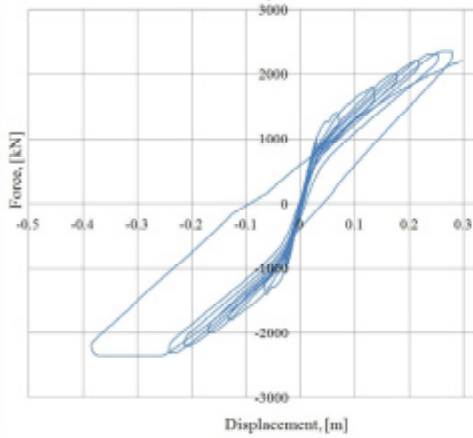
In this part of the article, comparative analyses were conducted on the slit walls and on a solid wall. The number of short connections is varied along the wall height and the height of the connections is kept 40 cm. Figure 9 shows the lateral load vs. displacement hysteresis diagrams of the studied walls: solid wall (Figure 9a), slit wall with 20 connections (Figure 9b), slit wall with 10 connections (Figure 9c), slit wall with five connections (Figure 9d), slit wall with four connections (Figure 9e), slit wall with three connections (Figure 9f) and slit wall with two connections (Figure 9g). From these hysteretic loops we can observe that by introducing a slit zone into the structural wall the behavior of the element is changed, a greater displacement being obtained by a sudden degradation of strength following the failure of the shear connections. The solid wall and the slit wall with 20 connections have almost the same behavior, both fails at a low displacement due to large crushing of the concrete at the base. Cracks due to bending are extended on less of the half of the solid wall (Figure 11). Before the ultimate load many shear cracks at 45° develop at the base of the wall. The slit wall with 10 connections fails as well due to large crushing of the concrete at the base and due to failing of five connections from the bottom zone that split the structural wall in two walls only to the middle. This mean that this slit wall has an undesired behavior because weakens the bottom zone and the slip doesn't appear on all height of the wall how should occur. As we can see from hysteresis loop for the reinforced concrete structural slit wall with five connections after the maximum load was reached and the short connections have crushed, the stiffness of the wall is drastically decreased and the slipping along the connections zone has appeared. After this point the hysteresis behavior of the slit wall became stable and a lot of hysteretic energy is dissipated.



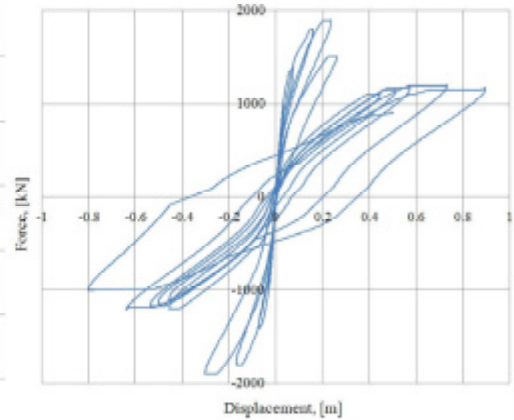
a)



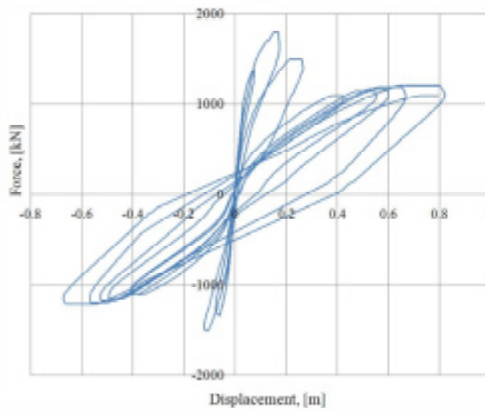
b)



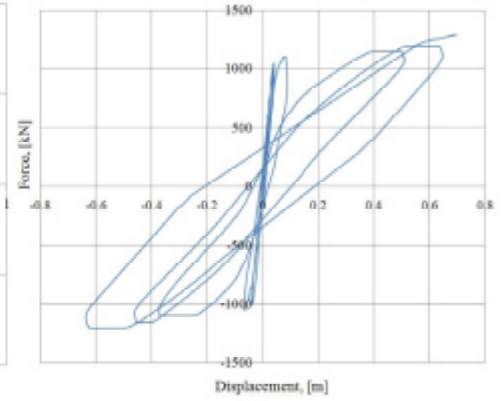
c)



d)



e)



f)

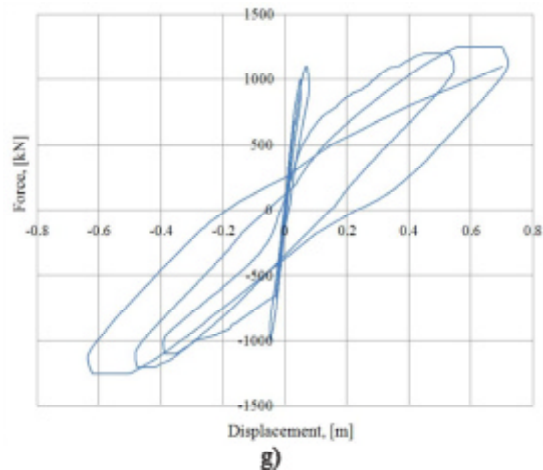


Figure 9. Cyclic behavior of the studied walls: a) solid wall, b) slit wall with 20 connections, c) slit wall with 10 connections, d) slit wall with 5 connections, e) slit wall with 4 connections, f) slit wall with 3 connections and g) slit wall with 2 connections

The behavior of the slit wall with four connections is almost identical with that of the slit wall with five connections having a lower maximum load and better hysteresis behavior with large loops after the short connections break. For slit walls with three and two connections the initial high stiffness decreases at a low lateral force and at a small displacement. These slit walls fail at a low number of cycles because each wall split in two slender walls very fast, and the plastic hinges appear concentrated at the base exactly as in the case of solid wall with a worst crack pattern. Figure 10 shows the comparison between strength envelopes of the studied walls.

Analyzing Figure 11 we can observe that the slit wall with five connections have a better crack pattern than solid wall before failure. In both walls the concrete is crushed on a length of 1.2...1.6 m on all border zones and on all height of first floor. To compare the behavior of the studied walls the ductility factor (μ) based on cyclic response and the hysteretic energy are calculated. Ductility is defined as the capacity of an element to undergo inelastic deformations with acceptable stiffness and strength reduction. Brittle elements fail after reaching their strength limit at very low inelastic deformations and ductile elements fail at large inelastic deformations. Most structures and elements are designed to behave inelastically under strong earthquakes for reasons of economy. The response amplitudes of earthquake-induced vibrations are dependent on the level of energy dissipation of structures, which is a function of their ability to absorb and dissipate energy by ductile deformations. For low energy dissipation, the structures may develop stresses that correspond to relatively large loads. These structures should be designed to withstand lateral forces of the same proportion of their weight to

remain in the elastic range. This is uneconomical in all practical applications with the exception of nuclear power plants, offshore platforms, water-retaining structures and other safety-critical structures [23].

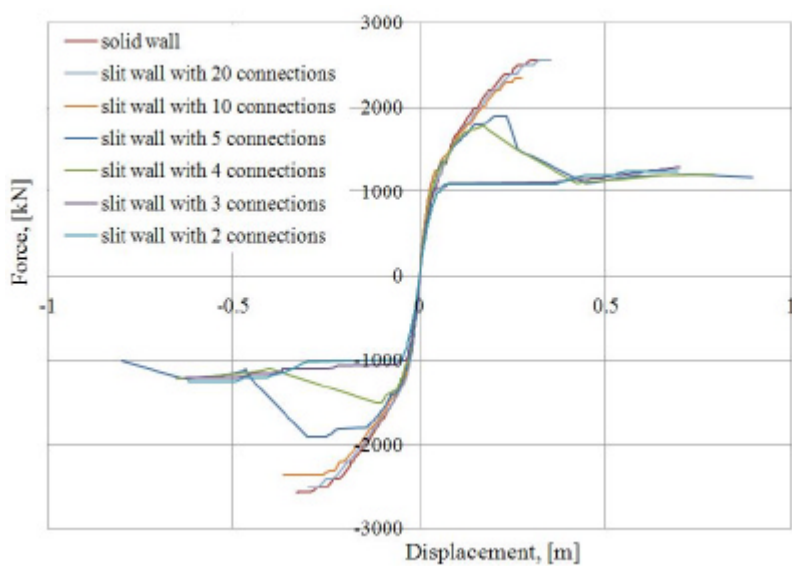


Figure 10. Comparison between strength envelopes of the studied walls

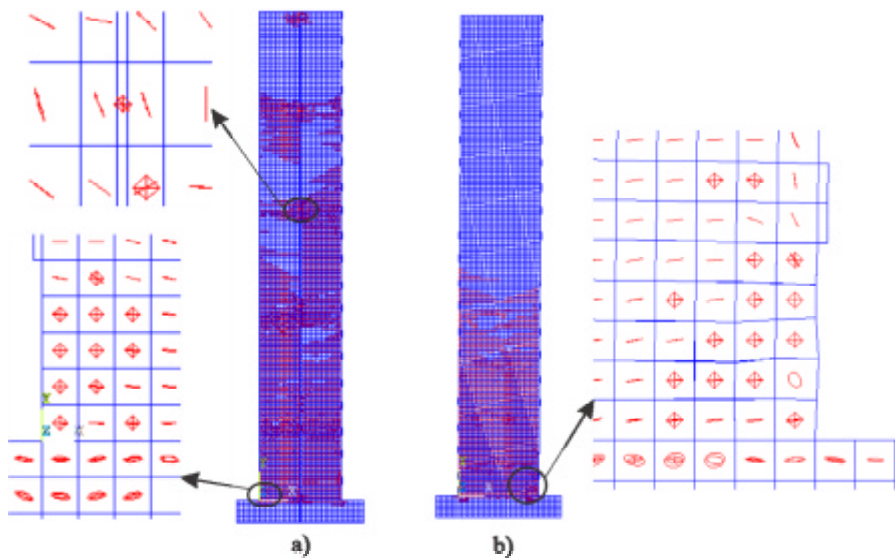


Figure 11. Crack pattern before collapse for: a) slit wall with 5 connections and b) solid wall

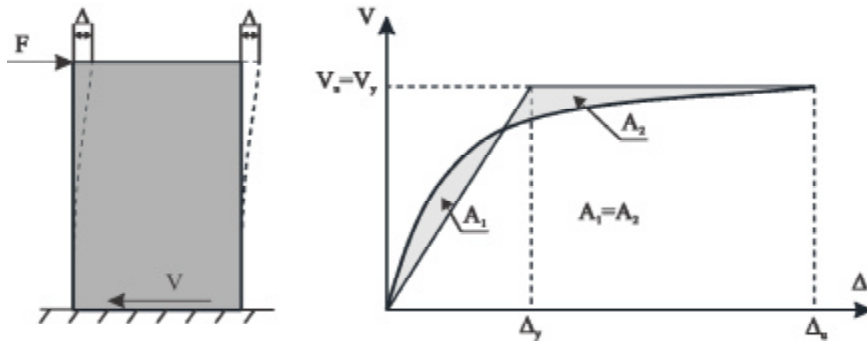


Figure 12. Yield point determination method

Definition of ductility factor based on cyclic response is given below and is related to the cyclic deformations:

$$m = \frac{|\Delta_{\max}^+| + |\Delta_{\max}^-|}{|\Delta_y^+| + |\Delta_y^-|} \quad (1)$$

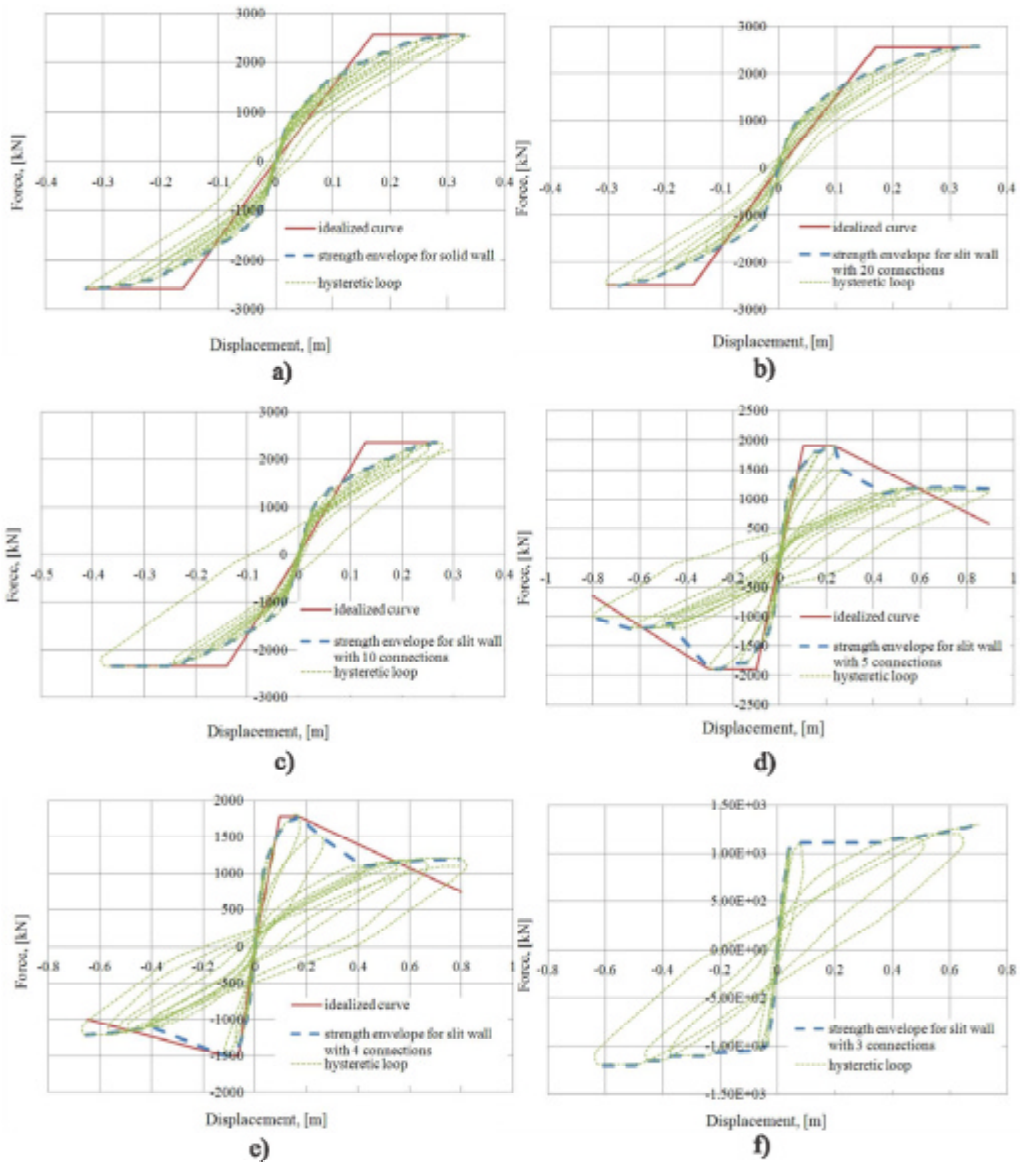
Where: Δ_{\max}^+ , Δ_{\max}^- - are the positive and negative ultimate displacements,

Δ_y^+ , Δ_y^- - are the positive and negative yielding displacements.

In seismic design, high ductility is essential to ensure plastic redistribution of actions among components of lateral resisting systems and to allow for large absorption and dissipation of earthquake input energy. Ductile structures may withstand extensive structural damage without collapsing or endangering life safety. The evaluation of the yield displacement from strength envelopes is not always straightforward.

Yield points are often wrong defined because of non-linearities and formations of plastic hinges in component elements. Response curves of reinforced concrete frequently do not present well-defined yield points because of cracking of concrete and sequential yielding of reinforcement bars. There are various definitions for yield displacements and in this paper we chose displacement corresponding to the yield point of an equivalent elasto-plastic system with the same energy absorption as the real system (Figure 12), [24]. Strength envelopes (Figure 13) are used to extract the yielding force and the ultimate displacement by replacing each strength envelope with the idealized curve. The case of slit walls with four and five short connections is a special one because the strength envelope has strength degradation and the idealized curve has to be tri-linear and, therefore, it was developed according to FEMA 440 [25]. The sum of the areas enclosed between the curve and the idealized curve must be zero. In the case of the slit walls with three and two

short connections is not necessary to replace the strength envelope with an idealized curve because the strength envelope has an idealized elasto-plastic shape (Figure 13f and g), and the yield point can be easily chosen. For these two walls the yield points are considered to appear when the short connections suddenly break and the stiffness drops close to zero.



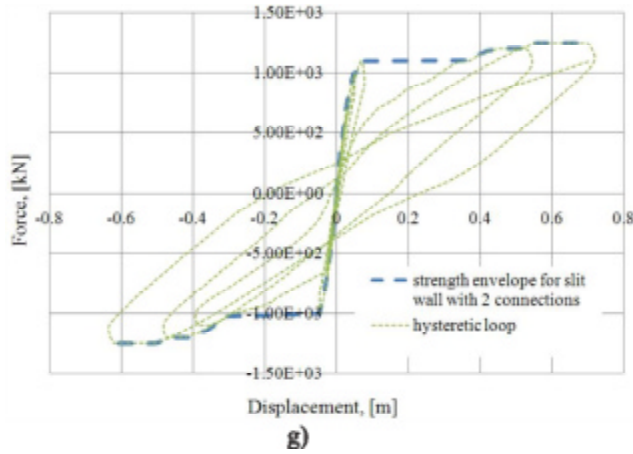


Figure 13. Idealized curves for the studied walls: a) solid wall, b) slit wall with 20 connections, c) slit wall with 10 connections, d) slit wall with 5 connections, e) slit wall with 4 connections, f) slit wall with 3 connections and g) slit wall with 2 connections

Table 3. The parameters required to calculate the ductility factor

Studied walls	Δ_{\max}^+	Δ_{\max}^-	Δ_y^+	Δ_y^-	μ
Solid wall	0.328	0.33	0.17	0.16	1.994
Slit wall with 20 connections	0.35	0.30	0.17	0.15	2.03
Slit wall with 10 connections	0.27	0.366	0.13	0.14	2.355
Slit wall with 5 connections	0.894	0.80	0.10	0.10	8.47
Slit wall with 4 connections	0.80	0.65	0.095	0.065	9.063
Slit wall with 3 connections	0.60	0.62	0.072	0.06	9.24
Slit wall with 2 connections	0.68	0.62	0.067	0.06	10.23

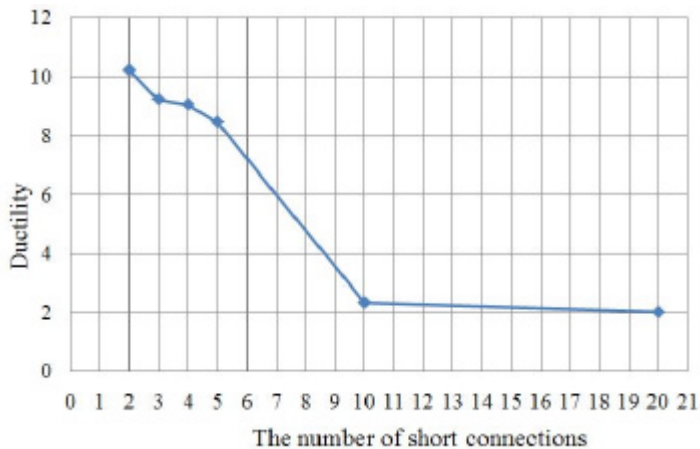


Figure 14. Ductility variation with the number of short connections

In Table 3 are introduced all the parameters required to calculate the ductility factor, these being extracted from idealized curves for the studied walls presented in Figure 13. Then, a graphic variation of ductility factor with the number of short connections disposed on the wall height is done (Figure 14). From this graphic we can see that the slit walls with 20 and 10 connections have a small ductility that is very close to the solid wall ductility, resulting that these structural elements are brittle. As we can see the ductility factor increases with the decrease of the number of short connections. For the slit walls with five, four, three and two short connections disposed on the wall height the ductility factor reaches high values.

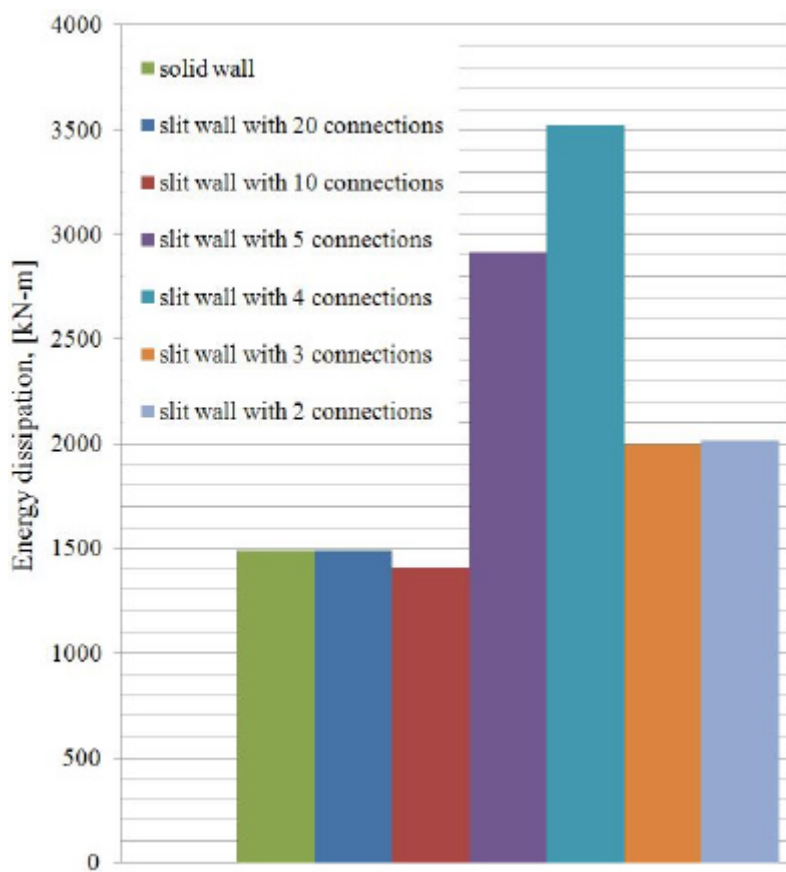


Figure 15. Comparison between cumulative hysteretic energy dissipated by slit walls and solid wall

Figure 15 shows the total energy dissipated of studied walls proposed in this analysis. The area enclosed by a hysteretic loop at a given cycle represents the energy dissipated by the wall during that cycle. It is found that the slit wall with four and five short connections have the highest energy dissipation capacity

resulted from the ability to withstand many cycles of loading. This is also due to energy dissipation mechanism that is different for these slit walls and other walls from this study. These slit walls dissipates seismic energy by cracks extended on all the surface of the wall and by crushing of the shear connections while the other slit walls and the solid wall dissipates seismic energy only by cracks at the base of the wall.

5. RESULTS INTERPRETATION

These analyses demonstrate that introducing a slit zone with short connections in a structural wall, with a rational disposal and a correct number of the short connections can significantly increase the dissipated hysteretic energy of this element. The seismic performance can be controlled by setting the short connections to satisfy different design criteria under different earthquake levels. Comparisons between the studied structural walls reveal that they have a different behavior. The solid wall is very stiff and the plastic zone is concentrated at the base, from this reason fails at a low displacement due to huge crushing of concrete. The slit walls with 20 and 10 short connections have a behavior close to the solid walls, because having a great number of connections disposed on the wall height no slipping appear in the slit zone and only a few connections from the base break, resulting that these slit walls fail as well at the base. On the other hand, the slit walls with four and five short connections have an initial stiffness compared with the solid wall but when the shear connections break, the strength starts to decrease, in this way the base of the walls being protected. The final displacement of these slit walls is much bigger than that of the solid wall. These slit walls have also a higher value of ductility factor than the solid wall. Reducing the number of short connections to three or two, the short connections break very fast at a small lateral displacement, resulting that the base of the walls remain in the elastic range, without cracks. In the calculation of the ductility factor for these walls it was considered that the yield displacement is the lateral displacement when the connection break and the stiffness is reduced. From this reason extremely high values for ductility factors emerge from these calculations. However, these two slit walls have a lower energy dissipation capacity because after the connections break the plastic hinges form quickly at the base and doesn't resist at many cycles of loading.

6. CONCLUSIONS

An economical design of buildings based on performance takes into account the dissipation of seismic energy accumulated in the structure. Reinforced concrete walls are frequently used as strength elements for structures designed in areas with high seismic risk. If ductility is a major concern, structural walls are not considered an efficient structural component. The main problems of these structural elements - low ductility and reduced energy dissipation capacity - are removed through the solutions presented in this article. The short connections disposed on the wall height in the slit zone prevent collapse of the structural element under extreme seismic excitations by dissipating hysteretic energy through an improved crack pattern. From these analyses we can conclude that the slit walls with four and five short connections have the best behavior, the highest ductility and the highest energy dissipation capacity. Also, it can be concluded that the number of short connections disposed on the wall height have a great influence on the ductility and on the energy dissipation capacity of the slit walls, that's why this number must be chosen wisely if we want to reach to the best behavior.

References

1. Muto, K., Ohmori, N., Itoh, T., *Composite building structure and walls therefor*, United States Patent 3736712, 1973.
2. Liou Y.W., Sheu S. M., *Prediction of lateral stiffness for fully slitted RC shear wall*, Journal of the Chinese Institute of Engineers, vol. 21, 1998, pp. 221-232.
3. Kwan, A.K.H., Dai, H., Cheung, Y.K., *Non-linear seismic response of reinforced concrete slit shear walls*, Journal of Sound and Vibration, vol. 226, 1999.
4. Lu X., Wu X., *Study on a new shear wall system with shaking table test and finite element analysis*, Earthquake Engineering and Structural Dynamics, vol. 29, 2000, pp. 1425-1440.
5. Lu X., Huanjun J., *Nonlinear earthquake response analysis and energy calculation for seismic slit shear wall structures*, Earthquake Engineering and Engineering Vibration, vol.1, no. 2 (2002), pp. 227-237.
6. Sabouri J., Ziyaeifar M., *Shear walls with dispersed input energy dissipation potential*, Asian Journal of Civil Engineering (Building and Housing), vol. 10, no. 5 (2009), pp. 593-609.
7. Labafzadeh M.S.R., Ziyaeifar M., *Seismic behaviour of RC dual ductility mode shear walls*, The 14th World Conference on Earthquake Engineering, Beijing, China, October 12-17, 2008.
8. Pavlik, V.S., Vasionkin, A.N., *Earthquake resistant building*, Patent nr.512279, URSS, 1976.
9. Aoyama H., *Dr. Kiyoshi Muto (1903-1989)*, Structural Engineering International, vol. 1, 2005, pp. 50-52.
10. Marin M., Roman O., *Hazardul seismic al Timisoarei*, Buletinul AGIR, no. 2-3 (2010), pp. 36-42.(in Romanian)
11. Code for seismic design of buildings P100-1/2006. (in Romanian)
12. Code for the design of buildings with reinforced concrete structural walls CR 2-1-1.1-2005. (in Romanian)
13. Sergiu Andrei Baetu, Ioan Petru Ciongradi, Georgeta Vasies, *Static nonlinear analysis of structural reinforced concrete walls energy dissipators with shear connections*, “Computational Civil Engineering 2010”, International Symposium, Iasi, Romania, May 28, 2010.

14. Greeshma S., Jaya K.P., Annilet S.L., *Analysis of flanged Shear Wall Using ANSYS Concrete Model*, International Journal for Civil and Structural Engineering, vol. 2, no. 2 (2011), pp. 454-465.
15. Kheyroddin A., Naderpour H., *Nonlinear Finite Element Analysis of Composite RC Shear Walls*, Iranian Journal of Science & Technology, vol. 32, no. B2 (2008), pp. 79-89.
16. Raongjant W., Jing M., *Finite Element Analysis on Lightweight Reinforced Concrete Shear Walls with Different Web Reinforcement*, The Sixth PSU Engineering Conference, May 8-9, 2008, 61-67.
17. Terec L., Bugnariu T., Pastrav M., *Analiza Neliniara a Cadrelor din Beton Armat cu Pereti Turnati in Situ*, Romanian Journal of Materials, vol. 40, 2010, pp. 214-221.
18. Wolanski J.A., *Flexural Behavior of Reinforced and Prestressed Concrete Beams Using Finite Element Analysis*, Master Thesis, Marquette University, Milwaukee, Wisconsin, 2004.
19. Kazaz I., Yakut A., Gulkan P., *Numerical simulation of dynamic shear wall tests: A benchmark study*, Computers & Structures, vol. 84, 2006, pp. 546-562.
20. ANSYS 12 Structural Analysis Guide, 2009.
21. Kachlakev D., Miller T., Yim S., *Finite Element Modeling of Reinforced Concrete Structures Strengthened with frp Laminates*, Oregon Dept. of Transp., USA, Res. Group, Final Report SPR 316, May 2001.
22. Proiectarea structurilor din beton, SR EN 1992-1-1:2004.
23. Elnashai A.S., Di Sarno L., *Fundamentals of earthquake engineering*, John Wiley & Sons, 2008.
24. Sittipunt C., Wood L.S., *Finite element analysis of reinforced concrete shear walls*, Research Grant BC 589-12992, University of Illinois, 1993.
25. FEMA 440 – Improvements of nonlinear static seismic analysis procedures 2005.

Probabilistic assessment of the seismic damage in reinforced concrete buildings

Alex H. Barbat¹, Yeudy F. Vargas¹, Lluís G. Pujades¹ and Jorge E. Hurtado²

¹ Universidad Politécnica de Cataluña, Barcelona, Spain

² Universidad Nacional de Colombia, Manizales, Colombia

Summary

The main objective of this article is to assess the expected seismic damage in reinforced concrete buildings from a probabilistic point of view by using Monte Carlo simulation. To do that, the seismic behavior of the building is studied by using random capacity obtained by considering the mechanical properties of the materials as random variables. Starting from the capacity curves, one can obtain the damage states and the fragility curves as well as to develop curves describing the expected seismic damage of the structures as a function of a seismic hazard characteristic. The latter can be calculated using the capacity spectrum and the demand spectrum according to the methodology proposed by the RISK-UE project. For defining the seismic demand as a random variable, a set of real accelerograms are obtained from the European and Spanish databases in such a way that the mean of their elastic response spectra is similar to an elastic response spectrum selected from Eurocode 8. In order to combine the uncertainties associated with the seismic action and the mechanical properties of materials, two procedures are considered for obtaining functions which relates the PGA to the maximum spectral displacements. The first one is based on a series of nonlinear dynamic analyses. The second one is based on the well known procedure named equal displacement approximation exposed in ATC 40. After applying both procedures, the probability density functions of the maximum displacement at the roof of the building are obtained and compared. The expected structural damage is finally obtained by replacing the spectral displacement obtained by using the ATC 40 and the incremental dynamic procedure. In the damage functions the results obtained from incremental static and dynamic analyses are finally compared and discussed from a probabilistic point of view.

KEYWORDS: Probabilistic seismic assessment, capacity curves, vulnerability, fragility curves, expected damage.

1. INTRODUCTION

The vulnerability of structures subjected to earthquakes can be evaluated numerically either by using incremental static analysis or pushover analysis or by means of nonlinear dynamic analysis performed in an incremental way. All the variables involved in such structural analyses, mainly the mechanical properties and the seismic actions, should be considered as random. The reason is that the randomness of the implied variables combined with the uncertainties in the seismic hazard, may lead to an underestimation or an overestimation of the actual vulnerability of the structure, but they are not always treated in this way. Due to the current capacity of the computers, a great number of structural analyses can be performed in order to study the behavior of buildings from a probabilistic standpoint within the framework of Monte Carlo simulation.

This study focuses on the nonlinear seismic response of reinforced concrete buildings and on their damage analysis considering the involved uncertainties (Fragiadakis & Vamvatsikos 2009). In the pushover analysis, previous studies already considered uncertainties (Bommer & Crowley 2006; Borzi et al. 2007; Fragiadakis & Vamvatsikos 2010) and evaluated the nonlinear behavior of structures considering uncertainties in the mechanical properties of materials and in the nonlinear static analysis (pushover) by means of the Monte Carlo method. Dolsek (2010) considered in this type of studies the seismic action as a random signal using real accelerograms roughly compatible with design spectra, but did not take into account the uncertainties associated to the structural characteristics. The present paper aims to assess the seismic vulnerability of the structure considering both the mechanical properties of the materials as random variables and the seismic actions as random signals. The seismic demand for the area is obtained in probabilistic terms starting from the response spectrum chosen from Eurocode 8. Afterwards, a procedure for selecting accelerograms whose response spectra are compatible, in a mean sense, with the mentioned response spectrum, is applied. In this study, we compare the results carried out by using the above mentioned analyses: 1) Incremental static analysis or pushover analysis (PA). 2) Nonlinear dynamic analysis (NLDA) in an incremental way, that is, an incremental dynamic analysis (IDA) (Vamvatsikos and Cornell 2002). PA and NLDA have been compared in previous studies (Mwafy & Elnashai 2001; Poursha et al. 2007; Kim & Kuruma 2008). The PA is used to determine the capacity curves of the structure and to obtain the expected displacement at the roof of the building for a given seismic area (Borzi et al. 2008; Barbat et al. 2008; Lantada et al. 2009; Pujades et al. 2011). The roof displacement obtained with this procedure will be considered as a random variable and will be compared with the displacement calculated via IDA. Finally, the results are discussed and compared from a probabilistic point of view.

2. DESCRIPTION OF THE STUDIED BUILDING

The reinforced concrete building selected for this study is shown in Figure 1. The building is located in Spain and, therefore, some of the selected accelerograms are taken from the Spanish database. However, due to the low seismicity of the area, we use additional accelerograms taken from the European database. The building is regular in plan, allowing the use of a 2D model. Nevertheless, this building has not a framed structure but a structure with columns and slabs which, in this case, are waffled slabs. In Spain, this type of building is frequently used for family housing and for offices and has been previously studied (Vielma et al. 2009; Vielma et al. 2010). For the purpose of this study, we use a simplified equivalent framed model. The main geometric characteristics of the building can be seen in Figure 1.

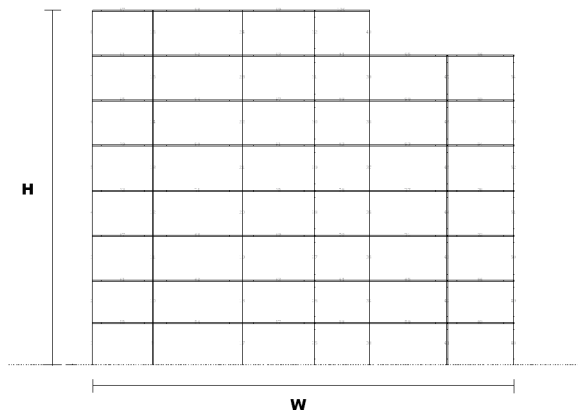


Figure 1. Equivalent frame of the reinforced concrete structure used in the probabilistic simulation

The constitutive law of the structural elements is elastoplastic without hardening or softening. In order to define the yield surfaces for the material of the columns and beams, it is necessary to create an interaction diagrams between the bending moment and the axial force, and between the bending moment and the angular deformation, respectively. Programs have been developed in MATLAB in order to calculate the yielding points which are necessary when defining the behavior of the structural elements used in the nonlinear static and in the dynamic analyses of the structures which, in this article, are performed by means of the RUAUMOKO computer software (Carr 2000).

3. MONTECARLO SIMULATION

3.1. Nonlinear static analysis

As mentioned before, the mechanical properties of the materials, such as the concrete compressive strength, f_c , and the reinforced yield strength, f_y , are random variables. The distribution assumed for these variables is Gaussian; the parameters that define these distributions, the mean value μ and the standard deviation σ , as well as the coefficient of variation \mathbf{r} , are shown in Table 1. These parameters correspond to the values given in the original blueprints of the structure.

Table 1. Characteristics of the probability distribution of the mechanical properties of the structural elements

	Col 1	Col 2	Col ..
f_c	30000	1000	3.33%
f_y	411510	22093	5.36%

It is important to note that, in each pushover analysis, the strength of the structural elements is not constant because, for each of them, a new stochastic data is generated. On the other hand, in the PA the results change depending on the variation of the load pattern with the height. Besides, it is very difficult to establish how much to increase the load; moreover, a load maintaining the pattern corresponding to the first mode of vibration of the elastic structure cannot capture the effect of higher-modes (Poursha et al. 2008). To overcome these difficulties, we use the so-called adaptive pushover method in its version proposed by Satyarno (1999) and it is this one which will be referred in the following as PA. The advantage of the PA is the independency of the results on the loading pattern, because this is calculated as a function of the mass, the equivalent frequency and the deformed shape of the structure; furthermore, the horizontal load limit is controlled by the current stiffness of the structure. Figure 2 shows a comparison among different capacity curves calculated for different load patterns.

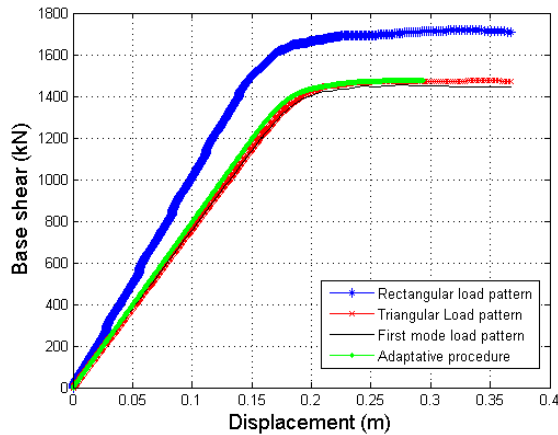


Figure 2. Capacity curves obtained with different load patterns

After generating 1000 samples of mechanical properties f_c and f_y by using the latin hypcube method, 1000 capacity curves are obtained and plotted in Figure 3 in which the uncertainties in the results can be seen.

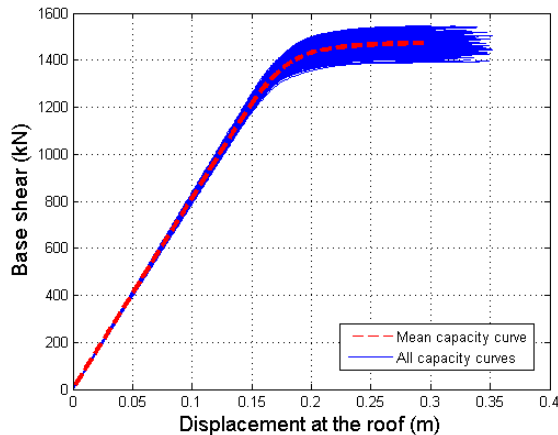


Figure 3. Capacity curves obtained via Monte Carlo simulation

3.1. Nonlinear static analysis

In order to consider the randomness of the seismic action, the response spectrum corresponding to EUROCODE 8 of type 1 and for soil type D is taken as target. Although we performed several tests using the type 2 spectra, we eventually used

in this article the type 1 spectrum for soil D, in order to achieve the nonlinear inelastic behavior of the structure, because for type 2 spectra the accelerograms require to be scaled for peak ground accelerations (PGA) higher than those expected in Spain; in the following, we will refer to this spectrum as the code spectrum. 20 acceleration records are selected whose mean 5% damped elastic response spectrum is in the range of $\pm 5\%$ of the code spectrum. There are several methods for selecting the accelerograms which describe the seismic hazard of an area (Hancock et al. 2008). In this paper we use a procedure based on least squares which consists in selecting a group of accelerograms whose mean spectrum minimize the error respecting the target spectrum (Vargas et al. 2012). In Figure 4, the code spectrum and the mean spectrum corresponding to the 20 selected accelerograms are shown.

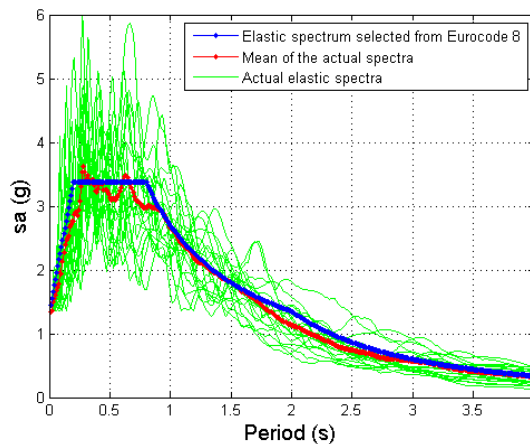


Figure 4. Comparison between the spectrum of EUROCODE 8 and the mean of the spectra of the earthquakes selected from the Spanish and European databases

The selected accelerograms are scaled to different levels of the peak ground acceleration and are then used to perform a series of NLDA within the framework of the incremental dynamic analysis, IDA. The scaling method used in this article consists of incrementing the acceleration ordinates by a scalar allowing to define the desired PGA levels. Even if in this way we maintain the initial frequency content of the seismic action, this scaling method is adequate for the purpose of this article, which is the comparison in a probabilistic way of the results obtained with static and dynamic nonlinear analysis methods considering uncertainties. Nevertheless, in the Monte Carlo simulation we considered 20 accelerograms scaled in this way, having their frequency content certain variability. The role of IDA in this article is to combine the uncertainties in the mechanical properties of the building with those involved in the seismic action. The objective is to obtain the evolution of a dynamic response variable, for instance the displacement at the

roof of the building, as a function of a variable describing the seismic action; we considered that this last variable is the PGA, which, in this case, is increased up to 0.25 g which is the maximum PGA value in the Spanish seismic design code. In the IDA, the variable which is related to the PGA is the expected spectral displacement (ESD). Obviously, as the seismic demand is obtained as a random variable, the ESD will also be random and, therefore, the values shown in Figure 5 are the mean values. This figure shows the variation of ESD, when PGA increases, together with the ± 1.65 standard deviation intervals that is, a confidence level of 95%. Figure 6 shows the evolution of the standard deviation of the ESD.

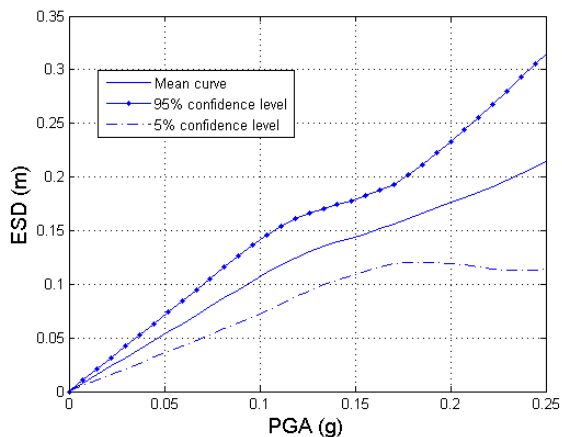


Figure 5. Relation between PGA and mean expected spectral displacement

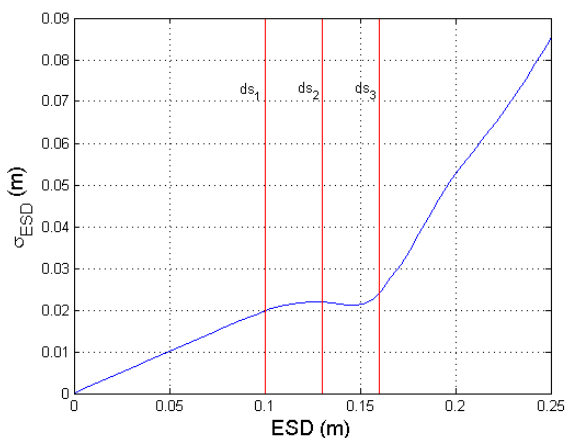


Figure 6. Relation between the mean expected spectral displacement and the standard deviation

In Figure 5, a major change in the slope of the curve approximately for 0.16 g can be seen, but other significant changes in the behavior of the structure can be not appreciated in this graph. However, Figure 6 shows three points related to significant changes in the slope of the curve; these points can be also seen in Table 2, where the first is related to the first change of the slope of the curve. The second point corresponds to the first maximum and the third one is related to the beginning of a straight line with maximum slope. Later on, we will use these points to discuss the damage states of the structure and, thus, its seismic behavior.

Table 2. Coordinates of the particular points which are identified in Figure 5

Point	X coordinates (m)	Y coordinates (m)
1	0.1	0.02
2	0.13	0.0294
3	0.16	0.0298

4. CAPACITY SPECTRUM, DAMAGE STATES AND FRAGILITY CURVES

4.1. Capacity spectrum and bilinear representation

Once calculated the capacity curve of the structure, it is useful transforming it in the capacity spectrum by means of the procedure proposed in the ATC-40 (1996). The capacity spectrum is represented in spectral acceleration-spectral displacement coordinates (*sa-sd*) and is often used in its simplified bilinear form, defined by the yielding point (D_y, A_y) and the ultimate capacity point (D_u, A_u), as it can be seen in Figure 7.

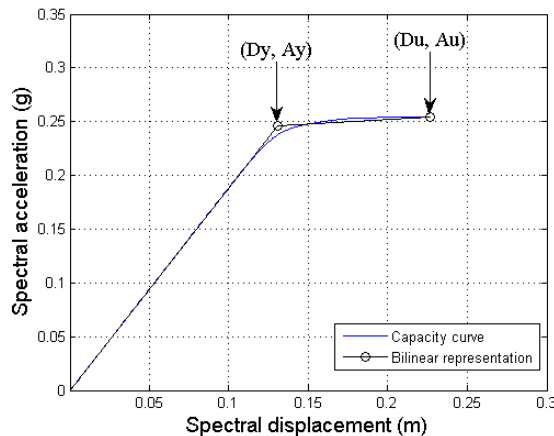


Figure 7. One of the capacity spectra of the studied building and its bilinear representation

4.2. Damage states

In order to analyze the expected damage we use simplified methods allowing to obtain the damage states thresholds ds and the corresponding fragility curves. Four non-null damage states are considered: (1) *slight*, (2) *moderate*, (3) *severe* and (4) *extensive-to-collapse*. For a given damage state, according to the hypothesis considered in the RISK-UE project (Milutinovic & Trendafiloski 2003), the damage state threshold is defined by the 50% probability of occurrence. This damage state threshold can be defined in the following simplified way from the bilinear capacity spectrum (Lantada et al 2008; Barbat et al 2010; Barbat et al 2011):

$$\begin{aligned}
 ds_1 &= 0.7 * Dy \\
 ds_2 &= Dy \\
 ds_3 &= Ds_2 + 0.25 * (Ds_4 - Ds_2) \\
 ds_4 &= Du
 \end{aligned}
 \tag{1}$$

The damage states thresholds have been established for all the capacity spectra calculated for the studied structure. Thus, considering the damage states thresholds as random variables, Figure 8 shows the results obtained and the mean values for each damage state. This figure also shows how the dispersion increases when the damage states increase. This fact indicates that, when the structure enters into nonlinear behavior, the uncertainties in the damage level increase. The mean and standard deviation of sa and sd of each damage state are shown in Table 3. It is important noting the agreement of these values with those of Table 2. The points 1, 2 and 3 of Table 2 correspond to the mean values of the damage state thresholds ds_1 , ds_2 and ds_3 ; the changes in the slope of the standard deviation calculated via IDA correspond to the damage state thresholds indicated in Figure 6.

Table 3. Mean and standard deviation of damage states.

ds	m_{sd} (m)	s_{sd} (m)	m_{sa} (g)	s_{sa} (g)
1	0.0985	0.0013	0.1878	0.0038
2	0.1314	0.0017	0.2504	0.0050
3	0.1583	0.0049	0.1878	0.0051
4	0.2212	0.0148	0.2504	0.0054

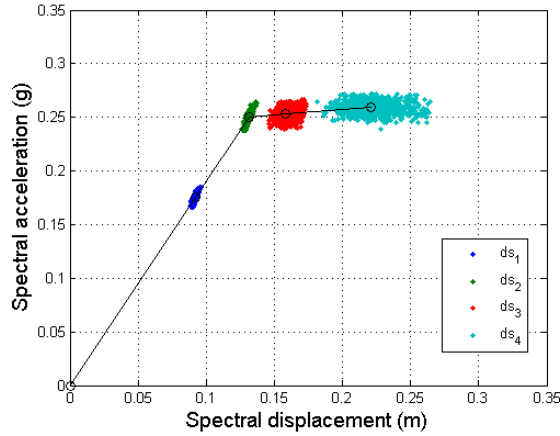


Figure 8. Damage states as random variables

For each damage state threshold, the corresponding fragility curve is defined by the probability of being exceeded the corresponding threshold as a function, in our case, of the spectral displacement. It is assumed that the fragility curves follow a standard lognormal cumulative distribution function.

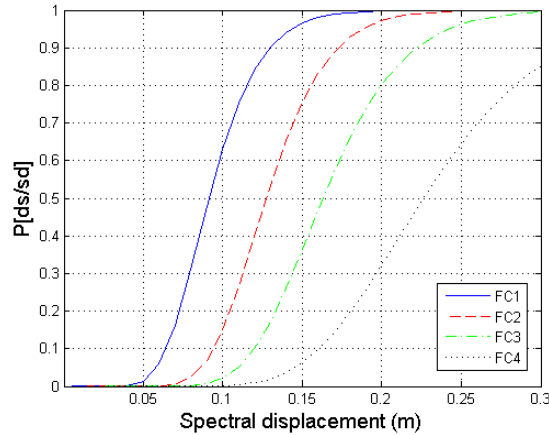


Figure 9. Example of one fragility curves for the building

Each fragility curve is then obtained by using the following equation:

$$P[i / sd] = f \left[\frac{1}{b_{ds_i}} \operatorname{Ln} \left(\frac{sd}{sd_{ds_i}} \right) \right] \quad (2)$$

where sd is the spectral displacement and \overline{sd}_{ds_i} is the mean value of the lognormal distribution which is the corresponding damage state threshold as defined above. b_{ds} is the standard deviation of the natural logarithm of the spectral displacement of ds . In equation 2, the mean values, \overline{sd}_{ds_i} , can be determined from the capacity spectrum and b_{ds} can be estimated by assuming that the damage follows a binomial distributions and, finally, by using a mean square procedure to fit the fragility curves (see Lantada et al. 2008). Notwithstanding, there is a correlation between the ductility of the building and the variables b_{ds} of each fragility curve, which has been found by relating the results obtained with the Monte Carlo Method. This correlation is very useful because one can obtain the fragility curves applying directly this method, avoiding the mean square procedure described in Lantada et al. 2008, being thus the calculation time considerably reduced. Figure 10 shows graphically this correlation.

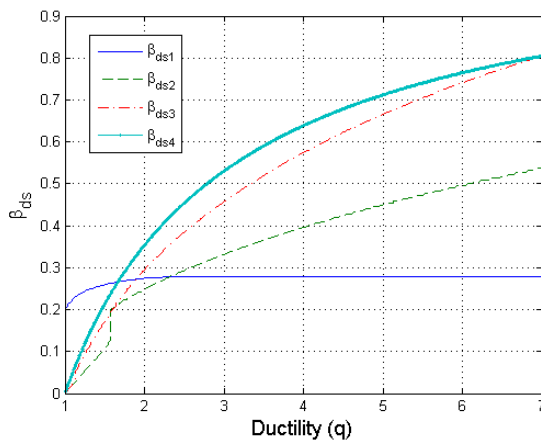


Figure 10. Correlation between ductility and the variables b_{ds}

Figure 11 shows 1000 fragility curves obtained for all the calculated capacity spectra applying the simplified method exposed above. Obviously, according to Figure 8, as the considered damage state increases, the uncertainties involved in the corresponding fragility curve also increase. As an example, the fragility curves corresponding to the damage states *slight* and *collapse* can be seen in Figure 11. Figure 12 shows the results of a sensitivity test on the influence of the mechanical properties of the materials and the damage state thresholds; the stiffness is used as an independent variable in this test.

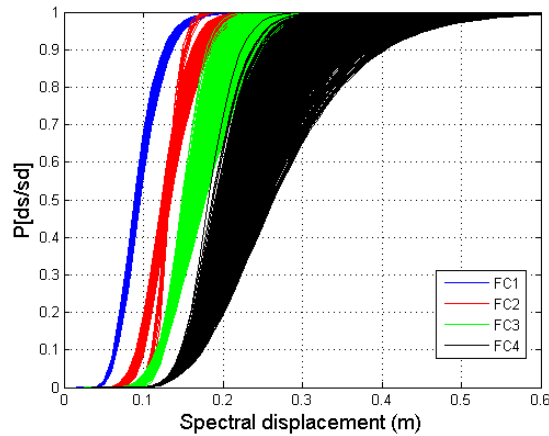


Figure 11. Fragility curves as random variables

ds_1 and ds_2 damage states are practically independent on stiffness, while for ds_3 and ds_4 the spectral displacement decreases with increasing stiffness, indicating that the probability of the corresponding damage states increases with stiffness. Figure 13 shows the mean fragility curves and Figure 14 shows the corresponding standard deviations as a function of sd .

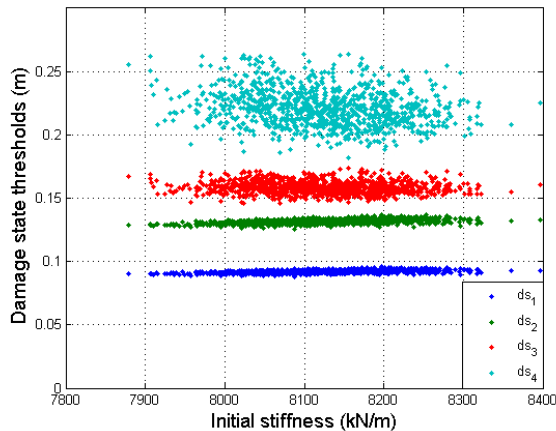


Figure 12. Sensitivity test for ds and the initial stiffness

Figure 13 clearly depicts the dependence of the uncertainties on the damage grades. For instance, the coefficient of variation of the damage state ds_4 may be greater than 10%, which means that, for a confidence level of 95%, the increase in the

probability of failure will be greater than 16.5%. This increase reaffirms the importance of analyzing the problem from a probabilistic viewpoint.

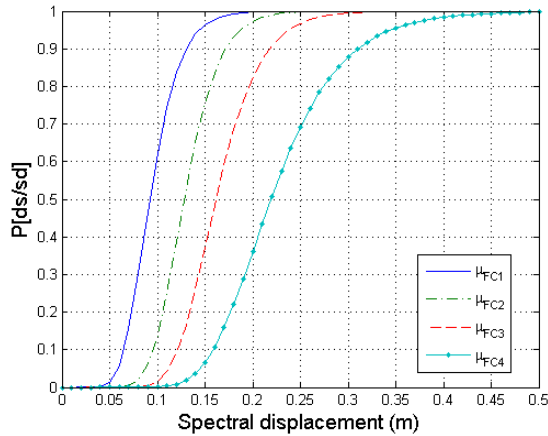


Figure 13. Mean fragility curves obtained via Monte Carlo simulation

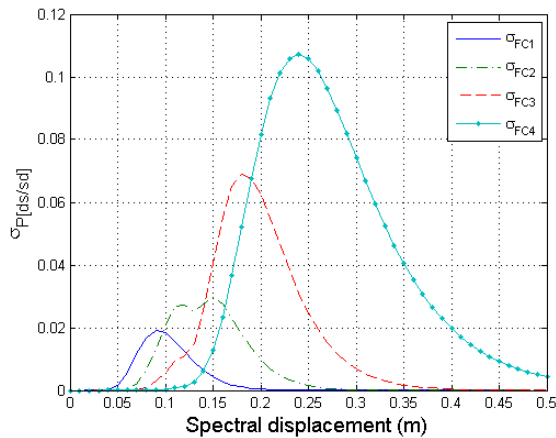


Figure 14. Standard deviation of the fragility curves

5. EXPECTED SPECTRAL DISPLACEMENT AND DAMAGE INDEX

The maximum expected spectral displacement in a building due to the seismic hazard of the area is obtained in section 4 using NLDA and the results were presented in figures 5 and 6. Different studies have searched for simplified procedures to estimate the expected spectral displacement (Kim et al 2008). A much more simplified procedure is the so-called equal displacement approximation, EDA, which is described in ATC-40 (1996) (see also Mahaney 1993). The EDA is performed by using the spectra corresponding to the selected accelerograms in order to perform a better comparison with the results obtained from the NLDA. Due to the fact that the EDA is a linear procedure, the results will be linear; for this reason, it is enough to scale the spectra for a single PGA. In order to express the expected spectral displacement as a function of the PGA, the spectra are scaled to 0.25 g obtaining the mean and standard deviation. Figure 15 shows graphically the EDA procedure considering the uncertainties associated to the seismic action and to the mechanical properties of the materials.

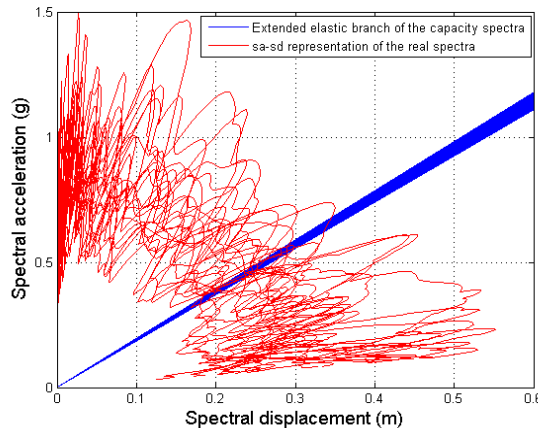


Figure 15. Equal displacement approximation considering the uncertainties associated to the seismic action and to the mechanical properties of the materials

These results are shown in figures 16 and 17, respectively, where the NLDA results are also given. The main conclusion of this analysis is that the EDA methodology provides an adequate approximation for the expected spectral displacement of the building, because it does not underestimate the expected displacement.

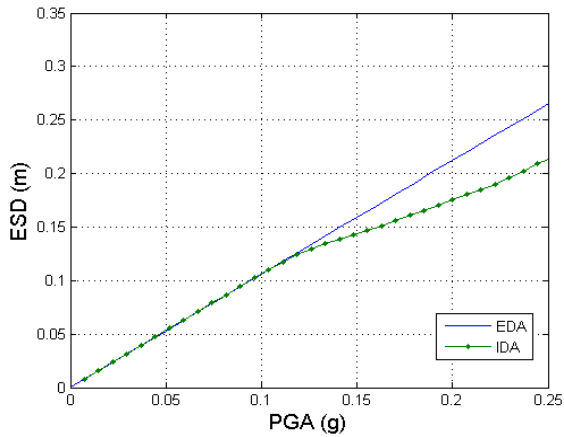


Figure 16. Comparison between the relation of the PGA to the expected spectral displacement obtained by using EDA and NLDA

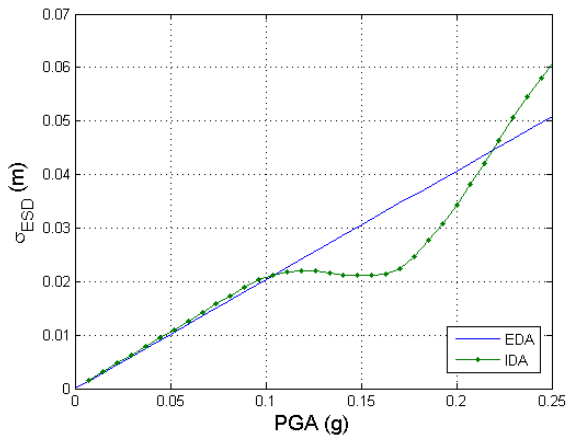


Figure 17. Comparison between the relations of the PGA to the standard deviation of the expected spectral displacement obtained by means of EDA and NLDA

Moreover, from a probabilistic viewpoint, this method is also conservative because, in the nonlinear range, the standard deviation obtained with EDA is higher than that obtained with NLDA. On the other hand, we can calculate a damage index, DI , which is defined by the following equation:

$$DI = \frac{1}{n} \sum_{i=0}^n iP(ds_i) \tag{3}$$

where n is the number of non-null damage states ($n=4$ in this case) and $P(dsi)$ is the probability of the damage state i which can be easily calculated from the fragility curves (see Figure 18). DI is the normalized mean damage grade which is a measure of the overall damage in the structure (Barbat et al. 2008). The authors proposed equation (3) for calculating the overall damage taking into account that the higher damage states ds_i have more influence on the global damage state DI of the structure and, also, because this equation provides the main parameter of the binomial distribution which allows obtaining the fragility curves in a simpler manner. Obviously, the values of the coefficients of the four probabilities of the damage states (0.25, 0.5, 0.75, 1.0) could be calibrated in order to improve DI if observed damage values would be available.

DI can be also plotted as a function of the expected spectral displacement. Thus, DI can be calculated for any spectral displacement but, in order to include the randomness associated to the seismic action, the comparison between DI obtained with EDA and with NLDA requires computing the PGA corresponding to each spectral displacement by using the relation shown in Figure 16. Figure 19 shows the obtained results, namely the mean values and the 95% confidence level curves. Again, our results confirm that the EDA is conservative respect to NLDA, even when considering a confidence level of 95% for random variables. But, if the variables were not treated by using a probabilistic approach, this would result in an underestimation of the actual damage that may occur in the building. In the case of the building analyzed in this article, the damage index estimated by using a deterministic approach is 0.25 lesser than that computed from a probabilistic viewpoint.

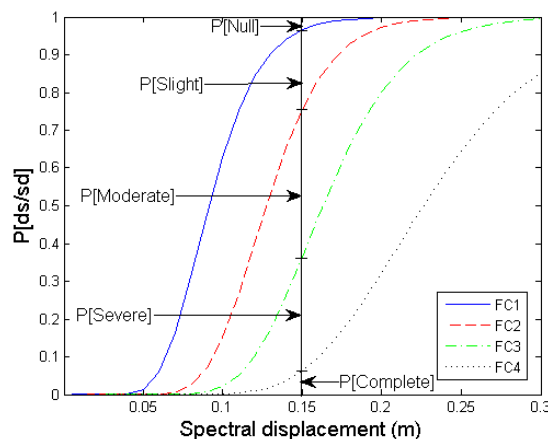


Figure 18. Probability of each damage state depending on the expected spectral displacement

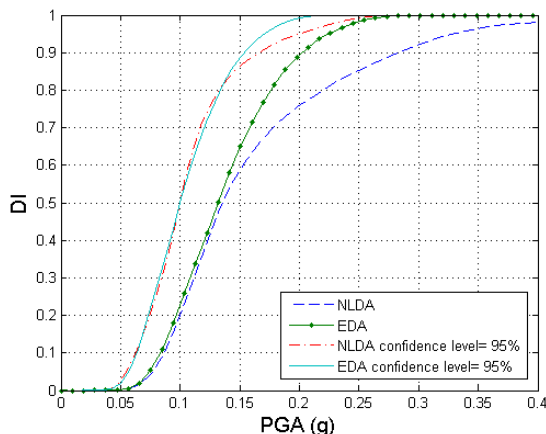


Figure 19. Damage index obtained with NLDA, EDA, and a confidence level of 95%

6. DISCUSSION AND CONCLUSION

The assessment of the vulnerability, fragility and expected damage in a reinforced concrete building is performed in this article. However, the results obtained herein go further and they compare, in a probabilistic way, nonlinear static and dynamic analysis procedures. We face the problem from a probabilistic point of view, since we consider the uncertainties in the parameters related to the mechanical properties of the materials and the seismic demands. A first hint is that, notwithstanding that incremental dynamic analysis is a powerful tool in the assessment of the structural behavior of buildings when submitted to seismic actions, this procedure has little sense if the seismic demand is not carefully and properly selected. We put special care in the selection of the accelerograms used in this study. We have selected accelerograms corresponding to seismic events from the Spanish and European strong motion records databases. In order to reach a wide range of spectral displacements, the Eurocode type 1 design spectrum for soil type D has been taken as target demand. The accelerograms have been selected according to this criterion and have been scales to cover PGA values until 0.25 g. We used standard pushover analysis to obtain probabilistic capacity curves. A modified adaptive technique has been used to define the horizontal incremental load limit in order to stop automatically the pushover analysis during the run of high number of structures, 1000 in this case. Starting from the capacity spectra, simplified methods allow obtaining damage states thresholds and probabilistic fragility curves. An interesting conclusion of this exercise is that uncertainties increase in the nonlinear range. For the *collapse* damage state, the uncertainties in the fragility curves may be greater

than 10%. EDA and NLDA are used to obtain the expected spectral displacement and its standard deviation as a function of the PGA. Again, uncertainties increase with increasing PGA. This fact can be attributed to the increase of the inelastic behavior of the building. EDA is a successful approach because it does not underestimate the actual displacement, but it can be too conservative in structures with higher ductility. Furthermore, the fact that both the expected spectral displacement and the standard deviation are greater when calculated with EDA than when calculated with NLDA, confirms that EDA is conservative. In the NLDA, the seismic action is the main responsible for uncertainties in the spectral response, being less significant the influence of the uncertainties in the mechanical properties of the building. However, as the damage state increases, a sensitivity test shows a correlation between stiffness and spectral displacement. For the damage states ds_3 and ds_4 , the spectral displacement decreases when stiffness increases, indicating that the probability of the corresponding damage state increases with the stiffness. This result is important since the damage states ds_3 and ds_4 have a high influence upon the calculation of the damage index. Finally, the comparison of the damage index as a function of PGA and the corresponding uncertainties shows that, for damage states from *severe* to *collapse* and for a confidence level of 95%, the uncertainties in the damage index may be higher than 0.25 units or 42% of the damage index. Thus, perhaps, the most important conclusion is that both static and dynamic structural analyses should be faced by using probabilistic approaches.

Acknowledgements

This work was partially funded by the Geological Institute of Catalonia (IGC), by the Spanish Government and by the European Commission with FEDER funds, through the research projects: CGL2008-00869/BTE, CGL2011-23621, CGL2011-29063, INTERREG POCTEFA 2007-2013/73/08, MOVE—FT7-ENV-2007-1-211590 and DESURBS-FP7-2011-261652.

References

1. ATC-40. 1996. *Seismic evaluation and retrofit of concrete buildings*. Applied Technology Council, Redwood City, California.
2. Barbat, A.H. Pujades, L.G. Lantada, N. and Moreno R., 2008. Seismic damage evaluation in urban areas using the capacity spectrum method: application to Barcelona. *Soil Dynamics and Earthquake Engineering*, 28, 851–865.
3. Barbat, A.H. Carreño, M.L. Pujades, L.G. Lantada, N. Cardona, O.D. and Marulanda, M.C., 2010. Seismic vulnerability and risk evaluation methods for urban areas. A review with application to a pilot area. *Structure and Infrastructure Engineering*, 6, 1–2, 17–38.
4. Barbat, A.H. Carreño, M.L. Cardona, O.D. y Marulanda, M.C., 2011. Evaluación holística del riesgo sísmico en zonas urbanas. *Revista internacional de métodos numéricos para cálculo y diseño en ingeniería*, 27(1), 3-27.
5. Bommer, J.J. & H. Crowley (2006). The influence of ground motion variability in earthquake loss modelling. *Bulletin of Earthquake Engineering* 4 (3), 231-248.

6. Borzi, B. Phino, R and Crowley H., 2008. Simplified Pushover analysis for large-scale assessment of RC buildings. *Engineering Structures*, 30, 804-820.
7. Carr, A.J., 2000. Ruaumoko-Inelastic Dynamic Analysis Program. Dept. of Civil Engineering. Univ. of Canterbury, Christchurch, New Zealand.
8. Eurocode 8. 2004. Design of structures for earthquake resistance. Part 1: General rules, seismic actions and rules for building.
9. Fragiadakis, M. and Vamvatsikos, D., 2009. Estimation of Uncertain Parameters using Static Pushover Methods. *The 10th International Conference on Structural Safety and Reliability, ICOSSAR 2009, Osaka, Japan*.
10. Hancock, J., J.J. Bommer & P.J. Stafford (2008). Numbers of scaled and matched accelerograms required for inelastic dynamic analyses. *Earthquake Engineering & Structural Engineering* 37 (14), 1585-1607.
11. Kim, S.P and Kuruma Y.C., 2008. An alternative pushover analysis procedure to estimate seismic displacement demands. *Engineering structures*, 30, 3793-3807.
12. Lantada, N. Irizarry, J. Barbat, A.H. Goula, X. Roca, A. Susagna, T and Pujades L.G., 2008. Seismic Hazard and risk scenarios for Barcelona, Spain, using the Risk-UE vulnerability index method. *Bulletin of Earthquake Engineering*, 8, 201-229.
13. Lantada, N. Pujades, L.G. and Barbat A.H., 2009. Vulnerability index and capacity spectrum based methods for urban seismic risk evaluation. A comparison. *Natural Hazards*, 51, 501-524.
14. MATLAB. The mathworks inc.
15. Mahaney, J.A. Paret, T.F. Kehoe, B.E. and Freeman, S.A., 1993. The capacity spectrum method for evaluating structural response during the Loma Prieta earthquake. *National earthquakes conference*, Memphis.
16. Mwafy, A.M. and Elnashai, A.S., 2001. Static pushover versus dynamic collapse analysis of RC buildings. *Engineering Structures*, 23, 407-424.
17. Milutinovic Z.V. and Trendafiloski G.S., 2003. *WP04 Vulnerability of current buildings*. RISK-UE project of the EC: an advanced approach to earthquake risk scenarios with applications to different European towns
18. Poursha, M. Khoshnoudian, F. & Moghadam, A.S., 2009. A consecutive modal pushover procedure for estimating the seismic demands of tall buildings. *Engineering Structures*, 31, 591-599.
19. Pujades, L.G. Barbat, A.H. González-Drigo, R. Avila, J. and Lagomarsino S., 2011. Seismic performance of a block of buildings representative of the typical construction in the Eixample district in Barcelona (Spain). *Bulletin of Earthquake Engineering*. (in press)
20. Satyarno I., 1999. Pushover analysis for the seismic assessment of reinforced concrete buildings. Thesis (PhD). University of Canterbury.
21. Vamvatsikos, D and Cornell, C.A., 2002. Incremental Dynamic Analysis. *Earthquake Engineering and Structural Dynamics*, 31(3), 491-514.
22. Vargas, Y. F., Pujades, L. G., Barbat A. H. and Hurtado, J. E., 2012, Evaluación probabilista de la capacidad, fragilidad y daño sísmico en edificios de hormigón armado. *Revista Internacional de Métodos Numéricos en Ingeniería*, 28(4) (in press).
23. Vielma, J.C. Barbat, A.H. and Oller, S., 2009. Seismic performance of waffled-slabs floor buildings. *Structures and Buildings (Proceedings of the Institution of Civil Engineering)*, 162(SB3), 169-18.
24. Vielma, J.C. Barbat, A.H. and Oller S., 2010. Seismic safety of limited ductility buildings. *Bulletin of Earthquake Engineering*, 8(1), 135-155.

Modelling of the line construction of building by the method network analysis

Renáta Bašková

*Institute of Civil Engineering Technology and Management
Faculty of Civil Engineering, Technical University of Kosice, Slovakia
e-mail: renata.baskova@tuke.sk*

Summary

The line method of work scheduling in construction of objects is characterized by smoothness and uniformity of work carried out simultaneously in time but by shift in space. Technological and organizational conditionality of processes, in the schedule processing by a computer, are entered by bonds in the network graph. The paper deals with mathematic apparatus of various methods of network analysis and its conformity with the requirements for planning, debugging, tracking and automatic update of the scheduling line construction.

KEYWORDS: line construction, scheduling, networks analysis methods

1. INTRODUCTION

For every computer software for scheduling of construction there is a specific method of the network analysis. From its mathematical program depends ability to meet the needs of its user, which arise in the creation, debugging, monitoring and automated updates of the schedule in pre-production, production and implementation phase of the construction.

2. METHODS OF BUILDING CONSTRUCTION

In the construction of multi-zones buildings construction works can be arranged on the principle of parallel, line, or a gradual method (Figure 1).

The line method of construction of the linear buildings or larger buildings of civil engineering is characterized by parallelism of many activities that take place at the same time at different zones of the building. Most of the work overlaps with a time lag depending on the size of the minimum work queue.

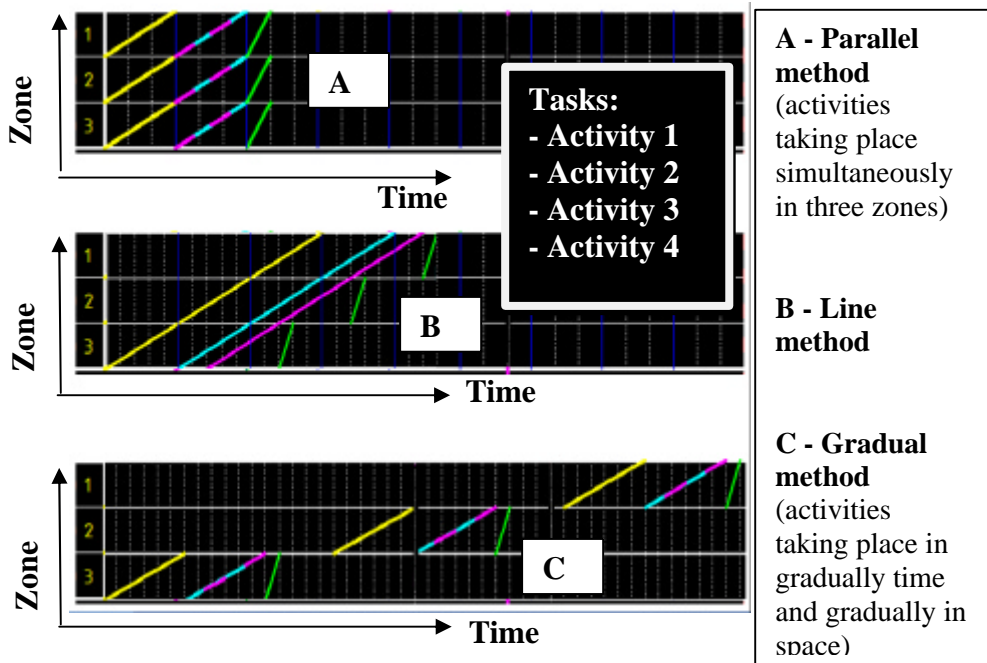


Figure 1: Time-space graph: a display of (A) parallel method, (B) line method and (C) gradual method construction of building

The line method is characterized by three principles in the scheduling of construction:

- **Continuity** - working parties should not interrupt their work in the transition between zones of the building.
- **Uniformity** - working parties should be uniformly labour loaded during the entire work. Building zones, through which the line passes, should have a comparable labour intensity so that working parties could work in a fixed composition throughout their deployment.
- **Rhythm** - working parties should stay at each construction zone the same length of time, technologically conditioned immediately consecutive activities should work with the same production rate.

3. BONDS IN THE METHODS OF NETWORK ANALYSIS

The base for automated modelling of time project course is always particular network analyses method. During the modelling of building time course by computer it is possible to define in the network topology technological or

organization activities relativities only by these mathematical bonds, which are defined in the particular network analyses method and its mathematical mechanism. [1] [2]

The mathematical bonds between activities/milestones are divided into:

- **Simple bonds** – these bonds express the connection between one event of previous activity and one event of next activity. There are connections: finish-start (FS), start-start (SS), finish-finish (FF) and the bonds, which are derived from them, such partial start-start and partial finish-finish. Each type of connections is characteristic also way of definition and time assessment of distance (for example $e_{ZZ} = 3$ days means that the subsequent activity begins 3 days after initiation of the predecessor). The definition of necessary the earliest date belongs among simple bonds too.

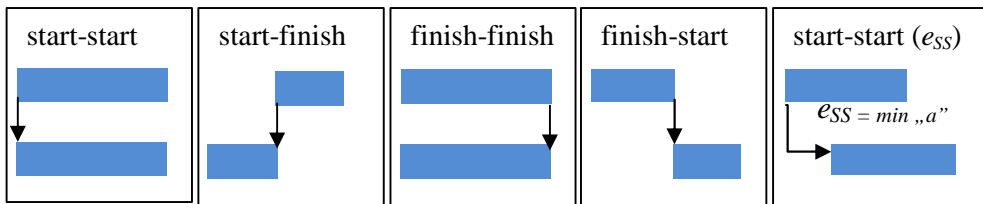


Figure 2: Simple bonds

- **Double bonds** – allow by one mathematical mechanism to express the connection between two events (also one) of previous activity and between two events (or one) of next activity. They are the mathematical connections of two simple bonds (SS+FF). Their elementary representative is critical approach bond. The construction-technological bond and line bond reflect activity development date and activity reduction date, as well as spatial parameters of structure, entered by value of the coefficient of the work queue.

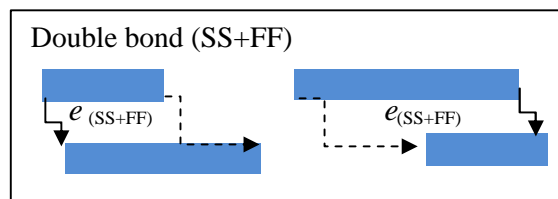


Figure 3: Double bond

- **Multiple bonds** – interconnects activities with defined number of events, such as a subdivision activity at part of the going in the area through various working zones. It can be bulk specified for the activity "in a line" (linking

parts of the same activity between zones) or between two activities, where is specified interconnection of activities parts in the individual zones.

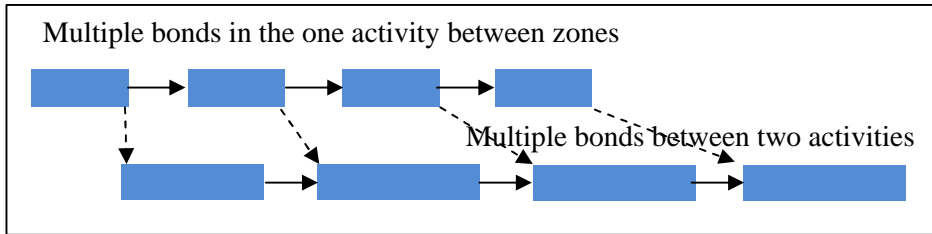


Figure 4: Multiple bonds

- Cyclic bonds** – these bonds express a feedback between event of next activity/milestone and event of previous activity/milestone. That is the bond, which has a given particular maximal possible value of time distance „b“ (where $b \geq 8$). Eventually, it can be a double bond between events of two activities, where first bond has given a maximal possible time distance and second bond has a maximal accepted time distance. The elementary representative of cyclic bond is a definition of the latest or stable necessary date. There belongs a stable activity connection without the interruption possibility of working teams (or with given maximal possible interruption) between two activities - finish work of one activity and start work of another activity.

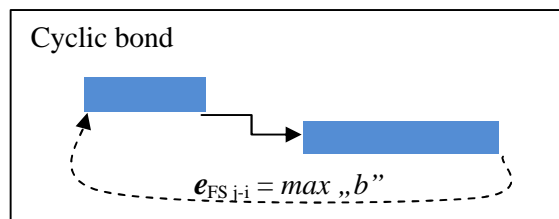


Figure 5: Cyclic bond

Specific bond types in a network diagram have the mathematical relationship to determine the latest date of activities in the earliest possible dates activity "forward calculation" and latest acceptable dates by "back calculation". Based on the "forward calculation" and "back calculation" to determine the activities lying on the critical path and are calculating a float time for non-critical activities.

Critical path in the nodes-defined network diagrams is sequence activities going from the beginning of the chart up to its end, the greatest sum of bonds specified intervals lying to her beginnings.

4. SCHEDULING OF CONSTRUCTION BY METHODS OF NETWORK ANALYSIS

In the construction of larger buildings parallel, gradual or line methods of work scheduling may be applied. The parallel method, as well as for the gradual methods of work scheduling, you can enter the sequence of work in scheduling in computer environment only through simple bonds. For planning of line organization of work scheduling double or multiple bonds are required, because single bonds using their mathematical formulas, do not allow to specify clearly the division of space structures on zones.

Software and their mathematical methods of network analysis that are used for scheduling construction can be divided into three groups:

- 1. group** – in this method only single bonds are used for interconnection of activities in network graph [3];
- 2. group** – method of network analyses allows to specify a single or double bonds between the processes, progress of work in space is specified by the coefficient work queue [8];
- 3. group** – single bonds and multiple bonds are used for scheduling processes, they enable you to add and connect activities, carried out at construction at multiple zones, and shots can be given size, volume or location within the building [7] [9] [10].

The second and third group of software in terms of scheduling of construction allows in the network graph to enter not only parallel and gradual, but especially a line activities execution. On the other hand, construction practice very often uses software for scheduling of construction, can use belonging to the first group, which creates the risk of non-conformity of schedules for automatic updates of the plan in time of the construction [5].

Produce a schedule with line organization of work is possible using only single bonds. Problematic, time consuming and technically demanding is but the subsequent debugging. During the implementation of construction projects, often occur to errors and irregularities in the auto-update schedule of work.

4.1 Network critical path and the line method of construction

By using simple bonds for planning of line method of construction may arise uncertainties in computer-generated during the activities on the critical path. Given the type of bonds and specified forced deadlines may be not duration of critical path directly dependent on the duration of critical activities. Extension or shortening their duration does not affect the proportion calculated the shortest duration of construction.

In terms of debugging schedule of work, critical activities may be threefold type:

- **Normal critical activities** – connect on critical path by bonds FS, critical path influence values $e_{FS\ i-j}$ a $e_{FS\ j-k}$ - change the duration of action varies the duration of the project;
- **Neutral critical activities** – connect on critical path by bonds ZZ, critical path influence value $e_{SS\ i-j}$ and $e_{SS\ j-k}$ -change their duration (of course, in the interval) does not change the duration of the project (Fig.6 - activity D and E);
- **Negative critical activities** - connect on critical path by bonds FF with previous activity and SS bond with the next activity, the critical path affects the value $e_{FF\ i-j}$ and $e_{SS\ j-k}$ - shortening their duration of the project is certainly not reduced, but their extension could lead to a reduction of the project (Fig. 6 - activity C).

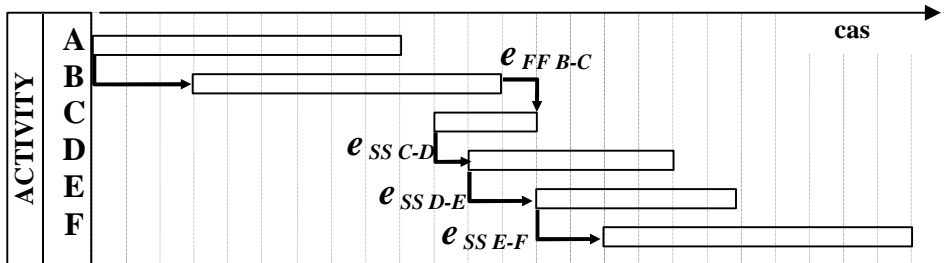


Figure 6: Activity interconnect by single bonds

It is clear that discernment of these three types of critical activities is not theoretical significance only, but their understanding, together with mastering of inputting the appropriate type and the time value of bonds, may have practical applications especially in the planning activities with the application of the principles of line methods of construction.

4.2 Scheduling of construction line method by software MS Project

SW MS Project has given simple bonds only. One way how to express by simple bond interval, less than the duration of the previous activity, is enter the time value of specific bond (Fig. 7-A), number or % of time predecessor. To change the duration of activity must always be reviewed and the time value of bond.

The second way assignments line implementation of activities is that work certain kind formally divided into more activities, going through individual zones of building, organization are linking activities by bond FS. Their linkage with following by especially dividing activities of another kind, allow to capture the real continuity with overlapping of work. FS bond connect at each zone the end of the previous frame with the start of the next activity (Fig. 7-B).

Concurrence of activities in the time but at price a considerable increase in the number of planning activities sometimes and even stronger growth in the number of bonds to their technological and organizational links. The downside is that so the divided work is not possible to specify the requirement for continuous work working parties.

In both cases shown in the figure (Fig. 6 and Fig. 7-A,B), it is possible to partially eliminate some disadvantages to balance periods of work working parties in the zones, in the line method is in a zone desirable comparable to the duration of subsequent works. If works on the building were planned with the same production rate, in the first case (Fig. 7-C) the reduced total time of implementation of works and in the second case (Fig. 7-D) would reduce the risk of interruption of work working parties in the transition between zones.

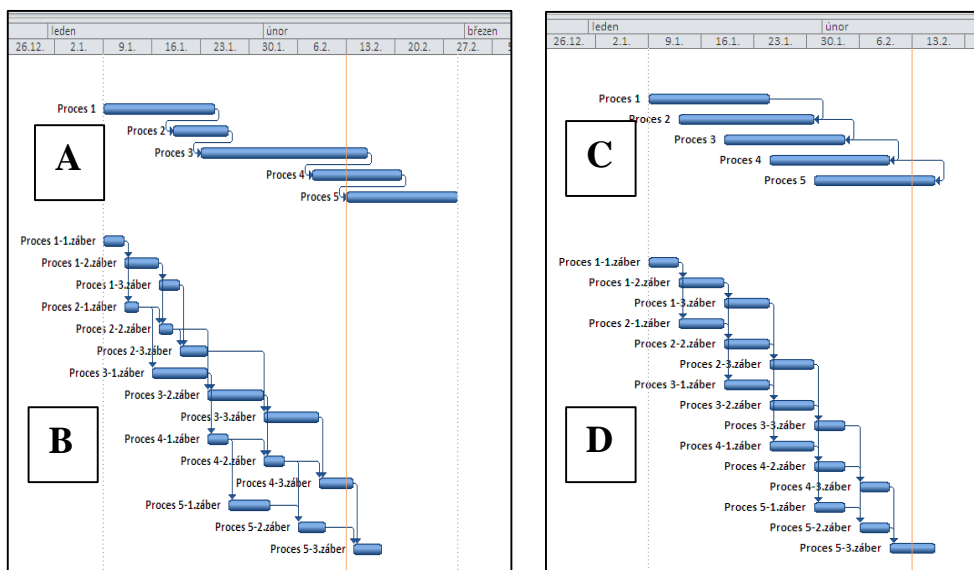


Figure 7: Specifying of the time course of the work on the three zones by single bonds only

In the figures (Fig. 8, 9) are samples of the errors in schedule after the automatic rescheduling of the project to the current date. Errors are due to a lack of conformity of network analysis methods, with the requirements for entering the technological conditionality of activities, running through multiple zones of structure. The duration of an unbalanced activities (Fig. 8 - A1), to enter the technological conditionality with one single bond only with a time interval, after the automatic update is not guaranteed that the predecessor created and released the workspace for successor. For example, at the figure (Fig. 8 - B1) activity no.2 after the rescheduling ends even earlier than his predecessor.

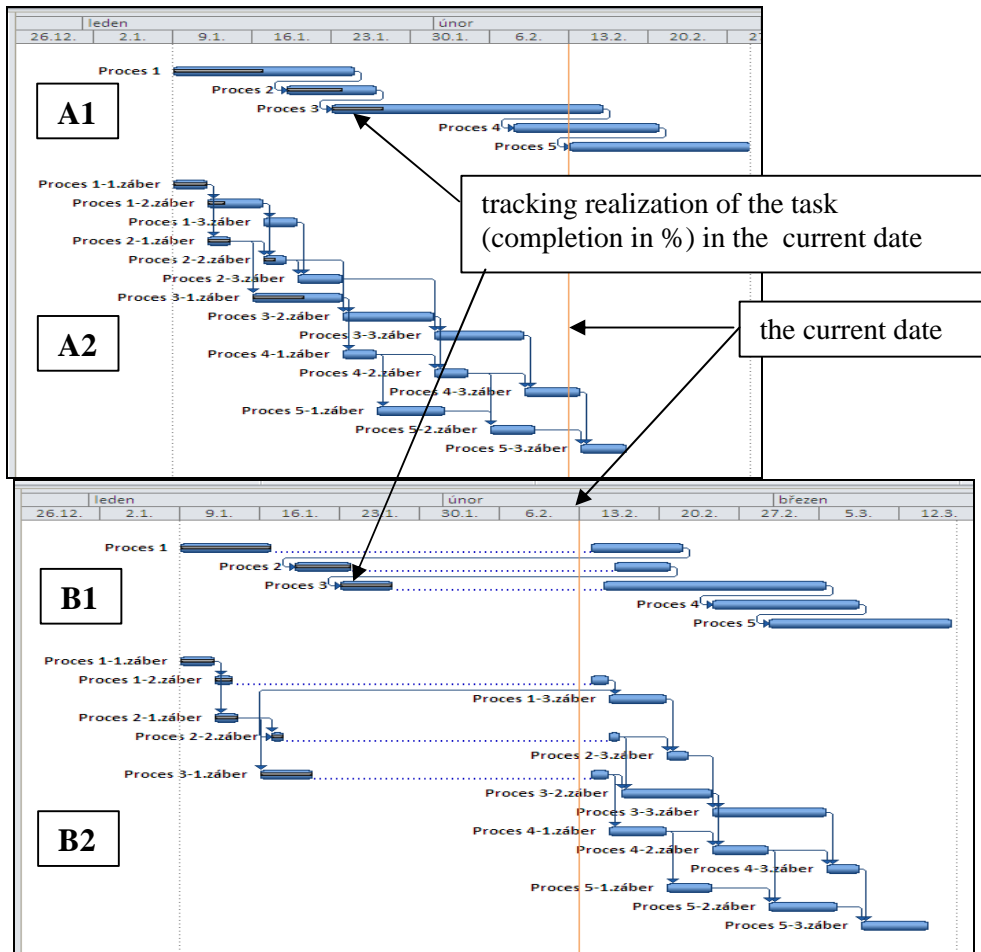


Figure 8: Automatic rescheduling activities with unbalancing duration to the current date

Neither the balancing of the duration of activities (Fig. 9 - C) does not guarantee a smooth upgrade schedule. Instead of the originally line organization of work can be scheduled after the update the implementation of several activity simultaneously at the same time and in the same area, what is from the organizational and technological site unacceptable (Fig. 9 - D1, D2). Conformity provides a FF bond only (Fig. 9 - D3), is less suitable for debugging of the schedule, as by percent specified the time value does not compute, at difference from other software, from duration of successor, but from duration of the predecessor.

Distribution of labor working parties to zones is not a suitable solution for high frequency of planned activities and labor intensive to compile a network diagram (Fig. 8 - A2; Fig. 9 - E).

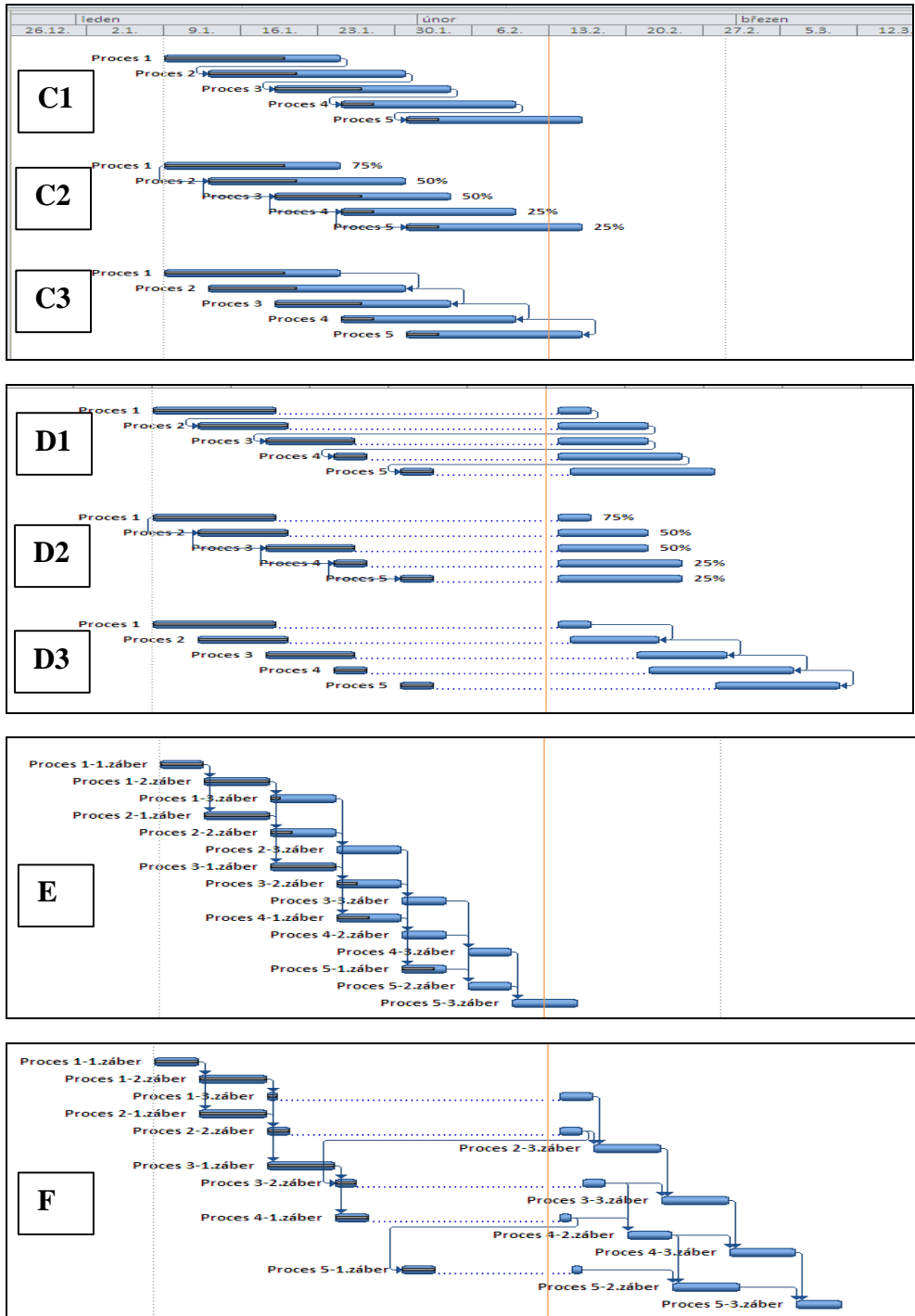


Figure 9: Rescheduling to the current date (work on zones with duration balanced)

There is a risk that in preparing the network diagram will not be given all the technological and organizational bonds (for 5 activities and 3 zones of the building is necessary to enter the 15 activities, 10-times organizational and 12-times technological bonds). Balancing of the duration of activities is no guarantee that crews will not interrupt a work between zones (Fig. 9- F) after the rescheduling.

CONCLUSION

When using a network diagram as a model of construction, where is technological conditionality of activities specified by single bonds only, use the automatic update of the project requires follow control of schedule of work and in most cases, treatment to eliminate errors and debugging of the updated schedule also.

Acknowledgements

Contribution was written within the implementation of the project VEGA 1/0840/11 Multi-dimensional approaches to support integrated design and management of construction projects.

References

1. Bašková, R.: Automation of building process time structure models. In: "INTERSECTIONS" International Journal. Vol.5, No.4, 2008, "Systemic Analysis". Iasi, Romania: Societatea Academica "Matei-Teiu Botez". p. 19-28, ISSN 1582-3024
2. Bašková, R.: Computational modeling of building process time behavior. In: "INTERSECTIONS" International Journal. Vol.3, No.6, 2006, "Construction Management". Iasi, Romania: Societatea Academica "Matei-Teiu Botez". p. 13-24, ISSN 1582-3024
3. Bašková, R.: Casové plánovanie výstavby v programe MS Project. Košice: TUKE, 2011. 64 strán
4. Makýš, P.: Optimization of Time Management Schedules for Construction Works. In: Geotechnical Engineering/Construction Technology & Management: Proceedings of the 8th International Congress on Advances in Civil Engineering, ACE 2008, Volume 2, North Cyprus, Famagusta, 09. 2008. - Famagusta: Eastern Mediterranean University Press, 2008. - S. 563-570
5. Kozlovská, M.: Space-time analysis of building process safety risks. In: Proceedings of Inter. Scientific Conference –Quality, environment, health protection and safety management development trends, NEUM (Bosna and Herzegovina). Brno: Tribun EU, 2008. p. 154-159
6. Makýš, P.: The Automation of Construction Scheduling Considering Variability of Working Environment. In: The 27th international symposium on automation and robotics in construction. Brno: Tribun EU, 06. 2010. Str. 534-543.
7. Kozlovská, M. –Sabol, L.: Using of the newest CAD/BIM tools in construction project. In: Design, technology, Refurbishment and Management of Buildings. Proceedings of 37th. IAHS World Congress on Housing Science, Santander (Spain), October 26 – 29, 2010. Florida (USA): International Association for Housing Science. pp 281 (CD-ROM, p. 1-6.)
8. <http://www.contec.cz/>
9. <http://www.astadev.com/software/>
10. <http://www.vicosoftware.com>

Composite materials in bridge consolidation

Gheorghita Boaca¹, Cristian-Claudiu Comisu²

¹*Department of Transportation Infrastructure and Foundation, "Gh. Asachi" Technical University of Iasi, Romania, boaca_gheorghita@yahoo.com*

²*Department of Transportation Infrastructure and Foundation, "Gh. Asachi" Technical University of Iasi, Romania, comisucristian@yahoo.com*

Summary

This article presents the technical solution for the rehabilitation of an arches bridge on an national road in Romania. The bridge is 61 years old and is in satisfactory condition and requires execution of building works.

The consolidation solution of bridge for taking current and future loads will be made with composite materials based on carbon fibers arranged to take over sectional efforts.

To determine the amount of material was made static calculation for the entire bridge structure. The values for sectional efforts have determined the carbon fiber amount necessary for taking requests.

Consolidation works will be done without being interrupted road traffic and pedestrian on bridge.

Finally, the bridge will have to take loads of traffic and to ensure appropriate gauge crossing national roads in Romania.

KEYWORDS: bridge, consolidation, composite materials.

1. INTRODUCTION

Since its appearance, composite materials have attracted special attention in the construction field due to its efficient behavior under tensile loading, their great resistance against external agents and the simplicity of their application, among other advantageous characteristics. These properties have allowed these materials to be considered for the repair and strengthening of concrete structures [1,2].

Since these products are new in the construction field, there is little available research on its behavior. On the other hand, the technical specifications given by the manufacturers are limited to its field of application.

The behavior of composite materials has been studied and characterization tests have been carried out in many international laboratories and to the Technical University of Iasi, at Faculty of Civil Engineering and Building Services, where have been prepared several PhD theses and reports. Studies have focused on the composite material independently analyzed and the elements and structures strengthened with composite material.



Figure 1. View of bridge on national road at Bicaz

2. BRIDGE ON DN 15 KM 287+062 AT BICAZ, OVER BICAZ RIVER

The bridge has a static undetermined structure made up of two double reinforced elastic arches recessed way up in collaboration with a concrete deck on the frame elastic continuous beams and two longitudinal beams solidarity transversely with beams at 5,00 m and plate concrete on top.

Concrete arches have a rectangular section of constant width 0,60 m and variable height, 1,40 m to 1,00 m at birth and key. Arches were length of 40.00 m measured on the birth line, providing a report $f / l = 1/5$, and were born in Piatra Neamt abutment 0,40m above in relation to the birth of the abutment Bicaz. In cross

section arcs are located at 5,00 m inter-axe symmetrically in relation to the longitudinal axis of the bridge directly.

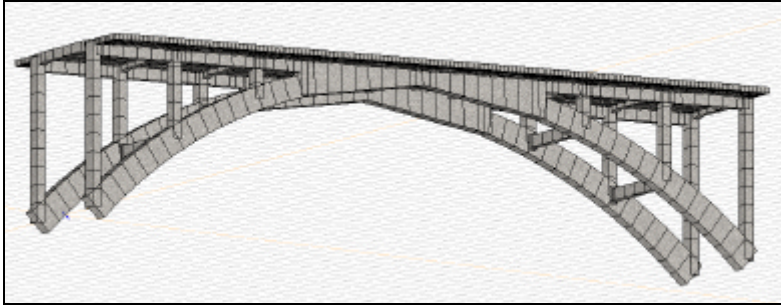


Figure 2. The model of bridge

The arches are solidarity together with reinforced concrete diaphragms with rectangular section 0,60 x 0,30 m in field and 1,00 x 0,30 m in recess, the front arches. The link between arcs is provided with four apertures located at 5,00 m from one another, along the bridge.

The key area for a length of 15.00 m arcs cast firmly attached to the deck beams, solidarity between the arches being covered deck spacers, and top plate of the deck concrete.

The resistance structure of deck consists of reinforced concrete frames with reinforced concrete columns keep the rectangular section 0,50 x 0,60 m and longitudinal beams of rectangular section 0,35 x 0,75 m, with reinforced concrete slab variable height on top. Working between the main beams is provided by beams of rectangular section 0,35 x 0,75 m bridge located along the inter-axe distance 5,00 m.

On top of beams network is secured by a reinforced concrete slab with fixed edges in the network of beams with variable thickness, 0,20 m in the longitudinal axis of the bridge and at least 0,16 m in the inner beams.

The road bridge is composed of the 7,0 m wide carriageway and two bumpy sidewalks each 1.5 m wide.

The bridge parapet covering a total length of 87.60 m. The connection the abutment embankments is provided by reinforced concrete frame type, the 10,50 m long, buried in embankments, foundations arcs with common foundations. Items collected are teaching the same elements as staff liaison between arches and deck.

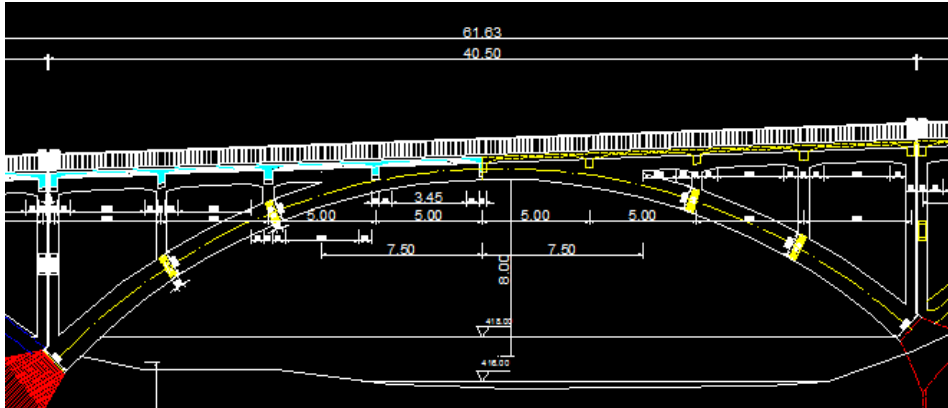


Figure 3. Bridge longitudinal section of bridge

The abutments are of reinforced concrete frame, frames with openings of 5,00 m with columns embedded in the foundation arches, common foundation, buried in embankments. This type of abutment embankments provides connection with a length of 10,50 m with slope 2/3.

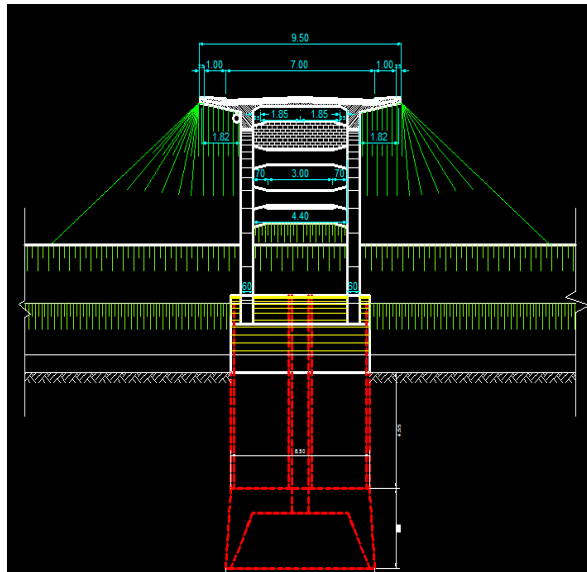


Figure 4. Cross section of the bridge

The foundations are such foundations directly taken to share with compressed air. Foundation block dimensions are 8,82 x 6,50 and the foundations were lowered 9,20 m at elevation 406,90 m Bicaz abutment and abutment 407,70 share Piatra

Neamt. To share the path, the sole foundation is 18,55 m to 19,35 m concerned, providing low-water line to about 9,50 m

The connection is done to the bridge embankments with quarter's cone of piers. Upstream quarters cone are in operation, and the embankment under the bridge embankments have collapsed. Left bank downstream quarter cone is in operation while the downstream quarter cone as completely destroyed. Due disposals embankment slope area covered the bridge was destroyed in the upper walls and embankments support was achieved with a dry underpinning of stone blocks with direct bearing on the existing embankments.

On the left bank upstream of bridge length of 50,0 m were provided of bank that is in operation, and a defense on the right bank downstream of the bridge was destroyed in floods.

3. CONSOLIDATION SOLUTIONS

The elements that need strengthening are:

- Reinforced concrete slab geometry of the deck and deck restoration.
- Consolidation and completion of structural reinforcement sections.
- Strengthening of the main beams and arches to increase the class's loading - truck convoy A30, and special vehicle on wheels V80.
- Strengthen and add structural elements to extend the life of the structure and bring it within the parameters imposed on the carrying capacity without affecting the existing aesthetic valences.
- Repair damaged areas of concrete infrastructure

3.1. Classical method - the bearing shirt

This solution takes into account to increase the bearing capacity of structure, using a well-known and common technology to strengthen the bearing. Since the bridge will have to take current and future traffic loads, the calculated arc section has insufficient carrying capacity. Taking over the efforts to ensure sectional efforts section is increased by the addition of concrete and reinforced all around the elements making a shirt section.

The calculations require a shirt sections on: arches, longitudinal beams and transversal beams. The shirt should have a thickness of 15 cm and two planes of reinforcement.

Strengthening the shirt structure leads to a significant additional load from the weight of the structure.

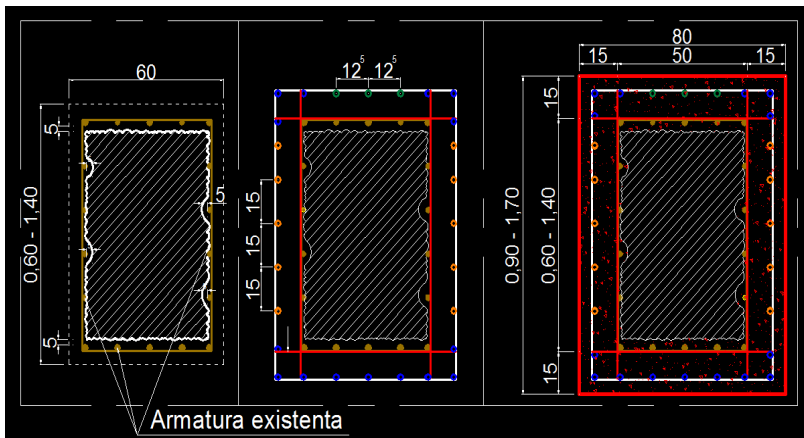


Figure 5. Consolidation of section with shirt

3.2. Modern method - Consolidation with composite materials

The solution of consolidation with composite materials has been studied to reduce the main disadvantage of traditional method, to reduce effort's from permanent loads.

Considered composite materials are based on carbon fiber with high resistance, low weight, corrosion resistance, durability.

Consolidation of resistance structure with carbon fiber associated with special high resistance mortars retain structural dimensions, reducing the completion time of work and perhaps most important contribution is their minimum weight.

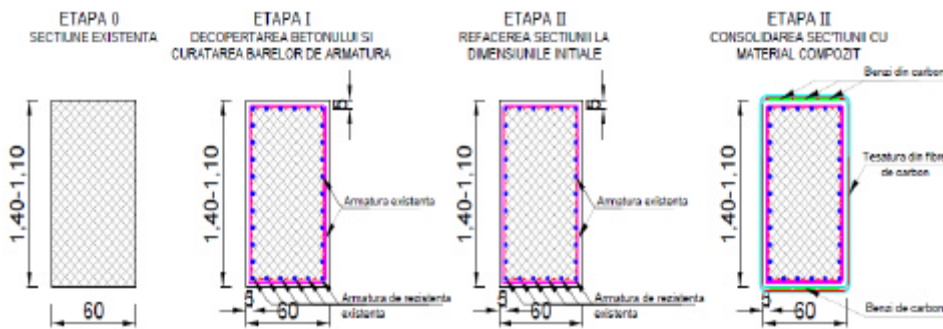


Figure 6. Section consolidation with carbon fiber

4. STRUCTURE CALCULATION

For exact quantity of composite material was necessary a structural modeling in a computer program. The structure was modeled in AxisVM 10 program, which resulted sectional efforts.

The calculation was done in several situations:

1. The first hypothesis was to determine the sectional efforts to bridge requested by its own weight, no route, no sidewalks and no parapets.
2. In the second hypothesis were calculated sectional efforts with self-weight produced by all consolidated bridge, sidewalks and fences.
3. A third case was the traffic loads, convoy of special vehicles V80 being the worst.

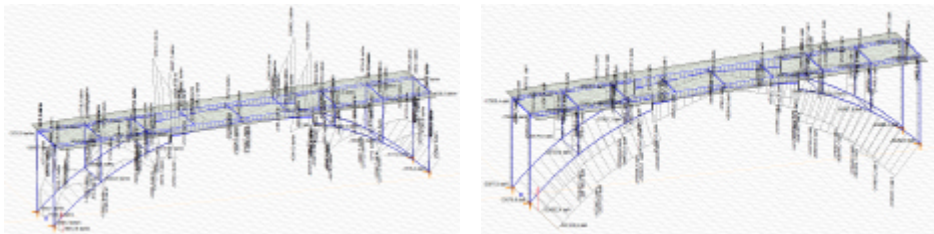


Figure 7 – Bending and axial force diagram from permanent loads

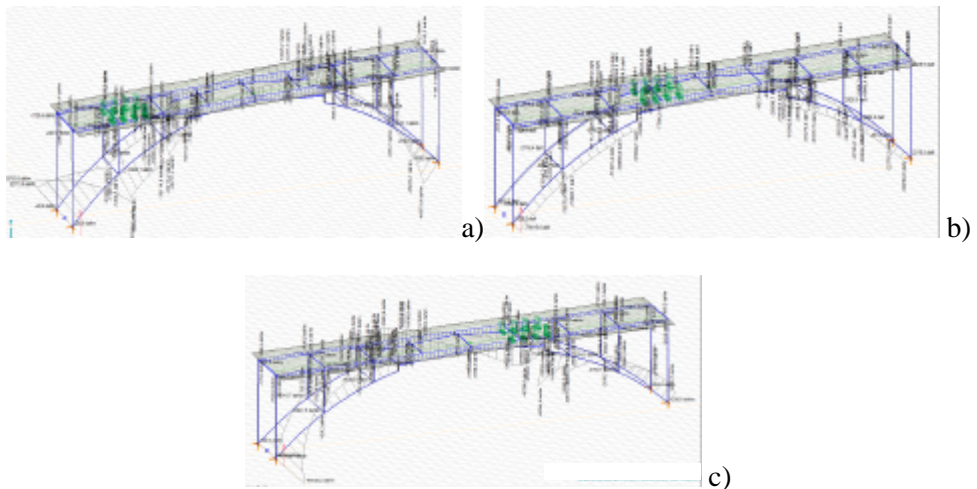


Figure 8 – Bending and axial force diagram from convoy V80 loads. a) Bending of superior fiber; c) Bending of inferior fiber

Knowing the sectional efforts can be dimensioned the necessary quantity of carbon strips for taking over the bending moment and the amount of carbon fiber for taking over the axial and shear force.

5. CONCLUSIONS

The composite materials for consolidation of bridges can often be legally viable technical and economical solution. The cost of new materials is greater than the classical ones, but by reducing the time and the necessary equipment can be saved, so that total costs are comparable.

The adoption of composite materials would not have done that support the concrete case; it would have been in an advanced state of decay.

Using composite materials not solve all solutions to consolidation of bridges, but can be taken into account when analyzing building solutions.

References

1. G. Ramos, J.R. Casas, A. Alarcon - Repair and strengthening of segmental bridges using carbon fibers – *Engineering Structures* 26 (2004), ISSN 609-618
2. Technical project „Rehabilitation of bridge on DN 15 km 287+062, at Bicaz ” – S.C: POD-PROIECT S.R.L., Aprilie 2012
3. *Tehnologii moderne de reabilitare a podurilor cu materiale compozite* – Workshop, Facultatea de Construc ii ? i Instala ii din Ia? i, Ia? i, 7 Martie 2000
4. Comisu, C. C., Boaca, G., „Design and Development of System Identification and Nondestructive Inspection of Bridges Network in Romania”, *Proceedings, PANNDT2011 5th Pan American Conference for NDT*, 2-6 October 2011, Cancun, 9 pg. , ISBN 978-968-9288-10-
5. Boaca, G., Comisu, C. C., „Rehabilitation of the bridge over the Danube river Iron Gate I – Romania”, *Proceedings, 11th International Scientific Conference VSU' 2011*, 2-3 June 2011, Sofia, Bulgaria, Vol II, pg. VI-60-65, ISSN 1314-071X

Experimental study regarding the induced ductility at the steel column base by the baseplate's flexibility

Mihai Budescu¹, Silviu Cristian Melenciuc² and Andrei-Ionut Stefancu¹

¹*Department of Structural Mechanics, "Gheorghe Asachi" Technical University of Iasi
Faculty of Civil Engineering and Building Services, Iasi, 700050, Romania*

²*Department of Civil and Industrial Buildings, "Gheorghe Asachi" Technical University of Iasi
Faculty of Civil Engineering and Building Services, Iasi, 700050, Romania*

Abstract.

The present design regulations postulate that the structural strength requirements should not prevail to the ductile ones in a design process. In case of steel columns, brittle failure of the bases (bolt's failure, concrete crushing) should be avoided. In this context, the ductility or the rotational capacity should be determined mainly by the flexibility of baseplates. Experimental studies may reveal specific local phenomena otherwise "invisible" (by numerical simulations, failure theories or other analysis methods). The main objective of this paper is to describe the overall structural behavior and evaluate the parameters involved in the connection design of two exposed rigid baseplates. The connections have been analyzed by means of full-scale tests that lead to failure modes validated by finite element models.

KEYWORDS: base column joint; base plate, ductility

1. INTRODUCTION

The column base represents one of the most important parts of a steel structure. It has the role of load transfer from the superstructure to the foundation system. When laterally loaded, exposed baseplate solutions for steel columns deform - under bending moments and (associated) shear forces - mainly by rotations. Behavior of connections in these regions is of major importance in the overall structural behavior under lateral loading conditions. Previous research studies, (Grauvilardell et al, 2005; Hamizi and Hamachi, 2007; Stamatopoulos and Ermopoulos, 2011), showed that connections between columns and foundation elements behave in a semi-rigid manner and, in most of the cases, heavily influence the overall structural system.

As stated above, experimental research studies may reveal specific local phenomena otherwise “invisible”. In this order, an experimental program involving full-scaled models of columns with exposed baseplates seconded a numerical analysis. The experimental tests evaluated the behavior of exposed baseplate steel columns connections under cyclic loading conditions with the aim of validating the numerically obtained results. Evaluation of parameters not possible to quantify by the numerical simulations was also of interest.

Nonlinear numerical analyses of the tested models were performed by the Finite Elements Method based ANSYS Workbench 12 software package (Ansys, 2009; Melenciuc, 2011).

2. EXPERIMENTAL PROGRAM AND TEST SET-UP SECOND CHAPTER

The experimental tests were performed in the dynamic and seismic test laboratory of the Structural Mechanics Department of the Faculty of Civil Engineering and Building Services of Iasi.

A specially designed stand completing the ANCO shaking table was used to test the column base ends connections (Fig. 1). The test set-up consisted in: stiff concrete slab supporting the shaking table, foundation system simulating foundation block - anchored to the laboratory ground slab using four M80 bolts. The acting member was equipped with a 200kN load cell.

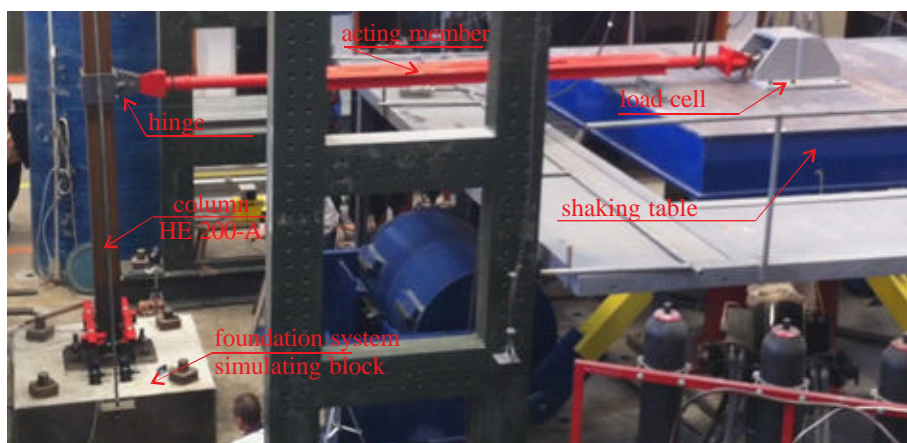


Figure 1. Experimental stand; load transmission system

The tests performed involved only lateral horizontal loading, without any axial components (excepting the column dead load). In this manner, the column' base behavior under extreme conditions was observed. It may be stated that this reflects the rather common situation of real structures, especially in case of perimetral columns in slender steel structures under seismic actions, when the axial components may be neglected. The horizontal action transmitted by the shaking table was applied at a 2.10m height with respect to the column base. A "sinus beat" type action was applied under displacement control, with maximum amplitudes (?) of 10, 20, 40, 60, 80 and 100 mm, (Fig. 2).

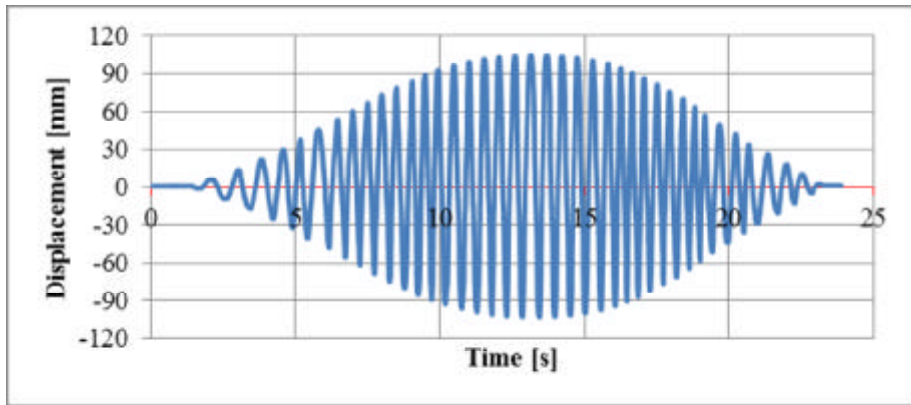


Figure 2. Imposed displacements, maximum amplitudes (?) 100mm

The action was indirectly applied by imposing successive displacements. The load applied to the steel column was monitored using a load cell placed at the end of the acting member, connected on the platform.

300mV/V/inch sensitivity, CELESCO thread type displacement transducers (T) were used in order to determine the structural response of the column models. The load-displacement curve at the level of load application (acting member level) was obtained using the readings of the T0, (Fig. 3).

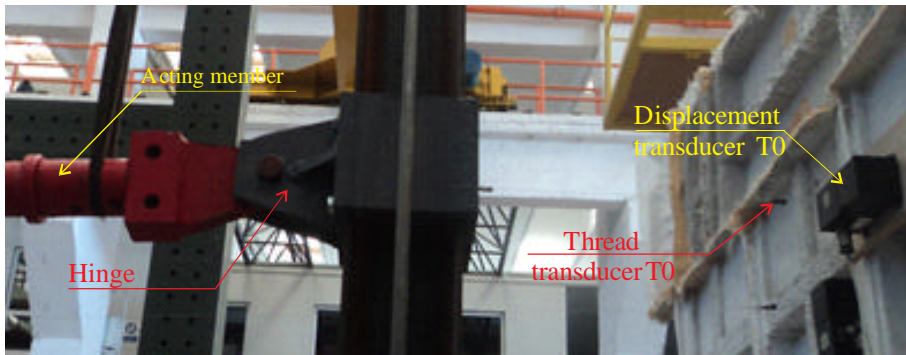


Figure 3. Horizontally placed displacement transducer (T0)

The other transducers were placed at the base level by connecting them to the steel column and measuring the relative displacements between the baseplate elements and the foundation system. The transducers were fixed on the column, at a 250mm span from the bottom face of the baseplate, in order to monitor the potential plastic hinge formation region, (Stamatopoulos and Ermopoulos, 2011).

Relative column base - foundation system displacements, in case of baseplated models, were monitored using T1 to T4 transducers; displacements of the baseplates were accounted using the T5 to T8 transducers, (Fig. 4), (Stamatopoulos and Ermopoulos, 2011).

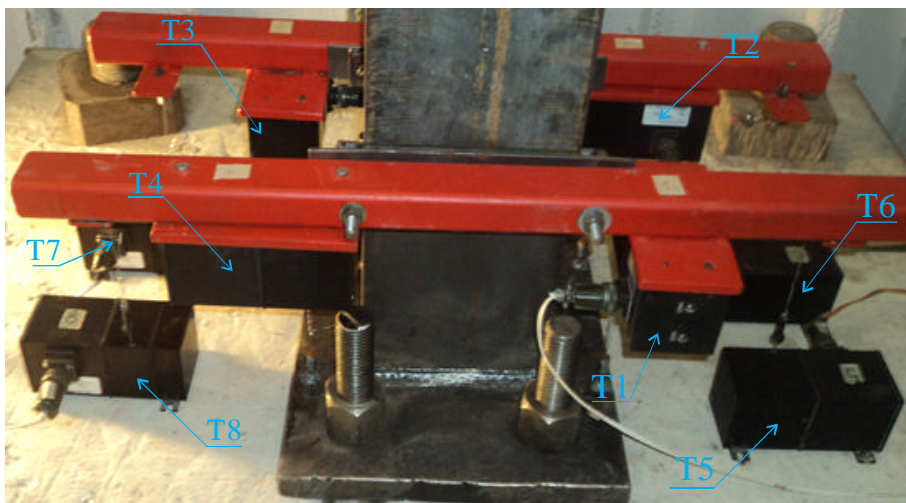


Figure 4. Baseplate transducers location

2.1. Test specimen

The experiments analyzed and compared the structural behavior of two specimens.

The first tested specimen is composed of a 2.10m high, HE 200-A cross-sectioned steel column and the baseplate, having the dimensions of 350x33-490, anchored in the reinforced concrete foundation block using four M36 bolts, (Fig. 5).

The second tested assembly used the same steel column and the baseplate having the dimensions 350x33-690.

The anchoring bolts were fixed in the foundation block with a clear deformation span of 360mm. The column and the baseplate were made of S355 steel while the concrete used for the foundation was of C20/25 class.

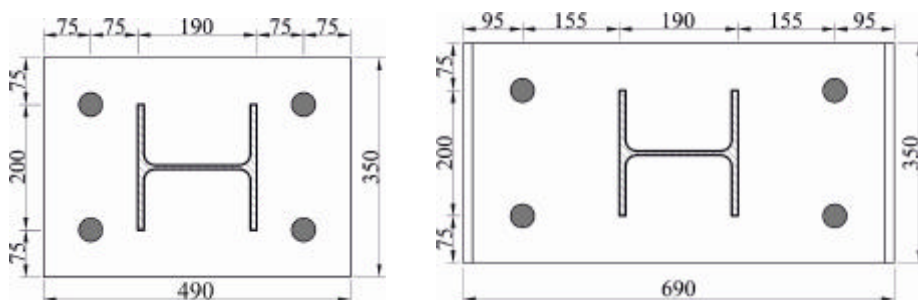


Figure 5. 350x490 mm steel column base plate

The connection' rotations were determined based on the vertical displacements of the baseplate at the column section flanges level and used the following relation, (Hamizi and Hamachi, 2007):

$$\mathbf{q} = (a - b) / x \quad (1)$$

where:

- \mathbf{q} - rotation of the column baseplate;
- a, b - vertical displacements of the column baseplate;
- x - span between the displacement measuring points.

2.2.1. Test results

For each of the loading cycles, graphs using the load readings of the load cell and the displacements given by the T0 transducer were plotted.

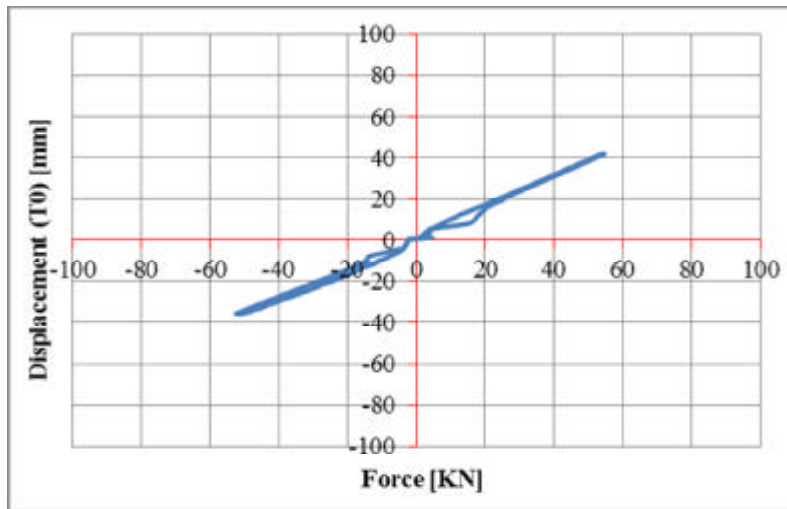


Figure 6. Load-displacement curve during the maximum amplitude cycle of 40mm

The specimen behaved in a linear elastic manner up to loading cycle of maximum amplitude of displacement of 40mm, (Fig. 6). The base plate presented a rigid behavior and presented no plastic deformations.

Starting with the load cycle of maximum displacement amplitude of 60mm, the behavior of the model became elastic-plastic, due to occurrence of plastic hinges at the column base level, (Fig. 7).

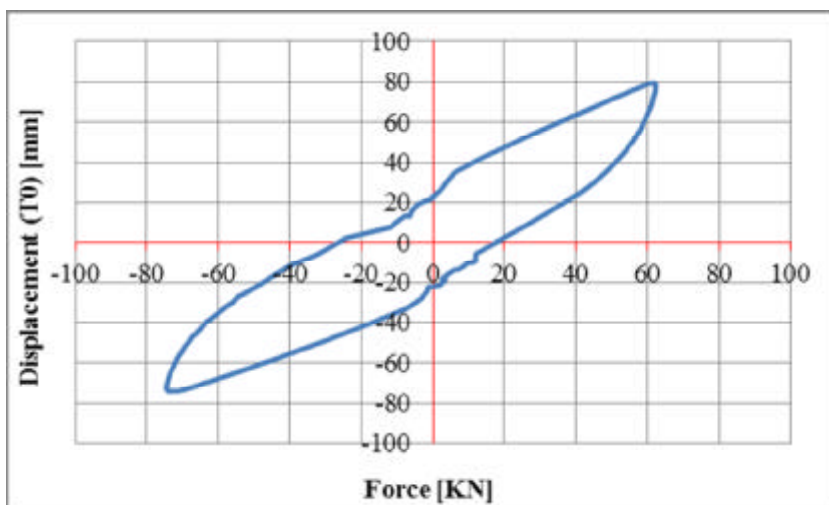


Figure 7. Load – displacement curve for the connection, $\Delta=80$ mm

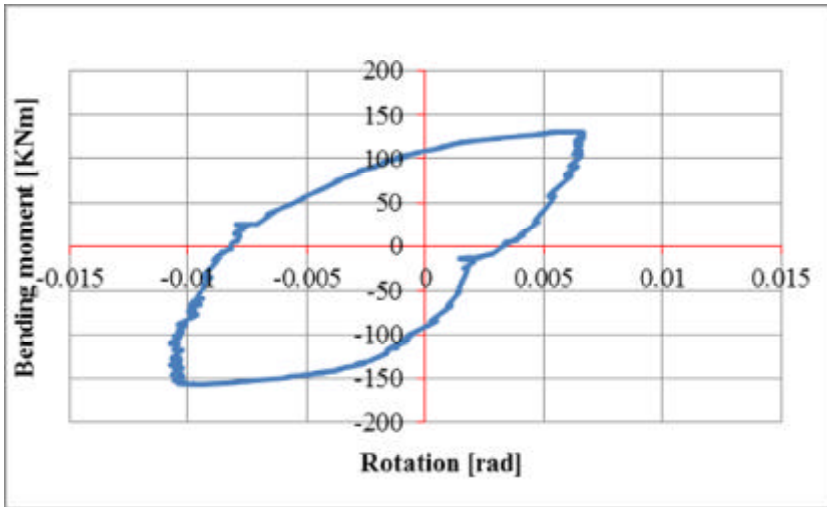


Figure 8. Bending moment – rotation curve for the connection, $\Delta=80$ mm

The bending moment-rotation curve of the connection is depicted in Fig. 8. The shape of the graph is not uniform; fact attributed to the loosening of nuts. The bending moment capacity of the connection was evaluated at 156.6 kNm, corresponding to a maximum baseplate rotation of 0.011 rad. The vertical displacements of the column baseplate were determined as arithmetic mean values given by the displacement transducers, when the amplitude of the action was of $\Delta = 80$ mm.

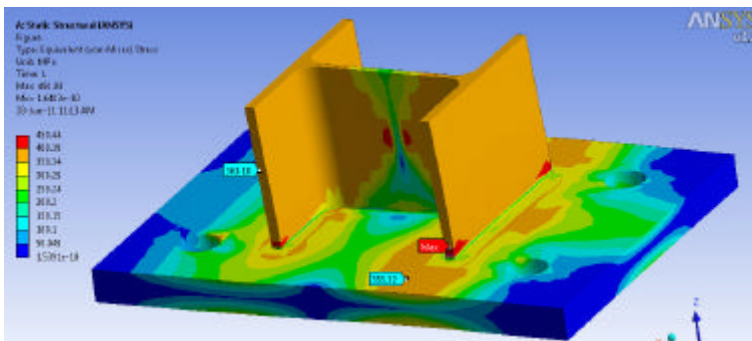


Figure 9. Von-Mises equivalent stresses distributions, $\Delta=100$ mm

The connection failed by the plastic hinge formation in the column due to the loss of the local stability of compressed flanges, (Fig. 10). The failure occurred at a load level corresponding to the maximum displacement of 80mm. The failure manner was also described by the numerical simulations, as the maximum Von-Mises equivalent stresses show in Figure 9, (Melenciuc, 2011).



Figure 10. Plastic hinge formation in the column

The second test specimen had the dimensions of the baseplate - 350x33-690 mm.

During the load cycle of maximum amplitude of displacement of 60mm, the behavior of the model became elastic-plastic without the degradation of the connection bearing capacity. When the displacements reach 60mm the plastic deformations appear in the baseplate.

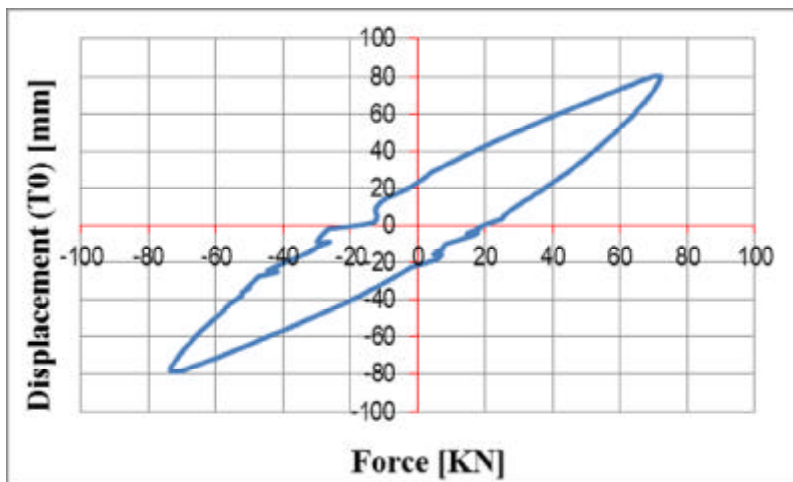


Figure 11. Load-displacement curve EXP 350x690x33, maximum amplitude $\delta=80$ mm

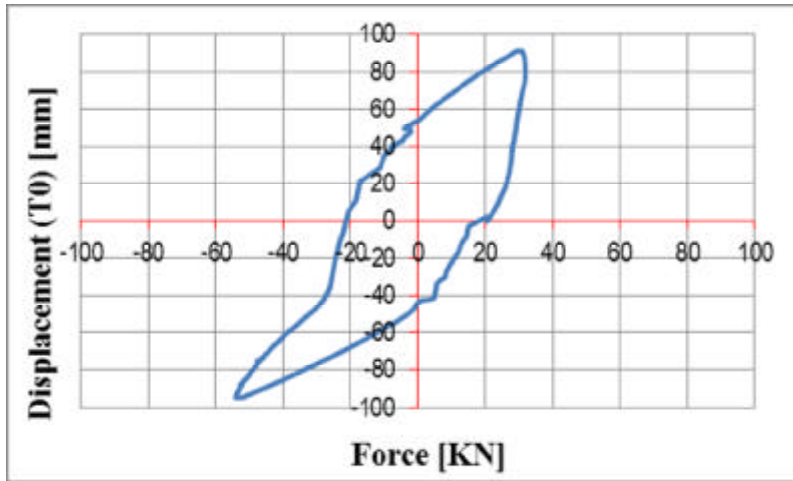


Figura 12. Load-displacement curve EXP 350x690x33, maximum amplitude $\delta = 100$ mm

A strong nonlinear behavior of the connection occurs during the load cycle with the maximum amplitude of the displacement of 80mm. The capable moment of the connection is 154.5kNm, with a 0.025 rad baseplate rotation.

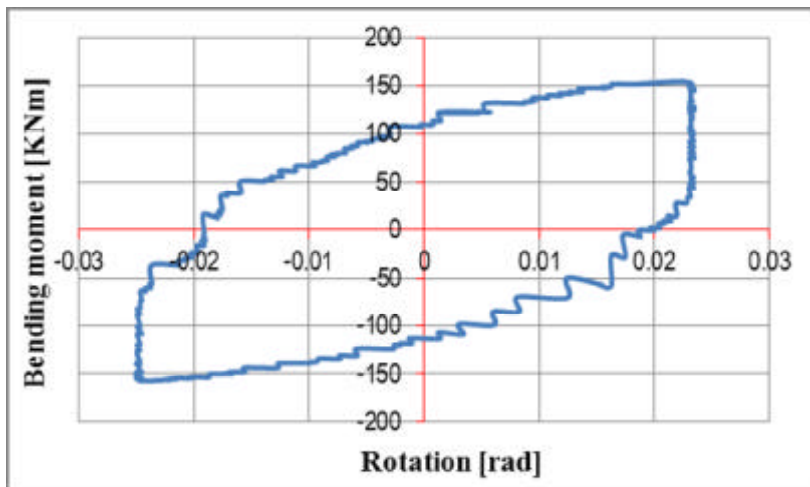


Figure 13. The bending moment-rotation curve EXP 350x690x33, maximum amplitude $\delta = 80$ mm

As the applied displacement increases the plastic deformations of the baseplate improves and the bearing capacity of the connection decreases. Thus, when the displacement is 100mm, the moment overtaken by the connection reaches the value 114.0 KNm

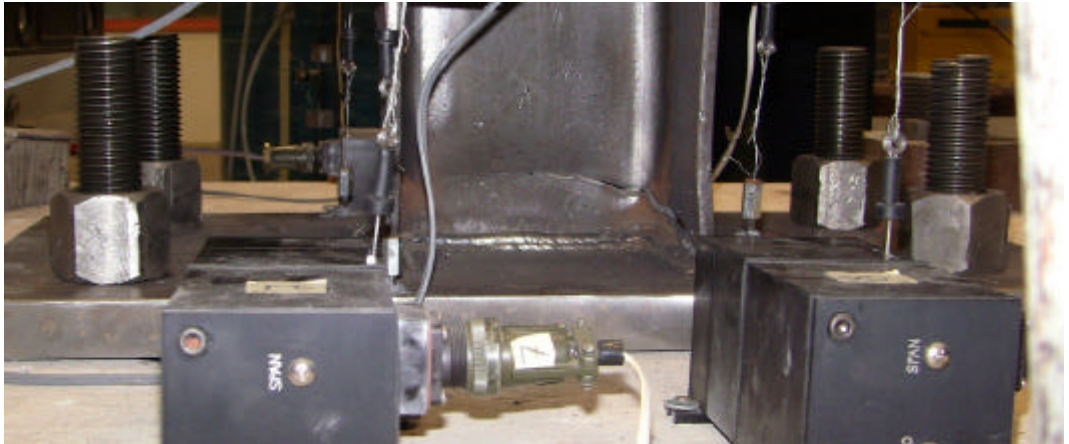


Figure 14. Model EXP 350x690x33 – web failure, $\Delta = 100$ mm

After 12 load cycles with the displacement of 100mm, a crack appears at the column pad subjected to extension in the thermal affected area. The crack is spreading suddenly, sectioning the column above the baseplate.

3. CONCLUSIONS

The behavior of exposed baseplate steel columns connections is highly influenced by the thickness of the baseplate. When using rigid baseplates, design parameters characteristic to full capacity connections may be obtained.

As a direct consequence of the baseplate increased stiffness – given by the large thickness and short outstands – the joint rotation was significantly influenced by the anchoring bolts deformation. This aspect should be avoided in case of structures likely to experience seismic actions during lifetime.

The experimental tests results for connections with the exposed, rigid baseplates, due to the large width and the reduced cantilever length, confirmed the numerical analysis results. The models had total resistance and a rigid behavior. The rotation was determined in the first place by the column's deformations and anchoring bolts' elongation and less by the baseplate bending.

The yielding occurred during 90's load cycles after the appearance of the plastic deformations.

The plastic hinge occurred after 15 full cycles having the imposed displacement magnitude of 80mm. The experimental tests confirmed the results obtained numerically and in the case of the connection with the large baseplate, but flexible because of large cantilever length. Thus, the connection presented total resistance and necessary rigidity in accomplishing the imposed ductility for structures located in seismic areas.

The baseplate flexibility had an important significance in the connection's rotation, a favorable aspect from the ductility point of view.

The connection yielding manner could not be numerical observed. After 130 load cycles and the plastic deformations appearance, a crack occurred at the tensioned column flange in the thermal affected area that spreaded suddenly in the column web.

References

1. ANSYS Inc., ANSYS Workbench 2.0 Framework Version: 12.0.1 (2009).
2. Grauvilardell, J. E., Lee D., Hajjar, J. F., Dexter, R. J., Synthesis of Design, Testing and Analysis Research on Steel Column Base Plate Connections in High-Seismic Zones. Structural Engineering Report No. ST-04-02, Department of Civil Engineering, University of Minnesota, October 1 (2005).
3. Hamizi M. si Hannachi N. E., Evaluation by a Finite Element Method of The Flexibility Factor and Fixity Degree for the Base Plate Connections Commonly Used. Strength of Materials, Vol. 39, No. 6 (2007).
4. Melenciuc S.C., Determinarea caracteristicilor de calcul a îmbinarilor stâlpilor metalici cu funda? iile de beton armat utilizând metoda elementelor finite. Volumul conferinței Creatii universitare 2011, Al IV-lea Simpozion National, Iasi, ISSN: 2247-4161, pag. 65-74 (2011).
5. Melenciuc S.C., Contributii privind imbunatatirea comportarii imbinarilor structurilor metalice amplasate in zone seismice. Politehnum, Iasi 2011, ISBN: 978-973-621-365-6 (2011).
6. Stamatopoulos G.N.,* , Ermopoulos J.Ch., Experimental and analytical investigation of steel column bases. Journal of Constructional Steel Research, Volume 67, Issue 9, september 2011, pp 1341-1357 (2011).

Probabilistic Seismic Risk Assessment of Barcelona, Spain

Omar D. Cardona¹, Mabel C. Marulanda², Martha L. Carreño², and Alex H. Barbat²

¹National University of Colombia, Manizales, Colombia

²International Center for Numerical Methods – CIMNE, Technical University of Catalonia, 08034, Spain

Summary

Understanding disaster risk due to hazard events, such as earthquakes, creates powerful incentives for countries to develop planning options and tools to reduce potential damages. The results of the seismic risk assessment of the city of Barcelona using CAPRA (Comprehensive Approach for Probabilistic Risk Assessment) presented in this paper involve the evaluation of probabilistic losses of the exposed elements using probabilistic metrics, such as the exceedance probability curve, the expected annual loss and the probable maximum loss, which are useful for multi-hazard/risk analyses. The outcomes obtained with techno-scientific methodologies like CAPRA are oriented to facilitate decision-making. Using CAPRA, it is possible to design risk transfer instruments; evaluation of probabilistic cost-benefit ratio, to consider the net benefits of risk mitigation strategies; land use planning, loss scenarios for emergency response, early warning, on-line loss assessment mechanisms and holistic evaluation of disaster risk based on indicators. These applications facilitate the integrated risk management by the different stakeholders involved in risk reduction decision-making.

KEYWORDS: probabilistic seismic risk assessment, average annual loss, pure premium, loss exceedance curve.

1. INTRODUCTION

A disaster is the materialization of existent risk conditions. The risk level of a society is related to its development achievements and its capacity to intervene the existing risk. Hence, urban planning and efficient strategies are necessary to reduce risk and improve sustainable development. Risk management is a fundamental development strategy that considers four principal policies: risk identification, risk reduction, disaster management and risk transfer.

From the financial point of view, it is essential to estimate and quantify potential losses in a given exposure time given that the budget for both emergency response and recovery and reconstruction could mean a fiscal exposure and a non explicit contingent liability for governments at city and country levels (Pollner 2001; Andersen 2002). Estimation of contingent losses provides information and permits to set out strategies *ex ante* for reducing or financing them (Marulanda et al 2008a, 2010a; Cardona 2010a; Cardona 2010b). Assessment of potential losses allows budget allocation for structural retrofitting to reduce damages and implementation of effective financial protection strategy to provide loss coverage of public infrastructure and private buildings to protect government resources and safeguard socioeconomic development; in summary, to achieve the greater awareness, security culture and economic prosperity, the financial protection must be a permanent and long term policy (Freeman et al. 2003).

Thus, one of the key strategic activities of disaster risk management is the assessment of the risk of disaster or of extreme events, which requires the use of reliable methodologies that allow an adequate calculation of probabilistic losses in exposed elements. The use of catastrophic risk models and the results obtained from risk analysis make feasible determining the potential deficit existing in case of the occurrence of an extreme event. Catastrophe risk models –based on metrics such as the Probabilistic Maximum Loss or the Average Annual Loss– are used to estimate, building by building, the probabilistic losses of different portfolios of exposed elements.

This paper performs a seismic risk assessment of the city of Barcelona, Spain. The probabilistic methodology Comprehensive Approach for Probabilistic Risk Assessment, CAPRA (Cardona et al. 2010a), is considered to be the most robust for this type of modeling and identifies the most important aspects of catastrophe risk from the financial protection perspective according to the fiscal responsibility of the states.

Vulnerability and risk analysis for Barcelona were developed starting from the seismic hazard information available for the city and the detailed cadastral information provided by the city administration in order to obtain the probable maximum losses (loss exceedance curve) and the pure risk premiums (average annual loss) of each building of the city. These risk metrics help to the knowledge of the contingency liabilities of the public sector and of the economic impact of the private sector, facilitating thus the consideration of risk transfer strategies for financial protection. Additionally, potential scenarios of damage can be obtained with the model, that can be used to develop emergency response plans and to implement risk reduction measures from physical, social and organizational point of view.

2. THE MODEL

The frequency of catastrophic seismic events is particularly low and this is the reason why very limited historical data are available. Considering the possibility of future highly destructive events, risk estimation has to focus on probabilistic models that can use the limited available information to best predict future scenarios and consider the high uncertainty involved in the analysis. Therefore, risk assessments need to be prospective, anticipating scientifically credible events that might happen in the future. The earthquake prediction models use the seismological and engineering bases for its development, allowing the assessment of the risk of loss given a catastrophic event. Since large uncertainties related to the severity and frequency characteristics of the events are inherent in models, the earthquake risk models have to use probabilistic formulations that incorporate this uncertainty into the risk assessment. The probabilistic risk model built upon a sequence of modules (Woo 1999, Grossi and Kunreuther 2005; Cardona et al 2008a/b/c/d), quantifies potential losses arising from earthquake events as shown in the Fig. 1.

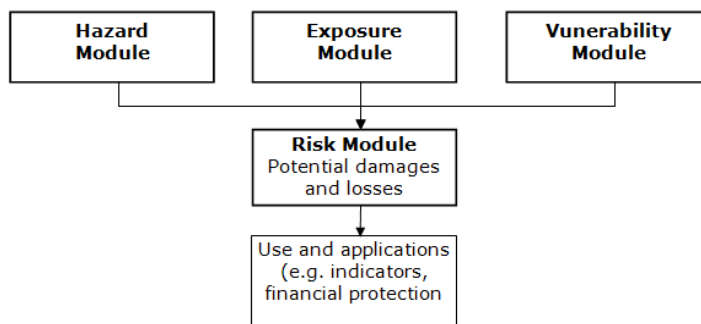


Figure 1. Probabilistic risk model

3. SEISMIC HAZARD MODULE

The hazard module of the probabilistic risk model defines the frequency and the severity of a hazard at a specific location. This is completed by analyzing the historical event frequencies and reviewing scientific studies performed on the severity and frequencies in the region of interest. Once the hazard parameters are established, stochastic event sets are generated which define the frequency and severity of thousands of stochastic events. This module can analyze the intensity at a location, once an event of the stochastic set has occurred, by modelling the attenuation of the event between its location and the site under consideration, and

evaluates the propensity of the local site conditions to either amplify or reduce the impact. The seismic hazard is quantified in terms of return periods (or exceedance rates) and the module provides the relevant seismic intensities necessary to evaluate the behavior of the structures. Its calculation includes the contribution of the effects of all seismic sources located in a certain influence area.

The application to the city of Barcelona takes into account the seismic sources for the Catalonia region of Spain identified by Secanell et al. (2004). Additionally, it considers the effects of the attenuation of the seismic waves by means of probabilistic spectral attenuation laws that include different source types Ambraseys (1996), as well as the local amplification effects based on microzonation studies. The site effects, considering the amplification of seismic hazard parameters according to the geological characterization of Barcelona, were established by Cid et al (2001) where a transfer function and an amplification factor for the acceleration level at the rock level characterized each zone (see Figure 2).

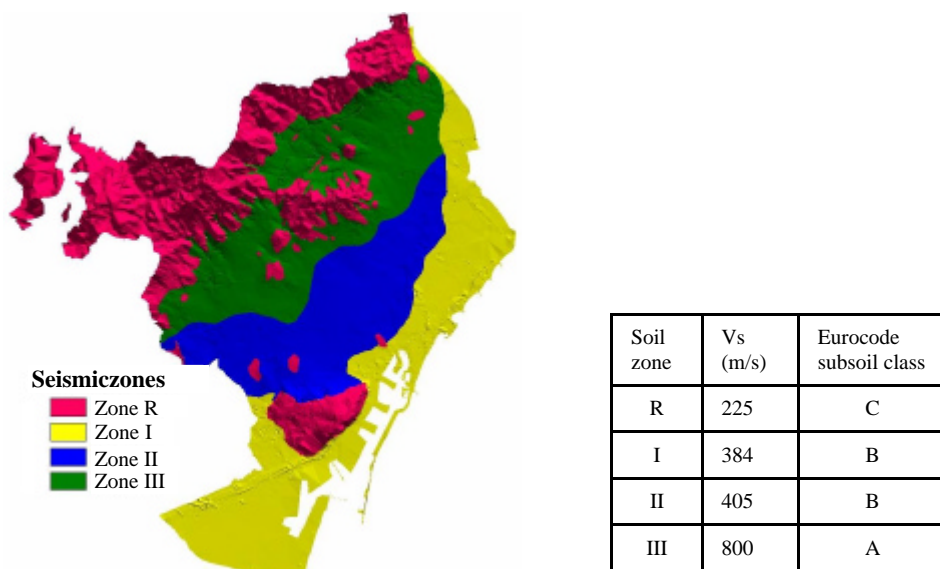


Figure 2. Seismic zonation based on local effects (Cid et al. 2001)

The seismic hazard was simulated by using the CRISIS 2007 code. The code allows estimating the hazard associated to all possible events that can occur, or to a group of selected events, or even to a single relevant event. Using the hazard module, it is possible to calculate the probable maximum value of the intensity, characterized for different exceedance rates or return periods. An .ame file type is created in this module (.ame comes from *amenaza* –hazard- in Spanish) which

includes multiple grids on the area of study, of the different parameters of intensity of the considered phenomena. Each grid is a scenario of the intensity level obtained from historical or stochastic generated events, with their frequency of occurrence. For this case, the parameter of seismic intensity selected is the spectral acceleration.

Further, the desired risk parameters such as percentages of damage, economic losses, effects on people and other effects are evaluated, in a probabilistic framework, for each of the hazard scenarios and then these results are probabilistically integrated by using the occurrence frequencies of each earthquake scenario. For Barcelona, 2058 seismic hazard scenarios were generated.

4. EXPOSURE MODULE

The *exposure* is mainly related to the infrastructure components or to the exposed population that can be affected by a particular event. The exposure module is based on files in *shape* format corresponding to the exposed infrastructure included in the risk analysis. To characterize the exposure, it is necessary to identify the individual components, including their location, their main physical, geometric and engineering characteristics, their vulnerability to hazardous events, their economic value and the level of human occupation that can have in a given analysis scenario. The exposure value of assets at risk is usually estimated from secondary sources such as available databases. The degree of precision of the results depends on the level of resolution and detail of exposure information.

The information used was compiled by Lantada (2007); the economic value of the exposed elements was supplied by the Cadastral Office of Barcelona, and 70655 buildings were considered (Figure 3). They are distributed in 10 municipal districts (Figure 4), 73 neighborhoods, 233 Basic Statistical Areas (in Spanish AEB– Áreas Estadísticas Básicas) and 1061 census sections. For each one of the buildings, the geographic location, economic value, year of construction, number of levels, structural type and human occupation, were defined. In order to proceed with the risk calculations, the results were calculated building by buildings, but they can be presented by considering any geographical level according to the required resolution.

In order to calculate the social impact, the general information related to building occupation is also estimated. Maximum occupancy and occupancy percentage at different hours of the day are also defined, allowing establishing different time scenarios of the event's occurrence. When no specific occupation information was available, an approximate occupation density by construction class was used to complete the information.

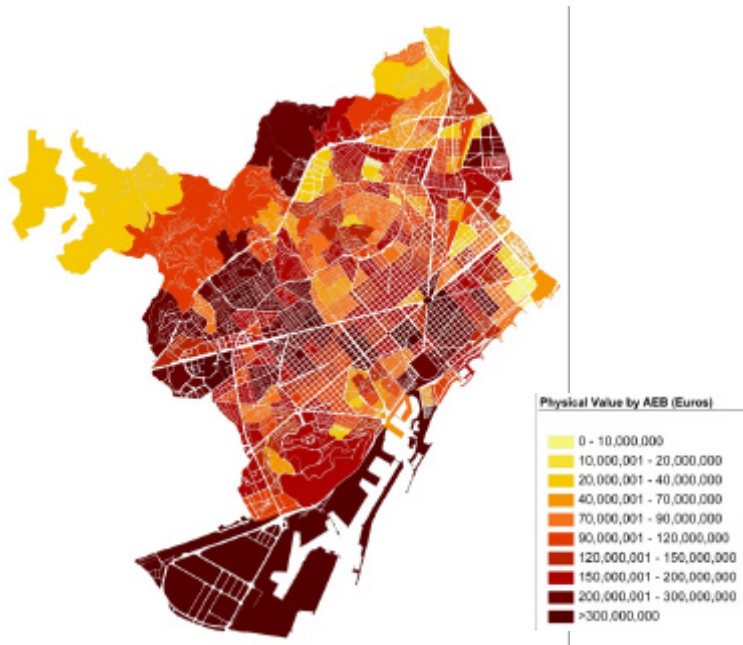


Figure 3. Exposed value of Barcelona by AEBs

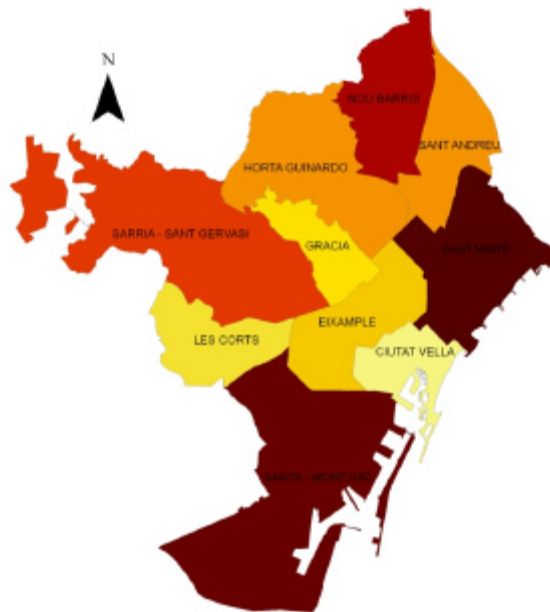


Figure 4. Administrative division of Barcelona

5. VULNERABILITY MODULE

The vulnerability module quantifies the damage caused to each asset class by the intensity of a given event at a site (Miranda, 1999). The classification of the assets is based on a combination of construction material, construction type (i.e. wall & roof combination), building use, number of levels and age. Estimation of damage is performed in terms of the mean damage ratio, MDR, which is defined as the ratio of the expected repair cost to the replacement cost of the structure. A vulnerability curve is defined relating the MDR to the earthquake intensity that can be expressed in terms of maximum acceleration (e.g. useful for 1-2 story buildings), spectral acceleration, velocity, drift or displacement (e.g. useful for multi-story buildings) at each location.

Most part of the building stock of Barcelona was constructed when no seismic-resistant construction codes existed. The combination of very old buildings constructed without seismic code with a highly populated and active produced a high vulnerability which can generate a significant risk even under the effects of a moderate earthquake. The vulnerability module of the ERN-CAPRA platform defines the vulnerability of the buildings in the city by using vulnerability functions. The assignment of the vulnerability function to each exposed element is carried out in the exposure module by means of a shape format file. There is a vulnerability function corresponding to each building typology; the most common structural system used in Barcelona is the unreinforced masonry, followed by the reinforced concrete, whose construction has increased rapidly in recent decades. Steel structures are less used and they are not usually used for residential buildings but for industrial buildings, markets, sports areas, among others. The used typologies were defined in RISK-UE (2004) and are shown in Table 1.

Each structural type is subdivided into 3 classes according to the height:

- *Low, L.* 1 to 2 floors for masonry and wood structures; and 1 to 3 floors for reinforced concrete and steel buildings.
- *Medium, M.* 3 to 5 floors for masonry and wood structures; and 4 to 7 floors for reinforced concrete and steel buildings.
- *High, H.* 6 or more floors for masonry and wood structures; and 8 or more floors for reinforced concrete and steel buildings.

Table 1. Building typology matrix for Barcelona (RISK-UE 2004)

UNREINFORCED MASONRY	M3.1	Unreinforced masonry bearing walls with wooden slabs
	M3.2	Unreinforced masonry bearing walls with masonry vaults
	M3.3	Unreinforced masonry bearing walls with composite steel and masonry slabs
	M3.4	Reinforced concrete slabs
REINFORCED CONCRETE	RC3.1	Concrete frames with unreinforced masonry infill walls with regularly infill frames
	RC3.2	Concrete frames with unreinforced masonry infill walls with irregularly frames (i.e., irregular structural system, irregular infill, soft/weak storey)
STEEL MOMENT FRAMES	S1	A frame of steel columns and beams
STEEL BRACED FRAMES	S2	Vertical components of the lateral-force-resisting system are braced frames rather than moment frames.
STEEL FRAMES WITH UNREINFORCED MASONRY INFILL WALLS	S3	The infill walls usually are offset from the exterior frame members, wrap around them, and present a smooth masonry exterior with no indication of the frame.
STEEL AND RC COMPOSITE SYSTEMS	S5	Moment resisting frame of composite steel and concrete columns and beams. Usually the structure is concealed on the outside by exterior non-structural walls.
WOOD STRUCTURES	W	Repetitive framing by wood rafters or joists on wood stud walls. Loads are light and spans are small.

Figure 5 shows the vulnerability functions used for unreinforced masonry buildings and Figure 6 shows the functions for other building typologies, for low (L), medium (M) and high (H) buildings. These functions relate the severity of the event, represented by the spectral acceleration with the average damage in the building.

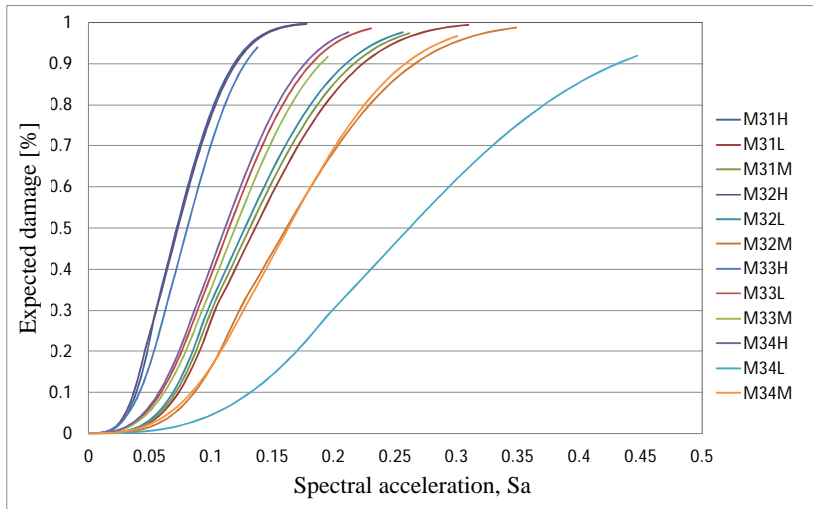


Figure 5. Vulnerability functions for unreinforced masonry buildings

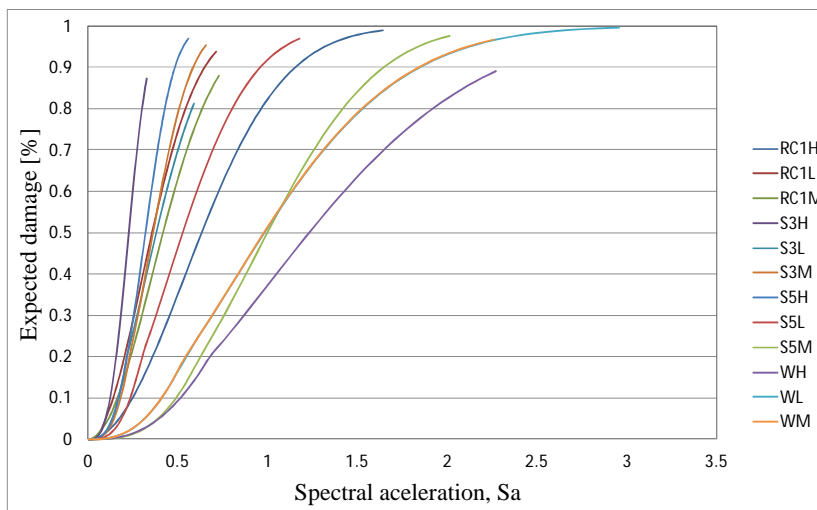


Figure 6. Vulnerability functions for reinforce concrete, steel and wood buildings

6. RISK MODULE

The physical seismic risk is evaluated by means of the convolution of the hazard with the vulnerability of the exposed elements; the results are the potential

consequences. Risk can be expressed in terms of damage or physical effects, absolute or relative economic loss and/or effects on the population.

Once the expected physical damage is estimated (average value and its dispersion) as a percentage for each of the assets or infrastructure components included in the analysis, one can make estimates of various parameters useful for the proposed analysis. Risk metrics calculated by using the model provide risk managers and decision makers with essential information required to manage future risks. One measure is the Average Annual Loss and the other is the Loss Exceedance Curve. Other measures, such as the Pure Risk Premium and the Probable Maximum Loss, can be computed based on the former.

- *Average Annual Loss.* AAL is the expected loss per year. Computationally, AAL is the sum of products of event expected losses and event annual occurrence probabilities for all the stochastic events considered in the loss model. In probabilistic terms, AAL is the mathematical expectation of the annual loss.
- *Pure Risk Premium.* PRP is the AAL divided by the replacement value of the asset, usually expressed as a rate per mill of monetary value.
- *Loss Exceedance Curve.* LEC represents the annual frequency with which a loss of any specified monetary amount will be exceeded. This is the most important catastrophe risk metric for risk managers, since it estimates the amount of funds required to meet risk management objectives. The LEC can be calculated for the largest event in one year or for all (cumulative) events in one year. For risk management purposes, the latter estimate is preferred, since it includes the possibility of one or more severe events resulting from earthquakes.
- *Probable Maximum Loss.* PML represents the loss amount for a given annual exceedance frequency, or its inverse, the return period. Depending on the stakeholder's risk tolerance, the risk manager may decide to manage for losses up to a certain return period (e.g. 1 event in 300 years). For that stakeholders (e.g. a public or private agency), the PML is the 300-year loss. For others, it may be 150 years or 500 years. It is noteworthy that it is frequent that certain stakeholders set the insolvency criterion at return periods between 150 years and 200 years. However, other involved stakeholders (e.g. governments or regulation agencies) have chosen much longer return periods, such as the Mexican Insurance Commission, which uses a return period of 1500 years to fix solvency margins of insurance companies in Mexico.

As previously said, the probabilistic risk analysis is done based on a series of hazard scenarios that adequately represent the effects of any event of feasible magnitude that can occur in the area of influence. Each of these scenarios has an associated specific frequency or probability of occurrence. The probabilistic

calculation procedure comprises the assessment using appropriate metrics, in this case the economic loss, for each exposed asset considering each of the hazard scenarios with its frequency of occurrence, and the probabilistic integration of the obtained results.

The Average Annual Loss for physical assets, fatalities and injuries are calculated for each building of the city. The probabilistic results for of Barcelona are shown in tables 2, 3 and 4. Figure 7 shows the PML curve obtained for Barcelona. Figure 8 shows the expected annual loss for each AEB of Barcelona. As it was previously mentioned, the expected annual economic loss was calculated building by building and Figure 9 shows the obtained results at this resolution. Figure 10 and Figure 11 show the expected annual loss for injured and deaths by AEB in Barcelona.

Table 2. Physical exposure

PHYSICAL EXPOSURE		
Exposed value	€x10 ⁶	31,522.80
Average Annual	€x10 ⁶	72.14
Loss	‰	2.29‰
PML		
Return period (Years)	Loss	
	€x10 ⁶	%
50	729.35	2.31%
100	1,770.16	5.62%
250	3,699.35	11.74%
500	5,172.26	16.41%
1,000	6,510.67	20.65%
1,500	7,021.14	22.27%

Table 3 Dead people

DEAD PEOPLE		
Exposed value	Inhab.	1,639,880.00
Average Annual	Inhab.	28.27
Loss	‰	0.017‰
PML		
Return period (Years)	Loss	
	Inhab.	%
50	101.41	0.01%
100	654.30	0.04%
250	2,069.97	0.13%
500	3,380.29	0.21%
1,000	4,898.39	0.30%
1,500	5,799.44	0.35%

Table 4. Injured people

INJURED PEOPLE		
Exposed value	Inhab.	1,639,880.00
Average Annual	Inhab.	113.55
Loss	‰	0.07‰
PML		
Return period (Years)	Loss	
	Inhab.	%
50	101.41	0.01%
100	654.30	0.04%
250	2,069.97	0.13%
500	3,380.29	0.21%
1,000	4,898.39	0.30%
1,500	5,799.44	0.35%

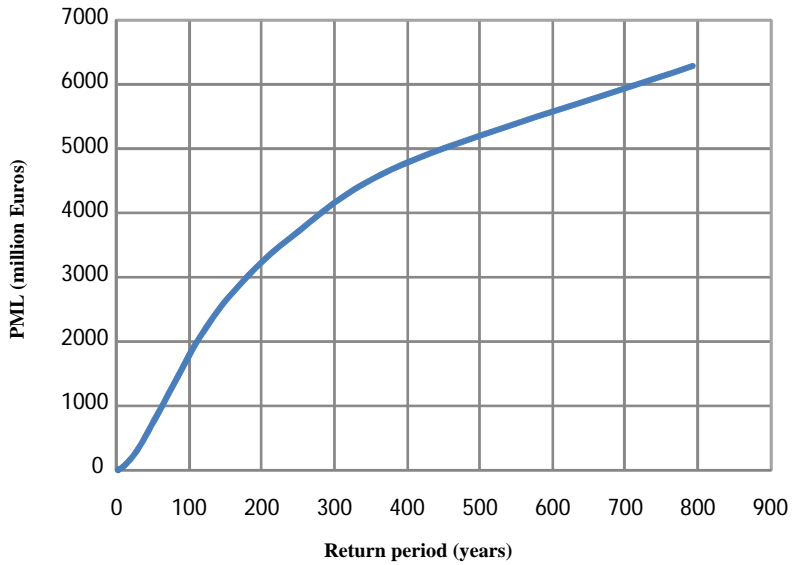


Figure 7. PML curve for Barcelona

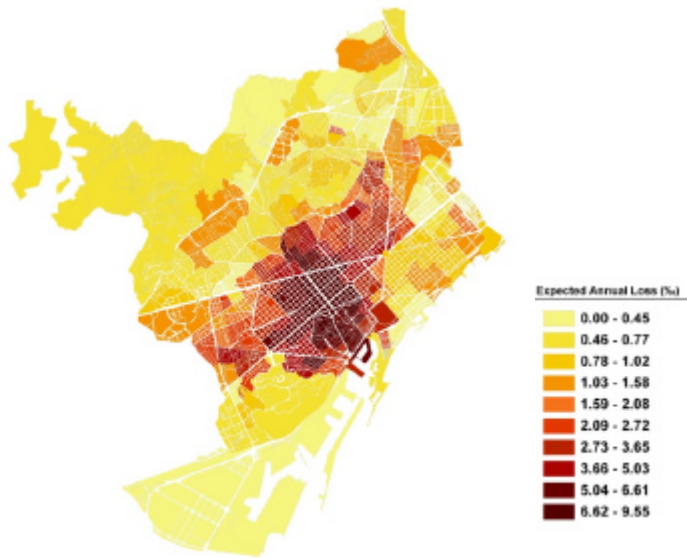


Figure 8. Expected annual loss for the AEBs of Barcelona

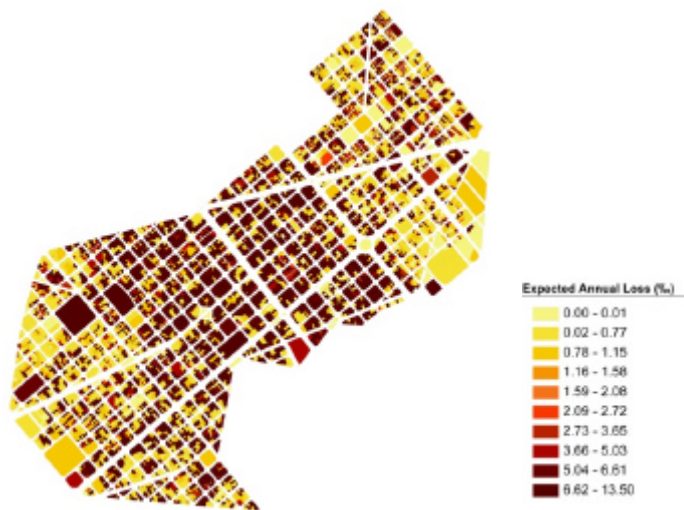


Figure 9. Expected annual loss for each building in the Eixample District of Barcelona

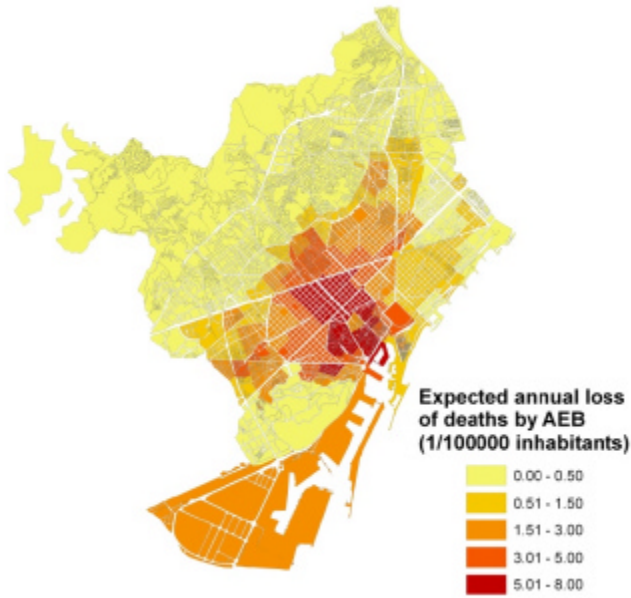


Figure 10. Expected annual loss for deaths by AEB in Barcelona

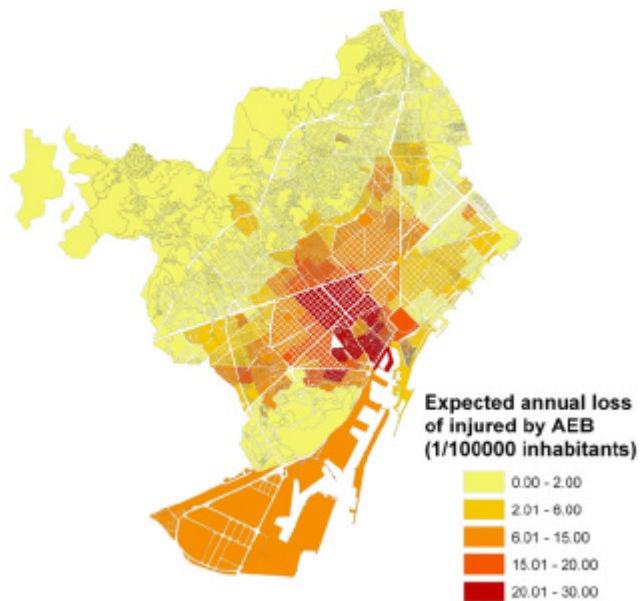


Figure 11. Expected annual loss for injured by AEB in Barcelona

In addition to the probabilistic economic figures, it is also relevant for the emergency response plans of the city to count with critical earthquake loss scenarios. In the case of Barcelona, a critical scenario for a loss with a return period of approximately 1000 years was chosen, to estimate the people that could lose their job or their houses. Assessments of these figures are based on the percentage of damage of each structure (greater than or equal to 20%). Table 6 presents the information of the critical scenario for Barcelona.

Table 6. Information of the critical scenario for Barcelona

N°	Scenario		Loss	
	Source	Magnitude	€x10 ⁶	%
600	Zona 4_SF2	6.56	6.78E+03	21

The Figure 12 and Figure 13 show the scenarios of homeless and jobless by AEB in Barcelona.

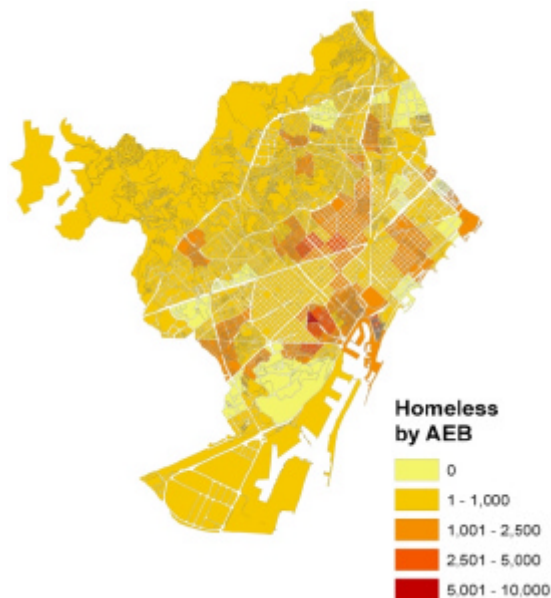


Figure 12. Homeless by AEB in Barcelona.

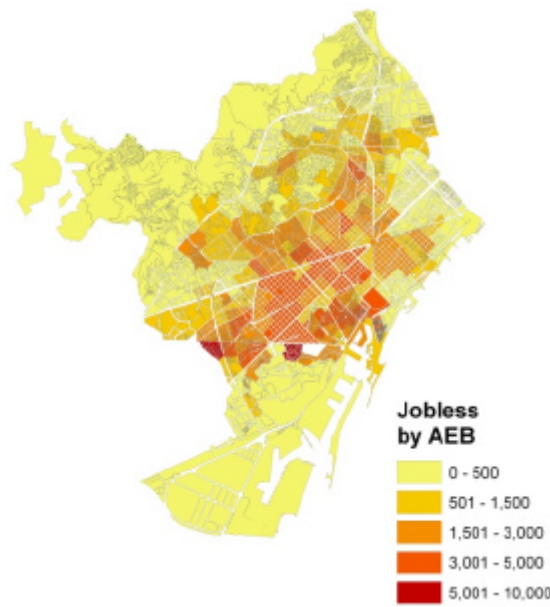


Figure 13. Jobless by AEB in Barcelona.

7. CONCLUSIONS

Catastrophic risks such as earthquake risk impose a dreadful threat not only for private insurers and reinsurers, but also for governments whom, in turn, are risk-takers for most of the uninsured and uninsurable risk. Therefore, seismic risk models become powerful tools for government officials in economic and financial planning institutions. The retention and transfer of risk should be a planned and somewhat controlled process, given that the magnitude of the catastrophic problem could represent a great governmental response and financial liabilities. For management purposes, the risk assessment should improve the decision-making process in order to contribute to the effectiveness of risk management, identifying the weaknesses of the exposed elements and their evolution over time. It is

expected that the application in Barcelona will be useful for the risk reduction and emergency preparedness plans in the city.

This study focuses on the risk assessment at urban level (by geographic units) due to the earthquake hazards, using as risk measure the Probable Maximum Loss (PML) for different return periods and the Average Annual Loss (AAL) or technical risk premium. The values of PML and AAL are the main results of this application. These measures are of particular importance for the future design of risk retention (financing) or risk transfer instruments, and therefore they will be a particularly valuable contribution to further studies to define a strategy for financial protection to cover the fiscal liability of the State.

References

1. Ambraseys, N.N., Simpson, K.A. and Bommer, J.J. (1996): "Prediction of horizontal response spectra in Europe". *Earthquake Engineering and Structural Dynamics* 25: 375-400.
2. Andersen, T. (2002). *Innovative Financial Instruments for Natural Disaster Risk Management*. Inter-American Development Bank. Sustainable Development Department. Technical Papers
3. Barbat, A.H.; Carreño, M.L.; Pujades, L.G.; Lantada, N.; Cardona, O.D. and Marulanda, M.C. (2010). "Seismic vulnerability and risk evaluation methods for urban areas. A review with application to a pilot area". *Structure and Infrastructure Engineering*. Vol. 6, Nos. 1-2, Taylor & Francis.
4. Cardona O.D., Ordaz, M.G., Reinoso, E., Yamín, L.E., Barbat, A.H. (2010a). *Comprehensive Approach for Probabilistic Risk Assessment (CAPRA): International Initiative for Disaster Risk Management Effectiveness*. in Proceedings of 14th European Conference on Earthquake Engineering, August 2010, Ohrid, Macedonia.
5. Cardona O.D., Marulanda, M.C. (2010b). *Mecanismos Financieros, Seguro y Reaseguro contra Desastres Naturales en América Latina y el Caribe: Experiencias Recientes*. Secretaría Permanente del Sistema Económico Latinoamericano y del Caribe, SELA, SP/SR-IPMFSRCDALC/DT N° 2-10, Caracas. Available at: http://www.sela.org/attach/258/EDOCS/SRed/2010/11/T023600004489-0-TDR_Estudio_Seguro_contra_Desastres_ALC_2010_REV-ODC.pdf
6. Cardona, O.D., Ordaz, M.G., Marulanda, M.C., & Barbat, A.H. (2008a). Estimation of Probabilistic Seismic Losses and the Public Economic Resilience—An Approach for a Macroeconomic Impact Evaluation, *Journal of Earthquake Engineering*, 12 (S2) 60-70, ISSN: 1363-2469 print / 1559-808X online, DOI: 10.1080/13632460802013511, Taylor & Francis, Philadelphia, PA.
7. Cardona, O.D., Ordaz, M.G., Yamín, L.E., Marulanda, M.C., & Barbat, A.H. (2008b). Earthquake Loss Assessment for Integrated Disaster Risk Management, *Journal of Earthquake Engineering*, 12 (S2) January 48-59, ISSN: 1363-2469 print / 1559-808X online, DOI: 10.1080/13632460802013495, Taylor & Francis, Philadelphia, PA.
8. Cardona, O.D., Ordaz, M.G., Marulanda, M.C., Barbat, A.H. (2008c). Fiscal Impact of future earthquakes and country's economic resilience evaluation using the disaster deficit index, *Innovation Practice Safety: Proceedings 14th World Conference on Earthquake Engineering, Beijing, China*.
9. Cardona, O.D., Ordaz, M.G., Yamin, L.E., Arámbula, S., Marulanda, M.C., Barbat, A.H. (2008d). Probabilistic seismic risk assessment for comprehensive risk management: modeling for

- innovative risk transfer and loss financing mechanisms, *Innovation Practice Safety: Proceedings 14th World Conference on Earthquake Engineering*, Beijing, China.
10. Cid J., Susagna T., Goula X., Chavarria L., Figueras S., Fleta J., Casas, A. y Roca, A. (2001): "Seismic Zonation of Barcelona Based on Numerical Simulation of Site Effects." *Pure Applied Geophysics* 158: 2559-2577.
 11. Cid J. (1998). Zonación sísmica de la ciudad de Barcelona basada en métodos de simulación numérica de efectos locales. Tesis doctoral. Dpto. Ingeniería del Terreno, Cartográfica y Geofísica. Universidad Politécnica de Cataluña, Barcelona. 215 pp.
 12. Freeman, P., Keen, M and Muthukumara, M. (2003). Dealing with Increased Risk of Natural Disasters: Challenges and Options. IMF – International Monetary Fund. Working Paper 03/197.
 13. Grossi P. & Kunreuther H. (2005). Catastrophe modeling: A new approach to managing risk, Springer Science.
 14. RISK-UE (2004). An advanced approach to earthquake risk scenarios with applications to different European towns. Project of the European Commission, Contract number: EVK4-CT-2000-00014.
 15. Lantada N. (2007): Evaluación del riesgo sísmico mediante métodos avanzados y técnicas GIS. Aplicación a la ciudad de Barcelona. Doctoral dissertation. Universidad Politécnica de Cataluña, Barcelona, Spain.
 16. Marulanda, M.C., Cardona, O.D., Barbat, A.H. (2010) Revealing the socio-economic impact of small disasters in Colombia using DesInventar database, *Disasters*, December 11/2009; 34(2): 552- 570, Overseas Development Institute, Blackwell Publishing, Oxford.
 17. Marulanda, M.C., Cardona, O.D., Ordaz, M.G., Barbat, A.H. (2008). La gestión financiera del riesgo desde la perspectiva de los desastres: Evaluación de la exposición fiscal de los Estados y alternativas de instrumentos financieros de retención y transferencia del riesgo. Monografía CIMNE IS-61, Universidad Politécnica de Cataluña, Barcelona.
 18. Miranda, E. (1999) Approximate seismic lateral deformation demands on multistory buildings, *Journal of Structural Engineering* 125:4, 417-425.
 19. Pollner, J. (2001). Managing Catastrophic Disaster Risks Using Alternative Risk Financing and Pooled Insurance Structures. World Bank Technical Paper, No. 495.
 20. Secanell, R., Goula, X., Susagna, T., Fleta, J. y Roca, A. (2004): "Seismic hazard zonation of Catalonia, Spain integrating uncertainties". *Journal of Seismology* 8 (1): 24-40.
 21. Woo, G. (1999): *The Mathematics of Natural Catastrophes*, Imperial College Press. Yamin, L.E., Gallego, M., Cardona, O.D., Phillips, C.A. (2004). "Recent Advances in Seismic Microzonation Studies, The Manizales-Colombia Case", 13th World Conference on Earthquake Engineering, Vancouver.

Integration of web-enhanced teaching tools in undergraduate construction and civil engineering higher education

Cristina Cosma

Department of Construction Management, Wentworth Institute of Technology, Boston, MA, 02115, USA

Summary

For the past several years web-based instructional technology has been constantly developed and used at Wentworth Institute of Technology to assist the face-to-face interaction. A first step was to use the Blackboard learning system to post syllabus, lecture handouts and laboratory assignments. A second step was to facilitate student assignment submission via Blackboard and use web-based assessments of student learning outcomes which offered just-in-time feedback both for instructor and students. In 2010 a third step towards on-line anytime anywhere learning was taken by developing a full set of video tutorials for laboratories.

The paper will describe and analyze the development of a complete set of on-line laboratories for CCEV 406 – Construction Project Scheduling which is offered every fall semester to the junior construction management students. The advantages and disadvantages of using these novel instructional methods will be assessed based on students' evaluations and comments and also on instructor's experience. The paper particularly outlines the technical challenges encountered in building the on-line course content, class assignments and student learning assessment tools.

KEYWORDS: Wentworth Institute of Technology, Web-enhanced learning, Blackboard, On-line laboratories, Video tutorials

1. INTRODUCTION

Located in Boston, MA, Wentworth Institute of Technology (WIT) is a private, coeducational college founded in 1904. Wentworth offers bachelor's degrees with majors in the fields of applied mathematics, architecture, computer science, construction management, design, engineering, engineering technology, and management. Wentworth provides a comprehensive interdisciplinary, project-based education that integrates classroom, laboratory, studio, cooperative and experiential learning resulting in a career-ready, skilled professionals and engaged citizens. Wentworth has a student body of more than 3,200 full time students from 33 US states and approximately 46 countries [1].

For the past ten years the teaching and learning landscape at Wentworth has been continuously changing in a sustained effort to satisfy the increasing demand for a more diversified and flexible type of higher education. Among the strategies used at Wentworth can be mentioned the integration of learning technology complemented by the changing face of instructional design, implementation of novel teaching strategies and the determination of meaningful learning objectives.

The Wentworth Laptop Program which started as a pilot in 2004 was one of the first initiatives aiming to accommodate the specific needs of students in terms of time and place of study. The program provides all full-time students and faculty members with a laptop computer (MacBook Pro for students in Architecture or Design and Facilities departments and Lenovo for all other departments). The computers are capable of running the high-end software that is customized to meet both the academic requirements and current industry demands for each specific major. To ensure that the students have the most updated hardware and software, each laptop is refreshed during the junior year. At the end of their senior year, once a student graduates, they take their computer with them. The cost of the laptop program is part of student tuition [1].

The laptop program is a fundamental tool highly needed to support the shift from a teacher-centric lecture model of instruction to a learner-centric, technology-enhanced learning model. The program was concurrently a key driving force towards the adoption of new teaching and learning methods and the effect of the dramatic growth of the internet and web-based applications for educators.

The Division of Technology Services (DTS) and the Division of Academic Affairs/Office of the Provost at Wentworth are the two main departments in charge to build on the educational innovations and also to inspire and offer support to faculty members to get involved and develop sound teaching strategies for the effective and stimulating utilization of technology in educational environments.

Figure 1 below shows a snapshot of the main website window with on-line resources available to faculty.

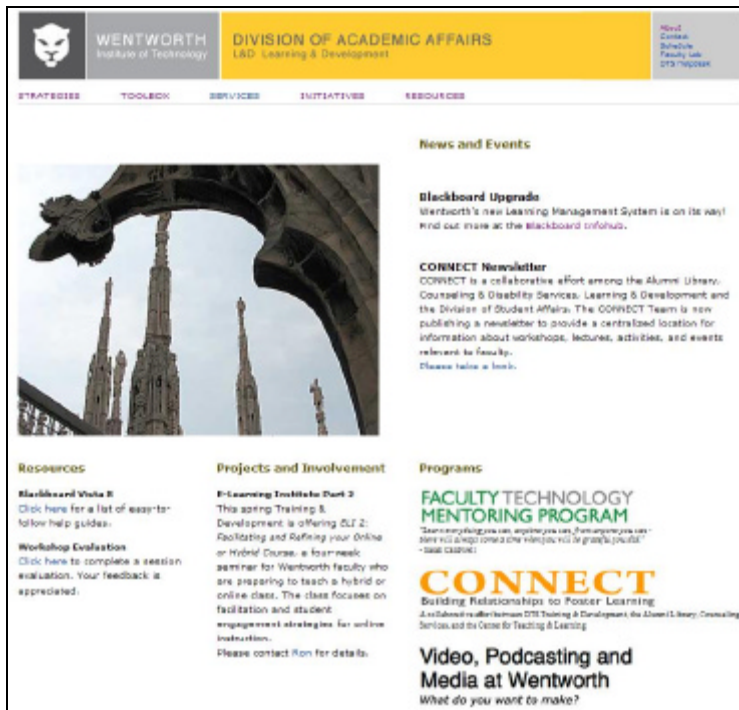


Figure 1. Learning and Development webpage

2. TRADITIONAL TEACHING FRAMEWORK

2.1. Existing situation

CCEV 406 “Construction Project Scheduling” (2-2-3) is offered once a year during the fall semester to junior CM students.

The learning goals of CCEV 406 are:

- Goal #1: to understand how schedules can be used to help plan, direct and control the construction process
- Goal #2: to manually develop a construction project schedule using the Critical Path Method (CPM)

- Goal #3: to use the computer as a tool to create and maintain a construction schedule
- Goal #4: to strengthen team building and communication skills.

The course consists of 2 hours traditional lecture time and 2 hours of laboratory-based instruction. In fall 2010 there were a total of 98 students registered for this course. The course is offered in 3 lecture sections having a maximum of 40 students each and 6 laboratory sections (2 laboratory sections for each lecture section) with a maximum of 20 students each.

In the past years during the laboratory hours the students were exposed to hands-on instruction on various planning and scheduling tools and software (Excel, Microsoft Visio, Microsoft Project, Primavera P6). The scheduling skills achieved by students in the first half of the semester were mastered through a class project assigned to teams of two students.

The laboratory hours were customary conducted on campus in a traditional manner. In most laboratory classes in the first part of the laboratory the instructor was offering a short review of the subjects presented during the lecture and was giving one or two additional examples of practical applications of the lecture subjects.

In the second part of the 2 hour laboratory the students were practicing on using various scheduling techniques, tools and software under the close supervision of the laboratory instructor.

In order to perform the assigned tasks the students were provided a Laboratory Manual which contained step by step instructions for each laboratory assignment. Also the instructor was performing the laboratory steps in the same time with the students and was projecting the output on the screen making it easier to follow. This instructional approach necessitated the laboratory instructor have an excellent knowledge of the tools and software presented and used. One of the implications of this particular skill requirement was the difficulty in finding adjuncts to teach the laboratory for CCEV 406.

The difficulty of the instructional approach used in the past was that the faster students were losing interest while waiting for the instructor (and the rest of the class) to reach a certain laboratory phase or step and sometimes were disturbing the class. Meanwhile the slower students ended up being left well behind and having to finish the laboratory on their own, outside the laboratory time.

The class project was introduced to the students in week 5 of classes and was due by the end of the semester. By this time students have been already introduced to the main notions and methods of scheduling and in the lab they have already practiced on using various scheduling software.

For the class project the students created teams of 2 students/each. All teams were given construction drawings for the same construction project. The main tasks of

the teams were to analyze the project, produce a Scope of Work (SOW), plan the construction of the building and the main construction packages, produce a Work Breakdown Structure (WBS), establish the logic sequence of construction the building, and finalizing the project by producing the construction schedule and various scheduling reports.

Due to the fact that most of the laboratory time was allocated to introducing and training the students on using scheduling tools and software, there was little time left for discussing class project and phases. Most of the feedback or answers to students' questions on class project were given during the office hours.

2.2. New training approach

In summer 2010 a Bistline Grant was awarded to research and extend the use of innovative distance learning techniques in order to create a hybrid laboratory for the fall 2010 semester. The course (CCEV 406 - “Construction Project Scheduling”) is offered to the junior Construction Management (CM) students. There were a total of 98 students registered for this course. The course is offered in 3 lecture sections having a maximum of 40 students each and 6 laboratory sections with a maximum of 20 students each.

The outcome of this research was a complete set of on-line laboratory classes for CCEV 406 “Construction Project Scheduling” (2-2-3). Ten on-line laboratories have been created. For each laboratory a set of video tutorials was developed. The videos are between 3 min to 18 min long.

One main objective of this project was to contribute to creating a student-centered learning environment where students are challenged to think critically, to be effective team players, and to be self-directed learners. This objective was achieved through the usage of video tutorials for the laboratory assignments. Students were given the opportunity to work on lab assignments anytime anywhere, perform the requested tasks at their own pace and also engage with peers in sharing, organizing and discovering the learning content.

Another objective of the research was to appeal to diverse learning styles by developing instructional materials based on a hybrid of Problem-Base Learning (PBL) and Active/Cooperative Learning (ACL) techniques that incorporate both visual, interactive teaching methods and extensive use of modern computational approaches. This objective was achieved by changing the focus of the laboratory class from training the students on the usage of various scheduling software to developing a team based and real-world project based learning environment.

3. DEVELOPMENT OF WEB-ENHANCED TEACHING

The research project had as a main goal to create a complete set of on-line laboratory classes for CCEV 406 “Construction Project Scheduling”. This goal was achieved in three main phases:

- Phase 1: Assessment of on-line laboratory delivery methods and strategies
- Phase 2: Training and practicing on on-line delivery tools
- Phase 3: Develop on-line laboratory tutorials
- Phase 4: Development of contingency plans in case of technical problems

3.1. Assessment of on-line laboratory delivery methods and strategies

The first step in developing the on-line laboratories was to analyze the existing laboratory subjects and plan the on-line delivery methods and strategies to be used. During this assessment phase the first step to be performed was to determine how much information from each laboratory should be uploaded to the online classroom.

With the support of the instructional designers from DTS a Course Map has been developed correlating the lecture subjects with the homework assignments, subject assessments (quizzes), laboratory assignments and project phases.

The second step was to determine what proportion of classroom interaction should occur online in the hybrid course. It was decided to offer on-line part of the class project and all laboratory assignments. The class project was divided into 3 phases. Each phase is concluded by an in-class team presentation. This organization resulted in 5 in-class scheduled meetings during the semester.

The third step was to determine how to evaluate levels of class participation. After discussing with the instructional designers it was decided that a scoring system based on three performance indicators (Need Improvement, Meet Expectations & Exceptional) will be used.

Next step was to establish what technological features of online courseware enhance the quality of online laboratory. With the support of DTS instructional designers the following software and technical equipment were identified to be useful for the laboratory:

- Camtasia Studio for producing video tutorials of laboratory assignments
- Blackboard discussion boards for facilitating group communication

- Blackboard learning modules for structuring the hybrid laboratory, class project particularly
- Flip cameras for video recording team presentations for the class project
- Digitizing Tablet for providing feedback for on-line assignments

Finally in conjunction with creating the Course Map the existing laboratory content had to be analyzed and alterations were performed in order to match the new approach to the existing lecture content. Additional materials were created for online delivery but also for the in-class parts of the laboratory and for assignments.

3.2. Training and practicing on on-line delivery

Three main tasks were performed during this phase: (1) Meetings with DTS instructional designers; (2) Participating to the Annual Sloan Consortium Emerging Technologies for Online Learning Symposium and (3) Practicing on producing pilot recordings and on-line laboratory tutorials.

3.2.1. *Training meetings with DTS instructional designers*

During the training phase the instructor interacted with DTS instructional designers during several meetings discussing the available resources and support for on-line teaching. Other subjects discussed were related to the technical aspects of video sharing on Blackboard and methods of student on-line engagement and interaction.

One potential problem that was identified was the fact that the available depositing space for files on Blackboard is limited. It was estimated that a number of almost 25 video files for the ten on-line laboratories (about 3 video recordings for each lab) can be recorded/produced. The pilot video recordings produced during this phase were quite large (20 MB/each or more). The estimated storage space needed for all the files was close to 1 GB (1,000 MB = 1 GB). The solution suggested by the instructional designers was to use the 2 GB storage space provided for free by TechSmith for Jing and Camtasia users on screencast.com.

3.2.2. *Practicing on producing pilot recordings and on-line laboratory tutorials*

At the end of this phase pilot recordings and on-line laboratory tutorials were produced. Blackboard digital tools for on-line communication (i.e. discussion boards) were used and a couple of short video tutorials using screen capture software (Jing and Camtasia Studio) were created.

After practicing both with Jing and Camtasia Studio it was decided to use Camtasia Studio for producing the laboratory video tutorials because this software offers a much wider variety of video effects than Jing.

Some of the video effects that can be used in Camtasia Studio and which definitely contribute to an increased quality of the laboratory video tutorials facilitating student learning are:

- Import images, recording files and video clips
- Apply SmartFocus and zoom-in keyframes on the recordings to draw viewers' attention to specific action in the video
- Make basic edits on the timeline like cut and split clips, move clips, add markers, etc.
- Record camera video or add a video clip as a Picture-in Picture on the timeline
- Add title clips and transitions
- Add callouts, captioning, mouse highlight, flash quizzes or surveys
- Edit the audio by removing noises, m-ms, etc.

Most of the above video effects have been used in the laboratory tutorials developed.

3.3. Development of on-line laboratory tutorials

During Phase 3 a full set of on-line laboratories was developed based on the laboratory course map created in Phase 1 by using the on-line tools and software (Camtasia Studio) learned in Phase 2.

Table 1 below shows the screen casts and sets of video tutorials that were created for each lab.

Table 1. Laboratory Video Tutorials

Laboratory	Video Tutorial
Lab Assignment 1 Build a Gantt/Bar Chart Schedule using Excel & Microsoft Project	1. PART A video (6 min) - Introduction to general scheduling concepts and Bar Charts. 2. PART B video (30 min) - shows students how to use Excel to build a Bar Chart 3. PART C video (12 min) - instructions on how to create a Gantt Chart schedule in Microsoft Project
Lab Assignment 2 Build a Gantt/Bar Chart Schedule using Primavera Project Manager (P6)	4. PART A video (13 min) - brief Introduction to the portfolio, OBS & EPS concepts and shows the steps students need to take to create these structures in P6 5. PART B video (16 min) - shows students how

Laboratory	Video Tutorial
	to use P6 to build a Bar Chart 6. PART C video (8 min) - instructions on how to create a Scheduling Report in P6
Lab Assignment 3 Build a Gantt/Bar Chart Schedule for a Renovation Project (32 activities) using Primavera Project Manager (P6)	7. PART A video (5 min) - brief Introduction to Lab Assignment 3 and project data. 8. PART B video (3 min) - reviews the steps on how to assign predecessors to activities in P6. 9. PART C video (6 min) - instructions on how to assign the holidays/non-work days to the schedule calendar and create the final schedule & the 2 lab submittals
Lab Assignment 4 Organizing & Sorting the Renovation Project Schedule in P6	10. PART A video (11 min) - brief Introduction to Lab Assignment 4 and instructions on how to create and assign activity/project codes. 11. PART B video (13 min) - steps on how to generate Submittals 1, 3 & 4.. 12. PART C video (7 min) - instructions on how to produce Submittal #2.
Lab Assignment 5 Customize the Renovation Project Schedule using Filters & Sorts in Primavera Project Manager (P6)	14. PART B video (10 min) - steps on how to generate Submittals 2, 3 & 4. 15. PART C video (5 min) - instructions on how to produce Submittal #5.
Lab Assignment 6 Review the use of P6 Create a WBS & OBS Structure	16. PART A video (14 min) - brief Introduction to Lab Assignment 5 and instructions on how to create Submittals 1 & 2. 17. PART B video (20 min) - instructions on how to create the new project and prepare for the Submittals 2 to 6. 18. PART C video (5 min) - instructions on how to produce Submittal #6.
Lab Assignment 7 Perform a Schedule Update on the Industrial Building Project	19. PART A video (8 min) - a brief Introduction to Lab Assignment 7 and on the importance and methods of updating a schedule 20. PART B video (18 min) - instructions on how to update the project and prepare for the Submittals 2 & 3. 21. PART C video (7 min) - instructions on how to produce Submittals 4 & 5.
Lab Assignment 8 Cost Load the Renovation Project	22. PART A video (3 min) - brief Introduction to Lab Assignment 8. 23. PART B video (17 min) - instructions on how to create cost accounts, resource codes, cost load a schedule and prepare for Submittals 1 through 4.

Laboratory	Video Tutorial
	24. PART C video (7 min) - instructions on how to produce Submittals 1 through 4..
Lab Assignment 9 Create Graphical Reports on Resource & Cost Usage for the Renovation Project	25. Video tutorial (8 min) – instructions on how to produce the required submittals
Lab Assignment 10 Create a short video training tutorial	No video tutorials were developed for this laboratory

3.4. Development of contingency plans in case of technical problems

During the last phase of this project potential pitfalls and troubleshooting associated with each laboratory were identified. Based on previous in-class experience with the lab assignments the instructor created several very short video tutorials (less than 5 min) showing how to redress from certain issues that students can encounter while using various scheduling software, Primavera Project Management (P6) particularly.

One main part of the contingency plan was to create and provide a Laboratory Manual for the lab assignments. The Manual contents are similar to the videos and offer step by step instructions on how to fulfill each assignment. Most of the written instructions in the Manual are also supported by pictures showing how to use the scheduling software and how the final submittals should look. The Manual is intended to overcome any problems related to internet connections and students access to the video tutorials.

4. TECHNICAL FINDINGS

4.1. Capturing team presentations using Flip camcorders

By offering the laboratory assignments on-line more lab time was opened to hands-on real-world project based learning and teamwork. Students were assigned in teams mimicking real organizational structure for project management. A team would have 3 to 4 students each of them being assigned a specific role in the team: project manager, estimator, scheduler and superintendent (for the teams of 4 students). Each team was assigned a real project that is being built in Massachusetts. The team has to study and analyze the project documents, drawings and specs and produce a complete schedule for it.

The first phase of the class project was finalized with a team presentation of the work, findings and submittals. The presentations were captured on camera and were available on you-tube for feedback and corrective actions. Two Flip camcorders were used to record the team presentations. One was a Flip MinoHD with a recording capacity of 60 min and the other was a Flip UltraHD with a recoding capacity of 120 min. The focus was on recording the presentations of the teams in the hybrid laboratory (3 teams which presented 15 min/each). Due to the remaining recording capacity the presentations in two other in-class laboratory sections were also recorded.

One of the limitations of using the camcorders was related to their recording capacity and to the large number of presentations taking place in the very same week. The lab sections are scheduled on Tuesday, Wednesday and Thursday. There was no time to download the videos to create space in the cameras in order to capture all presentations. Also the time to recharge a battery for a Flip camera can vary between 2 to 5 hours if a Flip charger is being used or up to 10 hours if charging is done through the computer. Some student teams expressed their disappointment of not being able to receive feedback related to their presentations.

4.2. Bandwidth usage

The video tutorials were made accessible to all the students registered for CCEV 406 and not only to the hybrid laboratory section. The videos were stored on screencast.com and they were made accessible to the students through a link created on Blackboard.

The tutorials were received very well by students. An indicator of student level of comfort with this new educational system is the large number of students that submitted the laboratory assignments well ahead of the required deadline.

Table 2 below shows student access of the video tutorials for the first three laboratories.

Table 2. Bandwidth usage

Laboratory	# Views	Bandwidth usage (GB)
Lab 1A	201	2,75
Lab 1 B	208	5.16
Lab 1 C	164	2.10
Lab 2 A	246	2.92
Lab 2 B	235	3.93
Lab 2 C	146	1.37
Lab 3 A	148	1.98
Lab 3 B	198	1.20
Lab 3 C	103	2.35

To be noticed that as students got more comfortable with the video tutorials and also with the scheduling software used, their access of the videos (measured by the # of views) started to drop. There were 98 students registered for CCEV 406. It can be noticed that the number of views per video varies between 1.05 to 2.5 views per student. Anecdotal evidence from several students showed that the opportunity to play back and listen again to the laboratory instructions was highly appreciated and welcomed.

An analysis of the bandwidth usage column shows that for each laboratory the range was between 5.53 GB to 10 GB total usage. This created an unexpected problem during the very first week of classes. TechSmith's provides a free video storage web space (screencast.com) of max 2 GB and also a max bandwidth allowance of 2 GB. For the first lab the 2 GB bandwidth was used in 48 hours. The solution was to buy additional bandwidth from TechSmith.

4.3. Using Wacom Cintiq 12WX digitizing tablet

A Cintiq 12WX was rented from DTS in order to grade and provide feedback to the students for some of the (homework) assignments. The usage of the digitizing tablet was quite easy and user-friendly but the installation time for the system took more than 30 min which suggests that renting this system for a limited period of time is not recommended.

The digitizing tablet facilitated the usage of a digital pen for writing comments on student assignments. Students were asked to save their assignment in Adobe/Pdf format and submit it on Blackboard. Once assignments were submitted the instructor opened and saved them her computer and after correcting and grading the assignments was sent back to the student(s) (also on Blackboard). The system worked quite efficiently despite the fact that due to opening of many Adobe files instructor's computer crushed a couple of times.

5. CONCLUSIONS AND RECOMMENDATIONS

The development of an on-line, hybrid or blended course requires a thorough advanced planning and training for the faculty involved in this type of teaching. There is the misconception that an on-line class can follow the traditional class format. Faculty interested in getting involved in developing an on-line class should be aware of the lack of flexibility of this particular type of class and the need to create a thoroughly structured course. It is difficult to improvise for on-line course delivery.

For a high quality well-structured on-line course planning should start two semesters in advance leaving a full semester for producing, editing and improving the on-line lectures/labs. Close co-operation and communication with the instructional designers during the planning, development and further while offering the on-line classes is the key to the success of such a class.

An on-line course should be the result of teamwork. The team members should be the faculty teaching that class and an assigned instructional designer for (that particular) course development. The support and involvement of the instructional designers in planning, development and delivery of on-line courses should go well above and beyond training and (technical) problem solving.

Both the planning and development phases require an extensive technical knowledge and skills which, if required from the faculty, can have either positive or negative effects. The positive effects would be extending faculty knowledge in high tech areas which can result in the reduced involvement of the instructional designer and an increased feeling of self-actualization for the faculty. One negative effect can be the reduced motivation of faculty feeling uncomfortable with high tech tasks. Another negative effect can be faculty losing interest in on-line education due to the altering of teaching tasks and skills and because faculty development initiatives might focus only on on-line technology skills.

Planning for on-line courses goes well beyond faculty involvement. There are many (technical) resources available for free but also at more or less affordable prices. Online education has to be looked at like an investment in the future. It needs a substantial “down payment” in order to bring profit on long term. The electronic resources available or to be used in on-line class development and implementation need more than anything storage space. An assessment should be made in order to decide the dimensions of this space (in GB or TB of course) and what are the financial implications of borrowing, leasing or owing it.

Another technical aspect to be considered when offering on-line classes is the rhythm of (electronic) resource usage. A particularity of these resources is that their usage comes at a price (the same way as electricity, water or gas). Strategies of lowering the usage can be developed. Reaching upstream into training the students not to waste these resources should be seriously considered maybe in combination with including the price of usage in the tuition fee.

Considerations should be made related to offering (technical) support to faculty delivering on-line classes in all locations where engagement in collaborative activities is necessary. The delivery of on-line classes requires both student and faculty access to the internet. Solutions should be considered for individuals with poor or occasional connectivity which limits the access to rich content and the engagement in collaborative activities.

Students can also be reluctant to taking on-line classes. If students are exposed to this particular learning environment without a preliminary preparation their engagement and involvement will be poor or missing totally.

Last but not least more training and faculty development is necessary in order to expand faculty “buy-in” and “stay-in” into the on-line/hybrid/blended educational systems. Teaching on-line requires a different pedagogy than face-to-face instruction and interactivity is very different in the on-line environment

References

1. Academic Support Services, Wentworth Institute of Technology, Office of Academic Affairs, <http://wit.edu/academic-affairs/index.html>
2. Cosma, C., *Development of on-line video tutorials*, Bistline Research Grant, Final Report, Boston, 2010.

Analytical method for axial– flexural interaction diagram in case of reinforced concrete columns confined with fibre reinforced polymers

Ciprian Cozmanciuc¹, Ruxandra Oltean²

¹*Department of Concrete Structures, Building Materials, Technology and Management, “Gh. Asachi” Technical University, Iasi, Romania*

²*Department of Civil and Industrial Engineering, “Gh. Asachi” Technical University, Iasi, Romania*

Summary

Reinforced concrete (RC) columns in buildings framing systems are structural members subjected to combinations of axial compression and bending moment, rather than pure axial loading. This type of action can be induced by several factors, such as vertical misalignments, unbalanced moments at connecting beams, or lateral forces resulting from wind or seismic actions.

Externally application of FRP jackets to RC columns can be used to increase strength and ductility of members, when subjected to inadvertent load eccentricities or combined axial–flexural (N–M) loading.

To design an axial load – bending moment diagram for an unconfined RC column, one needs the geometric properties of the cross – section, the internal reinforcement properties, quantity and placement in section and the concrete strength, this being described in all textbooks on RC design. For an FRP-confined RC column the design of N-M interaction diagram is not a common matter and limited experimental studies have been carried out. Because experimental tests on FRP-strengthened columns are difficult to perform, researches done so far do not comprise detailed interaction curves.

This paper presents a procedure that allows the development of a simplified N-M interaction diagram for FRP-confined RC columns for practical design applications. In the proposed method, the analysis of FRP-wrapped columns is carried out based on principles of equilibrium and strain compatibility equivalent to that of unconfined RC columns, the main difference being given by the use of stress-strain model developed by Lam and Teng for FRP-confined concrete.

KEYWORDS: concrete; fibre reinforced polymers, bond, finite element analysis, strengthening.

1. INTRODUCTION

Confining RC columns with FRP membranes is a frequently used technique, when it is desired to improve the load carrying capacity and/or ductility of such compression members. The necessity of enhanced strength is given especially by higher load capacity demands required by more restraining codes and changes in the structures use. The need of ductility enhancement is given by the energy dissipation reasons, which allows the plastic behaviour of the element and, finally, of the entire structure [1].

There has been a continuously increasing interest in the use of FRP materials over the past decade in the repairing, retrofitting, rebuilding, strengthening and new construction of columns in engineering structures. An important aspect for FRP membranes is that opposed from steel which applies a constant confining pressure after yield, FRP composites have an elastic behaviour up to failure and therefore exerts a (passive) confining action on concrete specimens under axial load [2,3].

Most columns, in practice, are eccentrically loaded, thus their sections are subjected to combined axial compression and bending moments. The FRP confining systems have proven their efficiency not only in case of axially loaded columns but also for eccentrically loaded columns [4, 5].

In literature there can be found several experimental studies analyzing the behaviour of FRP confined concrete cylinders, prisms and columns subjected to eccentric compression or combined axial and bending loads. It can be concluded that the load bearing capacity of the element improves when the number of confinement layers are increased, but is decreasing with the increasing of the eccentricity. The efficiency of the confining system is proportional to the stiffness of the FRP membrane, which controls the dilation of the concrete cross section and leads to a larger axial deformation capacity [6, 7].

The studies carried out so far on the behaviour of FRP strengthened RC columns eccentrically loaded have conducted to theoretical axial – flexural (N-M) interaction diagrams [8-11]. In this paper is presented an analytical method, based on ACI design guide lines, for realising the simplified N-M diagram in case of noncircular cross-section columns following the principles of equilibrium and strain compatibility, being limited to the compression-controlled region of the interaction diagram. An extensive experimental program carried out and some results referring to the performance of eccentrically loaded columns externally strengthened with FRP membranes are presented in the paper. Further on, there are described the N-M interaction diagrams for the tested columns according to the proposed analytical method [12].

2. DESIGN METHOD FOR THE N-M INTERACTION DIAGRAM

The interaction diagram for a RC element section is a graphic representation of all possible combinations between the axial forces (N_u) and the bending moments (M_u) which produces failure, as it can be observed from Figure 1. In order to design the interaction diagram it is necessary to know the dimensions of the cross-section and mechanical properties of the internal steel reinforcement and of the external confinement system [13].

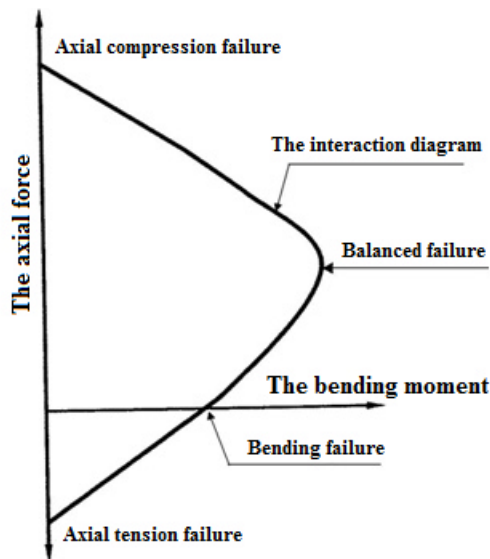


Figure 1. The interaction diagram for a RC element cross-section

The procedure for realising the interaction diagram in case of FRP confined elements is similar to the one for RC columns, except that the stress – strain model for FRP confined concrete is adopted in the compression region. For simplified computation, instead of a continuous curve, the N-M diagram can be obtained as a number of segment lines which are joining the axial force and bending moment values, resulting five characteristic points, as it can be seen in Figure 2.

In the interaction diagram, point A represents the pure compression case (with zero bending moment), while point E represents the pure bending moment case (with zero axial force), where position of the neutral axis is obtained by following the conventional RC beam theory. In case of points B, C and D, the neutral axis position (c) is determined by similar triangles in strain distribution corresponding to each case [10, 12].

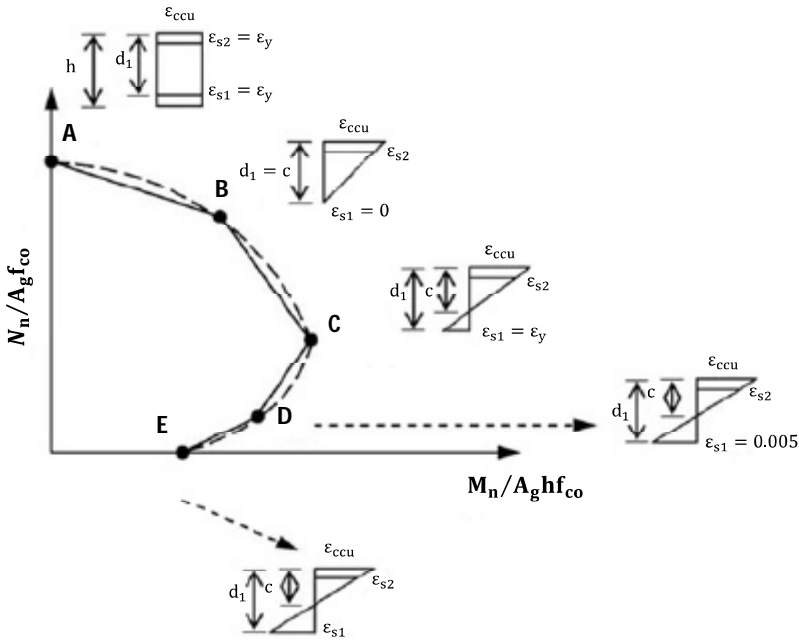


Figure 2. The interaction diagram for elements with circular and noncircular cross-sections

The nominal axial force (N_n) corresponding to point A can be determined by applying the following relation:

$$N_{n(A)} = [0.85f_{cc} (A_g - A_s) + f_y A_s] \tag{1}$$

Where f_{cc} represents the compressive strength of confined concrete, f_y is the yield strength of longitudinal steel reinforcement, A_g is the total cross-sectional area and A_s is the area of internal steel reinforcement.

The nominal axial force (N_n) and the nominal bending moment (M_n) for points B, C and D are evaluated by integrating the stresses over the noncircular cross-section of concrete, according to the following relations:

$$N_{n(B,C,D)} = \int_0^c (b)f_{co} (y)dy + \sum A_{si} f_{si} \tag{2}$$

$$M_{n(B,C,D)} = \int_0^c (b) \left(\frac{h}{2} - c + y \right) f_{co} (y)dy + \sum A_{si} f_{si} d_{si} \tag{3}$$

Where b and h are the dimensions of the noncircular cross-section, c is the distance from the extreme compression fibre to the neutral axis position of the cross-section, y is the variable of integration within the compression zone, d_{si} is the distance from the position of the “ i th” layer of longitudinal steel reinforcement to the geometric centre of the cross-section, f_{co} is the unconfined concrete compressive strength, f_{si} is the stress in “ i th” layer of longitudinal steel reinforcement and A_{si} is the cross-sectional area of the “ i th” layer of longitudinal steel reinforcement.

Starting from ACI 440.2R-08, in order to simplify the applications, Rocca et al. proposed a model which allows the development of a simplified axial – flexural interaction diagram for RC columns confined with FRP membranes [8, 10]. In the proposed model the analysis of FRP confined RC columns starts from the principles of equilibrium and strain compatibility taking into consideration the stress – strain model for FRP-confined concrete proposed by Lam and Teng [14, 15].

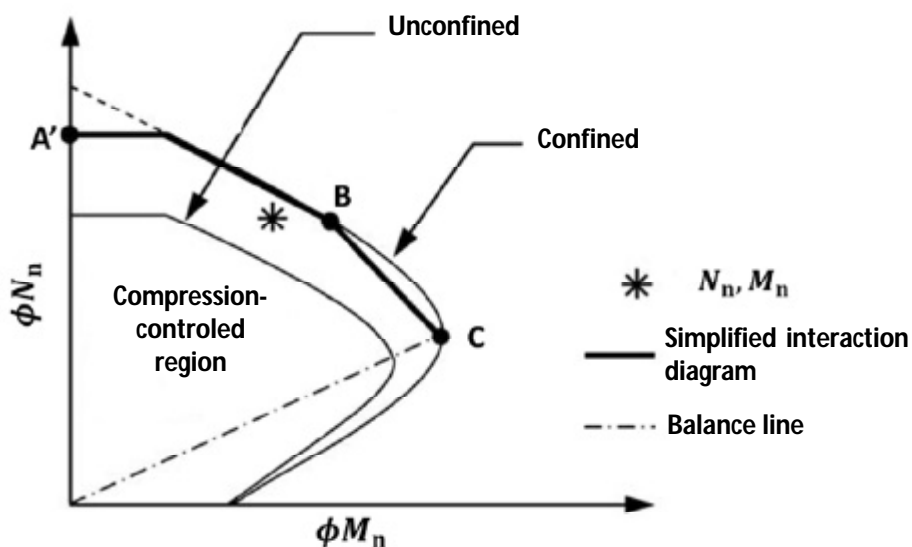


Figure 3. The simplified interaction diagram

The increase in strength can be considered only when the position of the point with the coordinates given by the applied ultimate axial force (N_n) and bending moment (M_n) is above the line connecting the origin and the balanced points of the interaction diagram for the unconfined member, or in the so called compression-controlled region. This limitation is given by the fact that strength enhancement can be significant for the elements only in case of a compression failure.

To simplify the design methodology, the interaction diagram can be reduced to two bilinear curves passing through the points A, B and C, for covering the compression-controlled failure region, as it is presented in Figure 3.

The coordinates of point A can be determined by applying equation (1), resulting the nominal axial force (N_n), while the nominal bending moment (M_n) is zero. For points B and C are applied the equation (2) and (3). By taking into consideration that elements have a rectangular cross-section, substituting Lam and Teng's stress-strain relationship in equation (3) and expressing the axial compressive strain at any point in the compression region in terms of the integrating variable y according to similar triangles principle, equation (2) and (3) will become as it follows:

$$N_{n(B,C)} = \int_0^{y_t} \left[E_c \left(\frac{e_{ccu}}{c} y \right) - \frac{(E_c - E_2)^2}{4f_{co}} \left(\frac{e_{ccu}}{c} y \right)^2 \right] b dy + \int_{y_t}^c \left[f_{co} + E_2 \left(\frac{e_{ccu}}{c} y \right) \right] b dy + \sum A_{si} f_{si} \quad (4)$$

$$M_{n(B,C)} = \int_0^{y_t} \left[E_c \left(\frac{e_{ccu}}{c} y \right) - \frac{(E_c - E_2)^2}{4f_{co}} \left(\frac{e_{ccu}}{c} y \right)^2 \right] b \left(\frac{h}{2} - c + y \right) dy + \int_{y_t}^c \left[f_{co} + E_2 \left(\frac{e_{ccu}}{c} y \right) \right] b \left(\frac{h}{2} - c + y \right) dy + \sum A_{si} f_{si} d_{si} \quad (5)$$

Where y_t represents the vertical coordinate within the compression region measured from the neutral axis and it corresponds to the transition strain (e_t'); E_c is the initial modulus of elasticity of concrete; E_2 is the slope of linear portion of stress-strain curve for the confined concrete and e_{ccu} is the ultimate axial compressive strain of confined concrete. With the following equation there can be determined c and y_t .

$$c = \begin{cases} d & \text{for point B} \\ d \frac{e_{ccu}}{e_{sy} + e_{ccu}} & \text{for point C} \end{cases} \quad (6)$$

$$y_t = c \frac{e_t'}{e_{ccu}} \quad (7)$$

By integrating, equations (4) and (5) can be expressed as in equations (8) and (9), where the coefficients A, B, C, D, E, F, G, H and I are determined with relations (10).

$$N_{n(B,C)} = [A(y_t)^3 + B(y_t)^2 + C(y_t) + D] + \sum A_{si} f_{si} \quad (8)$$

$$M_{n(B,C)} = [E(y_t)^4 + F(y_t)^3 + G(y_t)^2 + H(y_t) + I] + \sum A_{si} f_{si} d_{si} \quad (9)$$

$$A = \frac{-b(E_c - E_2)^2 \left(\frac{e_{ccu}}{c} \right)^2}{12f_c} \quad (10a)$$

$$B = \frac{b(E_c - E_2)}{12} \left(\frac{e_{ccu}}{c} \right) \quad (10b)$$

$$C = -bf_c \quad (10c)$$

$$D = bcf_c + \frac{bcE_2}{2} (e_{ccu}) \quad (10d)$$

$$E = \frac{-b(E_c - E_2)^2 \left(\frac{e_{ccu}}{c} \right)^2}{16f_c} \quad (10e)$$

$$F = b \left(c - \frac{h}{2} \right) \frac{(E_c - E_2)^2 \left(\frac{e_{ccu}}{c} \right)^2}{12f_c} + \frac{b(E_c - E_2)}{3} \left(\frac{e_{ccu}}{c} \right) \quad (10f)$$

$$G = - \left(\frac{b}{2} f_c + b \left(c - \frac{h}{2} \right) \frac{(E_c - E_2)}{2} \left(\frac{e_{ccu}}{c} \right) \right) \quad (10g)$$

$$H = bf_c \left(c - \frac{h}{2} \right) \quad (10h)$$

$$I = \frac{bc^2}{h} f_c - bcf_c \left(c - \frac{h}{2} \right) + \frac{bc^2 E_2}{3} e_{ccu} - \frac{bcE_2}{2} \left(c - \frac{h}{2} \right) e_{ccu} \quad (10i)$$

To prevent the possible accidental eccentricity, in the ACI design procedure, the nominal axial load capacity in case of RC columns with transverse reinforcement subjected to pure compression, represented by point A on the interaction diagram, is reduced with 20%. In Figure 3 this point is denoted as A' and equation (1) will become as it follows:

$$N_{n(A')} = 0.8[0.85f_{cc} (A_g - A_s) + f_y A_s] \quad (1)$$

3. DESIGN OF THE N-M INTERACTION DIAGRAM BASED ON EXPERIMENTAL TESTS

At the Faculty of Civil Engineering and Building Services of Iasi there was carried out an experimental program which studied the behavior of CFRP confined RC rectangular columns under eccentric compression loads [6, 12]. All columns were designed alike, with the height of 1000 mm and with an identical distribution of the internal reinforcement. The longitudinal steel reinforcement consisted of four deformed rebars 12 mm diameter. For transversal reinforcement, were provided steel stirrups of 6 mm diameter plain bars spaced at 200 mm in the middle region of the specimen and at 84 mm to the ends of the column.

The specimens were grouped in two series of three identical columns: a first group having the side of the cross-section of 250 mm, noted C2, and the second group with the cross-sectional dimension of 300 mm, noted C3. In each group, one specimen was unconfined and the other two specimens were confined with one, respectively two, layers of CFRP. All specimens were tested under eccentric compression, for the first group of columns the eccentricity was of 50 mm, while for the second group the eccentricity was of 75 mm.

A summary of column specimens' configuration and the resulted experimental maximum load are given in Table 1.

Table 1. Configuration of column specimens and the experimental maximum load

Group (cross-section) (mm)	Specimen	Confinement condition	Load eccentricity (mm)	Maximum Load (mm)
C2 (250 x 250)	C2-0	No wrapping	50	1391.1
	C2-1	1 layer CFRP	50	2133.8
	C2-2	2 layers CFRP	50	2004.9
C3 (300 x 300)	C3-0	No wrapping	75	2121.1
	C3-1	1 layer CFRP	75	2295.5
	C3-2	2 layers CFRP	75	2480.7

The comparative graphic for N-M interaction diagrams, based on the model proposed by ACI 440.2R-08 and discussed in this paper, for group C2 of columns is presented in Figure 4. In Figure 5 are represented the comparative N-M interaction diagrams graphic for group C3 of columns which had been tested during the experimental program.

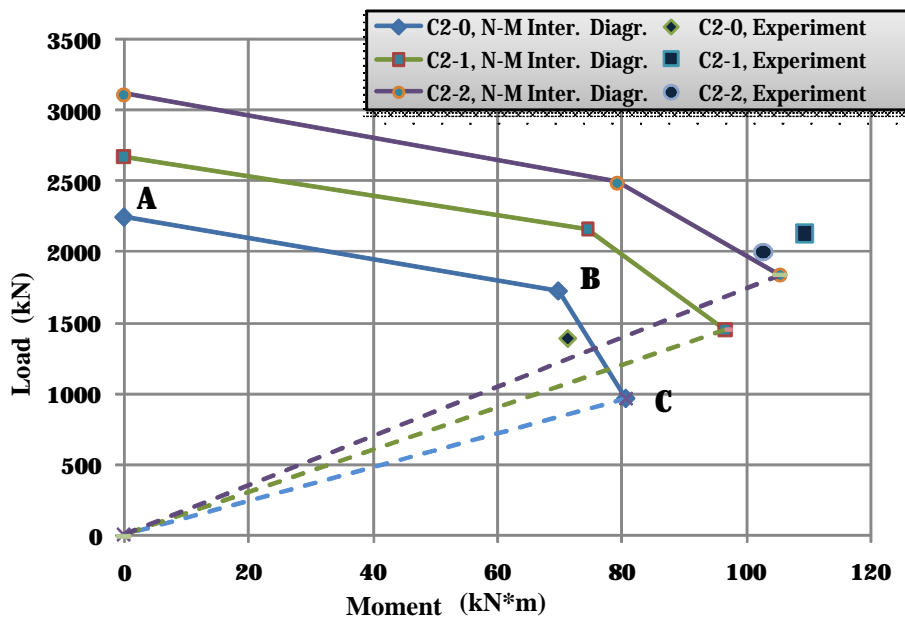


Figure 4. The N-M interaction diagrams for group C2 of columns

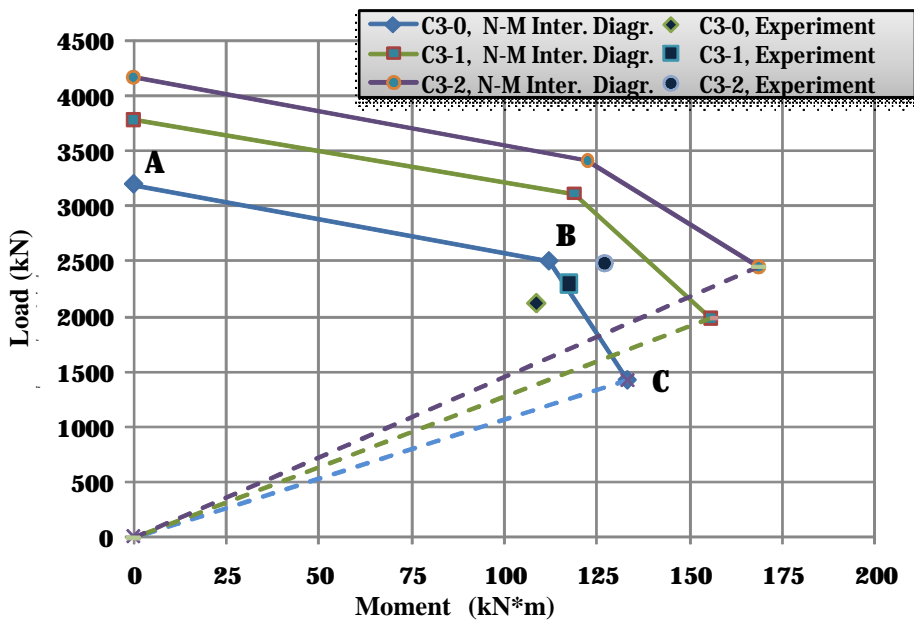


Figure 5. The N-M interaction diagrams for group C3 of columns

4. CONCLUSIONS

The proposed design approach for FRP-confined RC columns subjected to combined axial force and bending moment is responding to the need of a rational and simple method, by respecting the ACI requirements.

The design of the interaction diagram starts from principles of equilibrium and strain compatibility, equivalent to that of conventional RC columns but taking into consideration the Lam and Teng's stress strain model for FRP-wrapped concrete. For the compression-controlled region the N-M diagram is simplified to a series of straight segments which are joining only the characteristic points.

According to the experimental results the strength of rectangular FRP-confined RC columns under eccentric axial loads is improved as compared with identical unconfined columns.

In buildings many columns are subjected to eccentric loads and are influenced by slenderness effect. From this reasons it is important for design guidelines to establish slenderness limits and to outline procedures to deal with these loading types for RC columns strengthened with FRP materials.

References

1. Rocca, S., Experimental and analytical evaluation of FRP-confined large size reinforced concrete columns, Disertation, University of Missouri-Rolla, 2007.
2. Cozmanciuc, C., Oltean, R., Taranu, N., Analytical models for confinement systems of reinforced concrete columns with circular and noncircular cross sections utilizing composite materials, *Proceedings of the 8th International Symposium Computational Civil Engineering 2010*, „*New Computational Concepts in Civil Engineering*”, Iasi, Romania, 2010.
3. Cozmanciuc, C., Oltean, R., Munteanu, V., Strengthening Techniques of RC Columns using Fibre Reinforced Polymeric Materials, *Buletinul IPI*, Tomul LV (LIX), Fasc. 3, 2009.
4. Teng, J.G., Chen, J.F., Smith, S.T., Lam, L., *FRP-strengthened RC Structures*, John Wiley & Sons, Ltd, England, 2002.
5. Cozmanciuc, C., Comportarea stâlpilor din beton armat confinati cu membrane compozite solicitati la compresiune excentrica, *Creatii Universitare, Al IV-lea Simpozion National*, Iasi, 2011. (in Romanian)
6. Cozmanciuc, C., Oprisan, G., Taranu, N., Munteanu, V., Oltean, R., Budescu, M., Structural behaviour of eccentrically loaded reinforced concrete columns confined with carbon fibre reinforced membranes, *The 11th International Scientific Conference VSU*, Sofia, Bulgaria, 2011.
7. Quiertant, M., Clement, J.L., Behavior of RC columns strengthened with different CFRP systems under eccentric loading, *Construction and Building Materials*, 2011.
8. ACI Committee 440 Report, Guide for the Design and Construction of Externally Bonded FRP Systems for Strengthening Concrete Structures, *ACI Committee 440, Technical Committee Document 440.2R-08*, 2008.
9. El-Fattah, A., Rasheed, H., Esmaeily, A., A New Eccentricity-Based Simulation to Generate Ultimate Confined Interaction Diagrams for Circular Concrete Columns, *Journal of the Franklin Institute*, 2009.
10. Rocca, S., Galati, N., Nanni, A., Interaction diagram methodology for design of FRP-confined reinforced concrete columns, *Construction and Building Materials*, vol. 23, 2009.

11. Bisby, L., Ranger, M., Axial-flexural interaction in circular FRP-confined reinforced concrete columns, *Construction and Building Materials*, 24, 2010.
12. Cozmanciuc, C., *Consolidarea Stâlpilor din Beton Armat cu Sectiune Necirculara prin Confinare cu Materiale Compozite*, Editura Politehniun, Iasi, România, 2011.
13. Ghoneim, M., El-Mihilmy, M., *Design of Reinforced Concrete Structures, Second Edition, Volume 2*, 2008.
14. Lam, L., Teng, J.G., Design-oriented Stress-Strain Model for FRP-confined Concrete in Rectangular Columns, *Journal of Reinforced Plastics and Composites*, Vol. 22, No. 13, 2003.
15. Lam, L., Teng, J.G., Design-oriented Stress-strain Models for FRP-confined Concrete, *Construction and Building Materials*, 17, 2003.

Finite element analysis of square reinforced concrete columns confined with composite membranes subjected to eccentric compression

Ciprian Cozmanciuc¹, Ruxandra Oltean²

¹*Department of Concrete Structures, Building Materials, Technology and Management, "Gh. Asachi" Technical University, Iasi, 700050, Romania*

²*Department of Civil and Industrial Engineering, "Gh. Asachi" Technical University, Iasi, 700050, Romania*

Summary

Finite element method (FEM) is an accurate numerical technique utilized in simulating the structural response of a genuine application and is found to be an efficient method for studying a wide range of engineering and research problems.

Strengthening of reinforced concrete (RC) elements and structures with externally bonded fiber reinforced polymers (FRP) is becoming increasingly popular and widespread technique in civil engineering community.

Over the past three decades numerous studies have been developed in order to analyze the confining effect on concentrically loaded RC columns. In this matter, utilizing FEM satisfactory results were obtained, when analyzing the effect given by thickness of composite membranes, increase of load bearing capacity and ductility of the elements which resulted in a large energy absorption capacity.

Studies on eccentrically loaded FRP confined concrete columns are relatively new and limited in number making clear the need of investigating the behavior of columns under eccentric loads. However, the FEM analysis indicates a good behavior of RC columns subjected to eccentric loads when they are strengthened with externally bonded FRP materials. To evaluate the behavior of RC elements wrapped with carbon fiber polymeric (CFRP) sheets and to predict the behavior of such strengthened columns, a finite element analysis was performed using Ansys package software. There were modeled one meter height square concrete columns, with longitudinal and transversal internal steel reinforcement. The eccentricity of the compressive load was of 50 mm and it was applied at both ends. In this paper are presented the simulated results using the finite element analysis in case of RC column before and after confining it with one layer of CFRP.

KEYWORDS: fiber reinforced polymers, reinforced concrete columns; finite element analysis, confinement.

1. INTRODUCTION

In recent years the behavior of small concrete elements confined with composite materials was analyzed through FEM in several studies [1-9]. Also, few studies evaluated the influence of internal, longitudinal and transversal, reinforcement in concrete columns strengthened with CFRP membranes [10-13].

The behavior of columns with rectangular cross-section confined with CFRP materials was studied, by applying the FEM, by Parvin and Schroeder [14]. Their purpose was to check the effect given by the thickness of the confining system and the increase in load bearing capacity and ductility when subjected to axial compression. They realized a stress distribution over the element cross-section and concluded that by increasing the layers of composite membrane the confining system will be more efficient.

In the studies developed by Taranu et al. [15-17], a FEM was realized using LUSAS software to investigate the behavior of axial compressed noncircular RC columns confined with CFRP materials. They observed that the confined concrete and the unconfined one have a similar behavior until the compressive strength of unconfined concrete is reached. This is because the confining system has a passive behavior and it becomes active when concrete has a high level of lateral deformations. The wrapping layers are producing an increase of stresses and strains.

As far as the literature on eccentric compressed RC columns confined with FRP materials is concerned, there are many fewer studies. Parvin si Wang (2001) [4] studied using non-linear FEM the behavior of RC square section columns confined with FRP composites and subjected to eccentric loads. The column was modeled in MARC software program (*MARC Users Guide* 1994). When meshing the specimen 240 tri-dimensional solid elements (bricks) for the concrete column and 168 membrane elements (shell) for the composite strip were used. Between the composite system and the concrete member perfect bonding was defined, even if at the interface separation between materials was possible. They have concluded that in case of centric compression, the effective concrete area, influenced by the confinement system is situated in the central zone and in the corners, while for eccentric compressed columns the confining system influence is increased mostly in the compressed area of the element.

The behavior of elliptical columns confined with FRP membranes subjected to axial loads was analyzed in a study conducted by Parvin and Schroeder [18]. The finite element analysis was performed using MSC Marc 2005 software program and the results obtained by FEM were compared with the experimental model developed by Teng and Lam (2002). Thus, they noticed that increasing the bending moment leads to an increase in normal and circumferential deformations on the opposite side of the eccentric load.

2. FINITE ELEMENT MODELING

In order to analyze through FEM the behavior of concrete columns strengthened with composite membranes, in ANSYS v'12 software were defined two identical RC columns, one unconfined and the second one confined with CFRP materials. The geometrical and mechanical characteristics of columns were alike with the experimental program that was carried out at the Faculty of Civil Engineering and Building Services of Iasi, Romania [19, 20].

From geometrical point of view, the columns were 1000 mm in height with a rectangular cross-section (250 x 250 mm), corner radius of 35mm and an identical distribution of the internal reinforcement. The longitudinal steel reinforcement was made of four deformed rebars of 12 mm diameter, whereas the transversal reinforcement consists of steel stirrups of 6 mm diameter plain bars spaced at 200 mm in the middle region of the specimen and at 84 mm to the ends of the column. The concrete cover up to the surface of the longitudinal steel bars was 25 mm. Since in the experimental program there were fixed six linear variable differential transducers (LVDTs) at the mid-height of the specimen, the obtained results were expressed for that region of the columns. To compare the experimental results with the FEM ones, the model was divided into three slices. For eccentric loading application special steel plates were designed and positioned on both ends of the columns (Figure 1), the load eccentricity being of 50 mm. The mechanical characteristics of concrete, internal reinforcement and CFRP membrane are given in Table 1. Nevertheless, for the concrete it was adopted the simplified bilinear stress –strain curve (Figure 2).

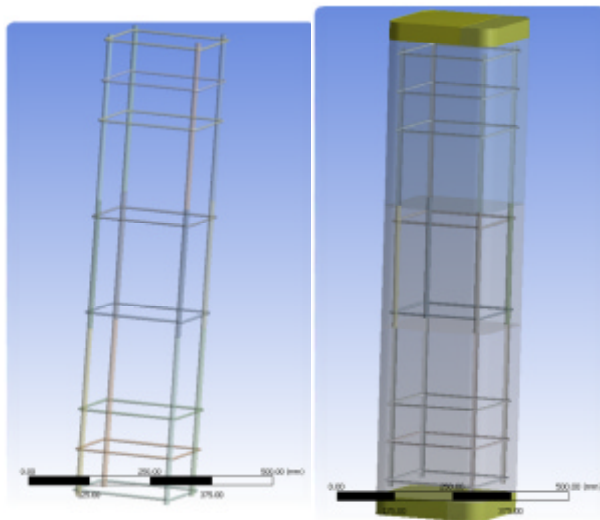


Figure 1. Column geometry defined with ANSYS software

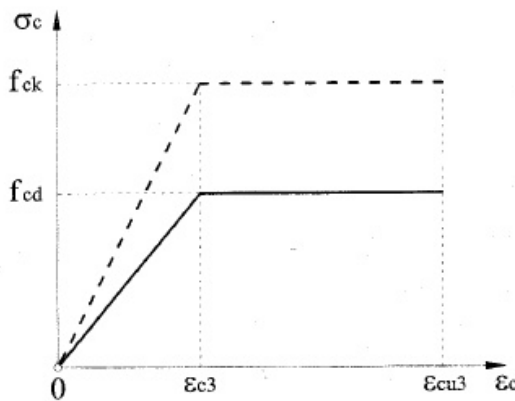


Figure 2. Simplified stress – strain curve for concrete

Table 1. Mechanical characteristics of materials defined in the model

	Unit of measure	Concrete	Longitudinal reinforcing bars	Transversal reinforcing bars	CFRP
Density	kg/m ³	2,300	7,850	7,850	-
Compressive strength	N/mm ²	32.34	-	-	750
Tensile strength	N/mm ²	3.05	355	255	800
Young modulus	N/mm ²	32,800	200,000	200,000	70,000
Poisson's ratio	-	0.2	-	-	0.25

The unconfined column was meshed using 248.043 nodes and 142.289 elements (Figure 3), while the confined column was meshed using 240.769 nodes and 134.468 elements. The eccentric loading of the elements was realized by assigning a linear uniformly distributed load at both ends of the column (Figure 4), equal with the maximum load obtained during the experimental tests. For the unconfined column the maximum experimental load was 5565 (N/mm), while for the confined column was 8467.5 (N/mm).

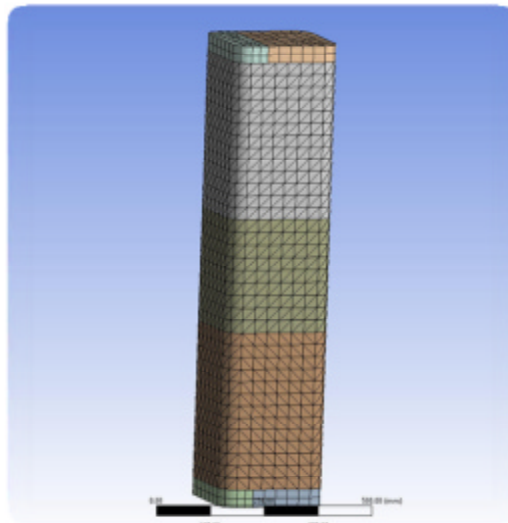


Figure 3. FE mesh

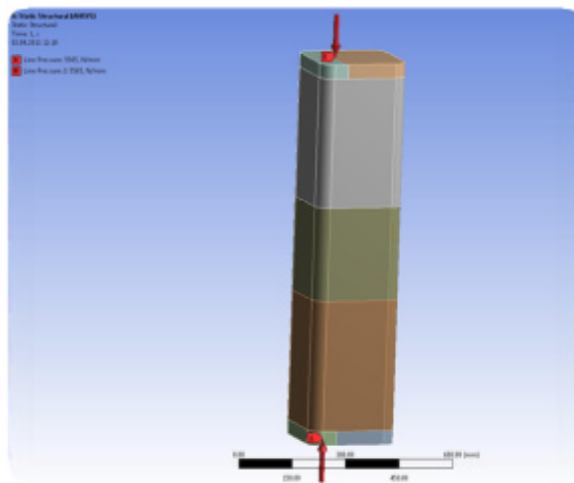


Figure 4. The eccentric loading of the elements

3. RESULTS AND DISCUSSIONS

After simulating the behavior of an unconfined and a CFRP confined RC column subjected to eccentric compression, a set of results were obtained and presented in this paper. After the FE analysis, in Figure 5 and Figure 6 are presented the

longitudinal and transversal displacements registered at the mid-height slice of the element, for the unconfined and the CFRP confined RC column. It can be stated that by applying the externally bonded confinement system the displacement for the RC columns increases.

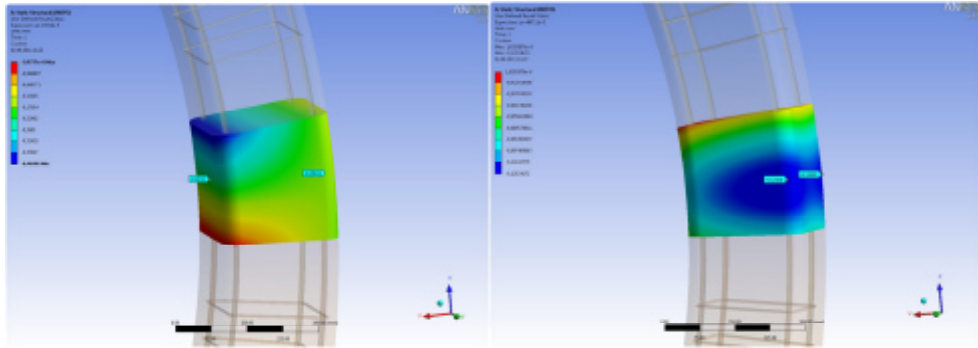


Figure 5. The longitudinal and transversal displacements for the unconfined element

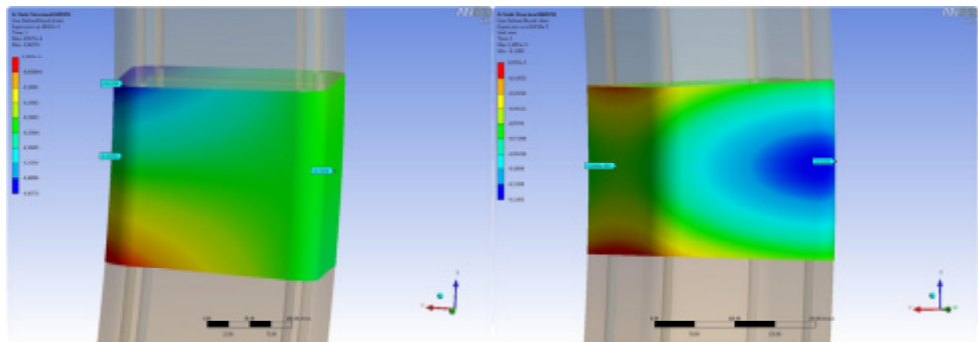


Figure 6. The longitudinal and transversal displacements for the CFRP confined element

In Figure 7 and Figure 8 are presented the axial stresses in a transversal cross-section, at the mid-height of the element, for the unconfined and the CFRP confined RC column. The FEM results are similar to the experimental ones. In the experimental program, the failure of the unconfined columns occurred in the compressed side due to concrete crushing. In the tensioned side, cracks developed in the transverse direction of the member, while in the compressed region it was observed the buckling of the longitudinal steel reinforcing bars. The externally strengthened columns failed by rupture of the CFRP jacket due to hoop tension and an important degree of concrete crushing was noticed, as well as, the buckled longitudinal steel bars. The CFRP jacket failure was initiated at a corner of the column at the most compressed side and occurred later on the tensile side [19]. It can be observed from Figure 7 and Figure 8 that the highest stress concentration is

at the compressed side of the elements and that by wrapping the RC column with one layer of CFRP membrane the elements can resist at higher loads and stresses.

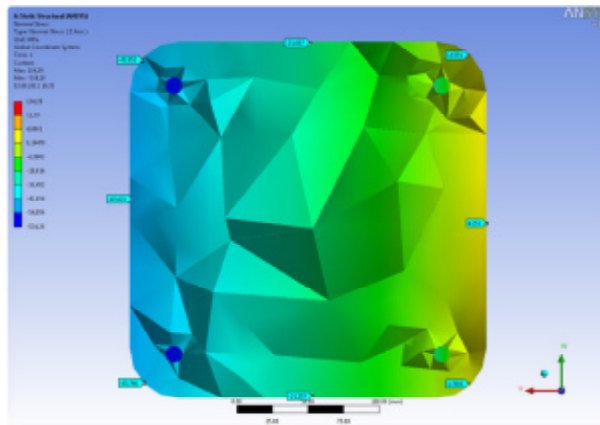


Figure 7. Axial stresses at the mid-height of the unconfined element, in the transversal cross-section

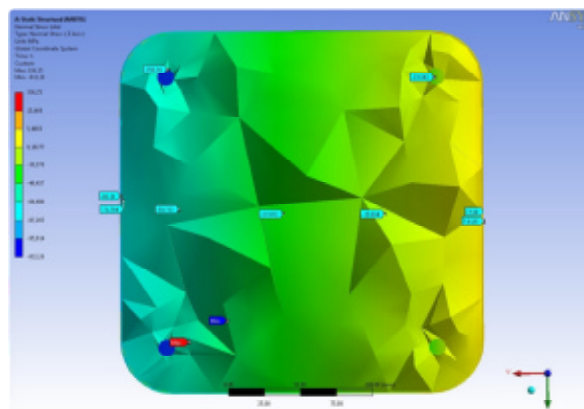


Figure 8. Axial stresses at the mid-height of the CFRP confined element, in the transversal cross-section

In Figure 9 are shown the comparative stresses for experimental and FEM for the unwrapped and wrapped RC columns with CFRP membranes.

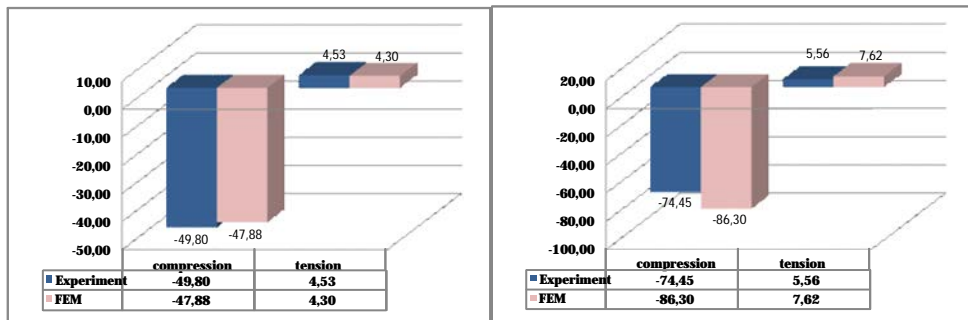


Figure 9. Axial stresses for the unconfined (left) and confined (right) RC columns

4. CONCLUSIONS

With FE analysis it is possible to model different elements with complex geometry, having various loading schemes and boundary, making it a very good alternative to the experimental programs and analytical approaches.

The evaluation of the structural response of rectangular RC columns confined with FRP composite membranes using FEM lead to satisfactory results, managing to describe in a satisfactory manner the confining effect of concrete using FRP systems. The simulations were performed using ANSYS v12 Workbench, finite element modeling program, in which the geometry configuration of the model closely approached to the experimental model, as well as the materials characteristics.

The confined column failed at a higher load level than the unconfined one. In case of elements subjected cu eccentric compression, by applying externally bonded CFRP membrane, the displacement and the stress level increased.

References

1. Rochette, P., Labossiere, P., A plasticity approach for concrete columns confined with composite materials, *Advanced Composite Materials in Bridges and Structures*, 1996.
2. Liu, J., Foster, S.J., Finite – Element Model for Confined Concrete Columns, *Journal of Structural Engineering*, Sept., 1998.
3. Mirmiran, A., Zagers, K., Yuan, W., Nonlinear finite element modeling of concrete confined by fiber composites, *Finite Elements in Analysis and Design*, 35, 2000.
4. Parvin, A., Wang, W., Behavior of FRP jacketed concrete columns under eccentric loading, *J. Compos. Constr.*, 5(3), 2001.

5. Montoya, E., Vecchio, F.J., Sheikh, S.A., Numerical evaluation of the behaviour of steel- and FRP-confined concrete columns using compression field modelling, *Engineering Structures*, 26, 2004.
6. Karam, G., Tabbara, M., Confinement effectiveness in rectangular concrete columns with fiber reinforced polymer wraps, *J. Compos. Constr.*, 9(5), 2005.
7. Chen, J.F., Pan, W.K., Three dimensional stress distribution in FRP-to-concrete bond test specimens, *Construction and Building Materials*, 20, 2007.
8. Banu, C., Taranu, N., Oltean, R., Cozmanciuc, C.I., Ionita, O.M, Finite Element Analysis of RC beams Reinforced with Fiber Reinforced Polymers Bars, *Proceedings of 7th International Symposium „Computational Civil Engineering 2009”*.
9. Koksai, H.O., Doran, B., Turgay, T., A practical approach for modelling FRP wrapped concrete columns, *Construction and Building Materials*, 23, 2009.
10. Nemecek, J., Padevet, P., Patzak, B., Bittnar, Z., Effect of transversal reinforcement in normal and high strength concrete columns, *Materials and Structures*, 38, Aug.-Sept., 2005.
11. Karabinis, A.I., Rousakis, T.C., Manolitsi, G.E., Three-Dimensional Finite Element Analysis of Reinforced Concrete Columns Strengthened by Fiber Reinforced Polymer Sheets, *FRPRCS-8*, University of Patras, Patras, Greece, July 16-18, 2007.
12. Karabinis, A.I., Rousakis, T.C., Manolitsi, G.E., 3D Finite – Element Analysis of Substandard RC Columns Strengthened by Fiber – Reinforced Polymer Sheets, *Journal of Composites for Construction*, ASCE, Sept./Oct., 2008.
13. Majewski, T., Bobinski, J., Tejchman, J., FE analysis of failure behaviour of reinforced concrete columns under eccentric compression, *Eng. Str.*, 30, 2008.
14. Parvin, A., Schroeder, J.M., FRP-confined rectangular concrete columns, *FRPRCS-8*, University of Patras, Patras, Greece, July 16-18, 2007.
15. Taranu, N., Munteanu, V., Oprisan, G., Budescu, M., Performance of FRP confined square RC columns, *FRPRCS-9*, Sydney, Australia, 2009.
16. Oprisan, G., Taranu, N., Munteanu, V., Experimental and numerical analysis of compressed concrete elements confined with FRP composites, *Computational Civil Engineering - International Symposium Iasi*, 2007.
17. Oprisan, G., Munteanu, V., Cozmanciuc, C., Taranu, N., Entuc, I., Particularities of structural response of confined RC columns with composite membranes, *Proc. of the International Scientific Conference VSU*, Sofia, 2009.
18. Parvin, A., Schroeder, J.M., Investigation of Eccentrically Loaded CFRP-Confined Elliptical Concrete Columns, *J. of Comp. for Constr.*, ASCE, 2008.
19. Cozmanciuc, C., Oprisan, G., Taranu, N., Munteanu, V., Oltean, R., Budescu, M., Structural behaviour of eccentrically loaded reinforced concrete columns confined with carbon fibre reinforced membranes, *The 11th International Scientific Conference VSU*, Sofia, Bulgaria, 2011.
20. Cozmanciuc, C., *Consolidarea Stâlpilor din Beton Armat cu Sectiune Necirculara prin Confinare cu Materiale Compozite*, Editura Politehniun, Iasi, România, 2011 (in Romanian).

Nonlinear analysis in finite element program Abaqus

Gabriela Dascalu

*Department of Concrete Structures, Building Materials, Technology and Management, "Gh. Asachi"
Technical University of Iasi, Faculty of Civil Engineering and Building Services, Iasi, 700050,
Romania,*

Summary

Nonlinear analysis is a research activity which assumes to establish the inelastic behavior of two principal components (steel and concrete) from which reinforced concrete is made and consider it in performing the numerical simulations and analytical calculations. The principal aim of this activity is to understand the real elastic-plastic response of structural assemblies in order to ensure the comfort and safety request and imposed by norms and standards through the design process. Presently, in construction domain, exists many programs for analysis, using the "finite element" concept, which facilitates the work of researches and design engineers and the obtained results are closed, or even identical, with those from reality. The present paper aims to describe such type of program, called Abaqus/CAE and to present results obtained on physical models based on reinforced concrete elements with voids.

Keywords: reinforced concrete, structural response, numerical simulation, stress states

1. INTRODUCTION

The structural analysis of an assembly has as first objective to establish the distribution either of stresses, either of strain and displacement which are developed inside of all structure or only in certain type of component elements. [4]

In order to make resistance calculation, according with existing norms and standard, it is necessary, in a first step, to model the geometry of analyzed structure, and also to model the constitutive materials behavior.

It is known that the reinforced concrete is a composite material, having 2 principal components (concrete and steel), each with higher properties to different type of loads. Thus, the concrete presents a higher resistance to compression and a small one to tension, while the steel has the capability to take the strong forces due to

tension efforts. To model the behavior of this material, it is absolute necessary to model separately his 2 components, so that to be respected the condition imposed through norms, according which the models created to be conformed to reality and to the problems analyzed.

Modeling the constitutive materials behavior is a process through which is schematic by characteristics curves using some simple deformed models. At the end of this processes result 3 principal categories of materials: with linear behavior, with plastic behavior and with nonlinear behavior.

The final objective of numerical simulations is to obtain the necessary information which can be used in order to determine the sectional efforts developed inside the structural elements. These simulations are often made with programs special designed, based on theoretical aspects, this use being justify by the advantages obtained: the possibility to create models with different shape and dimensions, possibility to modify the type and/or value of loads applied so that can be performed analysis in a short time and reduce work and also with economical efforts relatively low than in experiments and the conclusions and results in both situations being closely.

At international level, exist a variety of such programs, from which are mentioned few like: DIANA, ANSYS, ABAQUS/CAE, ROBOT, SAP etc.

2. GENERAL DESCRIPTION OF NONLINEAR MODELS

Abaqus/CAE software provides the capability of simulating the damage using either of the two crack models for reinforced concrete elements: (1) Smearred crack concrete model and (2) Concrete damaged plasticity model. [5]

In Abaqus/CAE software, reinforcement in concrete structures is typically provided by means of rebars, which are one-dimensional rods that can be defined singly or embedded in oriented surfaces and used with metal plasticity models to describe the behavior of the rebar material and are superposed on a mesh of standard element types used to model the concrete. With this modeling approach, the concrete behavior is considered independently of the rebar. Effects associated with the rebar-concrete interface, such as bond slip and dowel action, are modeled approximately by introducing some “tension stiffening” into the concrete modeling to simulate load transfer across cracks through the rebar.

2.1 Model CSC – Concrete smearred cracking

The “concrete smearred cracking” model (CSC) is intended for modeling and analysis of all types of reinforced concrete structures, including beams, trusses,

shells, solids etc. and it was created for applications that are subjected to monotonic straining at low confining pressures. Uses oriented damaged elasticity concepts (smeared cracking) to describe the reversible part of the material's response after cracking failure. [5]

A particularity of this model is that assumes the cracking to be the most important aspect of the behavior, and because of this reason the representation of cracking and postcracking behavior dominates the modeling. Cracking is assumed to occur when the stress reaches a failure surface so called the “crack detection surface”, which represent a linear relationship between the equivalent pressure stress, p , and the Mises equivalent deviatoric stress, q . [5]

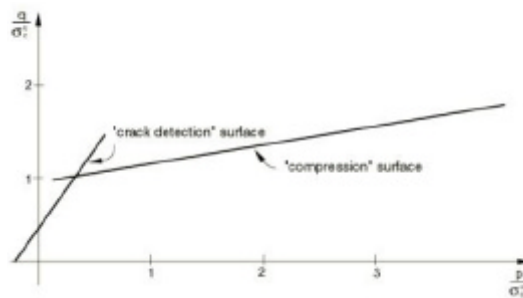


Figure 1 – Failure surface in (p-q) plane [5]

Cracks are irrecoverable: they remain for the rest of the calculation, but may be open and close. No more than three cracks can occur at any point (two in a plane stress case, one in a uniaxial stress case). Following crack detection, the crack affects the calculations because a damaged elasticity model is used. The concrete model is a smeared crack model in the sense that it does not track individual “macro” cracks. Constitutive calculations are performed independently at each integration point of the finite element model. The presence of cracks enters into these calculations by the way in which the cracks affect the stress and material stiffness associated with the integration point. [5]

The postfailure behavior for direct straining across cracks is modeled with tension stiffening, which allows defining the strain-softening behavior for cracked concrete. This behavior also allows for the effects of the reinforcement interaction with concrete to be simulated in a simple manner. Tension stiffening is required in the concrete smeared cracking model and it can be specified by means of: [5]

- a postfailure stress-strain relation (fig. 2a) – a specification of strain softening behavior in reinforced concrete generally means specifying the postfailure stress as a function of strain across the crack. In cases with little or no reinforcement this specification often introduces mesh sensitivity in the analysis results in the sense that the finite element predictions do not converge

to a unique solution as the mesh is refined because mesh refinement leads to narrower crack bands. This problem typically occurs if only a few discrete cracks form in the structure, and mesh refinement does not result in formation of additional cracks. If cracks are evenly distributed (either due to the effect of rebar or due to the presence of stabilizing elastic material, as in the case of plate bending), mesh sensitivity is less of a concern.

- a fracture energy cracking criterion (fig. 2b) – Hillerborg (1976) defines the energy required to open a unit area of crack as a material parameter, using brittle fracture concepts. With this approach the concrete's brittle behavior is characterized by a stress-*displacement* response rather than a stress-*strain* response. Under tension a concrete specimen will crack across some section. After it has been pulled apart sufficiently for most of the stress to be removed (so that the elastic strain is small), its length will be determined primarily by the opening at the crack.

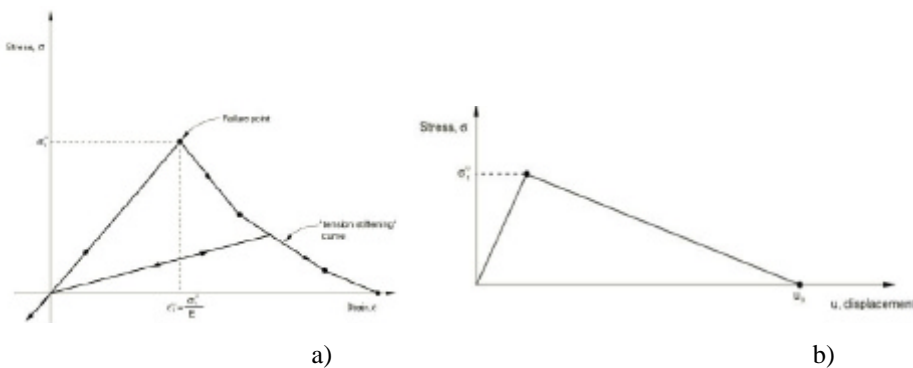


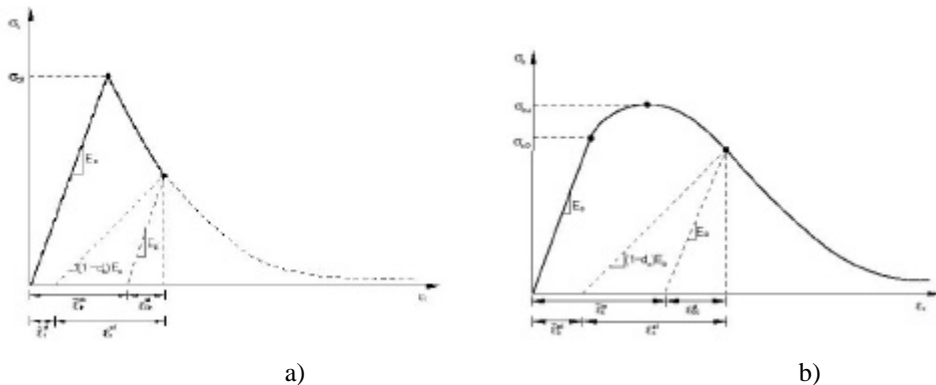
Figure 2 – Tension stiffening: a) stress-strain relation;
b) fracture energy cracking criterion [3]

2.2 Model CDP – Concrete damage plasticity

The “concrete damage plasticity” model (CDP) it was design for modeling all types of structures from reinforced concrete and other quasi-brittle materials, which are subjected to monotonic, cyclic, and/or dynamic loading under low confining pressures. Uses concepts of isotropic damaged elasticity in combination with isotropic tensile and compressive plasticity to represent the inelastic behavior of concrete and consists of the combination of nonassociated multi-hardening plasticity and scalar (isotropic) damaged elasticity to describe the irreversible damage that occurs during the fracturing process. [5]

The model is a continuum, plasticity-based, damage model for concrete. It assumes that the main two failure mechanisms are tensile cracking and compressive crushing of the concrete material (fig. 3). The evolution of the yield (or failure)

surface is controlled by two hardening variables, and linked to failure mechanisms under tension and compression loading, respectively.



a) cracking strain;
b) crushing strain in CDP model [5]

The degradation of the elastic stiffness is characterized by two damage variables, d_t and d_c , which are assumed to be functions of the plastic strains, temperature, and field variables. The damage variables can take values from zero, representing the undamaged material, to one, which represents total loss of strength.

Same as the other nonlinear model, the CDP model requires defining the tension stiffening and it can be done using the same concepts of stress-strain relation and stress-displacement relation. In reinforced concrete the specification of postfailure behavior generally means giving the postfailure stress as a function of cracking strain, ϵ_c^H , (fig. 3a) defined as the total strain minus the elastic strain corresponding to the undamaged material.

It can be defined the stress-strain behavior of plain concrete in uniaxial compression outside the elastic range. Compressive stress data are provided as a tabular function of inelastic (or crushing) strain, ϵ_c^M , (fig. 3b) and, if desired, strain rate, temperature, and field variables. [5]

The fracture energy cracking model can be invoked by specifying the postfailure stress as a tabular function of cracking displacement (fig. 4a) and alternatively, the fracture energy, G_f , can be specified directly as a material property; in which case, it has to be define the failure stress, σ_{t0} , as a tabular function of the associated fracture energy. This model assumes a linear loss of strength after cracking. (fig. 4b)

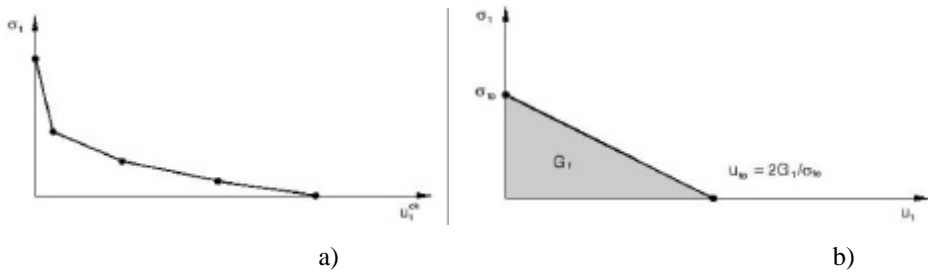


Figure 4 – Postfailure curve for tension stiffening: a) stress-displacement;
b) stress-fracture energy [5]

3. RESULTS OF ANALYSIS

The model analyzed in this study is represented by a strip, cut from the slab of an entire reinforced concrete structure, in order to simply the action of performing the nonlinear analysis and to reduced considerably the time that would be necessary to run the analysis. The length of this strip is $L=11250$ mm, the width is equal to 620 mm and the thickness of the voided slab is 230 mm, with 180 mm sphere diameter. The boundary conditions are placed in the zones which represent the contact area between the slab and the column.

Concrete used to design the strips in this study is C25/30 and the reinforcement is made from steel Pc52 with 18 mm diameter.

The physical model, together with the materials properties, was introduced in program and was run the nonlinear analysis, using both nonlinearity models consists in the program (CDP and CSC model). The results obtained in this two cases offers necessary information regarding the plastic deformations state (fig. 5) and load-displacement curve (fig. 6), information that is useful in the entire design process of these new constructive systems.

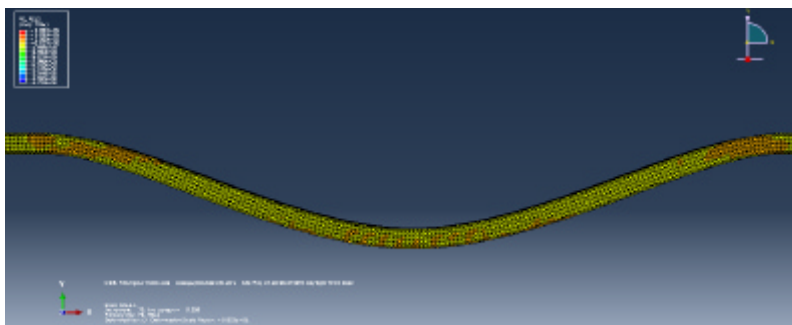


Fig. 5 – Plastic deformations state

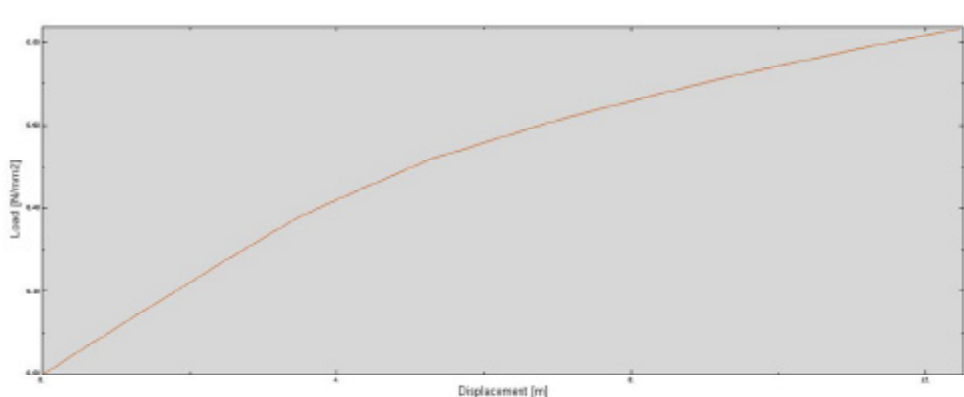


Fig. 6 – Load-displacement curve

3. FINAL CONCLUSIONS

Obtaining the deformation states in concrete elements is an important step in the design process because it provides essential information regarding assemblies' response to action of external loads. Based on the conclusions obtained, the designer defines the characteristics of the resistance structure and activities must be conducted so that the final products to ensure the comfort and safety wanted by the owners and imposed through the existing norms.

The nonlinear analysis performed using the finite element program Abaqus/CAE for the new voided slab system emphasizes the similarity with classical full slab system, so that the following research activities can be made using the theoretical aspects from the literature in domain, making, where is request, the necessary changes, in order to have accurate results, close to reality.

References

1. Pascu, R., *Comportarea si calculul elementelor din beton armat*, Ed. AGIR, Bucuresti, 2008.
2. Nilson, A.H., Darwin, D., Dolan, C., *Design of concrete structures*, Forth Edition, Mc Graw Hill, New York, 2010;
3. Ghali, A., Favre R., Elbadry, M., *Concrete structures-stresses and deformations*, Third Edition, Spon Press, New York, 2006;
4. ***Eurocod 2 – Proiectarea structurilor din beton armat
5. *** Manual de utilizare program Abaqus/CAE
6. www.simulia.com

Computer based assessment of building energy performance

Laura Dumitrescu, Dan Preda Stefanescu

Department of Civil and Industrial Engineering, "Gheorghe Asachi" Technical University of Iasi, Iasi, 700050, Romania

Summary

In the last decades, the tendency for energy-efficient construction became predominant in the building industry, because of the new regulations regarding resource conservation and environmental impact minimisation. The new standards refer both the construction of new buildings (passive houses, zero-energy buildings, etc.) and the rehabilitation of the existing ones with the target of energy savings.

The use of computer programs is a valuable aid in building energy calculations for two main purposes: (a) calculation of temperature distribution, heat streams and vapour diffusion streams within building elements, in two and three dimensional stationary and transient heat flow simulation, and (b) balance energy calculation for the entire building.

This paper presents a brief comparative study using two programs for thermal field simulation for a detailed thermal bridge calculation. A simplified method to include the thermal bridge effect into the assessment of the building energy performance is also proposed.

KEYWORDS: buildings, energy performance, thermal bridge, heat transfer.

1. INTRODUCTION

The energy conservation in buildings is the most important requirement for sustainable construction. It allows the reduction of the fossil fuel consumption and the correspondent pollutant emissions and opens the possibility of using locally produced clean renewable energy (solar, biogas, wind). This is a "sine qua non" condition for the new generation of low-energy houses and passive houses.

The building specialists from different countries made a significant effort to find global indicators to assess the energy performance of buildings and to unify national standards with European ones. Early performance indicators focused on thermal insulation of the building, and the most recent ones focus on primary energy needs - ‘primary energy’ means energy from renewable and non-renewable sources which has not undergone any conversion or transformation process [1].

Obviously, in this way reflects a multitude of factors: compactness of the building, composition of all elements of building envelope, heating, cooling, lighting, hot water, household equipment, solar collectors, photovoltaic devices, heat pumps, heat storage, urban networks for secondary energy transport (heat, electricity) and power plant where fuel is processed.

These indicators refer to the energy requirements in conventional conditions; the actual energy consumption also depends on the state of elements of construction and installation, climatic factors and the type of occupancy showing random variation.

2. NUMERICAL INDICATORS FOR ENERGY PERFORMANCE OF BUILDINGS

The main types of energy performance indicators that can be used to assess buildings are:

a) Indicators for assessing transmission heat losses through the building envelope, such as:

- *Transmission heat transfer coefficient*, H_T (W/K), which is the heat flow rate due to thermal transmission through the fabric of a building, divided by the difference between the environment temperatures on either side of the construction [2];

- Mean adjusted coefficient of thermal transmission U'_m and mean adjusted specific thermal resistance R'_m ($R'_m=1/U'_m$), used in the C107 series of Romanian norms [3] and calculated by the equation (1):

$$U'_m = \frac{\sum (A_i \cdot \tau_i \cdot U'_i)}{A}, [\text{W/m}^2\text{K}] \quad (1)$$

where:

A_i is the area of the element i of the building envelope, and $A=\sum A_i$ (m^2);

U'_i is the adjusted coefficient of thermal transmission of element i of the building envelope ($\text{W/m}^2\text{K}$);

τ_i is the coefficient for the temperature correction (-).

b) Indicators for assessing the overall heat losses in buildings:

According to [4], these indicators are the *volume coefficient of heat loss* F_V ($\text{W/m}^3\text{K}$) and the *surface coefficient of heat loss* F_S ($\text{W/m}^2\text{K}$); the surface can be, optionally, the area of the building envelope, the heated area, etc. Such an indicator, used in Romania and defined by the C107 regulations is the *global coefficient of thermal insulation* G (for dwellings) and $G1$ (for buildings other than dwellings destination). The value of G is a building characteristic and represents the energy necessary to compensate the heat losses through transmission and ventilation corresponding to 1 m^3 of heated volume, caused by a temperature difference of 1K and is calculated by the equation (2):

$$G = \frac{\sum \frac{A_i}{R'_i} \cdot \tau_i}{V} + 0.34 \cdot n, [\text{W/m}^3\text{K}] \quad (2)$$

where:

A_i is the area of the element i of the building envelope (m^2);

R'_i is the adjusted specific thermal resistance of element i of the building envelope ($\text{m}^2\text{K/W}$);

τ_i is the coefficient for the temperature correction (-);

V is the internal heated volume (m^3);

n is the natural ventilation rate of the building, i.e. the number of air changes per hour (h^{-1}).

c) Indicators for assessing the necessary of thermal energy

These indicators are based on the energy balance of building, and the most known method is the standard SR EN ISO 13790:2008 *Energy performance of buildings* –

calculation of energy use for space heating and cooling. There are also many buildings’ thermal simulation programs which use a short-time step in calculations (typically one hour) and which calculate at the same time the heating and cooling energy needs and the interior temperature (e.g. EnergyPlus, Lesosai, EPIQR, CASAnova, etc.).

According to the C107 norms, the annually necessary of thermal energy for 1 m³ of heated volume is estimated with the relation (3):

$$Q = \frac{24}{1000} CN_{12}^{\theta} G - (Q_i + Q_s), \text{ [kWh/m}^3\text{year]} \quad (3)$$

where:

C is the correction coefficient (-);

N_{12}^{θ} is the number of the degrees-days per year characteristic for the locality where the building is placed (Kdays);

G is the global coefficient of thermal insulation of the building (W/m³K);

Q_i is the usable energy gains resulted from the building habitation (kWh/m³year);

Q_s is the usable solar energy gains (kWh/m³year).

Calculation of heat balance of buildings is difficult because of the three-dimensional domain, the complexity of geometry and composition of envelope elements, the effect of air movement, sunshine, time variation in temperature and humidity, etc. Therefore, most foreign and Romanian norms support the following simplifying assumptions:

-Steady-state conditions;

-Physical characteristics are independent of temperature and humidity;

-There are no heat sources inside the building elements.

d) Indicators for assessing the necessary of primary energy

Such indicators have started to be used in technical regulations published after 2000. The necessity of using a numeric indicator of primary energy use, based on primary energy factors per energy carrier, which may be based on national or regional annual weighted averages or a specific value for on-site production is stated in the EU legislation [1].

For a more relevant and comprehensive assessment of buildings impact on the environment in terms of energy consumption, the performance indicator should relate to *specific primary energy consumption over the lifetime of the building*, i.e. taking into account the embodied energy. This is particularly so since the report embodied energy/exploitation energy has changed considerably in recent years,

decreasing from values of 1:7 for older buildings to values around 1:3 for new low energy buildings [5].

Use of each indicator has advantages and disadvantages, the choice must be made depending on the purpose of the study, the life cycle stage of construction (construction, use, refurbishment), the available simulation programs, etc.

3. EVALUATION OF TRANSMISSION HEAT LOSSES

Not all European countries consider the influence of thermal bridges in their regulations for new buildings and even less for the renovation of the existing ones, because the correct calculation of linear thermal transmittance is quite laborious. However, buildings can contain significant thermal bridges, their total impact on the heating energy need is in general considerable and can be as high as 30% [6].

The direct heat transfer coefficient between the heated space and the exterior through the building envelope is defined by the equation (4):

$$H_D = \sum_i A_i U_i + \sum_j l_j \psi_j + \sum_k \chi_k, \text{ [W/K]} \quad (4)$$

where:

A_i is the area of element i of the building envelope (m^2);

U_i is the thermal transmittance of element i of the building envelope ($\text{W}/\text{m}^2\text{K}$);

l_j is the length of linear thermal bridge j (m);

ψ_j is the linear thermal transmittance of thermal bridge j (W/mK);

χ_k is the point thermal transmittance of point thermal bridge k (W/K).

To apply the calculation method, building-element dimensions are usually measured according to one of three systems (Figure 1): internal (in France), overall internal (in Romania), and external (optional Germany). Therefore, the term $\sum_i A_i U_i$ and the values of ψ_j are different, so they will be noted below with $\psi_{j,i}$, $\psi_{j,oi}$, $\psi_{j,e}$ and $A_{i,i}$, $A_{i,oi}$, $A_{i,e}$, respectively (index i for internal, oi for overall internal, and e for external dimension system).

In Figure 1, the numbers have the following meaning:

- 1- internal dimension (measured from wall to wall and floor to ceiling inside a room of a building);
- 2- overall internal dimension (measured on the interior of a building, ignoring internal partitions);
- 3- external dimension (measured on the exterior of a building).

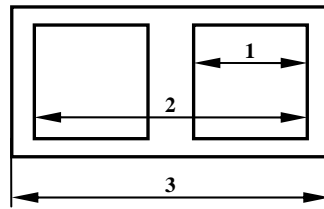


Figure 1. Dimensions systems

Using external dimensions may be preferred because it includes the total area of the envelope and is easier to calculate. It covers partly the additional losses due to thermal bridges. Consequently, the values of ψ_j are generally smaller for external dimensions, and can even be negative in some cases such as external corners. According to [2], when the main insulating layer (the layer with the highest thermal resistance in the elements flanking the potential thermal bridge) is continuous and of uniform thickness, with special attention to limit thermal bridge effect, the linear and point thermal transmittance may be neglected if external dimensions are used. This significantly simplifies the calculation, which is acceptable since a large number of parameters (thermal conductivity, thickness, climate regime, internal temperature, etc.) have random variation that deviate significantly from the conditions considered in the deterministic calculation. Corrections for other cases may be defined on a national basis. Traditionally, the alternatives available to designers for assessing thermal bridges have involved:

- to use thermal bridge atlases with ψ and χ values (for example, in C107 Romanian norms), but sometimes they are not a real help in solving specific problems;
- to perform detailed thermal bridge simulation, expensive and not at all part of the daily practice.

Other alternative could be the use of catalogs containing more flexible databases, such as the KOBRA software and EUROKOBRA database, offering a computerised thermal bridge atlas for 2-dimensional details. The main characteristics of this atlas is its user friendliness, the large flexibility of modifying the detail (layer thickness, materials, boundary conditions, etc.) and the way of presenting the results (e.g. color pictures showing the isothermal lines, the heat flux lines) [7].

4. COMPARATIVE STUDY REGARDING THE ENERGY PERFORMANCE OF A BUILDING

A typical dwelling building (Figure 2) was considered as a case study for the calculation of the thermal performance indicators.

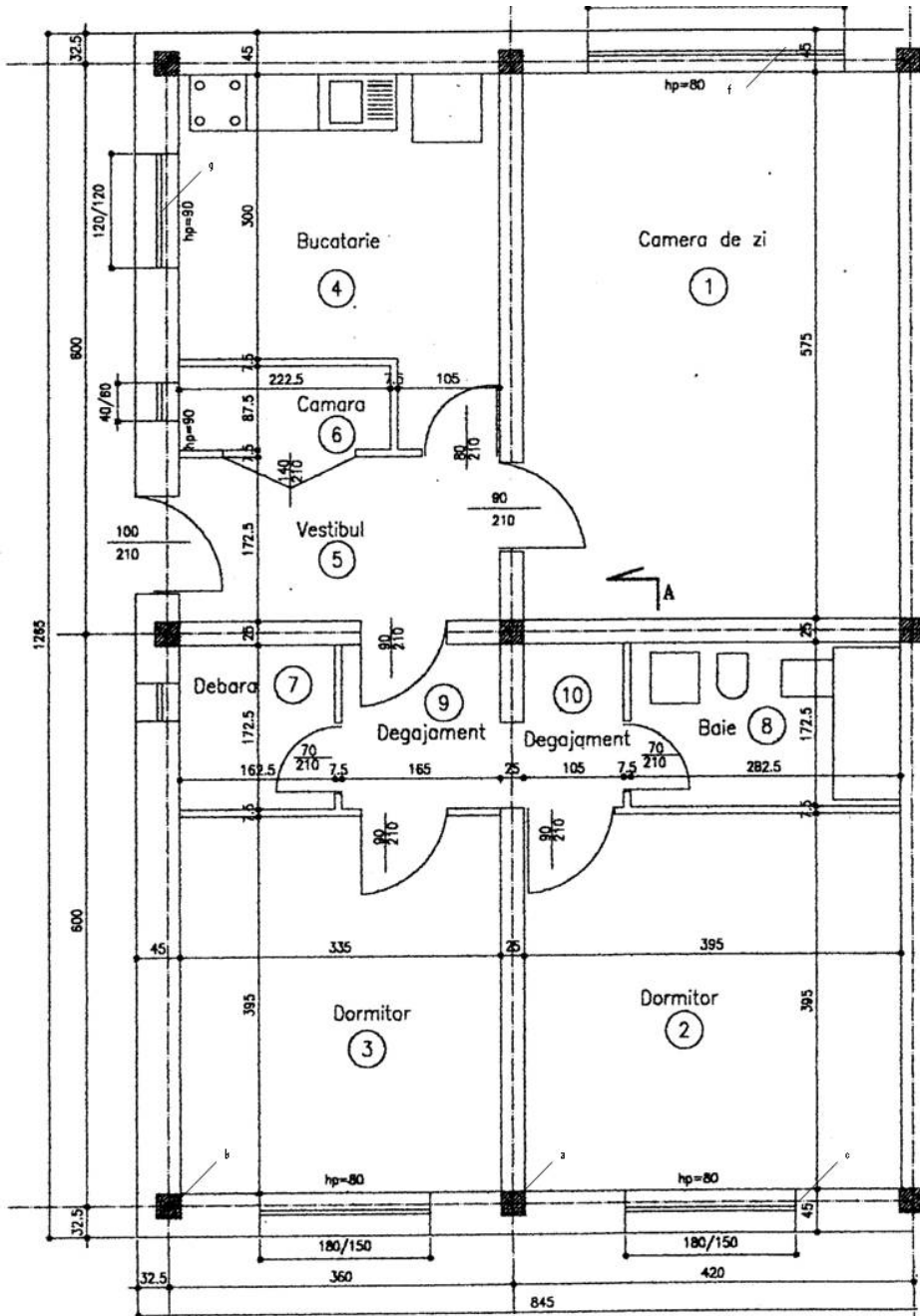


Figure 2. Ground floor plan

The building has two apartments of three rooms and it has ground floor, general basement and terrace roof. Bearing structure consists of bearing masonry of bricks and reinforced concrete cores of 25 cm thickness and reinforced concrete slabs of 15 cm thickness. Thermal insulation is from cellular polystyrene and it is protected by a half brick masonry. The quality of the constructive solutions is not covered by this analysis. The glazed areas have wooden frames and regular windows. The building is placed in the 2nd climatic zone ($T_e = -15\text{ }^\circ\text{C}$) and the temperature in the basement is $T_u = 2.5\text{ }^\circ\text{C}$. Given the symmetry of the building, all calculations are performed for an apartment. Building project has been drawn up in 1997. The thermal bridge details are presented in Figure 3.

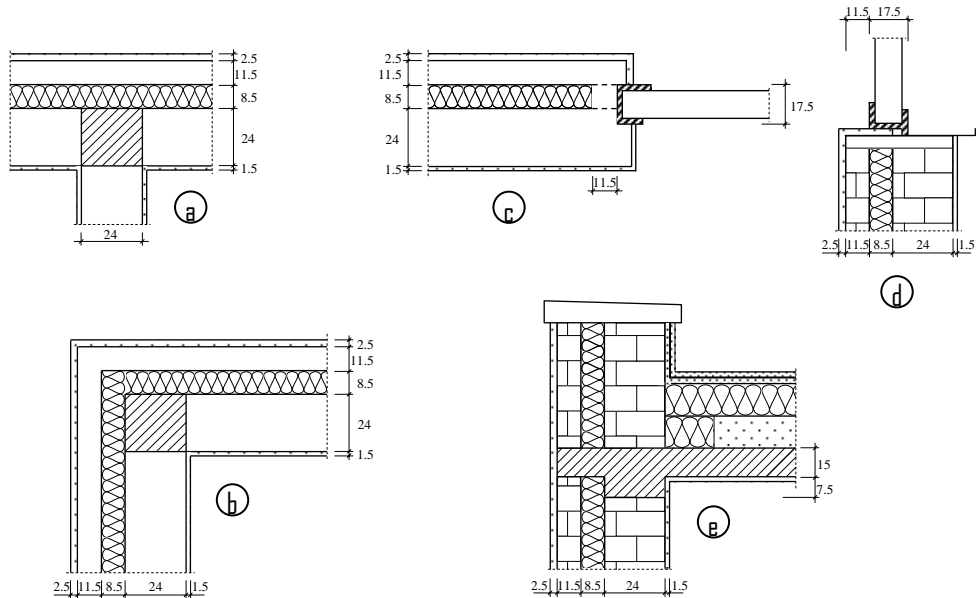


Figure 3. Thermal bridge details

The following energy efficiency indicators have been calculated:

- Mean adjusted coefficient of thermal transmission U'_m ($\text{W}/\text{m}^2\text{K}$);
- Global coefficient of thermal insulation G ($\text{W}/\text{m}^3\text{K}$);
- Annually specific energy demand for heating Q ($\text{kWh}/\text{m}^2\text{year}$).

The values of the linear thermal transmittance of thermal bridges have been determined both by numerical simulation and using EuroKOBRA program and the results are presented in Table 1, for the following methods of calculation:

- Case 1 – ψ_{oi} values according to the tables of normative C 107-2005;

- Case 2 – ψ_{oi} values obtained by numerical modeling;
- Case 3 – ψ_e values obtained by numerical modeling;
- Case 4 – ψ_i values according to EuroKOBRA thermal bridge catalog;
- Case 5 – ψ_e values according to EuroKOBRA thermal bridge catalog.

Table 1. Values of the linear thermal transmittance ψ (W/mK)

Thermal bridge	Scheme	ψ (W/mK)				
		Case 1	Case 2	Case 3	Case 4	Case 5
a – Wall „T” joint		0.01	0.019	0.003	0.055	0.005
b – External corner		0.09	0.093	-0.086	0.090	-0.090
c – Window reveal		0.06	0.047	0.047	0.030	0.030
d – Windowsill		0.17	0.218	0.218	0.210	0.200
e – Attic		0.27 0.35	0.366 0.534	0.340 0.147	0.680	0.370
f – Lintel, h=50cm		0.38 0.31	0.543 0.461	0.512 0.173	0.900	0.780
g – Lintel, h=70cm		0.40 0.31	0.603 0.490	0.570 0.209	0.980	0.860
h – Vertical joint with inferior slab		0.17 0.20	0.214 0.314	0.226 -0.130	-	-
i – Partition wall		0.11	0.202	0.166	-	-
j – Internal wall		0.25	0.369	0.332	-	-

The differences between values of the same coefficient (ψ_{oi} - cases 1 and 2, respectively ψ_e - case 3 and 5), are due to working assumptions adopted in each

case. Because EuroKOBRA catalog does not provide details for all types of thermal bridges of the building, energy efficiency indicators were calculated only for the first three cases, using ψ values, lengths and areas according to the correspondent dimensions system (overall internal and external, respectively). The results are presented in Table 2.

Table 2. The values of the thermal performance indicators of the building

	U'_m (W/m ² K)	G (W/m ³ K)	Q (kWh/m ² year)
Case 1	0.524	0.825	169.30
Case 2	0.579	0.883	183.66
Case 3	0.476	0.877	182.28

The results presented in Table 2 show relatively large differences between the values calculated using the same dimensional systems, depending on simulation software, work assumptions and simplifications adopted (cases 1 and 2) as follows: U'_m - 10.5%, G - 7 % and Q - 8.5%. Comparing the results obtained in cases 2 and 3, there is a big difference for U'_m indicator (21.6%), normal because the area varies greatly (overall internal dimensions, and external), but very similar values for G and Q indicators (difference of 0.7%).

To simplify calculations, it could be more convenient that all these indicators to be calculated using unidirectional thermal resistance values and applying an increase in U_m value. The calculation is made using external dimensions of the building and applying the following increases of the mean coefficient of thermal transmission U_m :

-For corrected thermal bridge: $\Delta U \leq 0.05$ W/m²K;

-For common thermal bridges: $\Delta U = 0.10$ W/m²K;

-For major thermal bridges: $\Delta U \geq 0.20$ W/m²K.

The mean adjusted coefficient of thermal transmittance U'_m for the analyzed building will be calculated with the relation (5):

$$U'_m = \frac{\sum \frac{A_i \cdot \tau_i}{R_i}}{\sum A_i} + \Delta U, \text{ [W/m}^2\text{K]} \quad (5)$$

where $\Delta U = 0.10$ W/m²K, supplement of unidirectional heat transfer coefficient, which takes into account the influence of thermal bridges.

The relation for calculating the G indicator is obtained from equations (2) and (5) and it is given by (6):

$$G = \frac{\sum \frac{A_i \cdot \tau_i}{R_i} + \Delta U \cdot \sum A_i}{V} + 0.34 \cdot n, [\text{W}/\text{m}^3\text{K}] \quad (6)$$

The values of the three energy performance indicators are $U'_m=0.468 \text{ W}/\text{m}^2\text{K}$, $G=0.867 \text{ W}/\text{m}^3\text{K}$, and $Q=179.79 \text{ kWh}/\text{m}^2\text{year}$, very similar (differences 1.1-1.7%) of those obtained by calculation based on numerical modeling of thermal bridges (external dimensions).

5. CONCLUSIONS

The necessity of energy conservation in buildings is an important requirement for achieving sustainable development in construction. The ambition of the European Commission is for new European buildings to become “near zero energy buildings” in 2020.

The impact of thermal bridges in energy performance of buildings cannot be neglected and should be included in the calculation methods, although the correct calculation of linear thermal transmittance is quite laborious.

In conclusion, besides the development of thermal bridge catalogs as large as possible and including current technical solutions, a very useful solution is to adopt a simplified methodology, allowing calculation of transmission heat losses using unidirectional thermal resistance values (much easier to calculate) with default values for including the increased thermal losses due to thermal bridges, as proposed in this paper.

References

1. Directive 2010/31/EU of the European Parliament and of the Council of 19 May 2010 on the energy performance of buildings
2. SR EN ISO 13789:2008 Thermal performance of buildings – Transmission and ventilation heat transfer coefficients – Calculation method
3. C107-2005 Regulation regarding thermal calculation of the construction elements of buildings (in Romanian)
4. SR EN ISO 7345:1995 Thermal insulation – Physical quantities and definitions
5. Tywoniak, J. – *Thermal performance of buildings and building components – Tool on the way to sustainable buildings*, First International Seminar on environmental compatibility of structures and structural materials, Prague, 4-5 May 2000
6. Erhorn-Kluttig, H., Erhorn, H. – *Impact of thermal bridges on the energy performance of buildings*, Information Paper P148 of EPBD Buildings Platform, 27.03.2009
7. Wouters, P., Schietecat, J., Standaert, P. – *Practical guide for the hygrothermal evaluation of thermal bridges*, a SAVE-KOPRACTICE-project document, 7.05.2003

Improvement proposal for URGENT1 - Software for planning and simulation of emergency evacuation using auto transport

Augustin-Ionut Gavrilă¹, and Neculai Scîntei²

¹ Computer Science Ph.D. Candidate, "Gh.Asachi" Technical University, Iasi, Romania

² Civil Engineering Ph.D. Candidate, "Gh.Asachi" Technical University, Iasi, Romania

Summary

The software URGENT1 was applied in a case study that simulated and planned decisions regarding population evacuation in emergency situations in a particular area. This program resolved the following problems: transportation plan, the making of the convoys, displacement itineraries, diagrams of population evaluation, it generated maps with information's regarding places, convoys, road segments, being of real use in training personnel that is responsible of population evacuation in cases of emergency.

KEYWORDS: emergency situation, population evacuation, simulation, deployment itinerary, evacuation diagrams, transport plans.

1. INTRODUCTION

The software for simulation, planning and optimization of decisions in risk and uncertainty conditions, considering population evacuation with auto transport means, took into consideration areas with different degrees of urgency, the road transport system, the existing and supplementary auto transport base using heuristics for a better time schedule of evacuation and having a final purpose of mineralizing risk taking.

The software URGENT1 was applied at a given study case for simulating, planning and optimizing decision making regarding population evacuation in emergency situations from an area affected for one day and 17 hours with a positive result. This software resolved the following problems: transport plan, map generation with information's referring to areas, convoys, road segments – at 10 minutes interval having the possibility of being of real help for personnel training in evacuation techniques (extended – of material property also) in emergency situations.

The purpose of this software is to be used at institutional level and also at the level of local administration for the preparation of personnel and population in case of disaster. Using this resource will lead to economy to budgets both financial and material and mainly it would save human life.

The program Urgent1 may be improved including new parameters and extending at regional and national level, eventually a distributed algorithmic approach can be used instead of the centralized-sequential existent solution. The software can contribute to the fulfillment of the imposed goal found in the National Strategy concerning prevention of emergency situations and national centralized evacuation of property and people. Also, it can be taken in consideration the dynamic adjustment of emergency degrees of different areas during running of the software. This will result in a rescheduling of the population evacuation concerning initially omitted information's that affect the current state of evacuation.

2. PROPOSED IMPROVEMENTS FOR STRATEGIES, METRICS AND EVACUATION ALGORITHM

2.1. Algorithm of evacuation example

It may be considered a meta-algorithm that must imply the automatic generation of possible strategies with the calculations made in parallel on a distributed calculus architecture (cluster/grid/cloud-computing).

Through the comparisons of the obtained results and retaining optimum values for the computed possible scenarios the following algorithm will appear:

```
bestStrategy=NULL;
MaximumUtility= - 8 ;
```

```
Foreach**(strategy ? GeneratedPossibleStrategies)
```

```
//computed in parallel, on a cluster/grid/cloud/other distributed systems
```

```
/**: examples of strategies:
```

```
//MaximumProfit:
```

```
MaximalDistance/MaximalPopulation/MaximalEmergencyDegreeEvacuation...
```

```
//MinimumRegret: MinimalTime for evacuation of local population from selected area
```

```

{
    while( $\exists i = \underline{UnsafeLocality}^*$  so that  $\underline{ActualPopulation}[i] > 0$ )
        /*test UnsafeLocality: population*EmergencyDegreeEvacuation*(1-safety)>0
        {
            i=ChooseUnsafeLocality(strategy**, distance***, EstimateTime,
            ActualPopulation, VehicleCover);
            /****distance – may be considered aproximate, on the shortest route possible,
            //or taking into consideration degrees and
            //time intervals to cover area arcs
            if( $\exists \underline{CoveringVehicles}[i]$ )
                {
                    j=EvacuationPlanning(i);
                    //considering:
                    //time for loading, transport and unloading
                    //anterior planning, degrees and intervals of occupancy
                    //of road arches from the road network involved in evacuation
                    EvacuationStart(i, j, SelectedPath, ComputedTimeIntervals, NecessaryStops);
                }
            else {
                j=ChooseSafeSource(AvailableVehicles,TimeIntervals,
                NeededSmallBusses,NeededBusses,NeededCoachBusses);
                SendHelp(j,i,way, TimeInterval, NeededSmallBusses,
                NeededBusses,NeededCoachBusses);
            }
        }
    currentUtility=function(maximumTimeNeededForLastEvacuatedPerson,
        exposedPeoplePeriodInAffectedAreas*
        fn2(EmergencyDegreeEvacuation,dangerType));
    Monitor.Enter(); //synchronized code for critical resources computed
    {
        if(currentUtility> MaximumUtility)
            {
                MaximumUtility= currentUtility;
                bestStrategy=strategy;
                save(EvacuationComputedPlans, convoysComponents,
                selectedRoutesForEachConvoy, plotsForGraphicsOfEvacuation,
                mapsInformations);
            }
    }
    Monitor.Exit();
}

```

2.2. Dynamic adaptation

The dynamic adaptation of the different degrees of emergency, of the affected areas and the available road sectors would permit adjusting the program run to real conditions, initially ignored or unpredicted.

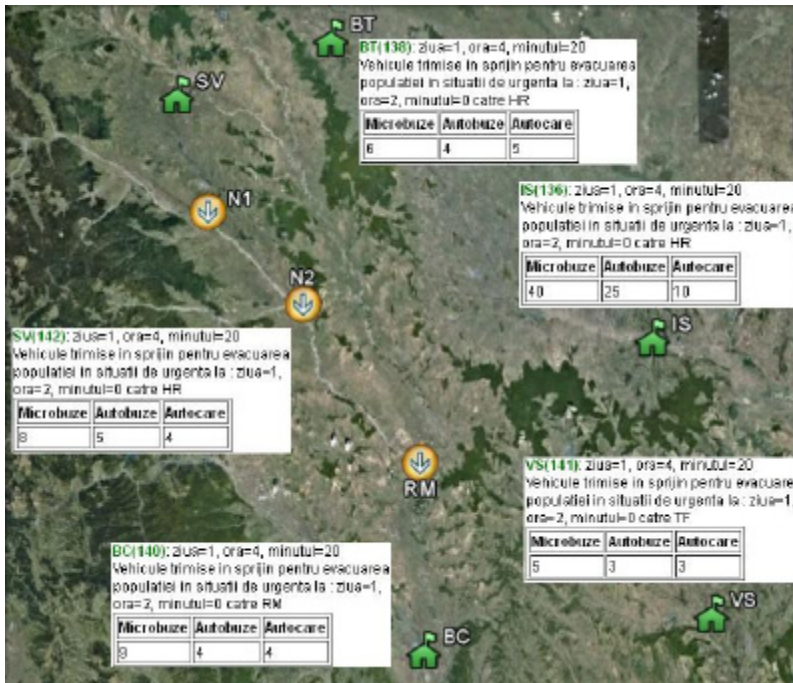


Figure 1. Transport vehicles requested and sent by the nearby support localities

2.3. Reducing of time divisions in the case of generated files containing information's regarding convoys, maps, road segments occupancy level

Having a better granularity, for example computations for each minute of program run, would permit a better follow-through of the simulation/planning of evacuation taking in consideration better decision making.

2.4. Continuous surveillance of the evacuation

Adding a software module for continuous surveillance of the obtained result, through 4-D visualization (space-time), allows good frame by frame run visualization on a desired area or road segment. Also this will permit a continuous monitoring of selectable characteristics for certain localities or road segments at any given time frame.

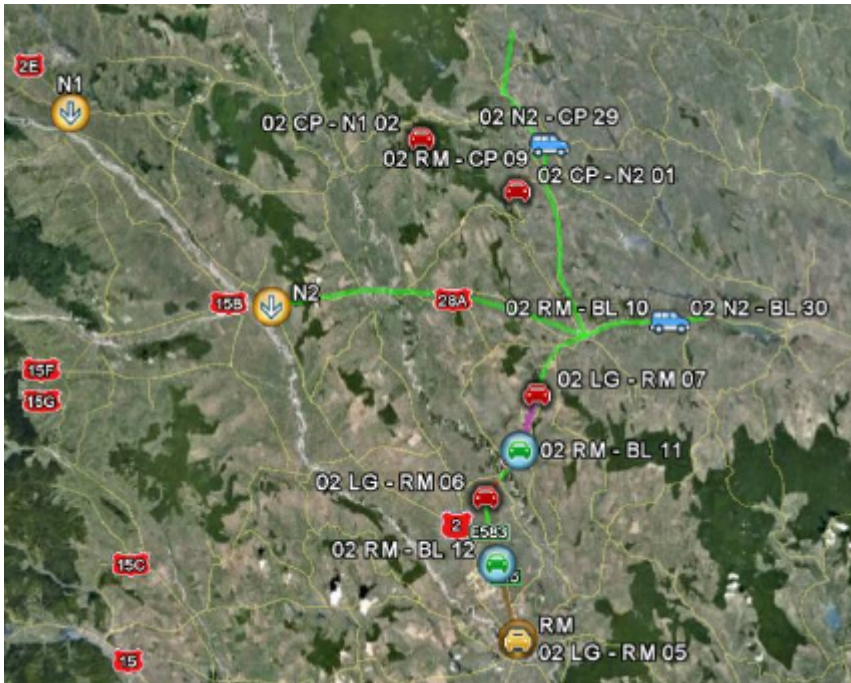


Figure 2. Convoys in motion at minute 1440 from evacuation start

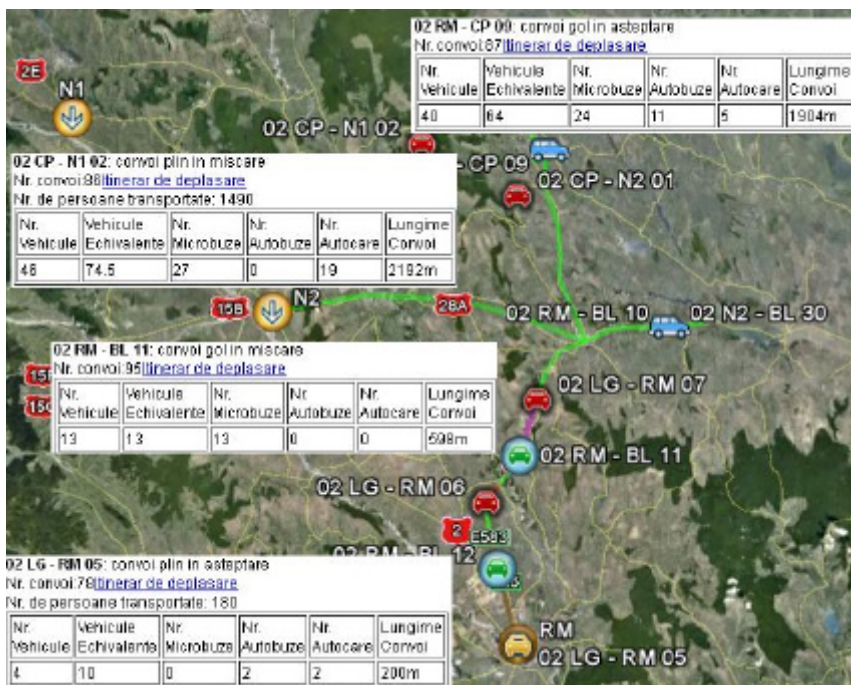


Figure 3. Information's concerning moving convoys at minute 1440 from evacuation start

2.5. Intermediary conclusion

Extending the follow-up of evacuation in simulated affected areas from a county level to a regional or national one through the partitioning of computations made for each area considering communication of data between simulated modules on different computation nodes (cluster, grid or cloud computing).

3. CONCLUSIONS

The software URGENT1 for simulation, planning and optimization of decisions in risk and uncertainty conditions, considering population evaluation with auto transport means, took into consideration areas with different degrees of urgency, the road transport system, the existing and supplementary auto transport base using heuristics for a better time schedule of evacuation and having a final purpose of mineralizing risk taking can be improved from the following perspectives: increase in number of scenarios through incorporation of variate evacuation strategies, independent parallel calculations, extension to regional and national level of emergency situations monitoring and evacuation from affected areas, inclusion of the human factor decision making and dynamic modification of different emergency degrees and available road segments.

References

1. Andrei Neculai: *Modele, programe de test si aplicatii de programare matematica*. Bucuresti: Ed. Tehnica, 2003. (in Romanian)
2. Buraga Sabin Corneliu: *Tehnologii Web*. Bucuresti: Ed. Matrix Rom, 2001. (in Romanian)
3. Cascaval Petru, Cascaval Doina: *Modelare si simulare*. Iasi: Ed. Gh. Asachi, 2002. (in Romanian)
4. Chitescu, S.: *Organizarea transporturilor auto*. Bucuresti: Ed. Tehnica, 1976. (in Romanian)
5. Craus Mitica: *Algoritmi pentru prelucrari paralele*. Iasi: Ed. Gh. Asachi, 2002. (in Romanian)
6. Croitoru Corneliu: *Tehnici de baza in optimizarea combinatorie*. Iasi: Ed. Univ. Al. I. Cuza, 1992. (in Romanian)
7. Ionescu Gh.Gh., Cazan Emil, Negruta Adina Letitia: *Modelarea si optimizarea deciziilor manageriale*. Cluj-Napoca : Ed. Dacia, 1999. (in Romanian)
8. Ionescu Tiberiu: *Grafuri-aplicatii*. Vol. I, Bucuresti: Ed. Didactica si Pedagogica, 1973. (in Romanian)
9. Ionescu Tiberiu: *Grafuri-aplicatii*. Vol. II, Bucuresti: Ed. Didactica si Pedagogica, 1974. (in Romanian)
10. Leon Florin, Zaharia Mihai Horia, Pal Cristea, Boronea Stefan Adrian, Didilescu Tudor: *Distributed Application for Traffic Control Using Intelligent Agents*, in Proceedings of the 9th WSEAS International Conference on Applied Informatics And Communications (AIC '09), WSEAS Press, 2009.

The effects of the seismic actions on bridge structures and structure control system

Adrian Haiducu, Elena Poida

Department of Structural Mechanics, Technical University of Civil Engineering, Bucharest, 020396, Romania

Summary

This work presents: the effects of the seismic actions on bridge structures and devices for limitation of the energy transfer namely seismic isolators, viscous dampers and a combination of the two systems.

A part same innovative systems for passive control through base isolation are presented, respectively oscillatory systems – laminated rubber bearings with or without lead core, non-oscillatory systems – systems type friction pendulum.

Advantages and disadvantages of different types of isolators applied to bridge structures are presented.

A numerical example is presented in the end of the work. Two bridge structures are analysed, a non-isolated structure and an isolated structure with two types of seismic isolators (oscillating systems - laminated rubber bearings with or without lead core).

KEYWORDS: *Base isolation; Seismic action; Passive control devices; Stiffness; Bridge structure; Bearings*

1. INTRODUCTION

The bridge is a work of art that supports a terrestrial communication way (road, railway, etc.) over a natural or artificial obstacle (river, channel, valley, etc.) ensuring continuity of the communication way and crossed obstacle.

The problem of bridges located in areas with severe seismic actions is that generally in piers there occur major seismic forces both on longitudinal and cross-section direction of the bridge. Therefore the problem is to find methods by which to reduce the influence of the deck mass on the bridge infrastructures (piers and abutments).

Chapter II presents the effects of earthquakes on bridge structures and the need for isolating them and Chapter III contains a brief overview of passive control devices

by isolating the base, namely, laminated rubber devices with or without lead core and the system of type friction pendulum.

Chapter IV presents the case study of a bridge structure analyzed with or without seismic isolation system, each type of structure being analyzed by help of three generated acceleration diagrams (acc1, acc2, acc3) and the acceleration diagram registered by Incerc on March 4,1977 (acc77) and Chapter V presents the conclusions.

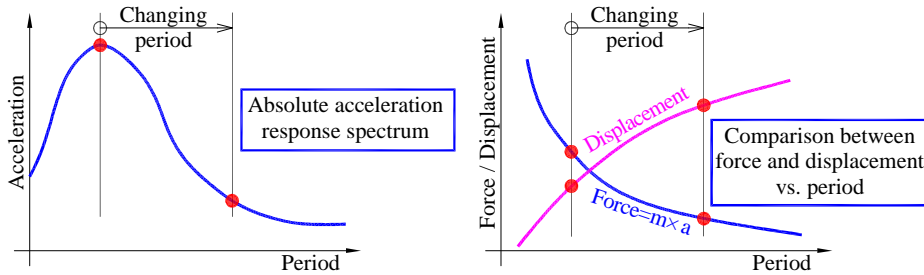


Figure1. Theoretic principle of base isolation

2. EFFECTS OF EARTHQUAKES ON BRIDGE STRUCTURES AND THE NEED FOR ISOLATING THEM

The images below present the effects of earthquakes on bridge structures. Effects depend on the intensity of the earthquake, depth where they can occur and the nature of the surface rocks.



Figure 2. Puente Viejo Pedestrian Bridge (the Veijo Bridge was restricted to pedestrian traffic two years before the earthquake) [4]; Figure 2. Bridges destroyed by the earthquake dated February 27, 2010 from Chile (8.8 degrees on the Richter scale, it lasted 9s, took place at a depth of 13km and was followed by 2 aftershocks bigger than 5 degrees) [5]



Figure 3. Crash of bridge decks at the motorway intersection way, earthquake Northridge Earthquake, January 17, 1994, California, 6.8 degrees on the Richter scale [6]; Figure 4. Crash of a bridge pile because of the insufficient confinement reinforcements, earthquake Northridge Earthquake, January 17, 1994, California, 6.8 degrees on the Richter scale [6]



Figure 5. Seongsu bridge from Seoul (South Korea) having a total length of 1160m, crashed on October 21, 1994 [7]; Figure 6. “La Democracia” bridge erected in 1963 over Uluá river, crushed during an earthquake of 7.1 degrees on the Richter scale [8]

In case of conventional non-isolated structures, major seismic forces can cause degradation through permanent deformations, cracks and eventually cracks in the structural elements. Forces are much reduced at isolated structures with or without damping, many of the movements taking place across the isolation system, while the structure moves almost as a rigid body. The isolation system provided with damping has an additional advantage as compared to the isolation system without damping because, due to additional damping, the maximum movement of the isolator is less, the maximum movement of the isolated and damped system is less than the maximum movement of the isolated system.

In the case of seismic isolated bridges, base isolation of bridges means to separate the deck, which is the largest mass, from infrastructures, which transmit the lateral loads induced by seismic loads to foundations. If the seismic input energy is zero, the structure doesn't need to be designed to support lateral loads.

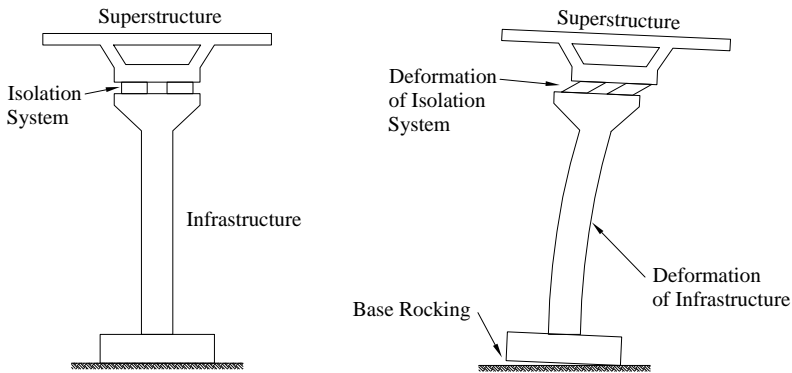


Figure 7. Actual lateral stiffness of the combined system, isolator-infrastructure

Generally, isolators are placed at the top of the infrastructures. This configuration reduces the overturning moment that would apply to the insulation devices. In addition, separating the superstructure from the infrastructure can be extremely beneficial because it eliminates the big moments that would otherwise be transmitted to piers from the superstructure, where it was fixed rigidly. Also, the design superstructure is simplified; it is reduced to a continuous, simply supported beam, or slab on elastic bearings both on longitudinal and cross-section direction of the bridge.

Seismic isolation systems combine two main component elements:

- an isolator, such as laminated rubber bearings with or without lead core or system type friction pendulum, mounted in the structure bearing area. Due to lateral stiffness much lower as compared to lateral stiffness of the structure, the isolator transfers the own lifetime of the structure beyond the most prevailing standard earthquakes.
- energy dissipation mechanism such as a damper, which dissipates the input energy and limits the forces transmitted to the structure through increased damping.

3. OVERVIEW OF PASSIVE CONTROL DEVICES BY ISOLATING THE BASE

This chapter presents a general study of various isolating devices that have been completed, successfully tested in laboratories and effectively implemented to bridge structures. This chapter highlights two main types of systems that have been

used extensively in the last twenty years, namely laminated rubber systems and systems type friction pendulum.

3.1. Laminated rubber bearing

Laminated rubber bearings, elastomeric bearings have been widely used in bridge superstructures to allow deformations and movements caused by temperature. In the last twenty years, the use of these bearings was extended to seismic isolation of buildings and bridge structures. Laminated rubber bearings can withstand high gravitational loads, providing only a fraction of the lateral stiffness of the superstructure that they support. As shown, a normal laminated rubber bearing is composed of alternating layers of elastomeric rubber and steel wheels joined tightly under pressure and at high temperature through a process of vulcanization.

Through alternation of steel and rubber layers, the capacity of laminated rubber bearing to resist gravity load is enhanced by reducing the thickness of individual layers of rubber. Although the lateral stiffness of the laminated rubber bearing depends only on the height and surface of the rubber in the unit, the vertical stiffness of the bearing is much enhanced by the presence of steel wheels. Steel wheels provide confinement and prevent rubber deformation during compression. Layers of steel wheels improve the stability of higher bearings during lateral load.

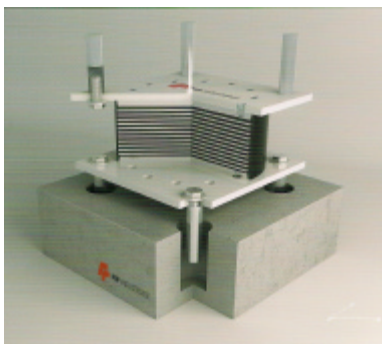


Figure 8. HDRB bearing [3];



Figure 9. HDRB bearing from Basarab passage

Key parameters in designing laminated rubber bearings are bearing capacity during gravity load, lateral stiffness and maximum relative movement that can be obtained between the top and bottom supports. Lateral stiffness of bearings influence directly the own lifetime of the isolated structure. Maximum relative acceptable movement is limited by admissible deformation of the rubber layers or by the general stability of the bearing during turnover.

A disadvantage of laminated rubber bearings is the relatively low damping provided by rubber. Lately rubbers with higher damping have been proposed for

laminated rubber bearings. It seems that layered rubber bearings with higher damping showed significantly higher energy dissipation than those made of rubbers with low damping. However, high damping rubber is sensitive to changes of properties related to heat produced during cyclic loading and wear effects that influence stiffness and energy dissipation capacity. This requires the provision of long and short term properties but also determination of appropriate limits of the bearing properties for the limited analyzes.

3.2. Laminated rubber bearing with lead core

One of the basic most developed isolation systems is the lead core laminated rubber. This system is composed of an elastomeric bearing incorporating a central core of lead. The lead core is inserted to enhance the damping through strong hysteretic shear deformation of the lead.

Main reason for choosing lead as the core material is that, at room temperature, lead is almost like an elastic-plastic solid and through shear it flows at a relatively low stress. Also, lead can be processed at hot, at room temperature. This means that lead properties are renewed continuously when subjected to an inelastic load cycle. Thus, lead has wear resistance properties. Another advantage of lead is high availability in high purity.

Key parameters in designing laminated rubber bearings with lead core are bearing capacity during gravity load, lateral stiffness, damping and maximum relative movement.

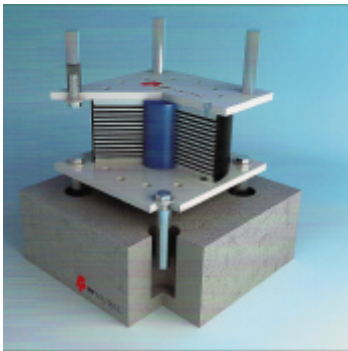


Figure 10. LRB bearing [3];



Figure 11. LRB bearing from Basarab passage

3.3. System type friction pendulum

The system type friction pendulum is a friction sliding bearing using gravity as a force for recovery. The system consists of an articulated friction slider moving on a consolidated concave spherical surface. The natural frequency of a structure isolated by help of friction system depends only on bearing radius. This advantage is significant since the period of isolation can be achieved no matter the superstructure weight.

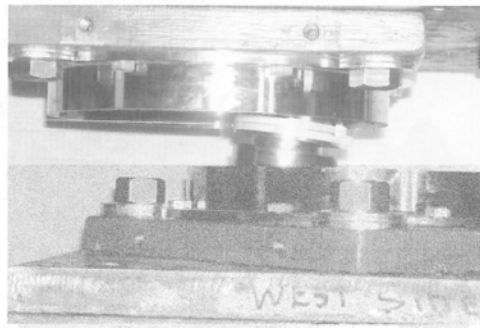


Figure 12. Seismic isolation with friction [2] Figure 13. System double friction pendulum [1]

Table 1. Types of isolators, advantages and disadvantages of these types

Types of base isolation systems	Advantages	Disadvantages
Natural rubber elastomeric isolators HDRB	- easy and inexpensive to manufacture; - easy to install; - not require replacement after a severe earthquake.	-should to be used in combination with systems that increase damping.
Natural rubber elastomeric isolators with lead core LRB	- easy and inexpensive to manufacture; - easy to install; - damping up to 30% of the fraction of critical damping; - takes over tensile forces.	-the system must be replaced after a severe earthquake.
Isolators type friction pendulum FPS	- re-centering provided by surface curvature; - properties depend less on the structure; - not require replacement after a severe earthquake; - small height of the device.	-stiffness variations induced sudden slip.

4. STRUCTURE MODELING. PERFORMED ANALYSES. RESULTS

The site is in Bucharest, where according to P100/2006 (National Annex) the peak acceleration of the designed soil is $a_g = 0.24g$. Local soil conditions at the location are provided by corresponding spectra defined by the (peak) control period value $T_c = 1,6s$. Seismic movement is described by response spectra in absolute normalized accelerations according to P100/2006, which have maximum coefficients of dynamic amplification $\beta_0 = 2,75$ and $\beta_{0v} = 3,0$.

Analysed structure consists of a reinforced concrete bridge, continuous beam on 5 spans of 50.00m each, having a total length $L = 5 \times 50.0m = 250.00m$. In cross-section, the superstructure consists of a reinforced concrete box with sloping walls.

Variant I-1 considers the classic propping superstructure with mobile and fixed bearing devices, fixed bearing being located on the pier. Variant I-2 considers the superstructure propped with laminated rubber isolators of high damping and variant I-3 considers superstructure propped with laminated rubber isolators having lead core. The infrastructure elevations are considered to be embedded in the base. There are used three generated acceleration diagrams (acc1, acc2, acc3) and the acceleration diagram registered by Incerc on March 4, 1977 (acc77).

Isolators have diameter $D = 1200mm$, height $H = 286mm$ and thickness of the neoprene $t_e = 120mm$ – I-2, diameter $D = 900mm$, height $H = 324mm$ and thickness of the neoprene $t_e = 144mm$ – I-3.

Analysed structure: elevation, joints of superstructure (5096 - abutment, 5092 - pier), joints of top infrastructure (3402 - abutment, 849 - pier) and joints of below infrastructure (3396 - abutment, 1 - pier).

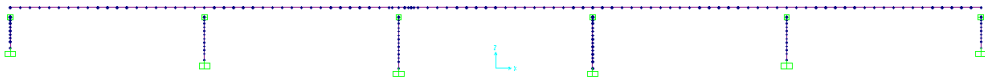


Figure 14. Structure analysed

Presentation of results: - vibration modules

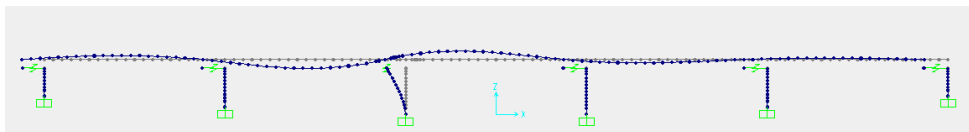


Figure 15. Structure I-1 – $T = 0.58s$

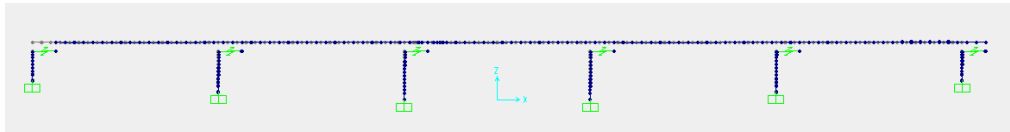


Figure 16. Structure I-2 – T=1.07s

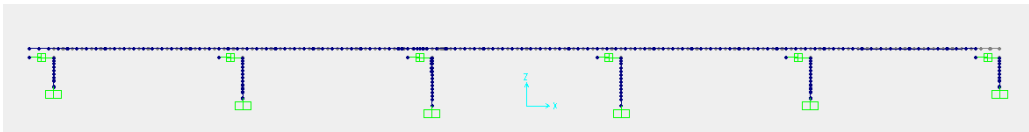


Figure 17. Structure I-3 – T=2.23s

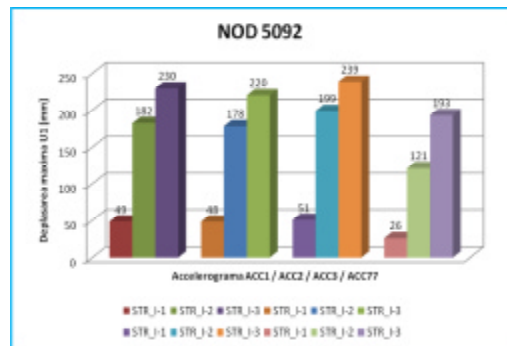
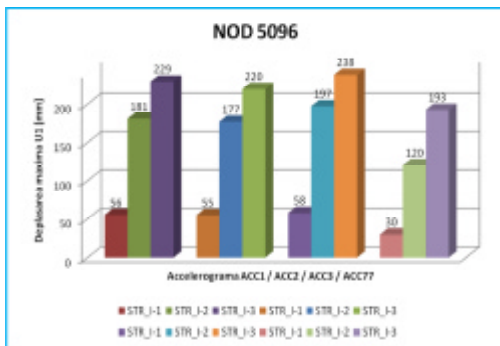


Figure 18. Maxim displacement - joints of superstructure (5096 / 5092)

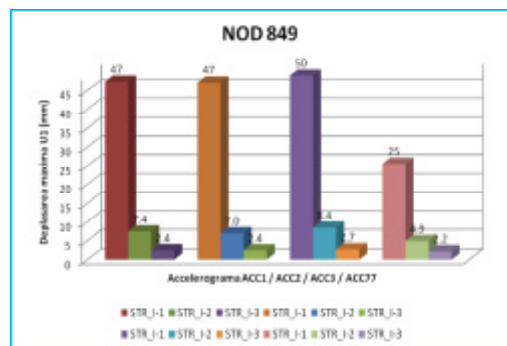
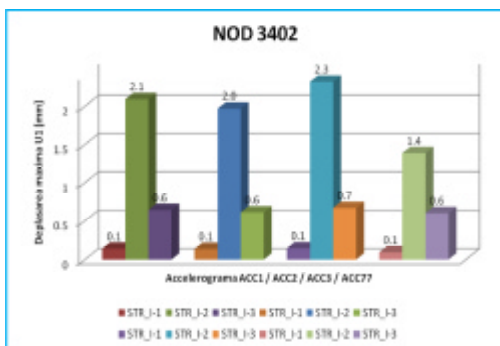


Figure 19. Maxim displacement - joints of top infrastructure (3402 / 849)

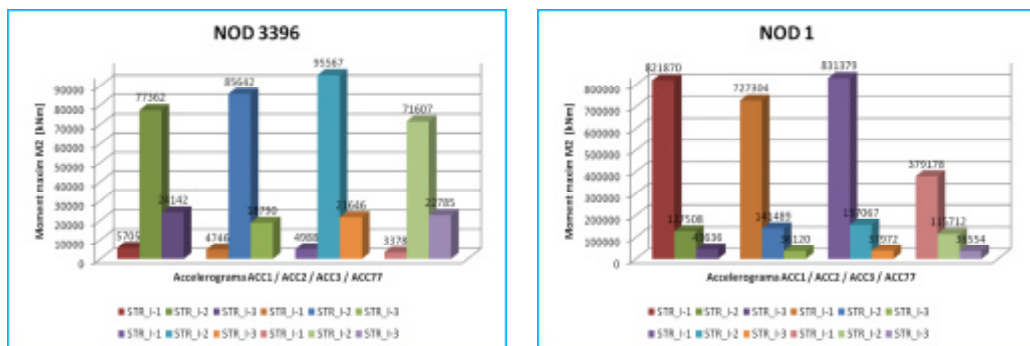


Figure 20. Maxim moment - joints of below infrastructure (3396 / 1)

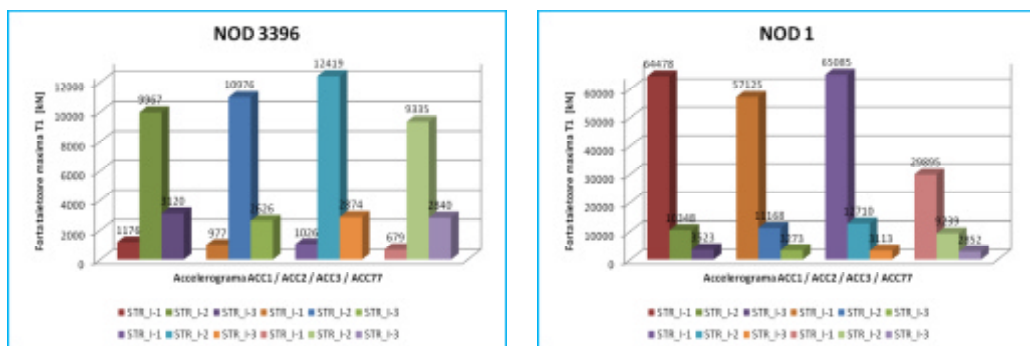


Figure 21. Maxim shear - joints of below infrastructure (3396 / 1)

5. CONCLUSIONS

In case the pier elevation is considered to be embedded in the base, when not taking into account the soil-structure interaction, the moments inside the piers can be much reduced via the seismic isolation and damping system, but the movements at the level of the superstructure increase.

As shown, at non-isolated structures (classic propping) is noticed that the movement at the level of the superstructure varies between 3 - 6 cm and at isolated structures the movement at the level of the superstructure varies between 12 - 24cm.

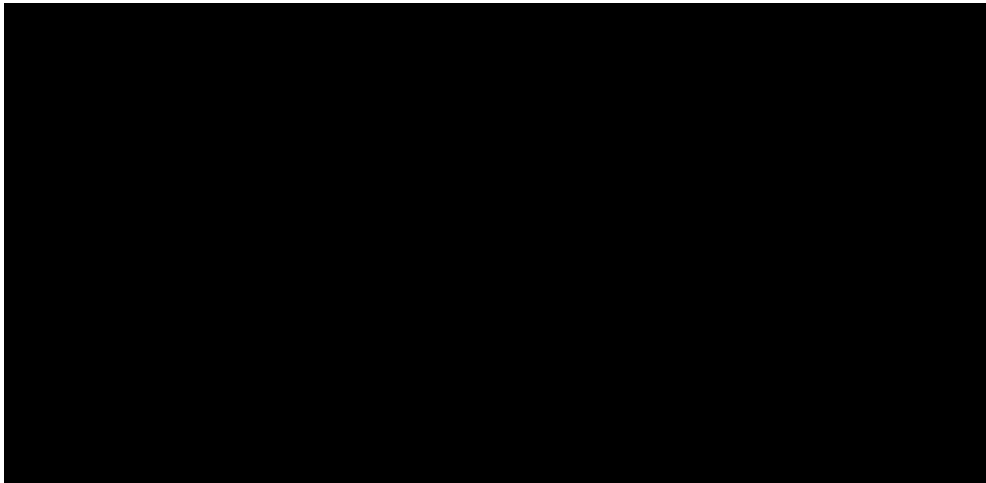
For the moments occurring at the elevation base, one can notice that at non-isolated structures (classic propping) the values vary between 379178 – 831379kNm for the

pier, and at isolated structures the values vary between 115712 – 157067kNm for the pier.

Insertion of isolators leads to reduction of the moments present at the base of piers and abutments but also increase of movements present at the ends of piers. This moment occurring at the base of piers is reduced up to 5 times and the deck movement increases up to 4 times.

With regard to the value of shearing force occurring at the base, also here one can notice a significant reduction in the case of isolated structures.

Table 2. Summarized table



References

1. [1] Christoponlos, C., Filiatrault, A., *Principles of Passive Supplemental Damping and Seismic Isolations*, Iuss Press, Pavis – Italy, 2006
2. Naeim, F., Kelly, J.M., *Design of seismic isolated structures*, John Wiley&Sous, New Yorg, 1995
3. [2] CONSTEL – Dispozitive telescopice si procedee tehnologice pentru consolidarea cladirilor prin controlul, linitarea si amortizarea oscilatiilor induse de activitatea seismica – Referat etapa I-a, 2008. Contract nr.32167/2008. beneficiarul Centrului National de Management Programe – programul: Parteneriate în domeniile prioritare; Director de proiect prof. dr. ing Dan Cretu.
4. [3] Catalog FIP INDUSTRIALE – Seismic Device – Elastomeric Isolators and Lead Rubber Bearings
5. Catalog ALGA – Seismic Devices – High Damping Rubber Bearings and Lead Rubber Bearings
6. [4] URL:< http://reidmiddleton.files.wordpress.com/2011/05/chili_4.jpg>
7. [5] URL:< <http://minnesota.publicradio.org/display/web/2010/02/27/chile-quake/>>
8. [6] URL:<http://whatiscivilengineering.csce.ca/structural_earthquakes.htm>
9. [7] URL:<<http://populargusts.blogspot.com/2009/10/dark-side-of-miracle-on-han.html>>
10. [8] URL:<<http://www.telegraph.co.uk/news/picturegalleries/pictures-of-the-year/6872613/Pictures-of-the-year-2009-disasters-earthquake-flood-fire-tsunami-and-plane-crashes.html?image=5>>

Aspects on building demolition waste and their impact on the environment

Vasile Iacob

¹ Faculty of Civil Engineering and Building Services, "Gheorghe Asachi" Technical University, Iasi, 700050, Romania

Summary

In the decade in which the cities face a chaotic urban development, by building residential houses and the demolition of the old buildings, the development of main streets, the construction and demolition waste are growing and must come up with a plan to reintegrate them.

Environment, built environment, natural environment are concepts that define the intervention to protect the environment on a global scale in construction and urban development.

Romanian and European concerns, on the recovery of demolition waste are summarized in this paper, with the declared intention to continue and deepen the problem.

KEYWORDS: concrete, air-placed concrete, durability, compacted, mixture, additive.

1. GENERAL ASPECTS

The wastes coming from buildings and demolitions are constituted from 2 individual components: wastes from buildings and wastes from demolitions. These wastes came from:

- materials resulting from buildings and buildings demolitions – cement, bricks, tiles, ceramic, stone, plaster, plastic, metal, cast iron, wood, glass, short ends, expired construction materials;
- materials resulting from the construction and the maintenance of roadways and afferent structures, tar, sand, rubble, bitumen, tarred substances, substances with bituminous or hydraulic bindings;
- excavated materials during the construction, decommissioning, spoil, decontamination activities: soil, gravel, clay, sand, rocks, vegetable remains.

Also, the wastes resulting from natural disasters are considered wastes from buildings and demolitions. Objects / materials easy to remove from a structure (furniture, electric equipment and other equipments) are not considered wastes from demolitions and buildings.

Among the wastes resulted from constructions and demolitions we can mention those which are dangerous and very dangerous:

- dangerous materials: asbestos, tars and paints, heavy metals(chromium, lead, mercury), varnishes, paints, adhesives, polyvinyl chloride, solvents, polychlorinated biphenyl compounds, different types of resins used for conservation, fireproofing, waterproofing;
- risk-less materials which were contaminated by mixture with dangerous materials, for example construction materials mixed with dangerous substances, mixed materials resulted from the activity of unselective demolition;
- soil and gravel contaminated with dangerous substances.

The construction wastes represent the wastes resulted from the activities of construction and/or demolition specified at art. 2, line 1 in accordance with The European List of Wastes transposed by H.G. nr. 856/2002 about The Evidence of wastes management and for approving the list which contains wastes, including the dangerous wastes, which are founded at 17th code.

Wastes from constructions and demolitions, including excavated soil from contaminated land are constituted of three individual components: wastes from constructions, wastes from demolitions and excavated soil from contaminated lands. The classification is mentioned in The Regional Plan of Wastes Management.

The Ministry of Environment and Sustainable Development together with the Ministry of Development for Public Works and Houses have initiated in 2007 a proposal of legislation for the management of wastes. Due to this proposal, wastes was clasified in this way:

- wastes from demolitions;
- wastes from building new constructions;
- wastes from renovation of constructions;
- wastes from activities of roads reparation;
- wastes from activities of bridges reparation;
- wastes from natural disasters.

Wastes from constructions and demolitions represent about 25% , the majority of them coming from renovation or demolition of old buildings.

Nowadays, just a part of the wastes from constructions and demolitions is reported, especially that from the citizens who request Construction authorization for renovations/demolitions/new constructions.

The majority, consisting usually in rests of concrete, bricks or composite (brick with mortar) come from the building companies which usually do not declare it, because either they crush it and reuse it for roads in the yard or for filling the pits from the comunal roads, fact more or less legal, or they store it in places unauthorized by the Environmental Agency, but accepted by the local authorities.

Concerning other components such as the wood resulting from the replacement of door and window cases, doors, parquet or of floors, of roof repairs, this is recuperated in a proportion of 95 percent by poor people, who use it as fuel.

The metal consists in reinforcement bars made from reinforcing steel which appear especially after the crushing of reinforced concrete blocks and is valorified by the REMAT unities.

In this stage plastic materials do not represent a significant procent, but it's expected that in the following years (2010-2012) this component which will come especially from waste PVC industry (of whom lifetime isn't bigger than 10-12 years, if it was new and even less if it was second hand) to become a problem.

We have to take into account that in this moment 90% of new buildings' joinery is made of PVC and less from natural wood or laminated wood.

The glass is a component which, because is very brittle, most of the times is mixed up and is eliminated with the garbage, when it comes from people or with mixt wastes when it comes from building companies.

An explanation for the selective uncollecting of this fraction may be the lack of a recycler interested in the taking over of this waste in order to recycle it, as well as the lack of interest among some institutions for this problem, that's way it has come to the establishment of some nongovernmental organizations which fight for this problem.

Table 1. Types of demolition and constructions wastes which are the study object

Waste code	Waste type
170101	Concrete
170102	Bricks
170103	Tiles and ceramics
170106*	Mixture or fragments separated from concrete, bricks, tiles or ceramics with dangerous content
170107	Mixture or fragments separated from concrete, bricks, tiles or ceramics, other than those specified at 170106*
170201	Wood
170202	Glass
170203	Plastic materials
170204	Glass, plastic materials or wood with content of/ contaminated with dangerous substances
170401	Copper, bronze, brass.
170402	Aluminum
170403	Lead
170404	Zinc
170405	Iron and steel

170406	Tin
170407	Metal mixtures
170409*	Metal wastes contaminated with dangerous substances
170410*	Cables with content of oil, tar or other dangerous substances
170411	Cables, other than those specified at 170410*

According to statistic references, in 2006, all over the country there were collected cca. 475.000 tons of wastes from constructions and demolitions, quantity that was entirely eliminated through storage.

2. EUROPEAN PREOCCUPATIONS CONCERNING CONSTRUCTIONS' WASTES.

The wastes coming from constructions and demolitions represent in the European Union countries approximately 25 percent of wastes. They are done from different materials, a lot of them being able to be recycled, one way or another, like: (Surse, EIONET 2005):

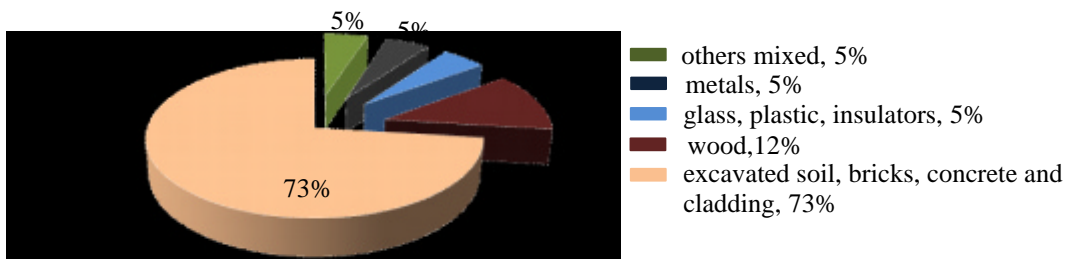


Figure 1. The structure of constructions and demolitions' wastes

A large number of the wastes coming from constructions and demolitions are recyclable and can be reused in producing materials for roads or reused in producing cement, if there are adequate facilities. The European Union reported a decrease in the storage of wastes coming from constructions and demolitions, since bigger depositing taxes were introduced, bigger than those cashed by the recycling companies. This thing was possible in Germany. It is suggested the onset of an European-level strategy because the wastes coming from constructions and demolitions can fill up spaces of 580.000 square km/year, supposing they are not totally recycled and recuperated.

This quantity may be significantly reduced by using a simple mincing and a sorting facility which can recuperate from 60 up to 70 per cent of the wastes coming from constructions and demolitions. Such facilities can cost between 3 and 4 million Euros for a structure that supports 500 tons of minced wastes per day. It is

suggested that this costs be smaller than the storage costs. This thing may be an initiative for the increase of recycling.

If Germany has made important steps concerning the urban ecology, integrating the problems of handling the wastes in a strategy of experimental ecological urban walling off, France is one of the first countries to have applied the European legislation of environment protection in the field of handling the yard wastes.

In France, ever since 1975, the law no. 75-633 of 15 July 1975, which constitutes in the application of directive no. 75/442/CEE concerning the wastes, has as objective the elimination of wastes and the recuperation of materials. This forbade the open air incineration of wastes and gave responsibility to the undertaking concerning the elimination of yard wastes, this demarche including the collecting, the transportation, the hoarding, the sorting, then the valorization through recycling or energetic capitalization.

Since 1992 – when law no. 92/646 of 13 July 1992 (Royal law), referring to the elimination of wastes and installations classified for the protection of the environment was adopted – until now, in France developed a system of planning the elimination of wastes through the regional plans (special industrial wastes) and departmental plans (municipal wastes).

3. ROMANIAN PREOCCUPATIONS CONCERNING CONSTRUCTIONS' WASTES

In Romania, the Ministry of Environment and Water Administration, through the Wastes and Hazardous Substances Management Division coordinates the elaboration, promotion, deploying and monitoring the deploying of the Wastes Management National Plan the National Strategy. These documents are the main instruments through which it is assured the deploying in Romania of European Union's politics concerning the wastes.

The Wastes Management National Strategy contains the national legislative frame and the stage of the deploying, the situation existent in the field of wastes management, general data concerning the wastes management, principles and strategic objectives. The strategic objectives are divided as following: general strategic objectives for wastes management, strategic objectives specific to certain flows of riskless wastes, general strategic objectives for hazardous wastes management and strategic objectives specific to certain flows of hazardous wastes.

The Wastes Management National Plan is made up from 3 parts: the first part – a general presentation, the second part – dedicated to municipal wastes and the third part – dedicated to production wastes, with a preponderant accent on hazardous wastes.

If the key elements of the National Strategy are the principles that stay at the basis of wastes management, as well as the general strategic objectives and those that are specific to certain flows of wastes, the National Plan attaches to the objectives

(which are provided in the Strategy) quantifiable targets where is the case and, in addition, it presents a number of alternatives of reaching the objectives and the afferent targets, respectively. The hierarchy of priorities in approaching wastes management in Romania is the one that stays at the basis of European politics and legislation, known internationally: the premonition and minimization of wastes generation, the material valorization through recycling, the energetic valorization, wastes' treatment in order to subtract the quantities and hazardous potential and at the end the storage. Among the general objective are to be mentioned: the development of organizational and institutional frame, the awareness of the implicated factors, the enhancement of preoccupations concerning the reducing of generated wastes' quantities, the exploitation of all technical and economical possibilities concerning the recuperation and recycling of wastes in order to reduce the quantity of eliminated wastes. A series of alternatives of reaching the strategic objectives is based, on short and medium term, on the usage of pilot-demonstrative installations. On their strength there will be made later evaluations and on the strength of the evaluations, the knowledge and the experience accumulated they will be able to extent for the implementation of a wastes management integrated system. Parallel with these there will develop population's informing and instruction campaigns in order to obtain the public acceptance necessary for later investments.

4. CONCLUSIONS

The wastes management problem is a complex problem. The correct understanding of the problems leads to the selection of their optimum resolving solutions and, in the end, to the rationally ecologic management and to the salvation of some natural resources, important for us, but mostly for next generations.

References

1. Maria Gheorghe, " *Turning waste and industrial by-products in building construction* ", Matrixrom, 2007;
2. Gabriel Stefan, " *Study on recovery of material from demolition and construction waste*", UTCB, Bucharest, 2003;
3. Ghecef I., " *Recovery technologies of concrete from demolition, an inevitable need for future* ", SINUC, Bucharest, 2005;
4. Queensland Government Environmental Protection Agency, Construction and Demolition Waste. *Waste management and resource use opportunities*, July 2002;
5. Departament of Environmental & Climate Change NSW, *Report into the Construction and Demolition Waste Stream Audit 2000-2005*;
6. EUROPEAN COMMISSION, *Management of Construction and Demolition Waste*;
7. Ministerul Mediului si Dezvoltarii Durabile din Romania, Ghid privind stocarea temporara a deseurilor periculoase din constructii si demolari (inclusiv soluri contaminate);

Improving mechanical and durability performances of air-placed concrete. Laboratory and situ researches.

Vasile Iacob

¹ Faculty of Civil Engineering and Building Services, "Gheorghe Asachi" Technical University, Iasi, 700050, Romania

Summary

This paper presents one modern and efficient method for the realization of concrete with low ration A/C, air-placing. In this paper we propose a modification for the traditional Romanian installation of dry mix air-placing, changes that lead to improved operation and reliability of the installation, increased quality and performances of air-placing concrete, reduced costs and material saved.

Through laboratory research mechanical and durability performances are highlighted and the results are analyzed compared with provided normative values and with performances of standard concrete or with other aditives.

KEYWORDS: concrete, air-placed concrete, durability, compacted, mixture, additive.

1. INTRODUCTION

Cement concrete quality, expressed by its mechanical performance and homogeneity of the mixture composition is determined by the composition factors (quality and proportion of components) and execution technology (cooking, transportation, work release, treatment after concreting). Compared with the factors of composition, execution technology offers several possibilities for improving the mechanical performance and durability of concrete. The durability of concrete, expressed mainly by the impermeability to water and resistance to repeated freeze-thaw cycles, structural compactness is determined by the nature and distribution of pores in concrete. The structural compactness is directly influenced by the amount of water in concrete and the ratio w/c , whose values must be as close as possible to the value 0.361 for structural porosity is determined only occlusive volume occupied by air (a) without the contribution volume occupied by water evaporated or evaporated. For $w/c = 0.361$, $A_e = 0$, so the structural compactness is maximum. The nature and distribution of pores in concrete can be controlled by the type of additive used at preparation, the thermal regime of hardening, especially in

the first period of curing and, especially, by concrete technological process used. In the present study were held technology superplasticizer concrete additives and concrete spraying, the technological processes that significantly influence the mechanical performance and durability of concrete.

2. SPRAYING OF CONCRETE

2.1. General issue.

Spraying is a special technological process of preparation and laying of concrete ratio w / c low pressure of compressed air and with a spraying installation. The process consists in the design pressure of the mixture moist microbeton or concrete, with a variable speed from 20 to 30 m / sec from 90 to 100 m / sec, through a nozzle, the support surface. The force of impact of jet material compacted in such a degree, that it remains alone, without sag or fall off the support surface, even if it is vertical or inclined .

Spraying is used to protect reinforcement tension around tubes, silos or prestressed tanks, the waterproofing works to repair damaged buildings or consolidation during the implementation or operation, the actual execution of construction and construction elements special, special shapes and pronounced slopes, which are difficult to execute with ordinary means laying and compaction. With this concrete are padded the tunnels, is achieved the wearing layers of floorings and roads, are executed construction elements. The gunite is applied in thin layers, the final thickness of concrete can reach 100 mm.

2.2. Micro concrete and shot concrete

Shot concrete must be waterproof, must have resistance to freeze-thaw and resistance to compression. Spraying process is giving high performance concrete in most cases. Micro concrete and gunite concrete composition is determined by class of concrete, gunite destination, type of cement and aggregates granularity; shot concrete composition design consist in to establish aggregates granularity and cement dosage.

For dry mixing process, the amount of water is added at dry mixture outlet from the nozzle, thus resulting in a homogeneous mixture, adherent and stable to the support surface.

Expected results depend to some extent and degree of training and specialization of person who work with the installation of spraying.

II/A-S32,5R cement dosage at the C18/22,5 gunite micro concrete class varies between 450 to 550 kg/m³, as the maximum diameter of aggregate is 5 mm or 3 mm; w/c ratio varies between 0.45 and 0.36.

I42,5 cement dosage at the gunite micro concrete class C18/22,5 varies from 425 to 450 kg/m³, as the maximum diameter of aggregate is 5 mm or 3 mm; w/c ratio varies between 0.47 and 0.44.

II/A-S32,5R cement dosage at the C18/22,5 gunite micro concrete class varies between 400 to 450 kg/m³, as the maximum diameter of aggregate is 16 mm, 10 mm or 7 mm; w/c ratio varies between 0.40 and 0.36.

I42,5 cement dosage at the gunite micro concrete class C18/22,5 varies from 385 to 415 kg/m³, as the maximum diameter of aggregate is 16 mm, 10 mm or 7 mm; w/c ratio varies between 0.41 and 0.38.

2.3. Spraying installation

There are two methods to making and implementation of shotcrete: dry mixing process and wet mixing process, each process uses specific spraying installations.

In Romania are used types of systems to spray dry mixture: drum installation spraying and cylinders and horizontal spraying installation with disc and alveoli.

The spraying installation with drum and cylinders has a flow rate of gunite by 3 m³/h at a pressure of (4-5) · 10⁵ Pa a required compressed air by 10 m³/min.

Shotcrete concrete is not uniform in structure or in thickness, due to pressure suppression variables.

Gunite layer surface does not appear uniform and flat. Cement losses occur and compressed air. Therefore, this facility cannot be used as a characteristic process equipment widely used in practice for a concrete who has a low ratio w/c.

3. RESEARCH TO IMPROVE SHOTCRETE PERFORMANCE

The research aimed to improve the gunite machine, to improve mechanical performance and durability of concrete and gunite in situ and laboratory testing of the performance levels achieved by the concrete gunite.

3.1. Facility improvement of spraying

The installation with horizontal disk and alveoli was modified by changing attack angle of compressing air connecting pipes, for processing continuous mixing portions of the alveoli, reducing friction and eliminating pulsations during operation.

During the experiments has been replaced the air compressor which had the flow by 10 m³/min (75 kW) with two compressors which had the flow by 1.5 m³/min

(total 30 kW); so, has improved the operation of the facility and was made energy saving for production of compressed air.

Also, was used a mixing nozzle and some auxiliary devices for concrete flow adjustment, to eliminate the compressed air jet and for reducing losses by ricochet.

3.2. Shot concrete performance test

Were designed and tested standard waterproof concrete compositions and with superplasticizer additive FLUBET - concrete cast - and the concrete and gunite micro concrete who at the same dosage of cement, were differentiated by reports w/c and by granules diameter of aggregates used in prestressed tested.

To design concrete compositions who was cast, it was used the absolute volume method and it resulted the compositions presented in table 1.

Table 1. Experimental concrete compositions

Code	Concrete type	W (l/m ³)	W/C	C Kg/m ³	Fl. l/m ³	A _g Kg/m ³	γ _b Kg/m ³
BS (standard)	C18/22,5/P ₈ ¹⁰ -T ₃ /T ₄ -II/A- S32,5R/31	205	0,50	410	-	1740	2355
BAF FLUBET	C18/22,5/P ₈ ¹⁰ -T ₄ /T ₅ -II/A- S32,5R/31 FLUBET	165	0,40	410	6,0	1725	2300
BT1 gunite	C18/22,5/P ₈ ¹⁰ -T ₃ /T ₄ -II/A- S32,5R/16 gunite	180	0,44	410	-	1815	2405
BT2 gunite	C18/22,5/P ₈ ¹⁰ -T ₃ /T ₄ -II/A- S32,5R/7 gunite	165	0,40	410	-	1855	2430

Mechanical performance and durability of concrete gunite were compared between them and with the performance of standard concrete and of concrete with superplasticizer additive Flubet cast and compacted by vibration. Have been compared the compressive strength test results determined at different time and different storage conditions of test piece, test results are presented in table 2.

Table 2. Evolution of compressive strength of experimental concrete

Mechanical resistance concrete type \ code	Standard BS	Additive BAF	Gunite BT1	Gunite BT2
R ₂₈ ^N	36,0	36,0	36,5	36,7
R ₉₀ ^N	42,0	43,6	44,0	45,0
R _{28+g} ^N	42,8	44,3	45,0	45,5
R _{28+g} ^{N+g}	38,7	41,1	42,2	43,1
R _{90+g} ^N	44,0	46,1	47,5	48,5
R _{90+g} ^{N+g}	41,0	44,2	46,3	47,4

The results of experimental concrete impermeability test were compared and this values are present in the table 3. Were tested concretes who were kept at normal

temperatures with concretes which have been subjected to repeated at freeze-thaw cycles, applied in terms of 28 days and 90 days.

Table 3. Evolution of experimental concrete permeability

Permeability concrete type \ code	Standard BS	Additive BAF	Gunitite BT1	Gunitite BT2
P_{8-28}^{10}	4,03	2,96	2,03	1,83
P_{8-28+g}^{10N+g}	5,30	3,72	2,76	2,10
P_{8-90+g}^{10N+g}	4,72	2,25	2,10	1,98

4. CONCLUSIONS

The compression resistances at 28 days, respectively at 90 days are higher (with 12.5- 15%) than the minimal values imposed by standards. This is due to the imposition of impermeability condition in P_8 class, which limits the value of w/c ratio to maximum 0.5 for standard concrete (w/c = 0.53 for realizing the class condition) and 0.4 – 0.44 for concrete with additive or for gunitite.

The compression resistances for concrete which were submitted to the G_{50} frost clefthness tests decrease with 7-10% at standard concrete, with 4 – 8% at concrete with superreducing water agent Flubet additive and with 3 – 7% at gunitite, which has the best behavior at this test. What is important is that the compression resistances of all the concrete tried after G_{50} test are higher than the minimal resistances accepted by the normative NE 012/99.

The gunitite micro concrete, as well as the concrete with superplastifiant Flubet additive behave very well at permeability – the value of permeability is approximately 5-6 times smaller than the maximum limit accepted. Even after the G_{50} frosting - defrosting test was performed – the value of permeability is approximately 4-5 times smaller than the maximum limit accepted.

The gunitite micro concrete with 0-7 mm aggregate behaves the best at the permeability test. The permeability of the concrete submitted to the endurance test increases with 6% up to 20% , but it remains 4-5 smaller at the micro-gunitite than the maximum limit accepted.

For the qualitative verification of the gunitite adhesion and the stand surface was experimentally applied a layer of gunitite on a stand surface made from carbonated concrete. After strengthening, on the attempt of breaking out, it was observed that the breaking was done through the layer of calcium carbonate and not at the gunitite - stand surface contact. The modification of the gunitite-gun provided a constant debit, an optimum dosed mixture and improved qualities of gunitite. The power consumption decreased by 2.5 times. The ricochet losses decreased by 2 times. The gunitite-jet has now a diameter of 10-20 cm at the contact with the stand surface, if

the application distance is 50-80 cm. The adhesion at the stand surface is now highly increased.

For the gunite's structural tightness improvement and for the costs' lowering, it is proposed the experimentation of some concrete compositions in which a 10-20 per cent of the cement's mix to be replaced with cementation additions such as micro-silica or steam power plant flier ash. For the production of ageing-proof gunites, the authors want to test as well gunite compositions made with dispersed reinforcement.

Also, the authors consider that the usage of the intense water reducing additives in composition of gunite may bring important improvements of the mechanical performances and of durability of gunite.

References

1. Ionescu, I., Ispas, T., *Proprietatile si tehnologia betoanelor*, Ed. Tehnica, Bucuresti, 1997;
2. Neville. A., M., *Proprietatile betonului*, Ed. Tehnica, Bucuresti, 1979;
3. Moldovan, V., *Aditivi în betoane*, Ed. Tehnica, Bucuresti, 1978;
4. Pamfil, E., s.a. *Influence de la température élevée durant la prise et la première période du durcissement sur la durabilité du béton*, Bul. IPIasi, 1995;
5. Chanvillard, G., D'Aloia, L., *Prévision de la résistance en compression au jeune âge du béton; application de la méthode du temps équivalent*, Bull. De LLPC, Paris, 1994;
6. Pamfil, E., *Procedee tehnologice moderne de îmbunătățire a performanțelor mecanice si de durabilitate ale betonului*, Conferinta Tehnologii moderne în constructii, vol. 1, Universitatea Tehnica a Moldovei, Chisinau, 2000;
7. Maidl, B., *Stahlfaserbeton*, Berlin, Ernst, Vrlag fur Architektur, 1991;

Nonlinear finite element analysis of masonry infill walls

Dorina Isopescu¹, Andrei-Ionut Stefanu² Silviu-Cristian Melenciuc¹

¹Department of Civil and Industrial Buildings, "Gheorghe Asachi" Technical University of Iasi
Faculty of Civil Engineering and Building Services, Iasi, 700050, Romania

²Department of Structural Mechanics, "Gheorghe Asachi" Technical University of Iasi
Faculty of Civil Engineering and Building Services, Iasi, 700050, Romania

Summary

Masonry or masonry infill walls have been widely used in the past and are still a common design solution for low rise building nowadays. The infill walls are most of the times considered to be nonstructural elements. However, the seismic response of concrete structures is strongly influenced by their presence. The hereby papers analysis, using the finite element method, the behavior of masonry infill reinforced concrete frames. Three design scenarios have been considered as well as two types of infill. Homogeneous materials models have been used. The seismic force has been statically applied at the top of frames, mimicking the real case. The purpose of analysis was to highlight the influence of the design solution and the infill material on the overall behavior of a reinforced concrete frame.

KEYWORDS: masonry infill wall, nonlinear finite element analysis.

1. INTRODUCTION

In seismic regions the aspect of seismic hazard shall be taken into account in the early stages of the conceptual design of a masonry building, for enabling the achievement of a structural system which, within acceptable costs, satisfies the fundamental requirements. Additionally, the masonry buildings with a durable and economical structure provide thermal and sound insulation and an acceptable fire resistance. Masonry buildings, which are classified in unreinforced masonry, confined masonry and reinforced masonry, shall be composed of floors and walls, which are connected in two orthogonal horizontal directions and in the vertical direction.

The infill walls in masonry buildings are provided within the reinforced concrete structures without being analyzed as a combination of concrete and units elements, though in reality they act as a single unit during earthquakes.

According to the design codes, the structure of a masonry building shall be designed and constructed to withstand a seismic action having a larger probability

of occurrence than the design seismic action, without the occurrence of damage and the associated limitations of use. The structure as a whole shall be checked to ensure that it is stable under the design seismic action. Both overturning and sliding stability shall be taken into account.

Masonry buildings are, usually, characterized by the existence of clear and direct paths for the transmission of the seismic forces, and the modeling, analysis, dimensioning, detailing and construction of these simple structures are subject to much less uncertainty and thus the prediction of its seismic behavior is much more reliable. In the design of masonry buildings the following norms are applied: P100/2006 [1], CR6/2006 [2], SR EN 1996 -1/2006 [3] and SR EN 1998 -1/2004 [4].

Masonry units should have sufficient robustness in order to avoid local brittle failure. Except in cases of low seismicity, the characteristic compressive strength of masonry modules, derived from normalized compressive strength of masonry units in accordance with SR EN 772-1 and mortar strength is:

$$f_k = K f_b^{0,70} f_m^{0,30} \tag{1}$$

- where: f_k = the characteristic compressive strength of masonry modules;
- f_b = the normalised compressive strength of masonry units;
- f_m = the mortar strength;
- k = constant that depends on the type of units used for masonry.

The characteristic compressive strength of masonry modules should be not less than the minimum values presented to table 8.1 from CR 6/2006. In Table 1 are presented the minimum requested values of the characteristic compressive strength of masonry modules f_k (N/mm²) for simple masonry buildings (strength wall from ordinary buildings, not belonging in the other categories, or from buildings of minor importance for public safety, e.g. agricultural buildings, etc).

Table 1- The minimum characteristic compressive strength values of masonry modules

Building height	Design ground acceleration a_g		
	0.08g ÷ 0.16g	0.20g ÷ 0.25g	0.30g ÷ 0.40g
= GF+2F	2.00	2.50	3.25
= GF+3÷4F	2.50	3.00	4.00

* GF=ground floor, F=current floor

A minimum strength is required for mortar, $f_{m,min}$, which generally exceeds the minimum specified in CR 6/2006. The value ascribed to $f_{m,min}$ for use may be found in the National Annex. The recommended value is $f_{m,min} = 5$ N/mm² for unreinforced or confined masonry and $f_{m,min} = 10$ N/mm² for reinforced masonry.

A linear analysis presumes that: the structural response is directly proportional to the loading, large displacements do not occur, supports do not fail, the stress –

strain relationship is linear, the loads are constant etc. [5]. This type of behavior can accurately describe a limited number of real cases. For the rest of them, a nonlinear behavior can be expected. This arises from a number of causes [6], among which the next could be mentioned:

- parts may come in/out of contact, contact areas may vary with loading, frictional interaction between moving elements may exist;
- displacement and/or rotations may be significant enough to require the static equilibrium equations be written for the deformed shape of the structure;
- materials may exhibit non-linear stress-strain relations;
- thermal conductivity may vary with temperature.

Consequently a problem may evolve from a linear to a highly nonlinear one. In structural mechanics, a problem is nonlinear if the stiffness matrix or the load vector depends on the displacements.

Nonlinearity in structures may be classified as:

- geometric nonlinearity - when the nonlinear behavior of the problem is given by significant changes in the geometry of the structure. This case includes, beside others, large displacements/strains [7];
- material nonlinearity – is associated to the nonlinear behavior of materials and includes the case of plastic materials [8] or hyper-elastic materials [9];
- contact nonlinearity – occurs when the contact surface between two parts changes during the analysis.

Nonlinearity makes a problem more complicated because the equations that describe the solution must incorporate conditions not fully known until the solution is known – the actual configuration, loading condition, state of stress and support conditions. Nonlinear problems are described using differential equations derived from continuum mechanics. Very often the solution of a set of differential equations may be hard to find. In these cases numerical methods are used to provide an approximate solution to the given equations. Approximate methods include the finite element method (F.E.).

Over the last decades a large number of software packages that solve nonlinear problems using the F.E. have developed. One of these programs is ANSYS [10]. ANSYS is a comprehensive general-purpose finite element computer program capable of performing static, dynamic, heat transfer, and fluid flow and electromagnetism analyses [11].

The current problem includes material nonlinearities given by the behavior of the masonry as well as contact nonlinearities due to the interaction between the concrete frame and the infill wall.

2. CHARACTERISTICS OF THE ANALYSED MODELS

2.1. Description of the models

Three types of models, common to concrete frame structures, have been considered as design scenarios. The key geometric features, as well as the meshing, are presented in Figure 1, starting from the upper corner left hand side, as follows: frame with infill wall – upper part, frame with infill wall and door opening – medium part and frame with infill wall and window opening – lower part.

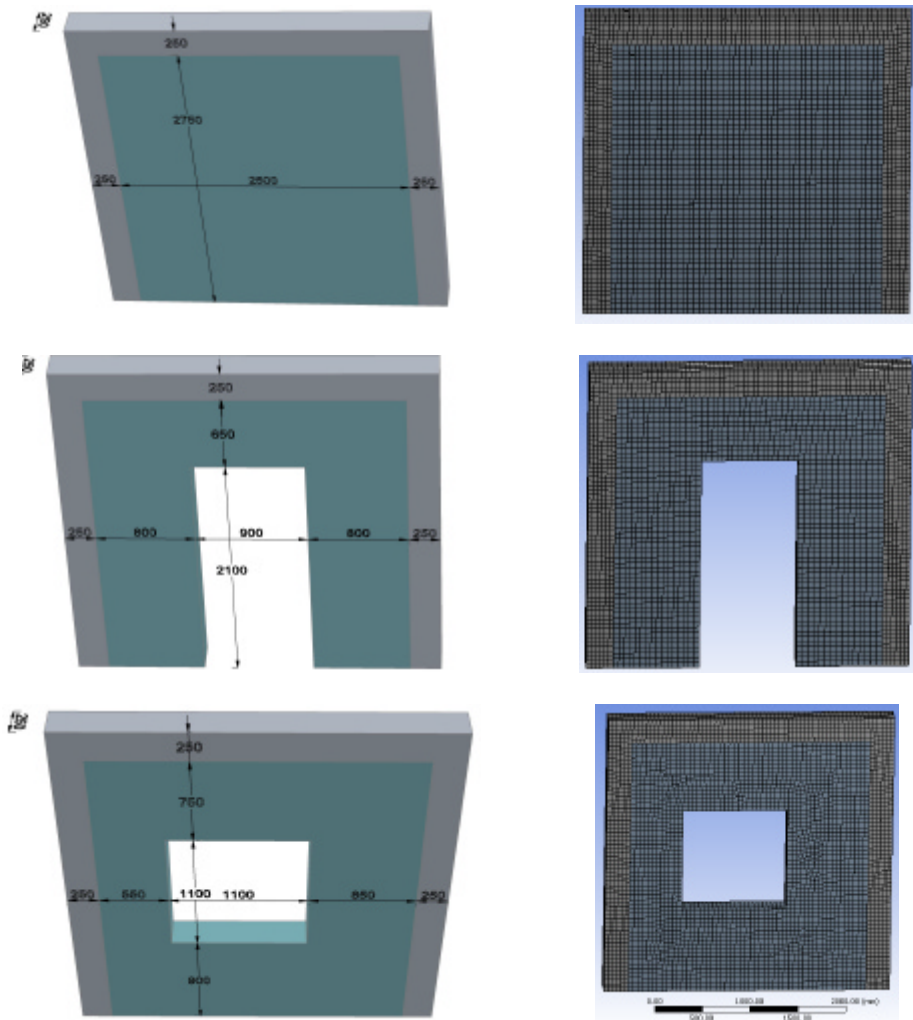


Figure 1. Layout of the analyzed configurations.

2.2. Materials used

The resistance and structural rigidity of masonry made of clay-bricks, are calculated using a parabolic – rectangular types of the stress – strain relationships "s-e" (constitutive laws) that show the real behavior of masonry (design, f_d , and characteristic values, f_k), Figure 2.

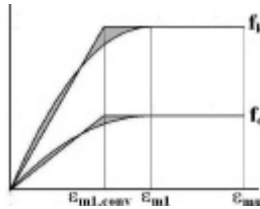


Figure 2. Parabolic - rectangular constitutive laws of clay-bricks.

The equation of constitutive law presented in Figure 2, is:

$$e = -\frac{1.1R}{E_0} \ln\left(1 - \frac{s}{1.1R}\right) \quad (2)$$

where: R = ultimate compression strength of the masonry modules;
 s = stress in the masonry modules;
 e = strain of the masonry modules;
 e_{m1} = initial strain (at first crack) of the masonry modules;
 e_{mu} = ultimate strain of the masonry modules;
 E_0 = initial elasticity modulus of the masonry modules.

The model of the stress – strain relationships "s-e" used for the autoclaved aerated concrete (AAC), also known as autoclaved cellular concrete (ACC) or autoclaved lightweight concrete (ALC) is presented in Figure 3.

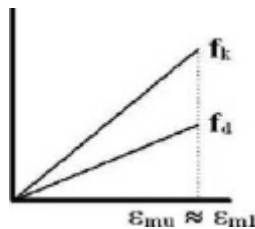


Figure 3. Linear - rectangular constitutive laws for AAC units.

The equation of constitutive law presented in Figure 3 is:

$$e = \frac{s}{E_0} \quad (3)$$

The materials are considered homogenous and isotropic and the values of their characteristics used in nonlinear finite elements analysis are presented in Table 2.

Table 2. The material characteristics used in nonlinear finite elements analysis.

Material characteristics	Clay-bricks	AAC	Reinforced concrete
Density [kg/m^3]	1600	700	2500
Young's Modulus [MPa]	10000	2420	25000
Poisson's Ratio	0.18	0.14	0.2

Besides the previous described design scenarios – geometry and materials, some additional information must be highlighted in what concerns the analysis, such as:

- the frame and the infill wall are fully restrained at the lower part;
- the interaction between the two structural components is realized using a frictionless contact (only compression stress between components are accounted for) ignoring thus the function of the mortar;
- two steps of analysis have been considered: during the first one the gravity is applied and during the second one a 100kN force is applied at the top part simulating thus transmitted by the flooring system to the frame in case of an seismic action.

The above are also presented in Figure 4.

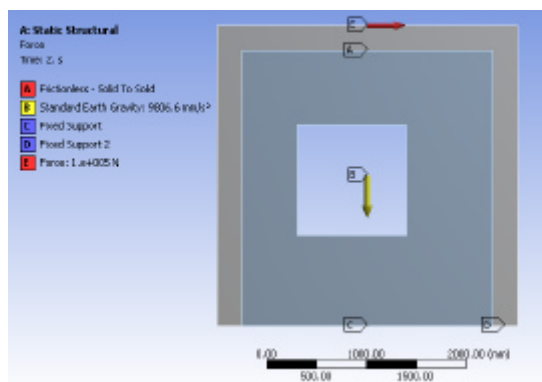


Figure 4. Boundary conditions and applied loads.

3. RESULTS OF THE ANALYSIS

The results of the analysis will be presented as contour plots. For each of the three geometries the stress distribution will be presented when using masonry (clay-bricks) and AAC as an infill material.

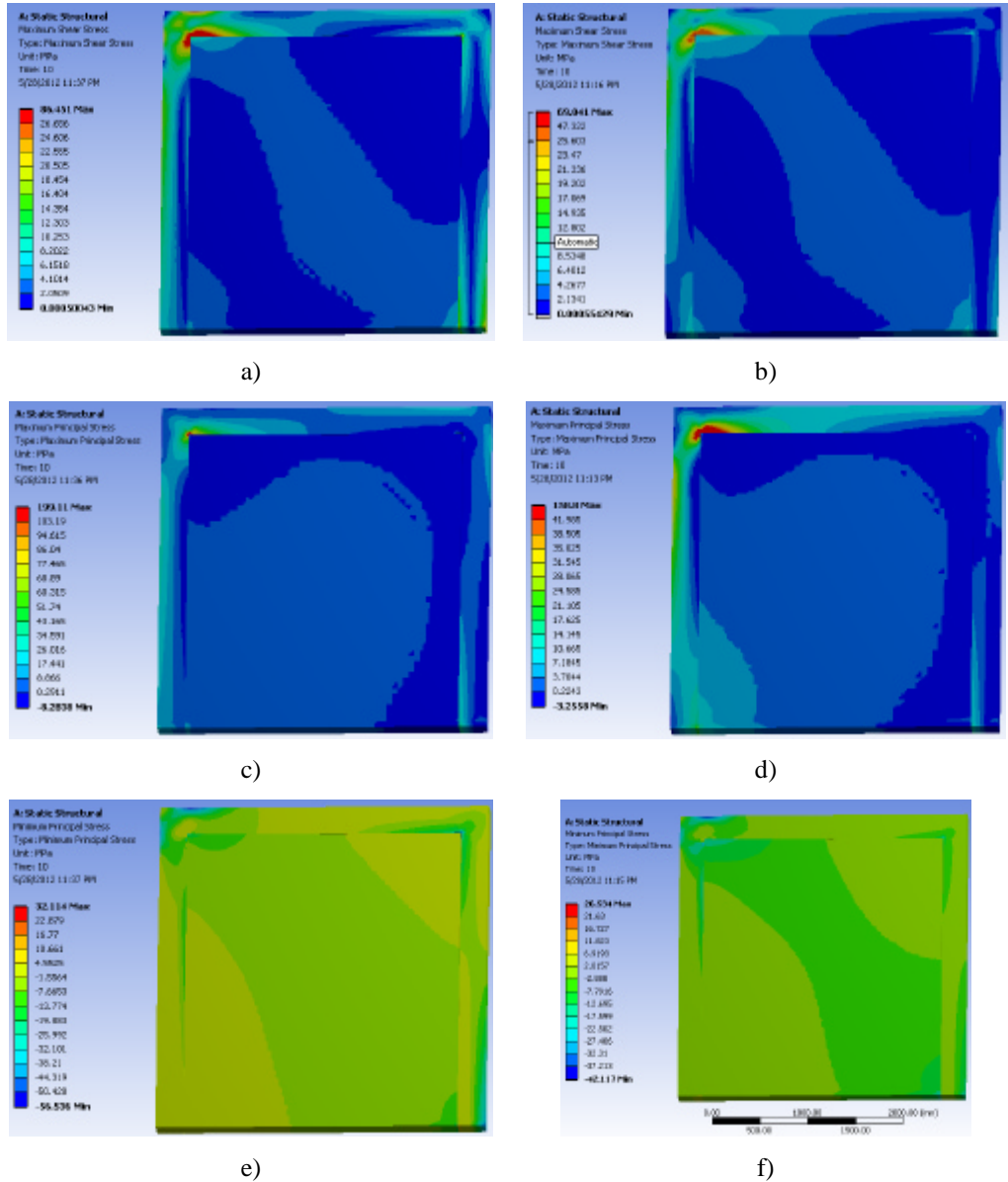


Figure 5. Contour plots:
 - maximum shear stress: a) AAC, b) masonry (clay-bricks);
 - maximum principal stress: c) AAC, d) masonry (clay-bricks);
 - maximum principal stress: e) AAC, f) masonry (clay-bricks).

The results will not be presented in a tabular manner given that their maximum values are influenced by stress singularities that occurs the interaction between the frame and the infill wall (the corner).

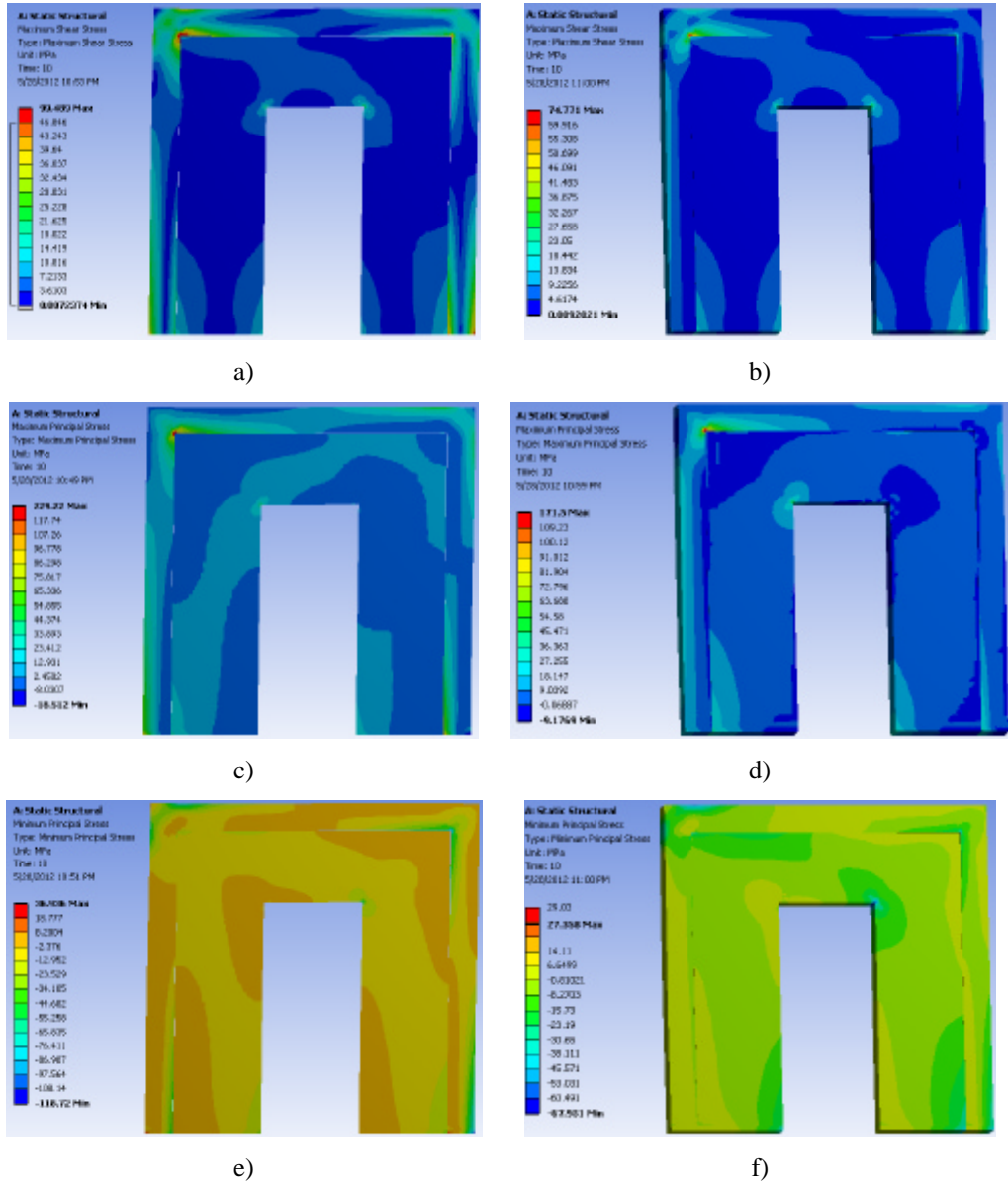


Figure 6. Contour plots:
 - maximum shear stress: a) AAC, b) masonry (clay-bricks);
 - maximum principal stress: c) AAC, d) masonry (clay-bricks);
 - maximum principal stress: e) AAC, f) masonry (clay-bricks).

As a general remark though, one could notice that the use of AAC (case that were and will be presented on the left hand side of Figures 5, 6 and 7) generally lead to higher value of stresses.

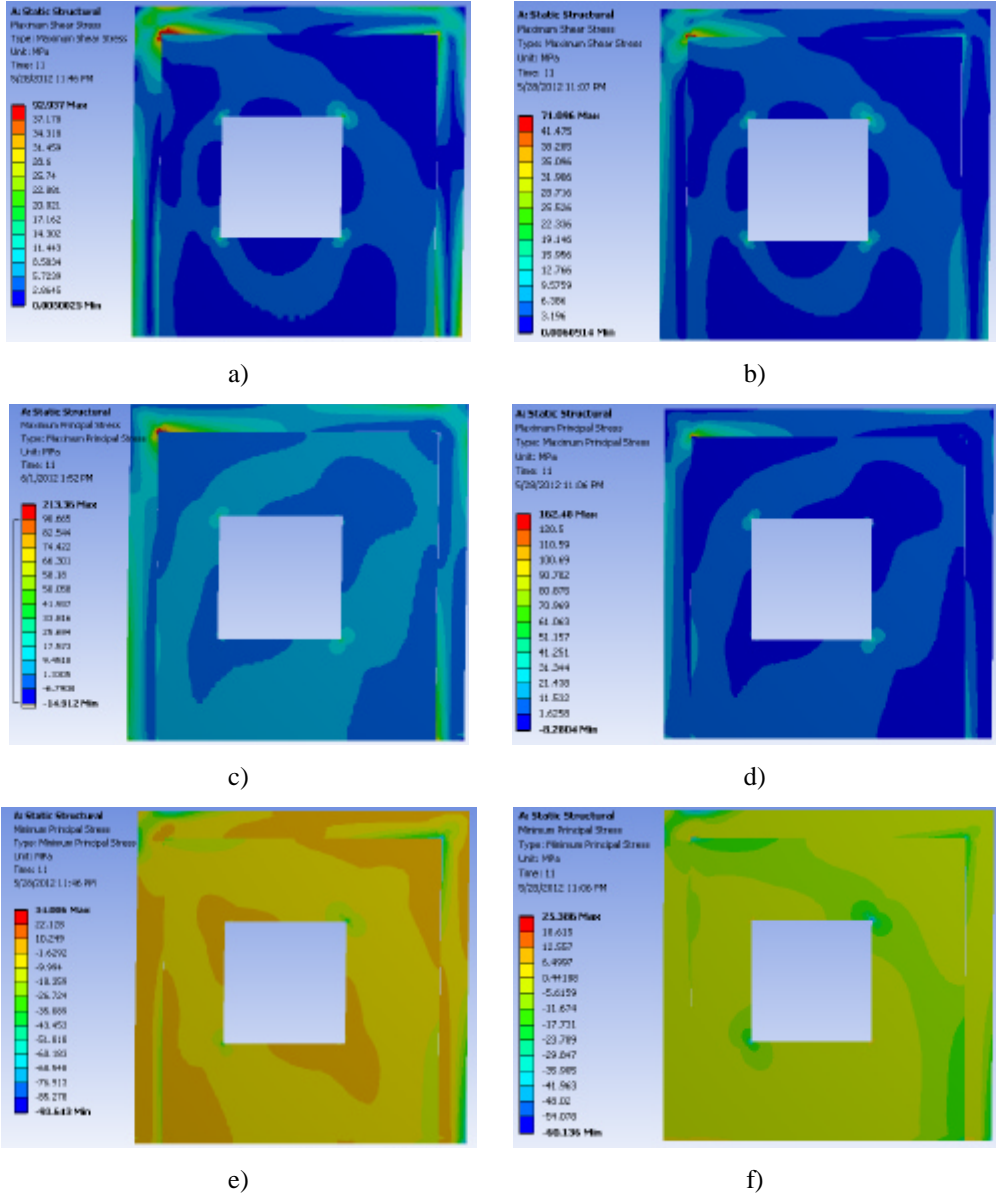


Figure 7. Contour plots:

- maximum shear stress: a) AAC, b) masonry (clay-bricks);
- maximum principal stress: c) AAC, d) masonry (clay-bricks);
- minimum principal stress: e) AAC, f) masonry (clay-bricks).

In terms of the overall behavior of the infill wall, as expected, it acts like a bracing system where a diagonal is tensed and the other one is compressed (as shown by the minimum and maximum principal stresses). High values of shear stresses occur along perpendicular planes (to the planes of principal stresses) with stress concentrations at corners (of door and window opening).

A more objective manner to evaluate the influence of geometry and infill material is given by the overall force reaction. In this way the influence of the stress concentration fades out and a more accurate evaluation of the phenomenon can be performed.

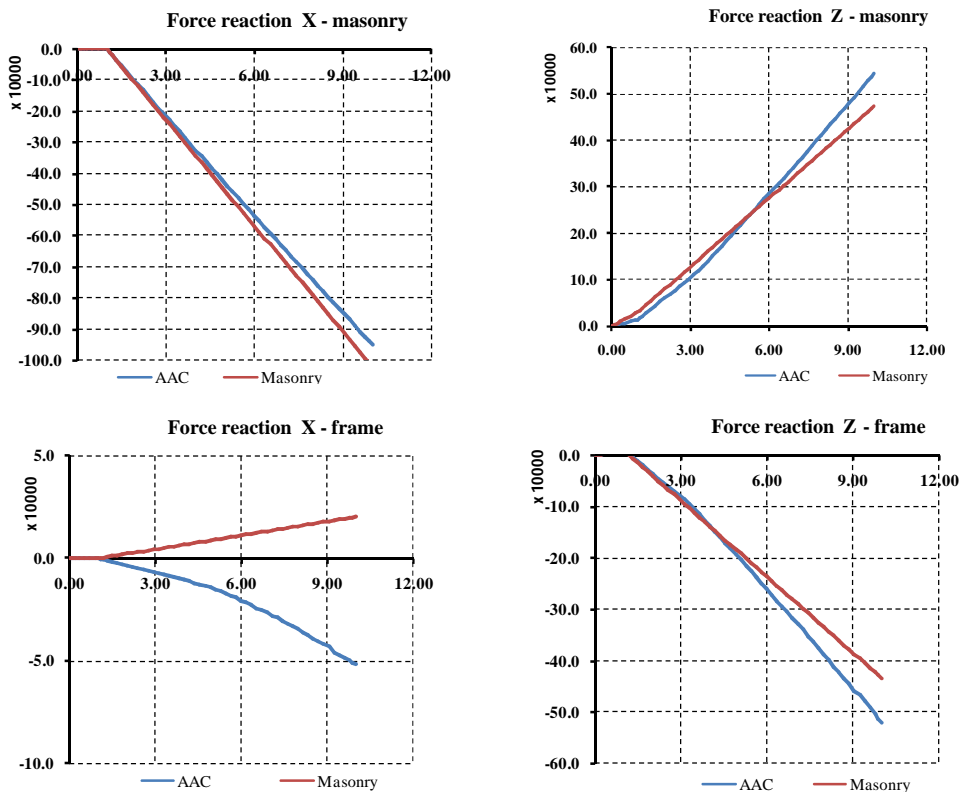


Figure 8. Force reactions at base for the frames without openings

As expected, given the material and geometric characteristics of the analyzed models (that lead to different lateral flexibilities of the two components – frame and infill) the biggest part of the exterior force is overtaken by the infill wall. Beside the X component, the applied action also leads to axial stress along Z. In this case the body forces acting upon the frame and the wall are equal but with opposite signs.

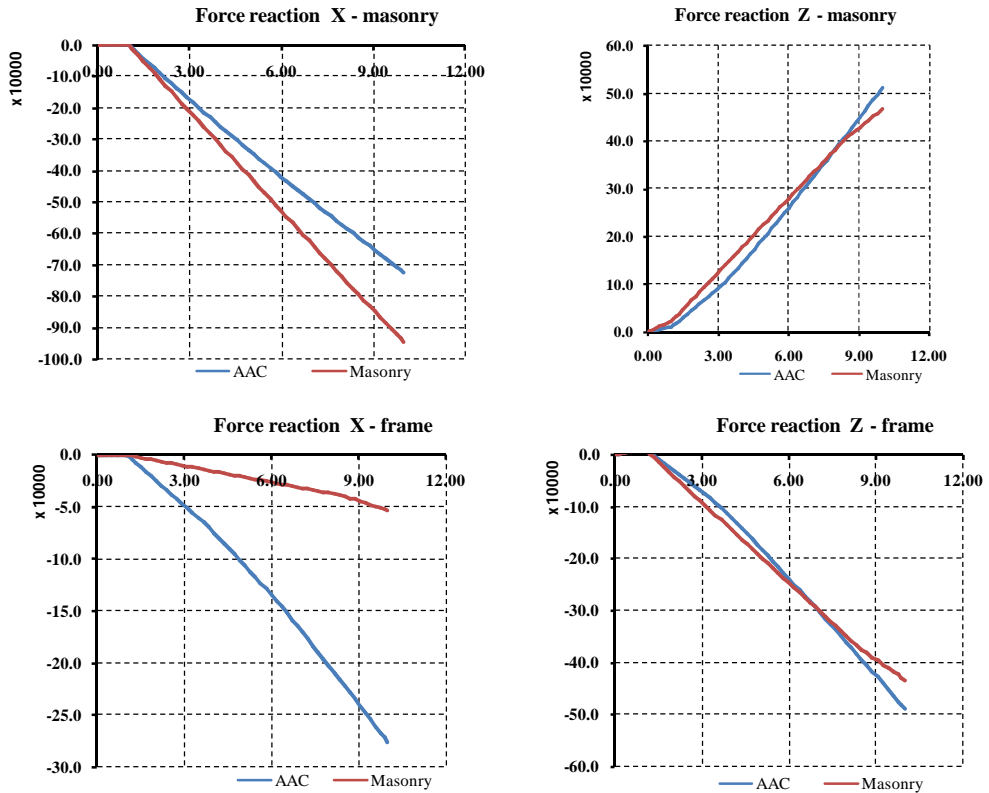


Figure 9. Force reactions at base for the frames with door opening

When comparing the effect of the infill materials one could notice that:

- the use of masonry as an infill material ensures that less horizontal forces are expected to be transmitted to the frame (in terms of reactions along X);
- considering that the amount of applied force is the same both cases, the previous statement implies that the infill material will be more stress out hence more prone to damage;
- since the AAC is less capable of sustaining significant stress the infill wall will fail faster when using it;
- given that the models do not account for material damage, and no cyclic loading has been applied the results provided by this type of analysis can only be used as a preliminary stress evaluation

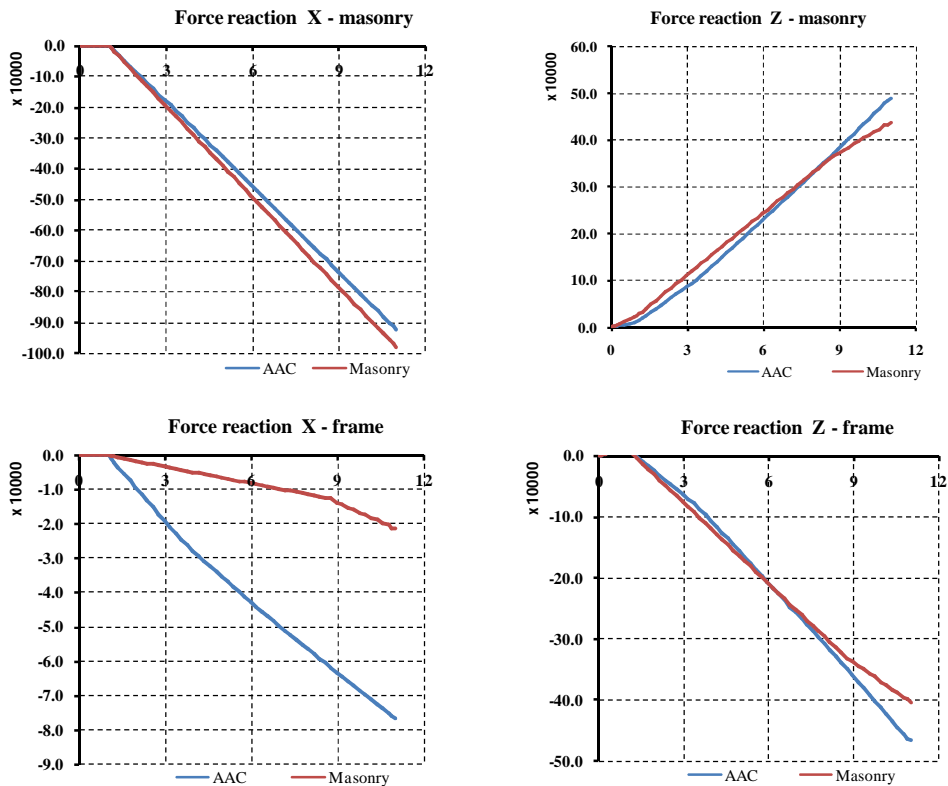


Figure 10. Force reactions at base for the frames with window opening

4. CONCLUSION

In light of the above one can conclude that using masonry as an infill material can improve the overall behavior of reinforced concrete structures if proper precautions are taken to limit the shear failure of the frames. The results show that the confining concrete frame increases the system ductility and the strength of the walls.

The structure behaves in different manner if openings are present in the wall. The force reactions in concrete frame (X direction) show considerable differences between wall without openings, wall with window opening and wall with door opening.

The use of AAC is likely to be efficient if appropriate measures are taken to limit local damages especially at the corners of the infill wall.

To overcome the limitations of the current study such as materials failure and stress concentrations due to contact between elements further studies must be performed to confirm the previously stated conclusions. Nevertheless, the step towards the development of reliable and accurate numerical models cannot be performed without a thorough material description and a proper validation by comparison with a significant number of experimental results.

5. References

1. **** - P100/2006, Romanian seismic code for design
2. **** - CR6/2006, Romanian codes for masonry design
3. **** - SR EN 1996 -1-1/2006, Romanian standards: Eurocode 6 – Design of masonry structures. General rules for masonry buildings.
4. **** - SR EN 1998 -1/2004, Romanian standard: Eurocode 8 – Building design in seismic area. General rules, seismic loads and rules for buildings.
5. Cook, R.D., Finite element modeling for stress analysis, John Wiley & Sons, 1995;
6. Cook, R. D., Malkus, D. S. and Plesha, M. E. (1989) *Concepts and applications of finite element analysis, Third Edition*, John Wiley & Sons.
7. Iu, C. K., Chan, S. L., A simulation-based large deflection and inelastic analysis of steel frames under fire, *Journal of Constructional Steel Research*, 2004;
8. Anandarajah, A., *Computational Methods in Elasticity and Plasticity: Solids and Porous Media*, Springer, 2010;
9. Bonet, J., Wood, R. D., *Nonlinear continuum mechanics for finite element analysis*, Cambridge University Press, 1997;
10. ANSYS Inc., ANSYS Workbench 2.0 Framework Version: 12.0.1, 2009/a;
11. Moaveni, S., *Finite element analysis – Theory and application with ANSYS*, Prentice Hall, 1999

Monitoring Steel Bearing Cables Using a Sound Scanning Technique

Ludovic Gheorghe Kopenetz¹, Dragos Florin Lisman²

¹Department of Structural Mechanics, Technical University of Cluj-Napoca, Cluj-Napoca, 400114, Romania

² Department of Structural Mechanics, Technical University of Cluj-Napoca, Cluj-Napoca, 400114, Romania

Summary

The paper presents a monitoring technique for structures composed of steel cables. The main idea behind this technique is the fact that wires that compose wire strands emit certain sound frequencies when their rupture occurs. In the majority of cases, steel cables do not fail totally in a sudden manner. As a result the authors propose a method for detecting the initial rupture of one or several wire strands.

By being able to detect these initial degradations, the monitoring system based on this technique will be able to instruct the users of the structures about the mandatory steps that have to be followed in order to limit or prevent material losses and to prevent any human life losses.

The entire sound scanning system depends on a set of accurate sound acquisition devices. The data acquisition devices or the sensors are the most sensitive part of the entire system. Besides the sensors which are mounted in key points along the structure, such as for example the pillars of a cable car, the system is composed of filtering and amplifying devices, preprocessing hardware/software, communication devices and a hardware platform on top of which a software application is permanently running in order to perform real-time detection and send instructions to the end users.

The authors hope to prove by several tests that this is a feasible and cost-competitive method for cable structure monitoring. There are several issues to be dealt with during the system development including permanent energy supply for the data acquisition devices, secure transmission and if necessary retransmission of sensor data and an accurate scale for assessing the magnitude of the initial degradations.

KEYWORDS: sound scanning, monitoring, real-time detection.

1. INTRODUCTION

Structures built using bearing cables can be met in many civil, infrastructure, military or mining applications. These are flexible structures that sustain and transfer predominantly tensile forces. They make use of the strength of the materials through intermolecular cohesion.

In a large number of application steel cables are used. The cables are manufactured using high quality steel and their use is, in principle, unlimited taking into account that their profitability increases with the increase of the spanning distances.

Due to the fact that these cables are subject to considerable efforts and also withstand the diverse actions of natural elements, they have to be subject to careful monitoring and any degradation or defect must be identified as soon as it may develop or even predicted, if possible.

Monitoring structures composed of bearing cables should be a permanent operation that supplies accurate information about the structural health of the objective. Any change in the cable's behaviour or of its physical properties should be available to the owners and especially to the current users of the structure.

2. MONITORING TECHNIQUES

The confirmation of the safety of bearing cable structures is based on a static and dynamic structural analysis, using beside other properties, real geometry, which means that the current observations are insufficient [1]. Real geometry for bearing elements depends on a series of aspects such as: intensity of the load, material type, operating conditions, etc.

Throughout history, different construction materials have been used for cables such as: papyrus, camel hair, flax and hemp until the 19th century, when the first steel wire cables were produced. Due to the particular properties of steel, such as high breaking strength compared to its sole weight, high flexibility and durability, steel wire cables became indispensable for a large number of structural engineering domains.

Cables used for bearing structures can have a classic or a special construction, using metallic insertion elements with three or five edges. Steel cables are produced from high quality carbon - steel with an average carbon content of 0.5% and a breaking strength of approximately 60daN/mm [2].

By wiredrawing, the circular section steel ingot is transformed into wire and the breaking strength increases up to 120 - 200daN/mm. After wiredrawing, the wires are subject to heat treating and thus the material regains its plastic properties. The

individual wires are twisted in a single or in multiple layers around a central wire forming a strand. In turn, strands are twisted around a central core forming the final cable rope [2].

The purpose of monitoring is to establish a relation between the values of the input quantity and the values of the output quantity. There are two possibilities for closed or open monitoring. The open monitoring system does not check or validate the relation between the input and output values. The closed monitoring system performs a validation of the relation between input and output values [3].

For in situ monitoring, the following methods are most frequently used: visual observation, electrochemical methods such as voltage method, magnetization method or mechanical sound method and non-electrochemical methods such as microscopic observation, gravimetry, infrared thermography, gammagraphy, radiography in the radar method [3].

In the context of the afore monitoring methods, the authors of this paper are developing a new monitoring technique based on sound scanning which they call SONCAB. The technique's test bench is pending patenting with national authorities.

3. SOUND SCANNING

This technique is based on capturing the acoustic signals emitted in the preceding moments and during the moments when elementary steel wires break. The breaking of composing wires of bearing cables can generate certain sounds and can represent an important signal of bearing strength degradation [4]. This sound signal propagates both through cable material and air. The intensity of the signal is proportional with the number of ruptured wires and thus appears the possibility of designing an efficient and strong structural control [5].

3.1. General architecture of the sound scanning system

The general architecture proposed for the SONCAB system under development has the main building blocks presented in Figure 1. These are:

- several sensing blocks;
- the trigger and signal identifier block;
- one or several data aggregation block;
- one or several data storage blocks;
- several data analysis and interpretation blocks.

The sensors that will be used in the test implementation of the system have to be robust, easy to mount and must have electromagnetic screening. The sensors are chosen in such a way that vibrations, environmental temperature and the effects of

electric or magnetic fields have a very small influence on their functioning. The main component of each sensing block is composed of at least one measurement microphone. A measurement microphone provides an analog output signal that is proportional to the variation in the acoustic pressure acting upon a flexible diaphragm.

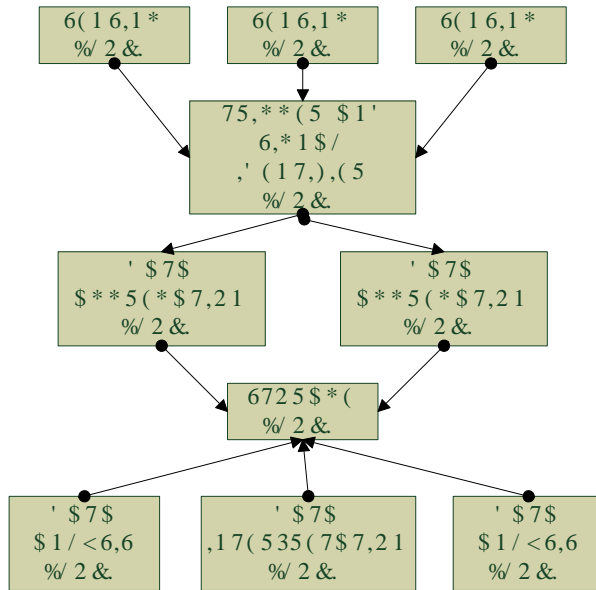


Figure 1. The building blocks of SONCAB system

3.1.1. Sensing blocks

As presented above, the measurement microphone is the most important component of the sensing block. These microphones are very different from those used in audio applications because their main feature is to accurately reproduce the sound waveform without distortion and with a linear relationship between the voltage and the pressure sensed by the microphone's diaphragm [6].

One of the most important properties of a good measurement microphone is sensitivity. Sensitivity is the ratio between its output voltage and the acoustic pressure sensed by the diaphragm. Sensitivity is measured in mV/Pa. For a microphone sound measuring system, the magnitude of the sensitivity is used to establish the minimum sound pressure that the microphone can measure accurately [7].

If there are variations of the sensitivity over the range of frequencies to be measured, these produce a distortion in the output signal compared to the acoustic

signal. The minimal requirements that a measurement microphone must comply to are:

- it has to exhibit a constant sensitivity over the range of frequencies to be measured; to have a flat frequency response;
- it has to have a nearly constant sensitivity over a wide range of temperatures and barometric pressures;
- the microphone sensitivity should exhibit the linearity property, namely, it should be nearly constant over a wide range of sound pressure levels. This produces a linear dependence between the microphone's output voltage and the sound pressure [6].

The composing elements of a sensing block are presented in Figure 2. These are the measurement microphone(s), cables, power supply and amplifiers.

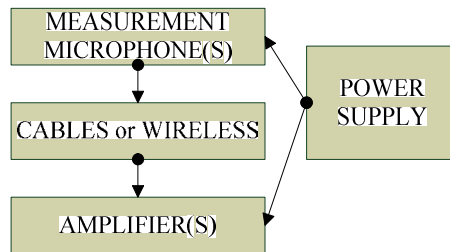


Figure 2. Sensing block

The most common measurement microphone types used in sound sensing applications are [8]:

- piezoelectric microphones;
- capacitive microphones;
- dynamic microphones.

Piezoelectric microphones are a good choice for a sound monitoring system like SONCAB due to the fact that they are often used in high pressure measurement situations. Still, there exists a disadvantage of using such a microphone: they have a low noise floor which limits their use in precision sound measurement applications [9].

Dynamic microphones are well suited for voice and audio applications but are not a good choice for sensing the sounds produced by the rupture of individual steel wire elements due to the following disadvantages: limited dynamic range, high sensitivity to vibrations and a frequency response that is not flat enough [6].

In the case of capacitive or condenser-based microphones, the movement of the diaphragm is relative to a fixed plate which produces a capacitance variation proportional to the sweep of the diaphragm. The capacitance variation is converted to a voltage variation. This type of microphone is the most appropriate choice for

the sound wave sensing component in the SONCAB monitoring system. The following characteristics make it the most appropriate choice: high stability, low internal noise, wide dynamic range, low distortion, high sensitivity and a flat frequency response.

In what concerns the connecting cables, usually these are the most error-prone component of the sensing block. Nevertheless, they should be able to support a wide temperature range and must accurately function under high humidity conditions. As an alternative to these cables, the sensing blocks can be equipped with wireless transmitters/receivers. This would imply that other blocks have to have the same wireless capabilities in order to be able to communicate with the sensing blocks.

The power supply must be temperature and time stable. It also has to resist to shocks and vibrations and have low susceptibility to magnetic and RF fields.

The amplifiers are responsible for providing gain, impedance matching, output drive current and for performing additional signal processing tasks. They also provide gain stability, linearity and they must have low residual noise and a zero temperature coefficient.

3.1.2. Trigger and signal identifier block

This block contains components responsible for sending the command signals to the sensing blocks. This is a complex process that takes as input the sound waves captured by a sensing device and decides based on their values to trigger the sound wave acquisition on other sensing devices.

This block is responsible for performing the function of an adaptive detection trigger which samples the signals received from a certain number of channels by comparing them to an adjustable reference voltage with the help of a set of voltage comparators.

3.1.3. Data aggregation blocks and the storage block

The data aggregation blocks are responsible for gathering the sensed and conditioned sound wave data from the sensing blocks. Several sensing blocks fan the data in an aggregation block. From the aggregation block data is routed to the storage block. An aggregation/storage block can be either a data acquisition system like the HBM MGCplus device available in the research team's experimental laboratory or it can be a PC or laptop equipped with proper extension boards and a storage interface to a memory capable of storing large amounts of data at high speeds, like for example a flash memory system [10], [11].

3.1.4 Data analysis and interpretation

The sound taken into account when performing data analysis and interpretation is the sound transmitted through the cable from the sound source (the breaking point of one or several elementary wires) to the sound sensors. For evaluation purposes, only the direct sound generated will be taken into account. For the directly transmitted sound, attenuation created by the cable mass has to be accounted for by using the mass laws specified in dB by Equation (1):

$$TL = k \log MS + r \tag{1}$$

The sound frequencies propagate through the cable material with a velocity of approximately 5000m/s towards the anchoring points of the cables [4]. The intensity of the sound signal is proportional to the number of broken wires or strands, thus having the possibility of developing an efficient structural control system.

A typical scenario of using the SONCAB steel cable monitoring system is presented in Figure 3.

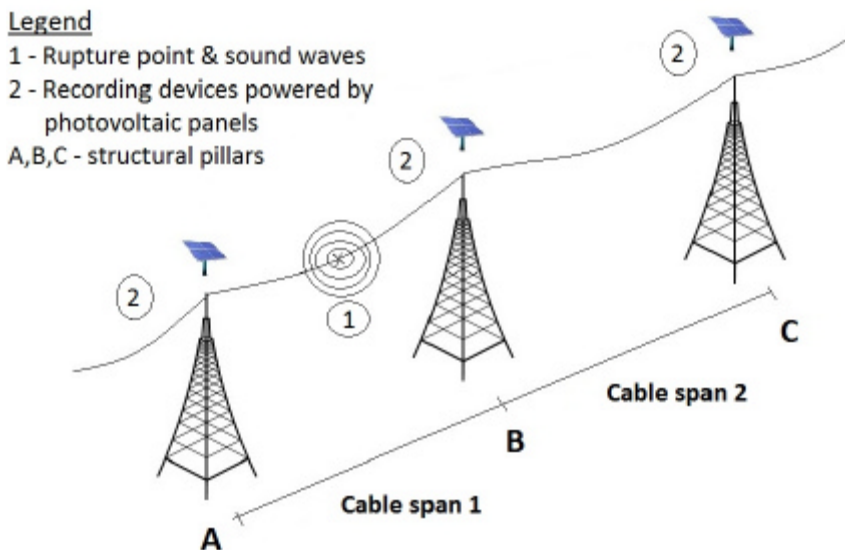


Figure 3. SONCAB scenario

This scenario presents a transport cable passing above a set of three structural pillars (A, B, C). On each pillar a sensing device along with a data recording device is mounted (2). The sensing devices have solar panels as energy supplies in order to be independent and in order to harvest the available luminosity. The calibration

tests for the sensor require intense work in order to obtain the required transfer function.

If a rupture event occurs at point (1) on the cable as suggested in Figure 3, the sound taken into account when measuring is the sound transmitted through the cable from the sound source, namely the breaking point of one or several elementary wires, to the sound sensors. For evaluation purposes, only the direct sound generated by the rupture, will be taken into account. The filtering of refractory components is assured through electronic screening.

The problems posed by the interpretation of data resulted from the sound monitoring of bearing cable structures are of great complexity, due to the multiple of random variables that intervene. As a result, the authors propose one interpretation method using fuzzy-logic based reasoning for interpretation and quantification of data resulted from monitoring [2].

4. CONCLUSIONS

With the increasing degree of complexity of constructions (high-rise and with large-spans) using bearing steel cables, an increase in the need of evaluating the associated risks appears.

Continuous, periodic or continuous-periodic monitoring helps analyze and mitigate these risks. The results of monitoring constitute a starting point when taking decisions concerning interventions to the structure in order to avoid local or chain collapse.

The authors hope to prove the feasibility of sound monitoring of steel bearing cables during the following months by testing a prototype of the SONCAB system out of the laboratory.

Up to now, several tests have been performed with different sensing devices in the faculty's experimental laboratory by sensing and recording the sound waves produced during the controlled rupture of different steel cables with diameters around 12mm.

References

1. Lazar-Mand, F. and Lisman, D.F., Practical aspects about linear dynamic analysis of cable structures, Proceedings of the 6th International Symposium "Computational Civil Engineering", Iassy, Romania, ISBN: 978-973-8955-41-7, 2008.
2. Kopenetz, L.G. and Gobesz, Zs., The Structural Expertise of Steel Cables, Transportation Infrastructure Engineering, edited by Intersections, Vol. 4, Iassy, Romania, pp. 49-62, 2007.

3. Kopenetz, L. and Lisman, D.F., Relatime Behavioral Monitoring of Cable Transport Structures, Journal of Applied Engineering Sciences, vol. 2(15), Issue 1/2012, Oradea, Romania, e-ISSN: 2284-7197.
4. Pellerin, G., Acoustique architecturale: Théories et pratiques, electronic version, 2006, http://assoacar.free.fr/archives/Cours/Ac%20des%20salles/Acoustique_Architecturale_CNAM.pdf, viewed at 07/03/2012 (in French).
5. Malet, T., Acoustique des salles - Le guide de référence du praticien, Publications Georges Ventillard, Neuilly sur Marne, France, 2005.
6. Townsend, C. and Arms, S., Test and Measurement Microphones, Chapter 18, pp. 481-501, from Sensor Technology Handbook, Elsevier Newnes, Oxford, UK, 2005.
7. Tashev, I.J., *Sound Capture and Processing: practical approaches*, John Wiley and Sons Ltd., West Sussex, UK, ISBN: 978-0-470-31983-3, 2009 .
8. Fraden, J., *Handbook of Modern Sensors, Physics, Designs and Applications*, 4th edition, Springer Science, New York, USA, ISBN: 978-1-4419-6465-6, 2010.
9. Brandstein, M. and Ward, D., *Microphone Arrays: Signal Processing Techniques and Applications*, Springer Verlag, Berlin, Germany, ISBN: 978-3-642-07547-6, 2010.
10. ***, Product web site, <http://www.hbm.com/en/menu/products/measurement-electronics-software/laboratory-test-stand/mgeplus/>, accessed on 05/03/2012.
11. ***, SD Association Homepage, <https://www.sdcard.org/consumers/speed/>, viewed on 03/03/2012

Possibilities of using the genetic algorithms to solve optimization tasks in construction projects

Marek Krajnák

Institute of Civil Engineering Technology and Management; Faculty of Civil Engineering, Technical University of Kosice, Slovakia. E-mail: marek.krajnak@tuke.sk

Summary

Article discusses the use of genetic algorithms to solve optimization problems in construction, focusing on the possibilities and limitations of their use in conditions of construction practice. The genetic algorithms bring new approaches to solutions and provide an interesting alternative to conventional optimization methods. It is an access solution with internal intelligence and ability to improvement. Contribution refers to specific application areas within construction resources optimization to increase efficiency of construction.

KEYWORDS: construction resources optimization, genetic algorithms, construction projects, effectiveness

INTRODUCTION

Currently, the increasingly frequent is use of evolutionary computing or evolutionary algorithms for solving complex mathematical, technical and non-technical problems. These methods, or rather algorithms basically simulate principles of biological evolution. As can be seen in living nature around us, evolution is basically simple, but on the other hand, very robust and powerful optimization tool. Biologists say that is valid for single-celled organisms as well as for most complex organisms consisting of thousands of billions of cells [1].

Genetic algorithms (GAs) are based on biological principles of evolution and provide an interesting alternative to “classic” gradient-based optimization methods. They are particularly useful for highly nonlinear problems and models, whose computation time is not a primary concern. Similar to other search methods they perform better than gradient-based methods in finding a global optimum if a problem is highly nonlinear and features multiple local minima. In general, GAs approach the entire design space randomly and then improve the found design points by applying genetics-based principles and probabilistic selection criteria [2], [3].

1. HISTORICAL EVOLUTION OF THE GENETIC ALGORITHMS

Scientists started to deal with these random genetic changes and natural selection and tried to bring these principles to solve practical problems that people face every day. Simulation of thousands to millions of evolutionary cycles, that occur in nature, requiring powerful computers, which in the early development of these methods were not available. Therefore, until the second half of the 20th century began at different locations around the world to solve different problems arise by natural evolution of the different design, but in some respects similar approaches. In Germany in the mid-60th years, Rechenberg and Schwefel have developed in optimizing engineering tasks so. evolutionary strategy. Lawrence Fogel in the U.S. introduced, during modeling and design of machines, a technique called evolutionary programming. As the beginning of genetic algorithms are considered working group led by John Holland of the University of Michigan in the USA in 70s the 20th century [1].

These discoveries, or several others, now cover the concept of evolutionary algorithms. All these approaches have evolved and still evolving and simultaneously influence each other, so the boundaries between them are more and more lost. All have common features, which form the basis of stochastic optimization based on changes in the individual competition and potential solutions. The most popular representative of this group is just genetic algorithms [1].

2. PRINCIPLES OF OPERATION OF THE GENETIC ALGORITHMS

GA is an universal browser and stochastic optimization approach, which is bordered by in the space of admissible solutions to the problem or be able to find at least closer to the global optimum [3] [4]. It shall apply when the nature of the principle of survival of strongest individuals and the necessity of termination the weakest or non-viable [5].

The genetic algorithm works with a group of several potential solutions of the problem - with a population. Each potential solution (also individual) is represented by an ordered set parameters or values that fully describes the properties and of which looking for the best combination. The elements of this set are called genes and can be binary-numeric, integer-numeric, real-number, symbol or mixed type depending on the nature of the problem. They are arranged in sequence, called a string or chromosome [6].

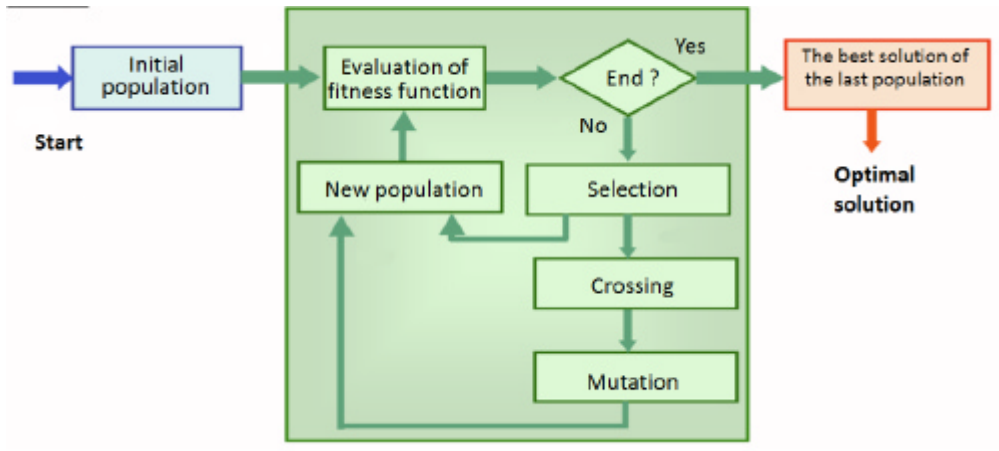


Figure 1: Block diagram of the genetic algorithm [8]

2.1 Operators of the GAs

The initial population of strings in the first calculation cycle (first generation) is obtained by randomly generating of genes within the planned boundaries. For each solution, which is decoded from the string into an existing computer model to quantify the calculation, is needed to determine value of objective function - fitness. Fitness is actually a measure of success or suitability of the string.

Another definition describes the objective function as an objective task, expressed by linear form, while the optimum form must ensure selected solution [7].

All individuals of the population compared to each other and then select a group of individuals into an unchanged new population. Also select a second group of individuals, which is designed to innovation by these operators:

- **Selection,**
- **Crossing over,**
- **Mutation.**

Operation of crossing randomly combines genes of two parents. In the ordinary way, crossing the two parent strings divided into one or more random locations and descendants receive alternately every second of the following substrings separated from each parent (Figure 2, Figure 3). Operation of mutation randomly changes the randomly selected genes randomly selected subjects (Figure. 4). Methods for selection of individuals into new populations are also several species differ in degree of preference and way the most successful individuals compared to

randomly selected individuals. The choice of all these genetic operations is influenced by the type of problem solving [5].

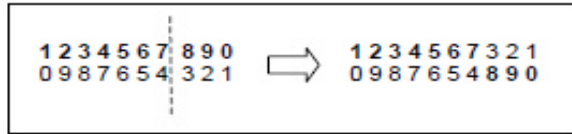


Figure 2: Example of one-point crossing of two integer strings [5]

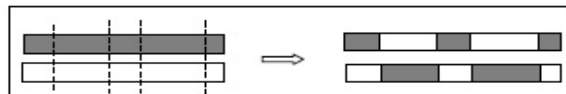


Figure 3: Example of multi-point crossover of two strings [5]

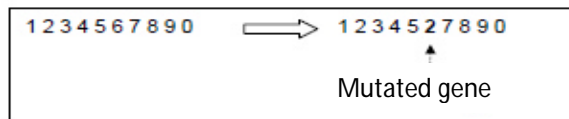


Figure 4: Example of integer string mutation [5]

2.2 Features of the GAs

As can be seen above, the primary usefulness of the GA is that it starts by sampling the entire design space, possibly enabling it to pick points close to a global optimum. It then proceeds to apply changes to the ranked individual design points, which leads to an improvement of the population fitness from one generation to another [2]:

The main advantages of GAs are:

- the nature of the optimization model does not need to be known. This makes GAs very interesting for complex problems or for users inexperienced in gradient-based optimization techniques,
- the optimization model and its constraints do not have to be continuous or even real values. No simplification of a problem is necessary to accommodate it to a particular algorithm (e.g. linearization),
- they are readily available and easily implemented.

The main disadvantages of GAs are:

- a large number of parameters need to be set. This is simplified by information from literature, but problem-specific adjustments might need to be made,
- due to the comparatively very large number of function calls, GAs require significant computational resources. This makes them unattractive for optimization problems with computationally demanding analyses.

3. APPLICATION OF THE GAS IN CONSTRUCTION PROJECTS

As indicated, genetic or evolutionary algorithms can be used to resolve a very wide range of tasks. The condition is the ability to formulate an objective function which is to be minimized or maximized. The minimization is usually to minimize the deviations (errors) from the desired state, minimizing energy consumption, fuel costs or losses, to minimize adverse effects and so on. The maximization can go to maximize efficiency, performance, profits etc. Another condition is the existence of their use of computer optimized representation of the problem. This means that for any point on the search space we can calculate the value of the objective function - evaluate it in terms of success rate in terms of meeting the desired objective [5].

3.1 Dividing of the optimization tasks in construction projects

There are several studies on distribution of optimization problems, in this paper are divided optimization problems based on economic-process model [9]:

- **resource optimization**
 - optimization sub deliveries purchasing,
 - optimization of acquisition costs of material,
 - optimization of storage costs,
 - optimizing purchasing policies,
- **process optimization**
 - optimization of continuous supply of material for construction,
 - optimization of the transfer of masses,
 - optimization of performance standards,
 - optimization of technological processes,

- optimization of organization works,
- optimization of resource consumption standards,
- **optimization of construction products**
 - optimization of the production program,
 - optimization of material composition of structures,
 - optimization of under construction,
 - optimization of construction activities in terms of production costs,
- **optimization of customer**
 - optimization of pricing policy,
 - optimization of marketing,
 - optimization of customer base.

4. ANALYSIS OF AVAILABLE SOFTWARE TOOLS

The following text gradual introduces three different software that use genetic algorithms to solve optimization problems. A common feature is the use of Excel as a workplace.

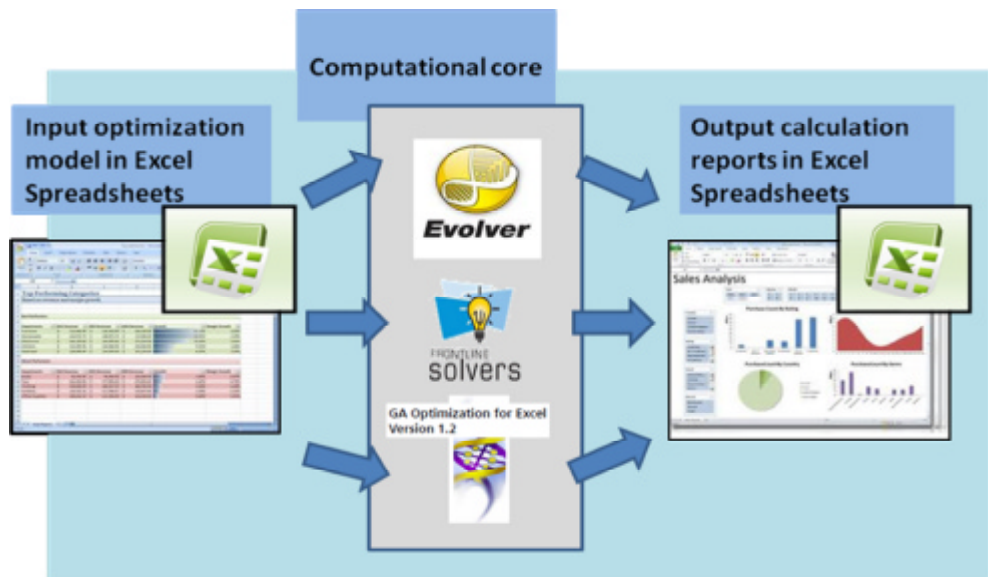


Figure 5: Optimization process using GA software (Source: Author)

4.1 Evolver (from Palisade Corporation)

Evolver is the genetic algorithm optimization add-in for Microsoft Excel. Evolver uses innovative genetic algorithms (GAs) technology to quickly solve optimization problems in finance, distribution, scheduling, resource allocation, manufacturing, budgeting, engineering, and more. Virtually any type of problem that can be modeled in Excel can be solved by Evolver, including previously unsolvable, complex nonlinear problems. Evolver is available by itself or as part of the software package - Decision Tools Suite.

Evolver is available in Professional and Industrial editions. The Professional edition allows up to 250 adjustable variables per model, while the Industrial edition allows unlimited variables. Use Evolver Industrial edition for largest models where we can control hundreds or thousands of adjustable cells [10].

4.2 Solver (from Frontline Systems)

Solver, within the software package Microsoft Office 2010, allows using a genetic algorithm, in addition linear and nonlinear algorithms that were available in earlier versions. Like Evolver uses the solver to work full compatibility with Excel. By means of solver can find the optimum (maximum or minimum) value of the formula in one cell (called the target cell) under the restrictions of values of other cells with formulas in the worksheet. Solver works with a group of cells called the decision variables or variable cell calculations involved in target cells and cells with a restriction. Solver adjusts the values in the cells of the decision variables so as to not exceed the limits in the cells with the restrictions and to obtain the desired result for the target cell [11].

4.3 GA Optimization for Excel (from A. Schreyer)

This program allows the user to take an Excel spreadsheet with any type of calculation data (no matter how complex) and optimize a calculation outcome (e.g. total cost). This is based on the selection of up to five design variables and up to five constraints. The optimization can be performed as maximization, minimization or the attempt to reach a target value. Applications for this technique lie in every field of work. If the problem can be modeled in Excel, it can be optimized using this program. The main advantage of this program is that it can solve highly nonlinear problems or problems that feature discontinuous functions. The software is the result of a term project in a class on engineering design optimization [12].

CONCLUSION

Genetic algorithms are powerful and perspective optimization tool, which uses the popularity and now clearly rising. It is a time and computationally consuming approach, but the current trend growth performance computing, this factor loses significance. In addition, GAs do not impose great demands on the user. They are quite able to solve a variety of universal problems, which can replace the need for knowledge of many other optimization methods and area of optimization of construction projects is an area where it could be the potential of these advanced methods fully exploited.

Contribution was written within the implementation of the project VEGA 1/0840/11 Multi-dimensional approaches to support integrated design and management of construction projects.

References

1. Špacek, J.: Concurrent Engineering. *Optimizing the implementation of PLM systems to companies using genetic algorithms*. Brno: Vysoké učené technické v Brne, Fakulta strojního inženýrství, 2006. 26 s.
2. Schreyer, A.: *GA Optimization for Excel Version 1.2. Genetic Algorithm Optimization in Excel Spreadsheets. Quick Start Manual*. 2006. available on the Internet: http://www.alexschreyer.net/blog/wp-content/uploads/2006/12/ga_optimization_for_excel_1_2.pdf
3. Goldberg, D.: *Genetic Algorithms in Search, Optimization and Machine Learning*. Addison-Wesley, 1989.
4. Z.Michalewicz: *Genetic Algorithms+Data Structures=Evolutionary Programs*. Springer, 1996
5. Sekaj, I., Foltin, M.: *Matlab Toolbox – Genetické algoritmy*. STU Bratislava.
6. Sekaj, I.: *Riešenie problémov pomocou genetických algoritmov*. Automatizace, vol. 47, 2004, No. 9, p. 552-555.
7. Bašková, R.: *Modelovanie procesov výstavby. Ekonomicko-matematické metódy – cast I. Lineárna optimalizácia a sieťová analýza*. Košice: SvF -TU Košice: október 2004. 150 s.
8. <http://www.posterus.sk/?p=3364>
9. Mesároš, F., Mesároš P.: *Process oriented approach on optimization of construction works costs*. In: *Ekonomika a manažment podniku*. - ISSN 1336-4103. - Roc. 5, c.1, 2007. s.74-84.
10. <http://www.palisade.com/devkits/edk.asp>
11. <http://office.microsoft.com/sk-sk/excel-help/definovanie-a-riesenie-problemu-pouzitim-riesitelu-HP010342416.aspx>
12. <http://www.alexschreyer.net/projects/xloptim/>
13. Bašková, R., Spišáková M.: *Diagram for leveling Formwork*. In: *Selected Scientific Papers: Journal of Civil Engineering*. - ISSN 1336-9024. - Roc. 5, c. 1 (2010), s. 97-104
14. Bašková, R.: *Dilef method for optimization of formwork*. In: *CzechSTAV 2010 : stavební systémy a technologie : sborník příspěvků z mezinárodní vědecké konference : 25. - 29.října 2010, Hradec Králové, Česká republika*. - Hradec Králové : Magnanimitas, 2010. - ISBN 978-80-86703-38-1. - P. 118-125

Design of Experiment Application in Thermal Bridges Assessment

Daniel Lepadatu, Adrian Iacob, and Adrian-Alexandru Ciobanu
Department of Civil and Industrial Engineering, Faculty of Civil Engineering and Building Services, "Gheorghe Asachi" Technical University, Iasi, 700050, Romania

Summary

Implementation of Energy Performance of Buildings Directive (EPBD) in national regulations demands an enhancement in envelope thermal efficiency requirements, and implicitly a higher consideration in thermal bridges assessment.

The purpose of this paper is to emphasize the significance of different factors involved in the effect of thermal bridges, subjecting to analysis critical areas of the envelope of prefabricated concrete large-panel apartment buildings.

Values for linear thermal transmittances and temperature factors are obtained by numerical analysis of steady-state bidirectional thermal field, using a heat transfer software. The parameters of thermal bridges are computed for variable values of thermal properties of materials and geometric characteristics of building details.

In order to render guidance for a good practice in building energy audits, a great variety of thermal bridges should be solved, leading to a high amount of work.

This study consists of an analysis of results obtained by numerical simulation, by means of statistical method of investigation. The method is based on an experimental plan, defined by limit values of ranges for factors that influence the energy performance and by the corresponding values for response parameters. Through a nonlinear regression model are established equations in order to determine the response factor for intermediate values of the variable factors. Therefore, a small number of numerical simulations for a type of thermal bridge offers the possibility to solve the more wide series of its configurations.

KEYWORDS: design of experiment, building envelope, thermal bridge, prefabricated concrete large-panel, energy efficiency.

1. INTRODUCTION

Although *Directive 2010/31/EU of the European Parliament and of the Council of 19 May 2010 on the energy performance of buildings* does not include explicit indications upon thermal bridges issue, under this aspect, still proves a great impact through national building codes, which follow European perspectives on energy efficiency. Thus, implementation of Energy Performance of Buildings Directive (EPBD) in Romanian national regulations demands an enhancement in envelope thermal efficiency requirements and implicitly a higher consideration in thermal bridges assessment.

A thermal bridge is defined as part of the building envelope where the otherwise uniform thermal resistance is significantly changed and which has a major effect on its thermal performance by giving rise to two- or three-dimensional heat flows (Janssens, 2007). Under the aspect of health and comfort a thermal bridge introduces an area with lower interior surface temperature, where the condensation of indoor moisture causes a high relative humidity, and furthermore the risk of mould growth (Gudum, 2008).

About 70% of apartment blocks in Romania are prefabricated concrete large-panels buildings constructed before 1989, this constructive solution being wide-spread in all eastern and central European states and also in many parts of the Soviet Union, with only a few local changes made (Ilomets *et al.*, 2011). Most of these buildings fail to meet today's energy performance standards, mainly because of low requirements for thermal performance in the previous construction standards and lack of attention to the quality of construction practices.

In energy envelope assessment there are many factors with high influence over thermal analysis results and reduced possibility of being precisely determined, thus giving rise to inaccurate calculation. In order to provide a more comprehensive evaluation of energy performance, there has to be taken into account the uncertainty of input parameters, which implies a lack of information about true value and also variability representing the heterogeneity of parameters (Jaraminiene & Juodis, 2006).

For this reason Design of Experiment method can be a useful tool in the investigation of those parameters. This method was introduced in the '20s by Sir R.A. Fisher, and the agronomists were among the first to understand its practicability. Towards the '60s, due to Taguchi's work, Design of Experiment is implemented in Japanese industry in order to take in consideration processes variance. Afterwards, this method was in the '80s assumed in U.S.A., and also in Europe in the '90s. Design of Experiment is applied to all “black box” phenomena, for which is intended an optimization (Lepadatu *et al.*, 2005; Lepadatu *et al.*, 2006) of response parameter by controlling of input factors.

2. DESIGN OF EXPERIMENT METHOD AND RESPONSE SURFACE METHODOLOGY

2.1. Design of experiments

The optimization process of different quality characteristics of a system is an essential one for every study, if the goal is to answer to the present requirements. This process refers to manipulating the most important process variables to levels or settings that result in the best obtainable set of operating conditions for the system. Response Surface Methodology (RSM) is a collection of mathematical and statistical techniques for empirical model building (Mayer & Montgomery, 1995; Cornell, 1990). The objective of experiments is to optimize a response (output variables) which is influenced by several independent variables (input variables). Originally, RSM was developed to model experimental response (Box *et al.*, 1978) and then migrated into modeling of numerical experiments which are less expensive. The difference is in the type of error generated by the response.

An important and simplified tool of RSM is the Design of Experiments (Box *et al.*, 1978), usually abbreviated as DoE. The objective of DoE is the selection of the point where the response should be evaluated. In a traditional DoE, screening experiments are performed in the early stages of the process, when it is likely that many of the design variables initially considered have little or no effect on the response. The purpose is to identify the design variables that have large effect for further investigation. To construct an approximate model that can capture interactions between N design variables, a full factorial approach (Montgomery, 2001) may be necessary to investigate all possible combinations. A factorial experiment is an experimental strategy in which design variables are varied together, instead one at a time. If the number of design variables becomes large, a fraction of a full factorial design can be used at the cost of estimating only a few combinations between variables. This is called fractional factorial design and is usually used for screening important design variables. Genichi Taguchi, a Japanese engineer, proposed several approaches to experimental designs that are sometimes called "Taguchi Methods." "Taguchi" designs (Taguchi & Konishi, 1987) are similar to our familiar fractional factorial designs. Taguchi introduced a new concept in industrial engineering that changed the way, where scientists reacting to new products. These concepts created a pragmatic approach to developing new products, namely Parameter Design and Tolerance Design (Ross, 1988).

In thermal bridges analysis an Ishikawa diagram (known also as fishbone diagram, or cause-and-effect diagram) presents in Figure 1 some possible causes that influence the response parameters of building junctions.

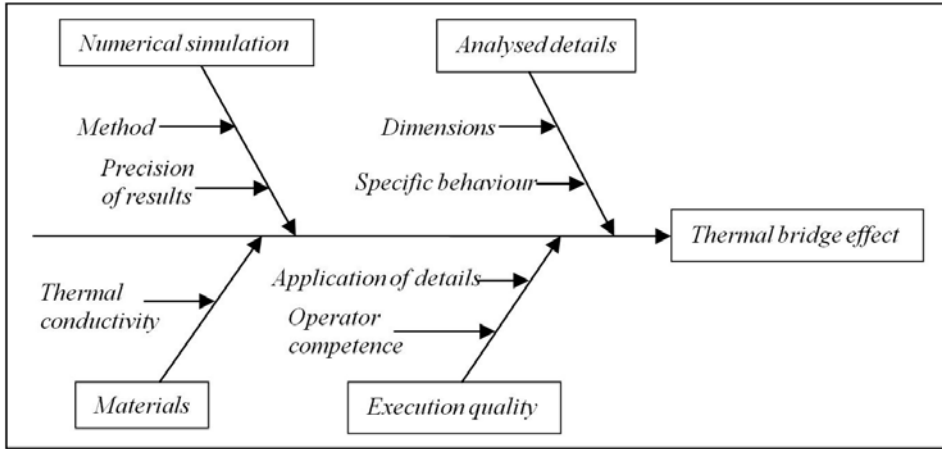


Figure 1. Fishbone diagram of factors affecting errors on thermal bridges.

2.2. Response surface methodology

The Response Surface Methodology (RSM) provides an approximate relationship between a true response Y and p design variables, which is based on the observed data from the process or system. The response is generally obtained from real experiments or computer simulations, and the true response y is the expected response. Thus, computer simulations are performed in this paper and the true response y can be written as:

$$Y = F(x_1, x_2, \dots, x_p) \tag{1}$$

where the variables x_1, x_2, \dots, x_p are expressed in natural units of a measurement, and are therefore called natural variables. The numerically obtained response Y differs from the expected value y due to random error, e .

In many cases, the approximating function F of the true response y is normally chosen to be either a first-order or a second-order polynomial model, which is based on Taylor series expansion. In general the second-order model is:

$$Y = b_0 + \sum_{j=1}^p b_j x_j + \sum_{j=1}^p b_{jj} x_j^2 + \sum_{i < j}^p b_{ij} x_i x_j + e \tag{2}$$

where $\beta_0, \beta_j, \beta_{jj}$ and β_{ij} are regression factors. For a first-order model with interactions, only β_0, β_j and β_{ij} are determined.

3. THERMAL BRIDGES ASSESSEMENT

3.1. Thermal Bridges Subjected to Analysis

Parametric studies were performed for two envelope solutions (Iacob *et al.*, 2011), with external walls (Figure 2) consisted of a load-bearing concrete inner layer, a coating concrete outer layer and autoclaved aerated concrete (AAC), respectively mineral wool (MW) in between.

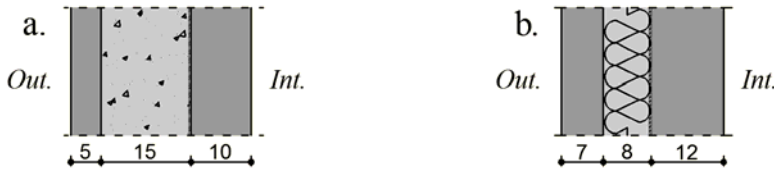


Figure 2. Configurations of prefabricated concrete large panels:
 a. with AAC insulation layer; b. with mineral wool layer.

Main locations of thermal bridges (Ilomets *et al.*, 2011) in apartment buildings composed of prefabricated concrete large panels, which are assessed in this study, are represented in Figure 3, for AAC solution.

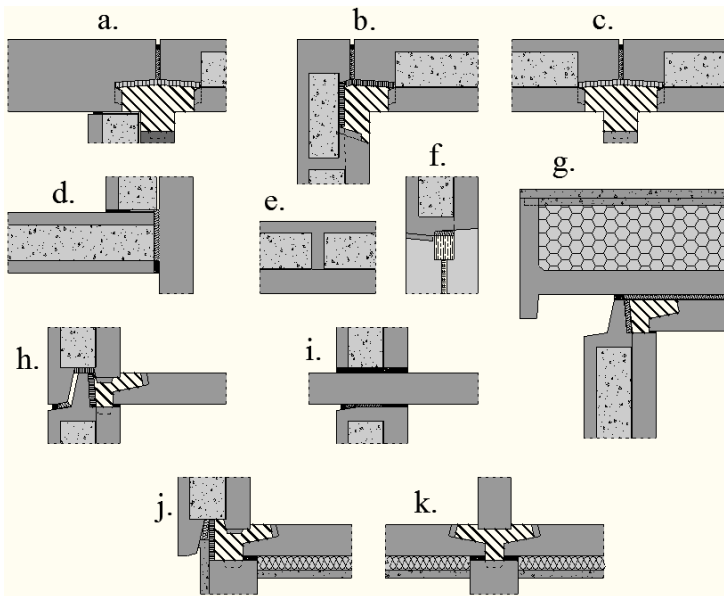


Figure 3. Specific details of thermal bridging: vertical junctions (a, b, c, d, e, f) and horizontal junctions (g, h, i, j, k).

For this configuration of external wall, there were brought a few changes (Figure 4) regarding the continuity of the insulating layer, by inserting thicker layers of polystyrene in wall junctions. The solution with mineral wool, as an improvement of the prefabricated large-panel concept, already had better design details (Figure 5.a).

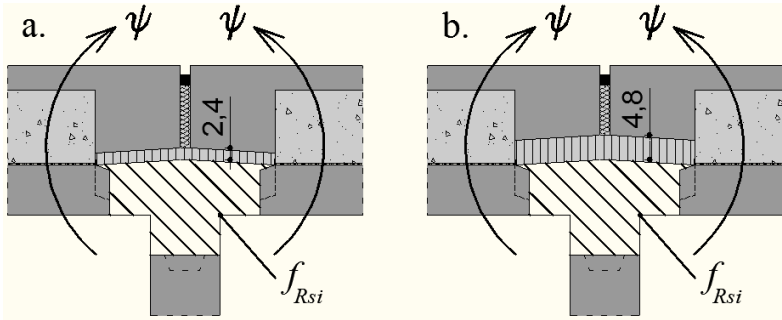


Figure 4. Initial and improved details for an external walls junction.

The major part of the existing building stock was constructed in times with lower requirements for thermal insulation. Therefore, the energy consumption for heating needs to be markedly reduced (Munch-Andersen, 2009).

The most efficient way to improve energy performance of existing buildings is applying exterior insulating layers (Figure 5). Along with hygrothermal aspects of this solution, other advantages that should be mentioned are the absence of another implication upon the interior space and the possibility to reform the aesthetic value of the building.

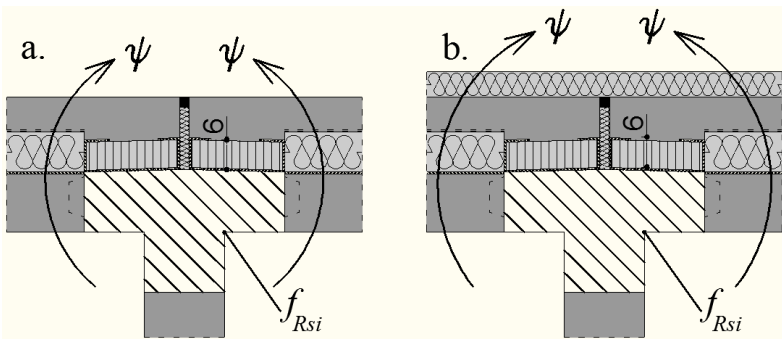


Figure 5. Walls junction details, before and after refurbishment.

3.2. Input factors: envelope design parameters

Building materials can fail meeting the heat conductivity values stated (Jaraminiene & Juodis, 2006), leading to deviations of envelope heat transfer coefficient from its design values. During the service life of a building, materials are exposed to weather conditions, as temperature and moisture, that contribute to its ageing by reductions in thermal resistance.

In Table 1 and Table 2, low and high values of the influential factors are selected for AAC solution, respectively MW solution, taking account of geometric variations from Section 3.1 and uncertainty considering thermal properties of autoclaved aerated concrete, mineral wool, polystyrene in junctions, but also of coating concrete outer layer.

Table 1. Low and high levels of factors – AAC solution

Parameter	Reduced parameter	Low	High
Polystyrene thickness, [cm]	X ₁	2.4	4.8
Coating concrete thermal conductivity, [W/mK]	X ₂	0.81	2.03
AAC thermal conductivity, [W/mK]	X ₃	0.24	0.34
Polystyrene thermal conductivity, [W/mK]	X ₄	0.04	0.05
External insulation thickness, [cm]	X ₅	0	20

Table 2. Low and high levels of factors – MW solution

Parameter	Reduced parameter	Low	High
Mineral wool thermal conductivity, [W/mK]	X ₁	0.042	0.052
Polystyrene thermal conductivity, [W/mK]	X ₂	0.04	0.05
External insulation thickness, [cm]	X ₃	0	20

The study is carried out by means of steady-state simulations, performed with ANSYS 12 program, obtaining values for surface temperature and values for heat flux corresponding to surfaces with non-adiabatic boundary conditions. With Equations (3) and (4) temperature factor and linear thermal transmittance values are obtained.

$$f_{Rsi} = (\mathbf{q}_{si} - \mathbf{q}_{out}) / (\mathbf{q}_{int} - \mathbf{q}_{out}) \quad (3)$$

$$\mathbf{y} = (\mathbf{F} - \mathbf{F}_u) / l \cdot (\mathbf{q}_{int} - \mathbf{q}_{out}) \quad (4)$$

where \mathbf{q}_{si} , \mathbf{q}_{out} and \mathbf{q}_{int} represent surface, outer and inner temperatures, measured in °C, \mathbf{F} and \mathbf{F}_u represent bidirectional heat flux passing through the thermal bridge and unidirectional heat flux passing through the building components in the absence of a thermal bridge, measured in W, and l represents the length of the thermal bridge, measured in m.

The number of simulations depends on the number of parameters. For two levels for each parameter of 11 thermal bridges, the number of simulations is 352 ($11 \cdot 2^5$) for AAC solution and 88 ($11 \cdot 2^3$) for MW solution. In this paper only some significant results are presented.

4. RESULTS AND DISCUSSION

The responses analyzed in the study can be identified by their coded notations: Y_1 (linear thermal transmittance β_1), Y_2 (linear thermal transmittance β_2) and Y_3 (temperature factor f_{Rsi}).

A standard statistical technique to carry it out, analysis of variance (ANOVA), is currently used to provide a measure of confidence. ANOVA results are given in Tables 3 to 8. This way, the significance of interaction effect of the five factors for AAC solution is expressed through p-value (lack-of-fit probability), which has to be smaller than 0,05, as is set out in the initial assumptions. Interactions with exceeding p-values can therefore be ignored. R-sqr coefficient is a statistical measure and expresses the approximation degree of the mathematical model, which is better as R-sqr value grows to 1. A low R-sqr value indicates that important and sistematic factors where ignored in the regression model. Similarly, adjusted R-sqr coefficient indicates the adjacency between hypothetical and real models.

Table 3. Summary of ANOVA for Y_1 (linear thermal transmittance β_1) – horizontal junction g, AAC solution

	Regr. Coefficients; Var.:Y1; R-sqr=,99997; Adj R-sqr:,99995					
	Regressn - Coeff.	Std.Err.	t(16)	p	-95,% - Cnf.Limt	+95,% - Cnf.Limt
Mean/Interc.	0,065603	0,007012	9,356	0,000000	0,050739	0,080466
(1)X1	-0,015779	0,000943	-16,734	0,000000	-0,017778	-0,013780
(2)X2	0,057851	0,001882	30,740	0,000000	0,053861	0,061841
(3)X3	0,104559	0,020218	5,172	0,000093	0,061699	0,147418
(4)X4	3,338847	0,144927	23,038	0,000000	3,031616	3,646077
(5)X5	0,001662	0,000117	14,232	0,000000	0,001415	0,001910
1 by 2	-0,000120	0,000140	-0,857	0,404267	-0,000416	0,000177
1 by 3	0,000671	0,001707	0,393	0,699419	-0,002948	0,004290
1 by 4	-0,032524	0,017070	-1,905	0,074867	-0,068710	0,003662
1 by 5	0,000816	0,000009	95,561	0,000000	0,000798	0,000834
2 by 3	-0,010396	0,003358	-3,096	0,006937	-0,017515	-0,003278
2 by 4	-0,086884	0,033580	-2,587	0,019842	-0,158070	-0,015698
2 by 5	-0,002706	0,000017	-161,167	0,000000	-0,002742	-0,002670
3 by 4	-0,130667	0,409673	-0,319	0,753888	-0,999134	0,737801
3 by 5	-0,005343	0,000205	-26,086	0,000000	-0,005778	-0,004909
4 by 5	-0,143440	0,002048	-70,027	0,000000	-0,147782	-0,139098

Table 4. Summary of ANOVA for Y_2 (linear thermal transmittance τ_2) – horizontal junction g, AAC solution

Regr. Coefficients; Var.:Y2; R-sqr=,99971; Adj R-sqr:,99944							
	Regressn	- Coeff.	Std.Err.	t(16)	p	-95,% - Cnf.Limt	+95,% - Cnf.Limt
Mean/Interc.	0,223924		0,027857	8,0384	0,000001	0,16487	0,282978
(1)X1	-0,023301		0,003746	-6,2197	0,000012	-0,03124	-0,015359
(2)X2	0,108280		0,007477	14,4816	0,000000	0,09243	0,124131
(3)X3	-0,387789		0,080325	-4,8278	0,000186	-0,55807	-0,217508
(4)X4	1,457049		0,575795	2,5305	0,022263	0,23642	2,677681
(5)X5	-0,011567		0,000464	-24,9265	0,000000	-0,01255	-0,010583
1 by 2	-0,000099		0,000556	-0,1776	0,861300	-0,00128	0,001080
1 by 3	0,002992		0,006782	0,4412	0,664964	-0,01138	0,017369
1 by 4	-0,009023		0,067818	-0,1330	0,895819	-0,15279	0,134745
1 by 5	0,001226		0,000034	36,1457	0,000000	0,00115	0,001298
2 by 3	-0,045136		0,013341	-3,3832	0,003792	-0,07342	-0,016854
2 by 4	-0,149352		0,133413	-1,1195	0,279462	-0,43217	0,133470
2 by 5	-0,004005		0,000067	-60,0319	0,000000	-0,00415	-0,003863
3 by 4	-0,233743		1,627635	-0,1436	0,887602	-3,68418	3,216689
3 by 5	0,023308		0,000814	28,6403	0,000000	0,02158	0,025033
4 by 5	-0,052506		0,008138	-6,4518	0,000008	-0,06976	-0,035254

Table 5. Summary of ANOVA for Y_3 (temperature factor f_{Rst}) – horizontal junction g, AAC solution

Regr. Coefficients; Var.:Y3; R-sqr=,99997; Adj R-sqr:,99995 ual=,0000007							
	Regressn	- Coeff.	Std.Err.	t(16)	p	-95,% - Cnf.Limt	+95,% - Cnf.Limt
Mean/Interc.	0,83913		0,010476	80,0979	0,000000	0,81692	0,861334
(1)X1	0,01142		0,001409	8,1052	0,000000	0,00843	0,014406
(2)X2	-0,05751		0,002812	-20,4505	0,000000	-0,06347	-0,051544
(3)X3	-0,11679		0,030208	-3,8661	0,001368	-0,18083	-0,052750
(4)X4	-1,38857		0,216542	-6,4125	0,000009	-1,84761	-0,929518
(5)X5	0,00693		0,000175	39,7363	0,000000	0,00656	0,007305
1 by 2	0,00028		0,000209	1,3511	0,195468	-0,00016	0,000726
1 by 3	-0,00052		0,002550	-0,2053	0,839890	-0,00593	0,004883
1 by 4	0,00565		0,025505	0,2215	0,827528	-0,04842	0,059716
1 by 5	-0,00059		0,000013	-46,1827	0,000000	-0,00062	-0,000562
2 by 3	-0,00238		0,005017	-0,4750	0,641209	-0,01302	0,008253
2 by 4	0,18254		0,050173	3,6381	0,002214	0,07617	0,288898
2 by 5	0,00232		0,000025	92,3376	0,000000	0,00226	0,002370
3 by 4	0,56517		0,612113	0,9233	0,369560	-0,73245	1,862791
3 by 5	0,00525		0,000306	17,1473	0,000000	0,00460	0,005897
4 by 5	0,03802		0,003061	12,4235	0,000000	0,03153	0,044511

Regression coefficients, obtained with the nonlinear regression model, are directly inserted in Equation (2), which gives predictions upon linear thermal transmittances and temperature factor, for any values of variable factors within the domains of definition.

Standard error of response is the average variability for the regression model at any given value of a factor, used in obtaining the t-ratio, a test statistics that gives more reliance in the regression coefficients as its value is higher.

Confidence limits are expressed in terms of confidence coefficients for the estimate. A narrow interval of $\pm 95\%$ confidence limits suggests that in 95% of the time the interval will contain the true parameter value.

Pareto charts obtained from the statistical analysis are presented in Figures 6 to 11, and have the role to reveal the importance order of the variables. The charts in Figures 6, 7 and 8 shows the statistical significance of factors and their interactions upon linear thermal transmittances τ_1 and τ_2 and temperature factor f_{Rsi} , for AAC solution, at a wall or roof slab connection. X_5 , X_2 and X_1 are leading factors in this order, whereas X_4 and X_3 have a lessened influence.

A physical interpretation of results will state that highest effects upon thermal bridges parameters are given by the additional external insulation thickness, the thermal conductivity of the outer layer of concrete and the thickness of polystyrene in the connection area. Furthermore, interactions between external insulation thickness with the other leading factors are shown as relevant, highlighting the importance of relating those three variables in thermal bridges assessment.

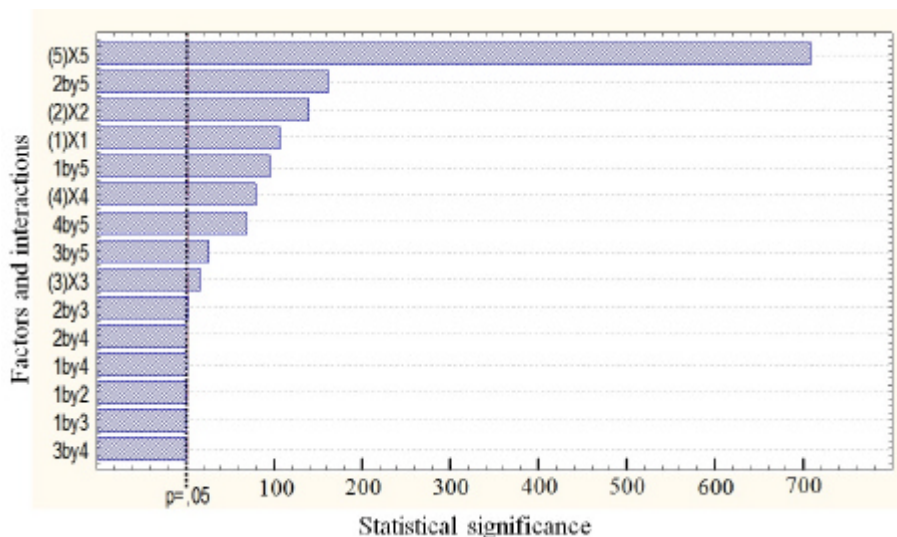


Figure 6. Pareto charts of standardized effect of Y_1 (linear thermal transmittance τ_1), for horizontal junction g , AAC solution.

Although previous statement might be seen as reasonable, it would be misleading to be taken as an absolute truth. Actually, the demonstrated influences are not characteristics of factors, but they reside in their variability. In other words, the range of variance for a specific factor weights in its statistical significance.

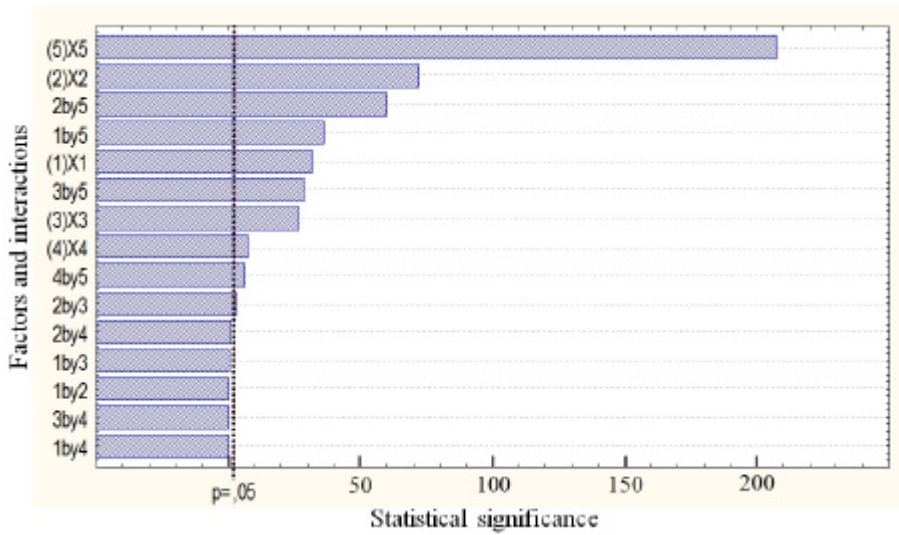


Figure 7. Pareto charts of standardized effect of Y_2 (linear thermal transmittance ? 2), for horizontal junction g, AAC solution.

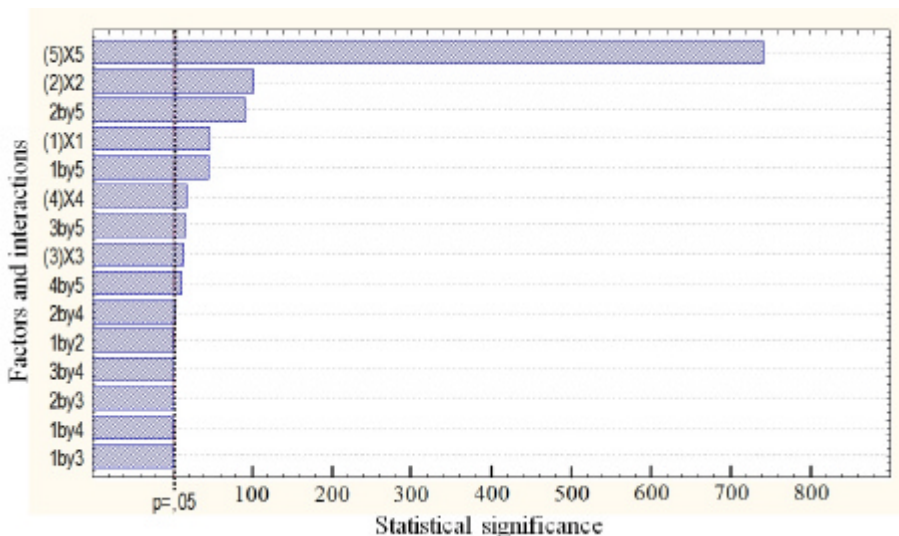


Figure 8. Pareto charts of standardized effect of Y_3 (temperature factor f_{Rsi}), for horizontal junction g, AAC solution.

If low-level and high-level values of variables are modified, so that wider intervals are defined for X_3 and X_4 , and narrower intervals for X_1 , X_2 and X_5 , it is to be expected for corresponding modifications in the statistical significances. Moreover, if all factors ranges would be very narrow, it will still have a meaning making observations upon statistical significances, even though Equation (2) will have a major β_0 coefficient and insignificant regression coefficients for factors.

Table 6. Summary of ANOVA for Y_1 (linear thermal transmittance τ_1) – vertical junction b , MW solution

Regr. Coefficients; Var.:Y1; R-sqr=1.; Adj R-sqr:1						
	Regressn	- Coeff.	Std.Err.	t(1)	p	-95,% - Cnf.Limt +95,% - Cnf.Limt
Mean/Interc.	0,52535		0,002451	214,357	0,002970	0,4942 0,55649
(1)X1	-3,58998		0,051572	-69,611	0,009145	-4,2453 -2,93469
(2)X2	3,14455		0,053810	58,438	0,010893	2,4608 3,82827
(3)X3	-0,02160		0,000037	-584,813	0,001089	-0,0221 -0,02114
1 by 2	-2,02112		1,132150	-1,785	0,325064	-16,4065 12,36421
1 by 3	0,15329		0,000566	270,798	0,002351	0,1461 0,16048
2 by 3	-0,14540		0,000566	-256,855	0,002479	-0,1526 -0,13821

Table 7. Summary of ANOVA for Y_2 (linear thermal transmittance τ_2) – vertical junction b , MW solution

Regr. Coefficients; Var.:Y2; R-sqr=1.; Adj R-sqr:1,						
	Regressn	- Coeff.	Std.Err.	t(1)	p	-95,% - Cnf.Limt +95,% - Cnf.Limt
Mean/Interc.	0,06303		0,001559	40,420	0,015747	0,0432 0,082838
(1)X1	-1,32145		0,032811	-40,275	0,015804	-1,7383 -0,904544
(2)X2	2,82536		0,034235	82,529	0,007714	2,3904 3,260351
(3)X3	-0,00275		0,000024	-117,100	0,005436	-0,0031 -0,002454
1 by 2	-4,10211		0,720293	-5,695	0,110657	-13,2543 5,050076
1 by 3	0,07719		0,000360	214,329	0,002970	0,0726 0,081766
2 by 3	-0,11843		0,000360	-328,833	0,001936	-0,1230 -0,113852

Table 8. Summary of ANOVA for Y_3 (temperature factor f_{Rsi}) – vertical junction b , MW solution

Regr. Coefficients; Var.:Y3; R-sqr=1.; Adj R-sqr:1						
	Regressn	- Coeff.	Std.Err.	t(1)	p	-95,% - Cnf.Limt +95,% - Cnf.Limt
Mean/Interc.	0,845066		0,001357	622,6941	0,001022	0,82782 0,862310
(1)X1	-0,389573		0,028557	-13,6419	0,046583	-0,75243 -0,026720
(2)X2	-0,519775		0,029796	-17,4442	0,036455	-0,89837 -0,141175
(3)X3	0,005438		0,000020	265,8154	0,002395	0,00518 0,005698
1 by 2	0,626912		0,626912	1,0000	0,500000	-7,33876 8,592582
1 by 3	0,024437		0,000313	77,9585	0,008166	0,02045 0,028419
2 by 3	0,024858		0,000313	79,3017	0,008027	0,02087 0,028840

The charts in Figures 9, 10 and 11 shows the statistical significance of factors and interactions upon linear thermal transmittances γ_1 and γ_2 and temperature factor f_{Rsi} , for MW solution, at a walls corner connection. While MW thermal conductivity proves a sufficient influence upon the two linear transmittances, f_{Rsi} factor is solely dependent on variance of external insulation thermal resistance.

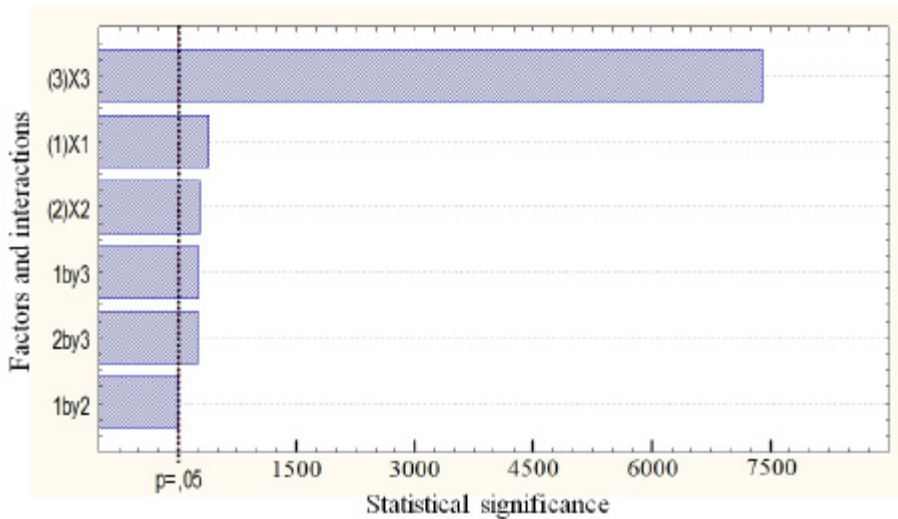


Figure 9. Pareto charts of standardized effect of Y_1 (linear thermal transmittance γ_1), for vertical junction b , MW solution.

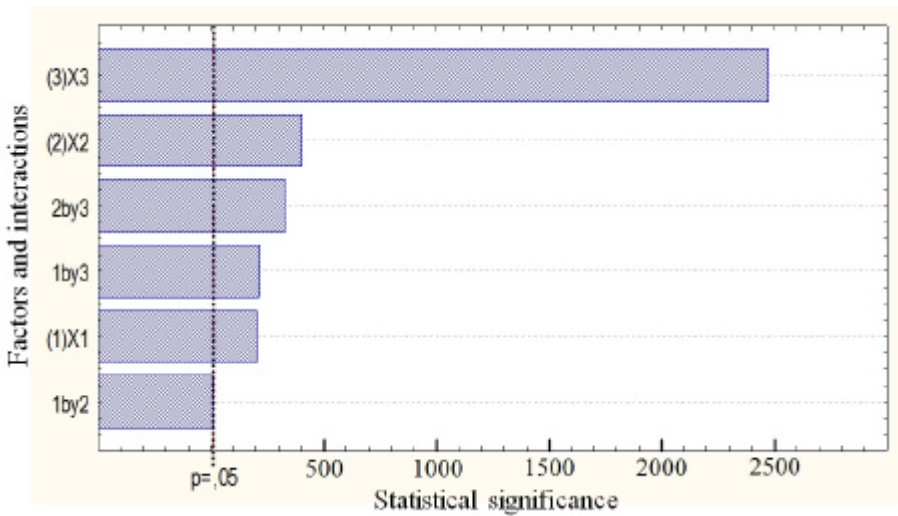


Figure 10. Pareto charts of standardized effect of Y_2 (linear thermal transmittance λ_2), for vertical junction b , MW solution.

Same as for AAC solution, a high f_{Rsi} value for MW solution is conditioned by a continuous insulation layer in thermal bridges areas, in order to minimize variations in inner surface temperature field. For linear thermal transmittances, in both cases, the geometric characteristic of thermal bridges renders a certain relevance also to minor factors.

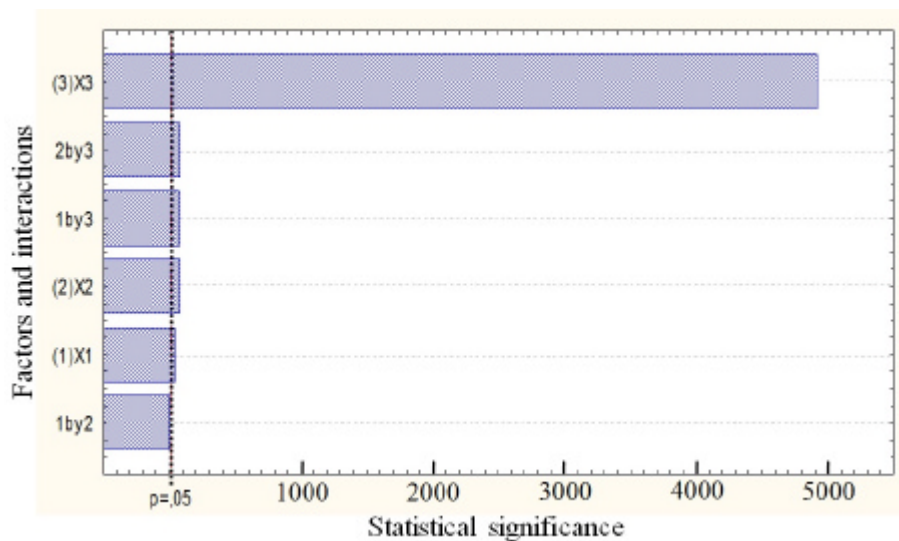


Figure 11. Pareto charts of standardized effect of Y_3 (temperature factor f_{Rsi}), for vertical junction b , MW solution.

5. CONCLUSIONS

In this paper a statistical analysis method was presented by applying it in a thermal bridges study. All factors were proved to be significant, but not for all the parameters of response studied. Thus, continuous insulation layer in thermal bridges areas, determined mainly by the additional external polystyrene layer and secondary by the coating concrete external layer, has a great influence upon linear thermal transmittances and temperature factor. AAC and mineral wool layers, being interrupted in thermal bridges area, have very low statistical significances for temperature factor, because of the low impact upon the variations in inner surface temperature fields.

This study reveals the possibility of obtaining a mathematical model to predict values for linear thermal transmittance and temperature factor, with a high precision on the domain of definition, but also outside of the domain, with an acceptable precision for current purposes.

References

1. Box, G.E.P., Hunter, W.G., Hunter, J.S., *Statistics for experimenters: An Introduction to Design, Data Analysis and Model Building*, John Wiley & Sons, New York, 1978.
2. Cornell, J.A., *How to Apply Response Surface Methodology*, vol. 8, ASQC, Wisconsin, 1990.
3. Gudum, C., *Evaluation of thermal bridges by means of numerical simulation*, Nordic Symposium on Building Physics 2008, Copenhagen, Denmark, 16-18 June 2008.
4. Iacob, A., Lepadatu, D., Ciobanu, A.-A., *Parametric statistical analysis of thermal bridges in buildings*, Proceedings of International Conference DEDUCON – Sustainable Development in Civil Engineering, Iasi, 11 November 2011.
5. Ilomets, S., Kalamees, T., Paap, L., *Evaluation of the thermal bridges of prefabricated concrete large-panel and brick apartment buildings in Estonia*, Proceedings of 9th Nordic Symposium on Building Physics – NSB 2011, Volume 3, Tampere, Finland 29 May – 2 June 2011.
6. Janseens, A., Van Londersele, E., Vandermarcke, B., Roels, S., Standaert, P., Wouters, P., *Developments of limits for the linear thermal transmittance of thermal bridges in buildings*, Proceedings of 10th Thermal Performance of the Exterior Envelopes of Whole Buildings Conference, ASHRAE, Clearwater Beach, Florida, U.S.A., 2-7 December 2007.
7. Jaraminiene, E., Juodis, E., *Heat demand uncertainty evaluation of typical multi-flat panel building*, Journal of Civil Engineering and Management, Vol XII, No 1, 2006.
8. Lepadatu, D., Hambli, R., Kobi, A., Barreau, A., *Optimization of springback in bending process using FEM and Response Surface Methodology*, International Journal of Advanced Manufacturing Technology, 27, pp: 40-47, 2005.
9. Lepadatu, D., Hambli, R., Kobi, A., Barreau, A., *Statistical investigation of die wear in metal extrusion process*, International Journal of Advanced Manufacturing Technology, 28, pp: 272-278, 2006.
10. Mayer, R.H., Montgomery, D.C., *Response Surface Methodology process and product optimization using design of experiments*, Wiley, New York, 1995.
11. Montgomery, D.C., *Design and analysis of experiments*, 5th edition, Wiley & Sons, Inc., New York., 2001.
12. Munch-Andersen, J., *Improving Thermal Insulation of Concrete Sandwich Buildings*, Indoor and Built Environment, 18, 2009.
13. Ross, P.J., *Taguchi Techniques for Quality Engineering*, McGraw-Hill, Inc., USA, 1988.
14. Taguchi, G., Konishi, S., *Orthogonal Arrays and Linear Graphs*, Dearborn, MI, ASI press, 1987.
15. The European Parliament and the Council of the European Union, *Directive 2010/31/EU of the European Parliament and of the Council of 19 May 2010 on the energy performance of buildings*, Official Journal of the European Union, May 2010.

Intelligent Sensor Networks Used for the Assessment of Structural Health

Dragos Florin Lisman¹, Ludovic Gheorghe Kopenetz²

¹Department of Structural Mechanics, Technical University of Cluj-Napoca, Cluj-Napoca, 400114, Romania

² Department of Structural Mechanics, Technical University of Cluj-Napoca, Cluj-Napoca, 400114, Romania

Summary

With recent developments in the field of wireless sensor networks the authors present in this paper a solution for complex monitoring systems, that can be used to perform continuous monitoring of different categories of bearing structures.

The system designed for the assessment of structural health is composed of the following main components: a data acquisition component, a data gathering component, a communication component, a storage component and a data interpretation and analysis component which also performs the computation and update of the structural model.

The data acquisition component is based on the use of a multitude of wireless sensors connected in network. There are several wireless sensor producers on the market today that supply sensors capable of acquiring information ranging from simple temperature, dust or humidity data to more complex sensors capable of detecting, cracks, crack propagation, linear displacements or image capturing sensors.

The system under testing uses such sensors and the main contributions of the research team are in customizing the hardware to deal with the time synchronisation of information received from several sensors, dissemination of sensor configuration information, storage of acquired data and the development of a software application able to interpret and present mandatory measures that have to be taken in order to maintain structural health.

The advantages of using a system based on wireless sensor networks range from the elimination of sensor wires and the associated installation costs to the possibility of using low-power, inexpensive nodes which in addition are able to provide redundancy in such a way that the failure of one sensor will have a very limited effect on the overall performance of the assessment system.

KEYWORDS: wireless, sensors, monitoring, structural health.

1. INTRODUCTION

On a global scale, a significant part of civil and commercial bearing structures are affected by certain degrees of deterioration. Due to the global crisis, it has become obvious to civil engineers the fact that there are insufficient funding solutions for immediate replacing or renovation of all affected structures. Thus, accurate information about the status of these structures is necessary in order to be able to optimize and prioritize the available resources. This information helps accurately classify which structures need replacement, which require immediate maintenance and which are in good condition and are normative compliant.

Integrating sensors into bearing structures is the main solution for performing periodical or continuous structural health monitoring. Structural health monitoring can be performed periodically or continuously based on the decision of structural engineers and experts. Both types of monitoring imply several activities like mounting the sensors, installing of power supplies or the connection of sensing devices to the mains of the structure or installing cable runs for the power supply and for the transmission of the data signals. On the long term, all the above mentioned activities can imply high installation and operation costs. Moreover, long bundles of wire cables or fiber optics are subject to periodic rupture or even connector failure. Wires also limit the number of sensors that can be mounted or there may be situations where cable runs cannot be mounted on certain parts or sections of the structure due to the structure's shape or its purpose.

Nevertheless, the integration of sensors into bearing structures has many benefits to the owners and users of the structures, including prediction of damages or catastrophic failures, improved emergency response, increased homeland security or reduced operation costs in the long term.

As a result, in the previous decade several private research companies, universities and international standardization institutions have started the development of wireless sensor networks. These networks are composed of devices called nodes having in their composition a processing unit, a wireless communication device and one or several sensors for data acquisition.

The recommended features of a wireless sensor network node are low power consumption, fast data acquisition capabilities, reliability, long term accuracy, reduced acquisition costs, very little or no maintenance over time and the possibility for remote configuration and programming. These features are not easy to implement because real-life structural monitoring applications and problems have different requirements. Selecting the appropriate sensors and the wireless communication protocol have a strong impact on the overall performance of a node and the lifetime of the energy source.

Nowadays a single integrated circuit is able to encompass a radio communication device, a processing unit and additional digital electronics. Very good example of such integrated circuits are produced by leading industry companies like Atmel, Texas Instruments or MicroChip [1], [2], [3].

According to the definition given in [4], a wireless sensor network is composed of a series of wireless nodes equipped with different types of sensors, placed in different locations on the structure, which communicate with one or several gateways using one or several different wireless communication protocols. A gateway or a basestation is the main collection point for the data sensed by the nodes. The data sensed by the nodes is transmitted directly or via other nodes to the gateway. In order to obtain small communication periods and thus lower energy consumption of nodes, the transmitted data is usually compressed. The data collected by the gateway is then fed as input to different software applications for further processing and information interpretation is performed by expert systems in conjunction with human experts in the structural engineering domain.

2. WIRELESS SENSOR NETWORKS PRINCIPLES

This chapter encompasses a brief description of the hardware components of a wireless sensor network node, the communication possibilities available, the energy supply options and power consumption related issues.

2.1. Node components

The basic hardware components that make up a wireless sensor network node are presented in Figure 1. and are compliant with the descriptions given in [4]. It can be observed that the components are modular and this architecture empowers the node's design with versatility and flexibility to requirements from different structural health monitoring applications.

The sensing devices are mounted on the prototyping board of the wireless node and can range from simple temperature, humidity, noise or dust sensors to more complex sensors able to detect cracks, crack propagation, linear displacements, accelerations or ultrasound sensors capable of distance measurement [5], [6]. The data acquired by the sensing devices is then fed into the conditioning module. This module is necessary because the sensed signal may be too weak or too noisy to be fed directly into the data storage devices. The most common circuits used for signal conditioning are conditional bridge circuits.

Multiplexing and amplifying circuitry is used in order to boost the conditioned signal which at the conditioning circuit's outputs can be as low as $10\mu\text{V}$ with

corresponding temperature drifts of $0.1\mu\text{V}/^\circ\text{C}$. The most common circuits used at this point are precision operational amplifiers. Multiplexers are used in order to combine the inputs from several sensing devices and then feed them as input to the analog digital (A/D) converters.

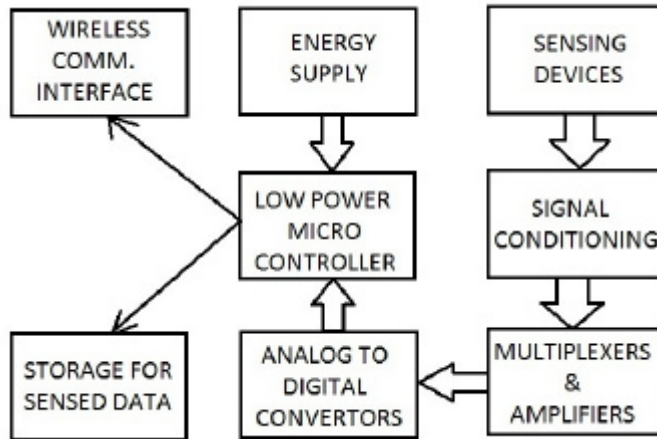


Figure 1. Node Components

The A/D converters are responsible for performing the digitization of the analog signals. The input signals are converted from an analog voltage range into a sequence of binary digits using several output channels of the A/D converters. Common resolutions for the A/D converters are 12, 14 or 20 bits.

The majority of nodes currently available on the market use 8-bit AVR RISC-based microcontrollers with operating frequencies between 8 - 16 MHz, capable of running in temperature conditions between -40°C and $+85^\circ\text{C}$ which fit the majority of bearing structure monitoring scenarios. The microcontroller mainly has the following functions [7]:

- wireless network protocol management;
- sensor data acquisition management;
- power supply management;
- transmission of data from the sensor interface to the physical communication layer;
- read/write controller operations for the local storage media.

The microcontroller units are directly coupled with different types of wireless communication interfaces. These include the IEEE 802.15.4 compliant interface, GSM/GPRS interface, Bluetooth or IEEE 802.11 interfaces.

In addition, the nodes provide the possibility for local data storage by using a flash memory mounted on the board. In the majority of node implementations SD,

miniSD or microSD cards are used. These cards have capacities ranging up to a few GBs but they also have some strict timing constraints [8]. Due to these constraints some of the sensor data can be stored to the flash memories if the timing constraints are not too strong for the flash memory write delay to comply to. For example, the flash storage is suitable for temperature sampling which is performed once every few minutes as opposed to acceleration sampling which may take place several times a second.

From the point of view of the energy supply, several options are available including: batteries (Li-Ion or Li-polymer rechargeable), fixed or flexible solar panels, auxiliary 3V no-rechargeable batteries or the possibility of connecting an AC/DC adapter to the mains, depending on the monitoring application.

2.2. Wireless communication options

A wireless sensor networks usually has no or very little infrastructure. It is composed of a given number of nodes ranging from a few to tens or even thousands working together in order to obtain information about the bearing structure under monitoring. Several standards and protocols have been developed to sustain the specific requirements of wireless sensor networks communication including:

- IEEE 802.15.4/ZigBee standard compliant [2], [9];
- IEEE 802.11 b/g /Wifi standard compliant;
- GSM/GPRS;
- Bluetooth;
- RFID/NFC.

In the following subchapters each of the standards/protocols from the previous list are detailed along with the advantages and disadvantages of using them in real-life implementations. A feature offered by the majority of hardware and software suppliers for wireless sensor networks is that the nodes can be simultaneously equipped with two different communication adapters. Thus the node is able to integrate radios allowing communication combinations like: IEEE 802.15.4/ZigBee with GSM/GPRS, IEEE 802.15.4/ZigBee with IEEE 802.11 b/g /Wifi, IEEE 802.11 b/g /Wifi with Bluetooth, etc.

2.2.1. IEEE 802.15.4/ZigBee

IEEE 802.15.4 is the standard proposed by the Institute of Electrical and Electronics Engineers along with leading industry companies for usage in low rate wireless personal area networks also called LR-PANs [10]. The main focus points of this standard are low power consumption, low deployment costs and low complexity.

From the topology point of view, the nodes of the wireless sensor network can be organized as a tree of nodes, a mesh of nodes or simply peer-to-peer nodes as described in Figures 2 (a) and 2 (b).

The 804.15.4 standard states the protocols and functionality at the lower, hardware levels of communication. ZigBee encompasses the higher, software levels of communication built upon the lower 804.15.4 levels. Zigbee ensures simple, low cost and low power communication protocols able to form mesh networks connecting thousands of nodes together [11]. ZigBee compliant devices have a very low power consumption and can operate on a battery for several years. The communication frequencies used at the physical layer of the communication stack are 2.4 GHz, which is practically a worldwide license-free frequency band, 868 MHz and 900 MHz.

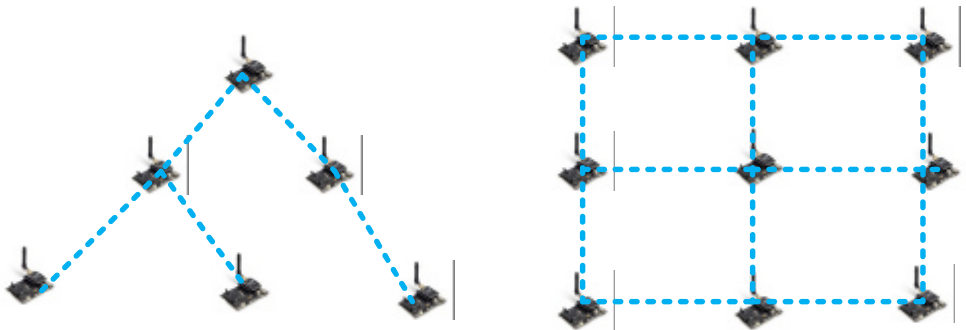


Figure 2. a) Tree node topology b) Mesh node topology

In line of sight conditions the communication range is from a few centimeters up to more than 10 km depending on the communication frequency and on the power of the dipole antenna. Lower distances between nodes require low power consumption in the range of 1 - 5mW, but for large distances of more than 4-5 km, power consumption tops to a few hundreds of mW [6], [11].

In terms of communication bandwidth, ZigBee ensures transmission rates starting from 20Kbps for the 868 MHz band, 40 Kbps for the 900 MHz band up to 250 kbps for the 2.4GHz band according to [4]. In addition, the standard provides the possibility to use the AES-128 encryption standard for the encryption of transmitted data. Thus, through encryption, the security of transmitted data is assured.

Currently, the IEEE 804.15.4/ZigBee standards are the most commonly accepted and employed standards in wireless sensor networks, especially for the low power consumption and due to the fact that nodes coming from sleep mode can achieve rapid synchronization to the network.

2.2.2. *IEEE 802.11 b/g /Wifi*

This is an older standard designed for local area networking between wireless personal computers or other wireless devices (e.g. smart phones) which is capable of relatively high transfer rates between the communication parties. The communication bandwidth ranges from 1Mbps up to 1Gbps (programmed for 2012 market release). The transmission range with simple dipole antennas is around 100m. By using high power directional high gain antennas higher distances can be obtained but with a considerable energy cost [11]. The requirement for time synchronization between 802.11 communicating nodes is performed by using periodic beacon transmissions [12].

Even if the transmission rates are appealing for wireless sensor networks, the main obstacles in the use of this technology on a large scale are high power requirements. Nevertheless, the technology still can be used for certain structural health monitoring applications, where energy supplies are not an issue, the distance between sensors is reduced and there is a strong requirement for high data rates. In addition, on top of the 802.11 communication stack, there are more security features that can be implemented in order to prevent any alteration of the transmitted data [13].

2.2.3. *GSM/GPRS*

This communication is based on the Global System for Mobile communication (GSM) standards and it uses a packet oriented mobile data service in 2G or 3G cellular networks called General Packet Radio Service (GPRS). Communication takes place in the quadband 850 MHz / 900 MHz / 1800 MHz / 1900 MHz typically used by GSM mobile phones. The data transmission rates are in the range 56 - 114 Kbps. These standards are considered to be suitable for long-distance communication between nodes.

This technology is suitable for communication of nodes which have to be placed at distances larger than the distances that can be covered by other technologies, but still in the range of a mobile basestation [14], [15]. Its advantage for use in structural health monitoring applications is the fact that the GSM/GPRS node does not have to be permanently connected to other nodes through a communication link and it can come up when an event has occurred (e.g. a crack appeared) and at that point it can place a call to a central monitoring station or it can send a SMS containing the data to be reported. This is feasible in applications that are not time-sensitive and for which the delivery of the data can be delayed for the time needed to connect to the closest GSM basestation and place the call or send the SMS message [12].

The features that are typically offered by a GSM/GPRS node are:

- place or receive calls;
- send or receive SMS;

- placing x-tone missed calls;
- TCP/IP server;
- HTTP service;
- FTP service for sending or receiving files [6].

2.2.4. *Bluetooth*

This is a personal area network (PAN) proprietary open standard that has a lower power consumption than 802.11x. It was initially intended for short-range data transfers between personal computers and other digital peripheral devices such as PDAs (personal digital assistants) or mobile phones [16]. The typical transmission range is from a few meters up to 100 meters. In the case of higher transmission distances just a limited set of services offered by Bluetooth are available.

Bluetooth communication devices generally operate in the globally license-free ISM band (Industrial, Scientific and Medical) at frequencies around 2.4GHz and it is based on a master - slave where one master can communicate to up to 7 slaves in a piconet [17].

Data transmission rates for general Bluetooth are around 1Mbps with the possibility for some applications to reach a 3 Mbps rate. According to [16] and due to the limited number of slaves and the master - slave communication method, Bluetooth based sensor networks are appropriate for a niche of structural health monitoring applications, such as monitoring in urban terrains which need intensive data exchange during a few important time intervals and within a time frame of around 7 to 10 days.

A functioning example of a sensor network node implemented based on the Bluetooth technology was developed by the Computer Networks and Engineering Laboratory at ETH Zürich, Switzerland during a research project [18]. The 3rd hardware version of this node has been successfully used in application having more than 70 nodes.

2.2.5. *RFID/NFC*

This standard will be covered just briefly due to the limited communication scope which is in the range of 1 - 5 cm [6]. This technology is based on the ISO 14443A standard and is primarily used in wireless sensor networks intended for the logistics, location based services, access management and electronic prepaid metering.

2.3. Energy supplies and power consumption

One of the major concerns if note the major concern in designing feasible wireless sensor network deployments for bearing structure's health monitoring are the node

power consumption and the available options for power supply for the node. According to studies performed in [4] and [11], from the total power consumption of a node a percentage around 80% is spent by the wireless transmitter/receiver, around 4-5% by the sensing devices and the rest is consumed by the processing unit and on board electronics.

Generally, structural health monitoring applications are continuous or span over long periods of time (e.g. one or several years). Thus, it is desirable that the energy source is able to serve the node without servicing for the entire monitoring period. In addition, a proper operational scheme has to be designed for the hardware of the node and tuned algorithms have to be implemented at the operating system and application level in order to minimize power consumption.

The most important concerns are with the wireless transmission/reception part and the related algorithms, due to the fact that it is the most power consuming component of the node. The following actions must be considered during implementation [4]:

- Implementation of strict power management strategies and functioning modes (sleep mode, power-down mode, suspend mode);
- Reduction of transmitted/received data through the use of compression algorithms and through data reduction;
- Reducing the frequency of data transmissions;
- Reducing the wireless transceiver duty cycle;
- Transmission of data only when sensor events occur (e.g. transmit displacement data or temperature data only when an increase/decrease of the sampled data occurs);
- Reduce the administrative overhead of the transmitted data (reduce the amount of data that is not related to the sensed data).

Significant research has been performed on the topic of energy sources for wireless sensing nodes. In the typical scenario, when the energy source of a node is almost depleted, the node will shut down and will disconnect from the network. This can have a limited or significant impact on the structural health monitoring system depending on the node placement and the initial redundancy considered in the network design [19]. As a solution researchers have sought energy harvesting solutions besides energy conservation techniques and algorithms.

The typical energy source for a wireless node is a rechargeable or non-rechargeable battery. The most common rechargeable batteries used in the nodes are Li-Ion or Li-polymer. The second category is preferred due to lower manufacturing cost, adaptability to a wide variety of packaging shapes, reliability, and ruggedness. In addition, the self-discharge rate is lower at around 5% per month as compared to 8% for classical Li-Ion batteries.

Even if rechargeable batteries are used in the design, they need servicing at certain time intervals by either replacing the batteries or recharging them. By using energy

harvesting there exists a solution for online recharging. Energy harvesting involves the replenishing of the energy capacity of a nodes energy source. Research has been conducted on different methods like use of solar energy, vibration, thermal energy, acoustic noise or fuel cells [11], [20], [21].

The current mature energy harvesting technology is using solar cells and panels. There exist rigid solar panels capable of supplying 500mA at a voltage of around 7V and flexible solar panels capable of supplying 100mA at the same voltage. The acquisition cost is still high with prices starting from 20-25 Euros/pc. Even if it is a mature technology, solar energy harvesting has the main drawback that the results of the harvesting is proportional to the existing sunlight or to the existing artificial light.

3. WIRELESS SENSOR NETWORK'S ARCHITECTURE

The network architecture of a wireless sensor network depends greatly on the type of structural health monitoring application to be implemented. Several factors influence the architecture chosen for in situ deployment including but not limited to the type of structure under monitoring, structural dimension, structural materials or expose of nodes to natural elements.

In the following subchapters first a presentation of the most commonly met topologies for wireless sensor networks is detailed, followed by a description of node roles and details about the software architecture and its main components.

3.1. WSN topologies

One of the most common topologies used in civil engineering structural health monitoring applications is the star topology, where all the sensor nodes transmit information directly to a special station called gateway [22]. The gateway or the basestation acts a direct data sink which receives all the information from the wireless nodes and can be accessed using a variety of internet communication options including Wifi, GSM/GPRS or broadband technologies. A star topology is presented in Figure 3.

Another topology used in case of monitoring applications that need strong connectivity between sensing nodes is the mesh topology already presented on Figure 2(b). In this topology nodes are connected to one another, to the closest neighboring nodes as well as to one of several gateways (data sinks). Such topology ensure that the redundancy criteria are met, but at a higher cost, due to additional hardware and energy cost in terms of wireless communication volume.

In all topologies the data sink nodes or the gateways require a computing device with enough processing power and enough storage space. In addition, they must act as a remote gateway for the users of the structural health monitoring system in order to allow remote connectivity, retrieval of data and data analysis software tools to run interpretation algorithms on the data. Last but not least, they must allow the structural expert to perform custom queries on the sensed data according to the criteria that he or she considers fit for the purpose of the monitoring.

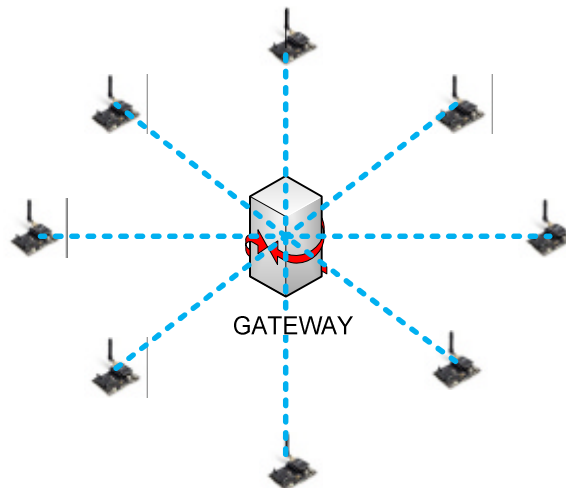


Figure 3. WSN star topology

Mesh topologies are especially appropriate for monitoring bridges and tunnels due to the fact that in these applications the primary concerns are to acquire data about the long-term changes in performance in a number of different locations on the structure. This requires a wireless sensor network composed of closely positioned nodes that sample data at a low time frequency of the order of minutes or even hours [23]. Due to the fact that in such monitoring application, nodes are closely positioned, it is not feasible to use wireless transmitters that need the power to communicate directly to the gateway. It makes sense using multi-hop communication inside a mesh topology whose nodes can communicate with one another as well as to the gateway in order to minimize the requirements in terms of transmission distance and thus reducing the overall energy consumption of the nodes.

3.2. Node types

In bridge or tunnel monitoring, as well as for other types of applications for bearing structures health monitoring, typically the following types of nodes are used:

- environmental nodes;
- deformation nodes;
- accelerations nodes [23];
- crack and crack propagation nodes [6], [25];
- inclinometer nodes [24].

3.2.1. *Environmental nodes*

Usually the steel wires and strands that compose the main cables of a bridge are exposed to the natural elements and it is important to have relative humidity information at the surface of the cables. This information can be obtained by directly mounting the sensors on the surface of the cables. In addition, environmental nodes are equipped with temperature sensors, particle and light sensors.

Humidity sensors can measure 0-100%RH with an accuracy of $\pm 4\%$ RH (at 25°C, range 30 ~ 80%), $< \pm 6\%$ RH (range 0 ~ 100) and a response time under 15s according to [25]. The temperature sensors can measure temperatures in the range between -40°C and +125°C with a stepping of 0.5°C and an accuracy of $\pm 2^\circ\text{C}$ (range 0°C ~ +70°C), $\pm 4^\circ\text{C}$ (range -40 ~ +125°C). These properties are sufficient to study temperature gradients across the cable length or at boundary regions. The light sensors have a spectral range between 400 - 700 nm and operate in environments with temperatures between -30°C and +70°C with a energy consumption closely to 0 μA .

3.2.2. *Deformation nodes*

Deformation nodes are nodes equipped with sensors able to measure the amount of deformation of the monitored structural element. In [24] the research team presents a fiber optics based sensor capable of performing the measurement. The idea behind this sensor is that it differentially measures the time required by a laser impulse to travel through a fiber optic wrapped around the monitored structural element. If the structural element suffers deformation, the time needed by the signal to travel becomes longer.

Some advantages of this type of deformation measurement device are the facts that it is a minimally invasive measurement method, it does not suffer from electromagnetic noise and it can be used to measure the deformations of a wide range of elements, for example from a single 1 foot element up to an entire structure [24].

Supplementary, this type of node contains a temperature sensor in order to measure the instantaneous temperature in order to perform coordination to the amount of deformation at the measurement point.

3.2.3. *Acceleration nodes*

The majority of nodes can be equipped with an acceleration sensor. Acceleration sensors are capable of measuring accelerations in the range: $\pm 2g$ (1024 LSB/g) / $\pm 6g$ (340LSB/g) at frequencies of 40Hz/160Hz/640Hz/2560Hz [6]. Acceleration data is high-volume data and has to be stored immediately after sampling. Acceleration nodes are able to sustain a 500Hz sampling rate while writing the data on the microSD card without loses. This requires nodes designed to support bursts of high-rate data having strict reliability requirements.

The acceleration sensor in the case of a wireless node is a MEMS device (micro-electro-mechanical system) with dimensions in the scale of maximum 1 millimeter. These are low-power inexpensive alternatives to classical sensors very suitable for implementation in a energy-constrained wireless sensor node.

3.2.4. *Crack and crack-propagation nodes*

These nodes are equipped with sensors capable of detecting the appearance of cracks and measure the magnitude and 2D orientation of these cracks. Crack detection gages have lengths between 15 and 56 mm and widths between 3 and 6 mm [25]. The operation temperature typical to this type of sensor is between -195°C and 120°C .

The sensor consists of a small conductive strand with a very low resistance value embedded in a fiber-glass film. In the case of a crack development, the sensor shall break thus interrupting a closed electric circuit. This event will be signaled to the node's central processing unit. In order to mount such a sensor to a surface, it has to be fixed using a special adhesive. The use of a protective coating is recommended in long term installations.

The crack-propagation sensor that is mounted on this type of node has the same operation principle, with the difference that it is composed of a small conductive strand which contains several parallel grid lines that break progressively with the propagation and enlargement of a crack's width. Several options are available for the distribution of the grids. There are sensors having: 10-grid lines with 0.25 mm between grids, 20-grid lines with 0.25 mm between grids, 20-grid lines with 0.51 mm between grids, 20-grid lines with 2.03 mm between grids, 20-grid lines with 1.27 mm between grids or other formats depending on the specifics of the structural health monitoring application in terms of crack propagation data [25].

3.2.5. *Inclinometer nodes*

These nodes are equipped with sensors able to measure the inclination sustained by structural elements. These nodes are especially used in the case of bridge, tunnel or

road structural elements with relatively high success in determining the changes that appear at the relative position of structural elements.

3.3 The software of wireless sensor nodes

On top of the hardware of wireless sensor nodes runs a very compact operating system (OS). This is a distributed operating system and must be perceived as a operating system working on the entire network as a whole. Abstracting the capabilities of the hardware is a basic OS responsibility.

The majority of OSs are developed using the nesC programming language which makes them portable on many types of hardware platforms.

The basic services provided by the OS are:

- hardware abstraction;
- timers/alarms;
- memory management;
- sensor primitives;
- communication primitives.

One of the main goals of an hardware abstraction is to provide programmers with the facility of easy traversing the software/hardware boundary by allowing some software components to be replaced by hardware components with real hardware modules and vice versa.

Timers and alarms are used by applications running on top of the OS in order to get an event or a piece of data when the timer expires. Alarms are used to signal the applications running on top of the operating system about events that have occurred and must be processed immediately by the monitoring software applications.

The memory management function is responsible for the allocation of memory to the structural health monitoring applications running on top of the operating system. It is also responsible for the efficient allocation of memory in order to reduce memory waste. The fact that the memory resources of the node are reduced as compared to smart phones for example, has to be noted at this point.

The sensor primitives provide an abstract interface to the physical hardware sensors and the underlying node platform. At least five functions of this interface can be called by a monitoring application: sensor activation, sensor deactivation, get sensor value, configure sensor and get sensor status. In addition, when sensors are deactivated, the sensor API has support for turning off the power to the sensors, thus conserving energy of the sensor board.

Communication primitives are abstracted under the form of messages. Messages are preceded by a small identifier that is attached to each message, specifying the action that needs to be taken on the receiver's side when a given message has been

received followed by sensed data, timestamps and other data fields. Usually the nodes transmitting the information are the sensing nodes and the receivers of information are the sink nodes. Nevertheless, communication can take place in the other direction too, for configuration and administrative related tasks.

In the test setup used in our research, the structural health monitoring applications are developed directly on top of the operating system by making use of the operating system's functions. Still, there exists in other implementations of monitoring application another layer between the OS and the user applications. This layer is called a middleware layer and performs further abstractions on top of the OS's abstractions [24].

4. CONCLUSIONS

Intelligent monitoring of bearing structures by using wireless sensor networks proves to be a cost-effective solution that can be deployed on a wide range of infrastructure projects including but not limited to water-supply and aerial sewage infrastructure, bridges, tunnels, towers or road segments. They can supply civil engineers with real-time critical data on the health status and the performance degree of the monitored structures.

In the test phase our research team is implementing a structural health monitoring application on a sewage-pipe in Cluj County. The pipe is suspended using bearing cables. Monitoring is performed on the health of the bearing cables by obtaining information about relative humidity, accelerations and deformations. This is done by using three types of wireless sensing nodes: environmental, acceleration and deformation nodes.

Environmental nodes sample humidity, temperature and dust readings. The purpose is to analyze the daily, weekly and seasonal temperature readings and match them to the contractions of the bearing cables. Humidity readings are performed in order to determine the exposure of sustaining and connection elements and braces to corrosion. Relative humidity values above 60% accelerate corrosion processes.

The acceleration nodes are recording information about the vibrations induced in the bearing cables by wind and nearby traffic. The analysis of acceleration records will be done by a custom application and will help understand the dynamic behavior of the suspended bearing structure. From the theoretical point of view, the vibration response of the test structure is not random, but it is situated along some frequencies known as natural frequencies.

Deformation nodes supply an average value of the last 20 deformation readings. This average is performed due to irrelevant character of single samples. These tend to fluctuate. Elongation of the vertical sustaining cables is an indication of a

deterioration and will be automatically detected and signaled by a software application under development.

Using a combination of data supplied by environmental, acceleration and deformation nodes a monitoring application will be developed in the next research phase, which will, hopefully, be able to perform strain analysis on the bearing cables. Nevertheless, there is a wide research field left uncovered when discussing about structural health monitoring applications based on intelligent networks composed of wireless sensing nodes.

References

1. ***, <http://www.atmel.com/devices/ATMEGA128RFA1.aspx>, viewed on 04/19/2012.
2. ***, <http://www.ti.com/lstds/ti/analog/zigbee.page>, viewed on 04/18/2012.
3. ***, http://www.microchip.com/stellent/idcplg?IdcService=SS_GET_PAGE&nodeId=2663, viewed on 04/17/2012.
4. Townsend, C. and Arms, S., *Wireless Sensor Networks: Principles and Applications*, Chapter 22, pp. 575-589, from *Sensor Technology Handbook*, Elsevier Newnes, Oxford, UK, 2005.
5. Basarna, C., Baydere, S., Bongiovanni G. and others, Research Integration: Platform Survey Critical Evaluation of platforms commonly used in embedded wisents research, Embedded WiSeNts - Project FP6-004400, 2006 available at: <http://www.embedded-wisents.org/studies/wisents/download/survey.pdf>, viewed on 02/15/2012.
6. ***, Libelium WaspMote technical guide (electronic version) available online at: http://www.libelium.com/documentation/waspmote/waspmote-datasheet_eng.pdf, viewed at 03/04/2012.
7. Arms, S.W., Newhard, A.T., Galbreath, J.H., Townsend, C.P., Remotely Reprogrammable Wireless Sensor Networks for Structural Health Monitoring Applications, ICCES International Conference on Computational and Experimental Engineering and Sciences, Medeira, Portugal, 2004.
8. ***, SD Association Homepage, <https://www.sdcard.org/consumers/speed/>, viewed on 03/03/2012
9. Jiang, X.D., Tang, Y-L, Lei, Y., Wireless Sensor Networks in Structural Health Monitoring Based on ZigBee Technology, Proceedings of the 3rd International Conference on Anti-Counterfeiting, Security and Identification in Communication (ASID'09), IEEE Press, Piscataway, NJ, USA, 2009, pp. 449 - 452.
10. Fasl, J. and Potter, D., Reliable Wireless Sensor Networks for Infrastructure Monitoring, Structural Health Monitoring: Proceedings of the 5th European Workshop on Structural Health Monitoring, DEStech Publications, Inc., Lancaster, PA, USA, 2010, ISBN: 978-60595-024-2, pp. 673 - 678.
11. Yick, J., Mukherjee, B., Ghosol, D., Wireless Sensor Network Survey, Elsevier B.V., Vol. 52, Issue 12, 2008, pp.2292 - 2330.
12. Lisman, D. F., Inter-Vehicle Communication Platform for Safety Applications - Communication Aspects, Diploma Thesis, Technical University of Cluj-Napoca, 2006.
13. Lisman, D. F., Securitatea Comunicatiei in Retele Vehiculare, Master's Thesis, Technical University of Cluj-Napoca, 2009. (in Romanian)
14. Jaman, G. and Hussain, S., Structural Monitoring using Wireless Sensors and Controller Area Network, Proceedings of the 5th Annual Conference on Communication Networks and Services Research (CNSR '07), IEEE Computer Society, Washington, DC, USA, 2007, pp. 26 -34.
15. Yan, B.Z. and Zhao, H.Y., A Low Cost GSM/GPRS Based Wireless Home Security System, *IEEE Transactions on Consumer Electronics*, May 2008, pp. 567-572.

16. Leopold, M., Dydensborg, M.B., Bonnet, P., Bluetooth and sensor networks: a reality check, Proceedings of the Sensys'03, Los Angeles, CA, USA, 2003.
17. Xiao, Y. and Pan., Y., *Wireless LANs & Bluetooth (Wireless Networks and Mobile Computing)*, Nova Science Publishers, Hauppauge, NY, USA, ISBN: 978-1594544323, 2005.
18. ***, BNode Platform Official Website, <http://www.bnode.ethz.ch/>, viewed on 02/14/2012.
19. Lisman, D.F. and Kopenetz, L.G., Advanced In Situ Monitoring Techniques for the Behaviour of Heritage Structures, *Journal of Applied Engineering Sciences*, University of Oradea Publishing House, Oradea, Romania, Vol. 2(15), Issue 1, 2012.
20. Kim, S., Pakzad, S., Culler, D. and others, Wireless Sensor Networks for Structural Health Monitoring, SenSys '06 Proceedings of the 4th International Conference on Embedded Networked Sensor Systems, ACM, New York, NY, USA, 2006, ISBN: 1-59593-343-3.
21. Seah, W.K.G., Eu, Z.A., Tan, H.P., Wireless sensor networks powered by ambient energy harvesting (WSN-HEAP) - Survey and challenges, 1st International Conference on Wireless Communications, Vehicular Technology, Information Theory and Aerospace & Electronic Systems, Aalborg, Denmark, 2009, ISBN: 978-1-4244-4066-5
22. Fasl, J., Helwig, T., Wood, S., Samaras, V., Potter, D., Lindenberg, R., Frank, K., Evaluation of Wireless Devices for Monitoring Fracture - Critical Bridges, 7th International Bridge Engineering Conference, San Antonio, TX, USA, December 2010.
23. Hoult, N., Bennett, P.J., Stoianov, I., Fidler, P., Maskimovic, C., Middleton, C., Graham, N., Soga, K., Wireless sensor networks: creating 'smart infrastructure', *Proceedings of ICE*, Civil Engineering, 162, 2009, pp.136 - 143
24. Ceriotti, M., Mottola, L., Picco, G.P., Murphy, A.L., Guna, S., Corrà, M., Pozzi, M., Zonta, D., Zanon, P., Monitoring Heritage Buildings with Wireless Sensor Networks: The Torre Aquila Deployment, *Proceedings of the 8th ACM/IEEE International Conference on Information Processing in Sensor Networks (IPSN/SPOTS)*, San Francisco, CA, USA, 2009.
25. ***, Libelium SmartCities technical guide (electronic version) available online at: http://www.libelium.com/documentation/waspmote/smart-cities-sensor-board_eng.pdf, viewed at 03/05/2012

Principles for design of wind turbine foundations. Case Study

Ana Nicuta, Razvan Mircea Chirila, Daniela Grigore

*Faculty of Civil Engineering and Building Services, Technical University "Gheorghe Asachi" to Iasi,
Code 70050, Romania,*

Summary

Foundation for special constructions represent a particular interest considering that the current state of development in renewable energy regeneration problem for Europe and the entire world is a special problem. From the category of special construction are also the wind turbins that became very efficient for generating electricity without producing carbon dioxide emissions that affect the ozone layer and global warming. The foundations for such construction are classified in direct foundations – general raft foundation and indirect foundation through piles. The case study refers to the design of foundations for a wind turbine located in two different areas of Romania, with different geotechnical characteristics

KEYWORDS: wind turbine, foundations on piles, general slabs foundation

1. INTRODUCTION

Wind energy has been exploited on land ever since the first windmill was build in ancient Persia in the seventh century. Around the fourteenth century the Germans have used passive wind energy to remove water from the flooded fields with a so-called windmill [11].

But the widespread exploitation appeared only in the twentieth century alongside the modern windmills, wind turbines that can generate energy ranging from 250 to 300 KW. Modern wind turbins became very efficient and now generates electricity for thousands of homes in Europe and worldwide, without producing carbon dioxide emissions that affects the ozone layer and the global warming.

The country with the highest percentage of electricity developed from wind energy is Denmark, with about 20%, and the country that produces the biggest quantity of energy is Germany.

The total global capacity of wind turbines is around 75.000 MW. Most turbines produce energy 25% of the time and this number increases during the winter when the winds are getting stronger.

2. TYPES OF WIND TURBINES

Wind energy is part of renewable energy. The aero-generator uses the wind’s kinetic energy to drive the rotor shaft: it is converted into mechanical energy, which in turn is converted into electricity by a generator that is mechanically coupled to the wind turbine.

2.1. Vertical axis wind turbines

The turbine pylons with vertical axis are quite small, with a height ranging between 0,1 – 0,5 of the rotors height. This allows placing the entire energy conversion equipment (multiplier, generator), at the foot of the turbine, thus facilitating the maintenance operations.

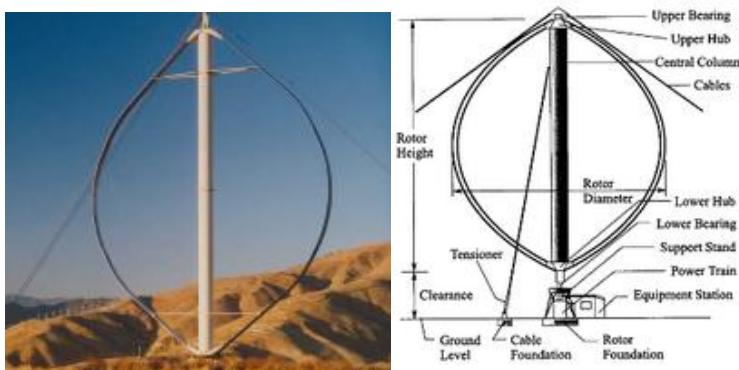


Fig.1. Types of wind turbins with vertical axis [13]

2.2. Horizontal axis wind turbines

The energy produced by the horizontal axis wind turbines is based on the principle of windmills. Most often, the rotor of these windmills have three blades with a certain streamlined profile, because in this way it achieves a good compromise between power ratio, cost and speed of rotation of the eolian transducer, as an aesthetic aspect improvement, compared with the rotor with two blades [10].

Horizontal axis wind turbines are mostly used because their aerodynamic performance is superior to the one of the vertical axis turbines, are less driven to significant mechanical stress and have a lower cost

There are two ways of positioning these horizontal axis turbines: upstream and downstream (Figure 2). The most widely used is placing the turbine axis upstream, with getting best results at high power.

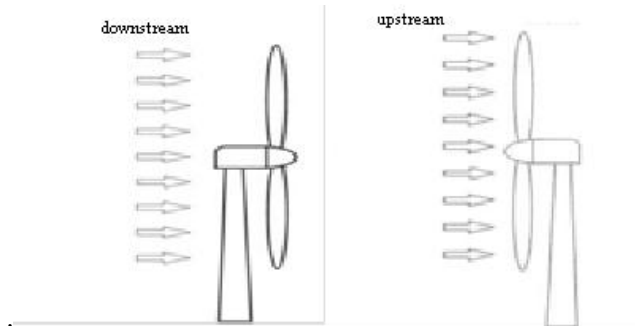


Fig.3. Scheme of horizontal axis wind turbine downstream and upstream

3. FOUNDATIONS FOR WIND TURBINE

The terrestrial wind turbines transfer the loads in to the ground through the foundation. Types of foundations for such constructions shall be chosen only after a detailed ground investigation has been made, through laboratory and in situ tests.

In preparation of the documentation for the geotechnical study it shall be take into consideration a more detailed site description in terms of geological, hydrogeological, climatic, seismic and framing development in the geotechnical category.

Land investigations provided by the geotechnical study should provide all the necessary data needed for designing in safety conditions, in compliance with the geotechnical design concept that ensures stability, strenght and durability of the construction.

The physical and mechanical characteristics of the ground where the wind turbines will be located, depending on the effort, usually governs the type of chosen foundation.

Before choosing the type of the foundation, the designer should check several important issues: the ground bearing capacity, the sliding and overturning stability, the resistance of the soil to degradation in terms of cyclic loads, compaction endings, differential compaction is more likely to develop because of the wind loads generated in the windmills, the possibility of soil erosion.

The foundations for such construction are classified as direct foundations – general raft foundation when the ground at the proposed foundation depth can support loads from the superstructure and indirect foundations – on piles, that are designed to transfer the loads in depth, to where the good ground foundation is located.

3.1. General slab foundations

Are surface foundations with varying sizes, with circular or octagonal shape in horizontal plane, with varying heights, depending on the size of the solicitations.

In calculating the raft foundation we must consider many factors from which the most important ones are the rigidity and foundation geometry, the size and distribution of loads, the deformation and strength characteristics of the ground and the execution phases.

The calculus follows the determination of contact pressures and deformations, bending moments and shear forces. In calculations, the raft foundation can be considered rigid or flexible.

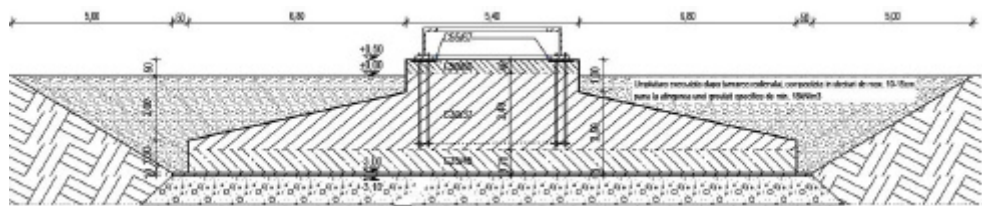


Fig.6. Example of general slab foundation

3.2. Indirect foundations through piles

Due to the important category of these types of buildings, large loads are transmitted to the foundation ground and the nature of the ground, force structure designers to choose many times the foundation through piles.

4. CASE STUDY

The case study refers to the design of foundations for a wind turbine located in two different areas of Romania.

The model for the wind turbine for which the calculus was made is VESTAS V90 – 1.8 MW VCS HH 105m [10]. The model characteristics are presented in Table 2.

The manufacturer provided data upon which the calculus is based. The data refers to a series of loads applied at the turbine base. The loads had extreme values, in order to observe the behaviour under worst circumstances.

Table 1. Loads on the foundation of the suprastructure

Extreme loads	Mx [kNm]	My [kNm]	Fz [kN]
	75407	-2295	-3666

Tabel 2. Geometric characteristic of wind turbine

General information about the suprastructure (turbine)	
Diameter propeller	90.0 m
Number of blades	3
Length of blades	44.0 m
Height of tower	105.0 m
Diameter at the base of the tower	4.0 m
Suprastructure weight	360.0 t

The foundation selection was based on several parameters, as it follows [7]:

- The foundation's own weight caused permanent, constant loads these loads were procentually reduced by the construction-foundation assembly.
- The weight of the frost deposits determined cvasipermanent loads, with a slow variation; these loads had low procentual values. But if irregularities occur to the frost deposits, the rotor unbalances and dynamic loads occur on a regular basis, but with low percentages.
- Wind action determined random variable loads which happen on a regular incidence, resulting in intense wear stresses (the percentage of this occuring is dominant and has extreme values). Wind action depends on electrical conducting power and rotor influence on direct force applied on pile.
- Seismic action caused short term loads, which were equivalent to an isolated impulse, with a higher procentage. The seismic action, even if different than the wind action, causes similar effects which sum up to a horizontal oriented group.

The rotor unbalance caused damaging forces (the shattering of blades), which provided violent loads.

All these loads were transmited to the foundation base. The special efforts on the foundation ground were oriented on the axes, having an intensity that can be predicted and included as a general rule.

The foundation calculus was made by means of a hypothesis considering the efforts provided by the manufacturer as the load in exploitation regime for the turbine. A simplified model will be used, combining this hypothesis with the seismic effect. Modeling was performed using an AxisVM software.

The solution for this foundation was based upon the transmission of all the loads from the suprastructure through a slab foundation to a pile system located on each side of the slab.

Calculations and analysis of the interaction between ground foundation and infrastructure has allowed a comparison of the stress and displacement values for the two cases that were analyzed. The design of the wind turbine foundations has been made taking into consideration the force normatives and SR EN 61400-1:2006, that is identical to IEC61400-1.

The raft foundation was calculated considering a reinforced concrete slab with the thickness of 250 cm and an octagonal shape with the sides of 800 cm. The bed-load coefficient k_s [1] had the following values: $k_s = 6,5 \text{ daN/cm}^3$ for location Galbiori (Constanta) and $k_s = 8 \text{ daN/cm}^3$ for location Valea Lupului (Iasi).

4.1. Location: Galbiori, Constanta

Foundation for wind turbine is the raft generally type, disposed on the 16 bored piles, $\text{Ø}1080 \text{ mm}$, embedded in the technical basis.

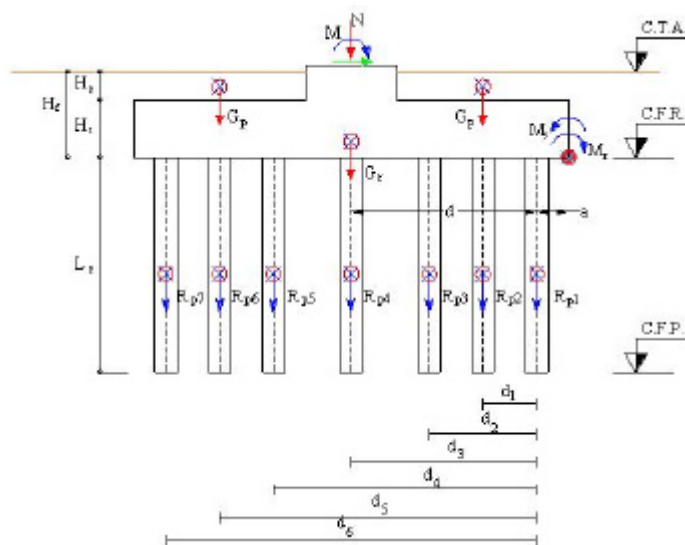


Fig.10 Cross section through the foundation

The factor of safety against overturning, is expressed: $M_s / M_r \geq 1,5$

$$M_s / M_r = 281761,27 / 105754,1 = 2,66 \Rightarrow 2,66 > 1,5$$

The calculation of bored piles was performed in according with [4], [5], [6], [7].

4.1.1. Ultimate compressive resistance from static load tests

$$\begin{aligned} R_{c;d} &= R_{b;d} + R_{s;d} = R_{b;k} / g_b + R_{s;k} / g_s \\ R_{c;d} &= 4561.025 \text{ kN} \end{aligned} \quad (2)$$

where:

$R_{c;d}$ - design value of the compressive resistance;

$R_{b;d}$ - design value of the base resistance;

$R_{s;d}$ - design value of the shaft resistance.

$$R_{b;d} = R_{b;k} / g_b \quad (3)$$

where:

$R_{b;k}$ - characteristic values of the base resistance;

g_b - partial resistance factor for bored piles on base.

$$R_{s;d} = R_{s;k} / g_s \quad (4)$$

where:

$R_{s;k}$ - characteristic values of the shaft resistance;

g_s - partial resistance factor for bored piles on shaft (compression).

The characteristic value may be obtained by calculating:

$$\begin{aligned} R_{b;k} &= A_b \cdot q_{b;k} \\ R_{b;k} &= 1570 \text{ kN} \end{aligned} \quad (5)$$

where:

A_b - area at the base pile;

$q_{b;k}$ - characteristic value of base resistance.

The characteristic values of the shaft resistance may be obtained by calculating:

$$\begin{aligned}
 R_{s;k} &= \sum A_{s;i} \cdot q_{s;i;k} = U \sum q_{s;i;k} \cdot l_i \\
 R_{s;k} &= 3.14(20 \cdot 0.50 + 42 \cdot 3 + 54.50 \cdot 1 + 60 \cdot 4 + 64.8 \cdot 1.80 + 68.50 \cdot 1.20 + \\
 &+ 70.60 \cdot 2.30 + 71.30 \cdot 0.70 + 77.80 \cdot 7.25 + 84.70 \cdot 2.0 \\
 R_{s;k} &= 4945.75kN
 \end{aligned}
 \tag{6}$$

where:

$A_{s;i}$ - shaft area of the pile in contact with the soil;

U - pile cross – section perimeter;

l_i - the thickness of “i” layer, which is in direct with “i” layer;

$q_{s;i;k}$ - characteristic value of the shaft resistance to “i” layer.

4.1.2. Ground tensile resistance

General relationship for calculating:

$$F_{t;d} \leq R_{t;d} \tag{7}$$

where:

$F_{t;d}$ - characteristic tensile value for the single pile corresponding to ULS;

$R_{t;d}$ - design value of the tensile resistance.

The characteristic value of tensile resistance may be obtained by calculating:

$$R_{t,d} = \frac{U \sum q_{s,k_2} l_i}{g_m \cdot g_{s_2}} = 4027.58kN \tag{8}$$

where:

q_{s,k_2} - characteristic values of shaft friction in the various layer obtained from values of ground properties;

U - pile cross – section perimeter;

l_i - the thickness of “i” layer, which is in direct with “i” layer;

g_{s_2} - values of the partial factor may be set by the National Annex;

g_m - values of the partial factor: $g_m = 2, 4$.

4.1. 3. Calculation of pressure on the slab foot

$$s = \frac{N + G}{A} + \frac{M}{W} = \frac{5746.9 + 276087.76}{763.96} + \frac{3138,8}{351.35} = 369.80 \text{ kPa} \quad (10)$$

4.2. Location: Valea Lupului, Iasi

The choice of the second location was made in order to highlight similar foundation types. These similarities provide a equal size, that would interact on soils with different characteristics. Therefore, on this location, the decision was to run the program with the same input data, the only difference being the elastic coefficient k_s , which in this case has the value of 8 daN/cm^3 .

There has been made a tabular centralization of data to compare the values obtained on the first location.

Table 3. Comparasions between the two locations efforts

			Galbiori, Constanta $k_s = 6,5 \text{ daN/cm}^3$	Valea Lupului, Iasi $k_s = 8 \text{ daN/cm}^3$
Total displacement	ez (mm)	Min	-2.654	-0.867
		Max	0.405	0.058
Shear Forces	V (kN)	Min	121.00	62.30
		Max	1181.00	1024.60
Bending Moments	My (kNm)	Min	7540.70	7526.30
		Max	10355.5	9876.53
React.	Rz (kN/m2)	Min	-212.30	-56.00
		Max	32.10	3.80

It ss observed a stress reduction of rafter surface for the lasi area compared to the soil from Galbiori

5. CONCLUSIONS AND RECOMMENDATIONS

In this paper were used models for the design of wind turbine foundations, the special construction which have taken a major role in our country.

Diversity of sites within the territory of Romania requires additional research to determine the correct bearing capacity of the foundation land and choice for the optimal system of the foundation. The case study was performed for the same type of wind turbine, but on two different sites, which have different stratification, from our country.

Different versions of the type foundation have been used for VESTAS V90 -1.8 MW VCS HH 105m. wind turbine model.

The raft foundation on piles applied on both sites allowed an accurate comparison between strains and stresses, shown in Table 3. The foundation designed presented the same dimensions and geometrical features.

The researches performed had aimed to highlight the fact that wind power would be a key factor in achieving the purpose established by the European Union for the year 2020, and to provide less consume, with 20% energy obtained through pollutant emissions.

European Wind Energy Association estimates that wind power will have an amount ranging between 13% and 16% of the electricity consumed in the European Union until the year 2020.

Therefore, the expansion of this energetic industry in Romania demands us a better understanding the behavior of the wind turbine and its infrastructure in relation to the foundation soil.

References

1. Stanciu, A., Lungu, Irina, - *Fundatii*, Editura tehnica, Bucuresti, 2006
2. Botu, N., Musat, V. – *Geotehnica*, Editura Societatii Academice “Matei – Teiu Botez, Iasi, 2003
3. Lungu, Irina, Stanciu, A., Boti, N – *Probleme speciale de Geotehnica si Fundatii*, Editura Junimea, Iasi, 2002
4. NP 123:2010 Normativ privind proiectarea geotehnica a fundatiilor pe piloti
5. SR EN 1536 –Executia lucrarilor speciale.
6. SR EN 1997-1:2006 – Proiectarea geotehnica. Partea 1 – Reguli de proiectare.
7. SR EN 61400-1:2006 - Turbine eoliene. Partea 1: Conditii de proiectare
8. www.consoft.ro – Manual AXISVM
9. <http://www.agp.ro>
10. <http://www.vestas.com/en/wind-power-plants.aspx#/vestas-univers>
11. <http://www.eoliene.eu/bazele-energiei-eoliene>
12. www.wikipedia.com
13. www. visual.merriam-webster.com

Dynamic response of a wind turbine considering soil - structure interaction

Cerasela-Panseluta Olariu

Structural mechanics Department, Gh. Asachi University, Iasi, Romania

Summary

In our country wind turbine construction is extending. Due to the fact that Romania is located in a seismic area it is necessary to consider wind as well as the seismic action when analyzing the towers of wind turbines. An evaluation method of structural response under dynamic actions is the knowledge of the natural modes of vibration of the structure. This aspect becomes of a high interest in a wind turbine analysis because it is necessary to avoid entering the resonance range. In order to highlight the soil structure interaction effects are usually used two methods, namely the substructure method when the soil stiffness is modeled through springs and the finite element method which analyses the entire structure including the foundation soil. In this paper it is presented a dynamic analysis of a 70 meters tall wind turbine considering 4 different types of soils using the finite element method.

KEYWORDS: soil structure interaction, wind turbines, natural modes of vibration, resonance ranges.

1. INTRODUCTION

The new tendency of sustainability requires that all unconventional sources of energy should be exploited. Therefore all around the world new techniques of achieving energy are developed. The construction of wind turbines is accelerating in the last decade all over Europe, as well as in Romania. This growth of wind turbines construction has revealed some design and building difficulties because care need to be taken when dealing with some particularities of these structures.

One of the aspects that should be treated carefully during the functioning of a wind turbine is that it is necessary to avoid entering the resonance range. This implies the knowledge and control of the natural frequencies of vibrations of the tower which should not coincide with the rotor and blade-passing frequencies.

In order to control the natural frequency of the tower particular solutions for the tower as well for the foundations has to be chosen. In this situation considering a rigid base for the tower can outcome misleading results. Studies have proved that when soil stiffness is taken into account in analyses the natural frequencies of the structures differ (usually are smaller) from the case when a rigid base is considered [1]. Therefore in order to choose the best design solutions as to avoid the resonance range it is necessary to consider soil - structure interaction.

This paper presents some theoretical methods to appreciate the foundation soil stiffness for analyzing a wind turbine and a case study using finite element method to analyze the entire soil/foundation/wind turbine system.

2. THEORETICAL BACKGROUND

The International Standard IEC 61400-1 - Wind turbines - Part 1: “Design requirements” was published in order to ensure the safety of wind turbines against damage for the entire life span. In 2005 it was reevaluated and it became the European standard EN 61400-1: 2005. This standard provides safety requirements and specifies the essential design requirements to ensure the engineering integrity of wind turbine [2].

On the other hand, countries with experience in this area of construction like Denmark, Germany have developed national standard for wind turbine design. Guidelines for Design of Wind Turbines, 2002 - Denmark is an example of design guide based on accumulated experience and research in this field. [3,4]

In Romania the European standard was completed with national design requirements and in 2006 it became the national standard SR EN 61400-1:2006. Wind turbines. Part 1: Design requirements. This standard includes also other parts which deal with different aspects of the wind turbines design.

2.1. Wind turbine modeling

The tower of a wind turbine supports the nacelle and the rotor and provides the necessary elevation of the rotor to keep it clear off the ground and bring it up to the level where the wind resources are. Most large wind turbines are delivered with tubular steel towers, which are manufactured in sections of 20-30 m length with flanges at either end. The sections are bolted together on the site. The towers are conical, their diameters increase towards the base, and thereby increasing their strength towards the tower base, where it is needed the most, because this is where the load response owing to the wind loading is largest. The tower is usually

connected to its supporting foundation by means of a bolted flange connection or a weld (figure1)[3].

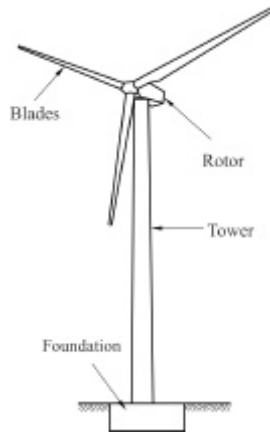


Figure 1. Main components of a wind turbine

On the entire life span of the wind turbine the tower has to withstand the operational vibrations. The rotor and blade-passing frequencies may cause increase of the forces acting on the tower which may lead to a highly insecure level of structural integrity.

The international design codes usually require that wind turbines should be designed for wind actions. On the other hand, in countries like Romania it is necessary to take into account apart from the wind action also the seismic action. When a wind turbine is to be designed for installation on a site which may be subject to earthquakes, the wind turbine has to be designed so as to withstand the earthquake loads.

Load calculations for a wind turbine structure are usually performed by means of a computer program based on an aeroelastic calculation procedure.

For analysis of the horizontal motions and accelerations, the wind turbine can be represented by a concentrated mass on top of a vertical rod. For a typical wind turbine, the concentrated mass can be taken as the mass of the nacelle, including the rotor mass, plus a part of the tower mass [5].

It is important to analyze the wind turbine tower for the earthquake-induced accelerations in one vertical and two horizontal directions. It usually suffices to reduce the analysis of two horizontal directions to an analysis in one horizontal direction, due to the symmetry of the dynamic system. The vertical acceleration may lead to buckling in the tower.

The way to avoid structural failures is to attain a natural frequency of the structure different from the operational frequency of the wind turbine. Usually the

operational frequency is smaller than the natural frequency of the tower. As the wind turbine blades start rotating their circular velocity is increasing and the induced vibration frequency increases. Depending on the power output capacity of the wind turbines, the blades rotate with rotational speeds that range from 30 to 60 rpm which correspond to some maximum operational frequencies from 0.5 to 1 Hz. Usually these operational frequencies are close to the natural frequency range of the soil-structure system [6].

A poor design decision can involve a maximum rotational speed that is very close to the natural frequency of the structural system resulting in a high likelihood of resonant amplification causing structural instability. Another poor design may have a rotational speed not very close to yet higher than the natural frequency of the structural system. In such cases, the structure would have to endure violent near-resonance vibrations as the operational frequency approaches the natural frequency while speeding up to and down from the maximum speed. This situation would result in very high dynamic forces which could cause immediate damage to the structure. Even if these dynamic forces do not exceed the structure's strength capacity, fatigue-induced failures could also be encountered [8].

A sound design would avoid allowing the operational frequency to approach the vicinity of the natural frequency by a certain safety factor. According to different design codes a safety factor ranging from 5% up to 15% of the natural frequency is recommended [1, 2, 3, 4; 5].

2.2. Soil structure interaction for wind turbines

Wind turbines are usually supported by either a slab foundation or a pile foundation. Soil conditions at the specific site usually govern whether a slab foundation or a pile foundation is chosen. A slab foundation is normally preferred when the top soil is strong enough to support the loads from the wind turbine, while a pile supported foundation is used when the top soil is of a softer quality and the loads need to be transferred to larger depths.

The overall foundation stiffness is dependent on the strength and stiffness of the soil as well as on the structural foundation elements. The foundation stiffness needs to be determined as a basis for predicting the dynamic structural response to wind, wave and earthquake loading. The foundation stiffness is in general frequency dependent. This is particularly important when predicting dynamic response to earthquake [7; 11].

The finite element method provides a precise computational mean for soil structure interaction. The foundation soil can be modeled throughout finite elements in stead of providing a global stiffness of the soil. Although in this method the soil parameters considered are the elastic modulus and the Poisson's ratio, the results are more realistic than using stiffness springs [6].

Various books are providing different equations to compute foundation stiffness depending on the shape, size and type of the foundation and on the soil properties. Table 1 presents some of these equations from three different sources to compute stiffness for a circular footing on stratum over bedrock (figure 2a.) and for circular footing embedded in stratum over bedrock (figure 2b.). There are also other equations to be used for other shapes of foundation and for pile foundations.

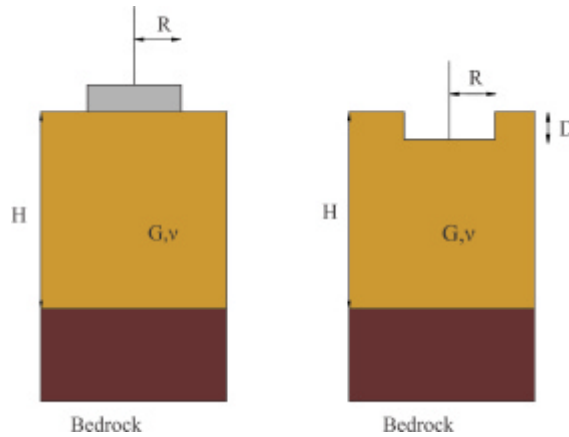


Figure 2. a. Circular footing on stratum over bedrock, b. circular footing embedded in stratum over bedrock

Table 1. Equations to compute stiffness for a circular footing on stratum over bedrock according to figure 2.a. [3, 9, 10]

Mode of motion	Circular foundation	
Source of references	Negoita and Fema 450	Guidelines for Design of Wind Turbines
Vertical	$k_z = \frac{4GR}{1-n}$	$k_z = \frac{4GR}{1-n} \left(1 + 1.28 \frac{R}{H} \right)$
Horizontal	$k_x = \frac{32(1-n)GR}{7-8n}$	$k_x = \frac{4GR}{1-n} \left(1 + 1.28 \frac{R}{H} \right)$
Rocking	$k_q = \frac{8GR^3}{3(1-n)}$	$k_q = \frac{8GR^3}{3(1-n)} \left(1 + \frac{R}{6H} \right)$
Torsion	$k_t = \frac{16GR^3}{3}$	$k_t = \frac{16GR^3}{3}$

Guidelines for Design of Wind Turbines provide the following formula to compute the foundation stiffness for a circular footing embedded in stratum over bedrock (figure 2b) [3]:

$$k_z = \frac{4GR}{1-\nu} \left(1 + 1.28 \frac{R}{H} \right) \left(1 + \frac{D}{2R} \right) \left[1 + \left(0.85 - 0.28 \frac{D}{R} \right) \frac{D/H}{1-D/H} \right] \quad (1)$$

$$k_x = \frac{8GR}{1-\nu} \left(1 + \frac{R}{2H} \right) \left(1 + \frac{2D}{3R} \right) \left(1 + \frac{5D}{4H} \right) \quad (2)$$

$$k_q = \frac{8GR^3}{3(1-\nu)} \left(1 + \frac{R}{6H} \right) \left(1 + 2 \frac{D}{R} \right) \left(1 + 0.7 \frac{D}{H} \right) \quad (3)$$

$$k_t = \frac{16GR^3}{3} \left(1 + \frac{8D}{3R} \right) \quad (4)$$

In figure 2 and in ale the equations the following notations were used:

- G –shear modulus,
- ν –Poisson’s ratio,
- R – foundation radius,
- D – embedment depth,
- H – the width of the soil stratum to the bedrock.

3. CASE STUDY

In order to highlight the importance of taking in to account soil - structure interaction in a dynamic analysis for a wind turbine it was chosen a particular case. Therefore in this chapter there are presented the results from a dynamic analysis for a 70 meters tall wind turbine considering 4 different types of soils.

The entire soil – foundation - wind turbine structure was modeled using finite element method. The model used is presented in figure 3. The analysis was performed using the computational program Sap 2000. The tower was modeled through ‘shell’ finite elements having variable diameter and thickness along the height of the tower. It is a 67.6 m tall tubular steel tower with a range of diameter from 4.2 m at the base to 1.85m at the top. The mass of the tower is 85.15 tones and the weight of the rotor and the blades are 47 tones. The rotor and the blades were modeled as a concentrated mass at the top of the tower. Also along the entire height of the tower the weight from interior stairs and platforms was applied.

The foundation used for this model is a circular footing having a 16 meters diameter (D) and a 3 meters thickness. The foundation soil considered for the analysis was extended around the foundation at a length of 2D and in depth for 6D.

It is considered that the wind turbine is operating with variable speed range from $n_{min} = 5,5$ rpm to $n_{max} = 29$ rpm.

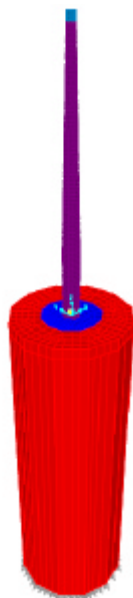


Figure 3. Model of the soil- foundation - wind turbine

Table 2 presents the characteristics of the 4 types of foundation soils used in the analysis. The names of the soils are given after their shear wave velocity. Also the soil classes correspond to the SR EN 1998-1:2004 standard.

Table 2. Foundation soils characteristics

Soil type	Shear waves velocity [m/s]	Soil class SR EN 1998-1:2004	Poisson's ratio , ?	Density, ? [N/m ³]	Elastic modulus, E [N/m ²]	Shear modulus, G [N/m ²]	kx N/m ³
V150	150	D	0.45	19620	4804940	1656875.9	3,5 *10 ⁶
V300	300	C	0.4	20000	13757818	4913506	6 *10 ⁶
V600	600	B	0.35	22000	23534400	8716444	35*10 ⁶
V900	900	A	0.3	25000	50000000	19230769	70*10 ⁶

From the dynamic analysis the natural frequencies of the tower considering the same type of foundation but different types of soils were determined. The variation range of the frequencies was considered to be at $\pm 10\%$.

Table 3 presents these results obtained from the dynamic analysis.

Table 3. Natural frequencies and periods of vibration of the model

Mode of vibration	Type of soil	Frequency Hz	Frequency+10% Hz	Frequency - 10% Hz	Period of vibration s
1	V150	0,445	0.4895	0.4005	2,242
	V300	0,499	0.5489	0.4491	2,002
	V600	0,514	0,5654	0,4626	1.942
	V900	0,521	0,5731	0,4689	1.917
2	V150	1.5743	1,73173	1,41687	0,635
	V300	2.5212	2,77332	2,2690	0.396
	V600	3,084	3,3924	2,7756	0,324
	V900	3,243	3,5673	2,9187	0,308

The diagrams of resonance presented in figures 4 to 7 were realized using the following equations:

$$\frac{f_R}{f_{0,1}} \leq 0.90 \text{ and } \frac{f_{R,m}}{f_{0,n}} \leq 0.90 \text{ or } \frac{f_{R,m}}{f_{0,n}} \geq 1.10 \tag{5}$$

where: f_R is maximum rotation frequency of the rotor in normal operation range;

$f_{0,1}$ – first eigenfrequency of the tower;

$f_{R,m}$ – pass frequency of the m rotor blades;

$f_{0,n}$ – the n -th frequency of the tower..

The frequencies f_f 1- f_f 15 from the resonance diagrams were computed with the following relation:

$$f_f = \frac{i \cdot n}{60} \tag{6}$$

Where: $i=1 \dots 15$ and $n= 1, 3, 5, 7, 9, 11, 13, 15, 17, 19, 21, 23, 25, 27, 29, 31$.

It is necessary that the first frequency f_f 1 avoid entering the variation range of the first frequency of the tower until the rotor reaches the speed of 29.18 rpm.

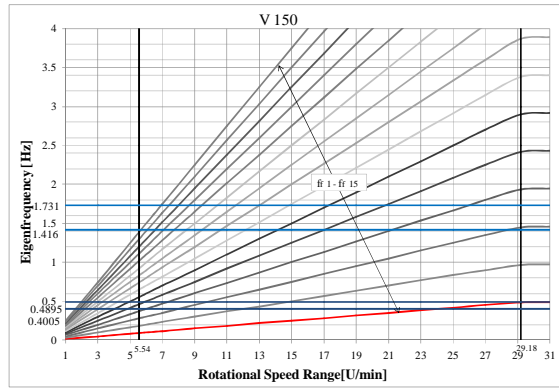


Figure 4. Diagram of resonance for model with soil V150

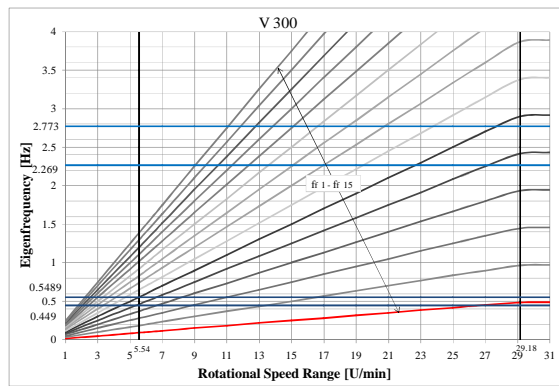


Figure 5. Diagram of resonance for model with soil V300

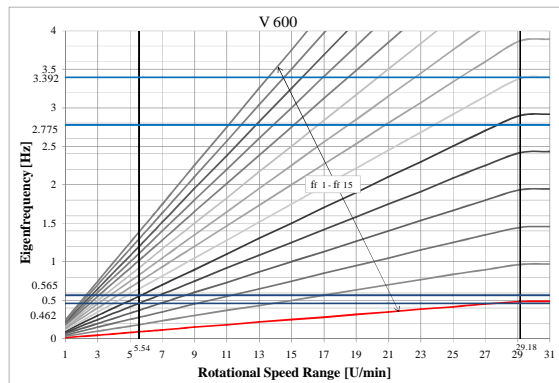


Figure 6. Diagram of resonance for model with soil V600

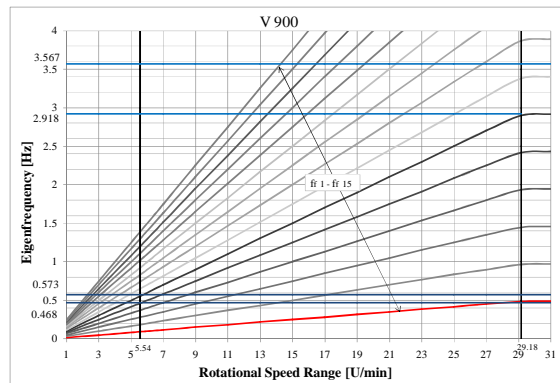


Figure 7. Diagram of resonance for model with soil V900

The resonance diagrams were performed in order to establish the minimum type of foundation soil on which this type of wind turbine can be placed.

From the resonance diagrams it can be noticed that the V150 type of soil is the most disadvantageous because the first operational frequency of the wind turbine is entering the resonance domain before the turbine reaches the maximum operational speed. Therefore the minimum type of soil to be used for this type of wind turbine and foundation system is V600 with the specific characteristics given in SR EN 1998-1:2004.

4. CONCLUSIONS

The natural modes of vibration and the frequencies of the entire soil - foundation- wind turbine system play an important role in wind turbine analysis. Based on this analysis it can be noticed that considering soil-structure interaction is a very important aspect in order to avoid entering the resonance range. Also by considering soil stiffness the entire system has smaller frequencies than considering the structure with a fixed base. This aspect is reflected in a lower limitation range of the tower’s frequencies which can imply a higher possibility for the operating frequency to coincide with the tower’s frequency. Therefore care must be taken when choosing the right foundation solution based on the type of soil it can be found on the construction site.

References

1. Olariu, C.P. Influenta deformabilitatii terenului de fundare asupra comportarii unor structuri de rezistenta, teza de doctorat , Universitatea Gh. Asachi, Iasi, 2011
2. The International Standard IEC 61400-1- Wind turbines - Part 1: Design requirements, 2005

3. Guidelines for Design of Wind Turbines, DNV/Ris? , Jydsk Centraltrykkeri, Danemarca, 2002.
4. Guideline for the certification of wind turbines, Germany, 2003.
5. Hau, E., Wind Turbines: Fundamentals, Technologies, Application, Economics; 2nd Edition Springer-Verl., Berlin, 2006;
6. Hartmann, F., Katz, C. - Structural Analysis with Finite Elements, Springer-Verl., Berlin, 2007;
7. Mohamed Al Satari, Saif Hussain, S.E – Vibration Based Wind Turbine Tower Foundation Design Utilizing Soil-Foundation-Structure Interaction, The 14th World Conference on Earthquake Engineering, Beijing, China, October, 2008
8. Pekka Maunu – Design of Wind Turbine Foundation Slabs, Master’s Thesis Lulea University of Technology, Hamburg, 2008
9. NEHRP recommended provisions for seismic regulations for new buildings and other structures, Part 1-15, Fema 450, Washington, D.C., 2003.
10. Negoita, Al., s.a. - *Inginerie seismica*, Editura didactica si pedagogica, Bucuresti, 1985
11. Olariu, C.P.- Influenta deformabilitatii terenului de fundare asupra raspunsului dinamic al unei turbine eoliene. “Creatii universitare 2011”, Al IV-lea Simpozion National Iasi, România, 2011.

Finite element analysis of bonding between carbon fibers reinforced polymeric composites (CFRP) and concrete

Ruxandra Oltean

Department of Civil and Industrial Engineering, "Gh. Asachi" Technical University, Iasi, Romania

Summary

Retrofit of reinforced concrete members using externally bonded fiber reinforced polymer composites (FRP) has become widely recognized. However, in many instances, the FRP strengthened element suffers a premature debonding failure between FRP and the concrete substrate before the concrete – FRP hybrid element reaches its bearing capacity. The FRP – concrete interface plays a major role in this strengthening method by providing effective stress transfer from the substrate to the FRP strips and guarantee the consistency of the hybrid systems made of FRP and concrete.

An experimental program has been carried out at the Technical University of Iasi, Romania to study the interfacial behaviour between carbon fibre reinforced polymer (CFRP) composite sheets and concrete as a preliminary required step to develop hybrid structures made of polymeric composites and traditional building materials.

In addition to the experimental work a finite element analysis was performed, using Ansys package software. Proper modeling of such hybrid structures require a significant effort made even assuming linear elastic behavior and problems exist when using finite elements to study the bonding between the FRP and the concrete due to the complexity of the materials. Therefore, most of the existing models in literature adopted a number of simplified assumptions. For example, the adhesive was often neglected and the bond layer was typically not modeled.

This paper focuses on predicting, by numerical modeling, the failure loads and stresses of concrete - CFRP hybrid elements utilizing three different CFRP plates.

The simulated results using the finite element analysis were found to agree well with experimental data from all sets of tests.

KEYWORDS: concrete; fiber reinforced polymers, bond, finite element analysis, strengthening.

1. INTRODUCTION

Since the beginning of structural restoration, architects and engineers have envisaged and actually applied a wide variety of repair or strengthening interventions to improve the structural response of the damaged concrete structures. Besides the usage of traditional techniques, modern techniques such as the application of FRP composites for strengthening are getting more attention nowadays. Modern practice in civil and structural engineering involves strengthening concrete structures by externally bonded FRP materials, which has become a common practice, widely recognized by modern design codes [1 – 6]. This type of reinforcing system has a significant number of advantages, such as lightness, noncorrosive, nonmagnetic, strong and highly versatile, FRP composite products being, in certain cases, the ideal materials for structural strengthening and rehabilitation [7 – 9].

The two general types of applications of externally bonded FRP composites on concrete substrate are generally known as contact-critical and bond-critical. In contact-critical applications, the load is transferred between FRP and concrete by contact stress across the interface, as in passive column confinement. In bond-critical applications, the load is transferred by shear stress as well as peeling-stress, as in flexural and shear reinforcements for beams [10]. Therefore the existing experimental work has been carried out using several set-ups, including single shear test [11 - 13], double shear tests [14 – 16] and beam tests [17] (Fig. 1). The current paper is concerned with the bond behavior in case of double shear test set-up using both experimental tests and the finite element (FE) analysis.

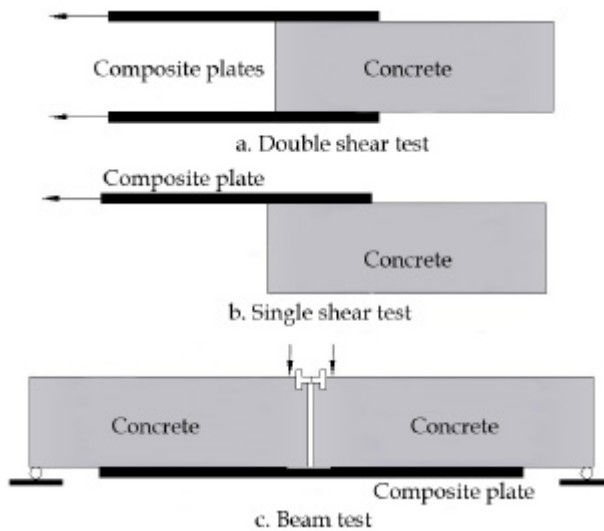


Figure 1. Bond test set-ups [17]

2. FINITE ELEMENT MODELING

Two identical CFRP plated concrete prisms 400 mm long and with a cross-section of 150 x 150 mm under tension were chosen as the benchmark specimen to be studied. Three simplified FE models with different types of CFRP reinforcement were built to analyze the bonding behavior using Ansys software package. For the first two models all components were assumed to be linear elastic, while for the third FE model the bilinear concrete behavior was considered. The materials properties of all components are given in Table 1 and the considered geometrical model can be observed in Figure 2. In order to reduce the solving time and to increase the precision the geometrical model was simplified using the symmetry of the elements, thus the simplified model is actually a quarter of the benchmark specimen.

Table 1. Properties of the constituent materials

Specimen series	C1	C2	C3
Type of CFRP plate	Sika Carbodur S1012	Sika Carbodur M1014	CFK 150/2000
Geometric characteristics (mm)	1.2x100	1.4x100	1.2x100
Density (kg/m ³)		1600	
Poisson's ratio		0.25	
Young's modulus (N/mm ²)	165000	210000	165000
Tensile strength (N/mm ²)	3100	3200	1000
Adhesive	Sikadur 30		
Density (kg/m ³)	1650		
Poisson's ratio	0.4		
Young's modulus (N/mm ²)	12800		
Tensile strength (N/mm ²)	25		
Compressive strength (N/mm ²)	75		
Concrete batch	Batch 1		
Density (kg/m ³)	2300		
Poisson's ratio	0.2		
Young's modulus (N/mm ²)	32000		
Tensile strength (N/mm ²)	2.2		
Compressive strength (N/mm ²)	31.6		

The FE modeling of all components was performed using 3D elements, solid elements. Namely, the specimens were modeled using 20 nodes solid elements, Solid 186, while for the interface area CONTA 174 were employed, elements which are currently used by Ansys in modeling the contact and slip between two surfaces. However, in this study perfect bond between materials was assumed. The

high strength of the epoxy used to bond the CFRP sheets to the concrete prisms supported the perfect bond assumption. More than that, the nodes of the CFRP solid elements were connected to those of adjacent concrete solid elements in order to satisfy the perfect bond assumption.

As an initial step, a fine FE mesh was employed especially in the area of CFRP bonding to the concrete substrate (Figure 3). In other words, the model was divided into a number of small elements, and after loading, stress and strain are calculated at integration points of these small elements [18].

The loading was applied taking into account the displacement control, thus it was imposed the ultimate value of the experimental displacement.

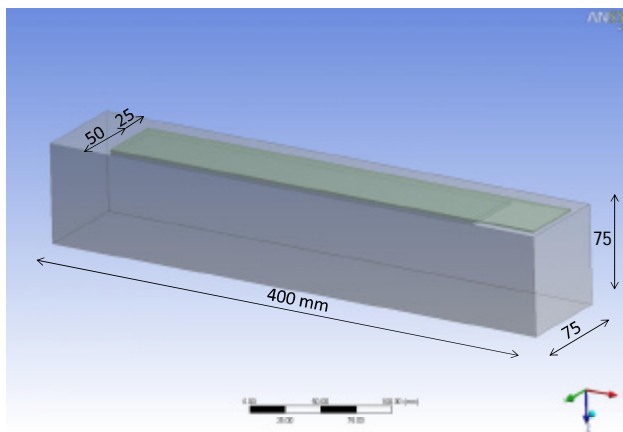


Figure 2. Simplified model

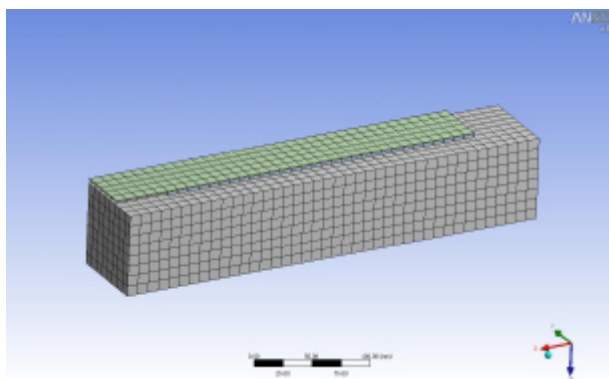


Figure 3. FE mesh

3. NUMERICAL RESULTS AND DISCUSSIONS

This chapter presents the numerical results obtained after simulating the behavior of a CFRP – concrete hybrid system subjected to tension. Thus, in Table 2 are summarized the maximum values of the following parameters: total displacement, principal stresses, equivalent, normal and shear stresses, as well as the frictional stresses, evaluated on three FE models corresponding to the considered groups, namely C1, C2 and C3.

Table 2. Numerical results

	C1	C2	C3
Total displacement [mm]	0.17	0.24	0.30
Maximum principal stress [N/mm ²]	350.19	466.72	450.29
Equivalent stress [N/mm ²]	355.09	474.35	456.71
Normal stress [N/mm ²]	350.08	466.57	450.17
Shear stress in the composite[N/mm ²]	16.43	22.41	21.69
Frictional stresses [N/mm ²]	24.17	34.51	27.63

The above presented numerical results were obtained after performing a considerable number of iterations, describing in a satisfying manner the general behavior of a hybrid system, in terms of maximum normal stresses and ultimate loads (Figure 4, Figure 5).

The accuracy of the models and accordance to the experimental program can be also confirmed by the resemblance between the shear stresses – slip comparative curves (Figure 6).

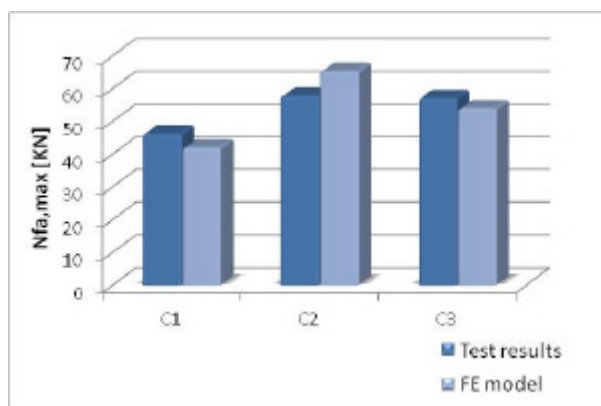


Figure 4. Experimental vs. FE analysis ultimate loads –

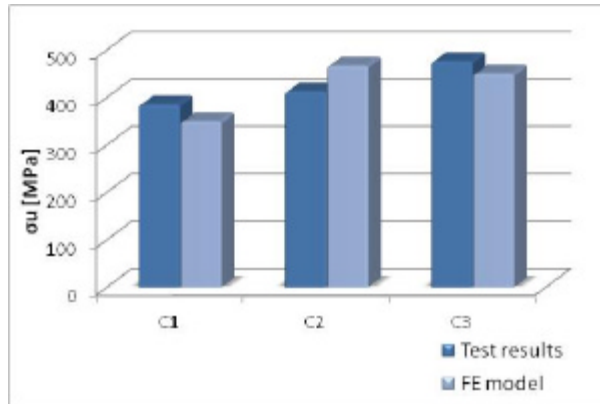


Figure 5. Experimental vs. FE analysis maximum normal stresses

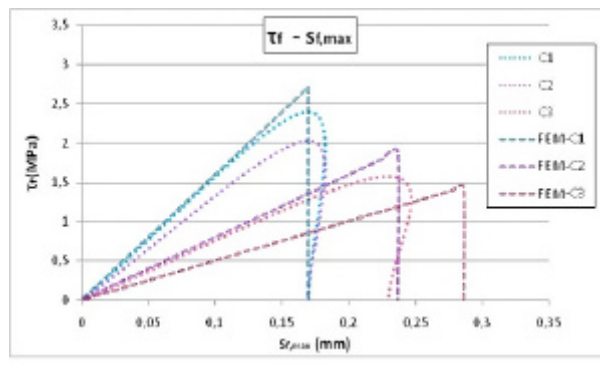


Figure 6. Experimental vs. FE analysis shear stresses – slip curve

4. CONCLUSIONS

Modern strengthening approaches are based on the idea that the strengthening should be light and removable and, if possible, it should not change the structural scheme or the construction; objective which can be achieved by using FRP composites. The FE analysis offers flexibility and precision, being possible to model different elements with complex geometry, having various loading schemes and boundary conditions. On this line, three FE models were carried out to establish the bonding behavior of a CFRP – concrete hybrid system. These models consisted in applying CFRP strips on two opposite sides of a concrete element, comprised of two identical prisms and subjected to tension. Analyzing the numerical results by comparing them to the experimental ones revealed a good correlation between the simulated structural behavior and the test results.

The FE analysis utilized in case of externally bonded FRP composites proved to be a powerful instrument in determining the general behavior of the considered element especially when the adhesive layer is included in the model.

References

1. JSCE, *Recommendations for upgrading of concrete structures with use of continuous fiber sheets. Technical Report*, Research Committee on Upgrading of Concrete Structures with Use of Continuous Fiber Sheets, Japanese Society of Civil Engineers, Japan, 2000.
2. Fib Bulletin 14, *Externally bonded FRP reinforcement for RC structures. Technical Report*, Federation Internationale du Beton, 2001.
3. ISIS, *Retrofitting concrete structures with fiber reinforced polymers*, ISIS, Canada, 2001.
4. ACI 440, *Guide for the design and construction of externally bonded FRP systems for strengthening concrete structures. Technical Report*, American Concrete Institute, 2002.
5. CNR – DT 200/2004, *Guide for Design and Construction of Externally Bonded FRP Systems for Strengthening Existing Structures. Materials, RC and PC structures, masonry structures*, National Research Council – Advisory Committee on Technical Recommendations for Construction, Rome, Italy, 2004.
6. CS 55, *Design guidance for strengthening concrete structures using fibre composite materials. Technical Report*, Concrete Society, UK, 2004.
7. Oprisan G., Munteanu V., Cozmanciuc C., Taranu N., Entuc I., *Particularities of structural response of confined reinforced concrete columns with composite membranes*, 9th International scientific conference VSU, Sofia, June 4-5, 2009, Vol. II, pp. 95-100, 2009.
8. Cozmanciuc C., Oltean R., Munteanu V., *Strengthening techniques of RC columns using fibre reinforced polymeric materials*, Bulletin of the Polytechnic Institute of Iasi, **LV (LIX)**, 3, pp. 85-92, 2009.
9. Cozmanciuc C., Oprisan G., Taranu N., Munteanu V., Oltean R., Budescu M., *Structural behaviour response of eccentrically loaded reinforced concrete columns confined with carbon fibre reinforced membranes*, 11th International Scientific Conference VSU, Sofia, 2-3 June 2011, Vol. I, II – 198 – 203, 2011.
10. Mirmiran A., Shahawy M., Nanni A., Karbhari V., *Bonded Repair and Retrofit of Concrete Structures Using FRP Composites. Recommended Construction Specifications and Process Control Manual*, NCHRP Report 514, Washington-DC, USA, Transportation Research Board, 2004.
11. Yao J., Teng J.G., Chen J.F., *Experimental study on FRP-to-concrete bonded joints*. Composites. Part B: Engineering, **36**, 2, pp. 99–113, 2005.
12. Aiello M.A., Leone M., *Interface analysis between FRP EBR system and concrete*. Composites: Part B, **39**, pp. 618 – 626, 2008.
13. Resende Balseiro A.M., Rautenstrauch K., *Bond behaviour of CFRP to timber beams in the end-anchorage situation*. Scientific Report within Cost Action E34 – Wood Adhesion, Bauhaus, Germany, 2007.
14. Aiello M.A., Sciolti M.S., *Bond analysis of masonry structures strengthened with CFRP sheets*. Construction Building Materials, **20**, 1-2, pp. 90 – 100, 2006.
15. Xiao J., Li J., Zha Q., *Experimental study on bond behaviour between FRP and concrete*. Construction Building Materials, **18**, 10, pp. 745 – 752, 2004.
16. Aprile A., Spacone E., Limkatanyu S., *Role of bond in RC beams strengthened with steel and FRP plates*. J Struct. Eng, **127**, 12, pp. 1445 – 1452, 2001.
17. Taranu, N., Oltean, R. Cozmanciuc, C., *Experimental investigation on bonding CFRP plates to concrete substrate*, Bulletin of the Polytechnic Institute of Iasi, **LVII (LXI)**, 3, pp. 47 – 56, 2011.
18. Bathe, K.J., *Finite Element Procedures*, Prentice-Hall, Inc., Upper Saddle River, New Jersey, 1996.

Bond behavior between fibers reinforced polymeric (FRP) strips and concrete – An analytical and numerical investigation

Ruxandra Oltean¹, Ciprian Cozmaniuc²

¹Department of Civil and Industrial Engineering, “Gh. Asachi” Technical University, Iasi., Romania

²Department of Concrete Structures, Building Materials, Technology and Management, “Gh. Asachi” Technical University, Iasi, 700050, Romania

Summary

Reinforced concrete (RC) structures, due to aging, material degradation, settlements, and structural alterations, often need to be strengthened to re-establish their performance. In this frame, fibre reinforced polymer (FRP) composites in the form of bonded strips applied to the external surface can be a convenient strengthening solution.

In flexural and shear strengthening cases, debonding between concrete and externally bonded FRP usually corresponds to the ultimate limit state of strengthened RC elements. This type of failure either decreases the strength efficiency of FRP materials or causes a deficiency in member ductility.

Since the structural performance relies on bond between FRP and concrete, the characteristics of bond and methods to evaluate it are critical to understanding and evaluating FRP- concrete hybrid elements.

Numerous analytical models were developed onwards to predict the interface bond strength or local bond stress – slip curve influences peak flexural or shear strength of RC elements strengthened with externally bonded FRP composites, generally on the basis of pull tests setup.

An accurate analytic model is of fundamental importance in the modelling of FRP strengthened RC structures. In this paper, a review of existing bond strength models and bond – slip models is first presented.

Further research was being conducted to simulate bond behaviour of external FRP reinforcement and concrete substrate, considering the double shear test set-up. Three-dimensional models based on finite element analysis were realised, using Ansys software. These results are then compared with the ones obtained by analytical models. The simulated results shown that the model can describe the static FRP-to-concrete bond behavior with good accuracy and mesh objectivity.

KEYWORDS: concrete; fiber reinforced polymers, bond, finite element analysis, analytical models.

1. INTRODUCTION

FRP composites are being successfully used for strengthening of degraded RC structures. Bond of the external FRP reinforcement to the concrete substrate is of critical importance for the effectiveness of this technique, since it is the means for the transfer of stresses between concrete and FRP in order to develop composite action. Indeed, a number of failure modes in FRP – strengthened RC elements are directly caused by debonding of the FRP from the concrete substrate. Therefore, for the safe and economic design of externally bonded FRP systems, a complete understanding of the behavior of FRP – concrete interface needs to be developed and reliable bond-slip model established.

In various debonding failure modes, the stress state of the interface is similar to that in a shear / double shear test specimen in which a laminate is bonded to a concrete prism and is subjected to tension (Figure 1). As a result, a large number of studies, both experimental and theoretical, have been carried out on simple and double shear test on adhesive joints. Existing studies suggest that the main failure mode of FRP – concrete hybrid systems in shear tests is concrete failure under shear, occurring generally at a few millimeters from the concrete – to – adhesive interface [1]. The current paper aims to predict, through both analytical and numerical analysis the bond behavior of a FRP – concrete hybrid system in double shear test.

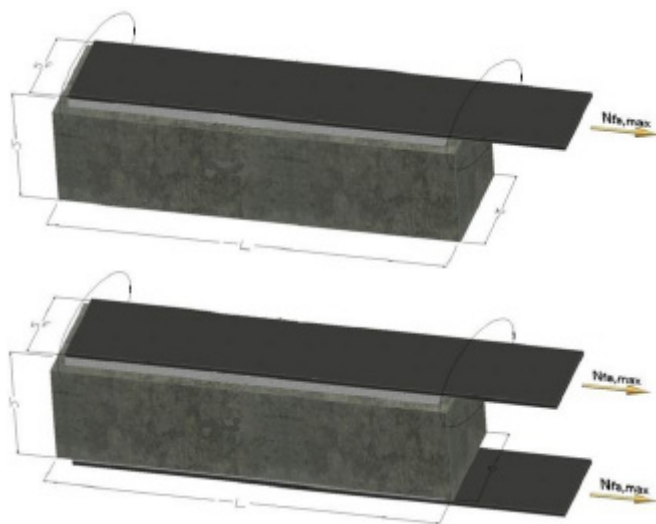


Figure 1. Single and double shear test setup

2. ANALYTICAL MODELS

2.1. Bond – slip models

Despite the difficulty in obtaining local bond–slip curves from pull tests directly, local bond–slip models for FRP to concrete interfaces have been developed based on strain measurements or load–slip curves.

Six local bond–slip models available in the existing literature are detailed below, where t (MPa) is the local bond (shear) stress, s (mm) is the local slip, t_{\max} (MPa) is the local bond strength (i.e. the maximum bond/shear stress experienced by the interface), s_{peak} (mm) is the slip when the bond stress reaches t_{\max} , s_{ult} (mm) is the slip when the bond stress reduces to zero, k_b is the geometry factor, f'_c (MPa) is the cylinder compressive strength of concrete.

- Neubauer and Rostasy [2]

$$t_{\max} = 1.8k_b f'_{ctm} \quad (1)$$

$$s_{\text{peak}} = 0.202k_b \quad (2)$$

$$k_b = \sqrt{1.125 \frac{2 - \frac{b_f}{b_c}}{1 + \frac{b_f}{400}}} \quad (3)$$

- Nakaba et al. [3]

$$t_{\max} = 3.5 f'_c{}^{0.19} \quad (4)$$

$$s_{\text{peak}} = 0.065 \quad (5)$$

- De Lorenzis et al. [4]

$$t_{\max} = 0.0182 \sqrt{n_f t_f E_f} \quad (6)$$

- Monti et al. [5]

$$t_{\max} = 1.8k_b f_t \quad (7)$$

$$s_{\text{peak}} = 2.5 t_{\max} \left(\frac{n_f t_f}{E_f} + \frac{50}{E_c} \right) \quad (8)$$

$$s_{ult} = 0.33k_b \tag{9}$$

$$k_b = \sqrt{1.5 \frac{2 - \frac{b_f}{b_c}}{1 + \frac{b_f}{100}}} \tag{10}$$

- Savoia et al. [6]

$$t_{max} = 3.5 f_c^{0.19} \tag{11}$$

$$s_{peak} = 0.065 \tag{12}$$

- Lu et al. [7 a, b]

$$t_{max} = 1.5k_b f_{ctm} \tag{13}$$

$$s_{peak} = 0.195k_b f_{ctm} \tag{14}$$

$$s_{ult} = 2 \frac{G_f}{t_{max}} \tag{15}$$

$$k_b = \sqrt{\frac{2.25 - \frac{b_f}{b_c}}{1.25 + \frac{b_f}{b_c}}} \tag{16}$$

$$G_f = 0.308k_b^2 \sqrt{f_{ctm}} \tag{17}$$

where,

E_c = elastic modulus of concrete;

G_f = fracture energy.

The model of Monti et al. [5] is comparable to that of Neubauer and Rostasy [2] but also gives the value of s_{ult} . The model of Savoia et al. [6] is similar to that of Nakaba et al. [3], and only the value of s_{peak} changes. Only the models of Monti et al. [5] and Lu et al. [7 a, b] give the three parameters t_{max} , s_{peak} , and s_{ult} , whereas, only the model of De Lorenzis et al. [4] considers t_{max} as a function of FRP stiffness. The other models consider t_{max} as a function of compressive or tensile strength of concrete, not depending on FRP stiffness [8]. Lu et al. [7 a, b] concluded that the model proposed by Chen and Teng [1] is the most accurate.

2.2. Bond strength predictions

Regardless the bond-slip model, the bond-strength of an FRP – concrete adhesive joint in terms of the interfacial fracture energy is given by Equation (18), which was developed by Holzenkämper [9] using a two-layered model.

$$P = b_f \sqrt{2G_f E_f t_f} \quad (18)$$

Based on a series of tests, Neubauer and Rostásy [10] found that the fracture toughness could be calculated by:

$$G_f = c_f f_{cm} \quad (19)$$

where, c_f was evaluated to 0.204 mm by a regression analysis of the test data. They further consider the effect of geometry of the specimen, and modified Holzenkämper's formula (Equation (18)) as:

$$P = \begin{cases} 0.64k_b b_f \sqrt{E_f t_f f_{cm}} \\ 0.64k_b b_f \sqrt{E_f t_f f_{cm}} \frac{L}{L_e} \left(2 - \frac{L}{L_e}\right) \end{cases} \quad (20)$$

where, $L_e = \sqrt{\frac{E_f t_f}{2f_{cm}}}$.

Monti et al. [5] conducted a parametric study using finite element analysis (FEA) in conjunction with experiments, and suggested the following formula for the bond capacity:

$$P = \beta_1 b_f \sqrt{\frac{E_f t_f t_{\max}}{3}} \quad (21)$$

where, $\beta_1 =$ the bond length factor $\begin{cases} = 1 & \text{- when } L > L_e; \\ < 1 & \text{- when } L < L_e. \end{cases}$

and $L_e = \sqrt{\frac{E_f t_f}{\sqrt{4t_{\max}}}}$.

Täljsten [11] considered a three-layered model with a crack in the adhesive layer. In this way, he obtained:

$$P = b_f \sqrt{\frac{2E_f t_f G_f}{1 + \mathbf{a}}}, \text{ with } \mathbf{a} = \frac{E_f t_f}{E_c t_c} \quad (22)$$

where,

t_c = the height of the concrete prism

Wu et al. [12] used nonlinear interfacial constitutive laws to analyze a three-layered model and deduced a similar formula:

$$P = b_f \sqrt{\frac{2E_f t_f G_f}{1 + \mathbf{b}}}, \text{ with } \mathbf{b} = \frac{b_f E_f t_f}{b_c E_c t_c} \quad (23)$$

It may be seen that when $E_c t_c \gg E_f t_f$ or $b_c E_c t_c \gg b_f E_f t_f$, Equations (21) and (22) have a similar form as Equation (18). However, neither one calculate the interface fracture energy G_c .

Lu et al. [7 a, b] used new bond-slip models which are based on their earlier work of meso-scale finite element predictions, and suggested another similar model:

$$P = \mathbf{b}_1 k_b b_f \sqrt{2G_f E_f t_f} \quad (24)$$

This definition follows Yuan et al. [13] equation for determining the effective bond length:

$$L_e = a + \frac{1}{2I_1} \ln \left[\frac{I_1 + \tan(I_2 a)}{I_1 - \tan(I_2 a)} \right] \quad (25)$$

where,

$$I_1 = \frac{t_{\max}}{s_{\text{peak}} E_f t_f}, \quad I_2 = \sqrt{\frac{t_{\max}}{(s_{\text{ult}} - s_{\text{peak}}) E_f t_f}} \quad \text{and} \quad a = \frac{1}{I_2} \arcsin \left[0.99 \sqrt{\frac{s_{\text{ult}} - s_{\text{peak}}}{s_{\text{ult}}}} \right]$$

Chen and Teng [1] proposed a simple expression for calculating the ultimate bond strength as follows:

$$P = 0.427 \mathbf{b}_1 k_b L_e b_f \sqrt{f'_c} \quad (26)$$

where,

$$k_b = \sqrt{\frac{2 - \frac{b_f}{b_c}}{1 + \frac{b_f}{b_c}}}, \quad L_e = \sqrt{\frac{n_f t_f E_f}{\sqrt{f_{cm}}}}$$

f_c' = the concrete compressive strength determined on cylinders (in MPa)

$$\beta_1 = \text{the bond length factor} \quad \left\{ \begin{array}{ll} = 1 & \text{- when } L > L_e; \\ \sin\left(\frac{\pi L}{2 L_e}\right) & \text{- when } L < L_e. \end{array} \right.$$

All the models based on fracture mechanics require the knowledge of interface or adhesive fracture toughness. Efforts have been made to relate the interface fracture toughness to the tensile strength of concrete [1, 10, 14], but the proposed relations are empirical and the forms by different authors are quite diverse [15].

3. FINITE ELEMENT ANALYSIS

In this chapter using Ansys software package was simulated the bonding behavior of a double shear test setup. In this line, two identical carbon fibers reinforced polymeric (CFRP) laminates bonded on two concrete prisms 400 mm long and with a cross-section of 150 x 150 mm under tension were chosen as the benchmark specimen to be studied. Simplified FEA models with different three types of carbon fibers laminated composites were built, resulting in three groups of models, namely C1, C2 and C3. For the first two models it was assumed that all components are linear elastic, while for the third model the bilinear concrete behavior was considered, their properties being given in Table 1. The geometrical model was simplified using the symmetry of the elements, in order to reduce the solving time and to increase the precision, thus the simplified model is actually a quarter of the benchmark specimen (Figure 2).

A 3D FE modeling was realized, namely, the specimens were modeled using 20 nodes solid elements, Solid 186, while for the interface area CONTA 174 were employed. However, in this study perfect bond between materials was assumed. The high strength of the epoxy used to bond the CFRP sheets to the concrete prisms supported the perfect bond assumption. After meshing the specimen, the loading was applied taking into account the displacement control.

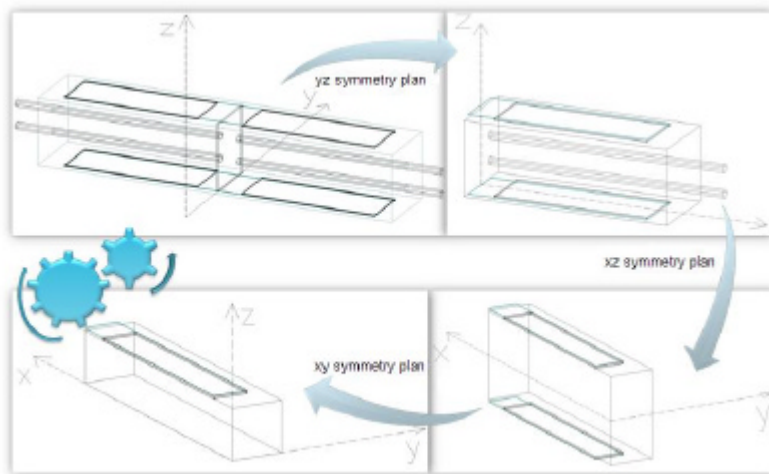


Figure 2. Reduced model obtained using symmetry plans

Table 1. Properties of the constituent materials

Specimen series	C1	C2	C3
Type of CFRP plate	Sika Carbodur S1012	Sika Carbodur M1014	CFK 150/2000
Geometric characteristics (mm)	1.2x100	1.4x100	1.2x100
Density (kg/m ³)		1600	
Poisson's ratio		0.25	
Young's modulus (N/mm ²)	165000	210000	165000
Tensile strength (N/mm ²)	3100	3200	1000
Adhesive		Sikadur 30	
Density (kg/m ³)		1650	
Poisson's ratio		0.4	
Young's modulus (N/mm ²)		12800	
Tensile strength (N/mm ²)		25	
Compressive strength (N/mm ²)		75	
Concrete batch		Batch 1	
Density (kg/m ³)		2300	
Poisson's ratio		0.2	
Young's modulus (N/mm ²)		32000	
Tensile strength (N/mm ²)		2.2	
Compressive strength (N/mm ²)		31.6	

4. COMMENTS AND RESULTS

In this section the authors present the numerical and analytical results obtained after simulating a double shear test setup for a hybrid CFRP – concrete element. Thus, in Figure 3 are illustrated the maximum loads corresponding to the considered series.

Regarding the bond – slip curve a summarized chart was realized for the presented analytical models (Figure 4), as well as for the simulated FEA models (Figure 5).

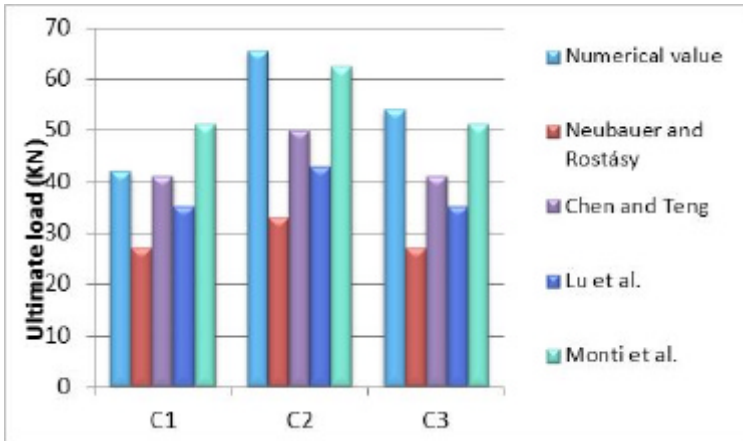


Figure 3. Numerical vs. analytical evaluation of ultimate load

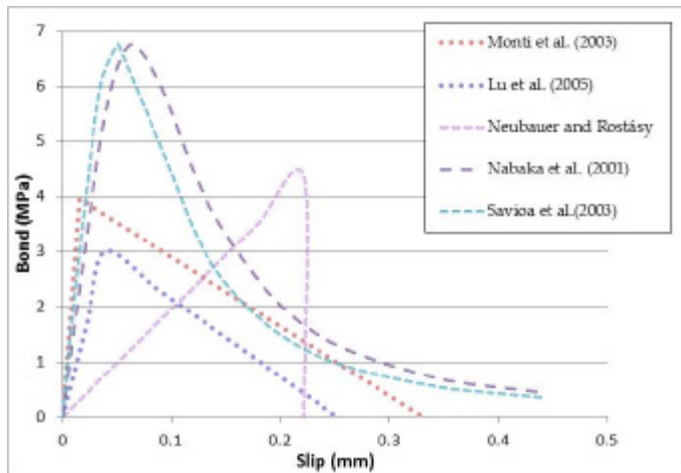


Figure 4. Bond – slip curve models

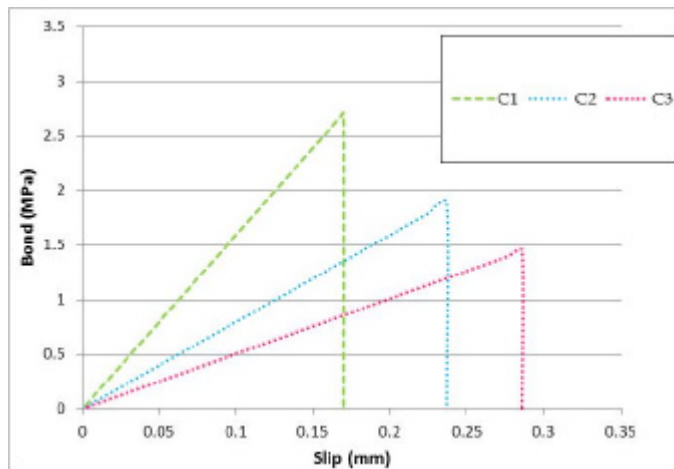


Figure 5. Numerical evaluation of the bond – slip curve

3. CONCLUSIONS

Clarifying the bond characteristics of the interface between concrete and externally bonded FRP strips is essential for designing externally bonded composite strengthening systems. Shear/ double shear tests are usually applied to obtain the bond characteristics of FRP – concrete interfaces in terms of overall or local interfacial bond properties. This paper analyses the analytical models showing how to obtain the main bond parameters necessary in engineering design and runs a numerical analysis for double shear tests of FRP – concrete interfaces.

Analyzing the results in terms of ultimate load one may state that the obtained numerical values are similar to the ones obtained using Monti et al. model. However, the numerical values overrate the values of the ultimate loads in two of the three studied cases.

References

1. Chen, J.F., Teng, J.G., Anchorage strength models for FRP and steel plates bonded to concrete, *Journal of Structural Engineering*, ASCE, Vol. 127, No. 7, pp. 784 – 791, 2001.
2. Neubauer, U., Rostasy, F. S., Bond failure of concrete fiber reinforced polymer plates at inclined cracks—Experiments and fracture mechanics model, *Proceedings of the 4th International Symposium on Fiber-Reinforced Polymer Reinforcement for Reinforced Concrete Structures*, SP-188, American Concrete Institute, Farmington Hills, Mich., pp. 369–382, 1999.

3. Nakaba, K., Kanakubo, T., Furuta, T., Yoshizawa, H., Bond behavior between fiber-reinforced polymer laminates and concrete, *ACI Struct. J.*, Vol. 98, No. 3, pp. 359–367, 2001.
4. De Lorenzis, L., Miller, B., Nanni, A., Bond of fiber reinforced polymer laminates to concrete, *ACI Mater. J.*, Vol. 98, No. 3, pp. 256–264, 2001.
5. Monti, M., Renzelli, M., Luciani, P., FRP adhesion in uncracked and cracked concrete zones, *Proceedings of the 6th International Symposium on FRP Reinforcement for Concrete Structures, FRPRCS-6*, World Scientific, Singapore, pp. 183–192, 2003.
6. Savoia, M., Ferracuti, B., Mazzotti, D., Nonlinear bond–slip law for FRP-concrete interface, *Proceedings of the 6th International Symposium on FRP Reinforcement for Concrete Structures, FRPRCS-6*, World Scientific, Singapore, pp. 163–172, 2003.
7. a. Lu, X. Z., Teng, J. G., Ye, L. P., Jiang, J. J., Bond–slip models for FRP sheets/plates bonded to concrete, *Eng. Struct.*, Vol. 27, pp. 920–937, 2005.
b. Lu, X. Z., Teng, J. G., Ye, L. P., Jiang, J. J., Meso-scale finite element model for FRP plates/sheets bonded to concrete, *Eng. Struct.*, Vol. 27, No. 4, pp. 564–575, 2005.
8. Pellegrino, C., Tinazzi, D., Modena, C., Experimental Study on Bond Behavior between Concrete and FRP Reinforcement, *Journal of Composites for Construction*, ASCE, Vol. 12, No. 2, pp. 180 – 189, 2008.
9. Holzenkämpfer, P., *Ingenieurmodelle des verbundbes geklebter bewehrung für betonbauteile. Dissertation*, TU Braunschweig, 1994. (in German)
10. Neubauer, U., Rostásy, F. S., Design aspects of concrete structures strengthened with externally bonded CFRP plates, *Proceedings of 7th International Conference on structural faults and repairs*, Vol. 2, pp. 109–118, 1997.
11. Täljsten, B., Strengthening of concrete prisms using the plate bonding technique, *Internat J Fract*, 1996, Vol. 82, No. 3, pp. 253–266.
12. Wu, Z. S., Yuan, H., Niu, H. D., Stress transfer and fracture propagation in different kinds of adhesive joints, *J Eng Mech*, Vol. 128, No. 5, pp. 562–573, 2002.
13. Yuan, H., Teng, J. G., Seracino, R., Wu, Z. S., and Yao, J., Full range of FRP-concrete bonded joints, *Eng Struct*, Vol. 26, No. 5, pp. 553–565, 2004.
14. Taranu, N., Oprisan, G., Isopescu, D., Entuc, I., Munteanu, V., *Solutii compozite de realizare a structurilor ingineresti*, Editura Stef, 2006. (in Romanian)
15. Wu, Y., Zhou, Z., Yamg, Q., Chen, W., On shear bond strength of FRP-concrete structures, *Engineering Structures*, Vol. 32, pp. 897–905, 2010.

Computer aided optimization of a mixed structure

Ioana Olteanu¹ and Alexandru Stanila²

¹ Department of Structural Mechanics, Gheorghe Asachi Technical University, Iasi, 700050, Romania

² Department of Civil and Industrial Engineering, Gheorghe Asachi Technical University, Iasi, 700050, Romania

Summary

Modern architecture tends to propose structures with challenging shapes for the structural designer. These structures, beside their aesthetic properties, must fulfil some strength and stability requirements.

The technical content of the study refers to the structural configuration of an innovative flexible 5-storey building having the destination of a Students' Activity Centre, located in Iasi.

The structure has a pyramid shape with a centre core as structural system realized mainly of reinforced concrete. Radial disposed cantilevered floors, resembling with the branches of a tree, discharge on the centre core.

Several analyses were conducted in SAP2000 in order to find the most suitable configuration that satisfies strength, serviceability and stability requirements.

KEYWORDS: finite element analysis, mixed structure, structure optimization.

1. INTRODUCTION

Earthquakes effects from past years reveal the necessity to design considering the multi-hazard effect on structures. The studied project is located in Iasi, in an area where the most unfavorable situation is represented by the seismic action.

The earthquake effect is controlled by: structural deep central foundation with double function taproot system, central core made of concrete, flat plate frames and radial disposed cantilevered floors.

The architectural aspect of the building mimics the nature in plane and facades, layouts, elevation, and details of out-of-the-box architecture. The natural tree aspect integrates the building in the natural landscape.

The innovation of the structure consists of the challenge to realize a structure that satisfies the structural safety requirements and does not influence the environment conditions. Besides adopting reinforced concrete structural system, several ecological elements were considered, like special glazing curtain façade walls, special foundation, but they do not make the subject of the current paper.

The aims of structure modeling by FEM model are: to understand the global behavior of structure, to design each element and to optimize the overall behavior of the structure. Prescriptions from current regulations were considered.

2. STRUCTURE DESCRIPTION

2.1. Structure dimensions

The building central's core is 6.2 m x 6.2 m wide with a ground floor high of 4 meters and 3 meters high for the superior floors.

The surface of the first slab is 24.2 m x 24.2 m, the second slab have a surface of 19.7 m x 19.7 m, the third slab of 15.2 m x 15.2 m, the fourth one of 10.7 m x 10.7 m, and the last one of 6.2 m x 6.2 m.

The maximum high of the pyramid in top of the building is 2.3 meters.

2.2. Materials properties

The proprieties of the used materials are presented in table 1

Table 1. Material characteristics

No	Material	Density [daN/m ³]	Coefficient of elasticity [N/mm ²]	Poisson's coefficient [-]	Strength [N/mm ²]	
					reduction	expansion
1.	C 25/30	2500	32500	0.2	24.3	-
2.	S235	7850	270000	0.3	-	235

2.3. Structural system

The symmetrical geometry looking like a tree needed a specific structural conception in order to fulfill strength and stability requirements.

The configuration was for a flexible 5-storey building having the destination of a Students' Activity Centre. From structural point of view, the building has a central

core where the circulation function is located, that carries large, radial disposed cantilevered floors. As closing elements, translucent heat-saving panels were used.

The foundation is based on a rectangular foundation raft carried by four piles, placed on the corner of the main foundation raft, figure 1. The foundation raft dimensions are 21 by 21 m.

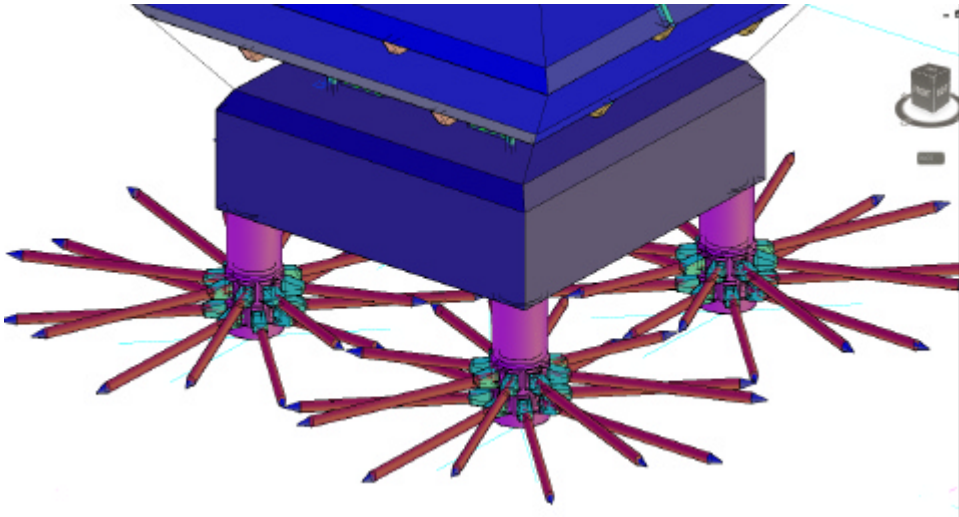


Figure. 1 Foundation detail

The central core is composed of four reinforced concrete columns having a L shape with the following dimensions 100 x 100 x 40 mm. The plan dimensions of the main central core are 6.2 x 6.2 meters as it can be seen in the Figure 2. The circulation core is enforced with structural walls of 15cm thickness.

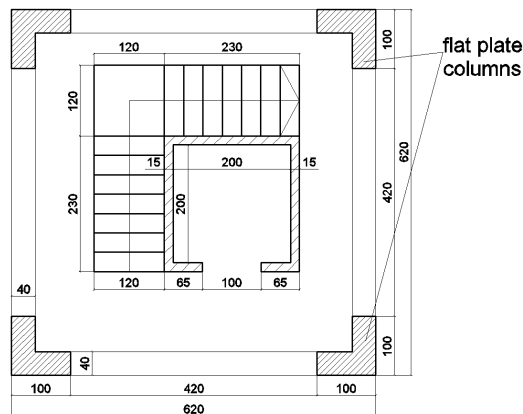


Figure. 1 Central core; horizontal and vertical section

In the final version, coffered slabs were adopted for the first and second floors of the structure in order to take over internal efforts. The contour beams are made of INP 400 steel profiles cross section. The slabs panels are 1.00 m x 1.00 m wide and the secondary beams that split the slab into panels have the section as presented in Figure 3.

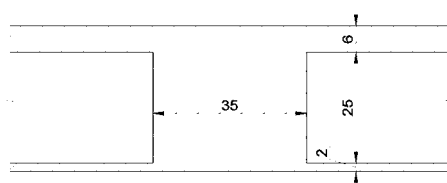


Figure 3 Coffered slab detail

The slabs over the second and the third floor are reinforced concrete, rested also on INP 240 steel profiles. The considered thickness of the slabs is 0.15 meters.

The last slab is also a 0.15 m reinforced concrete wide slab, which discharge on reinforced concrete beams of 0.3 x 0.4 m cross section.

All the slabs direct their load to the central core through principal reinforced concrete beam of 0.3 x 0.4 m cross section.

The biggest radial cantilever is of 9 m and in order to limit the vertical displacement of the slabs additional reinforced concrete columns were introduced. Reinforced concrete columns of 30 x 30 m were considered in the numerical simulation.

3. NUMERICAL SIMULATION

To understand the behavior of the structure and to design the elements, a model was made in FEM software SAP 2000, version 14.2. The program allows creating structural models rapidly and intuitively without long learning curve delays. Complex models can be generated and meshed with powerful built in templates.

Advanced analytical techniques allow for step-by-step large deformation analysis.

Eigen and Ritz analyses based on stiffness of nonlinear cases, buckling analysis, progressive collapse analysis, energy methods for drift control, base isolators and support plasticity. This finite element model had been developed to obtain the expected maximum stresses and the behavior of the structure under the load combinations detailed below.

The final structural model satisfies safety and stability requirements. For the considered model several analysis were performed in order to obtain the final results: modal analysis, static analysis and response spectrum.

3.1. Applied load

Beside the self weight of the structure, the taproot was also subjected to a 200 daN/sqm dead load and a 250 daN/sqm live load. The response spectrum analysis was performed using the normalized response spectrum from the Romanian seismic code, P100-1/2006, presented in figure 4.

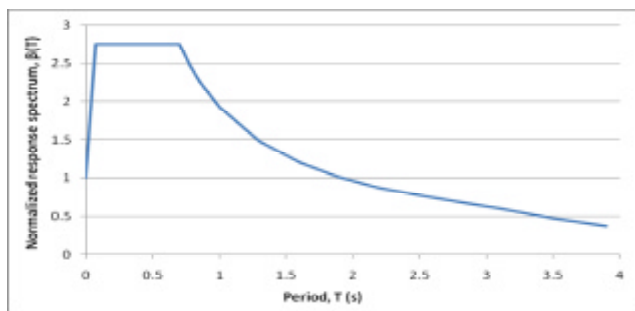


Figure 4. Considered response spectrum according to P100-1/2006

Other important parameters considered in the response spectrum analysis are: peak ground acceleration for Iasi $a_g=0.2g$, corner period, $T_c=0.7s$, importance factor for ordinary building, $\gamma_I=1.0$ and a behavior factor of 6.15. The behavior factor is characteristic for a medium ductility and for frame and dual structural systems. The seismic action is applied on X axis, Y axis and on a 45 degree angle directions.

3.2. Considered combinations

Table 2. Considered combinations

Nr	Name	Dead	Live	RS x	RS y
0	C1 (modal analysis)	1	0.4	0	0
1	C2 (fundamental ULS)	1.35	1.5	0	0
2	C3 (seism x, ULS)	1	0.4	1	0
3	C4 (seism y, ULS)	1	0.4	0	1
4	C5 (seism 45, ULS)	1	1	0.707	0.707
5	C6 (characteristic, SLS)	1	0.4	0	0

Combinations for the Ultimate Limit States (ULS) and Serviceability Limit States (SLS) were considered, as showed in table 2. The combinations are according to CR0-2005 code.

3.3. Structural analysis results

3.3.1. Modal analysis results

The model analysis was performed considering masses from elements and gravitational loads, using C1 combination.

A comparison in terms of period, frequency and circular frequency between two versions of the structure was performed. The first version contains pre-stressed concrete columns only in the slab’s corners; meanwhile the second version has pre-stressed columns on each façade in order to diminish the vertical displacement of the slab. Figure 5a shows that the first version has a period of 0.6225 s and that the slab over the ground floor vibrates significantly in vertical direction, in comparison with the second version for which the fundamental period is 0.26 s, almost 3 times smaller, and the characteristic vibration for mode 1 is torsion, figure 5b.

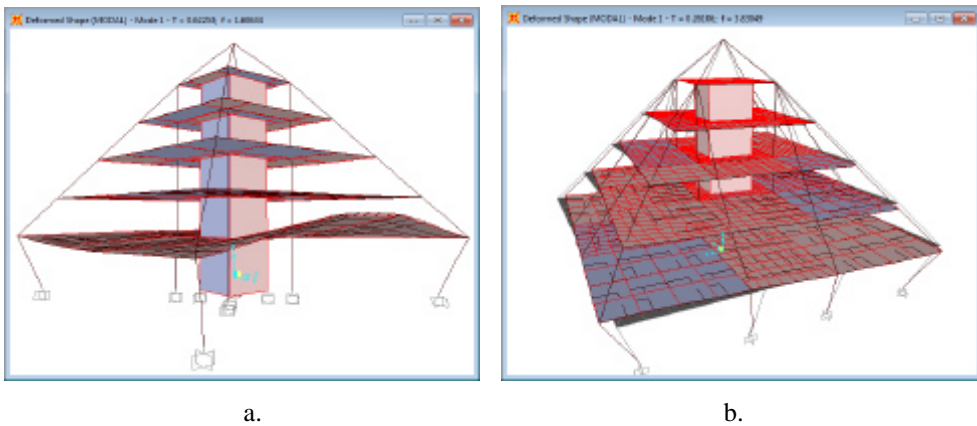


Figure. 5 a. First mode of vibration for version 1; b. First mode of vibration for version 2

Table 3 presents complete results for the first 5 vibration modes for second structure, which was also considered in the rest of the analysis.

Table 3. Modal analysis results

Step number	Period [s]	Frequency [Hz]	Circular frequency [rad/sec]	Eigenvalue [rad ² /s ²)
1	0.261063	3.8305	24.068	579.25
2	0.181716	5.5031	34.577	1195.6
3	0.180717	5.5335	34.768	1208.8
4	0.176748	5.6578	35.549	1263.7
5	0.167240	5.9794	37.570	1411.5

3.3.2. *Static analysis results*

Considering the static combinations, C2 and C6, the following results were obtained for the slab in terms of stresses on the principal and secondary axis respectively, figure 6 and figure 7.

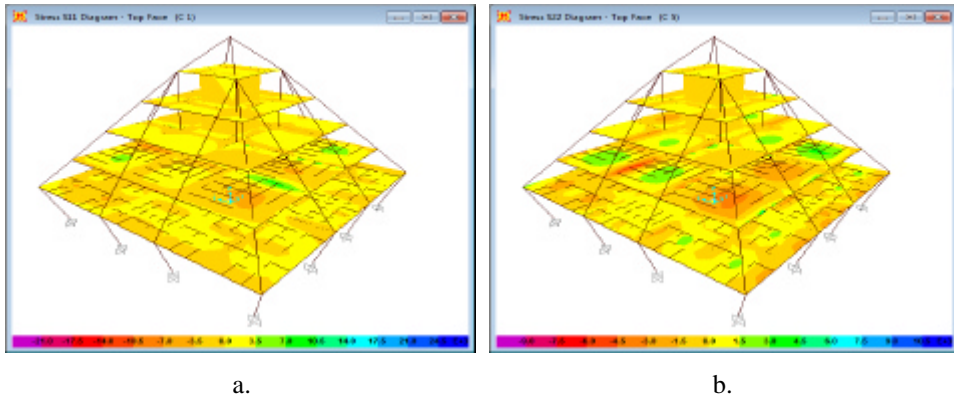


Figure 6. Stresses on shells for C1 combination: a. S11 stresses; b. S22 stresses

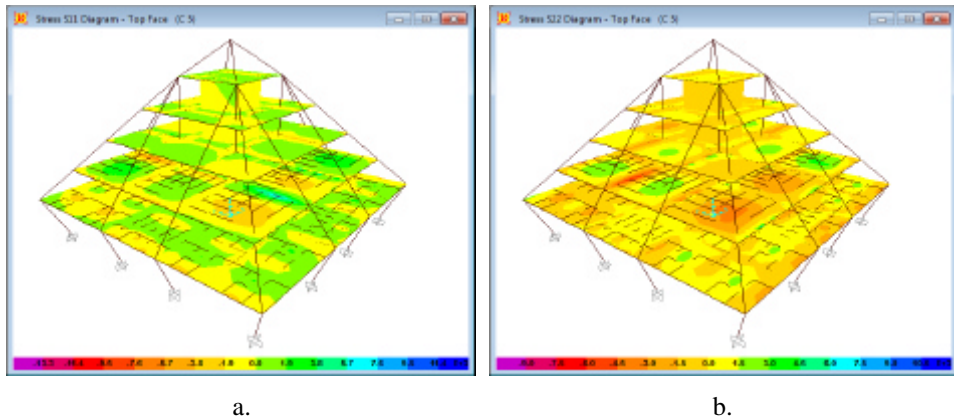


Figure 7. Stresses on shells for C5 combination: a. S11 stresses; b. S22 stresses

Figure 8 presents the bending moment diagrams for a plane frame of the structure.

The performed analysis offer sufficient information in order to design and check the structural elements.

Considering the stresses which appear on the structural elements and comparing them with the material strength, it can be concluded that the selected cross section are enough to take over the internal efforts.

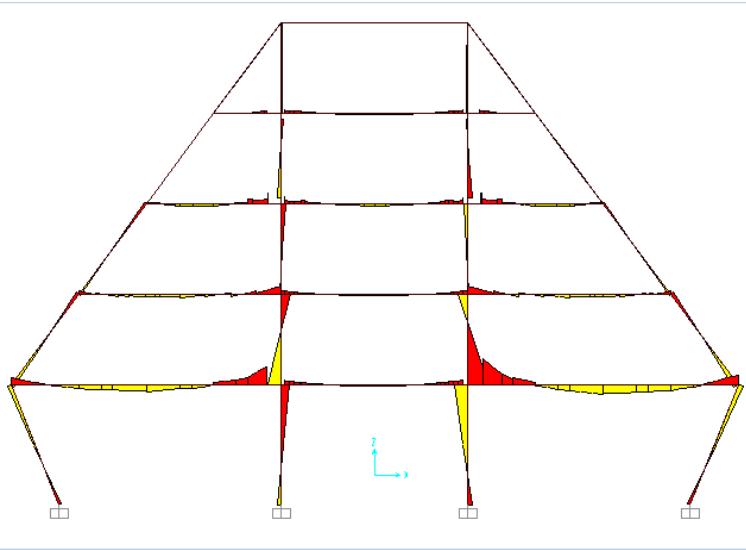


Figure 8. Bending moment diagram for C1 combination

3.3.3. Response spectrum analysis results

Antiseismic codes offer a wide variety of seismic analyses which can be applied on a structure. The analysis can be linear or nonlinear, static or dynamic. The most accurate one is considered the dynamic seismic analysis. Even though, researches in this field show that the response spectrum analysis can be considered a good approximation for the seismic analysis. Three seismic cases were considered – on X axis, on Y axis and on a 45 degree angle. Comparisons of the results for the stresses on both directions are made in the following figures.

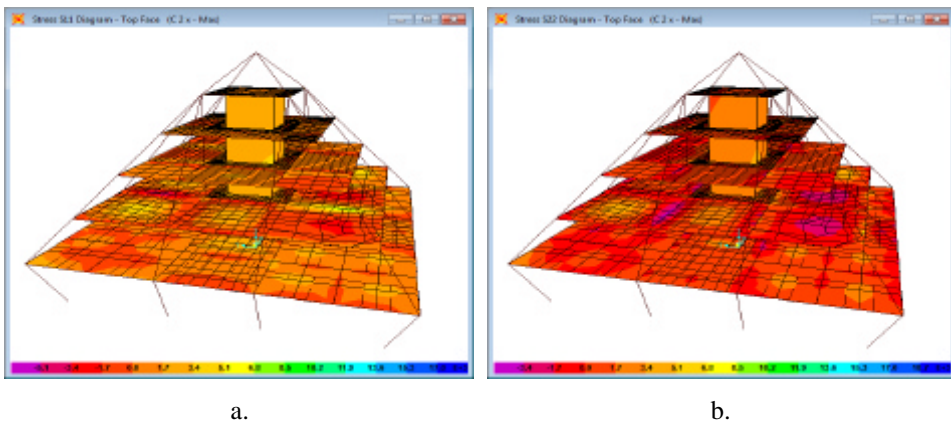


Figure 9. Stresses on shells for C 2 combination: a. S11 stresses; b. S22 stresses

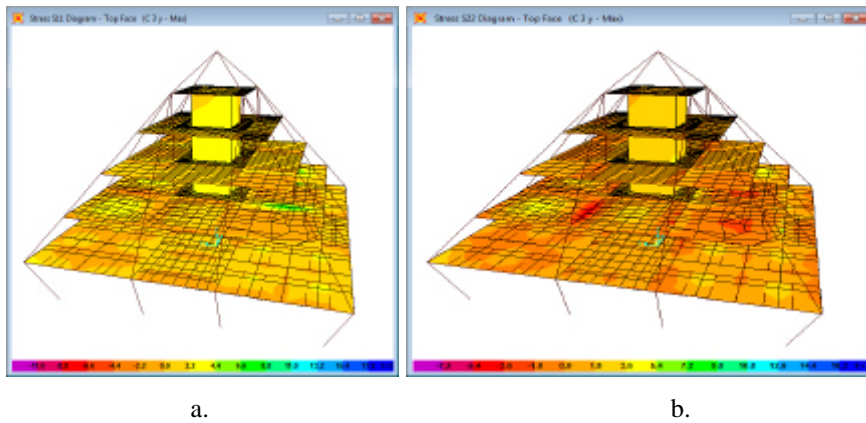


Figure 10. Stresses on shells for C3 combination: a. S11 stresses; b. S22 stresses

Table 4 represents a synthesis of the maximum internal efforts for the structural elements, specifying the combination in which they occur.

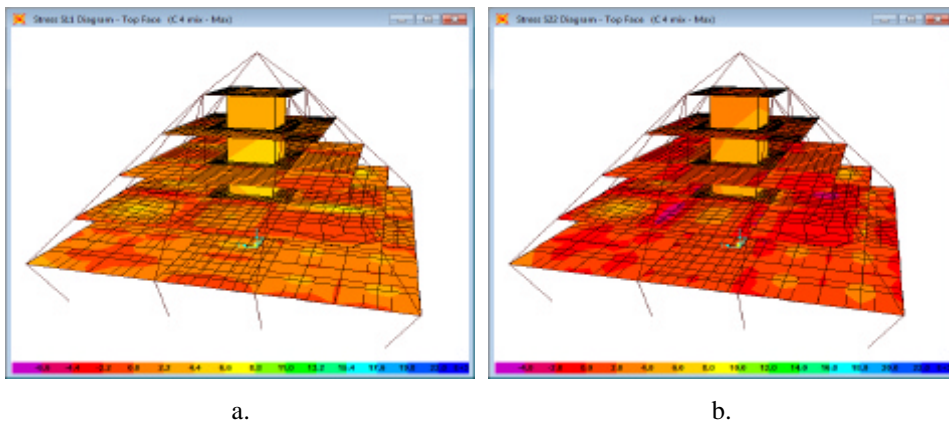


Figure 11. Stresses on shells for C5 combination: a. S11 stresses; b. S22 stresses

Table 4. Maximum internal efforts

Maximum effort	Element	Combination	Magnitude
P (kN)	ground floor column	C4	-1483.841
V2 (kN)	ground floor beam	C2	-264.883
V3 (kN)	ground floor beam	C4	-683.439
M2 (kN*m)	ground floor column	C3	-581.0212
M3 (kN*m)	ground floor column	C2	-563.996
T (kN*m)	ground floor beam	C2	-28.2257

Table 4 is making a synthesis of the most loaded elements and the combination in which they appear. These values were considered for the checking of the elements.

4. CONCLUSIONS

The paper aim was to find the most suitable solution for the structural elements in order to satisfy seismic requirements from P100/2006. In order to do this, several analysis were performed.

The chosen solution is a mixed structure with a period of 0.26 s.

The structure satisfies two main conditions: aesthetical ones, from architectural point of view, and strength and safety ones from structural point of view.

References

1. Euro code 1 - EN 1991 parts 1-3, 1-4;
2. P100-1/2006 The Romanian Standard For Design Of Structures For Earthquake Resistance;
3. C107/1-3/2005 - Romanian standard for the calculus of the global thermal insulation coefficients for the civil residences;
4. CR0-2005 –Romanian standard – Design principles for structures in construction.

Numerical simulation approach to estimate the ground level wind action near a prismatic building

Radu-Aurel Pescaru, Georgeta Vasies, Hasan Ali Ahmad Akileh,
Adrian Radu

*Department of Civil and Industrial Engineering, "Gheorghe Asachi" Technical University of Iasi,
Iasi, 700050, Romania*

Summary

Buildings, with their shape or setting, have a strong influence on the wind flow in their proximity. The presence of large or high rise buildings can often modify the airflow, creating unpleasant and sometimes dangerous windy conditions at the pedestrian level around them.

Considering all these aspects mentioned above in many developed towns as Boston, San Francisco, Paris, Montreal, London, Tokyo e.a., city authorities require wind tunnel testing and numerical simulations of new built developments to estimate their impact to local wind environment. For already existing situations the city planners need some information, guidebooks, and practical means to control and manage the pedestrian level wind conditions.

The paper presents some results, regarding the pedestrian level wind environmental conditions around single rectangular shape buildings, from studies on numerical model of the structures. The researched was carried on at the Building Aerodynamics Laboratory of the Faculty of Civil Engineering and Building Services from Iasi, using a CFD analysis sub-program of the finite element program ANSYS 12.

KEYWORDS: wind activity; buildings; pedestrian level airflow; CFD analysis, numerical model.

1. INTRODUCTION

Wind is one of the most active climatic factors; in addition, both in Romania and throughout Europe, climate change caused an increase of the wind activity characterized by strong winds, frequent storms etc. Meanwhile, in the last 20 years, it is found in our country the expansion of urban areas and the agglomeration of

existing ones with new high buildings of various shapes and sizes, resulting heterogeneous urban space geometry.

In this context the wind "flow" through the streets and generally at ground level becomes more mixed, and could adversely affect pedestrian comfort, dispersion of pollutants, snow accumulation etc. in open spaces, such as plazas, squares, and recreation grounds.

The urban expansion projects should take into consideration these adverse effects incompatible with the sustainable development. Therefore the ground level wind has to be estimated whether it may cause any intolerable consequence to pedestrian due to the construction of a proposed building or structure.

Studies regarding wind climate in built up areas are recommended to be completed in the phase of urban-development planning. This requirement is however difficult because every wind environment is unique due to the interaction of wind and the building form, local topology, predominant wind features. Especially the characteristics of wind instability and turbulence are difficult to estimate by conventional design means. Therefore specialists in wind engineering and building aerodynamics have developed different methods of prediction and assessment of the pedestrian level wind environment using experiments at model-scale in boundary layer wind tunnel (B. L. W. T.) reproducing the specific natural wind.

However the studies on physical models in boundary layer wind tunnel are generally not accessible or attractive to architects and design engineers for common projects, due to high additional costs imposed by the construction and maintenance of special testing equipments and of the tested building models. With the progresses in the computer science, the techniques of computational fluid dynamics (CFD) became an attractive alternative for wind studies developed on numerical models.

The paper presents a study aimed to provide information about ground level wind environment conditions for preliminary building design situation, using a commercial CFD. The numerical simulation in the study was developed under ANSYS_12 CFX , at the Building Aerodynamics Laboratory of our Faculty.

2. THE NUMERICAL SIMULATION APPROACH

In a numerical simulation, the size of a computing domain has to be determined as a first step [1]. Specifications from the literature suggest that the size of a domain must be a multiple of building dimensions [2]. For example the distance from the edge of the domain to any side of a building must be more than five times of the tallest building's height [3].

Three prototypes of prismatic buildings were considered. Their base is 30 m x 30 m and the height is, in succession, 45 m (building no. 1), 60 m (building no. 2) and 75 m (building no. 3).

The initial input data for numerical simulation were the computational space dimensions, the building size and position; the upstream wind speed is 14 m/s and the turbulence intensity of 5%.

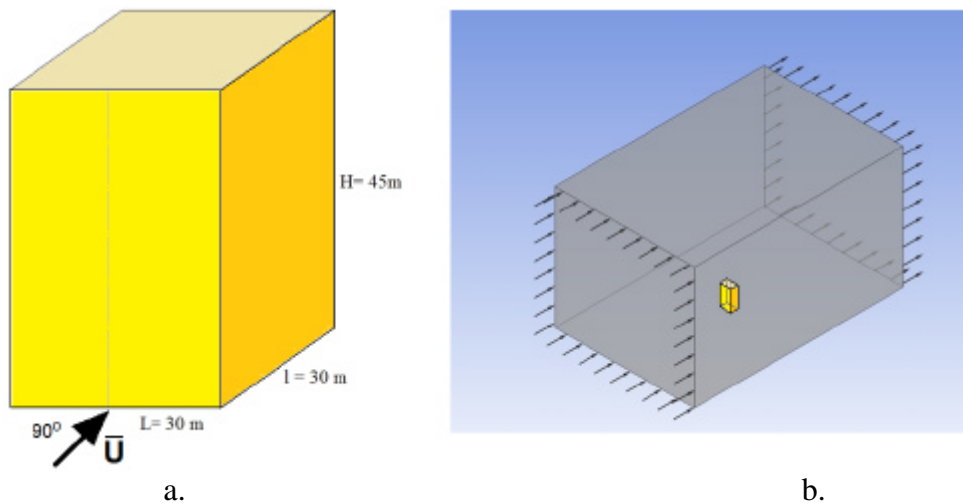


Figure 1. a. - building No1, geometry and wind direction; b – the computational domain

The computer simulation study, using the CFD modelling, provided the following information:

- the power lines of air flow at ground level, or the flow pattern around the building, marked with collared fillets;
- the possibility to establish the wind flow velocity field (in m/s) and to represent it graphically as a coloured map, where different areas of equal speed has the same colour;
- the values of the wind induced dynamic pressure (Pa) in various points of interest situated at the ground level, or on the building surface.

The images below shows the flow lines of pedestrian level wind flow as derived from the numerical simulation, for each of the three types of buildings previously described (building no.1, building no. 2 and building no.3).

From the analysis of flow lines charts for the three types of prismatic shape building, with the base of 30x30 m and height of 45 m, 60 m and 75 m, results a thickening of the flow lines along the sides of buildings. This thickening reflects an increasing of the wind speed with the increasing of the building height.

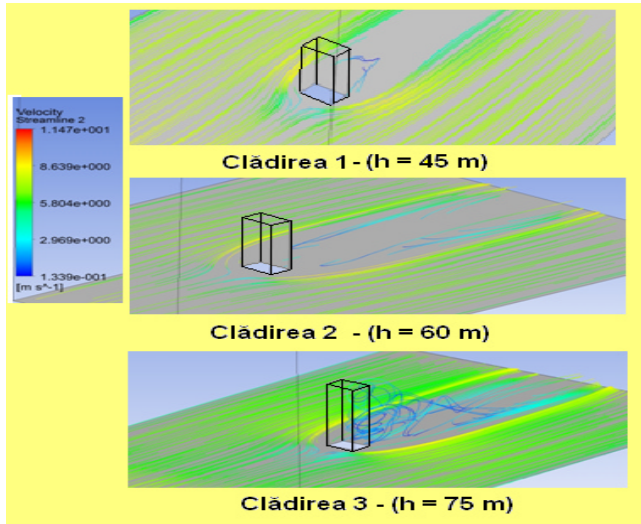


Figure 2. Flow stream lines at the ground level for the studied buildings

In case of building no.3, behind the structure corners from the downstream, can also be seen the presence of Von Karmán vortices. These vortices are stemming from the corners of the structure and are moving down to the trail of building wake. The presence of Von Karmán “vortex street” determine an acceleration of wind flow and increases the local turbulence, which can extend downstream up to a distance of about $1.5 H \dots 2H$, (where H is the height of the building).

	R1	R3	R5	R7	R9	R11	R13	R15	R17	R19	R21	
linia 1	1 22 43	84 95 136 127 148 169 187 205 223 241 258 268 284 301 322 341 351 365 402										
linia 2	2 23 44	85 96 137 128 149 170 188 206 224 242 259 269 285 302 323 344 354 368 403										
linia 3	3 24 45	86 97 138 129 150 171 189 207 225 243 260 270 286 303 324 345 355 369 404										
linia 4	4 25 46	87 98 139 130 151 172 190 208 226 244 261 271 287 304 325 346 356 370 405										
linia 5	5 26 47	87 98 139 130 152 173 191 209 227 245 262 272 288 305 326 347 357 371 406										
linia 6	6 27 48	89 99 141 132 153 174 192 210 228 246 263 273 289 306 327 348 358 372 407										
linia 7	7 28 49	70 91 132 133 154 175 193 211 229 247 264 274 290 307 328 349 359 373 408										
linia 8	8 29 50	71 92 133 134 155 176 194 212 230 248 265 275 291 308 329 350 360 374 409										
linia 9	9 30 51	72 93 134 135 156 177 195 213 231 249 266 276 292 309 330 351 361 375 410										
linia 10	10 31 52	73 94 135 136 157 178 196 214 232 250 267 277 293 310 331 352 362 376 411										
linia 11	11 32 53	74 95 136 137 158 179 197 215 233 251 268 278 294 311 332 353 363 377 412										
linia 12	12 33 54	75 96 137 138 159 180 198 216 234 252 269 279 295 312 333 354 364 378 413										
linia 13	13 34 55	76 97 138 139 160 181 199 217 235 253 270 280 296 313 334 355 365 379 414										
linia 14	14 35 56	77 98 139 140 161 182 200 218 236 254 271 281 297 314 335 356 366 380 415										
linia 15	15 36 57	78 99 140 141 162 183 201 219 237 255 272 282 298 315 336 357 367 381 416										
linia 16	16 37 58	79 100 141 142 163 184 202 220 238 256 273 283 299 316 337 358 368 382 417										
linia 17	17 38 59	80 101 142 143 164 185 203 221 239 257 274 284 300 317 338 359 369 383 418										
linia 18	18 39 60	81 102 143 144 165 186 204 222 240 258 275 285 301 318 339 360 370 384 419										
linia 19	19 40 61	82 103 144 145 166 187 205 223 241 259 276 286 302 319 340 361 371 385 420										
linia 20	20 41 62	83 104 145 146 167 188 206 224 242 260 277 287 303 320 341 362 372 386 421										
linia 21	21 42 63	84 105 146 147 168 189 207 225 243 261 278 288 304 321 342 363 373 387 422										
		R2	R4	R6	R8	R10	R12	R14	R16	R18	R20	

Figure 3. The building base and measurement points around the structure

Based on the results of the simulation for the three numerical models described above, was created a pivot table, figure 3, which shows the longitudinal component of pedestrian level wind speed values, measured in 422 points arranged in 21 columns (R1 R21 ...) and 21 lines (line 1 line 21) around the building base.

With wind speed values registered in the pivot table can draw graphs of the flow speed in different areas near the building. To save space are presented below only a few significant cases.

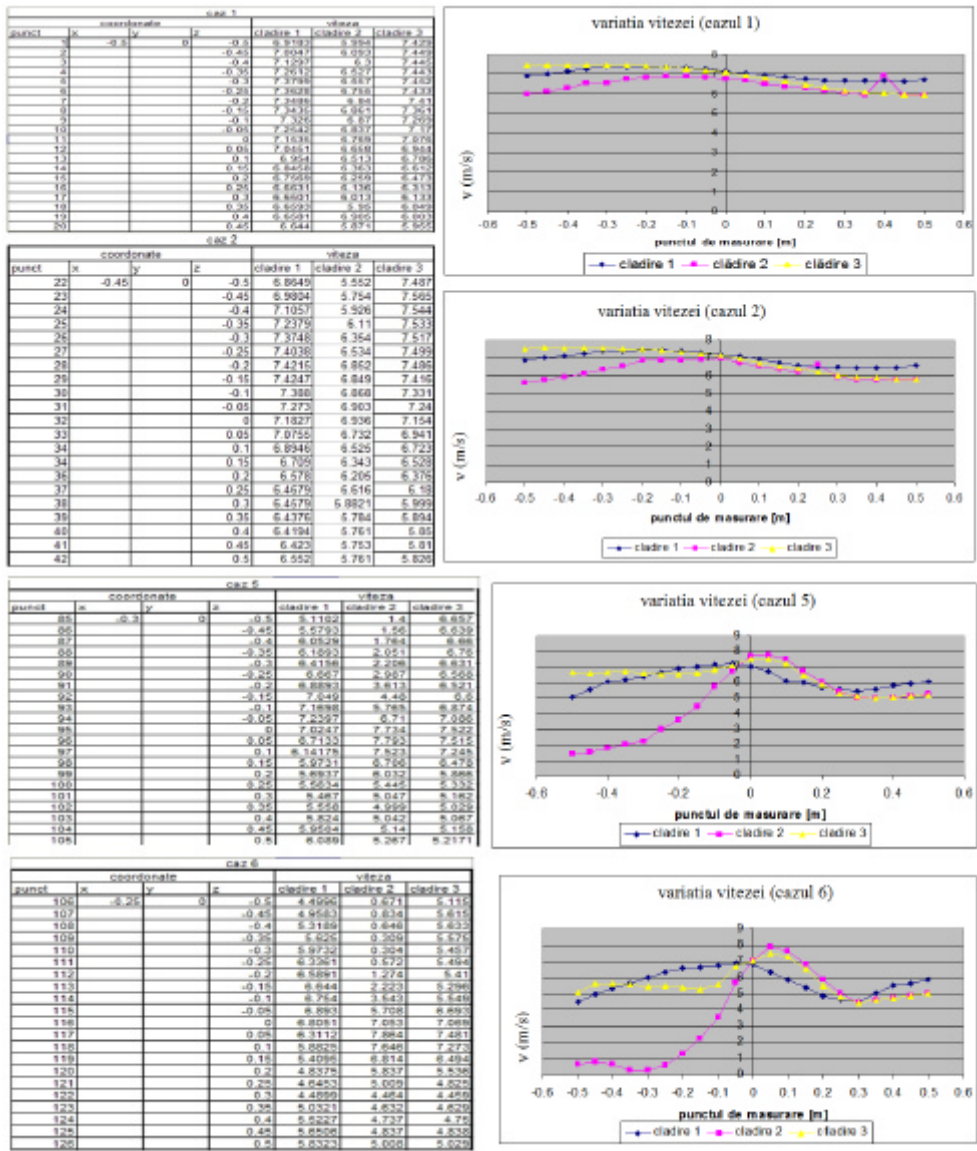


Figure 3. Speed values on columns (R1, R2, R5, R6)

3. THE WIND REDUCTION COEFFICIENT

The data obtained by CFD modelling can be used to calculate for each point by a Reduction Coefficient, $R_{c_{ij}}$, as proposed by WM Cornelis for windbreak screens in

his dissertation [4, 5]. The value of Reduction Coefficient reflects the reduction of the wind speed, and it is estimate using the equation:

$$Rc_{ij} = 1 - \frac{\bar{u}_{ij}}{\bar{u}_{0,ij}} \tag{1}$$

with :

- i = height above the windbreak (in barrier height H),
- j = distance from the windbreak (in barrier height H),
- \bar{u}_{ij} = arithmetic mean wind speed disturbed by the windbreak (m×s-1),
- $\bar{u}_{0,ij}$ = arithmetic mean wind speed in absence of windbreak (m×s-1).

According to the value of the speed Reduction Coefficient can say that:

- if the value is positive and is close to 1 means that the area is heavily sheltered;
- if the value is close to 0, means that the wind speed on that area is similar to the speed free stream and the presence of the obstacle do not influence the flow;
- if value is negative results an acceleration of the flow on that area.

The values of the wind reduction coefficient can be plotted to create maps with sheltered or wind accelerated areas around the building.

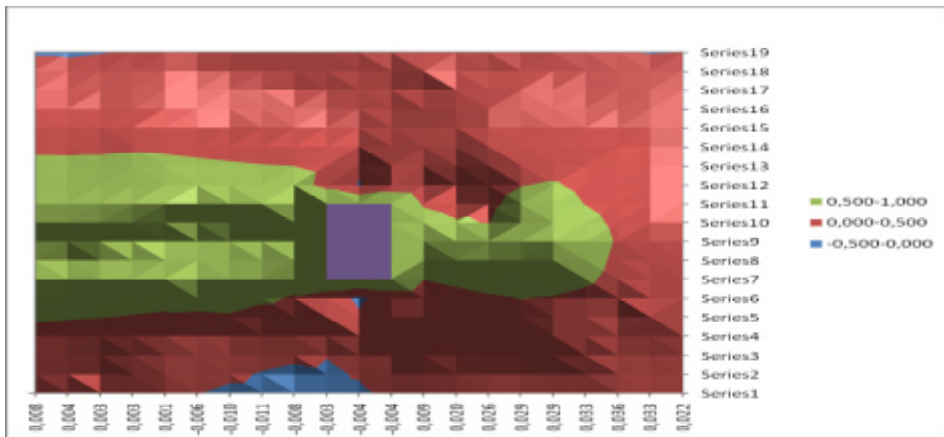


Figure 4. Reduction Coefficient map around building no. 1, H=45 m

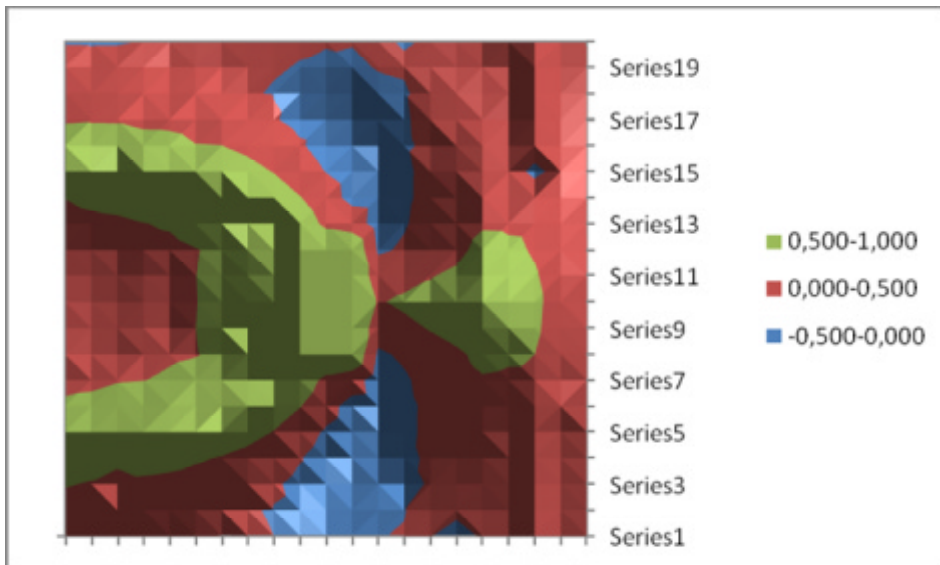


Figure 4. Reduction Coefficient map around building no. 2, H=60 m

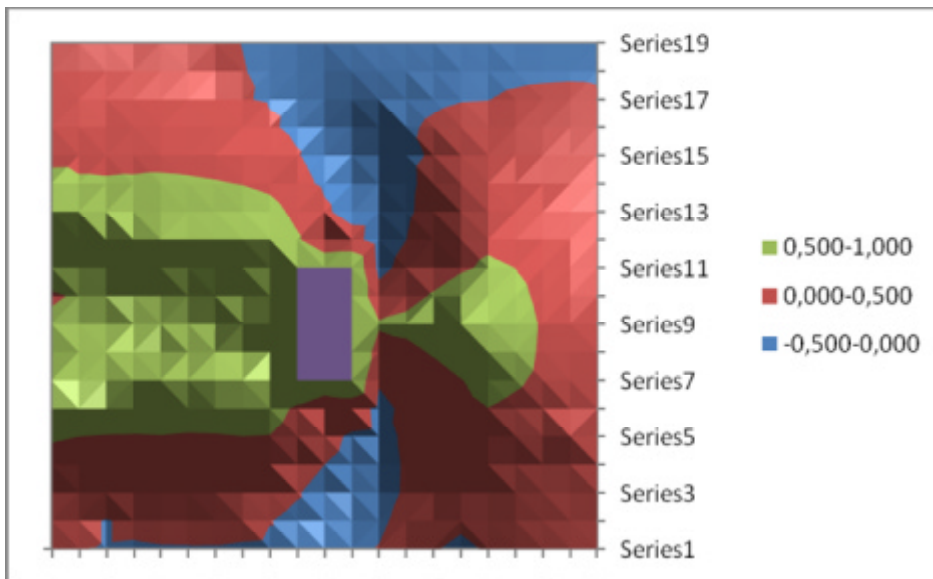


Figure 4. Reduction Coefficient map around building no. 3, H=75 m

For building no.2 (H = 60 m) can see the emergence of areas, starting at the downstream corner, where air velocity is increased reaching values up to 1,5 times the reference speed of the incident wind. This acceleration of flow due to Von

Karmán vortex is shaded downstream alternatively from the building corners, followed the general direction of the flow. In the case of building no. 3 ($H = 75$ m) the area covered by the trail of vortices expands significantly.

3. CONCLUSIONS

Conclusion extracted from this CFD wind application exercise is that although Computational Wind Engineering is still under development, techniques presented in the paper appear to be sufficient for external comfort assessment of pedestrian level wind environmental design.

It is important to make parallel researches for similar examples with boundary layer wind tunnel tests on physical models and with numerical simulations, any time when it is an opportunity, in order to validate an efficient CFD model for wind environmental design and to know the degree of errors that are critical in understanding, interpreting and presenting CFD results.

References

1. Baskaran A. and Kashef A. Investigation of airflow around buildings using computational fluid dynamics. *Engineering Structures* 1996, Vol. 18, No. 11, pp. 861-875.
2. Franke J., et al. Recommendation of the use CFD in wind engineering. *Proceeding of the International Conferences on Urban Wind Engineering and Building Aerodynamics*, Belgia, 2004.
3. Hall R. C. Evaluation of modelling uncertainty – CFD modelling of near-field atmospheric dispersion, *Project EMU final report, WS Atkins Consultants Ltd*, UK, 1996.
4. Cornelis W.M. - A wind-tunnel study on the reduction coefficient of synthetic windscreens. *M.Sc. Thesis*. University of Ghent, Belgium. 96 p, (1994).
5. Pescaru, R.A, Akileh, H.A.A., Radu, A., Laboratory measurements of wind velocity field behind windbreak screens, *Bul. Inst. Polit. Iasi*, t. LVII (LVII), f. 4, 2011

Seismic hazard of Romania: overview for the probabilistic approach

Elena Poida, Adrian Haiducu

Department of Structural Mechanics, Technical University of Civil Engineering, Bucharest, Romania

Summary

The seismic hazard analysis is concerned with getting an estimate of the strong-motion parameters at a site for the purpose of earthquake resistant design or seismic safety assessment. There are two main approaches for the seismic hazard analysis: Deterministic Seismic Hazard Analysis (DSHA) and Probabilistic Seismic Hazard Analysis (PSHA). In the deterministic method the seismic events are generated for a specific site considering information known such as seismic sources that could affect the area, historical earthquakes and geological conditions. The probabilistic approach takes into account the deterministic information and integrates the effects of all the earthquakes expected to occur at different sites during a specified life period, considering also the uncertainties and randomness involved.

A methodology to perform a probabilistic seismic hazard analysis for Romanian districts is presented in this paper. The Vrancea intermediate-depth earthquakes are considered as seismic sources and the specific attenuations relationships are presented. The results of this analysis are released through hazard maps and hazard curves representing the probability of exceeding different ground motion values at a site.

KEYWORDS: *Seismic hazard, probabilistic analysis, Vrancea intermediate-depth earthquakes*

1. INTRODUCTION

Romania is one of the world countries exposed to a persistent, periodical and severe seismic regime produced by various tectonic type sources: shallow or normal depth sources and intermediate depth sources. The intermediate depth sources ($70 \leq H \leq 170$ km) are located in Vrancea region and affect 2/3 of the Romania territory, while the shallow sources contribute to local seismicity.

The potential for dangerous, earthquake – related phenomena such as ground shaking, fault rupture or soil liquefaction are described by seismic hazard analysis.

The seismic hazard analysis is concerned with getting an estimate of the strong-motion parameters at a site for the purpose of earthquake resistant design or seismic safety assessment. There are two main approaches for the seismic hazard analysis: Deterministic Seismic Hazard Analysis (DSHA) and Probabilistic Seismic Hazard Analysis (PHSA).

In the deterministic method the seismic events are generated for a specific site considering known information such as seismic sources that could affect the area, historical earthquakes and geological conditions: “the earthquake hazard for the site is a peak acceleration of 0.35g resulting from an earthquake of magnitude 6.0 on the Balcones Fault at a distance of 12 miles from the site” [1].

The probabilistic seismic hazard approach, first addressed in 1968 by C. Allin Cornell in “Engineering Seismic Risk Analysis”, takes into account the deterministic information and integrates the effects of all the earthquakes expected to occur at different sites during a specified life period, considering also the uncertainties and randomness involved: “the earthquake hazard for the site is a peak ground acceleration of 0.28g with a 10 percent probability of being exceeded in 50-year period” .

The result of the probabilistic seismic hazard analysis is the seismic hazard curve, representing the rate of probability of exceedance related to a ground motion parameter such as peak ground acceleration. The level of probability in building design codes is usually associated to a 50 year period.

The European seismic design codes consider two performance levels for buildings, Life Safety (LS) and Immediate Occupancy (IO) associated with two seismic hazard levels. This European approach was adopted in the new Romanian seismic code P100-1/2011, which considers a mean recurrence interval of 475 for high importance building and a mean recurrence interval for 100 years for the current buildings [2]. The reference return period of 475 years correspond to a 10 percent probability of being exceeded in 50 years and the return period of 100 years correspond to a 10 percent probability of being exceeded in 10 years [3].

If a series of seismic curves is developed for a range of different parameters (e.g., PGA, 1 sec spectral acceleration, 0.2 spectral acceleration, etc.) and values are extracted for a certain constant probability (say a 10% in 50 years probability of exceedance), then a design response spectrum may be created by plotting the parameter magnitude vs. period. A complete response spectrum, where each point has the same probability to being exceeded in a given period is called a uniform hazard spectrum (UHS). These spectra could then be used in a response spectrum analysis of the structure.

2. METHODOLOGY OF PROBABILISTIC SEISMIC HAZARD ANALYSIS

The probabilistic seismic hazard analysis (PSHA) of Romania is completed on seismicity, geology and attenuations characteristics available in the current scientific literature, using CRISIS2007 v7.2 computer code.

CRISIS2007 was developed at the Engineering Institute of the National University of Mexico (UNAM), by M. Ordaz, A. Aguilar and J. Arboleda and use as calculation base for the seismic hazard the standard probabilistic approach defined by Cornell in 1968. CRISIS allows the definition of two seismic models for the hazard assessment: Poisson and characteristic. The seismic sources are modeled as area sources, faults (modeled as lines in the space) or point sources and the seismic hazard assessment is computed through attenuation relations and seismic parameters defined by user.

Considering α a random variable describing the intensity of earthquake ground shaking at a site (in this analysis $\alpha = S_a(T)$, the response spectral ordinate at vibration period T), CRISIS computes the annual exceedance rate of the value α (events per year), caused by earthquakes in the i -th seismic source, through the equation 2 obtained by discretization of the equation 1. The exceedance rate of value α^* , calculated with equation 2, is used in CRISIS for computing the seismic hazard curve.

$$\alpha_i(\alpha^*) = \sum_{i=1}^N \alpha_{0i} \int_{M_{\min_i}}^{M_{\max_i}} \int_R P[\alpha > \alpha^* | M, R] f_{M_i}(M) f_{R_i}(R) dM dR \tag{1}$$

$$\alpha_i(\alpha^*) = \sum_{i=1}^N \alpha_{0i} \sum_{M_{\min_i}}^{M_{\max_i}} \sum_R P[\alpha > \alpha^* | M, R] f_{M_i}(M) f_{R_i}(R) \Delta M \Delta R \tag{2}$$

where: α^* is the certain value of the seismic ground motion parameter α ;

α_i is the annual probability of exceedance of selected ground motion parameter α^* , occur to the seismic source considered;

I_{0i} is the rate of exceedance of reference earthquake in the seismic source i , corresponding to earthquakes with magnitude larger or equal with the minimum magnitude consider in the source i , (M_{\min_i})

$f_{M_i}(M)$ si $f_{R_i}(R)$ are the probability density function for magnitude and source to site distance, considering that magnitude and distance are independent;

$P[g \geq g^* | M, R_i]$ is the probability of exceeding of a particular value, g^* , calculated with attenuation relations related to magnitude M and distance to site R ;

M_{\max_i} is the ground motion maximum magnitude considered in the seismic source i ;

N is the number of seismic sources.

2.1. Magnitude recurrence

CRISIS admits two types of seismicity models. They essentially differ in the way in which the earthquake magnitude exceedance rate, $\lambda(M)$ is described. The two models are: Poisson and characteristic. The Romanian hazard analysis is computed using the Poisson model. The earthquake magnitude exceedance rate is given by equation 3 and the probability density of the earthquake magnitude is given by equation 4, [4]:

$$\lambda(M) = \lambda_0 \frac{e^{-\beta M} - e^{-\beta M_{\max}}}{e^{-\beta M_{\min}} - e^{-\beta M_{\max}}} \quad (3)$$

$$f_{M_i}(M) = b \frac{e^{-bM}}{e^{-bM_{\min}} - e^{-bM_{\max}}}, \quad M_{\min} \leq M \leq M_{\max} \quad (4)$$

Where: λ_0 is the exceedance rate of magnitude M_{\min} ;

β is a parameter equivalent to the "b-value" for the source i (except that it is given in terms of the natural logarithm);

M_{\max} is the maximum magnitude for the source.

2.2. Attenuation relations

The attenuation relations (predictive relationships) allow estimating the probability of exceedance of value g^* in the site during a ground motion with M magnitude and R source to site distance. Considering the seismic hazard parameter with a lognormal distribution with known magnitude and distance, the probability $P[g \geq g^* | M, R_i]$ is calculated with the equation 5, [4]:

$$P[g \geq g^* | M, R_i] = 1 - F \left[\frac{\ln g^* - \ln g_m(M, R)}{S_{\ln A}} \right] \quad (5)$$

where: Φ is the cumulative distribution function of the ground motion parameter;

$m(M,R)$ is the mean value of the ground motion parameter γ (given the specific attenuation relation for magnitude M and site to source distance R)

$s_{\ln A}$ is standard deviation of natural logarithm of the ground motion parameter, $\ln \gamma$

The equation 5 is represented in the Figure 1 as the area under the curve, for the case magnitude M is established, $M=M^*$ and the source to site distance is known, $R=R^*$.

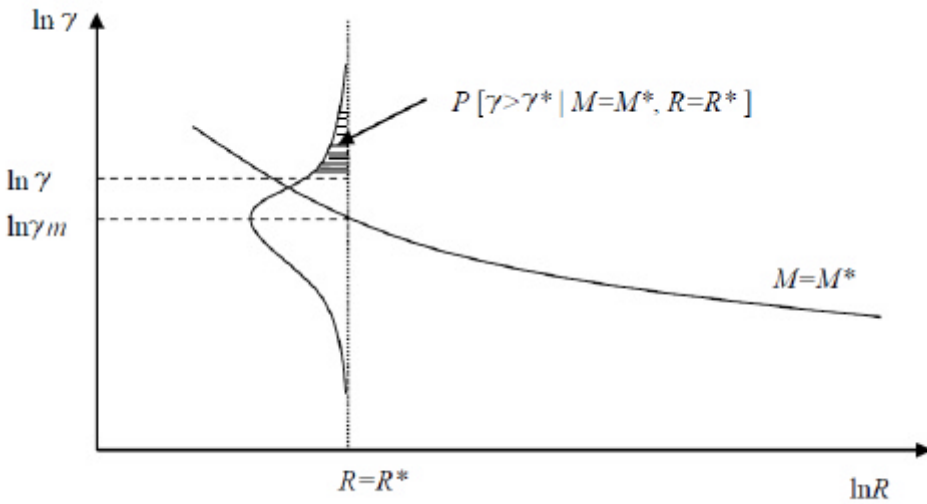


Figure 1. Estimate the exceedance of the ground motion parameter γ^* using the seismic attenuation relation, in the case $M=M^*$ and $R=R^*$ [5]

3. COMPUTING THE SEISMIC HAZARD

3.1. Maps

For graphic identification of the site, CRISIS allows input of a map in *shape file* format (*.shp*) and mention of cities as reference points. A map for Romanian districts and cities, projected in World Geographic System 1985(WGS1984) was realized using the ArcGIS 3.3 software and input into CRISIS (Figure 2).

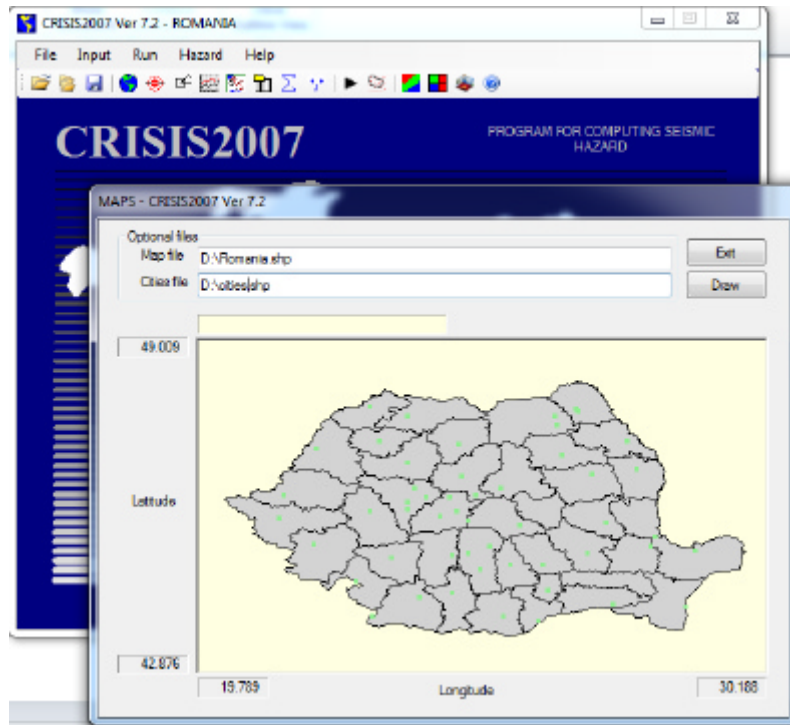


Figure 2. Romania district and cities input to CRISIS2007

CRISIS request the definition of the area for which the seismic hazard will be computed. In the current analysis the area of Ilfov district, including Bucharest city, was selected for validating the current results with the previews hazard analysis that have been completed for Bucharest city. The grid was defined with longitude and latitude increment of 0.05. Hazard will be computed at the nodes of this grid.

3.2. Vrancea seismic source

Vrancea seismic source is located to the Carpathian curvature and affect 2/3 of the Romania territory. Even though CRISIS admit a maximum number of seismic region of 400, in this analysis only the seismic region Vrancea was considered.

Vrancea source was modeled as point source and area source, considering an epicentral area of 40x80 sq. km. and the epicenter of the destructive ground motion of March 1977, the focal depth is between 60 and 170km (Figure 3). The seismicity of the source was selected as Poisson process.

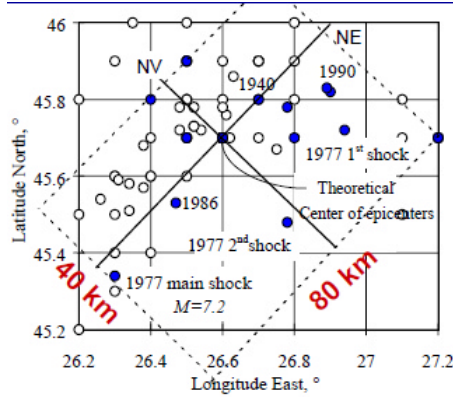


Figure 3. Epicenter position of Vrancea seismic source [6]

Taking into account the N45°E directionality of the seismic field produced by the Vrancea source, the attenuation analysis consider two orthogonal directions (the average direction of the rupture surface N45°E and the normal to this direction E45°S) [7]. The following type model is selected for attenuation analysis in Bucharest sector [7]:

$$\ln PGA = 1.685 + 1.181M_w - \ln R + 0.002R - 0.005h + e \tag{6}$$

where: PGA is the peak ground acceleration at the site, M_w is the moment magnitude, R is the hypocentral distance to site, h the focal depth and e is a random variable with zero mean and standard deviation $s_e = s_{\ln PGA} = 0.461$.

The main data for Vrancea seismic source input are: Expected value of maximum magnitude 8.1; Standard deviation of maximum magnitude 0.3; Maximum observed magnitude 7.8; Threshold magnitude $M_0=5.0$; Expected annual rate with magnitude $\lambda(M_0)=1.29$; Expected value of $\beta=0.73$ [7].

3.3. Results

Table 1. The prediction of PVGA for different mean recurrence intervals of Ilfov district

Hypothesis for Vrancea seismic source	PGA(cm/s ²)		
	50 years	100 years	475 years
1.Point source 1977 earthquake location 26.3 long E, 45.3 4lat N, h=110km	254	275	397
2.Area source Source rupture area 40x80km ² Horizontal, h=130km	192	232	326

CRISIS provides the results of the analysis graphic or through several output files. The graphic results for the current analysis are plotted in figure 4 and figure 5. The prediction of PGA for Ilfov district, considering different mean recurrence intervals are centralized in Table 1.

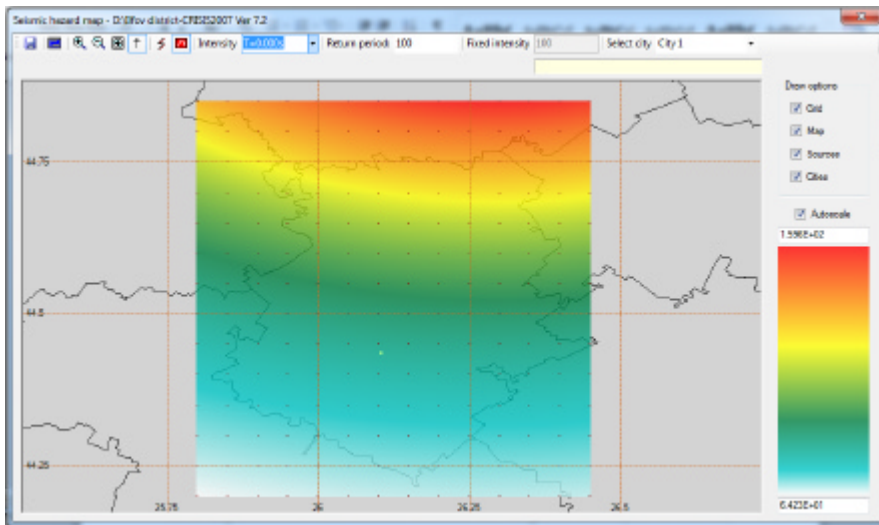


Figure 4. CRISIS2007 ver 7.2. Graphic output - Hazard map for Ilfov district

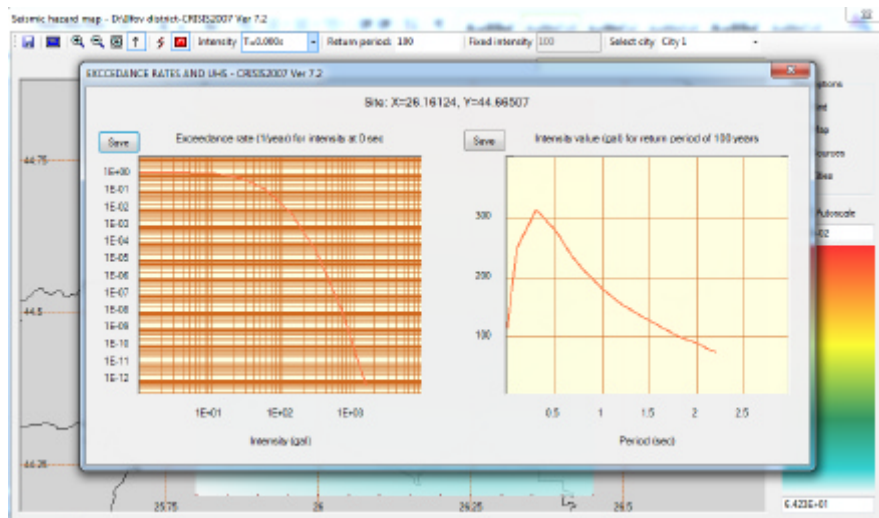


Figure 5. CRISIS2007 ver 7.2. Graphic output - Exceedance rate and UHS for Ilfov district

4. CONCLUSIONS

The seismic hazard analysis is concerned with getting an estimate of the strong-motion parameters at a site for the purpose of earthquake resistant design or seismic safety assessment. The probability seismic hazard analysis (PSHA) takes into account the deterministic information and integrates the effects of all the earthquakes expected to occur at different sites during a specified life period, considering also the uncertainties and randomness involved.

CRISIS computes seismic hazard using a probabilistic model that consider the rates of occurrence, attenuation characteristics and geographical distribution of earthquakes. Earthquake occurrence can be modeled either as a Poissonian process or as a Characteristic Earthquake process. Sources can be modeled as areas, lines or points, attenuation models are furnished by the user or built-in in. [4]

Romania is one of the world countries exposed to a persistent, periodical and severe seismic regime produced by various tectonic type sources: shallow or normal depth sources and intermediate depth sources. The intermediate depth sources are located in Vrancea region and affect 2/3 of the Romania territory, while the shallow sources contribute to local seismicity. For hazard analysis of the Romanian region the attenuation relations furnished by user should be considered. The results obtain with Crisis are validated through the preview hazard analysis studies. Crisis2007 is a powerful tool in computing a probabilistic hazard analysis.

References

1. FEMA 451, *Instructional Material Complementing FEMA 451 Design Examples–Seismic Hazard Analysis*, FEMA Publications Center, 2007
2. P100-1/2011, *Prevederi de proiectare pentru cladiri*, 2011. (in Romanian)
3. Solomos, G., Pinto, A., Dimova, S., *A review of the seismic hazard zonation in national building codes in the context of Eurocode 8*, EUR 23563EN, 2008.
4. Ordaz, M., Aguilar, A., Arboleda, J., *CRISIS 2007, ver. 7.2. Program for computing seismic hazard*, UNAM, Mexico, 2007.
5. Melendez, A., *Evaluation probabilista del riesgo sismico de edificios en zonas urbanas*, Tesis doctoral, Universidad Politecnica de Catalunya, 2011. (in Spanish)
6. Dubina, D., Lungu, D., *Constructii amplasate in zone cu miscari seismice puternice*, Editura Orizonturi Universitare, Timisoara, 2003. (in Romanian)
7. Lungu, D., et al, *Synthesis report for the City of Bucharest, RISK-UE An advanced approach to earthquake risk scenario with application to different European town*, 2004
8. Lungu, D., Vacareanu, R., Aldea, A., Arion, C., *Advanced Structural Analysis*, Conspress 2000
9. Vacareanu, R., Aldea, A., Lungu, D., *Structural Reability and Risk Analysis*, Conspress 2007
10. Aguilar, A., Pujades, L., Barbat, A., Lantada, N., *A probabilistic model for the seismic risk of buildings. Application to assess the seismic risk of building in urban area*, *9th US National and 10th Canadian Conference on Earthquake Engineering*, Toronto, 2010.

Maple 12 a Reliable Tool for Physics Learning

I. Radinschi¹, B. Aignatoiaei²

¹Department of Physics, "Gheorghe Asachi" Technical University University, Iasi, 700050, Romania

²Faculty of Automatic Control and Computer Science, "Gheorghe Asachi" Technical University University, Iasi, 700050, Romania

Summary

In this work we explain and give examples how powerful algebra systems like Maple 12 gives the possibility to the students to improve their knowledge about physics phenomena. The applications are made using physical quantities from the Physics I course that is designated to the first-semester at the Faculty of Civil Engineering and Building Services of "Gheorghe Asachi" Technical University of Iasi, and have been developed with the aid of the Graphics package of Maple 12 program.

The Maple 12 program can be used for graphical representations at a high level. The students work in a simple manner with the program and draw the graphs for many physical phenomena. Moreover, this algebra system yields a very good environment for calculus, algebra, basic mathematics, differential equations, linear algebra, mathematical functions, packages, power series, physics, and also contains a student package that is very useful and "is designed to provide an introduction to the power of the full Maple system".

We present at the course some applications of the Maple 12 program that we have prepared in our PowerPoint presentation. After this, we give to the students the possibility to use it for some calculations and to make graphs. The program is useful at seminars for solving problems and can be also used in campus for a deeper understanding of the physical phenomena presented at the course of physics.

This tool enables our students to improve their learning process and obtain better results. The Maple 12 program becomes a more powerful tool for learning physics if it is used in connection with lectures, seminars and our Virtual Physics Laboratory.

In this paper we present examples of plotting 2d and 3d for some chapters of physics contained in our course of physics. We give examples of plotting physical quantities from Classical Mechanics and Waves chapters. For making the plots we use important physical quantities like the mechanical work, force, momentum, wave vector, period and pulsation.

KEYWORDS: Maple 12, physics, plots, graphs.

1. INTRODUCTION

Nowadays, the Maple 12 program [1] is considered as one of the most reliable products in term of technology that helps the students to improve their learning process.

We develop a method that takes into account the students knowledge and their performance in the use of Maple 12 program. After the implementation of the Maple 12 program in our Physics course, our students consider this an easy way of accessing this technology for their purposes. We point out that only a percentage of our students use this algebra system. This percentage is higher than last years. A greater percentage of students who have chosen to work with this computational program indicates an increasing of their interest for this type of learning.

With the aid of Maple 12 the students can make the connection between physical phenomena and mathematical formalism and graphical representations. Before using Maple 12 we used Maple 9.5 program [1], but now we choose the new version because of its improvements. The students can also use the Maple Calculator that is attached to the Maple 12 program. They can use it for graphs, data, variables, math and settings. Concerning the plotting, some of the many features introduced in Maple 12 [1] are “new abilities that include dual axis plots, polar plots, and specialized engineering plots such as frequency domain responses and root-locus plots”.

Our experience over the last decade in the use of computational programs [2]-[7] allows us to implement in our Physics course and seminars new algebra systems for improving the learning process.

2. MAPLE 12 A POWERFUL TOOL FOR PLOTTING

We present some applications of Graphics package of the Maple 12 program that we use at our Physics course. The plot and plot3d commands are used. We plot physical quantities from Classical Mechanics and Waves chapters [8].

2.1. Plotting the mechanical work, force and momentum

The commands in Maple 12 for plot and plot3d in the case of the mechanical work, force and momentum are given by

a) `plot3d(F*r, r = 1 ...10, F = 1 ...10)`; and the graph is in Figure 1.

We have elementary mechanical work

$$L = F \cdot dr \tag{1}$$

and the mechanical work between two points A and B

$$L_{A \rightarrow B} = \int_A^B F \cdot dr . \tag{2}$$

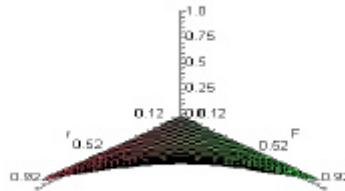


Figure 1. The plot3d for the mechanical work

The expression for the force is given by the second law of dynamics

$$\vec{F} = m\vec{a} . \tag{3}$$

b) plot3d(m*a, m = 1 ...10, a = 1 ...40); and the plotting is given in Figure 2.

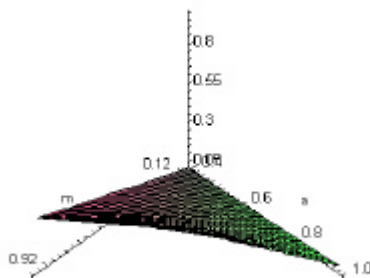


Figure 2. The plot3d for the force

The momentum has the expression

$$\vec{p} = m\vec{v} . \tag{4}$$

c) `plot(1*v, v = 1 ...100)`; and the graph is presented in Figure 3. We choose for the mass the value $m=1$ (kg).

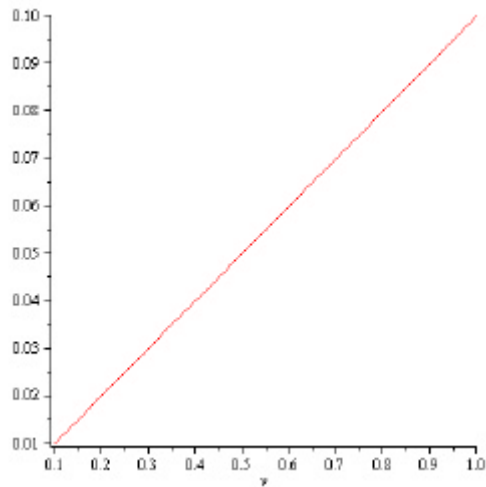


Figure 3. Plot for the momentum

d) `plot3d(m*v, m = 1 ...7, v = 10 ...70000)`; and the plotting is given in Figure 4.

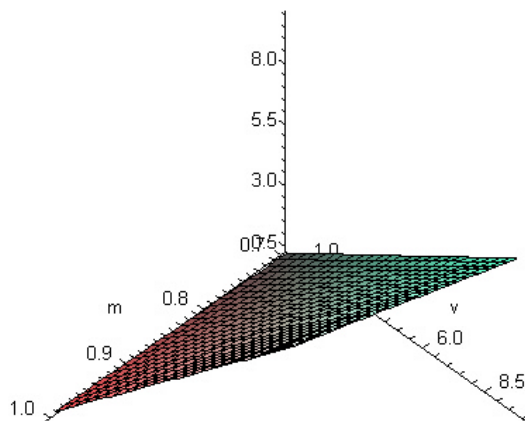


Figure 4. Plot3d for the momentum

2.2. Plotting the wave vector, period and pulsation

The wave vector is given by

$$k = \frac{w}{n} . \tag{5}$$

e) `plot3d(w/n , w = 1 ...10, n = 1 ...100)`; and the graph is plotted in Figure 5.

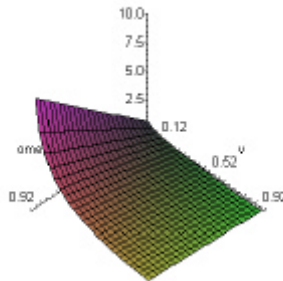


Figure 5. Plot3d for the wave vector

The period is

$$T = \frac{2p}{w} . \tag{6}$$

f) `plot(2*Pi/w , w = 1 ...10)`; and the plotting is given in Figure 6.

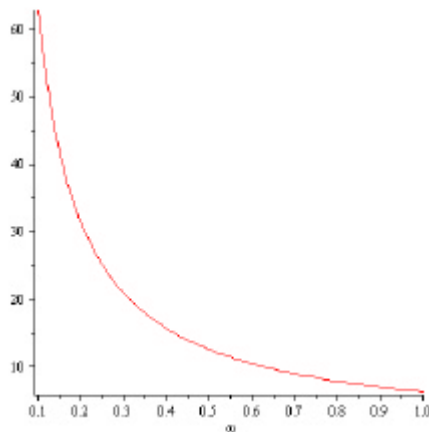


Figure 6. Plot for the period

The pulsation is given by

$$w = 2\pi n . \quad (7)$$

g) `plot(2*Pi*n , n = 1 ...10)`; and the graph is presented in Figure 7.

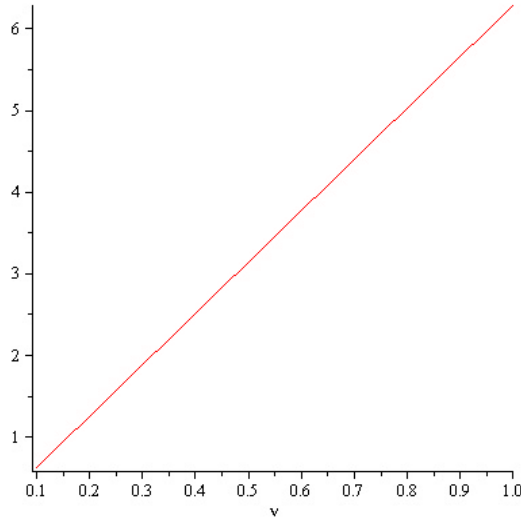


Figure 7. Plot for the pulsation

These are some examples of graphs developed in Maple 12. The students will also use other packages and performing calculations for seminars.

3. CONCLUSIONS

One of the newer versions of the Maple program, the Maple 12 provides new functions and packages presenting in this way many advantages. The program is a proper environment for calculus, plotting and animation.

When we implemented this algebra system in our Physics course we also give to our students the possibility to achieve a good training for using the program in the case they are beginners. In this case we started with simple applications and after this we introduced new problems to be solved. For the students who already know to work with Maple 12 we also offer some more advanced problems. In this way, all the students have made progresses at their levels of knowledge. We use the Maple 12 program in order to make plots for different important physical quantities and for physics laws. After they become more familiar with the program, the students have used it for solving equations and making other calculus improving

the learning process and preparing in a modern way for the seminars. The students will also be capable to develop their ability to learn physics without the guidance of the teacher. The program can be used outside class and this contributes to the improvement of the knowledge of physics laws and phenomena, and for the improving of the final mark at the exams.

References

1. <http://www.maplesoft.com/>
2. Radinschi, I., Ciobanu, B., *Physics Tests*, Junimea Publishing House Iasi, Romania, 2006.
3. Radinschi, I., Damoc, C., Aignatoaie, B., Cehan, V., *Improving the e-Learning of Engineering Physics with the Aid of Adobe Flash*, 8th International Symposium “Computational Civil Engineering 2010”, Iasi, Romania, May 28, 2010, published in *New computational concepts in civil engineering*, editors Rodian Scinteie, Costel Plescan, "Matei - Teiu" Publishing House, Iasi, Romania, pp. 219-226, 2010.
4. Radinschi, I., Damoc, C., Cehan, A., Cehan, V., *Computer Simulations of Physics Phenomena Using Flash*, 5th International Conference on Hands-on Science Formal and Informal Science Education, October 13-17, 2008, Espaço Ciência, Olinda-Recife, Brazil, Edited by Manuel Filipe Pereira da Cunha Martins Costa (Universidade do Minho), José Benito Vazquez Dorrío (Universidade de Vigo), António Carlos Pavão (Espaço Ciência), Mikiya Muramatsu (Universidade de São Paulo), pp. 147-151, 2008.
5. Radinschi, I., Ciobanu, B., *Improving Civil Engineering Physics Teaching-Learning with Mathematica 5.1*, Proceedings of 5th International Symposium “Computational Civil Engineering 2007”, CCE 2007, Iasi, Romania, May 25, pp. 180-190, 2007.
6. Radinschi, I., Frunza M., D., Ciobanu, B., *Online Virtual Model for Testing the Knowledge*, Proceedings of International Technology, Education and Development Conference INTED 2007 edited by IATED, Valencia, Spain, March 7-9, pp. 42-47, 2007.
7. Radinschi, I., Ciobanu, B., *Implementation of Computational Methods in Physics Learning*, Proceedings of 4th “International Symposium Computational Civil Engineering 2006”, CCE 2006, May 26, Iasi, Romania, pp. 251-256, 2006.
8. Radinschi, I., Course of Physics, <http://www.ce.tuiasi.ro/english/index.html>

Optimization methods for steel girders using EUROCODE 3

Victoria E. Rosca, Elena Axinte, and Elena C. Telesman

Department of Civil and Industrial Engineering, "Gheorghe Asachi" Technical University of Iasi, 700050, Romania

Summary

Plate girders are used either on long spans where a rolled section would need to be spliced and as a result may be inefficient, or to support heavy loads. It is important to note that although plate girders may be lighter than other forms of compound beams, fabrication costs are likely to be much higher.

The design of a built-up steel girder is a tedious and time-consuming job for the designer. In common practice, steel plate girders are designed by a trial-and error approach due to the complexity of the design rules.

Standard optimal design formulation of steel plate girder respecting Class restriction is discussed. The design, resistance and deflection inequality constraints for steel built-up welded beams were defined in accordance with the European Standards Eurocodes (EN 1990; EN 1993-1-1; EN 1993-1-5) in order to satisfy the requirements of both the ultimate and the serviceability limit states.

Efficient procedures for minimum weight design of unstiffened steel plate girders using analytical and numerical approach are presented.

Analytical optimization method should prove useful to structural designers and is expected to advance existing design practices of steel beams.

The nonlinear optimization problem is formulated also on the basis of the current Eurocode 3 specification.

Results of numerical calculations for optimal shapes of three steel-grades and various beam length are presented.

By means of simple formulae derived above and using a simple spreadsheet program, it is possible to compare the characteristics of various length, steel grades and section Classes, which can be useful for designer.

KEYWORDS: steel beam, EC3, bending and shear, optimal design, nonlinear optimization.

1. INTRODUCTION

Optimization is the process of obtaining "the best" solution to a problem based on a given criterion. Structural optimization, therefore, is the process of obtaining the "optimum" solution to a structural problem. This optimization is obtained by using analysis and design theory and an optimum seeking method suited to the problem.

The optimization of girders has been extensively approached in the past by using minimum weight as the measure of effectiveness (Arora, 1997; Farkas & Jármai, 1997, Bauer, 1994).

In this paper, the minimization method approach are initially briefly described. The procedure has been to minimize the cross-sectional area of the girder. This in turn minimizes the weight of the structure. Then the standard optimal design formulation of steel plate girder with Class restriction is discussed. Numerical implementation in a spreadsheet program like Excell using Solving Toolbox and the conversion of the design criteria in inequality constraints is illustrated.

The design, resistance and deflection inequality constraints for steel built-up welded beams were defined in accordance with the European Standards Eurocodes (EN 1990; EN 1993-1-1; EN 1993-1-5) in order to satisfy the requirements of both the ultimate and the serviceability limit states.

2. RESEARCH METHODOLOGY IN COST OPTIMIZATION OF PLATE GIRDERS

In this section, design of a welded plate girder is solving on the basis of the European Standards (EN 1993-1-1).

Formulation of an optimum design problem uses the following steps (Arora, 1997):

- 1) Identification and definition of independent variables;
- 2) Identification and definition of an objective function;
- 3) Identification and definition of constraints.

The dependent variables for the problem that can be evaluated once the design of girder is specified are identified as follows:

The objective is to minimize the total mass or equivalently, the cross-sectional area A of the girder. The independent variables consists of four design variables, depth (h), width (b), flange thickness (t_f) and web thickness (t_w), as shown in Figure 1.

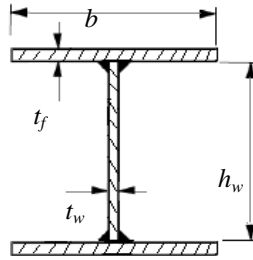


Figure 1 – Cross-section of plate girder

The objective function in the optimization problem is associated with a set of constraints. In the context of structural optimization, these constraints fall into two categories: behavior constraints that limit the plastic/elastic moment, shear force or stability conditions; and design constraints imposed on design variables to put practical limits on some dimensions of elements. Further, to simplify the formulation, it is necessary to introduce dependent design variables. These variables give rise to additional constraints, called equality constraints.

The mathematical programming can be expressed as follows:

$$\begin{aligned} \text{Min } z &= f(\mathbf{x}) \\ \text{subjected to: } &\begin{cases} h(\mathbf{x}) = 0, & (\text{NLP}). \\ g(\mathbf{x}) \leq 0 \end{cases} \end{aligned} \quad (1)$$

where \mathbf{x} is a vector of continuous variables, defined within the compact set X .

To find the mathematical formulation, two major steps are formulated (Arora, 1997; Farkas & Jármai, 1997), namely:

- a) To determine the major decision variables affecting the design of composite beams.
- b) To formulate the objective of cost optimization of composite beams in optimization model.

3. DESIGN CONSTRAINTS DERIVED FROM EC3

Girders of the length L , depth h , simply supported and carry a concentrated force P_k at the middle span are considered in his paper.

The moment, shear, and concentrated load bearing resistances of beams whose plate elements are slender may be significantly influenced by local buckling

considerations. The moment, shear, and concentrated load bearing resistances of beams whose plate elements are slender may be significantly influenced by local buckling considerations. Because of this, beam cross-sections are classified as Class 1, 2, 3, or 4, depending on the ability of the elements to resist local buckling. Sections are classified by comparing the slenderness $\lambda = (c/t)\sqrt{235/f_y}$ of each compression element with the appropriate limits of Table 5.2 of EN 1993-1-5. In this example, only cross-section of Class 1, 2 and 3 are considered.

The local web buckling constraint is expressed by

$$\lambda_w = \frac{h_w}{t_w} \leq \lambda_{0w} \tag{2}$$

where limiting web slenderness has the following values

$$\text{for elastic design: } \lambda_{0w} \leq 124\epsilon \tag{3}$$

$$\text{for plastic design: } \lambda_{0w} \leq 83\epsilon \tag{4}$$

For the compression flange the limiting plate slenderness is:

$$\text{for elastic design: } \lambda_{0f} \leq 14\epsilon \tag{5}$$

$$\text{for plastic design: } \lambda_{0f} \leq 10\epsilon \tag{6}$$

For the moment resistance check of a beam that has adequate bracing against lateral buckling, the inequality:

$$M_{Ed} \leq M_{c,Rd} \tag{7}$$

$$M_{c,Rd} = \begin{cases} M_{pl,Rd} = W_{pl} \frac{f_y}{\gamma_{M0}} & \text{for Class 1 and 2} \\ M_{el,Rd} = W_{el,min} \frac{f_y}{\gamma_{M0}} & \text{for Class 3} \end{cases} \tag{8}$$

must be satisfied, in which M_{Ed} is the maximum design moment, $M_{c,Rd}$ is the design section moment resistance, W is the appropriate section modulus (elastic or plastic, depending on section Class), f_y the nominal yield strength for the section, and $\gamma_{M0} = 1$ the partial factor for section resistance.

For the shear resistance check, the inequality:

$$V_{Ed} \leq V_{c,Rd} \tag{9}$$

must be satisfied, in which V_{Ed} is the maximum design shear force, and $V_{c,Rd}$ the design shear resistance. For a stocky web with $h/t_w = 72\sqrt{235/f_y}$ and for which the

elastic shear stress distribution is approximately uniform (as in the case of an equal flanged I-section), the uniform shear resistance $V_{c,Rd}$ is usually given by:

$$V_{c,Rd} = h_w t_w \frac{f_y / \sqrt{3}}{\gamma_{M0}} \quad (10)$$

in which $f_y / \sqrt{3}$ is the shear yield stress and A_v is the shear area of the web defined in Clause 6.2.6(3) of EN 1993-1-1 [5].

The shear resistance of slender unstiffened webs for which $h/t_w > 72e$ decreases rapidly from the value in Equation (10) as the slenderness h/t_w increases. Neglecting the contribution of the flanges, for these.

$$\begin{aligned} V_{c,Rd} &= V_{bw,Rd}, \\ V_{bw,Rd} &\geq \eta h_w t_w \frac{f_y / \sqrt{3}}{\gamma_{M1}} \end{aligned} \quad (11)$$

where $V_{bw,Rd}$ is the design resistance governed by buckling of the web in shear, c_w is a factor for the shear area that can be taken as 1,2 for steels up to S460 and 1,0 otherwise, and g_{M1} (=1) is a partial resistance factor based on buckling. The buckling resistance of the web is given in EC3 as

$$V_{bw,Rd} = \chi_w h_w t_w \frac{f_y / \sqrt{3}}{\gamma_{M1}} \quad (12)$$

in which the web reduction factor on the yield strength $h_w t_w f_y / \sqrt{3}$ due to buckling is:

$$\chi_w = \begin{cases} \eta; & \bar{\lambda}_w < 0,83 / \eta \\ 0,83 / \bar{\lambda}_w; & \bar{\lambda}_w \geq 0,83 / \eta \end{cases} \quad (13)$$

where the modified web plate slenderness for an unstiffened web, is:

$$\bar{\lambda}_w = \frac{h_w}{t_w} \frac{1}{37,4\epsilon \sqrt{k_\tau}} \quad (14)$$

Since for unstiffened webs $k_\tau = 5,34$, the reduced web slenderness became:

$$\bar{\lambda}_w = \frac{1}{86,425\epsilon} \frac{h_w}{t_w} \quad (15)$$

Thus, the constraints on shear can be rewritten as:

$$V_{bw, Rd} = \begin{cases} h_w t_w \frac{f_y / \sqrt{3}}{\gamma_{M1}} & \text{for } \frac{h_w}{t_w} < \frac{71,733}{\eta} \\ 71,733 t_w^2 \frac{f_y / \sqrt{3}}{\gamma_{M1}} & \text{for } \frac{h_w}{t_w} \geq \frac{71,733}{\eta} \end{cases} \quad (16)$$

With no web stiffeners the web should be sized to avoid the flange undergoing local buckling due to the web being unable to support the flange. This is known as flange induced buckling (EN 1993-1-5).

$$\frac{h_w}{t_w} \leq k \frac{E}{f_y} \sqrt{\frac{A_w}{A_{fc}}} \quad (17)$$

where f_y is the yield strength of the compression flange, A_{fc} is the effective area of the compression flange and A_w is the area of the web.

The parameter k takes values of 0,3 where plastic hinge rotation is utilized, 0,4 if the plastic resistance is utilized and 0,55 if the elastic resistance is utilized. Thus for rigid (continuous) design $k = 0,3$ unless the analysis is elastic with no redistribution. For simply supported beams k may be taken as 0,4.

Considering the serviceability limit state, the vertical deflections is calculated and checked.

The total deflections d_{max} subjected to the overall load and the deflections subjected to the variable imposed load is:

$$\delta_{max} = \frac{L^3}{384 \cdot 10^6 EI} (8P_k + 5q_k L) \quad [\text{m}] \quad (18)$$

The allowable deflection ratio, e.g. for simply supported beams in buildings, according to EC3, is $L/300$. The deflection beam constraints $d_{max} \leq L/300$ can be expressed as:

$$I \geq I_o = \frac{C_w}{300} \quad (19)$$

where

$$C_w = \frac{5q_k L^3}{384E} + \frac{P_k L^3}{48EI} \quad (20)$$

4. ANALYTICAL OPTIMIZATION FOR OF THE GIRDERS WITHOUT CONSTRAINTS

4.1 Optimization of Classes 1 and 2

The moment is resisted by the complete section, when the moment capacity is given by that due to the flanges (Equation (21)) and the additional plastic capacity of the web:

$$M_{Ed} \leq M_{c, Rd} \approx bt_f h_w f_{yd} + \frac{t_w h_w^2}{4} f_{yd} \quad (21)$$

where $f_{yd} = f_y/\sqrt{3}$ is the design strength of the flanges, t_f and b_f the thickness and width of the flange plates and h_w the distance between the internal faces of the flanges.

The cross-sectional area A is given by

$$A = 2bt_f + h_w t_w \quad (22)$$

Eliminate $b_f t_f$ between Equation (21) and (22) to give

$$A = \frac{2M_{Ed}}{h_w f_{yd}} + h_w t_w - 2 \frac{t_w h_w}{4} = \frac{2M_{Ed}}{h_w f_{yd}} + \frac{t_w h_w}{2} \quad (23)$$

Defining the web slenderness ratio λ_w/t_w (Equation (2)), then Equation (23) becomes

$$A = \frac{2M_{Ed}}{\lambda_w t_w f_{yd}} + \frac{\lambda_w t_w^2}{2} \quad (24)$$

For an optimum solution, $dA/dt = 0$, so Equation (24) becomes,

$$\frac{dA}{dt_w} = -\frac{2M_{Ed}}{\lambda_w f_{yd} t_w^2} + \lambda_w t_w = 0 \quad (25)$$

Optimal solution of the thickness is given now by

$$t_w = \sqrt[3]{\frac{2M_{Ed}}{\lambda_w^2 f_{yd}}} \quad (26)$$

and:

$$h_w = \sqrt[3]{\frac{2\lambda_w M_{Ed}}{f_{yd}}} \quad (27)$$

The area of the web, A_w is then given by

$$A_w = \sqrt[3]{\frac{4M_{Ed}^2}{\lambda_w f_{yd}^2}} \quad (28)$$

Using Equation (22), the flange area, A_f is given by

$$A_f = b t_f = \sqrt[3]{\frac{M_{Ed}^2}{\lambda_w f_{yd}^2}} \cdot \left[\sqrt[3]{\frac{1}{2}} - \sqrt[3]{\frac{1}{16}} \right] \quad (29)$$

or,

$$\frac{A_f}{A_w} = \frac{\sqrt[3]{\frac{M_{Ed}^2}{\lambda_w f_{yd}^2}} \cdot \left[\sqrt[3]{\frac{1}{2}} - \sqrt[3]{\frac{1}{16}} \right]}{\sqrt[3]{\frac{4M_{Ed}^2}{\lambda_w f_{yd}^2}}} = \frac{1}{4} \quad (30)$$

Thus the area of the web is equal four times that of a single flange.

4.2 Optimization of Classes 3

The moment is resisted by the complete section, when the moment capacity is given

$$M_{Ed} \leq M_{Rd} \approx b t_f h_w f_{yd} + \frac{t_w h_w^2}{6} f_{yd} \quad (31)$$

where f_{yd} is the design strength of the flanges, t_f and b_f the thickness and width of the flange plates and h_w the distance between the internal faces of the flanges.

Eliminate $b_f t_f$ between Equation (22) and Equation (31) to give

$$A = \frac{2M_{Ed}}{h_w f_{yd}} + h_w t_w - 2 \frac{t_w h_w}{6} = \frac{2M_{Ed}}{h_w f_{yd}} + \frac{2t_w h_w}{3} \quad (32)$$

Define the web slenderness ratio h_w/t_w (eqs. (2) and (3)), then Equation (32) becomes:

$$A = \frac{2M_{Ed}}{\lambda_w t_w f_{yd}} + \frac{2\lambda_w t_w^2}{3} \quad (33)$$

For an optimum solution, $dA/dt = 0$, so Equation (33) becomes,

$$\frac{dA}{dt_w} = -\frac{2M_{Ed}}{\lambda_w f_{yd} t_w^2} + \frac{4}{3} \lambda_w t_w = 0 \quad (34)$$

or,

$$t_w = \sqrt[3]{\frac{3}{2} \cdot \frac{M_{Ed}}{\lambda_w^2 f_{yd}}} \quad (35)$$

and

$$h_w = \sqrt[3]{\frac{3}{2} \cdot \frac{\lambda_w M_{Ed}}{f_{yd}}} \quad (36)$$

The area of the web, A_w is then given now by

$$A_w = \sqrt[3]{\frac{9 \cdot M_{Ed}^2}{4 \cdot \lambda_w \cdot f_{yd}^2}} \quad (37)$$

Using Equation (31), the flange area, A_f is given by

$$A_f = b t_f = \sqrt[3]{\frac{M_{Ed}^2}{\lambda_w f_{yd}^2}} \cdot \left[\sqrt[3]{\frac{2}{3}} - \frac{1}{6} \sqrt[3]{\frac{9}{4}} \right] \quad (38)$$

thus:

$$\frac{A_f}{A_w} = \frac{\sqrt[3]{\frac{M_{Ed}^2}{\lambda_w f_{yd}^2}} \cdot \left[\sqrt[3]{\frac{2}{3}} - \frac{1}{6} \sqrt[3]{\frac{9}{4}} \right]}{\sqrt[3]{\frac{9 M_{Ed}^2}{4 \lambda_w f_{yd}^2}}} = \frac{1}{2} \quad (39)$$

Thus the area of the web is equal twice that of a single flange.

4.3 Optimum Design of The Flanges

Thickness of the flange t_f must satisfy minimum requirements:

$$\begin{aligned} t_w + 2 \text{ mm} &\leq t_f \leq (2 \dots 3) \cdot t_w \\ 12 \text{ mm} &\leq t_f \leq 30 \text{ mm} \end{aligned} \quad (40)$$

Shear lag in flanges may be neglected if $c < L_e/50$ where c is taken as the flange outstand or half the width of an internal element (Figure 1) and L_e is the length between points of zero bending moment. Where the above limit for c is exceeded the effects due to shear lag in flanges should be considered, accordingly EN 1993-1-5. Therefore, the wide of the flange is restricted to:

$$b \approx 2c \leq \frac{L_e}{25} \tag{41}$$

Dimensions of the flange are established now from optimum requirements:

$$\begin{aligned} b_f &\approx 2c \leq 2\lambda_f t_f \\ A_f &= b t_f = 2\lambda_f t_f^2 \\ t_f &\leq \sqrt{\frac{A_f}{2\lambda_f}} \end{aligned} \tag{42}$$

It should be noted that flange area of the girder must fulfill resistance conditions, Equation (8) thus,

$$b \approx \frac{M_{Ed}}{h_w t_f f_{yd}} - \xi \frac{t_w h_w}{t_f} \tag{43}$$

where ξ is 1/4 for Class 1 and 2 and 1/6 for Class 3.

5. OPTIMIZATION OF THE GIRDERS VIA NUMERICAL TECHNIQUES

The advantages of computer technology have been incorporated in the optimization of girder steel design; most notably is the use of spreadsheets. Spreadsheets are user friendly and exceedingly powerful but are not being exploited as much as they could be in structural engineering design.

In structural optimization, various mathematical programming techniques have been extensively applied, with most of the applications based upon one of following algorithms. The method of moving asymptotes, sequential quadratic programming (*SQP*), penalty function methods or feasible direction methods. Many spreadsheet programs have the capability of solving constrained nonlinear problems. In the present work, the Solver tool of Microsoft Excel™ is used. No effort has been made to study the mathematical programming methods used in the structural optimization procedures and the nonlinear algorithm is used here essentially as a black box.

In this section optimization of the weight objective function associated with a set of constraints derived from EC3 requirements, is presented, i.e:

$$\begin{aligned} \min \quad & G = (ht_w + 2bt_f) \cdot L \\ \text{subject to} \quad & \begin{cases} M_{Ed} \leq M_{c, Rd} \\ V_{Ed} \leq V_{c, Rd} \\ \text{if } \frac{V_{Ed}}{V_{c, Rd}} \geq 0,5 \text{ then } V_{Ed} \leq V_{bw, Rd} \\ \lambda_w \leq \lambda_{0w} \\ \lambda_f \leq \lambda_{0f} \\ \delta_{\max} \leq \frac{L}{300} \end{cases} \end{aligned} \quad (44)$$

6. NUMERICAL EXAMPLES

A parametric study is presented to investigate the effects of beam spans on the cost optimization of steel girders. The optimization also considered different economic conditions: different structural steel grades, three defined spans, $L = 15\text{m}$, 18m and 25m , subject to a concentrated imposed load $P_k = 104\text{ kN}$ (dead) and a dead weight $q_k = 2,70\text{ kN/m}$ (Figure 2). In this formulation, bearing stiffeners, welded connections, and transverse stiffeners are not taken into account.

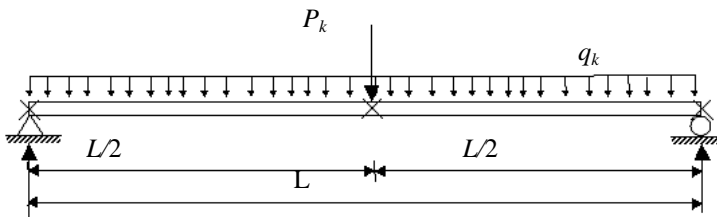
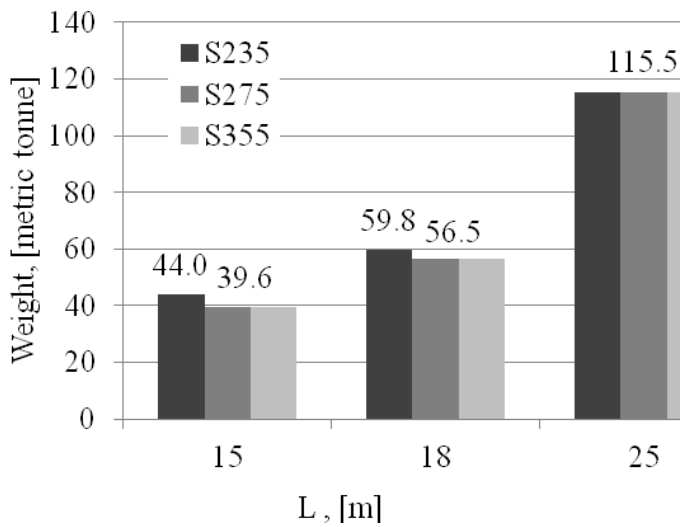
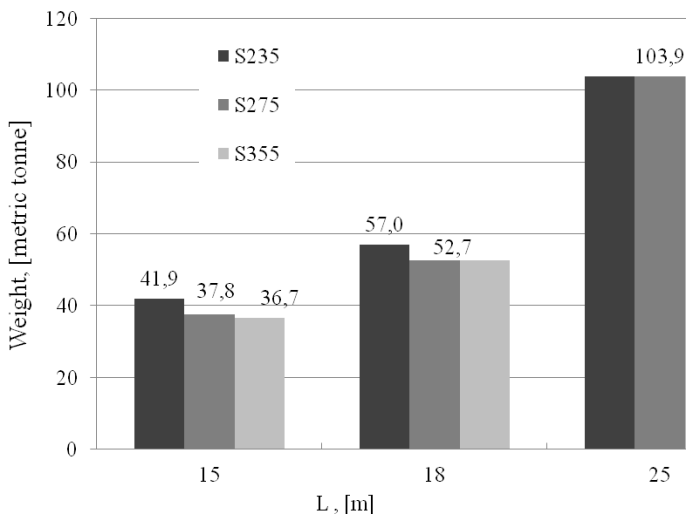


Figure 3 – Variable imposed load and the span of the girder

Characteristics of the optimum cross-section design are also compared with analytical solutions (Farkas & Jármai, 1997) with stress constraints and deflection constraints, respectively. Figure 2 and Figure 3 show differences about 20% for section Class 1 and 2 and 10% for elastic design (Class 3), when only stress constraints are active for analytical solution.

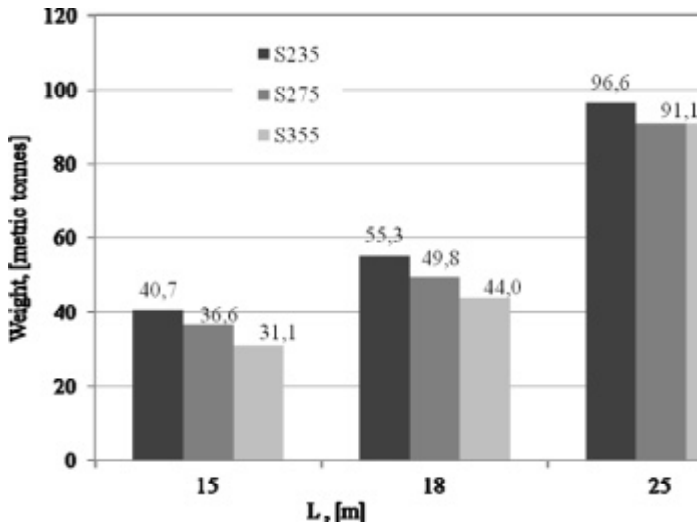


a.



b.

Figure 2 – Minimum weight of optimized cross section in function of beam length and steel grade. a. –Class 1; b. –Class 2



c.

Figure 3 – Minimum weight of optimized cross-section Class 3 in function of beam length and steel grade.

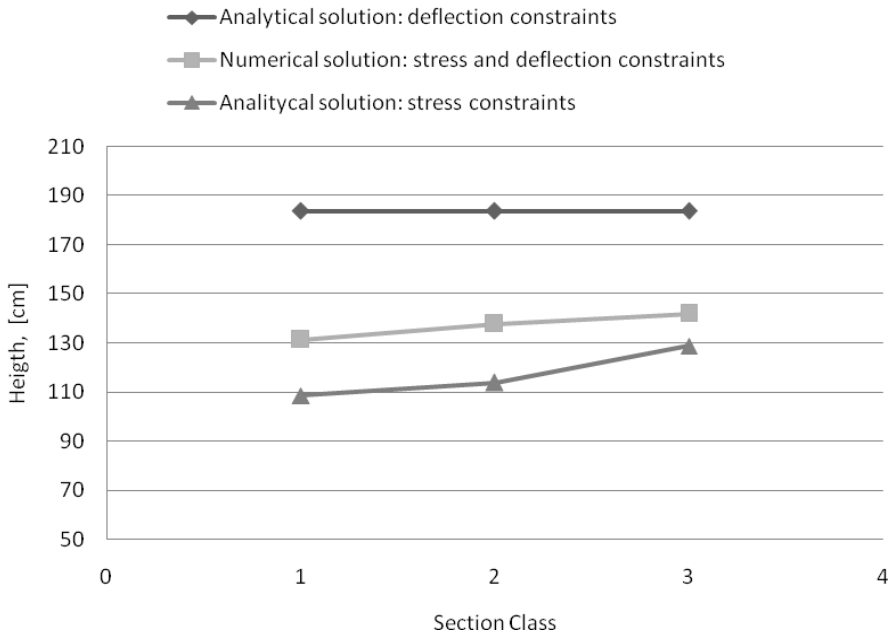


Figure 4 – Optimized height of welded I – beam for S235 steel grade

Note, however, that the optimum height values obtained by numerical solution using both constraints are smaller than the values for the case where only deflection constraint is included in the analytical formulation. Whenever, more constraints are imposed on the system, the optimum cost function value can be expected to increase.

Figure 4 summarizes numerical solutions of optimum design with four discrete variables formulations, for three Classes and steel grades, respectively. Due to the large span, for $L = 25$ m, prevail deflection constraints and the optimum solution not depend on steel grade for Class 1 and 2. Active constraints are given by section 3.

7. CONCLUSIONS

Effective and simple methods of finding minimum (near minimum) weight of a structure, applying requirements from EC3 code, is presented. The paper proposes the cost optimization of I steel girders by means: (i) analytical method and (ii) numerical method. Analytical optimization method should prove useful to structural designers and is expected to advance existing design practices of steel beams. By means of simple formulae derived above and using a simple spreadsheet program, it is possible to compare the characteristics of various length, steel grades and section Classes, which can be useful for designer.

References

1. Arora J.S., *Guide to Structural Optimization*. ASCE Manuals and Reports on Engineering Practice, ASCE, New York, 1997.
2. Farkas, J., Jármai, K. *Analysis and Optimum design of Metal Structures*, A.A. Balkema, Rotterdam, Netherlands, 1997.
3. Bauer, J. A survey of methods for discrete structural design. *Computer Assisted Mechanics and Engineering Sciences*, vol. 1, 27–38, 1994
4. *** Basis of design and actions on structures, EN 1990.
5. *** Design of steel structures, Part 1-1: General rules and rules for buildings, EN 1993-1-1
6. *** Eurocode 3: Design of steel structures - Part 1-5: General rules - Plated structural elements, EN 1993-1-5.
7. *** Microsoft Excell 2007 Spreadsheet
8. Pacurar V., Aribert J.M., (Eds.) *Design of Steel Structures*, Tempus Phare Complem. Meas. Project 01198, Implem. of Struct. Eurocodes in Romanian Civil Engineering Standards, 1997.
9. Axinte E., Rosca V.E., Teleman E.C., *Elements for Steel buildings 2*, Ed. Academic Society “Matei Teiu Botez”, Iasi, Romania, 2011. (in Romanian)

Some Considerations Regarding the Complex Eigenvalues in Structural Analysis

Octavian Victor Rosca

Structural Mechanics Department, Technical University "Gh. Asachi", Iasi, 700241, Romania

Summary

Most of the engineering problems in vibrations are leading to the eigenvalue problem, in the simple or generalized format. It is commonly accepted and convenient to use the real eigenvalues; therefore the matrices of the dynamic system are symmetric and positive defined. Moreover, in the case of the time history analysis the equations of motion are decoupled, based on the assumption that the damping is proportional (Rayleigh type) to the mass or stiffness or both. Under these circumstances the time responses obtained separately can be superimposed using the modal participations.

In the structural analysis there are situations when the eigenvalues and eigenvectors of non- symmetric matrices are requested, even of the complex matrices. Non- proportional damped structures are a part of these systems. The hypothesis of proportional damping is advantageous from the numerical point of view and the experimental tests show that this approximation leads in most cases to acceptable results. However it is not demonstrated yet the proportional behavior of the damping.

This paperwork deals with the numerical problem of the complex eigenvalues. A structural case study of a 3 storey frame tested on the master shaking table of the Laboratory of Earthquake Engineering from the Structural Mechanics Department of the Faculty of Civil Engineering and Building Services from Iasi it is presented.

The analysis conducted to the complex eigenvalues and modal shapes of vibration.

In the end the conclusions of the analysis and the computational effort are depicted.

KEYWORDS: Structural Analysis, Modal Analysis, Complex Eigenvalue Problem.

1. INTRODUCTION

Most of the engineering problems in vibrations are leading to the eigenvalue problem, in the simple or generalized format. It is commonly accepted and convenient to use the real eigenvalues; therefore the matrices of the dynamic system are symmetric and positive defined. Moreover, in the case of the time history analysis the equations of motion are decoupled, based on the assumption that the damping is proportional (Rayleigh type) to the mass or stiffness or both. The damping matrix C is then written as a linear combination of M and K ($C = \alpha M + \beta K$). Under these circumstances the time responses obtained separately can be superimposed using the modal participations.

In the structural analysis there are situations when the eigenvalues and eigenvectors of non-symmetric matrices are requested, even of the complex matrices. Non-proportional damped structures are a part of these systems. The hypothesis of proportional damping is advantageous from the numerical point of view and the experimental tests show that this approximation leads in most cases to acceptable results. However it is not demonstrated yet the proportional behavior of the damping.

Let us consider the solution of the N d.o.f.s dynamic system in the linear vibration:

$$M \ddot{X} + C \dot{X} + K X = 0 \tag{1.}$$

The solution can be written in the vector form:

$$x = q e^{st} \tag{2.}$$

The substitution of (2) in (1) leads to the equation:

$$\left(s^2 M + s C + K \right) q = 0 \tag{3}$$

that has to be provided with the zero determinant in order to obtain a non-trivial solution

$$\det \left(s^2 M + s C + K \right) = 0 \tag{4.}$$

The characteristic eq. (4) is also known as the quadratic form of the eigenvalue problem. The solution leads to $2 N$ eigenvalues and the corresponding $2 N$ eigenvectors (with N components). The general solution of the motion is obtained after the modal superposition of the $2 N$ solutions:

$$x = \sum_{i=1}^{2 N} \xi_i q_i e^{s_i t} \tag{5}$$

where ξ_i are arbitrary constants that are find out from the initial coditions. The eigenvalues are obtained as complex conjugated pairs $s^m = \mu_m + i v_m$ si $s^*m = \mu_m - i v_m$ and the corresponding eigenvectors are written as $q_m = a_m + i b_m$ si $q^*m = a_m - i b_m$. The sollution that corresponds to the “m” DDOF is written:

$$x_m(t) = (c_m + i d_m) e^{(\mu_m + i v_m)t} (a_m + i b_m) + (c_m - i d_m) e^{(\mu_m - i v_m)t} (a_m - i b_m) \tag{6}$$

wher c_m and d_m are arbitrary constants. In order to obtain a damped oscillation in time it must that

$$\mu_m < 0 \tag{7}$$

If all the roots of the eigenvalue problem are complex conjugated, then there will be N solutions of the type and the total response shall be provided by:

$$x = \sum_{m=1}^N x_m \tag{8}$$

The eq. (6) can also be expressed in tthe exponent form:

$$x_m(t) = e^{\mu_m t} (v_m \sin v_m t + w_m \cos v_m t) \tag{9}$$

where:

$$v_m = -2 (d_m a_m + c_m b_m) \tag{10.a}$$

$$w_m = 2 (c_m a_m - d_m b_m) \tag{10.b}$$

and c_m si d_m are arbitrary constants that are calculated from the 2 N initial conditions. The final solution is of real type.

The quadratic eigenvalue can be transformed into a linear or standard problem. The transformation to the generalized (linear) form is presented. A displacement and velocity vector will be assembled, in a similar manner as that used in the state-space:

$$z = \begin{bmatrix} \dot{x} \\ x \end{bmatrix} \tag{11}$$

and the equations of motion are written:

$$\begin{cases} M \dot{x} - M \dot{x} = 0 \\ M \ddot{x} + C \dot{x} + K x = 0 \end{cases} \tag{12}$$

or, in matrix format:

$$\begin{bmatrix} 0 & M \\ M & C \end{bmatrix} \begin{bmatrix} \ddot{x} \\ \dot{x} \end{bmatrix} + \begin{bmatrix} -M & 0 \\ 0 & K \end{bmatrix} \begin{bmatrix} \dot{x} \\ x \end{bmatrix} = \begin{bmatrix} 0 \\ 0 \end{bmatrix} \tag{13}$$

that leads to:

$$A \dot{z} = B z \tag{14}$$

where

$$A = \begin{bmatrix} 0 & -M \\ -M & -C \end{bmatrix} \tag{15}$$

$$B = \begin{bmatrix} -M & 0 \\ 0 & K \end{bmatrix} \tag{16}.$$

and

It is selected a solution of the form $z = v e^{s t}$. The replacement in (14) leads to the generalized eigenvalue problem

$$B v = s A v \tag{17}$$

Just like in the case of undamped vibrations, the v_i vectors are orthogonal with respect A and B:

$$v_i^T A v_j = 0 \quad , \quad s_i \neq s_j \tag{18.a}$$

$$v_i^T B v_j = 0 \quad , \quad s_i \neq s_j \tag{18.b}$$

and are normalized over the A matrix, thus leading to:

$$v_m^T A v_m = 1 \quad , \quad m = 1, 2, \dots, 2 N \tag{19}.$$

If we define the modal matrix V and the spectral matrix S of the 2 N eigenvectors v, like in the case of the standard eigen problem, we obtain:

$$V^T A V = I \tag{20},$$

$$V^T B V = S \tag{21}.$$

The shift from the generalized problem to the standard one is performed by pre-product of B^{-1}

$$B^{-1} A v = \frac{1}{s} v \tag{22}$$

thus leading to:

$$D v = \gamma v \tag{23}.$$

wher $D = B^{-1} A$ and $\gamma = 1 / s$. The D is the dynamic matrix and is defined thereby:

$$D = \begin{bmatrix} 0 & I \\ -K^{-1} M & -K^{-1} C \end{bmatrix} \quad (24)$$

where $K^{-1} M$ is the dynamic matrix in the case of the free undamped vibrations.

2. CASE STUDY

It is considered the modal analysis of a 3 storey steel frame as depicted in the Figure no.1. For the dynamic model 3 translational DOFs are granted along the OX direction and numbered as shown. In order to simplify numerically the case study the masses, the storey stiffnesses and the damping coefficients are scaled and the system matrices are defined below.

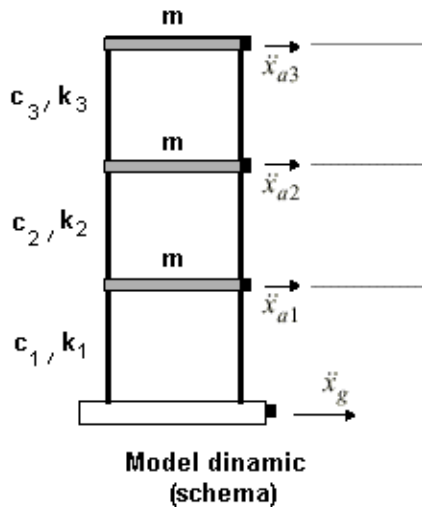


Figure 1

The mass matrix is considered diagonal, with equal uncoupled masses at each level. Masses are normalized to unit.

$$M = \begin{bmatrix} 1 & 0 & 0 \\ 0 & 1 & 0 \\ 0 & 0 & 1 \end{bmatrix} [I] \quad (25)$$

The stiffness matrix (scaled):

$$K = \begin{bmatrix} 398.6465 & -199.3233 & 0 \\ -199.3233 & 398.6465 & -199.3233 \\ 0 & -199.3233 & 199.3233 \end{bmatrix} [I] \quad (25)$$

The modal analysis in the field of real eigenvalues was performed by taking into account a stiffness proportional damping (i.e. $C = \beta K$, $\beta = 0.01$ (1%)). It resulted a proportional damping matrix:

$$C = \begin{bmatrix} 3.9865 & -1.9932 & 0 \\ -1.9932 & 3.9865 & -1.9932 \\ 0 & -1.9932 & 1.9932 \end{bmatrix} [I] \quad (26).$$

Using this model as basis, a non- proportional damping shall be added. We consider the first diagonal term of C affected by an arbitrary coefficient (ex. ff = 8.5)

$$C_{np}(1, 1) = ff * C(1, 1) \quad (27);$$

thus the non- proportional damping matrix becomes:

$$C_{np} = \begin{bmatrix} 33.8850 & -1.9932 & 0 \\ -1.9932 & 3.9865 & -1.9932 \\ 0 & -1.9932 & 1.9932 \end{bmatrix} [I] \quad (28).$$

Now, by applying the complex eigenvalue process described in the previous chapter one obtains:

- The complex spectral matrix:

$$\Lambda_{np} = \begin{bmatrix} -3.5787 + 22.5706i & 0 & 0 & 0 & 0 & 0 \\ 0 & -3.5787 - 22.5706i & 0 & 0 & 0 & 0 \\ 0 & 0 & -14.6445 + 8.7259i & 0 & 0 & 0 \\ 0 & 0 & 0 & -14.6445 - 8.7259i & 0 & 0 \\ 0 & 0 & 0 & 0 & -1.7091 + 7.0185i & 0 \\ 0 & 0 & 0 & 0 & 0 & -1.7091 - 7.0185i \end{bmatrix} \quad (29)$$

After sorting descending the diagonal elements and the computation of their modullus, one obtains:

- the circular frequency vector:

$$\omega_{np} = \begin{bmatrix} 7.2236 \\ 7.2236 \\ 17.0471 \\ 17.0471 \\ 22.8526 \\ 22.8526 \end{bmatrix} [\text{rad/s}] \quad (30).$$

- The complex modal matrix:

$$V_{np} = \begin{bmatrix} 0.0217 - 0.0368i & 0.0217 + 0.0368i & -0.0024 + 0.0550i & -0.0024 - 0.0550i & -0.0045 + 0.0102i & -0.0045 - 0.0102i \\ 0.0701 - 0.0365i & 0.0701 + 0.0365i & -0.0121 + 0.0138i & -0.0121 - 0.0138i & -0.0312 - 0.0183i & -0.0312 + 0.0183i \\ 0.0976 - 0.0348i & 0.0976 + 0.0348i & -0.0080 + 0.0007i & -0.0080 - 0.0007i & 0.0202 + 0.0084i & 0.0202 - 0.0084i \\ 0.2209 + 0.2151i & 0.2209 - 0.2151i & -0.4441 - 0.8260i & -0.4441 + 0.8260i & -0.2140 - 0.1371i & -0.2140 + 0.1371i \\ 0.1367 + 0.5545i & 0.1367 - 0.5545i & 0.0568 - 0.3083i & 0.0568 + 0.3083i & 0.5250 - 0.6383i & 0.5250 + 0.6383i \\ 0.0774 + 0.7443i & 0.0774 - 0.7443i & 0.1112 - 0.0809i & 0.1112 + 0.0809i & -0.2627 + 0.4259i & -0.2627 - 0.4259i \end{bmatrix} \quad (31)$$

The above matrix is computed for the standard problem of 2N order, $D_{np} v_{np} = \gamma_{np} v_{np}$ and the eigenvectors are transformed for the real system with N GLD.

- The complex shapes of vibration are:

$$X_{np} = \begin{bmatrix} 0.3165 - 0.2638i & 0.3165 + 0.2638i & 1.0000 - 0.0000i & 1.0000 + 0.0000i & -0.0364 - 0.3054i & -0.0364 + 0.3054i \\ 0.7560 - 0.1050i & 0.7560 + 0.1050i & 0.2608 + 0.2091i & 0.2608 - 0.2091i & 1.0000 & 1.0000 \\ 1.0000 - 0.0000i & 1.0000 + 0.0000i & 0.0198 + 0.1453i & 0.0198 - 0.1453i & -0.5999 + 0.0819i & -0.5999 - 0.0819i \end{bmatrix} \quad (32)$$

The complex modal shapes of the first and second mode of vibration are depicted in the complex space in the Figure No.2.

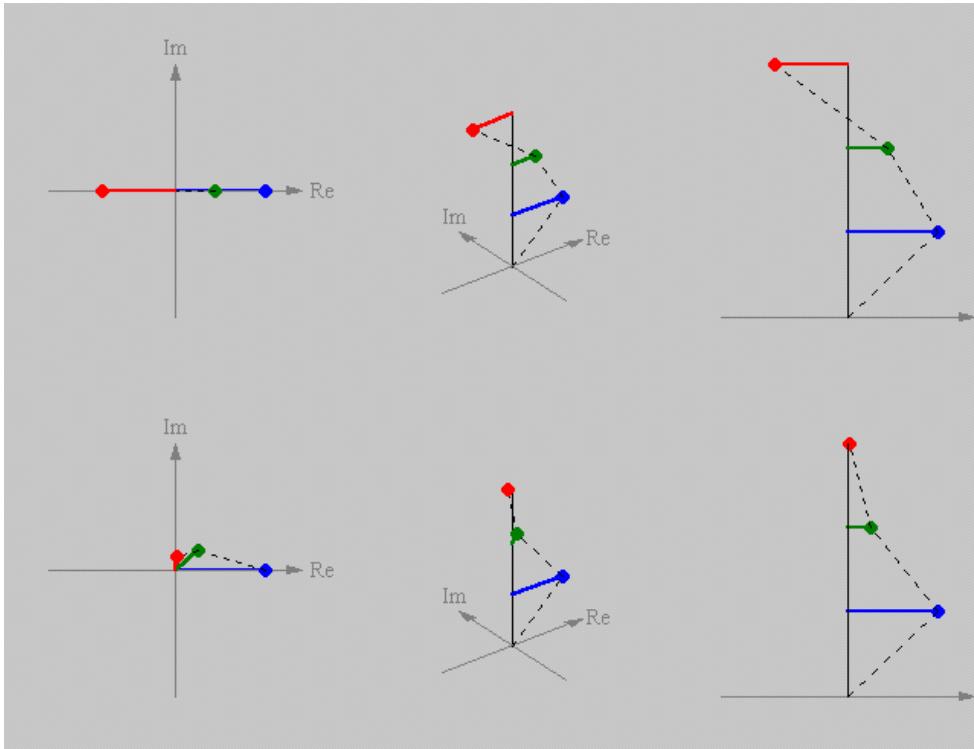


Figure 2 The complex modal shapes of vibration

3. CONCLUSIONS

This method is suitable for the solution of problems with non-proportional damping and it consumes a lot of operations. Broadly speaking, the solution of an eigenvalue problem consumes N^3 operations (3rd order problem). The quadratic problem requires the solution of a $2N$ order system and it follows that the number of operations is 8 times bigger. In the case of a large eigenvalue problem, the performance of the solver is dramatically decreased. Under these circumstances, a balance between the costs and the Rayleigh assumption might be useful, thus leading to good results, but not necessarily exact.

References

1. J. L. Humar, Dynamics of Structures, Prentice-Hall, N.J., 1990.
2. K. J. Bathe, Edward L. Wilson, Numerical Methods in Finite Element Analysis, Prentice-Hall Inc., Englewood Cliffs, New Jersey, 1976.
3. K.J. Bathe, Finite Element Procedures in Engineering Analysis, Prentice-Hall Inc., Englewood Cliffs, New Jersey, 1982.
4. J. H. Wilkinson, C. Reinsch, Linear Algebra, vol. II of Handbook for Automatic Computation, Springer Verlag New York, 1971.
5. J. H. Wilkinson, The Algebraic Eigenvalue Problem, Clarendon Press, Oxford, 1978.
6. P. Hood, “Frontal Solution Program for Unsymmetric Matrices”, Int. J. Num. Meth. Engng, 10, 379-399, (1976).
7. K. J. Bathe, E.E. Wilson, “Large Eigenvalue Problems in Dynamic Analysis”, J. Engng Mech Div., ASME, 1972, 98, pp.1471-1485.
8. A. Perdon, G. Gambolati, “Extreme Eigenvalues of Large Sparse Symmetric Matrices by Rayleigh Quotient and Modified Conjugate Gradients”, Comput. Meth. Appl. Mech. Engng., 1986, 56, 251-254.
9. X. Wang, J. Zhou, “An Accelerated Subspace iteration Method for Generalized Eigenproblems” Comps. & Struct., 1999, 71, pp. 293-301.
10. Octavian V. Rosca, Ioan P. Ciongradi, “Metode numerice utilizate în programele de calcul automat al structurilor” Ed. Acad. Society “Matei-Teiu Botez”, Iasi, 2003.

URGENT1 - Software for planning and simulation of emergency evacuation using auto transport

Neculai Scîntei, Augustin-Ionu? Gavrila
"Gh.Asachi" Technical University, Iasi, 70050, Romania

Summary

The program URGENT1 was applied in a case study that simulated and planned decisions regarding population evacuation in emergency situations in a particular area. This program resolved the following problems: transportation plan, the making of the convoys, displacement itineraries, diagrams of population evaluation, it generated maps with information's regarding places, convoys, road segments, being of real use in training personnel that is responsible of population evacuation in cases of emergency.

KEYWORDS:emergency situation, population evacuation, simulation, deployment itinerary, evacuation diagrams, transport plans.

1. INTRODUCTION

Motto: "Human safety should be the supreme law."

Marcus Tullius Cicero

Population protection, of property and implementation of safety measures regarding the environment are the responsibilities of every human trough his actions.

Opportune and effective intervention is no longer possible trough the standard procedures that are based on approximate evaluations and experimental based decisions. In this case it is necessary to have knowledge in probabilistic evaluation regarding nature, content and quantity parameters of the phenomena that can produce calamity. Following this new parameters well based decisions can be made.

Intensified disasters and human crisis will lead to a raise in need of the *Inspectorate for Emergency Situations*, component of the National Emergency Situations Management system, to prevent and manage emergency situations, especially the capacity of the operative structures from within the system.

Prevention and risk reduction in the case of disasters, population and property protection against the negative effects of the emergency situations are a part of the specific activities of civil protection that must have permanently the capacity of a credible response, corresponding to the degree of danger in which the population is.

A strategic objective from the National strategy of civil protection in Romania is accomplishing preventively the measures of civil protection through population evacuation, protection of property and cultural or archival values having in mind minimal destructive effect and/or military intervention. This objective can be accomplished through firm and opportune measures, enhancing the capacity of intervention of the forces and resources, through the mobilization and requisition of resources and using the protection and intervention plans drawn in peace time, after reviewing and updating them.

This paper wants to be a stepping stone for the analysis, design and implementation of a integrated informatics system, capable to plan and simulate terrestrial transportation in the case of a disaster that requires population evacuation, material property moved from an affected area or one in the process to be affected, all being done well organized, and assuring their safety in an area with better conditions.

2. PLANNING AND ORGANIZING TRANSPORTATION ON THE TRAFFIC ROUTE IN EMERGENCY SITUATIONS

Traffic management of the transports is made having a good knowledge and operative skills on all the phenomena specific to these activities. The complexity of traffic management determines the replacement of the methods based on intuition and experience with scientific methods, all this being made for rationalizing the technical potential of execution transport missions in case of an emergency. Traffic management can have the following systemic approach: decisional subsystem – its role is regulatory in the system; operational subsystem of execution – which has the role of moving the decision in the action plan; information subsystem – which has the role to link the other two subsystems.

Organizing the evacuation procedure consists of: analysis of the emergency situation, prognosis regarding the evolution of the situation, determination of the destructive effects of the emergency, establishing first-aid emergency actions, recognition of the itinerary and areas where the evacuation is in effect, updating the evacuation plan and applying it, elaboration and transmission of the order/disposition of evacuation.

Traffic management on terrestrial routes will have as objective harmonizing the activities and correlation between decisional entities and execution ones.

The complexity and dynamic of the activities during an emergency situation imposes the amplification of collaboration between the decisional factors from the structure of the Ministry of Administration and Internal Affairs with other organs from state administration and public institutions with attributions in mobilization and evacuation.

3. SOFTWARE FOR PLANNING AND SIMULATION OF EMERGENCY EVACUATION USING AUTO TRANSPORT - URGENT1

Taking into consideration that lately there are more and more emergency situations, therefore more victims and affected areas, it is necessary to find more effective ways of intervention and saving population in dire situations through the evacuation in safer districts/areas using the advantages of modern techniques in planning, organizing, development and leading interventions.

The goal is making a software for optimized planning of population evacuation and rescue from a clearly marked area using traffic management in the given terrestrial transportation situation considering different degrees of emergency for affected districts. Taking into consideration that the railway infrastructure is underdeveloped in the endangered area it is considered that the model should contain only pedestrian evacuation with auto means of transportation using the national, regional and rural network of roads. Also the main concern is follow-through on every step of the evacuation regarding the support needed for the human decision factors with the purpose of ensuring the necessary information in taking decisions in respect to the given manpower and ways of intervention.

4. STRATEGIES, METRICS AND THE ALGORITHM OF EVACUATION

```
while( $\exists i = \underline{UnsafeLocality}^*$  so that  $\underline{ActualPopulation}[i] > 0$ )
/**test UnsafeLocality: population*EmergencyDegreeEvacuation*(1-safety)>0
{
  i=ChooseUnsafeLocality(strategy**, distance**, EstimateTime, ActualPopulation,
VehicleCover)
/**: examples of strategies:
//MaximumProfit:
MaximalDistance/MaximalPopulation/MaximalEmergencyDegreeEvacuation...
```

```

//MinimumRegret: MinimalTime for evacuation of local population from selected area
//***distance – may be considered aproximate, on the shortest route possible,
//or taking into consideration degrees and
//time intervals to cover area arcs
if( $\exists$ CoveringVehicles[i])
{
j=EvacuationPlanning(i);
//considering:
//time for loading, transport and unloading
//anterior planning, degrees and intervals of occupancy
//of road arches from the road network involved in evacuation
EvacuationStart(i, j, SelectedPath, ComputedTimeIntervals, NecessaryStops)
}
else {
j=ChooseSafeSource(AvailableVehicles,TimeIntervals,
NeededSmallBusses,NeededBusses,NeededCoachBusses)
SendHelp(j,i,way, TimeInterval, NeededSmallBusses,
NeededBusses,NeededCoachBusses)
}
}

```

5. CASE STUDY

In this paper it was considered for exemplification a coded locality TF with a maximum degree of emergency evacuation and with a population of 13.573 people at which it is added the population of the nearby codified villages, 2.696 people.

Comparing the available auto transport capacities with the necessary of transport of the existing population in the locality TF at the initial moment T_0 it was decided to solicit help for supplementary transport capacity for a number of 1.020 people like this: from the codified locality VS – 370 places representing 5 small buses with 20 seats each, 3 buses with 40 seats each and 3 coach buses with 50 seats each from the coded locality RM – 650 places given by 10 small buses, 5 buses and 5 coach buses.

Following the diagram of the effective number of people situated in the coded locality TF it is observed that evacuation time, in minutes, of the 2.696 people from the nearby villages that are using for displacement pedestrians convoys and auto transport evacuation and the fact that the last convoy leaves at the minute 504.

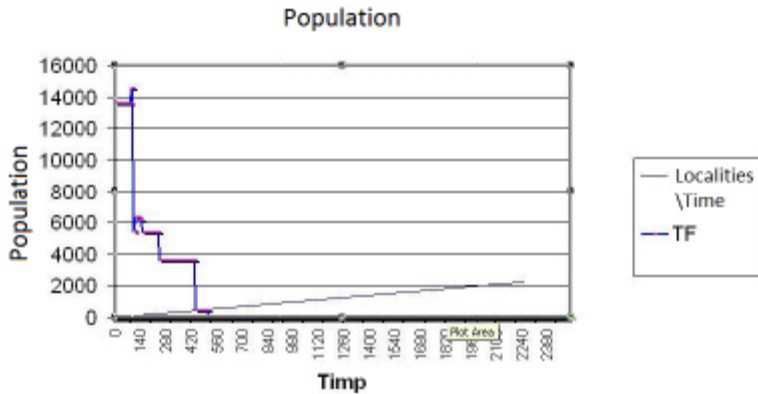


Figure 1. Diagram of the population evacuation development in TF coded locality

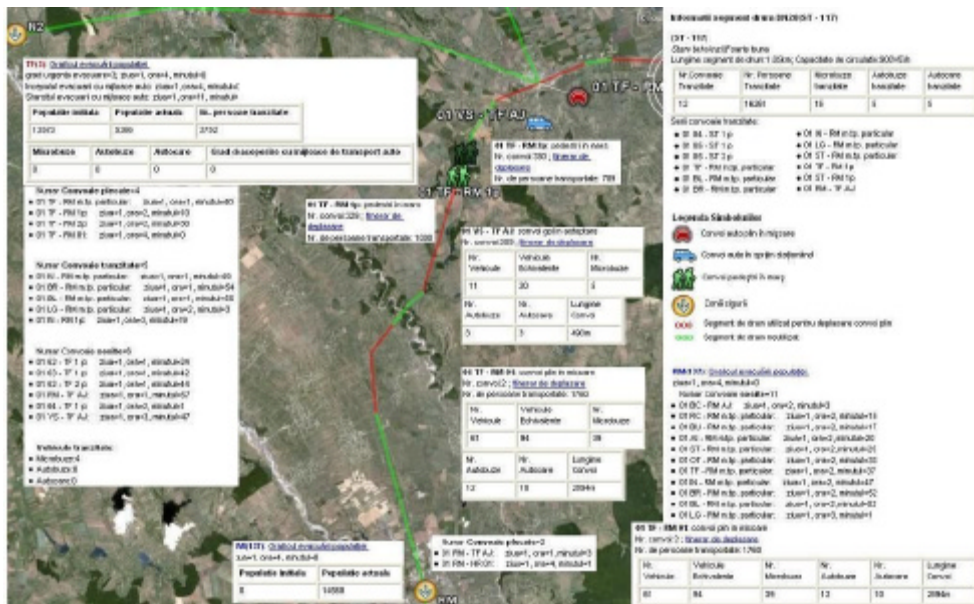


Figure 2. Population evacuation status in the given situation at minute 240

At minute 540 it is observed the 21 small buses convoy moving the last batch of 416 people from the coded TF locality; in this way at minute 561 the operation of evacuation with auto transport is finalized following that in the minute 663 the last pedestrian convoy, 01 TF – RM 02 p, to reach the safe coded locality RM.

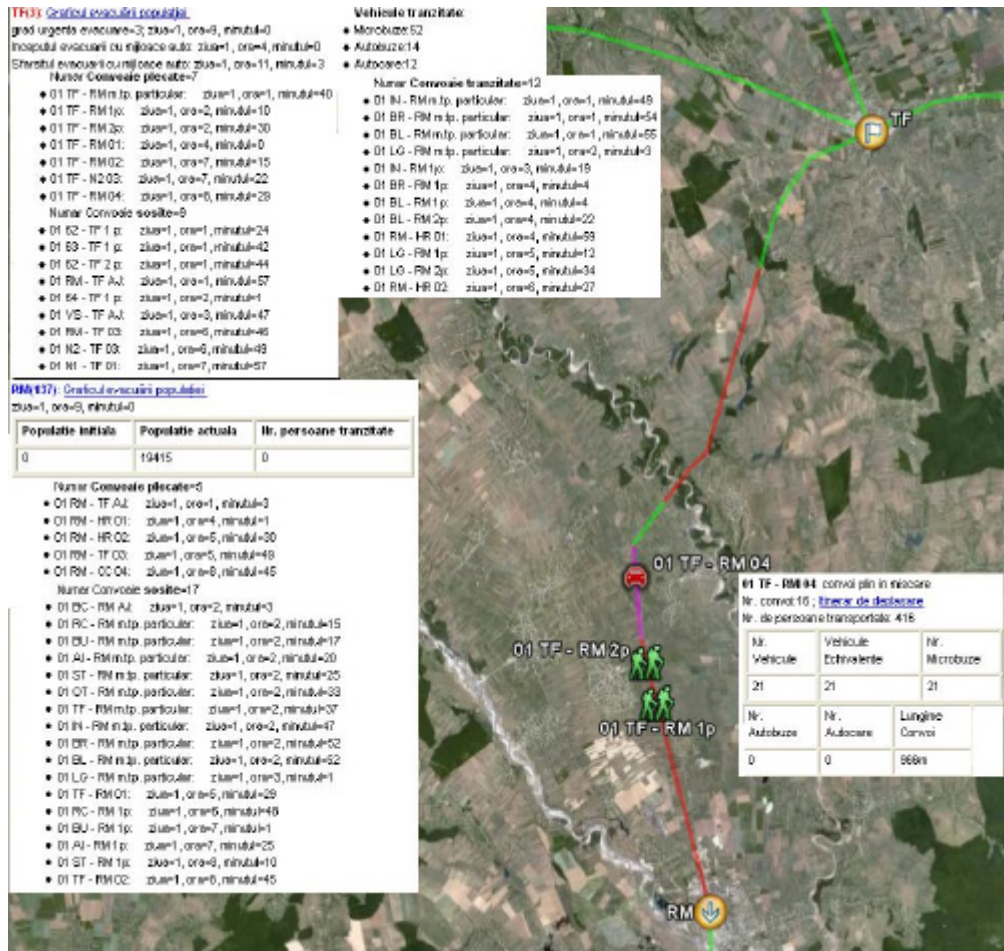


Figure 3. Population evacuation status at minute 540 in the given TF coded locality

6. CONCLUSIONS

The authors of this paper feel that the proposed goal was acquired, the design of a software for simulation, planning and optimization of risk and uncertainty condition decision making involving population evacuation using auto transport in emergency situations – URGENT1. This was made taking into consideration areas with different levels of danger, the terrestrial road system, the existing and supplemented road transportation using heuristics for time optimization in evacuating with minimal risk taking.

The software URGENT1 was applied at a given study case for simulating, planning and optimizing decision making regarding population evacuation in emergency situations from an area affected for one day and 17 hours with a positive result. This software resolved the following problems: transport plan, map generation with information's referring to areas, convoys, road segments – at 10 minutes interval having the possibility of being of real help for personnel training in evacuation techniques (extended – of material property also) in emergency situations.

The purpose of this software is to be used at institutional level and also at the level of local administration for the preparation of personnel and population in case of disaster. Using this resource will lead to economy to budgets both financial and material and mainly it would save human life.

References

1. Cascaval Petru, Cascaval Doina: *Modelare si simulare*. Iasi: Ed. Gh. Asachi, 2002. (in Romanian)
2. Croitoru Cornelius: *Tehnici de baza în optimizarea combinatorie*. Iasi: Ed. Univ. Al. I. Cuza, 1992. (in Romanian)
3. Hagi Victor: *Managementul executiei proiectelor de constructii*. Iasi: Ed. Dosoitei. 2003. (in Romanian)
4. Ionescu Gh.Gh., Cazan Emil, Negruta Adina Letitia: *Modelarea si optimizarea deciziilor manageriale*. Cluj-Napoca : Ed. Dacia, 1999. (in Romanian)
5. Ionescu Tiberiu: *Grafuri-aplicatii*. Vol. I, Bucuresti: Ed. Didactica si Pedagogica, 1973. (in Romanian)
6. Ionescu Tiberiu: *Grafuri-aplicatii*. Vol. II, Bucuresti: Ed. Didactica si Pedagogica, 1974. (in Romanian)
7. Luban Florica: *Modelarea si simularea proceselor economice în transporturi*. Bucuresti: Ed. Academia de Studii Economice, 1997. (in Romanian)
8. Lupescu Titus, Rosu Alexandru, Cerchez Mihai: *Programarea matematica cu aplicatii militare*. Bucuresti: Ed. Militara, 1965. (in Romanian)
9. Zarojanu Gh. : *Elemente de tehnica traficului rutier*. Iasi: Ed. Societatii Academice Matei – Teiu Botez, 2002. (in Romanian)
10. Andrei Neculai: *Modele, programe de test si aplicatii de programare matematica*. Bucuresti: Ed. Tehnica, 2003. (in Romanian)
11. Legea nr. 481 din 08.11.2004 privind protectia civila, cu modificarile si completarile ulterioare.
12. Hotărârea Guvernului României nr.547 din 09.06.2007 pentru aprobarea Strategiei nationale de protectie civila. (in Romanian)
13. Hotărârea Guvernului României nr.762 din 16.07.2008 pentru aprobarea Strategiei nationale privind prevenirea situatiilor de urgenta. (in Romanian)
14. Ordinul ministrului administratiei si internelor nr. 1184 din 06.02.2006 pentru aprobarea Normelor privind organizarea si asigurarea activitatii de evacuare în situatii de urgenta. (in Romanian)

Implementation of a Geotechnical GIS Database for 3D Modeling of the Layer Limit Surfaces

Ana-Luciana Tofan, Vasile Musat

Department of Roads, Railways, Bridges, and Foundations, Technical University "Gh. Asachi", Iasi, 700050, Romania

Summary

The existing plans and maps can be one of the methods for data acquisition needed for implementing a geotechnical GIS database. They contain a large amount of qualitative and quantitative information, available at different scales. Graphic data collection on plans and maps can be achieved by scanning, digitizing or automatic vectorization, processes in which the collected data are converted from analog to digital format.

The first stage of this work used information from 9 topographic plans at 1:1000 scale in analog (scanned) format, covering the center of Iasi, resulting the 3D terrain model, which is also the surface of the filling layer. In this sense, were through the stages of georeferencing, digitization, delimitation of the study area, entry of known rate points found on the scanned plans, ending with the implementation of 3D model and contour levels for the surface layer. Autodesk Map 3D, GTX and TopoLT platforms were used for these achievements.

Similarly, using the other stratification data, which has been classified as loess layer, water bearing layer, impermeable layer and lower layer, extracted from the existing geotechnical data of the boreholes performed on the study area, the steps of introducing corresponding rates were driven again, resulting the 3D models and contour levels.

KEYWORDS: GIS database; geotechnical data; Z-coordinate; 3D Model; contour levels.

1. INTRODUCTION

Currently, the Internet is known as the most efficient way through which large amounts of information circulating throughout the world with amazing speed and trough information technology were developed and develops data management systems with spatial location. The technology that purchases, integrates and

provides spatial data is called "Geographic Information System" (GIS) and nowadays it is continuously growing, serving as a computerized tool for mapping and analysis of all elements that exist and events happen in the world. It integrates common database operations such as query and statistical analysis with unique advantages of maps for viewing and analyzing geographic spatial data.

Since maps are the most important way to represent graphic information, a GIS is combining their data, satellite images and aerial photos with alphanumeric databases containing information on graphical data. Geographic Information Systems allow to create maps, integrate information, visualize scenarios, solve problems with high difficulty and developing effective solutions in a new easy to use approach.

In order to obtain real-time spatially referenced data, it is necessary to achieve an integrated computerized support. This paper uses as a means of digital graphic data acquisition 1:1000 scale topographic plans, resulting from scanning and on-screen digitizing.

The main purpose of this paper is to present a method for integration of geotechnical data in a Geographical Information System to highlight changes in 3D surface models of stratification limits.

According to the specialized literature, a solution for solving this problem can be given by geostatistical methods, which can be used to better understand the spatial variations of soil characteristics (Akbarzadeh & Taghizadeh, 2010), by providing tools for analyzing spatial data and estimating unknown values (Isaaks & Srivastava, 1989).

Generally, these approaches using Geographic Information Systems technology involves difficulties when estimating 3D spatial variables due to loss of the Z-coordinate information (Choi & Park, 2006).

1.1. Study area

The considered study area for processing and synthesis of geotechnical data for 3D stratifications developing represents the part of Iasi with the highest occupancy of buildings, this forming the nucleus around which the city has been developed over time. The built background on the area under discussion incorporates both historical buildings, most of them being declared monuments (Palace of Culture, Three Hierarchs Church, Metropolitan Cathedral, National Theatre, Roznovanu Castle, Philharmonic Moldova, Union Museum, V. Alecsandri Museum, Natural Sciences Museum, Armenian, Barboi, Banu, Lipovenian Churches, etc.) and recent buildings (residential, administrative establishments, banks, hotels, family homes, public buildings and social services, catering, etc.).

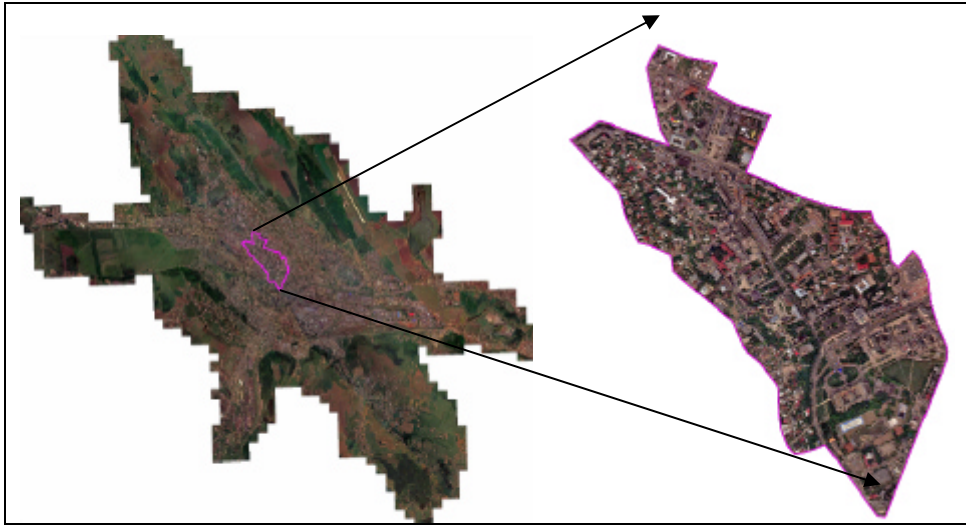


Figure 1. Location of study area in Iasi county

1.2. Sources for both graphic and alphanumeric data acquisition

This paper uses the following sources as means for digital graphic data acquisition:

- a) orthophotomap of Iasi, air-photographed in 2005;
- b) topographic plans in analog format at 1:1000 scale;
- c) the layout of boreholes plans, according to geotechnical documentation;
- d) boreholes stratification sheets, according to geotechnical documentation (figure 2).

The corresponding Z-coordinate for each layer were extracted in a first stage from the geotechnical boreholes sheets (insufficient), and for the 3D Model implementation of the filling layer surface, leveling network points whose rate is specified on the scanned maps and plans are used (figure 2.b).

However, for achieving the 3D Models of the other layer limit surfaces (loess layer, bearing water layer, impermeable layer, lower layer), the problem occurs in determining the Z coordinate of the points whose rate is known in the filling layer, but not known for the other layers and only the insufficient data from geotechnical boreholes sheets can be used.

involves the use of specialized GIS software functions for data cleaning, data integration and topologies establishment. (Bofu & Chirila, 2007)

Graphic information was taken using raster format topographic plans (trapezoids) at the scale 1:1000 (data acquisition from existing maps and plans), image air-photographed in 2005 (data acquisition from photogrammetry) and the layout of boreholes plans in accordance with geotechnical documentation.

2.1. GIS data acquisition

The existing maps and plans are the main source for the achievement of a GIS application and the graphic data can be obtained by scanning, digitizing and vectorization, the graphics being converted from analog to digital format.

The achievement of graphic database involves obtaining the digital format for the analyzed study area through various stages. In this chapter are presented other methods different than those used in the paper for data acquisition such as:

2.1.1. *Data acquisition from remote sensing*

Remote sensing data is represented by satellite images obtained by collecting electromagnetic radiation transmitted by objects and transforming them into digital format. The main known data sources are the two remote sensing systems: the U.S. Landsat and SPOT of France.

2.1.2. *Data acquisition from direct measurements*

In this case, data are acquired by direct measurement, which can be performed with total station or GPS equipment. These type of works involves performing measurements in order to identify ownerships or large-scale plans to highlight the planimetric and elevation details. (Bofu & Chirila, 2007)

2.2. Achievement of digital graphic support of the study area by data processing

The 1:1000 scale topographic plans are obtained in analog format by scanning, so still must be processed with specialized software (Autodesk Map and RasterCad GTX Plus) to obtain digital format for the area. In this sense, several steps are performed as follows:

2.2.1. *Calculation of the topographical plans cartographic elements*

a. Inventory of existing database

Cadastral territory of the study area is placed within the municipality on a number of 2 plans at 1: 5000 scale, 5 plans at 1:2000 scale and 9 plans at 1: 1000 scale (table 1).

Table 1. Plans inventory of the study area

Scale	No	Name	Editing year	Edited by	Projection
1:5000	2	L-35-32-A-c-4-III L-35-32-C-a-2-I		I.P.T.A.N.A.	Local-Iasi
1:2000	5	L-35-32-A-c-4-III-3 L-35-32-A-c-4-III-4 L-35-32-C-a-2-I-1 L-35-32-C-a-2-I-2 L-35-32-C-a-2-I-4		I.P.T.A.N.A.	Local-Iasi
1:1000	9	L-35-32-A-c-4-III-3-d L-35-32-A-c-3-III-4-c L-35-32-C-a-2-I-1-b L-35-32-C-a-2-I-2-a L-35-32-C-a-2-I-2-b L-35-32-C-a-2-I-2-c L-35-32-C-a-2-I-2-d L-35-32-C-a-2-I-4-a L-35-32-C-a-2-I-4-b	1982/1983	I.P.T.A.N.A.	Local-Iasi

b. The connection scheme of the topographical plans

This scheme contains the plans shown in table 1 along with the (f , ?) geographical coordinates (figure 3).

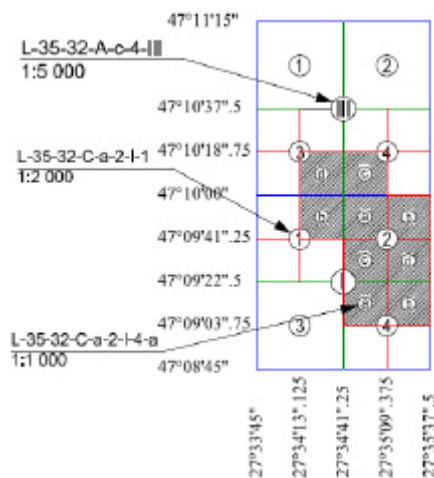


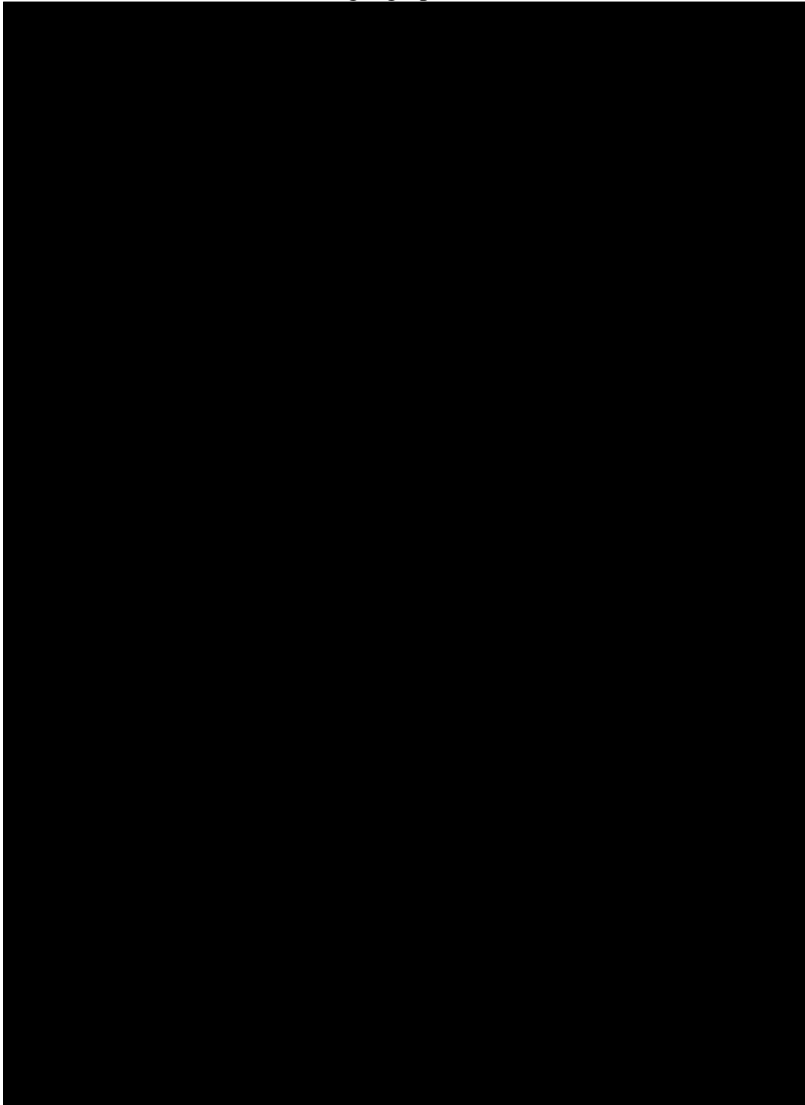
Figure 3. Connection scheme and (f , ?) geographical coordinates

c. The calculation of the (X, Y) stereo-70 coordinates

Based on the geographical coordinates of the topographic plans on Krasovski-1940 reference ellipsoid, it is necessary that they be transformed into rectangular coordinates in stereo-70 projection system applied to our country. This could be achieved using the formulas with constant coefficients as presented in a previous paper. (Tofan, 2011)

The calculus was performed for each 1NW, 2NE, 3SW and 4SE corners of 1:1000 scale topographic plans and are presented in table 3.

Table 3. Stereo-70 and geographical coordinates database

The table content is completely redacted with a solid black box.

d. Attaching and georeferencing raster images

Raster images attaching and georeferencing were conducted in AutoCAD Map using the special functions in the Map menu.

Trapezoids scanned georeferencing is the process through which the images are brought into their spatial position and is of great importance in terms of accuracy and continuity of graphic information as support for future GIS application. Figure 4 shows in left the continuity of the scanned topographic plans obtained by georeferencing and in the right the detachment of the study area in digital format obtained by on-screen digitizing.

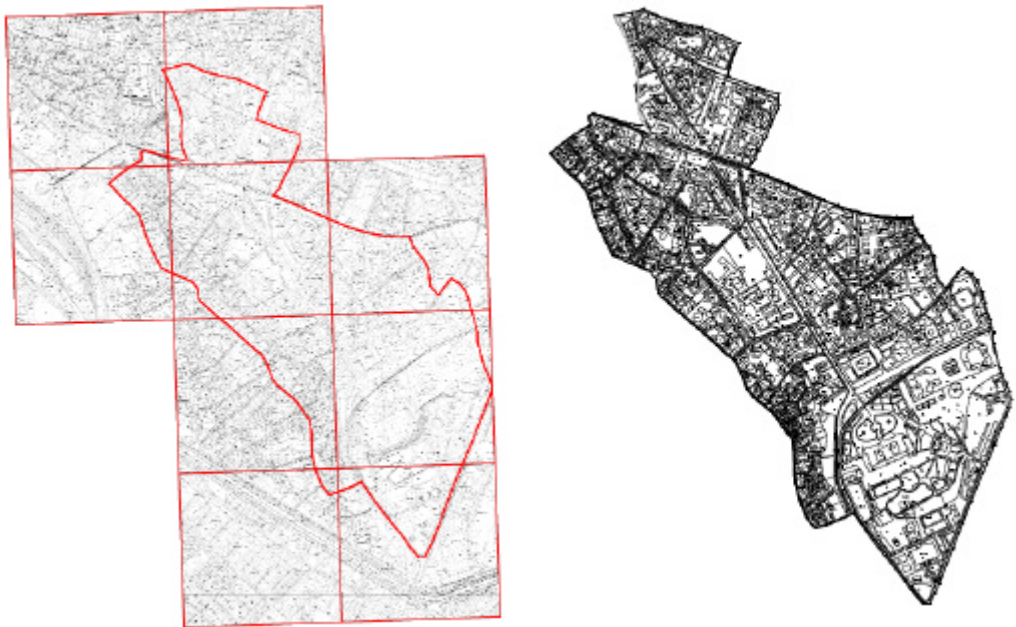


Figure 4. Graphic data processing for the achievement of digital format of the study area

In addition to the steps outlined above, the steps of defining name layers, on-screen digitizing, database defining for each digitized plan and projection system definition are detailed described in the mentioned paper. (Tofan, 2011)

3. IMPLEMENTATION OF ALPHANUMERIC DATABASE AND COUPLING IT WITH GRAPHICS BY DATA CONVERSION

Further, the alphanumeric data and 3D models of layer limits surfaces will be achieved by attaching TopoLT application to Autodesk Map platform.

The TopoLT specialized program provides tools for 2D and 3D applications with which you can create topographical or cadastral plans, 3D terrain model and contour levels, calculate volumes or georeferenced images can be inserted. Functioning of this program is possible for most CAD platforms (Autodesk, Bricscad, CADian, CMS IntelliCAD, progeCAD, ZwCAD), supporting Windows 98 / Me / NT / 2000 / XP / Vista / Windows 7 operating systems.

Under the Autodesk platform, but also for the other programs, TopoLT uses its drawing functions, plus specific program functions necessary to achieve topographical or cadastral plans in digital format. (<http://topolt.com/>)

3.1. Unknown rate point interpolation for each layer using known rate points

In this paper, Z coordinates of unknown points were determined by accessing the interpolation function from the TopoLT program menu. Thus, having the spatial coordinates (X, Y, Z) of a number of 470 points covering the study area and actually forming alphanumeric database, the next step is to convert and attach it to the graphics database.

The calculated rates for each layer (filling layer, loess layer, bearing water layer, impermeable layer, lower layer) were determined “on-screen” (in screen space) and the “.rtf” (rich text format) type files were downloaded accessing the function “Coordinates » Create coordinates table”. Based on them, the “.txt” type files containing PN (point name), X, Y, Z coordinates and code were created for each layer.

In this way, database can always be verified, completed or updated as new information regarding other performed boreholes in the study area are available.

After verifying, completing or updating the alphanumeric database, the next step is to couple it with graphics. This can be done by opening a new “.dwg” file and accessing the function “Coordinates » Draw points” from TopoLT menu, so all points with name, coordinates and code in accordance with those entered in the “.txt” type files are brought into screen space to visualize.

3.2. Coupling alphanumeric database with graphics

For 3D modeling and contour levels achievements, must first relate points of the “.txt” files with Autodesk platform. In this sense, five “.dwg” files were made, one for each surface.

Using the function “Coordinates » Draw Points” from TopoLT menu, must choose the “.txt” file corresponding to each layer. After making all settings and choosing the import method, click OK, and points will be visualized in the screen space. (<http://topolt.com/>)

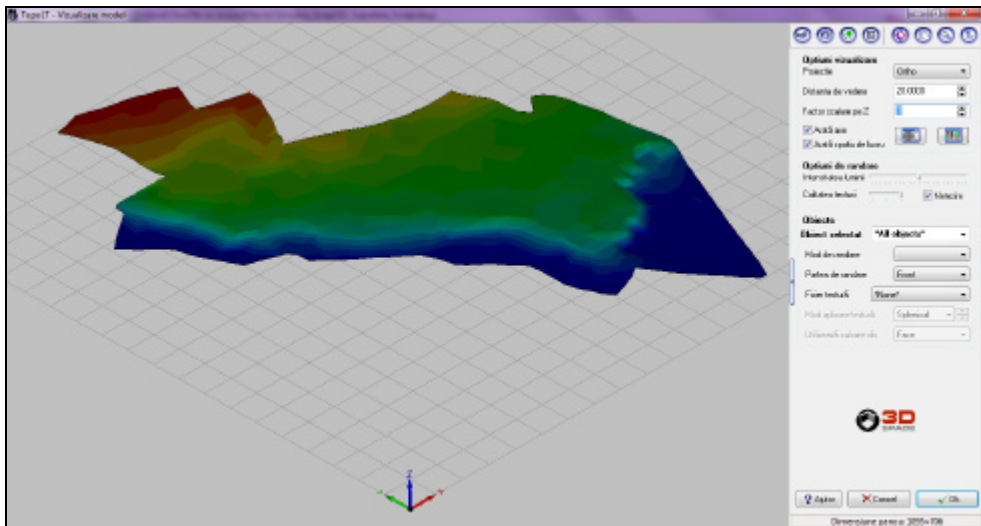
To raise the other entities at their rate, "Transformations Lift-up to points elevations" function must be used.

3.3D MODELS AND CONTOUR LEVELS

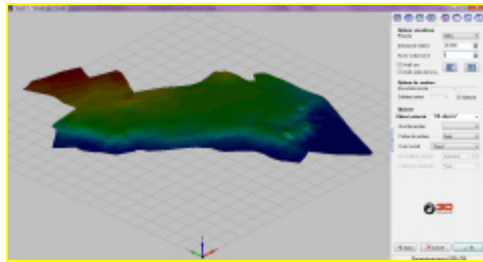
Using the function "3D Model » Build 3D", must select the points, delete points with elevation 0.000 m, select lines or polylines of forced change of the slope (breaking lines), select 3D model boundary (which is the outline of the study area) and models are generated automatically. Finally, a new window is shown where you can view the models, make renderings, choose the projection method, light intensity, quality of texture, whether smooth or not 3D objects, textures (<http://topolt.com/>). The resulting 3D models are presented in figure 5.

To visualize all the 3D models of each layer at once, they have to be brought in a single ".dwg" file using the commands "Edit » Copy", "Edit » Paste to original coordinates" and "3D Model » View 3D model" (figure 6).

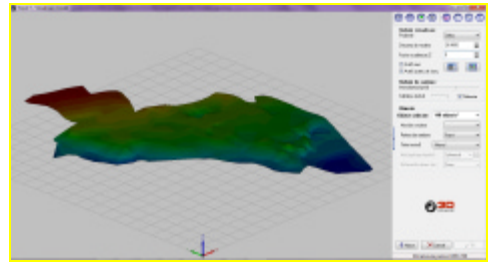
The contour levels are also automatically generated for each layer based on fairness, colors and thicknesses chosen in Program Options (figure 7) by accessing the function "3D Model » Draw contour levels" (<http://topolt.com/>).



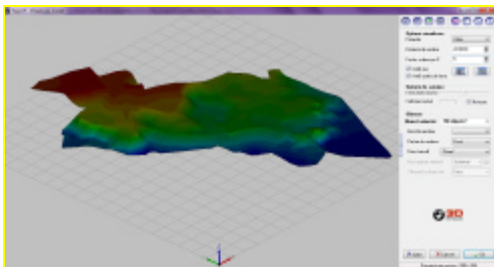
FILLING LAYER



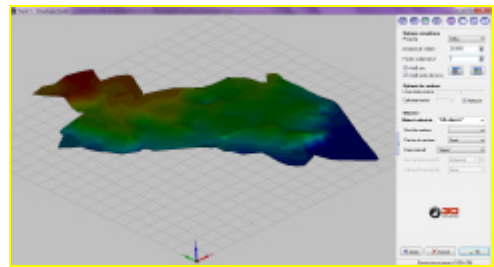
LOESS LAYER



WATER BEARING LAYER



IMPERMEABLE LAYER



LOWER LAYER

Figure 5. 3D Models of the layer limit surfaces

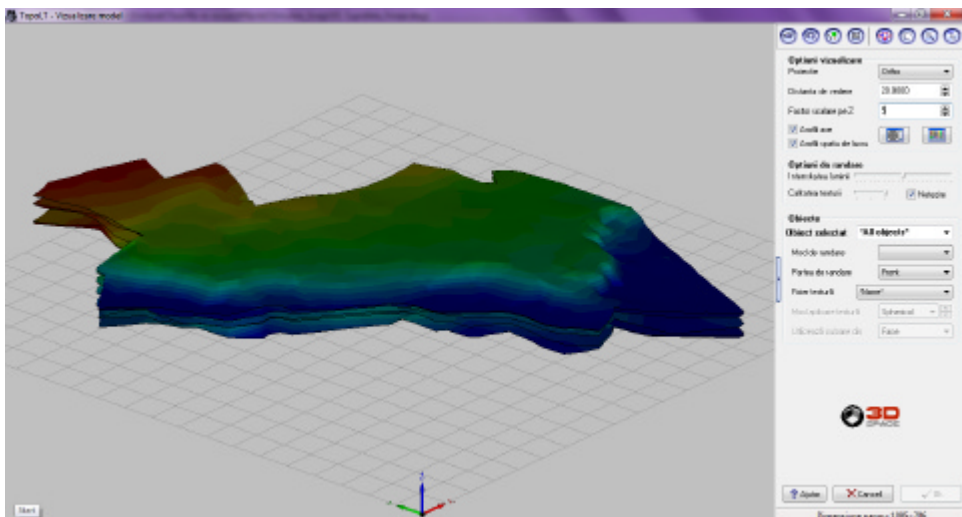


Figure 6. The 3D Model view of all the layer limit surfaces

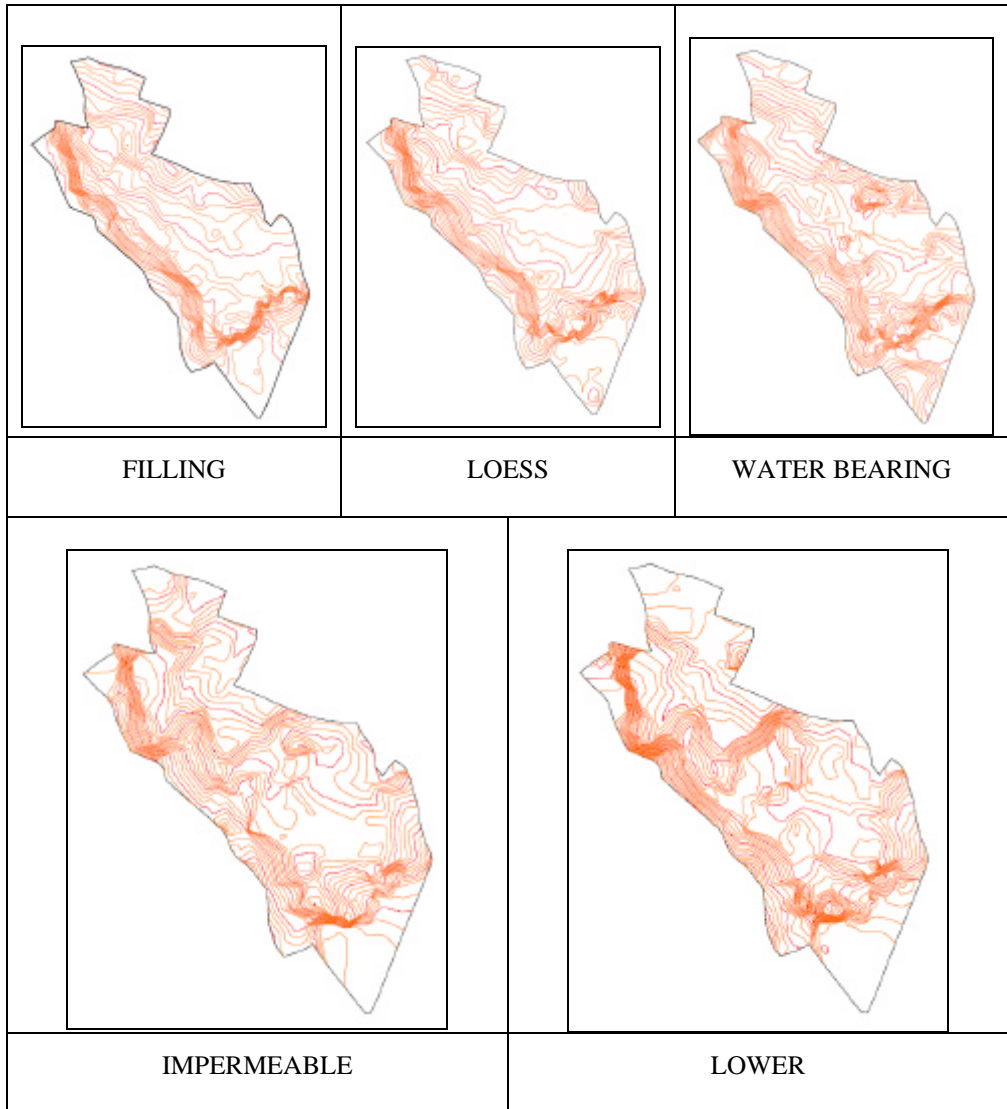


Figure 7. Contour levels of the layer limit surfaces

4. CONCLUSIONS

A system through which is collected, stored, handled, processed, analyzed and visualized all the necessary data at any time determines also a better organization of the existing information for a particular study area.

Such a system can also be achieved for geotechnical engineering by Geographical Information Systems technology, this paper presenting a way to implement a database containing information from scanned maps and plans, as well as from boreholes sheets, to 3D modeling and corresponding contour levels implementation of the layer limit surfaces.

Also these results can be used in establishing the points for factor of ground condition that is taken into account when estimating geotechnical risk.

References

1. Akbarzadeh, A., & Taghizadeh, M. R. (2010). Distributia spatiala a unor proprietati ale solului prin utilizarea metodelor geostatistice în regiunea Khezrabad (Yazd) din Iran. *ProEnvironment* 3 (2010) , 227-236.
2. Bofu, C., & Chirila, C. (2007). *Sisteme Informationale Geografice. Cartografierea si editarea hartilor*. Iasi: Editura Tehnopress.
3. Choi, Y., & Park, H.-D. (2006). Integrating GIS and 3D geostatistical methods for geotechnical characterization of soil properties. *IAEG 2006 Paper number 532* , 1-8.
4. <http://topolt.com/> . (n.d.).
5. Isaaks, E. H., & Srivastava, R. M. (1989). *Applied Geostatistics*. New York.
6. Tofan, A.-L. (2011). Integrarea datelor grafice pentru un areal din zona centrala a municipiului Iasi într-un Sistem Informational Geografic în vederea evaluarii si monitorizarii riscului geotehnic. Al IV-lea Simpozion National "Creatii universitare 2011" .

Numerical Evaluation of the Seismic Behavior of a Load-Bearing Masonry Condominium Structure Specific for Romanian Urban Areas

Ana-Maria Toma¹, Gabriela M. Atanasiu², and Ionut-Ovidiu Toma²

¹*Department of Graphical Communication, "Gheorghe Asachi" Technical University of Iasi, Iasi, 700050, Romania*

²*Department of Structural Mechanics, "Gheorghe Asachi" Technical University of Iasi, Iasi, 700050, Romania*

Summary

The paper presents preliminary results related to the numerical evaluation of the seismic behavior of a load-bearing masonry condominium structure widely met in the Romanian urban areas by means of SAP2000 computer software. The numerical model follows closely the geometry and the loading conditions of a real structure. The seismic behavior was analyzed from the point of view of the fundamental period of vibration, by means of the degradation coefficient, and lateral displacements at the level of each floor. The model was subjected to various earthquake scenarios all of which took place during the life-time of the structure. The obtained results show that there are minor degradations in the structure and, therefore, the safety of the occupants is not jeopardized.

KEYWORDS: non-linear time history analysis, masonry structure, seismic behavior, degradation coefficient.

1. INTRODUCTION

An increase in the number of natural disasters occurring all over the world has been recorded for the past decade. Natural disasters are extreme geological, meteorological or hydrological events that exceed the ability of a community to cope with that specific event. They result, more often than not, in great human, property, and environmental losses, along with social and economic disruptions [1].

Assessing the impact of a natural disaster upon a community is important for many reasons [2-4]. One of the reasons is that the information about disaster impacts can be used to identify specific segments of the community that have been affected or might be affected in the future. Additionally, decision makers can develop disaster impact scenarios before they even occur in order to assess the potential

consequences [5-9]. Due to the increased public awareness to the effects of natural disasters, with particular focus on earthquakes, great emphasis is being placed on the role of disaster mitigation and vulnerability assessment in planning for sustainable development. Communities can use risk and vulnerability assessment results to reduce the impacts from hazards through the development or revision of emergency response, disaster recovery and hazard mitigation strategies [4, 6, 10].

Evaluating the seismic hazard in a region is of critical importance in the field of structural engineering. Although the first scientific efforts in earthquake parameter prediction date back to 67 years, advances made in this field can best be described as sporadic, as described by Panakkat and Adeli, 2008 [11].

Buildings have partially or totally collapsed during recent earthquakes in Turkey 1999, India 2001, Italy 2009, Haiti 2010, Chile 2010 and Japan on March the 11th, 2011. Many of these collapses occurred in older buildings designed according to what nowadays are considered inadequate design standards. Others have been attributed to mistakes made during the design and execution stages. However, several of the collapses took place in buildings that were designed and constructed in accordance with modern seismic design principles. Therefore, as demonstrated by the on-site investigations, it is possible that many of the observed collapses have been the result of deficiencies in our knowledge of the regional seismic hazard, the behavior of structural materials under dynamic loads, and the post-elastic behavior of structural systems [12].

Therefore, from the structural engineering point of view, it is important to assess the behavior of a building during seismic excitations in order to determine whether or not supplementary measures should be taken before such an event occurs in order to prevent the possible collapse of the building. The assessment can be performed either by means of experimental works on scaled down [13] or full-scale models mounted on shaking tables [14, 15] or by means of numerical simulations using advanced software packages. Numerical simulations by means of the Finite



Figure 1. Load-bearing masonry structure

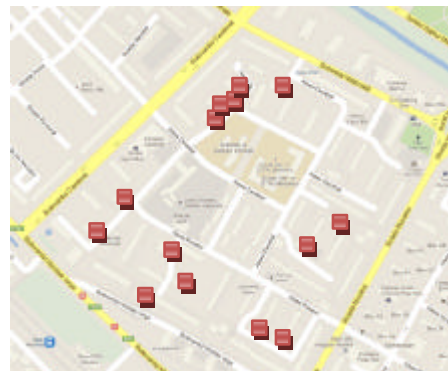


Figure 2. Selected urban sample

Element Method have become a valuable and important tool in the field of Civil Engineering. The application of suitable mathematical algorithms and nonlinear material models allow for the identification of the damage and possible failure modes of a structure subjected to any type of loading scenario [16-20].

The paper presents partial results from the numerical evaluation of the seismic behavior of a load bearing masonry condominium largely used in the Romanian urban areas. The structure is a four-story high load bearing masonry structure, Figure 1, built during the late 1960s and it is a typical condominium type of structure for the city of Iasi and other urban areas in Romania. The selected urban sample is presented in Figure 2. The model was subjected to different earthquake scenarios, all of which took place during the life-time of the structure, and the behavior was investigated from the point of view of the degradation coefficient [21] and peak lateral displacements at each storey level. The paper brings its contribution to the pre-disaster mitigation which is essential to the long-term sustainable development of communities. Risk assessment is an integral part of disaster mitigation. It provides critical information on the characteristics of potential disasters in a region and allows planners to identify and prioritize mitigation opportunities [22, 23].

2. NUMERICAL MODEL

2.1. Geometry, Sections and Materials

A 3D view of the numerical model is shown in Figure 3. It has been generated by means of the performant computer software SAP2000 v.14 [24] following the specifications of Project 1497/1966 [25]. Linear beam elements were used to model the beams and the monolith concrete columns between the masonry panels. The walls and the stair-case, Figure 4, were modeled by means of *Shell Layered / Nonlinear* elements.

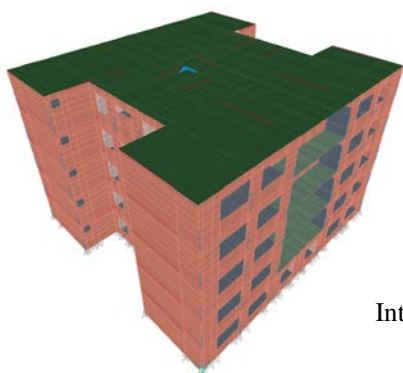


Figure 3. 3D view of the model

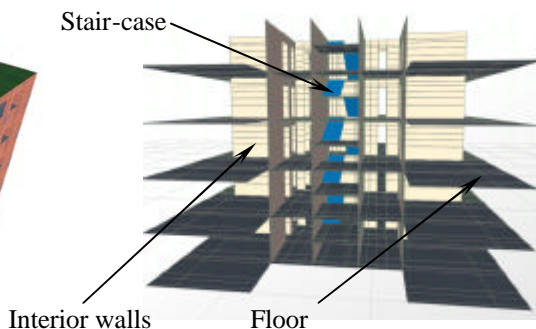


Figure 4. Details of the numerical model

Since floors are generally considered to have an infinite rigidity, only translational degrees of freedom were allowed in the numerical model. All other rotational degrees of freedom were restrained. Additionally, the floors were assumed to behave elastically and were, therefore, modeled using *Thin Shell* elements.

The loggias, floors, stairs and the terrace were made of reinforced concrete class C8/10. The interior and exterior walls were made of masonry. The masonry was modeled as an equivalent concrete material with a mass per unit volume of 1845 kg/m³ and a design compressive strength of 6.1 MPa [26].

2.2. Loading Scenarios

The static loads, except the self weight which is automatically computed by the program, were defined as *Superdead* loads and their design values were selected in accordance to STAS 10101/1-78 [27]. The effect of the snow was also taken into account according to the code prescriptions [28].

The load combinations were defined following the guidelines from CR0-2005 design code [29] both for the fundamental and the special group of loads. In the case of load combination taking into account the effect of the earthquakes, several earthquake scenarios were considered by means of their accelerograms. The considered earthquakes were Vrancea 1977, 1986, 1990 and 2004. All the recordings of the accelerograms were for the city of Iasi [30] with the sole exception for the 1977 earthquake. In this case, the recording made in Bucharest at the headquarters of the Romanian Institute for Building Research was considered [31].

The identification data for each earthquake is presented in Table 1 whereas Table 2 outlines the characteristics of each recording used in the numerical model.

Figure 5 shows the time-history in terms of ground acceleration for the first earthquake from 1990, depicting both the longitudinal and the transversal components. The recording was done at the IAS2 station, as mentioned in Table 1.

Table 1. Identification data for each earthquake scenario considered

Location	Depth [km]	Earthquake code	Code of recording station	Date	Magnitude [Mw]	PGA [m/s ²]
1	109	771	INC1	1977.03.04	7.5	1.95
2	133	861	IAS2	1986.08.30	7.3	1.46
3	91	901	IAS2	1990.05.30	7.0	1.26
4	91	902	IAS2	1990.05.31	6.4	0.46
5	100	041	IAS4	2004.10.27	6.0	0.66

Table 2. Characteristics of the recorded earthquakes

Earthquake Code	Duration [s]	Peak Ground Acceleration (PGA) values				
		Longitudinal component [m/s ²]	Time stamp [s]	Transversal component [m/s ²]	Time stamp [s]	
1	771	40.14	1.62	5.58	1.95	6.12
2	861	21.15	0.641	20.385	1.46	19.93
3	901	31.18	1.262	14.33	1.095	14.61
4	902	26.45	0.389	12.025	0.458	0.52
5	041	73.09	0.582	22.72	0.658	22.81

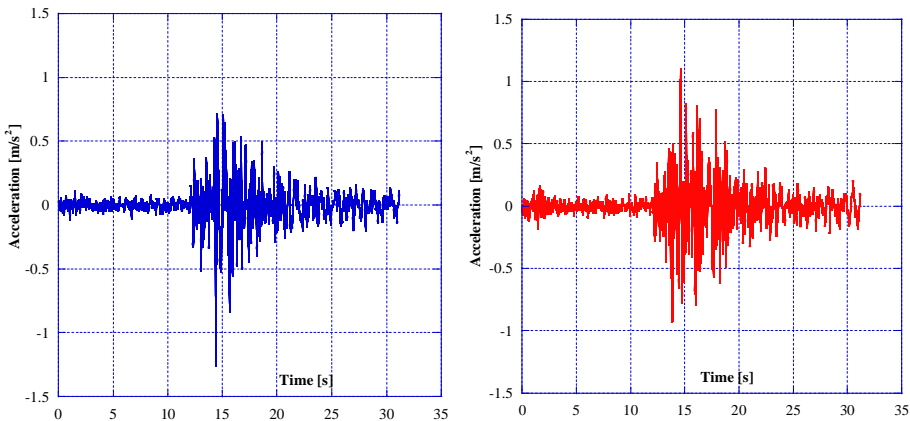


Figure 5. Sample of the first 1990 earthquake recording made at the IAS2 station: longitudinal component (left); transversal component (right)

The non-linear time history analysis was performed by using the Hilber-Hughes-Taylor time integration method [32]. This is an implicit method that allows for energy dissipation and second order accuracy both of which are not possible with the regular Newmark method. As presented in the literature [33], the method preserves the stability and numerical damping properties of the trapezoidal method while achieving a second order accuracy when used in conjunction with the second order differential equations.

3. RESULTS AND DISCUSSIONS

3.1. Degradation Coefficient

The coefficient of degradation, as defined in the scientific literature [21], depends of the natural period of vibration of the structure in its initial state, T_0 , and in its degraded state, T_{degr} . The classification of the structures depending on the

coefficient of degradation has been made according to the reference intervals [8, 21].

Figure 6 presents the change in the fundamental period of vibration of the considered structure after being subjected to each earthquake scenario. The cumulative damage of the structure, evaluated by the change in the fundamental period of vibration, is shown to increase with each earthquake scenario that the structure is subjected to. Figure 7 shows the displacement distribution in the X direction corresponding to the fundamental mode of vibration, $T_0 = 0.171807$ seconds. It can be observed that, although the in-plane shape of the structure is a symmetric one, the first mode of vibration is not a translational one but it exhibits some rotation as well. This is caused by the fact that the stiffness is not symmetrically distributed over the floor surface due to the presence of the stair case. Hence, one half of the building exhibits positive translation, shown in blue with a maximum value of $u_x = 0.1877$ mm, whereas the other half is characterized by a negative displacement, shown in red with a minimum value of $u_x = -0.2063$ mm. However, the difference between the extreme positive and negative values of displacements is so small that the torsional effect induced by the presence of the stair case can be neglected in this case.

Table 3 summarizes the obtained results from the numerical analysis in terms of values for the degradation coefficient. This, in turn, falls within a certain reference interval that indicates the degradation state of the considered structure. Even after all earthquake scenarios, the structure shows only minor degradations. This is very important since the collapse of the structure is prevented. As it is well known, collapse prevention is one of the objectives of a performance-based design [34, 35]. One of its key features is the assurance of an adequate safety margin against collapse under the expected maximum seismic load [36].

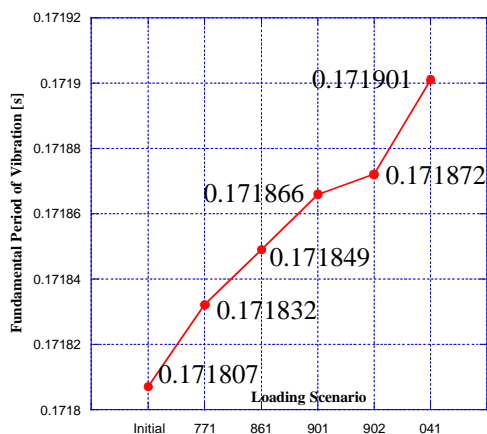


Figure 6. Variation of T for different earthquake scenarios

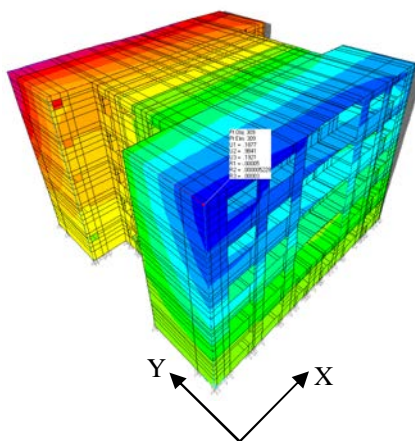


Figure 7. Displacements in x direction for the first mode of vibration

3.2. Extreme Storey Displacements

Figure 8 presents the extreme values of the recorded storey displacements in both X and Y directions. It can be observed that for the first considered earthquake scenario, 771, de extreme values of the displacements in both X and Y directions are the same. However, following the next scenario, the displacements in Y direction become slightly larger, by as much as 12%.

The general observation is that the values of displacements in Y direction are on average 19% larger compared to those in X direction. The percentage is lower for early earthquake scenarios and increase with the number of earthquakes the structure is subjected to. It should be pointed out that the maximum measured value of the displacement at the top of the structure was 3.24 mm. Such a small value of the peak displacement could be explained by the high stiffness of the structure and by the fact that only minor degradations occurred in the model after being subjected to all scenarios, Table 3.

Table 3. Degradation coefficient and degradation state

Earthquake Scenario	Fundamental Period of Vibration [sec]	Degradation Coefficient [21]	Degradation State [8]
771	0.171832	1.455×10^{-4}	Minor Degradations
861	0.171849	2.444×10^{-4}	
901	0.171866	3.433×10^{-4}	
902	0.171872	3.782×10^{-4}	
041	0.171901	5.468×10^{-4}	

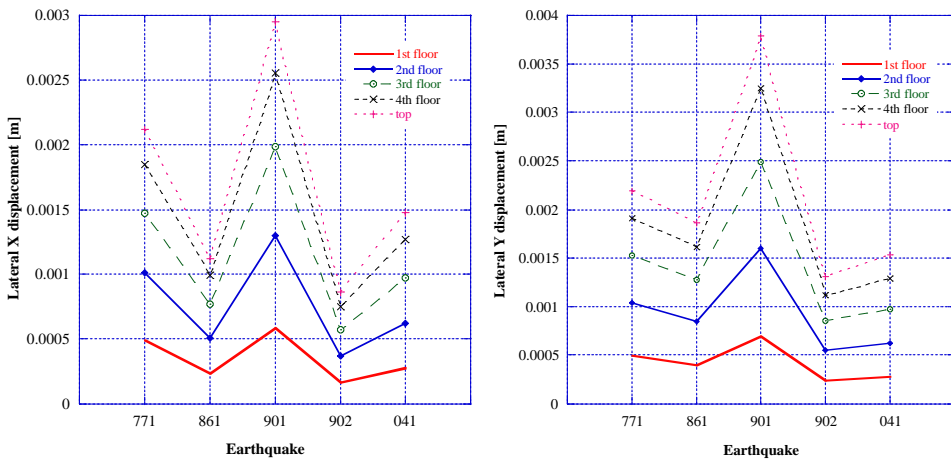


Figure 8. Extreme storey displacements in X and Y directions

3. CONCLUSIONS

The paper presents a numerical assessment method of the seismic behavior of a load bearing structure that is widely met in the Romanian urban areas. The method is based on the non-linear time history analysis of the considered model. The considered earthquake scenarios are based on the seismic actions recorded during the life time of the real structure. The seismic behavior is analyzed from the point of view of the degradation coefficient and the extreme values of the lateral displacements corresponding to each storey.

Based on the obtained results for the degradation coefficient it can be concluded that even though the structure suffered minor degradations produced by the earthquakes during its life time, those degradations do not endanger the life of inhabitants.

The analysis of the maximum storey displacements in both in-plane directions confirm that the structure did not exhibit large lateral displacements and, as a result of that, the degradations should not be important. The maximum recorded value at the top of the structure is 3.24 mm, being lower than the limit value prescribed by the design codes [37].

References

1. Geis, D.E., By Design: The Disaster Resistant and Quality-of-Life Community, *ASCE Natural Hazard Review*, vol. 1(3), pp. 151-160, 2000.
2. Maksud Kamal, A.S.M., Earthquake Risk Assessment and Corresponding Contingency Plans of the Major Cities of Bangladesh, *Proceedings of the 8th International Conference on Urban Earthquake Engineering (8CUEE)*, Tokyo, Japan, paper ID: 12-291, 2011.
3. Luna, R., Hoffman, D., Lawrence, W.T., Estimation of Earthquake Loss due to Bridge Damage in the St. Louis Metropolitan Area. I: Direct Losses, *ASCE Natural Hazard Review*, vol. 9(1), pp. 1-11, 2008.
4. Faccioli, E., Seismic Hazard Assessment for Derivation of Earthquake Scenarios in Risk-UE, *Bulletin of Earthquake Engineering*, vol. 4, pp. 341-364, 2006.
5. Lindell, M.K., Prater, C.S., Assessing Community Impacts of Natural Disasters, *ASCE Natural Hazard Review*, vol. 4(4), pp. 176-185, 2003.
6. Odeh, D.J., Natural Hazards Vulnerability Assessment for Statewide Mitigation Planning in Rhode Island, *ASCE Natural Hazard Review*, vol. 3(4), pp. 177-187, 2002.
7. Atanasiu, G.M., Toma, A.M., Managing the Seismic Risk of Some Residential Buildings of Romanian Urban Infrastructure, *Proceedings of the 14th European Conference on Earthquake Engineering (14ECEE)*, Ohrid, Republic of Macedonia, paper ID: 439, 2010.
8. Toma, A.M., Atanasiu, G.M., Seismic Risk Evaluation Based on Digital Mapping of a Romanian Urban Area, *Proceedings of the 8th International Conference on Urban Earthquake Engineering (8CUEE)*, Tokyo, Japan, paper ID: 12-124, 2011.
9. Toma, A.M., Atanasiu, G.M., Toma, I.O., GIS-Based Seismic Risk Evaluation of Tall Residential Buildings of Romanian Urban Areas – Case Study for the City of Iasi, *Proceedings of the International Conference on Engineering UBI2011 – Innovation and Development*, Covilha, Portugal, 2011.

10. Meli, R., Alcocer, S.M., Implementation of Structural Earthquake-Disaster Mitigation Programs in Developing Countries, *ASCE Natural Hazard Review*, vol. 5(1), pp. 29-39, 2004.
11. Panakkat, A., Adeli, H., Recent Efforts in Earthquake Prediction (1990-2007), *ASCE Natural Hazard Review*, vol. 9(2), pp. 70-80, 2008.
12. Villaverde, R., Methods to Assess the Seismic Collapse Capacity of Building Structures: State of the Art, *ASCE Journal of Structural Engineering*, vol. 133(1), pp. 57-66, 2007.
13. Toma, I.O., Budescu, M., Albu, G., Seismic Behavior of an Experimental Model Made of Thin-Walled Cold Formed Steel Profiles – Hardell Structures, *Bulletin of the Polytechnic Institute of Iasi, Construction. Architecture Section*, Tome LV(LIX), pp. 67-78, 2009.
14. Moon, F.L., Yi, T., Leon, R.T., Kahn, L.F., Testing of a Full-Scale Unreinforced Masonry Building Following Seismic Strengthening, *ASCE Journal of Structural Engineering*, vol. 133(9), pp. 1215-1226, 2007.
15. Di Ludovico, M., Manfredi, G., Mola, E., Negro, P., Prota, A., Seismic Behavior of a Full-Scale RC Structure Retrofitted Using GFRP Laminates, *ASCE Journal of Structural Engineering*, vol. 134(5), pp. 810-821, 2008.
16. Konstantinidis, K., Kappos, A.J., Izzuddin, B.A., Analytical Stress-Strain Model for High-Strength Concrete Members under Cyclic Loading, *ASCE Journal of Structural Engineering*, vol. 133(4), pp. 484-494, 2007.
17. Palermo, D., Vecchio, F.J., Simulation of Cyclically Loaded Concrete Structures Based on the Finite Element Method, *ASCE Journal of Structural Engineering*, vol. 133(5), pp. 728-738, 2007.
18. Kim, U., Leon, R.T., Galambos, T.V., 3-D Nonlinear Dynamic Behavior of Steel Joist Girder Structures, *Engineering Structures*, vol. 31, pp. 268-274, 2009.
19. Ivorra S., Pallares, F.J., Adam, J.M., Dynamic Behavior of a Modern Bell Tower – A Case Study, *Engineering Structures*, vol. 31, pp. 1085-1092, 2009.
20. Grange, S., Kotronis, P., Mazars, J., Numerical Modelling of the Seismic Behavior of a 7-Story Building: NEES Benchmark, *Materials and Structures*, vol. 42(10), pp. 1433-1441, 2009.
21. DiPasquale, E., Cakmak, A.S., Seismic Damage Assessment Using Linear Models, *Soil Dynamics and Earthquake Engineering*, vol. 9(4), pp. 194-215, 1990.
22. Talaslidis, D.G., Manolis, G.D., Paraskevopoulos, E., Panagiotopoulos, C., Pelekasis, N., Tsamopoulos, J.A., Risk Analysis on Industrial Structures under Extreme Transient Loads, *Soil Dynamics and Earthquake Engineering*, vol. 24(6), pp. 435-448, 2004.
23. Romeo, R.W., Bisiccia, C., Risk-Oriented Microzoning Study of an Urban Settlement, *Soil Dynamics and Earthquake Engineering*, vol. 26(10), pp. 899-908, 2006.
24. Computers and Structure Inc., SAP2000 Integrated Software for Structural Analysis & Design, Berkeley, California, USA (2005), available at: http://www.csiberkeley.com/products_SAP.html
25. Project no. 1497/1966 – Blocuri de locuinte P+4 cu pereti structurali din zidarie de caramida, *ICPROM Iasi archives*. (in Romanian).
26. CR6-2006, Cod de proiectare pentru structuri din zidarie, *National Institute for Research and Development in Construction – INCERC*, 2006 (in Romanian)
27. STAS 10101/1-78, Actions upon structures. Technical Weights and Dead-Loads, *Romanian Association for Standardization (ASRO)*, 2010. (in Romanian)
28. CR1-1-3-2005, Cod de proiectare: Evaluarea actiunii zapezii asupra constructiilor, *Universitatea Tehnica de Constructii Bucuresti*, 2005. (in Romanian)
29. CR0-2005, Cod de proiectare: Bazele proiectarii structurilor în constructii, *Universitatea Tehnica de Constructii Bucuresti*, 2005. (in Romanian)
30. Borcia, I. S., Procesarea înregistrarilor miscarilor seismice puternice specifice teritoriului României, *Ph.D. Thesis, Universitatea Tehnica de Constructii Bucuresti*, 2006. (in Romanian).
31. National Institute for Research and Development in Construction, Urban Planning and Sustainable Spatial Development, URBAN-INCERC, <http://www.incerc2004.ro/accelerograme.htm> (last accessed, March 2012).
32. Hilber, H.M., Hughes, T.J.R., Taylor, R.L., Improved Numerical Dissipation for Time Integration Algorithms in Structural Dynamics, *Earthquake Engineering and Structural Dynamics*, vol. 5, pp. 282-292, 1977.

33. Negrut, D., Rampalli, R., Ottarsson, G., Sajdak, A., On the Use of HHT Method in the Context of Index 3 Differential Algebraic Equations of Multibody Dynamics, *Journal of Computational and Nonlinear Dynamics*, vol. 2(1), pp. 73-86, 2007.
34. Fajfar, P., A Nonlinear Analysis Method for Performance Based Seismic Design, *Earthquake Spectra*, vol. 16(3), pp. 573-592, 2000.
35. Moehle, J.P., Nonlinear Analysis for Performance Based Earthquake Engineering, *The Structural Design of Tall and Special Buildings*, vol. 14(5), pp. 385-400, 2006.
36. Ghobarah, A., Performance-Based Design in Earthquake Engineering: State of Development, *Engineering Structures*, vol. 23(8), pp. 878-884, 2001.
37. P100-1-2011, Seismic Design Code P100 – Part I – Design Specifications for Buildings, *Universitatea Tehnica de Constructii Bucuresti*, 2011. (in Romanian)

Numerical simulation of wind action on solar panels inclined with 30° and different wind directions

Georgeta Vasies, Elena Axinte, Claudiu Romila, and Adrian Radu

Technical University Gh. Asachi" Iasi, Faculty of Construction & Building Services. 43 Dimitrie Mangeron Str., 700050, Iasi, Romania

Summary

Solar panels are increasingly being used to convert solar energy into thermal energy (solar collectors) and electricity (photovoltaic panels). In the last decade, their number has increased considerably. Therefore, more research on these systems is needed, especially in the aerodynamic domain. The wind represents the main action that determines the design of support systems for solar panels, wherever they are located, on flat roofs, pitched roofs or at ground level. Computational Fluid Dynamics (CFD) simulations can be performed in order to estimate the wind pressure on solar panels. In this study, the wind pressure on 12 solar panels in an arrayed configuration, mounted on ground level, with an angle of 30° and seven wind directions (0°, 30°, 45°, 60°, 90°, 135°, 180°) have been analyzed with the computer code ANSYS 12 CFX.

KEYWORDS: wind action, solar panels, wind degree, numerical simulations and pressure distribution.

1. INTRODUCTION

The techniques for capture and conversion of solar energy are in continuous development. Installation of solar plant involves important financial resources and the economic criteria that have an important role in design of supporting systems [1]. The determination of wind forces on the support systems of solar panels is the subject of many research studies. The behavior of solar arrays immersed in an aerodynamic field has made the subject of several studies in the wind tunnel with atmospheric boundary layer and numerical simulations using specialized software of fluid flow. In the last decade numerous studies were performed in order to determine pressure distributions and wind forces of size on solar panels located on flat and pitched roofs, building envelope or at ground level. Design of the anchoring systems must be done so that the extreme values of wind will not affect

the integrity of the solar panels. The main problem in designing of the anchoring systems is to determine the correct uplift forces and pressure field, and the solutions to reduce them.

In case of solar panels located at ground level, the assessment of the wind loads proves to be an easier task than for panels installed on the roof top.

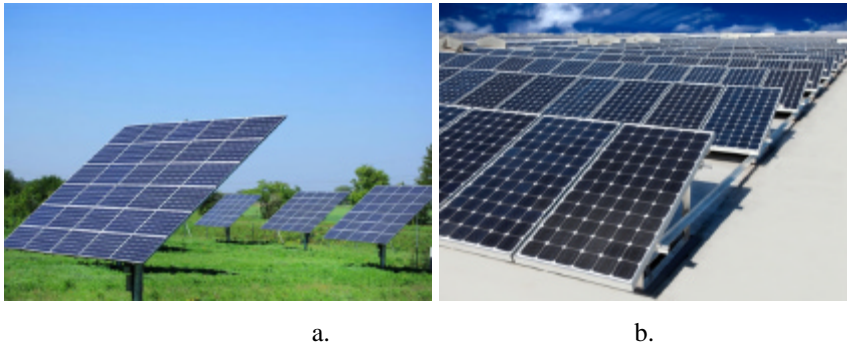


Figure 1. Solar panels installed at ground level: a. in a solar array configuration; b. in consecutive rows

In this study, wind action on twelve solar panels arranged in a 4x3 array, placed at ground level was analyzed. In the Romanian standard SR EN 1991-1-4:2006 the procedure for evaluating the wind loads on publicity boards is presented, but it cannot be extended to solar panels installed on ground level because publicity boards have a vertical position and wind acts perpendicular on their surface while solar panels are tilted under a particular angle. In Romania, due to the sunlight conditions, it is recommended that the solar panels should be disposed at an angle tilted between 30° and 40° to the plane of the ground. Also, in the scientific literature, is recommended that solar panels should be facing south direction with small deviations to southeast and southwest. This study aims to determine the loads produced by wind action on a solar panels array under different angles of attack.

2. SOLAR PANELS DISPOSED AT GROUND LEVEL

At ground level, the air flow disturbance is not only a consequence of solar panels presence, but it is also influenced by location (open field, bordering area and neighborhood buildings) and terrain topography [2]. Intensity of wind loads depends of the arrangement of solar panels (in consecutive rows or isolated solar arrays), the incidence of wind and the distance between panels rows/arrays. Wind speed decreases at the lower part of the atmospheric boundary layer (figure 2), but

when turbulence intensity is large enough and when wind speeds high, damages can occur on anchoring systems of solar panels.

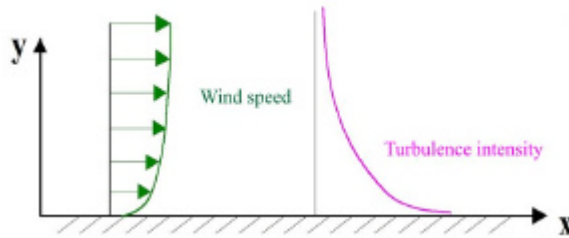


Figure 2. Profile of wind velocity and turbulence in atmospheric boundary layer

In order to determine the average wind speed and the velocity profile, the influence of orography and roughness factors (specific for each terrain type), is fundamental. In urban and suburban areas, it is interesting to see how roughness characteristics change the air flow conditions. According to roughness conditions (different types of vegetation and constructed areas) Roumanian standard SR EN 1991-1-4:2006 divides ground surface in five categories of exposure [5]:

Table 1. Terrain categories and terrain parameters (SR EN 1991-1-4:2006)

Terrain category		z_0 (m)	z_{min} (m)
0	Sea or coastal area exposed to the open sea	0.003	1
I	Lakes or flat and horizontal area with negligible vegetation and without obstacles	0.01	1
II	Area with low vegetation such as grass and isolated obstacles (trees, buildings) with separations of at least 20 obstacle heights	0.05	2
III	Area with regular cover of vegetation or buildings or with isolated obstacles with separations of maximum 20 obstacle heights (such as villages, suburban terrain, permanent forest)	0.3	5
IV	Area in which at least 15 % of the surface is covered with buildings and their average height exceeds 15 m	1.0	10

Velocity variation with height can be better observed from the velocity profiles proposed by Davenport [3] for three different types of terrain roughness (figure 3).

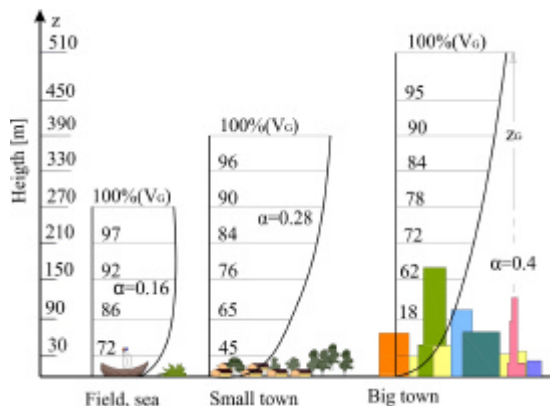


Figure 3. Ideal velocity profile established by Davenport for characterizing the boundary layer of Earth's atmosphere

3. CFD SIMULATION CASES

In the present study, CFD techniques have been used to investigate the aerodynamic features of a stand-alone ground mounted solar panels modules, arranged in a 4x3 array. The pressure distribution was evaluated for the entire array and also for every individual solar panel. Seven different incidence angles of attack were considered, listed in Table 2. The solar array has 17.641 sqm and it is compose by twelve solar panels (figure 5a) with: 1.482 m length, 0.992 m width and 0.045 m thickness.

Table 2. CFD simulation cases

Cases	Panel type	Panel inclination	Angle of attack
Case 1	Arrayed	30°	0°
Case 2	Arrayed	30°	30°
Case 3	Arrayed	30°	45°
Case 4	Arrayed	30°	60°
Case 5	Arrayed	30°	90°
Case 6	Arrayed	30°	135°
Case 7	Arrayed	30°	180°

The numerical simulation was developed using ANSYS 12 CFX code. The solar array is immersed in the computational domain (figure 4), whose minimum

dimensions respect the specifications from the scientific literature [4]. The solar array is lifted at 0.6m height above the ground level. On the surface of the array, the pressure is measured in 144 points for each face, arranged in 9 lines (figure 5 b). Overall resultant pressure has also been calculated.

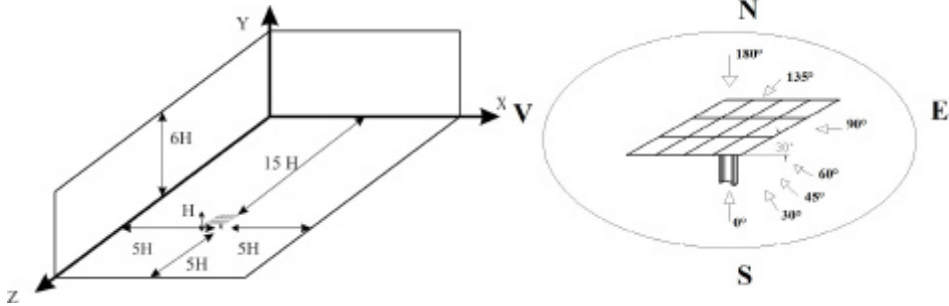


Figure 4. Computational domain and angles of attack

During the numerical simulation season, the considered wind speed was of 18 m/s and the turbulence intensity 10 % for all the seven analyzed cases. The pressures values on both faces of the exposed solar panels array were registered.

4. RESULTS AND DISCUSSIONS

In the analyzed cases a global analysis for determining the average pressure on solar array, and a local analysis for determining the critical panels of solar array have been made. Angle of attack which produces the largest wind loads has been determined by comparing the results.

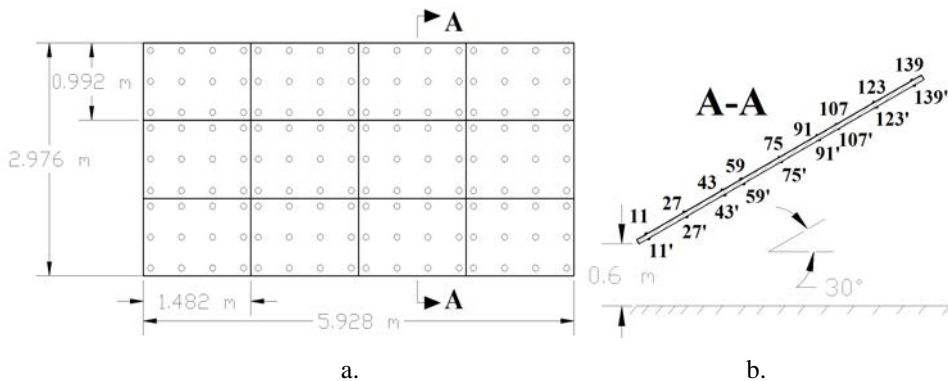


Figure 5. Pressure points distribution on the surface of the solar array

4.1 Case 1: Wind angle of attack at 0°

The highest pressures occur on surfaces of panels 9, 10, 11 and 12, that are positioned on the top of the solar array (figure 6 and 8). Panel number 2 is the least loaded, with a mean pressure of -23.7 Pa and the most loaded is panel number 12 with a mean pressure of -177.85 Pa (figure 7). The mean pressure on surface of solar array is -103.25 Pa.

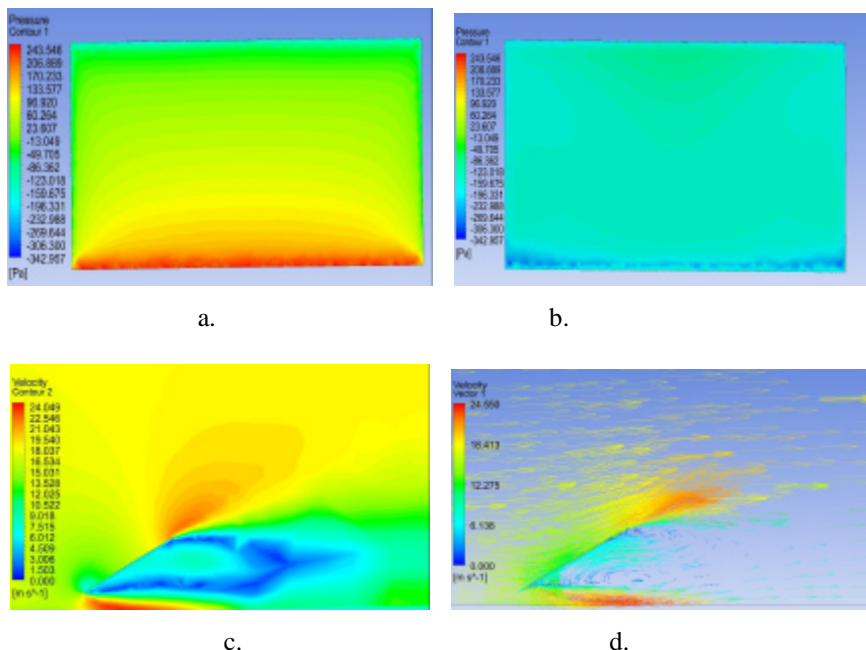


Figure 6. Pressure distribution on upper face (a.) and underside face (b.) of solar array, velocity contour (c.) and velocity vectors (d.) for an angle of attack of 0°

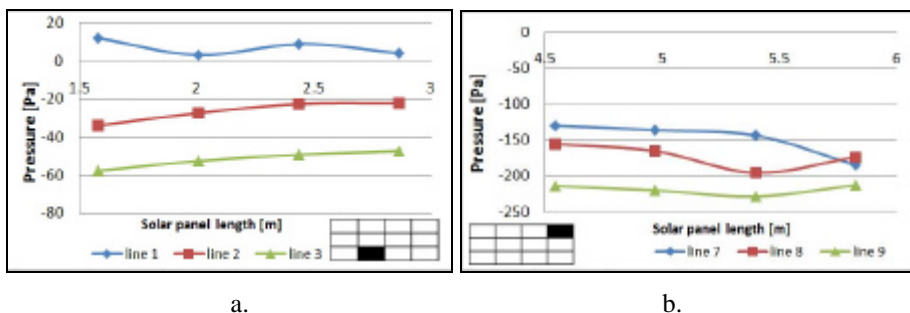
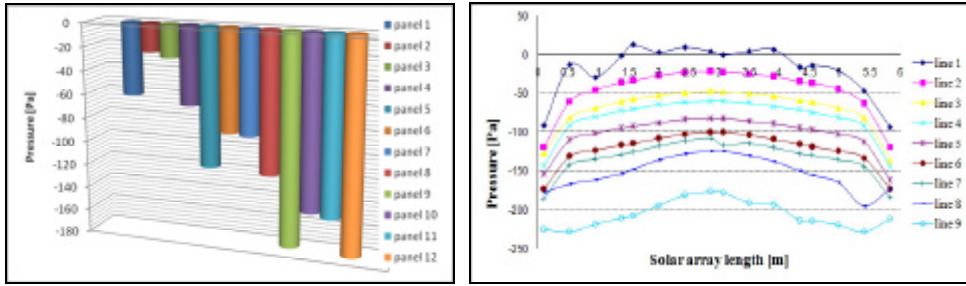


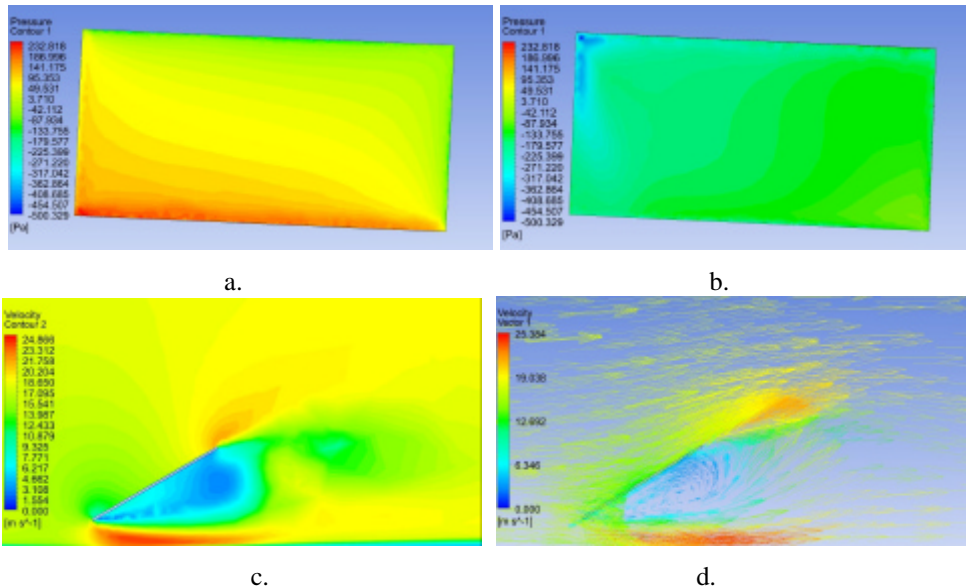
Figure 7. Pressure variation on panels 2 and 12



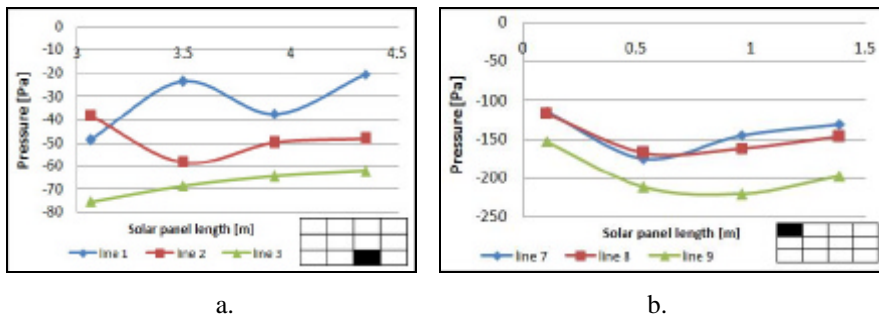
a. b.
Figure 8. Mean pressure on: a. panels of solar array; b. solar array surface

4. 2 Case 2: Wind angle of attack at 30 °

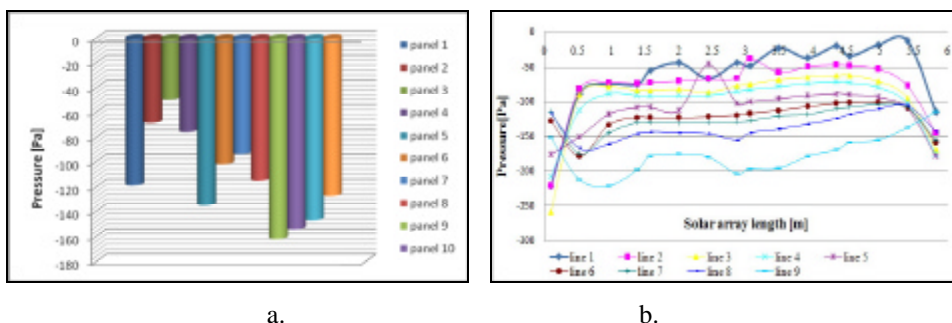
When the wind angle is at 30°, the left part of the solar array is more loaded than right one (figure 9). Like in the previous case, pressure values are negative on entire solar array with a mean value of -112.33 Pa (figure 11).



a. b. c. d.
Figure 9. Pressure distribution on the upper face (a.) and the underside face (b.) of solar array, velocity contour (c.) and velocity vectors (d.) for an angle of attack of 30°



a. b.
Figure 10. Pressure variation on panels 3 and 9



a. b.
Figure 11. Mean pressure on: a. panels of solar array; b. solar array surface

Panel number 9 is the most loaded, with a mean pressure of -161.99 Pa, followed by panel 10 with a mean pressure of -154.15 Pa. Panel number 3 is the least loaded, with a mean pressure of -49.68 Pa (figure 10).

4.3 Case 3: Wind angle of attack at 45°

Like in the previously analyzed cases, over the entire surface of the solar array negative pressure have been found (figure 12 and 14 b). The mean pressure obtained for the solar array is -118.88 Pa. The suction developed on the left side are up to 45% higher that the values of the right one. Panel number 1 is the most loaded, with a mean negative pressure of -291.35 Pa. The least loaded is panel number 4, with a mean pressure of -69.1 Pa (figure 13).

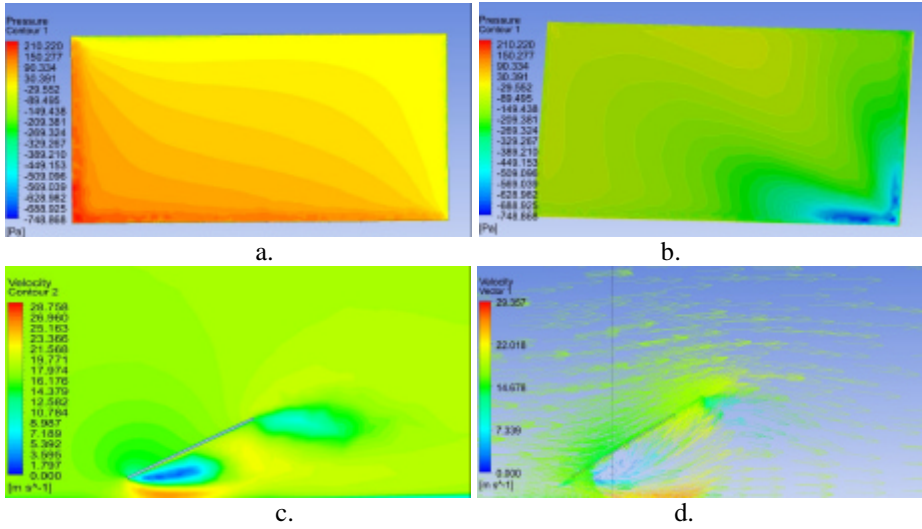
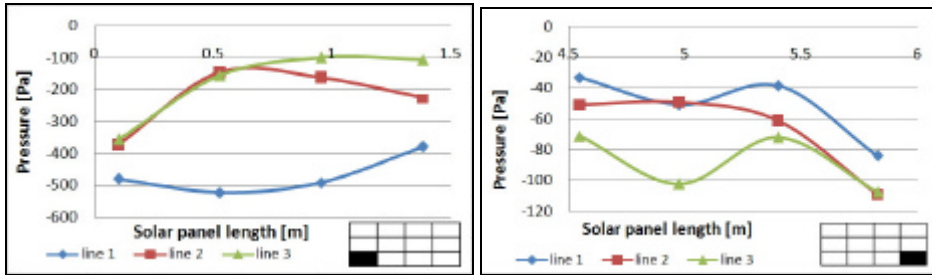
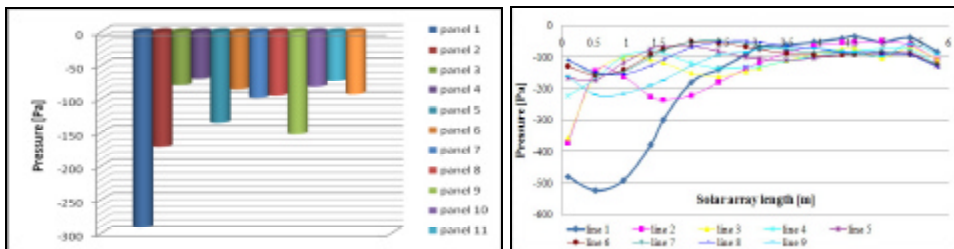


Figure 12. Pressure distribution on the upper face (a.) and the underside face (b.) of solar array, velocity contour (c.) and velocity vectors (d.) for an angle of attack of 45°



a. b.
Figure 13. Pressure variation on panels 1 and 4



a. b.
Figure 14. Mean pressure on: a. panels of solar array; b. solar array surface

4.4 Case 4: Wind angle of attack at 60°

The pressures obtained in all analyzed points are negative, the measured mean pressure on solar array being -96.13 Pa (figure 17). The left one is again more loaded than the right one (figure 15). The least loaded are panels number 11 respectively 12 and the most loaded is panel one (figure 16).

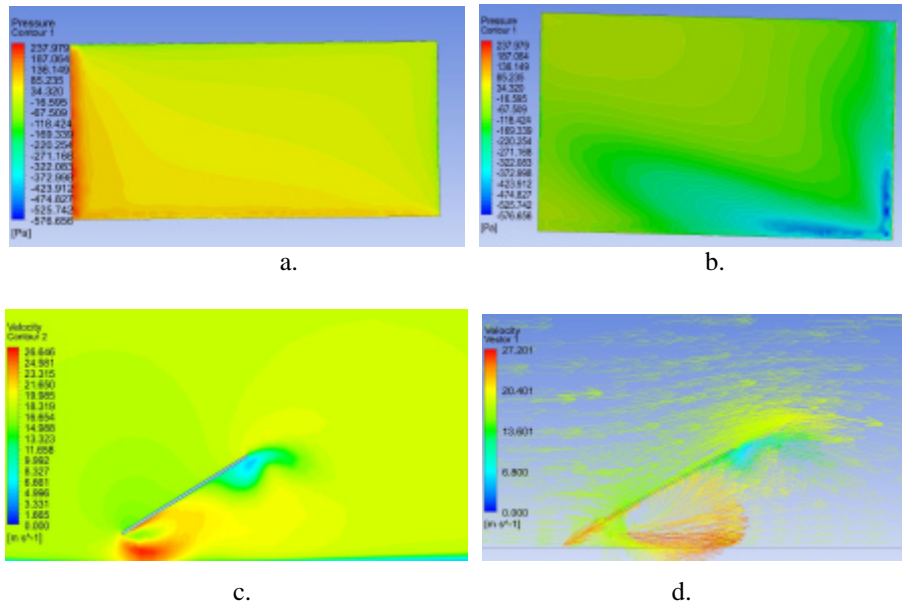


Figure 15. Pressure distribution on the upper face (a.) and the underside face (b.) of solar array, velocity contour (c.) and velocity vectors (d.) for an angle of attack of 60°

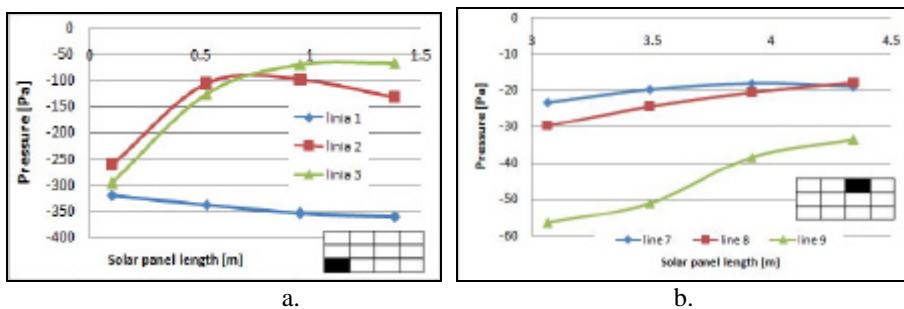
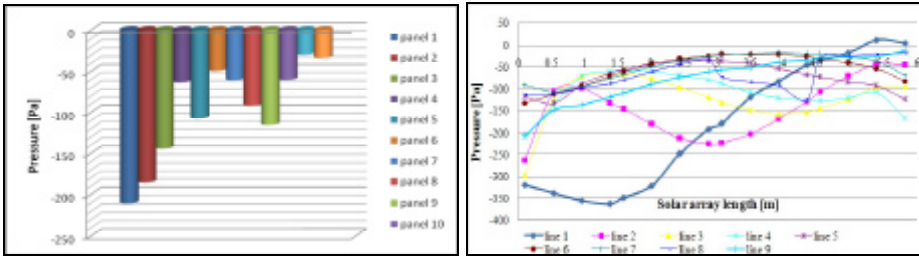


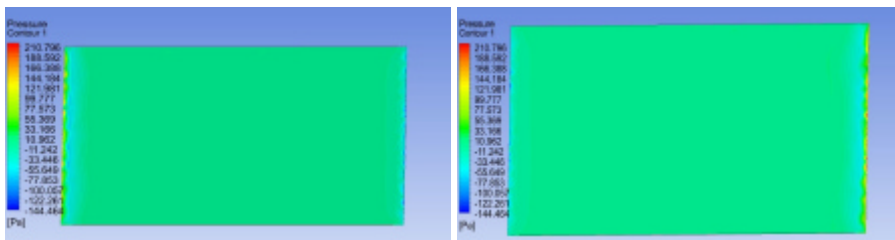
Figure 16. Pressure variation on panels 1 and 11



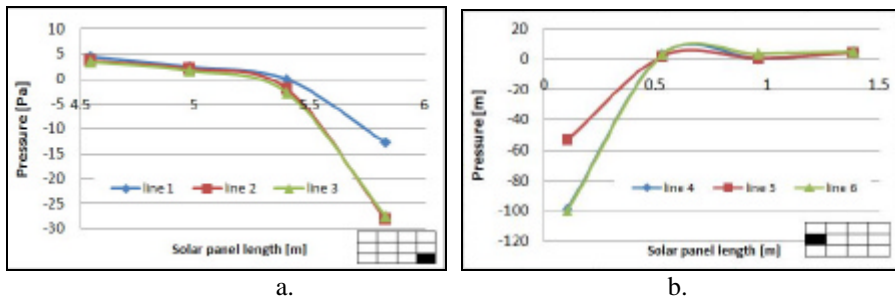
a. b.
Figure 17. Mean pressure on: a. panels of solar array; b. solar array surface

4.5 Case 5: Wind attack angle at 90°

The solar array has the smallest loads when the attack angle is at 90° (figure 18). The resultant pressures are both positive and negative, according to the position on solar panels in the array (fig. 20). The pressures developed on the left side (panels 1, 5, and 9) and on the right side of solar array (panels 4, 8, 12) are entirely negative, while the pressures developed on central panels have positive values. Though, the mean pressure on solar array has a negative value of -2.26 Pa. The biggest negative pressure (-18.74 Pa) was found on panel number 5, and the lowest negative pressure (-4.64 Pa) on panel number 10 (figure 19).



a. b.
Figure 18. Pressure distribution on the upper face (a.) and the underside face (b.) of solar array, velocity contour (c.) and velocity vectors (d.) for an angle of attack of 90°



a. b.

Figure 19. Pressure variation on panels 4 and 5

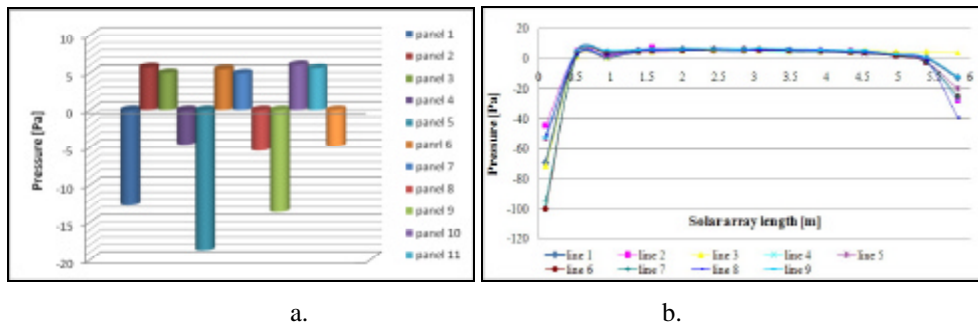


Figure 20. Mean pressure on: a. panels of solar array; b. solar array surface

4.6 Case 6: Wind angle of attack at 135°

For an attack angle of 135°, the mean pressure on solar panels has both positive and negative values. Negative pressures appear on panels positioned on the extremities, while the pressures on central panels are positive (figure 21 and 23). The mean pressure on solar array surface is -62.8 Pa. Panel number 12 (figure 22) has the highest mean negative pressure (-257.89), and panel number 7 has the lowest positive pressure (16.25Pa).

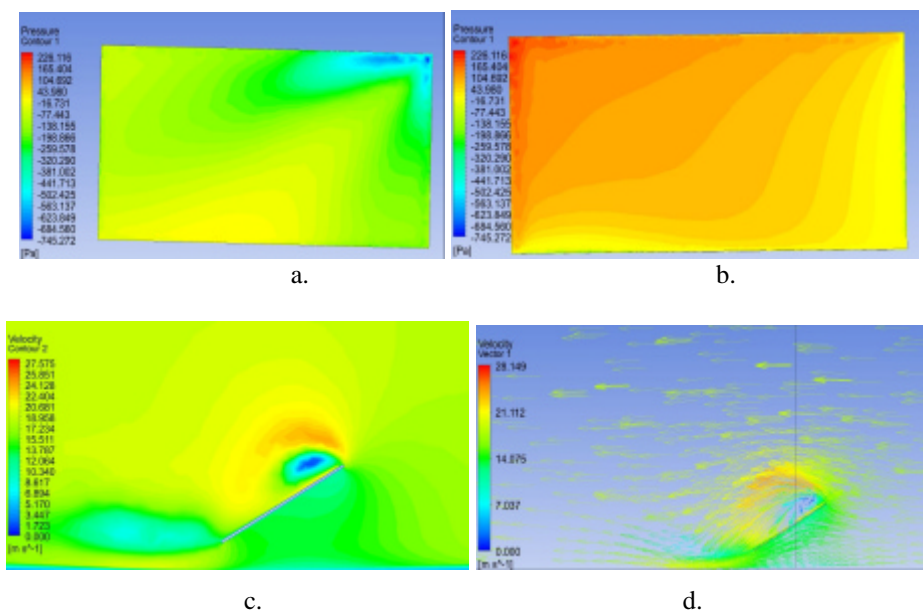


Figure 21. Pressure distribution on the upper face (a.) and the underside face (b.) of solar array, velocity contour (c.) and velocity vectors (d.) for an angle of attack of 135°

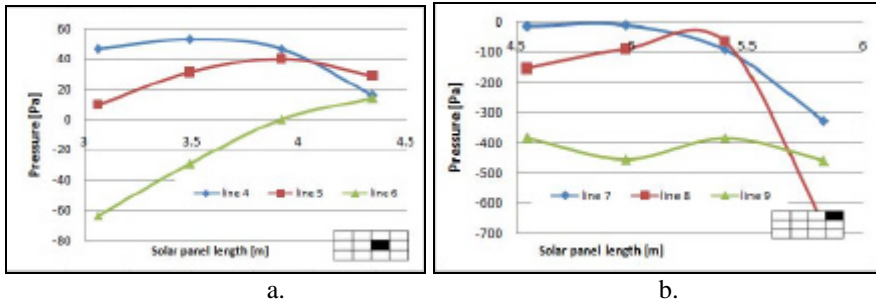


Figure 22. Pressure variation on surface of panels 7 and 12

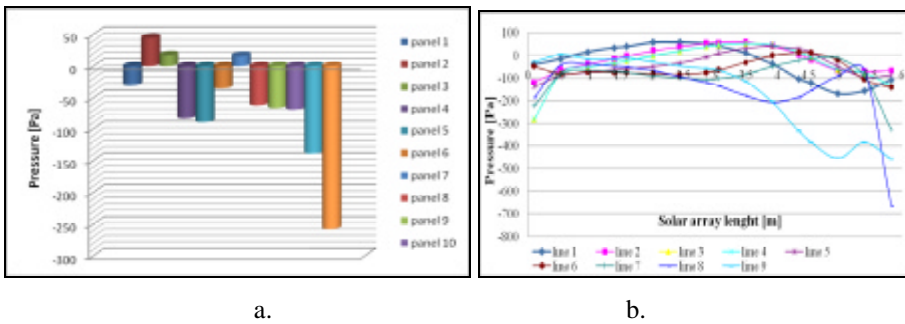
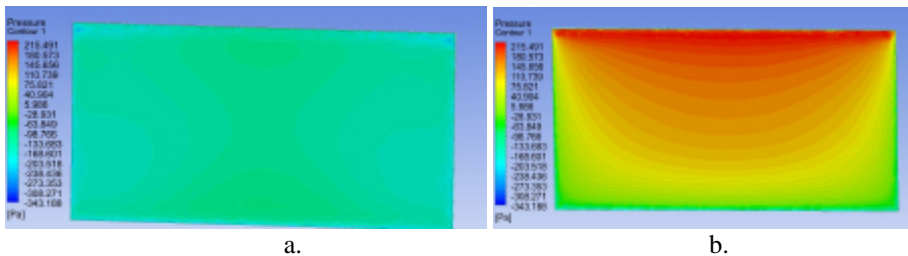


Figure 23. Average pressure on: a. panels of solar array; b. solar array surface

4.7 Case 7: Wind angle of attack at 180°

The mean pressure measured on the solar array surface has a negative value (-39.7 Pa). The most loaded panel is panel number 1, with a value of mean negative pressure of -140.95 Pa (figure 22a). The least loaded panel is number 6, with a mean pressure of 1.77 Pa (figure 22b). The resultant pressures at the lowest and lateral sides of solar array are negative, while in the central zone, positive pressures are obtained.



a. b.

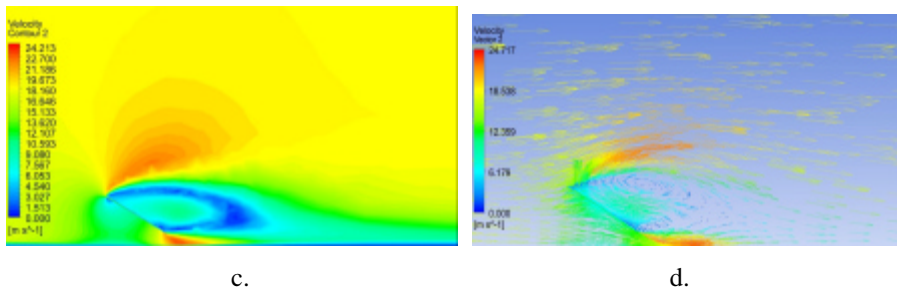


Figure 24. Pressure distribution on the upper face (a.) and the underside face (b.) of solar array, velocity contour (c.) and velocity vectors (d.) for an angle of attack of 180°

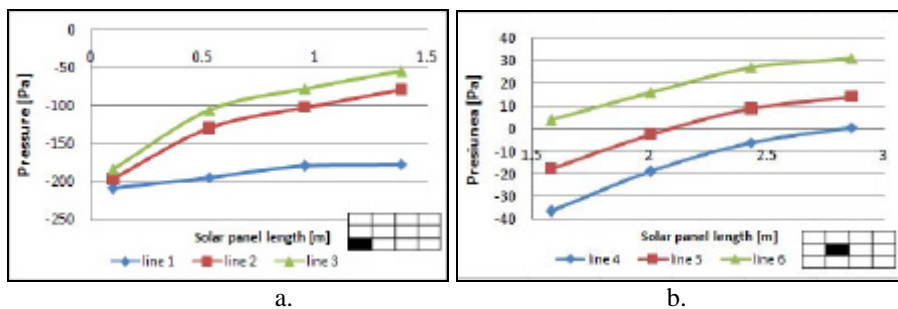


Figure 22. Pressure variation on panels 1 and 6

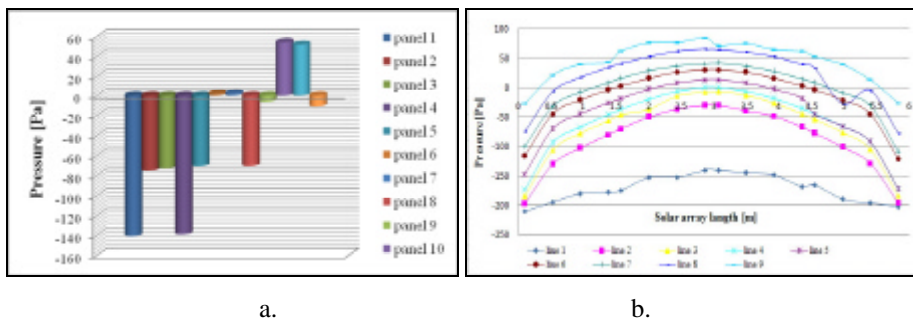


Figure 23. Mean pressure on: a. panels of solar array; b. solar array surface

5. CONCLUSIONS

Wind direction has a major influence on the pressure distribution on solar arrays. Suctions have higher values for wind directions of 30°, 45°, 60° and 135°, when the incidence angles create conical vortices on surface of solar array. These vortices

appear in pairs, one on each edge of solar array. The center of each vortex is at the area where high suction occurs. The obtained results for each analyzed case were used to make a comparison between mean pressures developed on each panel of the solar array. A global analysis was performed; the mean pressure was compared for each considered attack angle. The biggest suction occurs for an attack angle of 45° respectively 30° .

References

1. Vasies, G., Axinte, E., Teleman, E.C., *Numerical simulation of wind action on solar panel placed on flat roofs with and without parapet*, Buletinul Institutului Politehnic din Iasi, Sectia Constructii. Arhitectura, Tomul LVIII (LXII), Fasc. 1, Editura Politehnicum, ISSN 1224-3884 (p), ISSN 2068-4762 (e), p 139-155, Iasi, 2012.
2. Bitsuamlak, G.T., Dagnew A.K., Erwin J., *Evaluation of wind loads on solar panel modules using CFD*, The Fifth international Symposium on Computational Wind Engineering (CWE2010), Chapel Hill, North Carolina, USA, May 23-27, 2010.
3. Radu, A., Radu, V., *Aerodinamica constructiilor. Îndrumator pentru lucrari de laborator la Constructii civile si industriale*, Ed. Institutului Politehnic, Iasi, 1981.
4. Franke J. et al., *Recommendations of the Use CFD in Wind Engineering*. Proc. of the International Conference on Urban Wind Engineering and Buildings Aerodynamics, Belgium, 2004.
5. ***SR EN 1991-1-4:2006, Eurocod 1: Actiuni asupra structurilor. Partea 1-4: Actiuni generale-Actiuni ale vântului.

Wind action on solar panels placed on flat roofs with parapets

Georgeta Vasies, Elena Axinte, and Elena Carmen Teleman

Technical University Gh. Asachi" Iasi, Faculty of Construction & Building Services. 43 Dimitrie Mangeron Str., 700050, Iasi, Romania

Summary

Wherever they are located, on flat roofs, pitched roofs or at ground level, the wind represents the main action that determining the design of support systems for solar panels. Increasing the number of solar panels used in the world, determine behavior research on these systems in the aerodynamic field. In the specialty literature is recommended orientation of solar panels to south, south-east, respectively south-west, for benefit of a better sunlight. In Romania the dominant wind direction is from north, north-east or north-west, in which case the wind blows behind the field of panels. It is aimed the highlight of shielding effect produced by the building, respectively by building and parapet on the pressure distribution on the solar panels surface. Numerical simulations are performed in ANSYS 12 CFX, for an incidence wind angle of 135 °.

KEYWORDS: wind direction, solar panels, CFD simulation, flat roof, shielding effects

1. INTRODUCTION

The techniques for capture and conversion of solar energy are in continuous development. Determination of wind forces on the support systems of solar panels is the subject of many research studies. The behavior of solar arrays immersed in aerodynamic field, makes the subject of several studies in wind tunnel with atmospheric boundary layer and numerical simulations using specialized software in fluid flow. In the last decade numerous studies was performed for determinate the pressure distributions and the size of wind forces on solar panels located on flat roofs, pitched roofs, building facades or at ground level.

Wood, Denoom and Kwok [1] investigated the behavior of solar collectors located on the flat roof, parallel with the roof line. In their studies the distance between roof and collectors and the distance between rows of collectors was varied, proving that none of these parameters have a considerable influence on the pressure distribution. The experiments showed that the distance between solar modules and

roof edges, orientation of panels toward the wind direction and the shape and size of the building, can influence or even change the wind loads on solar collectors placed on flat roofs. Blackmore [2] using his studies, has published a design code for solar panels placed on flat roofs, but he did not consider the maximum pressure that occur for different wind angles. In Romania, Radu, Axinte and Theohari [3] have made studies on solar collectors located on flat roofs, using a wind tunnel with open circuit. The collectors were arranged in compact group and two distinct groups and the pressure distribution was analyzed for the main wind directions. The net pressure was determined for each collector and for each row of panels was calculated the average pressure. Also was showed the shelter effect produced by the first row of collectors. Radu and Axinte [4] have investigate the effect of the parapet on collectors modules placed on roof top, showing that it's presence reduces the both pressure and suction in the corner areas of the flat roof. The collectors have been placed on the flat roof of a five story building, reduced to the scale of the model. The height and the permeability of the parapet were varied. The experiments demonstrated that the presence of parapet reduces the pressure up to 45% and the uplift forces up to 25 %, for the first row of collectors. Making comparison between various situations, the authors concluded that the reduction of pressure and wind forces is dependent by the building height; if the height increases, this reduction become insignificant. Solar panels exposed to wind action involves issues such as determining the influence of air flow on energy efficiency and designing the support systems for satisfy the requirements in service with minimal use of materials [5]

Since the wind tunnel experiments and full-scale measurements require time and significant financial resource, in wind engineering has developed the numerical simulation of wind action, based on computational fluid dynamics. Increased processing speed of computers has led the development of specialized computers programs in fluid flow and numerical simulation results are often comparable with data collected in the wind tunnel experiments.

3. NUMERICAL SIMULATION USING ANSYS CFX

The numerical simulation in the study presented here was developed using ANSYS 12 CFX. The building is immersed in the computational domain, its minimal dimensions respecting the specifications from the literature [6]. Solar panels rows are arranged in compact group on the flat roof of a building with parapets (figure 1). The rows have 27.5 m length, 1.58 m height and 0.008 m thick and are titled by 35° to the roof plan. The distance between two rows of panels is 1.0 m and the distance from the roof edge to the first row is 3.0 m. Numerical simulation was done considering the wind angle by 135° . Solar panels are facing to south, while the wind direction is northeast (figure 2).

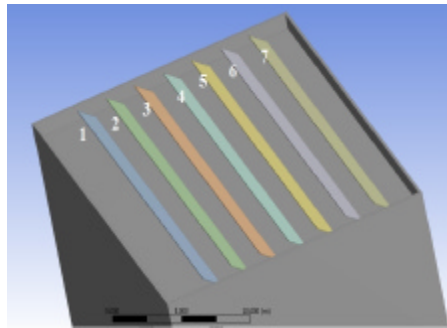


Figure 1. Arrangement of solar panels on flat roof

The building equipped with solar panels on the roof is a regular one, 30 m x 20 m in plane dimensions and 15 m height; an attic of 1.0 m is placed on the roof perimeter. The solar panels are lifted at 0.2m height from the level of the roof and situated in consecutive rows, respecting the recommendations from the scientific literature [7]: the distance between these rows and the edge of the attic is about $e/10$, where:

$$e = \min(b, 2h) \tag{1}$$

The significance of the symbols being:

b - the dimension of the face normal to the wind direction,

h - height of the building.

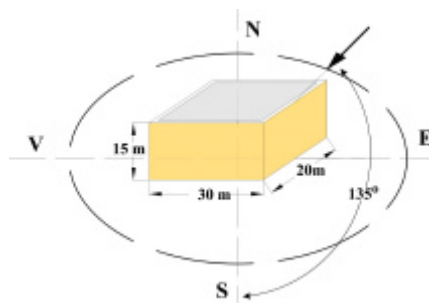


Figure 2. Dimensions of the building and the wind action angles

During the numerical simulation season, the wind speed considered is 14 m/s and the turbulence intensity is 10 %. As a result of the numerical simulation for the two analyzed cases, the pressures coefficients on both faces of the exposed solar panels were registered.

4. DISCUSSIONS AND RESULTS

In the case of the plane solar panels mounted on supports the local pressure coefficients will act on both faces of the panel and the resultant of the normal component will be obtained with the sum[4]:

$$c_{LR} = \pm c_{ns} \pm c_{ni} \tag{3}$$

where c_{ni} is the pressure coefficient on the in wind surface of the panel and c_{ns} is the pressure coefficient from the leeward face (Fig. 3 b).

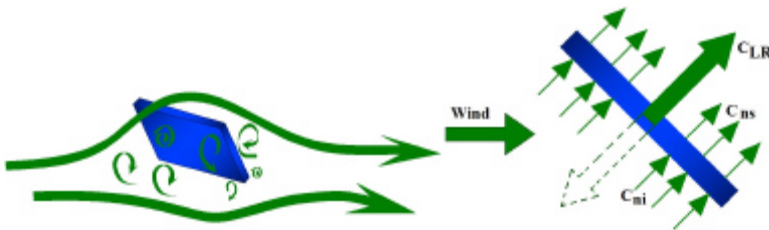


Figure 3. The air flow around the plane surface of the solar panel and the computation of the coefficient c_{LR}

The Romanian wind standard does not give information available for design of solar panels systems.

4.1 Analysis of the results obtained during the numerical simulation

For every row of solar panels, the pressure produced by wind action was measured in 45 points, placed in 5 lines respective 9 columns, according to figure 4.

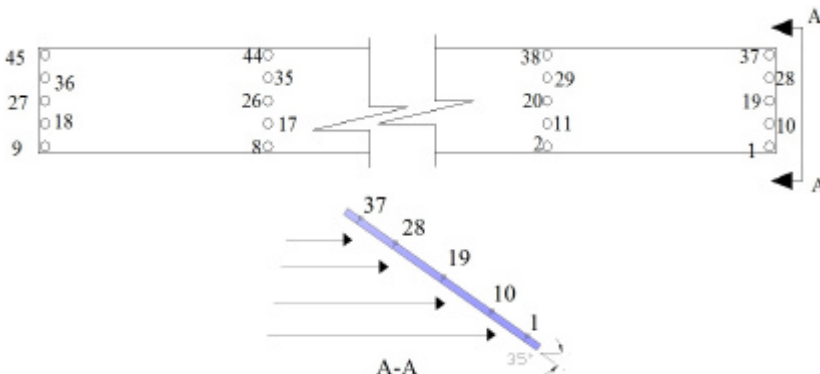


Figure 4. Distribution of the points on the surface of the solar panels where the local wind pressure was measured

For each point was measured the pressure values on both sides of the solar panels and calculated the resulting pressure. With the values obtained in every point, graphics were traced and has been made observations regarding pressure variations on every row of solar panels. The resultant pressures in all points analyzed is negative. The mean pressure values obtained from the 45 points located on each side of panel’s rows are entirely negative. The lower suction appears in the points of first row of solar panels and increasing gradually until the penultimate row.

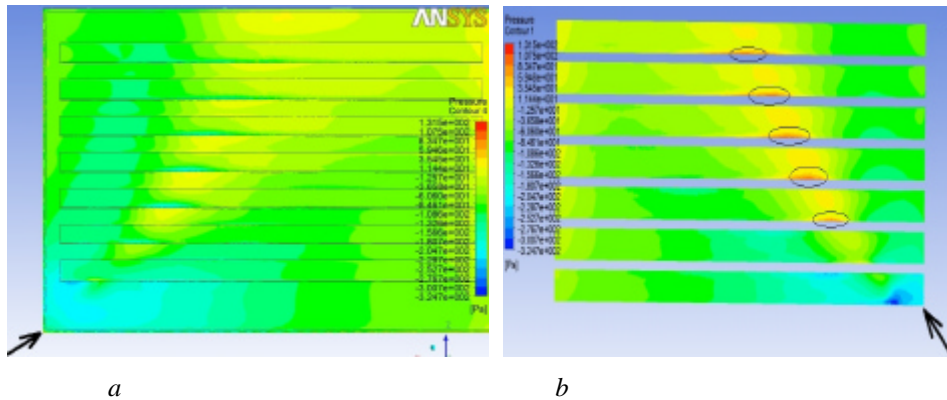


Figure 5. Pressure distribution on solar panels face: a - upper (active) face, b - underside (exposed) face

The negative pressures measured in the first column of rows number 1, 2 and 3 (right side) are double compared with negative pressure values measured on the panels located in the left side of this rows (column 9). Starting with row number 4, the pressures measured on left side grow, compared with values measured on right side. The difference gets up to 60 % higher in case of the sixth row and 110 % higher in case of the last row of solar panels.

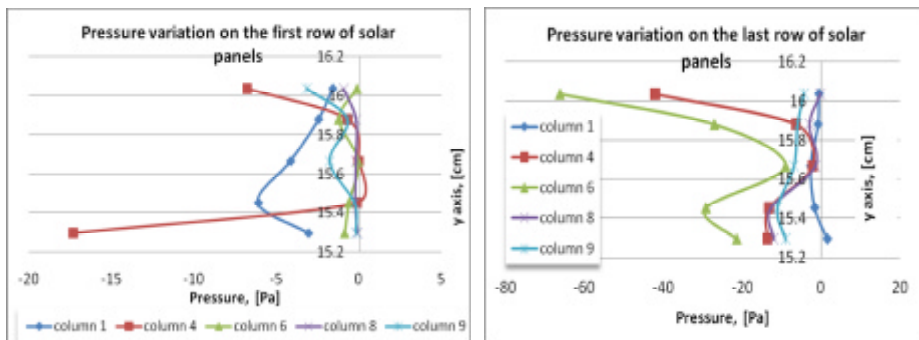


Figure 6. Pressure variation on the first and last rows of solar panels

Positive pressure, lower in value, appear in the central area of the solar panels group. These positive values appear in points 7 and 16 on the third row, in points 6 and 7 on the fourth and fifth row, respectively in points 5 and 14 on the last row of solar panels. The positive values appear only on active face of solar panels, while the resultant pressure is negative.

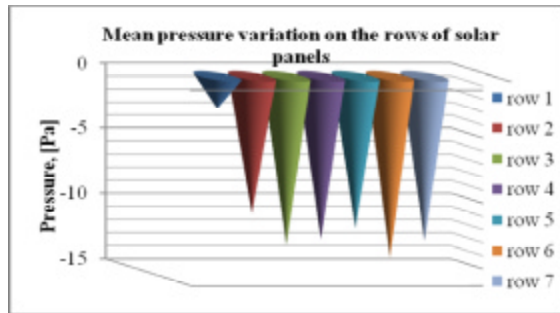


Figure 7. Mean pressures variation on the rows of solar panels

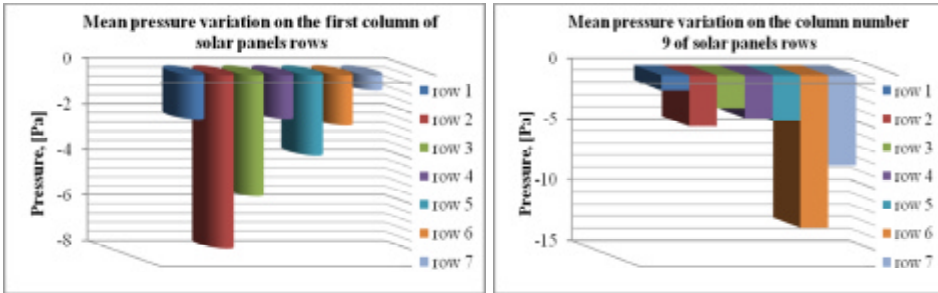


Figure 8. Mean pressure variation on the first and last column of solar panels rows

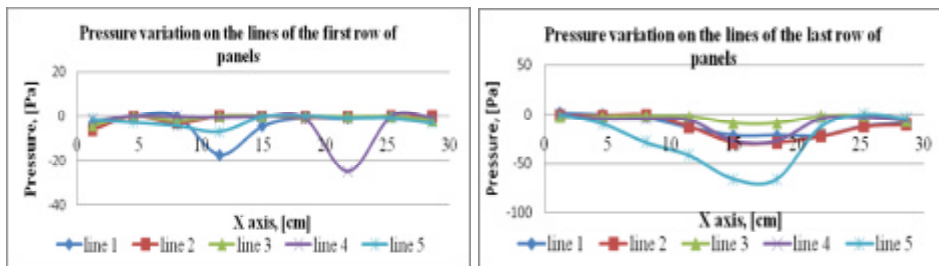


Figure 9. Pressure variation on lines of first and last rows of solar panels

4.2 Discussions

Wind direction has a major influence on the pressure distribution on flat roof surface and also on faces of solar panels arrays. Local suction is more intense for wind direction of $\pm 45^\circ$ and that wind acts from N-E direction, behind the solar arrays, leads to negative pressure on both sides of panels. Considering the incidence angle of 135° , would create conical vortices (delta-wing vortex) at the roof level. These vortices are usually in pairs, one on each roof edge, and the center of each vortex is an area where high suction is occurring.

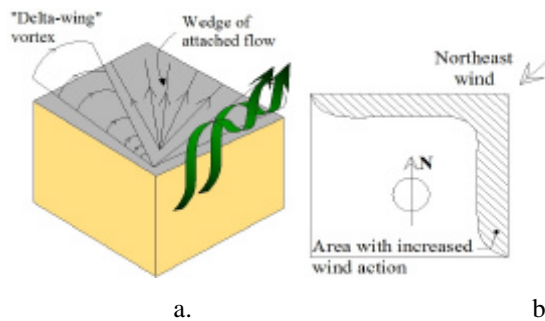


Fig. 10 – Development of conical vortices for angle of incidence wind between 30° and 60° (by Cook, 1985) and their action area

Conical vortices action leads to development of high uplift forces, which means a biggest load on support systems of solar panels.

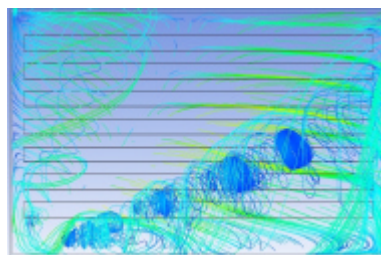


Fig. 11 – Streamline on roof level

The shape and size of the building have a big influence in pressure distribution on solar panels mounted on building roof. Placement of solar panels on the roof top favors the appearance of local turbulence with changes of pressure distribution and reduces uplift force by down force. Though, wind incidence can create wake vortices and then suction effects are more obvious. By their position, solar panels can shield each other, phenomenon amplified by attic presence.

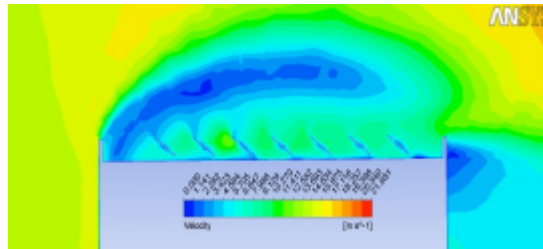
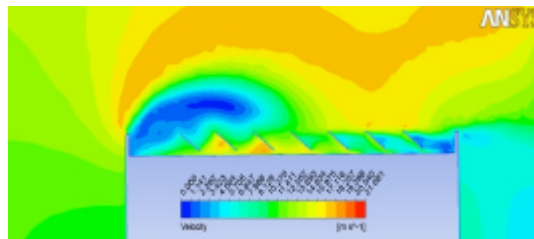
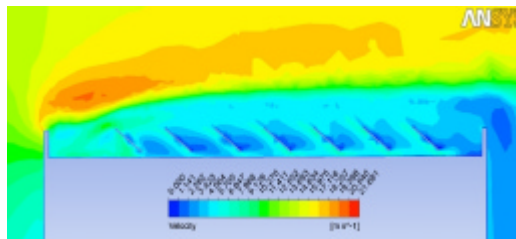
*a**b**c*

Figure 12. Velocity counter in: *a* - right extremity, *b* - central zone, *c* - left extremity of solar panels rows, for building with parapet

5. CONCLUSIONS

Oblique direction of wind action is an unfavorable case, generating high intensity of uplift forces in the corner areas of the flat roof, forces which bring an additional load on support systems of solar panels. Placement of solar panels to a height of 20 cm above the roof level, allows infiltration of streamlines under rows of solar panels. In the middle of the roof, where conical vortexes influence is lower; on active face of solar panels appear positive values of pressure. Building height has an important role in the pressure distribution on the roof and panels arrays.

Presence of the parapet helps to mitigate the wind loads, and increase the shelter effect.

References

1. Wood G.S., Denoon R.O., Kwok K.C.S., *Wind Loads on Industrial Solar Panel Arrays and Supporting Roof Structure*. Wind & Structure, 4, 6, 481-494 , 2001.
2. Blackmore, P., BRE Digest 498, Wind loads on roof-based photovoltaic systems, 2004
3. Radu A., Axinte E., Theohari C., Steady wind pressures on industrial solar collectors on flat-roofed buildings, Journal of Wind Engineering and Industrial Aerodynamics vol. 23, pp 249-258, 1986
4. Radu a., Axinte E., Wind forces on structures supporting solar collectors, Journal of Wind Engineering and Industrial Aerodynamics vol. 32, pp 93-100, 1989
5. Axinte E., Modelarea fizica a interactiunii vant-structura pentru proiectarea captatoarelor solare, teza de doctorat, Universitatea Tehnica “Gheorghe Asachi”, Iasi, 1988
6. Franke J., et al., Recommendation of the use CFD in wind engineering, Proceeding of the International Conferinces on Urban Wind Eneering and Building Aerodybamics, Belgium, 2004
7. **** SR EN 1991-1-4/2006, Eurocod 1: Actiuni asupra structurilor. Partea 1-4: Actiuni generale- Actiuni ale vantului

Multidirectional energy dissipative columns

Vasile-Mircea Venghiac

Department of Structural Mechanics, "Gh. Asachi" Technical University, Iasi, 700050, România

Summary

The Slimdek composite flooring system was created and is widely used in Great Britain where there is no seismic activity. In recent years, countries situated in seismic areas showed great interest in this type of composite flooring system. This raises the problem of energy dissipation. Plastic hinges cannot develop in the beams due to the fact that they are encased in concrete. Thus, the behaviour of the Slimdek flooring system is similar to the behaviour of flat slabs. In order to absorb the seismic energy, multidirectional dissipative columns are proposed. These columns show great potential for energy dissipation in new or existing buildings with Slimdek composite floors or flat slabs.

KEYWORDS: yielding steel damper, energy dissipative column, cyclic loading, Slimdek, composite floor.

1. INTRODUCTION

The Slimdek composite floor was conceived and is widely used in Great Britain. It consists of encasing asymmetric section beams in concrete by placing the steel decking on the bottom flange of the beams as shown in figure 1.

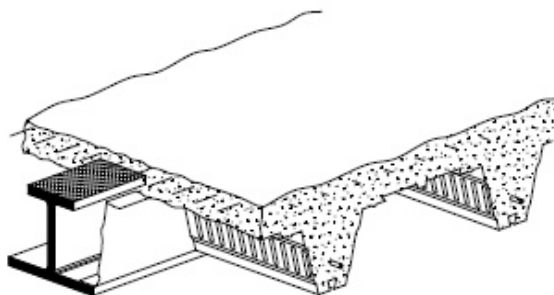


Figure 1. Slimdek composite flooring system [4].

The floors can reach up to 9 m spans without the need of secondary beams. This type of composite flooring system presents many advantages, as the following:

- Reduced height of the structural system. This reduces the cost of claddings;
- Ease of service integration. The services can be accommodated within the thickness of the slab, between the ribs of the decking;
- Good fire resistance. A fire resistance of 60 minutes can be achieved without any supplementary fire protection [3].

Countries in seismic areas, such as New Zealand, showed great interest in this type of composite floor. Plastic hinges cannot develop in the beams of the Slimdek composite floor, making this system similar to flat slabs. The seismic energy must be absorbed by using damping devices. There are many types of dampers available, such as ADAS (Added Damping and Stiffness), TADAS (Triangular plate Added Damping and Stiffness), DFMD (Dual Function Metallic Damper), Pall, Damptech, Sumitomo etc.

2. OBJECTIVES AND SCOPE OF WORK

The author proposes a new type of metallic damper called “multidirectional energy dissipative column” or MDC. This type of device has the advantage of absorbing the seismic energy within the column, without the need of additional braces which can obscure the window area.

The main objective is to investigate the capacity of energy dissipation of the proposed device. The hysteretic behaviour of the device is also analyzed.

3. MDC MODELS

Unlike “energy dissipative columns” analysed before [5-7], the MDC device is capable of dissipating the seismic energy on all directions. It consists of using a circular hollow section with dissipative elements placed at each end of the column. The dissipative elements are made of circular hollow sections with different types of holes. The size, shape and position of the holes are designed so that the plastic stresses would appear on the whole dissipative element in order to achieve good energy dissipation.

Eight models are considered with different types of holes in the dissipative element (figure 2), as follows:

- Model MDC1: 24 slits (10x200 mm);

- Model MDC2: 24 slits (10x30 mm) on 5 rows;
- Model MDC3: 24 circular holes (Ø10 mm) on 8 rows;
- Model MDC4: 24 circular holes (Ø15 mm) on 8 rows;
- Model MDC5: 24 circular holes (Ø20 mm) on 8 rows;
- Model MDC6: 24 circular holes (Ø20 mm) on 8 rows with cross layout;
- Model MDC7: 24 circular holes (Ø20 mm) on 10 rows;
- Model MDC8: 24 circular holes (Ø20 mm) on 15 rows.

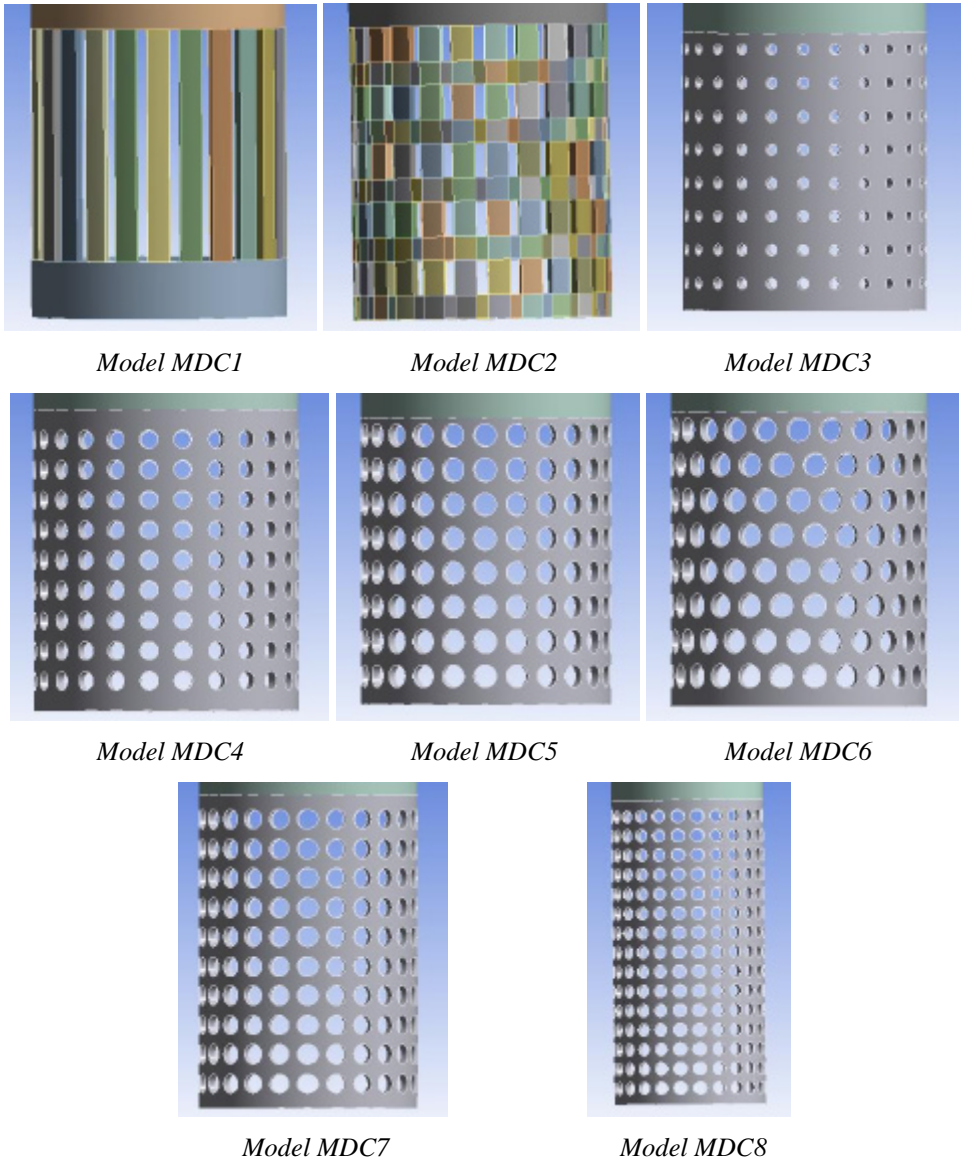


Figure 2. MDC models in ANSYS [1].

The program used for the analysis is ANSYS v12. The considered models have the following characteristics:

- the circular hollow section is 219.1x8 mm [2];
- the height of the column is 3.00 m;
- the steel grade is S235;
- the action is an imposed displacement of 25 mm according to the graph shown in figure 3.

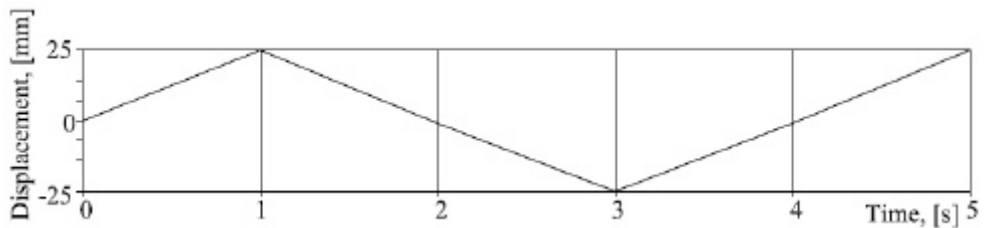


Figure 3. Imposed displacement.

4. RESULTS

The hysteretic loops for models MDC1 and MDC2 are presented in figure 4. Model MDC2 has a better energy dissipation capacity and also a bigger rigidity. The disadvantage of this model is the difficulty of creating the slits.

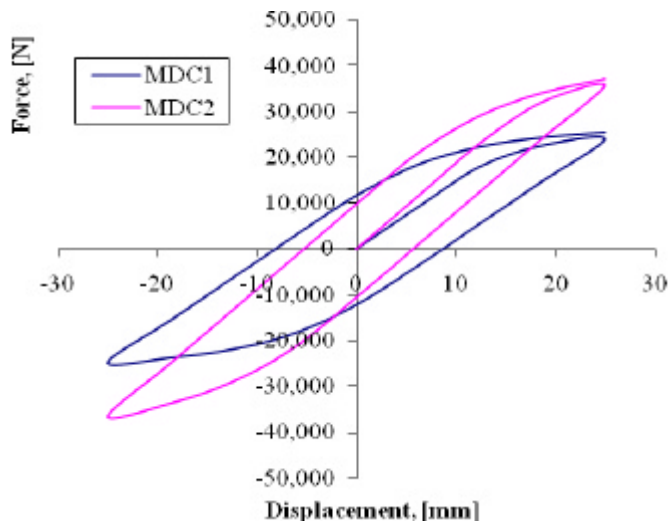


Figure 4. Hysteretic loops for models MDC1 and MDC2.

Models MDC3, MDC4 and MDC5 differ in hole size. The hysteretic loops are presented in figure 5.

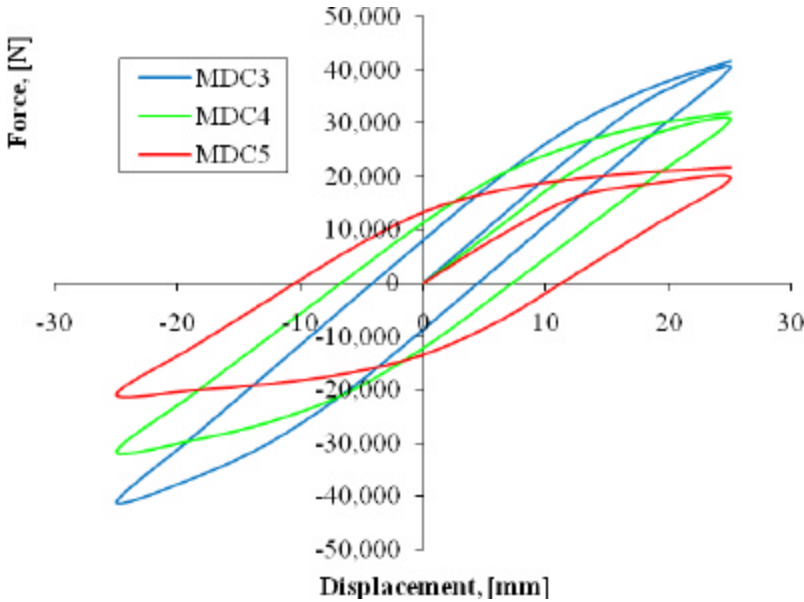


Figure 5. Hysteretic loops for models MDC3, MDC4 and MDC5.

Models MDC5 and MDC6 have different types of hole layouts. By analyzing their hysteretic loops (figure 6) it can be concluded that model MDC5 has a better energy dissipation capacity. Also, the different hole layouts have no influence on the rigidity of the element.

Models MDC5, MDC7 and MDC8 differ by the dissipative element length. The hysteretic loops in figure 7 outline the fact that plastic deformations are better distributed on a shorter dissipative element. Also, the rigidity of the device is decreased by increasing the length of the dissipative element.

The equivalent stresses (von-Misses) of the MDC models are presented in figure 8 and the values of the total dissipated energy for each model are presented in table 1.

Table 1. Total dissipated energy

Model	MDC1	MDC2	MDC3	MDC4	MDC5	MDC6	MDC7	MDC8
Total dissipated energy [J]	1111.7	1183.6	1178	1234.1	1147.5	1092.5	1080.9	956.7

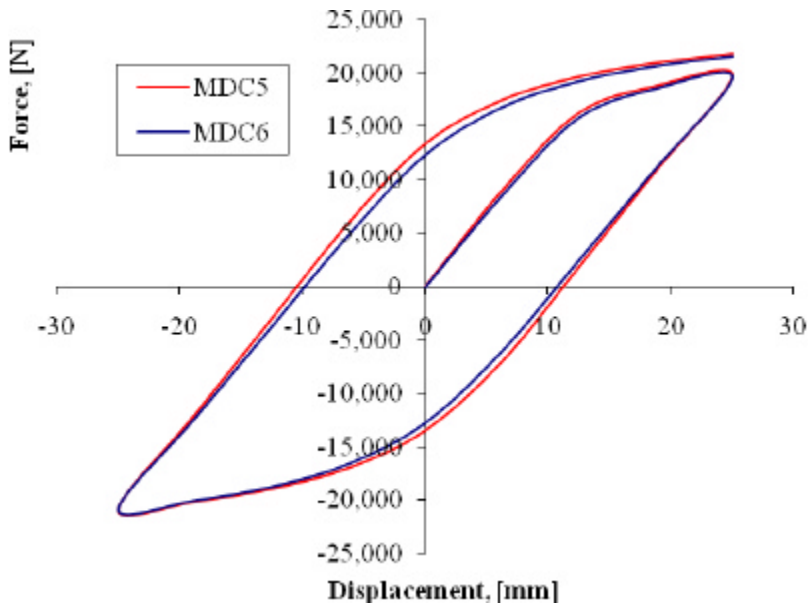


Figure 6. Hysteretic loops for models MDC5 and MDC6.

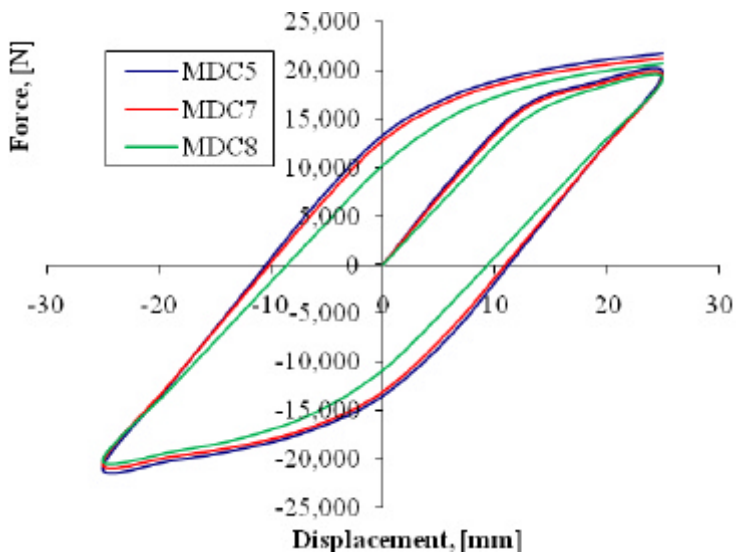


Figure 7. Hysteretic loops for models MDC5, MDC7 and MDC8.

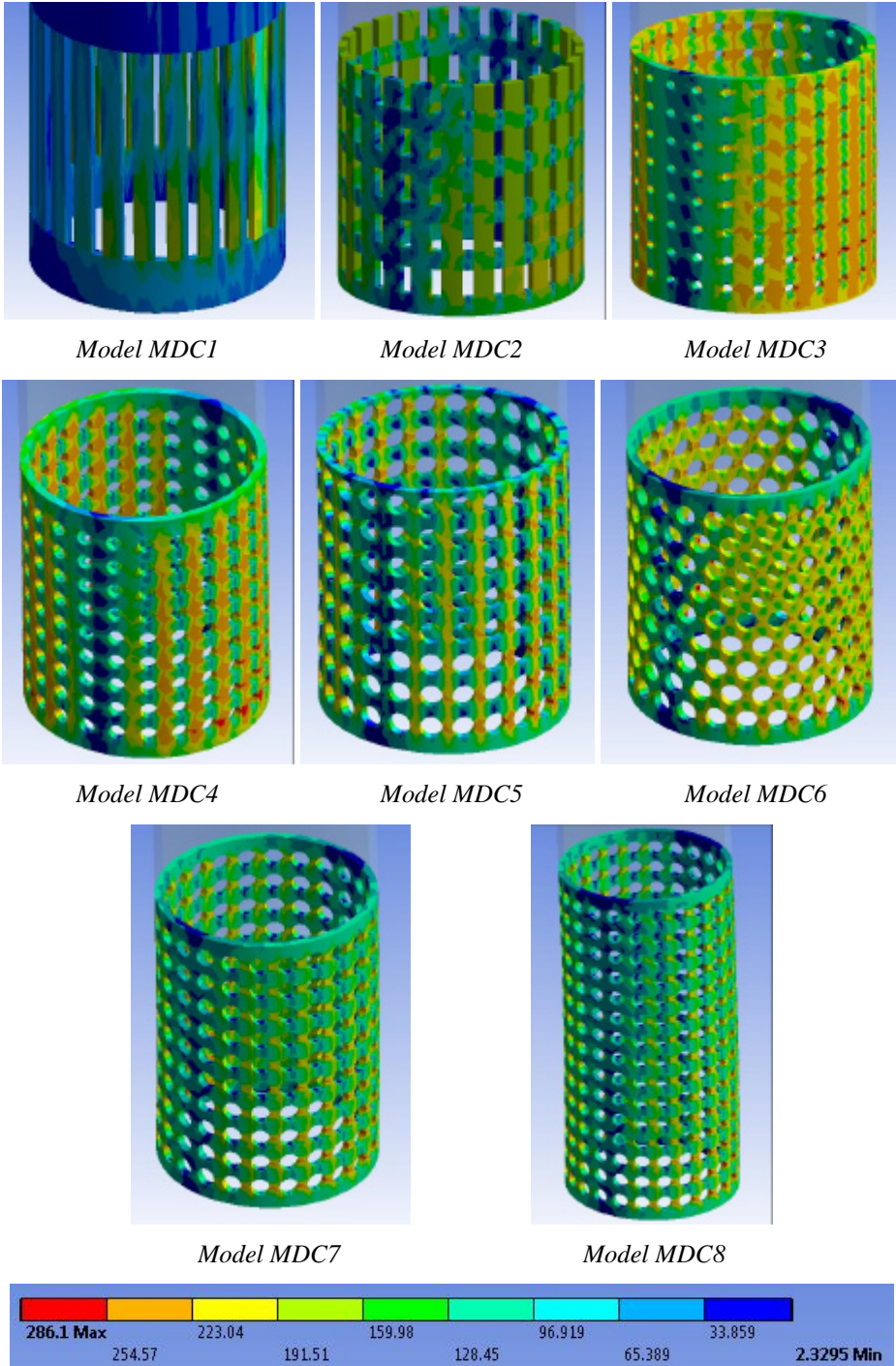


Figure 8. Stresses in MPa in the dissipative elements of the MDC models [1].

5. CONCLUSIONS

The multidirectional energy dissipative columns show great potential for energy dissipation at structures with Slimdek composite floors. The shape of the hysteretic loops of all MDC models analyzed in this paper is symmetric, which means that the behaviour of these devices is stable and predictable in time. These devices can be used either as earthquake dampers or as wind dampers. The variety of hole shapes and sizes allows the structural engineer to fully control the rigidity and energy dissipation capacity of the MDC device.

References

1. ANSYS, User's Manual Revision 11, ANSYS, Inc., Canonsburg, PA, 2009.
2. DIN EN 10210-2. *Hot finished structural hollow sections of non-alloy and fine grain steels – Part 2: Tolerances, dimensions and sectional properties*, Beuth Verlag, Berlin, Germany, 2006.
3. Hicks, S. J., Lawson, R. M., Rackham, J. W., Fordham, P. *Comparative structure cost of modern commercial buildings – Second Edition*, The Steel Construction Institute, UK, 2003.
4. Rackham, J.W., Couchman, G.H., Hicks, S.J. *Composite Slabs and Beams using Steel Decking: Best Practice for Design and Construction (Revised Edition)*, The Steel Construction Institute and The Metal Cladding & Roofing Manufacturers Association, ISBN: 978-1-85942-184-0, UK, 2009.
5. Venghiac, V.M., Budescu, M. *Optimization methods of energy dissipative columns*, Buletinul Institutului Politehnic din Iasi, Sectia Constructii. Arhitectura, Tomul LVII, Fasc. 4, ISSN 1224-3884, pp. 33-41, 2012.
6. Venghiac, V.M., Ciongradi, I.P., Budescu, M. *Steel structures with composite floors and energy dissipative columns*, Proceedings of The 8th International Symposium „Computational Civil Engineering 2010 – New Computational Concepts in Civil Engineering”, Editura Societatii Academice „Matei – Teiu Botez”, ISBN 978-973-8955-87-5, pp. 459-466, Iasi, 2010.
7. Venghiac, V.M., Melenciuc, S.C., Ciongradi, I.P., Budescu, M. *The influence of solid dry friction damping at columns with compound sections*, Buletinul Institutului Politehnic din Iasi, Sectia Constructii. Arhitectura, Tomul LVII, Fasc. 1, ISSN 1224-3884, pp. 47-54, 2011.

